TU Delft

Delft University of Technology

Document Version
Final published version

Citation (APA)
Hartanto, D. (2026). *A systematic and validated framework for selecting greener entrainers towards eco-efficient extractive distillation*. [Dissertation (TU Delft), Delft University of Technology]. https://doi.org/10.4233/uuid:271b4b53-2793-43e0-9a55-7776a98db4b3

Important note
To cite this publication, please use the final published version (if applicable).
Please check the document version above.

Copyright
In case the licence states “Dutch Copyright Act (Article 25fa)”, this publication was made available Green Open Access via the TU Delft Institutional Repository pursuant to Dutch Copyright Act (Article 25fa, the Taverne amendment). This provision does not affect copyright ownership.
Unless copyright is transferred by contract or statute, it remains with the copyright holder.

Sharing and reuse
Other than for strictly personal use, it is not permitted to download, forward or distribute the text or part of it, without the consent of the author(s) and/or copyright holder(s), unless the work is under an open content license such as Creative Commons.

Takedown policy
Please contact us and provide details if you believe this document breaches copyrights.
We will remove access to the work immediately and investigate your claim.

*This work is downloaded from Delft University of Technology.*

# A systematic and validated framework for selecting greener entrainers towards eco-efficient extractive distillation

Dhoni Hartanto

# A systematic and validated framework for selecting greener entrainers towards eco-efficient extractive distillation

Dissertation

for the purpose of obtaining the degree of doctor
at Delft University of Technology
by the authority of the Rector Magnificus,
Prof.dr.ir. H. Bijl,
chair of the Board for Doctorates
to be defended publicly on
Monday, 7 September 2026 at 12:30

by

**Dhoni HARTANTO**

This dissertation has been approved by the promotors.

Composition of the doctoral committee:

| | |
|---|---|
| Rector Magnificus, | chairperson |
| Prof.dr.ir. A.B. de Haan, | Delft University of Technology, promotor |
| Prof.dr.ir. A.A. Kiss, | Delft University of Technology, promotor |

Independent members:

| | |
|---|---|
| Prof.dr.ir. T.J.H. Vlugt, | Delft University of Technology, Netherlands |
| Prof.dr. F.C. Grozema, | Delft University of Technology, Netherlands |
| Prof.dr.ir. B. Schuur, | University of Twente, Netherlands |
| Prof.Dr.-Ing. M.B. Franke, | University of Twente, Netherlands |
| Prof.dr.ir. J. van der Schaaf, | Eindhoven University of Technology, Netherlands |

This research was funded by LPDP (Indonesia Endowment Fund for Education), Ministry of Finance of the Republic of Indonesia.



Key words : greener entrainers, screening framework, eco-efficient, extractive distillation
Cover by : Dhoni Hartanto and Riyan Zulmaniar Vinahari
Copyright : © 2026 by Dhoni Hartanto
ISBN : 978-94-6518-372-5
An electronic version of this dissertation is available at: http://repository.tudelft.nl

# A systematic and validated framework for selecting greener entrainers towards eco-efficient extractive distillation

Proefschrift

ter verkrijging van de graad van doctor
aan de Technische Universiteit Delft,
op gezag van de Rector Magnificus,
Prof.dr.ir. H. Bijl,
voorzitter van het College voor Promoties,
in het openbaar te verdedigen op
Maandag, 7 September om 12:30 uur

door
**Dhoni HARTANTO**

Dit proefschrift is goedgekeurd door de promotoren.

Samenstelling promotiecommissie:

| | |
|---|---|
| Rector Magnificus, | voorzitter |
| Prof.dr.ir. A.B. de Haan, | Technische Universiteit Delft, promotor |
| Prof.dr.ir. A.A. Kiss, | Technische Universiteit Delft, promotor |

Onafhankelijke leden:

| | |
|---|---|
| Prof.dr.ir. T.J.H. Vlugt, | Technische Universiteit Delft, Netherlands |
| Prof.dr. F.C. Grozema, | Technische Universiteit Delft, Netherlands |
| Prof.dr.ir. B. Schuur, | University of Twente, Netherlands |
| Prof.Dr.-Ing. M.B. Franke, | University of Twente, Netherlands |
| Prof.dr.ir. J. van der Schaaf, | Technische Universiteit Eindhoven, Netherlands |

Dit onderzoek werd gefinancierd door LPDP (Indonesia Endowment Fund for Education), Ministerie van Financiën van de Republiek Indonesië.



Kernwoorden : groenere entrainers, screeningkader, coëfficiënt, extractieve destillatie
Omslag : Dhoni Hartanto en Riyan Zulmaniar Vinahari
Copyright : © 2026 by Dhoni Hartanto
ISBN : 978-94-6518-372-5
Een elektronische versie van dit proefschrift is verkrijgbaar op: http://repository.tudelft.nl

*What we contribute through our PhD may enter the world quietly,*
*but knowledge is not built by greatness alone.*
*It grows through countless sparks of inquiry, persistent effort, shared discovery, and*
*steadily built until they become the ground beneath humanity's next leap.*

(*This page is intentionally left blank*)

# Table of contents

## Summary

Extractive distillation (ED) is a key technology for separating close-boiling and azeotropic mixtures by introducing an entrainer that modifies intermolecular interactions within the mixture. Through selective affinity toward specific components, the entrainer increases the non-ideality of the system, enhances relative volatility, and eliminates close-boiling and azeotropic behavior. However, conventional entrainers such as N-methyl-2-pyrrolidone (NMP) raise significant environmental and health concerns, including reproductive toxicity. Meanwhile, many greener candidates, including biobased and greener organic entrainers, as well as natural deep eutectic solvents (NADESs), remain insufficiently evaluated for ED applications. Nevertheless, systematic and validated entrainer selection strategies, supported by reliable vapor-liquid equilibrium (VLE) data and rigorous process performance comparisons for the close-boiling methylcyclohexane-toluene mixture and the azeotropic n-hexane-ethanol mixture containing these underexplored greener entrainers, are unavailable. Therefore, this thesis aims to develop a framework for screening greener entrainers, along with generating reliable VLE data and performing process performance comparison, to identify effective alternatives to NMP for these two representative separation challenges.

To achieve this objective, a multi-stage entrainer selection methodology was developed, integrating initial screening, predictive modelling, experimental validation, and process performance comparison. In Chapter 2, potential greener entrainers were screened using an initial screening phase, which identified potential greener entrainers based on high boiling temperatures, favorable solvency, and compliance with green chemistry principles. Subsequently, key separation metrics, such as selectivity and capacity at infinite dilution, and performance index, were predicted using quantum chemical calculations (COSMO-RS). In addition, relative volatility was predicted using both COSMO-RS and group contribution methods (UNIFAC and modified UNIFAC Dortmund). Promising candidates were then evaluated experimentally through miscibility tests and relative volatility measurements. Selected greener entrainer candidates, along with benchmark entrainer NMP in both mixtures, were examined for their vapor-liquid equilibrium (VLE) data. Chapters 3 and 4 focus on generating reliable VLE data for both mixtures in the presence of each selected greener entrainer at various entrainer-to-feed ratios (E/F) and operating pressures. The experimental data were examined through thermodynamic consistency tests. Moreover, the data were regressed using activity coefficient models (NRTL and UNIQUAC) to obtain the optimum binary interaction parameters. In Chapter 5, these parameters were implemented in Aspen Plus V.12 for ED process simulations. Greener entrainers were evaluated according their performance compared to NMP using economic indicator (total annual cost) and sustainability metrics, such as energy

requirements, water consumption, and $CO_2$ emissions. In addition, the use and limits of predictive tools for ED entrainer screening were evaluated.

The screening results in Chapter 2 identify promising greening entrainers. For the methylcyclohexane–toluene mixture, gamma-valerolactone (GVL), n-butyl-2-pyrrolidone (NBP), and dimethyl isosorbide (DMI) were selected for VLE data experimental evaluation, while NBP, DMI, and guaiacol were selected for the n-hexane–ethanol mixture. Some NADESs and other biobased and greener organic entrainers exhibited favorable predicted selectivity but showed immiscibility issues in the investigated mixtures and were therefore excluded from further evaluation. In Chapters 3 and 4, the measured VLE data for both mixtures containing each entrainer passed the thermodynamic consistency test, indicating the reliability of the data. The VLE data confirmed that the selected greener entrainers significantly increase the relative volatility of the mixtures and effectively remove close-boiling and azeotropic behavior. Process simulations discussed in Chapter 5 indicate that for the separation of methylcyclohexane-toluene, GVL reduces total annual cost (TAC) by 5.6% compared to NMP, while also having a lower energy intensity of 6.1%. In contrast, DMI and NBP exhibit slightly higher TAC values of 6.2% and 15.2%, respectively, along with slightly higher energy intensity of 3.0% and 18.2%. For $CO_2$ emissions and water consumption, GVL remains comparable to NMP, with both exhibiting values of 0.04-0.05 $kg_{CO2}/kg_{products}$ and 0.05 $m^3_{water}/kg_{products}$. For the n-hexane-ethanol mixture, NBP shows a comparable TAC, with 1.6% slightly higher than that of NMP, with a 3.1% increase in energy intensity. Meanwhile, guaiacol and DMI demonstrate increasing TAC by 10.9% and 14.0%, respectively, along with energy intensity that are 12.5% and 18.8% higher. In addition, $CO_2$ emissions for these options remain comparable at around 0.05-0.06 $kg_{CO2}/kg_{products}$ and water consumption is similar at approximately 0.05-0.07 $m^3_{water}/kg_{products}$. Importantly, these greener entrainers have significantly lower toxicity profiles than NMP. Furthermore, the TAC deviation threshold of 32% from predictive models compared to the experimental-based NRTL model makes them suitable for early-stage entrainer screening. However, experimental validation remains necessary for detailed process design.

Overall, this thesis provides a systematic and experimentally validated framework for selecting greener entrainers in extractive distillation. The work delivers new and reliable VLE data along with optimum binary interaction parameters and a comparison of process-level performance. The findings demonstrate that replacing conventional entrainers, such as NMP, with greener alternatives is technically feasible, economically viable, and environmentally sustainable. This supports the transition toward more eco-efficient extractive distillation processes.

## Samenvatting

Extractieve destillatie (ED) is een belangrijke technologie voor de scheiding van mengsels met dicht bij elkaar liggende kookpunten an azeotrope mengsels. Bij deze techniek wordt een entrainer toegevoegd die de intermoleculaire interacties in het mengsel verandert. Door een selectieve affiniteit voor bepaalde componenten te vertonen, verhoogt de entrainer de niet-idealiteit van het systeem, vergroot hij de relatieve vluchtigheid en maakt hij het mogelijk om zowel dicht bij elkaar liggende kookpunten als azeotropie te doorbreken. Conventionele entrainers, zoals N-methyl-2-pyrrolidone (NMP), brengen echter aanzienlijke milieu-en gezondheidsrisico's met zich mee, waaronder reproductietoxiciteit. Tegelijkertijd zijn veel groenere alternatieven, waaronder biogebaseerde en andere milieuvriendelijkere organische entrainers evenals natuurlijke diepe eutectische oplosmiddelen (natural deep eutectic solvents, NADESs), nog onvoldoende onderzocht voor toepassingen in extractieve destillatie. Systematische en gevalideerde strategieën voor de selectie van entrainers, ondersteund door betrouwbare damp-vloeistof-evenwichts gegevens (vapor-liquid equilibrium, VLE-data) en grondige procesvergelijkingen voor de methylcyclohexaan-tolueen en n-hexaan-ethanol mengsels met deze onderbelichte groene entrainers, ontbreken echter. Het doel van dit proefschrift is daarom een raamwerk te ontwikkelen voor de screening van groenere entrainers, gecombineerd met het genereren van betrouwbare VLE-gegevens en een vergelijking van procesprestaties, om effectieve alternatieven voor NMP te identificeren voor deze twee representatieve scheidingsproblemen.

Om dit doel te bereiken werd een meerstapsmethodologie voor entrainerselectie ontwikkeld, waarin initiële screening, voorspellende modellering, experimentele validatie en procesvergelijking worden geïntegreerd. In Hoofdstuk 2 werden potentiële groenere entrainers geïdentificeerd via een eerste screening op basis van hoge kookpunten, gunstige oplosbaarheidseigenschappen en naleving van principes van groenere chemie. Vervolgens werden belangrijke scheidingsparameters, zoals selectiviteit en capaciteit bij oneindige verdunning, een prestatie-index, voorspeld met behulp van kwantumchemische berekeningen (COSMO-RS). Daarnaast werd de relatieve vluchtigheid voorspeld met zowel COSMO-RS als groepsbijdragen modellen (UNIFAC en modified UNIFAC Dortmund). Veelbelovende kandidaten werden vervolgens experimenteel geëvalueerd door middel van mengbaarheidstesten en metingen van relatieve vluchtigheid. De geselecteerde groenere entrainers, samen met de conventionele entrainer NMP, werden vervolgens onderzocht op hun VLE-gegevens in beide mengsels. Hoofdstukken 3 en 4 richten zich op het genereren van betrouwbare VLE-gegevens voor beide systemen in aanwezigheid van de geselecteerde entrainers bij gegevens werden beoordeeld met behulp van thermodynamische

consistentietesten. Daarnaast werden de gegevens gecorreleerd met activiteit coëfficiënt modellen (NRTL en UNIQUAC) om optimale binaire interactieparameters te bepalen. In Hoofdstuk 5 werden deze parameters toegepast in processimulaties van extractieve destillatie in Aspen Plus V.12. De prestaties van de groenere entrainers werden vergeleken met die van NMP op basis van economische indicatoren (totale jaarlijkse kosten, total annual cost, TAC) en duurzaamheidindicatoren, zoals energieverbruik, $CO_2$-emissies en watergebruik. Daarnaast werden het gebruik en de beperkingen van voorspellende methodieken voor de screening voor extractieve destillatie geëvalueerd.

De screening in Hoofdstuk 2 identificeerde verschillende veelbelovende groenere entrainers. Voor het methylcyclohexaan-tolueen mengsels werden gamma-valerolactone (GVL), n-butyl-2-pyrrolidone (NBP), en dimethyl isosorbide (DMI) geselecteerd voor experimentele evaluatie van VLE-gegevens, terwijl voor het n-hexaan-ethanol mengsel, NBP, DMI en guaiacol werden geselecteerd. Sommige NADESs en andere biobased entrainers vertoonden weliswaar gunstige voorspelde selectiviteiten, maar bleken onvoldoende mengbaar met de onderzochte systemen en werden daarom uitgesloten van verdere evaluatie. In Hoofdstukken 3 en 4 bleek dat de gemeten VLE-gegevens voor beide mengsels met de verschillende entrainers voldeden aan de thermodynamische consistentietesten, wat de betrouwbaarheid van de gegevens bevestigt. De VLE-gegevens tonen aan dat de geselecteerde groenere entrainers de relatieve vluchtigheid van de mengsels aanzienlijk verhogen en effectief zowel dicht bij elkaar liggende kookpunten als azeotropie opheffen. Processimulaties, besproken in Hoofdstuk 5, laten zien dat voor de scheiding van methylcyclohexaan en tolueen GVL de totale jaarlijkse kosten (total annual cost, TA) met 5.6% verlaagt ten opzichte van NMP, terwijl ook de energie-intensiteit met 6.1% afneemt. Daarentegen vertonen DMI en NBP respectievelijk 6.2% en 15.2% hogere TAC-waarden en een iets hogere energie-intensiteit van respectievelijk 3.0% en 18.2%. Wat betreft $CO_2$-emissies en watergebruik blijft GVL vergelijkbaar met NMP, met waarden van ongeveer 0.04-0.05 $kg_{CO2}/kg_{products}$ en 0.05 $m^3_{water}/kg_{products}$. Voor het n-hexaan-ethanol-mengsel vertoont NBP een TAC die vergelijkbaar is met die van NMP, namelijk slechts 1.6% hoger, met een toename van 3.1% in energie-intensiteit. Guaiacol en DMI leiden daarentegen tot hogere TAC-waarden van respectievelijk 10.9% en 14.0% met energie-intensiteiten die respectievelijk 12.5% en 18.8% hoger zijn. De $CO_2$-emissies blijven voor alle opties vergelijkbaar, rond 0.05-0.06 $kg_{CO2}/kg_{products}$, en ook het waterverbruik is vergelijkbaar met waarden van ongeveer 0.05-0.07 $m^3_{water}/kg_{products}$. Belangrijk is dat deze groenere entrainers aanzienlijk minder toxisch zijn dan NMP. Verder maakt de TAC-afwijkingsdrempel van 32% voor predictieve modellen ten opzichte van het op experimentele gegevens gebaseerde NRTL-model deze

modellen geschikt voor screening van entrainers in een vroeg stadium en voor voorlopig ontwerp van extractieve destillatie. Voor gedetailleerd procesontwerp blijft experimentele validatie echter noodzakelijk.

Samenvattend biedt dit proefschrift een systematisch en experimenteel gevalideerd raamwerk voor de selectie van groenere entrainers voor extractieve destillatie. Het onderzoek levert nieuwe en betrouwbare VLE-gegevens, optimale binaire interactieparameters en een vergelijking van procesprestaties op procesniveau. De resultaten tonen aan dat het vervangen van conventionele entrainers, zoals NMP, door groenere alternatieven technisch haalbaar, economisch verantwoord en milieukundig duurzamer is. Daarmee ondersteunt dit werk de transitie naar meer eco-efficiënte extractieve destillatieprocessen.

# Ikhtisar

Distilasi ekstraktif (DE) merupakan teknologi unggul untuk pemisahan suatu campuran dengan titik didih berdekatan maupun azeotrop dengan penambahan entrainer yang dapat memodifikasi interaksi intermolekular di dalam campuran. Melalui afinitas selektif terhadap komponen tertentu, entrainer meningkatkan ketidakidealan campuran, volatilitas relatif, serta menghilangkan titik didih berdekatan maupun azeotrop. Tetapi, penggunaan pelarut konvensional seperti N-metil-2-pirolidon (NMP) sebagai entrainer menimbulkan masalah lingkungan dan kesehatan yang serius, khususnya toksisitas reproduksi. Di sisi lain, banyak alternatif yang lebih ramah lingkungan yang masih belum dievaluasi secara memadai untuk diaplikasikan di DE, termasuk pelarut berbasis bio dan pelarut organik yang lebih ramah lingkungan, serta *natural deep eutectic solvents* (NADESs). Meskipun demikian, strategi pemilihan entrainer yang sistematis dan tervalidasi, yang didukung oleh data kesetimbangan uap-cair (VLE) yang akurat serta perbandingan kinerja proses yang tepat masih belum tersedia. Khususnya untuk campuran metilsikloheksana-toluena yang memiliki titik didih berdekatan dan campuran azeotropik n-heksana-etanol dengan penambahan entrainer ramah lingkungan yang belum banyak dieksplorasi. Oleh karena itu, penelitian ini bertujuan untuk mengembagkan kerangka kerja untuk seleksi entrainer yang lebih ramah lingkungan, disertai dengan produksi data VLE yang akurat, dan mengevaluasi perbandingan kinerja proces untuk mengidentifikasi entrainer alternatif yang efektif sebagai pengganti NMP pada dua campuran yang diteliti.

Untuk mencapai tujuan penelitian, dikembangkan metode pemilihan entrainer ramah lingkungan bertahap yang mengintegrasikan seleksi awal, perhitungan dengan model prediktif, validasi eksperimental, dan perbandingan kinerja proces. Pada Bab 2, entrainer yang lebih ramah lingkungan diseleksi menggunakan tahap penyaringan awal, yang mengidentifikasi entrainer potensial berdasarkan titik didih tinggi, daya larut yang baik, dan kepatuhan terhadap prinsip-prinsip kimia ramah lingkungan. Selanjutnya, metrik pemisahan utama seperti selektivitas dan kapasitas pada pengenceran tak terbatas, dan indeks kinerja diprediksi menggunakan perhitungan kimia kuantum (COSMO-RS). Selain itu, volatilitas relatif juga diprediksi menggunakan metode COSMO-RS dan metode kontribusi kelompok (UNIFAC dan UNIFAC Dortmund termodifikasi). Kandidat entrainer ramah lingkungan yang berpotensi kemudian dievaluasi secara eksperimental melalui uji kelarutan dan pengukuran volatilitas relatif. Kemudian, data VLE diukur untuk dua campuran dengan kandidat entrainer yang terpilih dan NMP sebagai entrainer acuan.

Bab 3 dan 4 berfokus pada pengukuran data VLE yang akurat untuk kedua campuran yang mengandung entrainer ramah lingkungan yang terpilih. VLE diukur pada berbagai komposisi entrainer (rasio entrainer terhadap bahan baku

(E/F)) dan tekanan operasi. Data eksprimen yang diperoleh diuji menggunakan uji konsistensi termodinamika. Selain itu, data tersebut diregresi menggunakan model koefisien aktivitas yaitu NRTL dan UNIQUAC untuk memperoleh parameter interaksi biner yang optimal. Pada Bab 5, parameter-parameter ini diaplikasikan ke Aspen Plus V12 untuk digunakan pada simulasi proses DE. Kinerja entrainer ramah lingkungan dievaluasi dan dibandingkan dengan NMP menggunakan indikator ekonomi (total biaya tahunan) dan metrik keberlanjutan, seperti kebutuhan energi, air, dan emisi $CO_2$ yang dihasilkan. Selain itu, pada penelitian ini juga dilakukan evaluasi terhadap penggunaan dan batasan penggunakan model prediktif untuk seleksi entrainer pada DE.

Hasil seleksi entrainer pada Bab 2 mengidentifikasi bahan entrainer yang berpotensi untuk digunakan. Untuk pengukuran data VLE pada campuran metilsikloheksana-toluena, entrainer yang dipilih antara lain gamma-valerolakton (GVL), n-butil-2-pirolidon (NBP), dan dimetil isosorbide (DMI). Sedangkan pada campuran n-heksana-etanol, entrainer yang dipilih adalah NBP, DMI, dan guaiacol. Beberapa NADESs dan entrainer berbasis bio dan organik yang lebih ramah lingkungan lainnya juga menunjukkan selektivitas yang baik. Akan tetapi, terdapat kendala pada penerapannya yaitu entrainer tidak dapat larut dengan baik saat diimplementasikan di kedua campuran sehingga pada penelitian ini entrainer-entrainer tersebut tidak dievaluasi lebih lanjut. Data VLE yang telah diperoleh pada Bab 3 dan 4 untuk kedua campuran dengan kandungan entrainer di dalamnya menunjukkan data yang konsisten berdasarkan uji konsistensi termodinamika. Hal ini menunjukkan bahwa data VLE yang diperoleh akurat. Data VLE tersebut juga menunjukkan bahwa entrainer ramah lingkungan dapat meningkatkan volatilitas relatif campuran secara signifikan sekaligus menghilangkan titik didih berdekatan serta titik azeotrop secara efektif. Simulasi proces yang dibahas pada Bab 5 menunjukkan bahwa pada pemisahan campuran metilsikloheksana-toluena, GVL dapat menurunkan total biaya tahunan hingga 5,6% dengan intensitas energi yang lebih rendah 6,1% dibandingkan dengan NMP. Sebaliknya, DMI dan NBP menghasilkan total biaya tahunan yang sedikit lebih tinggi yaitu masing-masing 6,2% dan 15,2% dengan intensitas energi yang juga sedikit lebih tinggi yaitu masing-masing 3,0% dan 18,2% dibanding NMP. Untuk emisi $CO_2$ dan kebutuhan air, GVL sebanding dengan NMP. Keduanya menunjukkan nilai 0,04 – 0,05 $kg_{CO2}/kg_{produk}$ dan 0,05 $m_{air}/kg_{produk}$. Untuk campuran n-heksana-etanol, NBP menunjukkan total biaya tahunan yang sebanding tetapi sedikit lebih tinggi (1,6%) dibandingkan dengan NMP. Untuk intensitas energi, nilainya lebih tinggi 3,1%. Sementara itu, peningkatan total biaya tahunan untuk guaiacol dan DMI masing-masing sebesar 10,9% dan 14,0%. Intensitas energi lebih tinggi sebesar 12,5% dan 18,8%. Sedangkan emisi $CO_2$ sebanding dengan NMP yaitu 0,05 – 0,06 $kg_{CO2}/kg_{produk}$. Kebutuhan air juga menunjukkan nilai yang sebanding pada sekitar

0,05 – 0,07 $m_{air}/kg_{produk}$. Meskipun demikian, hal yang sangat penting adalah bahwa entrainer ramah lingkungan ini mempunyai profil toksisitas yang jauh lebih rendah dibandingkan dengan NMP. Hasil evaluasi penggunaan model prediktif untuk proses simulasi menunjukkan bahwa ambang batas penyimpangan total biaya tahunan sebesar 32% dibandingkan dengan model berbasis eksperimen yaitu NRTL. Hal ini menunjukkan bahwa model prediktif dapat digunakan untuk seleksi entrainer tahap awal. Namun, validasi melalui eksperimen tetap diperlukan untuk perancangan proces yang lebih detail.

Secara keseluruhan, disertasi ini menyajikan kerangka kerja yang sistematis dan tervalidasi secara eksperimental untuk menyeleksi entrainer yang lebih ramah lingkungan dalam distilasi ekstraktif. Penelitian ini menghasilkan data VLE yang baru dan akurat, disertai dengan parameter interaksi biner yang optimal serta perbandingan kinerja proces DE. Temuan-temuan tersebut menunjukkan bahwa penggantian entrainer konvensional seperti NMP dengan alternatif yang lebih ramah lingkungan dapat dilakukan dengan pertimbangan teknis, ekonomis, dan lingkungan. Hal ini dapat mendukung transisi menuju proces distilasi ekstraktif yang lebih ramah lingkungan.

# Chapter 1

## Introduction

*Part of this chapter has been published in:*
*Journal of Chemical & Engineering Data 64 (38), 18927-18937 (2025)*
*Fluid Phase Equilibria 605, 114694 (2026)*

## 1.1.Motivation and extractive distillation technology

In chemical industries, separation is one of the most important processes, as it contributes to more than 50% of the total energy and costs.[1,2] Distillation is the most widely used separation method in the chemical industry, offering several advantages. It can operate across a wide range of feed flow rates and concentrations, demonstrates high mass transfer efficiency,[3] can handle various complex mixtures,[4] and produces high-purity products.[5] Currently, more than 100,000 distillation columns are in operation worldwide, and they account for 40-50% of the plant's total cost.[4,6] However, conventional distillation is not capable to separate azeotropic mixture and require very large number of stages to separate the close-boiling mixture. Therefore, it is not effective to separate these challenging mixtures. Consequently, finding an effective separation process has received increasing focus over the last years. To overcome these challenges, extractive distillation (ED) is commonly employed. ED is a hybrid technology combining heat and entrainer as an energy and affinity separation agent, respectively.[7,8] The separation performance of the entrainer significantly impacts the sustainability of the ED processes by affecting energy efficiency, $CO_2$ emissions, and water consumption, while ensuring cost competitiveness. In addition, ED relies on high-boiling entrainers that circulate continuously within the process. Therefore, the environmental and toxicological profiles of entrainers influence the sustainability of the separation process. ED has been demonstrated as a more effective technology compared to other separation methods, such as azeotropic distillation (AD), liquid-liquid extraction (LLE), and pressure swing distillation (PSD), for various industrial implementation.[9,10] The comparison between these technologies is provided in Table 1.

**Table 1.** Comparison among azeotropic and close-boiling mixture separation technology[11–14]

| **Separation technology and their main principle** | **Advantages** | **Disadvantages** |
|---|---|---|
| *Extractive distillation (ED):* Addition of a high-boiling entrainer, complete miscibility in the mixture, modify relative volatility, not forming new azeotrope. | Larger capacity than liquid liquid-liquid extraction, not limited by pressure sensitivity, industrially mature and widely applied, high product purity achievable, flexibility in design as more degree of freedom, less entrainer required compared to AD, entrainer recovery is in the bottom of entrainer recovery column therefore, vaporization of entrainer is not required | Requires entrainer recovery column, energy intensive, entrainer screening is crucial, possible thermal degradation of entrainer |

| Separation technology and their main principle | Advantages | Disadvantages |
|---|---|---|
| *Azeotropic distillation (AD)*: Addition of an entrainer, which forms a new azeotrope and phase splitting to allow separation work | Capable of effectively separating dilute concentration, highly volatile components | Complex phase behavior, higher entrainer losses possible, requires large amount of entrainer, targeted product as volatile component and entrainer is vaporized |
| *Liquid-liquid extraction (LLE)*: Separation achieved based on different solubility in immiscible liquid phases | Suitable for separation of low decomposition component separation, non-volatile component, and component with spanning a broad boiling-point range, operates at low temperature | Effective operation depends on the formation of two partially immiscible liquid phases, more complex equipment and costly than other methods, possible fouling in the equipment, less purity product compared to ED, need subsequent purification to separate trace solvent. |
| *Pressure-swing distillation (PSD)*: Exploits pressure dependence of azeotrope composition | No entrainer required, prevents entrainer handling, no contamination risk in the targeted product | Only applicable if azeotrope is pressure-sensitive, operation and control is complex |

ED involves the addition of entrainers that improve the separation process. Entrainers interact more effectively with specific components in the mixture, increasing relative volatility, and thereby facilitating separation by breaking the azeotropic point and removing the close-boiling behavior in the mixtures. Consequently, this approach reduces energy and water requirements, $CO_2$ emissions, and costs. A conceptual extractive distillation process design is provided in Figure 1. The entrainer and the feed mixture (A+B) are added to the extractive distillation column. Light component (A) will be vaporized and condensed as a high-purity top product. The heavier component (B) will be at the bottom of the product as a mixture with the entrainer. The entrainer will be separated from component B in an entrainer recovery column, and the high-purity entrainer will be recycled to the extractive distillation column.

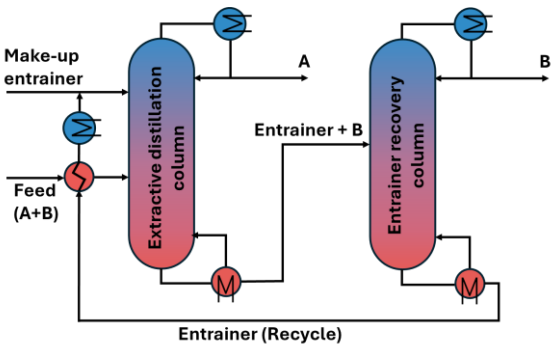


**Figure 1**. Extractive distillation process scheme.

## 1.2. Entrainer for extractive distillation

The performance of ED strongly depends on the selection of suitable entrainers. An effective entrainer should[15–17]:

- Significantly increase relative volatility
- Fully miscible in the feed mixture
- Exhibit high thermal and chemical stability.
- Possess low volatility and viscosity
- Noncorrosive and economically feasible
- Easily recoverable without forming new azeotropes

While conventional organic entrainers can fulfil many of these criteria, they often suffer from drawbacks such as high volatility, toxicity (including reproductive toxicity), lack of eco-friendliness, and increasing regulatory restrictions.[18,19] Recent research has therefore focused on developing greener entrainers with more sustainable characteristics. These new entrainers are less toxic or non-toxic, eco-friendly, and derived from bio-based or sustainable materials.[16,20] By adopting greener entrainers, process sustainability can be increased by mitigating the negative environmental and hazard effects while providing lower or comparable cost, energy, $CO_2$ emission, and water requirements of conventional organic entrainers.

Examples of such green entrainers that have been extensively studied include ionic liquids (ILs),[21–24] biological buffers,[25,26] bio-based entrainers,[27–29] and deep eutectic solvents (DESs)/low transition temperature mixtures (LTTMs).[30–38] However, each alternative presents limitations. The use of ILs on an industrial scale is limited due to their high cost, toxic potential, and low biodegradability.[39,40] According to our miscibility tests described in Chapter 2, Section 2.5.6, some bio-based entrainers, such as Cyrene, face miscibility issues in non-polar mixtures. While DESs/LTTMs are promising, not all can significantly increase relative volatility and effectively remove the azeotropic point.[41–43] They also encounter miscibility issues when applied to the mixtures containing non-polar components.[44] Additionally, biobased compounds such as dl-limonene, butyl propanoate, and butyl butanoate are limited by their low boiling points.[45–47] A high boiling point of an entrainer is a crucial feature for ED, as it prevents entrainer vaporization, thus ensuring a high-purity product. Moreover, a significant boiling point difference between the entrainer and the heavy component facilitates easier separation in the entrainer recovery column. The miscibility of the entrainer in the mixture is also vital, as homogeneous mixtures provide effective interactions between molecules and therefore impacts the effectiveness of the separation.

Despite increasing interest in greener entrainers, systematic evaluation of high-boiling points and environmentally benign entrainers remains limited. Many

potentially suitable candidates combining high boiling points, favorable solvency, and environmental profiles have not yet been comprehensively assessed for ED applications. These potential entrainers include biobased and greener organic entrainers, as well as natural deep eutectic solvents (NADESs), which could lead to the identification of new green entrainers to replace conventional organic entrainers in ED.[48,49]

## 1.3. Entrainer screening methodology

Selecting the right entrainer is crucial for the optimum ED design. Heuristics, or rules of thumb, have been developed to rank entrainers and facilitate the decision-making process for selecting the most effective one. While qualitative selection can help identify a suitable entrainer, this approach has a lack of accuracy. Experimental methods typically produce reliable results; however, they require significant effort, are costly, and can be time-consuming.[50] In contrast, alternative methods, such as Computer-Aided Molecular Design (CAMD), are gaining popularity. While these methods are more effective and widely accepted, they tend to be less accurate than experimental methods. CAMD relies on a molecule structure that allows for property predictions of solvents using group contribution methods. Among the CAMD approaches, UNIQUAC Functional-group Activity Coefficients (UNIFAC) along with its related model (modified UNIFAC Dortmund), and UNIFAC-Lei models demonstrate strong solvent selection capabilities.[51–57] Nonetheless, a significant challenge with these models is the availability of functional group parameters, particularly for new solvent types.[58,59] Another CAMD-based model is the COnductor-like Screening MOdel for Realistic Solvents (COSMO-RS) and COnductor-like Screening Model for Segment Activity Coefficient (COSMO-SAC). These models predict thermophysical properties based on unimolecular quantum chemical calculations. One of their main advantages is that they can be applied to molecules for which group contribution parameters are not available.[58,60]

Various screening strategies have been reported in the literature. Jeon et al. conducted an experimental screening of ILs using relative volatility to separate ethylbenzene from p-xylene. Their study identified 1,2,4 trichlorobenzene:maleic anhydride (2:1) as the best entrainer.[61] In another report, Cignitti et al. employed the UNIFAC model to screen potential entrainers, such as ethylene glycol, water, and dimethyl sulfoxide, for acetone-methanol separation. Their findings indicated that ethylene glycol provided the best driving force, which means the best separation performance.[62] Brouwer et al. evaluated greener solvents for separating methylcyclohexane-toluene and n-heptane-1-heptene. They screened entrainers using predicted relative volatility calculated with the modified UNIFAC Dortmund and compared these results with experimental results. The modified

UNIFAC Dortmund model showed good agreement with experimental values. Based on their screening results, Cyrene was selected due to its high relative volatility.[28] Additionally, they explored several biobased solvents for the separation of acetone and diisopropyl using predicted relative volatility from the modified UNIFAC Dortmund model, which was further validated with experimental results. They found that a bio-based entrainer named, DL-Limonene exhibited a higher relative volatility compared to the conventional organic solvent dimethyl sulfoxide (DMSO) and other alternative solvents such as ethylene carbonate and water, which yield relative volatility lower than 1.[27] For the ILs screening, the UNIFAC-Lei model was utilized, which identified two effective ionic liquids of 1-Ethyl-3-methylimidazolium tetrafluoroborate [EMIM][BF4] and 1-Buthyl-3-methylimidazolium tetrafluoroborate [BMIM][BF4], for ethanol-water separation.[57] Although group contribution methods offer favorable predictions, they are limited by the unavailability of parameters for certain solvents. This restriction affects their application for novel solvents, particularly those lacking functional group parameters.

COSMO-RS has been extensively utilized in entrainer screening. Previous studies have shown that COSMO-RS performs well in predicting thermophysical properties of novel solvents, such as ILs and DESs. For example, Gutiérrez et al. reported the preselection of various ILs as entrainers by predicting selectivity and activity coefficients at infinite dilution using COSMO-RS for the separation of 1-hexane from n-hexane, as well as methylcyclohexane and toluene.[63] Malik et al. investigated the selection of ILs as entrainers by calculating selectivity, capacity, and activity coefficient with COSMO-RS for the separation of ethanol from water.[21] Additionally, selectivity, capacity, and performance index derived from activity coefficients at infinite dilution were predicted using COSMO-RS to screen DESs for the separation of cyclohexane from benzene.[64] COSMO-RS was also employed to predict the distribution coefficient, selectivity, and performance index of 49 DESs with various combinations of hydrogen bond donor (HBD), hydrogen bond acceptor (HBA), and their ratio in the context of extractive desulfurization. Based on the prediction results, the DES with the highest performance index was experimentally tested for its desulfurization efficiency. The results revealed that COSMO-RS predictions align well with experimental data.[65] Salleh et al. studied the selection of DESs for cyclohexane-benzene separation using COSMO-RS, screening 40 DESs that include choline BF4-, ChCl, choline nitrate, methyltriphenylphosphonium bromide, benzyltriphenylphosphonium bromide, N,N-diethylenethanolammonium chloride, tetrabutylammonium bromide, and tetramethylammonium chloride as HBAs, along with various greener HBDs. From this screening, 5 DESs were selected.[64] Therefore, COSMO-RS can serve as a reliable tool for early-stage

entrainer screening. However, validation with experimental data is necessary, as this work shows that COSMO-RS tends to underpredict TAC performance, with larger deviation for associating systems, as discussed in Chapter 5.

Another type of COSMO-based model, known as COSMO-SAC, has been widely used for entrainer screening. The COSMO-SAC model predicts the activity coefficient at infinite dilution, which is then used to calculate the selectivity, capacity, and performance index DESs in isopropanol-water mixture.[32] One study indicated that selectivity at infinite dilution, calculated using COSMO-SAC, can serve as a parameter for selecting biobased entrainers for isobutanol and isobutyl acetic acid separation.[66] The COSMO-SAC method has also been employed to select conventional organic entrainers, taking into account various constraints, such as boiling point, melting point, material prices, and toxicity. This selection process was followed by VLE data measurement and process simulation.[67] Similarly, Li et al. used relative volatility and COSMO-SAC molecular analysis to identify effective organic entrainers.[68] Bio-based entrainers, such as propyl propionate, and butyl propanoate, have been screened using the COSMO-SAC model for the separation of n-hexane/cyclohexane-ethanol. The model predicted the selectivity of the mixture when incorporating butyl butanoate, propyl propionate, and butyl propanoate. In both systems, butyl butanoate was predicted to have the highest selectivity. VLE data for the binary system was measured to obtain binary interaction parameters, indicating that, this new bio-based entrainer is a viable entrainer option for alcohol-hydrocarbon separation.[29] Furthermore, Zhan et al. utilized molecular simulation, including dissipative particle dynamics and density functional theory, to screen conventional organic entrainers for separating dimethyl disulfide and methyl tert-butyl ether. They discovered that DMSO exhibited the strongest interaction with dimethyl disulfide among the solvents investigated, suggesting that DMSO offers the best separation capability.[69]

In addition to CAMD and experimental methods, other screening techniques were employed, including Infinitely Sharp Split (ISS) method. This approach combines VLE data for a pseudo-ternary mixture with the driving force concept, to select an appropriate entrainer. Through to this method, methyl salicylate was identified as the most effective entrainer for separating an azeotropic mixture of methanol-dimethyl carbonates. Moreover, the ranking of entrainers aligned with the optimization results of ED.[70] Sethi et al. developed process-driven approach for entrainer selection that combines screening of entrainer properties, heuristics criteria, and ED design using the UNIFAC model. Their findings indicate that 1,1,2,2-tetrabromoethane is the most effective entrainer for separating ethylbenzene-styrene.[71] Cheng et al. investigated conventional organic entrainers using relative volatility predictions derived from activity coefficient models, such

NRTL and UNIQUAC. Their results showed that ethylene glycol is the most effective option for single-entrainer processes for separating methanol-tetrahydrofuran, tetrahydrofuran -water, and n-butanol-water.[72] Xu et al. explored relative volatility predicted using the NRTL model along with thermophysical properties, including specific heat, latent heat, and boiling point, as criteria for screening conventional organic entrainers.[73] Additionally, relative volatility predictions using the NRTL model, along with sigma profile analysis calculated by COSMO-SAC, were used to screen conventional organic entrainers for cyclohexane-isopropanol, cyclohexane-water, and isopropanol-water separations. The results revealed that ethylene glycol yielded the highest relative volatility for the cyclohexane-isopropanol separation, while DMSO was the most suitable for isopropanol-water. Both ED and DMSO provided effective results for the cyclohexane-water separation.[74]

## 1.4. Process performance comparison

Process performance comparison studies between green entrainers and conventional entrainers for the separation of azeotropic and close-boiling mixtures are limited in the literature. Only view relevant studies available. For instance, Brouwer et al. compared bio-based entrainers and conventional organic entrainers for separating methylcyclohexane-toluene using extractive distillation and liquid-liquid extraction. At both low and high toluene concentrations, ED with Cyrene was more efficient than ED with sulfolane, the benchmark entrainer. This suggested that Cyrene is a suitable bio-based alternative entrainer for separating aromatic and aliphatic mixtures.[75] Additionally, Minor et al. studied DES-based ED compared to conventional organic entrainer-based ED. Choline chloride:urea [ChCl:Ur] (1:2) and choline chloride:triethylene glycol [ChCl:TEG] (1:3) for the ethanol-water and isopropanol-water separations, respectively, were evaluated and compared with the conventional entrainer, ethylene glycol. DES-based ED exhibited improved performance, potentially saving up to 20% in energy requirements and 16% in total annual cost compared to conventional organic entrainer-based ED. Furthermore, DES can save up to 6% of energy requirements when compared to IL-based ED.[76]

Nevertheless, the selection methods, vapor-liquid equilibrium data, and process performance comparison of overlooked biobased, green organic entrainers, and NADESs in the studied mixtures are limited and need to be established. To address this gap, this study develops a systematic and validated framework through a multi-stage process. It integrates initial screening according to high-boiling point, solvency, and green entrainer criteria; molecular-level screening metrics, such as predicted selectivity and capacity at infinite dilution; predicted and experimental relative volatility; miscibility tests; experimental vapor-liquid equilibrium and

thermodynamic consistency test; thermodynamic model correlation; and process performance comparisons between greener and conventional entrainers, as illustrated in Figure 2. This framework is required, as it enables effective selection for greener entrainers, allowing for the identification of suitable entrainers in the early stages while also eliminating unsuitable options. Consequently, this approach reduces the time and effort required to evaluate all entrainers experimentally.

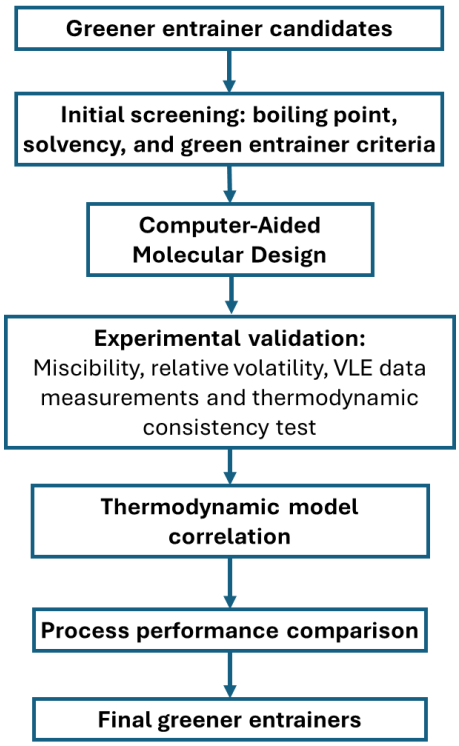


**Figure 2**. Entrainer screening approach.

## 1.5. Scope of research

### 1.5.1. Polarity-based classification of mixtures

Azeotropic and close-boiling mixtures cannot be efficiently separated by conventional distillation. The polarity of the components plays a key role in determining intermolecular interactions and separation behavior. According to molecular polarity, mixtures can generally be classified into three categories: non-polar/non-polar, non-polar/polar, and polar/polar mixtures.

This study specifically focuses on two representative types of mixture: non-polar/non-polar and non-polar/polar mixtures. These mixtures are selected because polar entrainers are commonly used in extractive distillation and can

potentially interact differently with each type of mixture. However, separation of such mixtures can be challenging because strong polarity differences between entrainers and mixture compounds may lead to heterogeneous phase formation. Therefore, investigating these mixtures allows the evaluation of entrainer performance under different intermolecular interaction regimes.

Polar/polar mixtures, such as alcohol – water, are not considered in this study. This exclusion is primarily due to the hygroscopic nature of NADESs, which are one of the entrainer types investigated in this study. The presence of water in the NADESs can significantly influence the physicochemical properties and diminish their effectiveness as entrainers for mixtures containing water.

### 1.5.2. Case studies

Two representative mixtures were selected: methylcyclohexane-toluene and n-hexane-ethanol. The methylcyclohexane-toluene mixture represents a non-polar/ non-polar mixture, which has become one of the most important separation processes in the petrochemical industry.[77] Methylcyclohexane and toluene are a binary hydrocarbon mixture with a close–boiling behavior. Methylcyclohexane ($T_b$ = 374.15 K[78]) and toluene ($T_b$ = 383.15 K[79]) exhibit a narrow boiling point difference. It is further reflected in their VLE profile,[80] where the vapor and liquid phase compositions are closely aligned. These characteristics make it challenging to separate the mixture into high-purity products using conventional separation technologies, such as conventional distillation. Therefore, it is necessary to separate this close-boiling mixture using advanced separation technology to achieve the desired specification of high-purity methylcyclohexane and toluene, respectively. Methylcyclohexane has been used in a wide range of applications, such as fuel additives to improve combustion performance, chemical intermediates, and hydrogen carriers, and it has also been used in industrial separation processes as an extraction solvent.[81–84] Toluene also has a broad range of applications, such as fuel, hydrogen carriers, and extraction solvents.[85–87] In addition, this system can represent a wide range of separations in complex hydrocarbon mixtures.[28] The n-hexane-ethanol mixture represents a non-polar/polar mixture that forms a homogeneous azeotrope. This mixture is commonly found in various industries, including petrochemicals.[88] Ethanol, as one of the low-carbon alcohols, is generated from syngas derived from natural gas or coal. This direct syngas-to-ethanol pathway inherently produces $C_{2+}$ hydrocarbons, including n-hexane.[89,90] Likewise, Fischer-Tropsch synthesis yields oxygenated compounds, including ethanol, together with hydrocarbons, such as n-hexane.[91] Since both n-hexane and ethanol are extensively used as solvents across a broad range of applications, achieving their effective separation is essential to obtain high purity of each component, considering the azeotrope inherent in the

mixture.[92] A summary of the selected mixtures and the possible separation technology applied is provided in Table 2.

**Table 2**. The specification of the mixtures

| Binary mixture | Polarity | Type of mixture | Separation technology applied |
|---|---|---|---|
| Methylcyclohexane-toluene | non-polar/non-polar | Close boiling mixture<br>Aliphatic - Aromatic | extractive distillation and liquid-liquid extraction[75]<br>membranes[93,94]<br>azeotrope distillation, liquid-liquid extraction, crystallization by freezing, adsorption[95] |
| N-hexane-ethanol | non-polar/polar | Homogenous azeotrope<br>Aliphatic - Alcohol | liquid-liquid extraction [88,96–98]<br>extractive distillation[29,99]<br>membrane[100] |

## 1.6. Overview of research

The aim of this research is to establish a systematic and validated framework for screening greener entrainers, along with accurate VLE data and process performance comparison, to define effective alternatives to the conventional solvent NMP in the separation of the methylcyclohexane-toluene and n-hexane-ethanol mixtures. This study systematically evaluates several greener alternatives, including biobased and greener organic solvents, as well as NADESs, to serve as sustainable replacements for NMP. The research focuses on two representative systems: methylcyclohexane–toluene (close-boiling components) and n-hexane–ethanol (azeotropic). A multi-stage green entrainer selection methodology has been developed. This framework integrates initial green entrainer screening, predictive thermodynamic models, experimental work, thermodynamic consistency test and model correlation, and process performance comparison through process simulations. The initial green entrainer screening involved selecting suitable green entrainers according to their high boiling points, solvency, and green chemistry properties. The selected green entrainers are categorized into two groups: (i) biobased and greener organic entrainers and (ii) NADESs. Subsequently, quantum chemical calculations were performed using COSMO-RS and group contribution methods, including UNIFAC and modified UNIFAC Dortmund, to predict key separation parameters, such as selectivity (relative volatility), capacity, and performance index. Experimental work consisted of conducting miscibility tests, as well as measuring relative volatility and VLE data. The obtained VLE data were tested for thermodynamic consistency and correlated with the NRTL and UNIQUAC models to obtain optimum binary interaction

parameters. Furthermore, process simulations using Aspen Plus software V.12 were used to assess the overall process performance of the selected green entrainers in comparison to NMP. The process performance was evaluated based on the key performance metrics, including economic (total annual cost) and environmental impacts (energy intensity, $CO_2$ emissions, and water consumption).

## 1.7. Research questions

According to the challenges explained above, this thesis addresses the following research question:

1. How can a systematic screening framework be implemented to identify promising greener entrainer candidates for separating the close-boiling methylcyclohexane-toluene mixture and the azeotropic n-hexane-ethanol mixture?
2. Which greener entrainers are potential candidates for these separation systems based on screening evaluation?
3. How reliable are the measured vapor-liquid equilibrium data for the investigated mixtures containing the selected entrainers?
4. How do the selected greener entrainers affect the vapor-liquid equilibrium behavior of the mixtures, particularly for increasing relative volatility and removing azeotropic or close-boiling behavior?
5. Do the selected greener entrainers provide comparable or improved economic and sustainability performance compared with benchmark entrainer NMP in extractive distillation processes?

Addressing these research questions allows the development of a systematic framework for identifying effective greener entrainers as alternatives to benchmark entrainer NMP while ensuring technical feasibility, economic competitiveness, and sustainable viability in extractive distillation processes.

## 1.8.Thesis outline

To achieve the primary objective outlined in the above section, this thesis is organized into six chapters, as follows:

**Chapter 1** introduces the research by providing the scientific and industrial background of ED and the role of entrainers. It reviews the current state of the art of greener entrainers and entrainer selection strategies, as well as thermodynamic measurements and modelling, and process performance comparisons through process simulation. Additionally, this chapter discusses the research scope, provides an overview of the study, and lists research questions.

**Chapter 2** establishes a systematic approach for selecting greener entrainer candidates to replace the conventional solvent NMP. A multi-stage methodology was employed, integrating initial green entrainer screening, quantum chemical calculations and group contribution methods, and experimental validation to identify promising candidates. The selected greener entrainers were then assessed for their effect, alongside NMP, on the VLE behavior in methylcyclohexane-toluene and n-hexane-ethanol mixtures, which is explored in Chapters 3 and 4.

**Chapter 3** reports the VLE data of the close-boiling methylcyclohexane-toluene mixture in the presence of selected entrainers, including gamma-valerolactone (GVL), dimethyl isosorbide (DMI), 1-butylpyrrolidin-2-one (NBP), along with the benchmark entrainer NMP. This data was measured at various entrainer-to-feed ratios and pressures. For GVL and NMP, the NRTL and UNIQUAC models were used for data correlation, while the NRTL model was applied for DMI and NBP. In this chapter, the separation performance of each entrainer in removing close-boiling behavior is assessed and compared.

**Chapter 4** provides the VLE data for the azeotropic n-hexane-ethanol mixture in the presence of selected entrainers (NBP, DMI, guaiacol) and the benchmark entrainer NMP, under varying entrainer-to-feed ratios and pressures. The VLE data of each mixture were regressed using the NRTL model. The effectiveness of each entrainer in eliminating azeotropic behavior was analyzed and compared.

**Chapter 5** presents the comparison of ED process performances for both the azeotropic n-hexane-ethanol mixture and the close-boiling methylcyclohexane-toluene mixture containing the selected entrainers. Process performance was evaluated through process simulation that developed based on the VLE data from Chapters 3 and 4, along with the optimum binary interaction parameters derived from this data. The economic and sustainability performances of the selected greener entrainers were assessed and benchmarked against NMP. Additionally, the evaluation of the use and limitations of predictive tools for ED entrainer screening was performed.

**Chapter 6** concludes the thesis by summarizing the main findings and highlighting the scientific and practical contributions of the work. Recommendations for future study are also provided.

## References


(1) de Haan, A. B.; Eral, H. B.; Schuur, B. *Industrial Separation Processes*; De Gruyter, 2025. https://doi.org/doi:10.1515/9783111063812.

(2) Chavez Velasco, J. A.; Tawarmalani, M.; Agrawal, R. Systematic Analysis Reveals Thermal Separations Are Not Necessarily Most Energy Intensive. *Joule* **2021**, *5* (2), 330–343. https://doi.org/https://doi.org/10.1016/j.joule.2020.12.002.

(3) Rico-Ramírez, V.; Diwekar, U. Distillation, Multicomponent Distillation; Wilson, I. D. B. T.-E. of S. S., Ed.; Academic Press, 2000; pp 1071–1081. https://doi.org/https://doi.org/10.1016/B0-12-226770-2/00691-8.

(4) Kiss, A. A.; Lange, J.-P.; Schuur, B.; Brilman, D. W. F.; van der Ham, A. G. J.; Kersten, S. R. A. Separation Technology–Making a Difference in Biorefineries. *Biomass and Bioenergy* **2016**, *95*, 296–309. https://doi.org/https://doi.org/10.1016/j.biombioe.2016.05.021.

(5) Smith, R.; Jobson, M. Distillation; Wilson, I. D. B. T.-E. of S. S., Ed.; Academic Press: Oxford, 2000; pp 84–103. https://doi.org/https://doi.org/10.1016/B0-12-226770-2/00041-7.

(6) Kiss, A. A. Design, Control and Economics of Distillation. In *Advanced Distillation Technologies: Design, Control and Applications*; John Wiley & Sons, Inc., 2013; pp 37–65. https://doi.org/https://doi.org/10.1002/9781118543702.ch2.

(7) Doherty, M. F.; Knapp, J. P. Distillation, Azeotropic, and Extractive. In *Kirk-Othmer Encyclopedia of Chemical Technology*; 2004. https://doi.org/https://doi.org/10.1002/0471238961.0409192004150805.a01.pub2.

(8) Lei, Z.; Chen, B.; Ding, Z. Chapter 2 - Extractive Distillation; Lei, Z., Chen, B., Ding, Z. B. T.-S. D. P., Eds.; Elsevier Science: Amsterdam, 2005; pp 59–144. https://doi.org/https://doi.org/10.1016/B978-044451648-0/50002-1.

(9) Gerbaud, V.; Rodriguez-Donis, I. Chapter 6 - Extractive Distillation; Górak, A., Olujić, Ž. B. T.-D., Eds.; Academic Press: Boston, 2014; pp 201–245. https://doi.org/https://doi.org/10.1016/B978-0-12-386878-7.00006-1.

(10) Zhu, J.; Sun, Y.; Chen, Y.; Wu, N.; Shi, R.; Ren, Z.; Li, Q.; Zhao, H. Isobaric Vapor–Liquid Equilibrium Experiments of Methyl Propionate + Ethanol with Different Ionic Liquids at 101.3 KPa. *J. Chem. Eng. Data* **2025**, *70* (1), 427–438. https://doi.org/10.1021/acs.jced.4c00517.

(11) Speight, J. G. 4 - Distillation; Speight, J. G. B. T.-T. R. of the F. (Second E., Ed.; Gulf Professional Publishing, 2020; pp 125–159. https://doi.org/https://doi.org/10.1016/B978-0-12-816994-0.00004-X.

(12) Luyben, W. L. Importance of Pressure-Selection in Pressure-Swing Distillation. *Comput. Chem. Eng.* **2021**, *149*, 107279. https://doi.org/https://doi.org/10.1016/j.compchemeng.2021.107279.

(13) Ma, Y.; Cui, P.; Wang, Y.; Zhu, Z.; Wang, Y.; Gao, J. A Review of Extractive Distillation from an Azeotropic Phenomenon for Dynamic Control. *Chinese J. Chem. Eng.* **2019**, *27* (7), 1510–1522. https://doi.org/https://doi.org/10.1016/j.cjche.2018.08.015.

(14) Seader, J. D. .; Henley, E. J.; Roper, D. K. *Separation Process Principles: Chemical and Biochemical Operations*, Third edit.; John Wiley & Sons, Inc.: New Jersey, 2010.

(15) Lee, F.-M.; Joseph C, G. Don't Overlook Extractive Distillation. *Chem. Eng. Prog.* **1997**, *93* (10).

(16) Lei, Z.; Dai, C.; Chen, B. Chapter 2 - Extractive Distillation; Lei, Z., Dai, C., Chen, B., Ding, Z. B. T.-S. D. P. (Second E., Eds.; Elsevier, 2022; pp 65–154. https://doi.org/https://doi.org/10.1016/B978-0-12-820507-5.00003-8.
(17) Kyle, B. G.; Leng, D. E. Solvent Selection for Extractive Distillation. *Ind. Eng. Chem.* **1965**, *57* (2), 43–48. https://doi.org/10.1021/ie50662a007.
(18) Kerton, F. M. Solvent Systems for Sustainable Chemistry. In *Encyclopedia of Inorganic and Bioinorganic Chemistry*; 2016; pp 1–17. https://doi.org/https://doi.org/10.1002/9781119951438.eibc2417.
(19) George Wypych, E. Handbook of Solvents: Use, Health, and Environment 3rd Ed; Wypych, G. B. T.-H. of S. (Third E., Ed.; ChemTec Publishing, 2019; pp 1203–1253. https://doi.org/https://doi.org/10.1016/B978-1-927885-41-3.50006-1.
(20) Yilmaz, E.; Soylak, M. Chapter 5 - Type of Green Solvents Used in Separation and Preconcentration Methods; Soylak, M., Yilmaz, E. B. T.-N. G. G. S. for S. and P. of O. and I. S., Eds.; Elsevier, 2020; pp 207–266. https://doi.org/https://doi.org/10.1016/B978-0-12-818569-8.00005-X.
(21) Malik, H.; Khan, H. W.; Hassan Shah, M. U.; Ahmad, M. I.; Khan, I.; Al-Kahtani, A. A.; Sillanpää, M. Screening of Ionic Liquids as Green Entrainers for Ethanol Water Separation by Extractive Distillation: COSMO-RS Prediction and Aspen plus Simulation. *Chemosphere* **2023**, *311*, 136901. https://doi.org/https://doi.org/10.1016/j.chemosphere.2022.136901.
(22) Qi, L.; Li, J.; Yang, A.; Yi, X.; Shen, W. Toward a Sustainable Azeotrope Separation of Acetonitrile/Water by the Synergy of Ionic Liquid-Based Extractive Distillation, Heat Integration, and Multiobjective Optimization. *Ind. Eng. Chem. Res.* **2022**, *61* (27), 9833–9846. https://doi.org/10.1021/acs.iecr.2c01285.
(23) Yan, L.; Li, J.; Ye, Q.; Jian, X.; Li, X.; Xie, L.; Zhang, J. Sustainable Wastewater Treatment via Extractive Distillation Process with Ionic Liquid as Entrainer for the Separation of Ethyl Acetate/Isopropanol/Water. *Process Saf. Environ. Prot.* **2022**, *160*, 527–540. https://doi.org/https://doi.org/10.1016/j.psep.2022.02.046.
(24) You, X.; Zhao, K.; Li, L.; Qiu, T. Ionic Liquids as Entrainer in Extractive Distillation for Effectively Separating 1-Propanol–Water Azeotropic Mixture. *Chinese J. Chem. Eng.* **2022**, *49*, 224–233. https://doi.org/https://doi.org/10.1016/j.cjche.2021.12.007.
(25) Taha, M. Designing New Mass-Separating Agents Based on Piperazine-Containing Good's Buffers for Separation of Propanols and Water Azeotropic Mixtures Using COSMO-RS Method. *Fluid Phase Equilib.* **2016**, *425*, 40–46. https://doi.org/https://doi.org/10.1016/j.fluid.2016.05.011.
(26) Hartanto, D.; Gupta, B. S.; Taha, M.; Lee, M.-J. Isobaric Vapour–Liquid Equilibrium of (Tert-Butanol+water) System with Biological Buffer TRIS at 101.3kPa. *J. Chem. Thermodyn.* **2016**, *98*, 159–164. https://doi.org/10.1016/j.jct.2016.03.013.
(27) Brouwer, T.; Schuur, B. Biobased Entrainer Screening for Extractive Distillation of Acetone and Diisopropyl Ether. *Sep. Purif. Technol.* **2021**, *270*, 118749. https://doi.org/https://doi.org/10.1016/j.seppur.2021.118749.
(28) Brouwer, T.; Schuur, B. Bio-Based Solvents as Entrainers for Extractive Distillation in Aromatic/Aliphatic and Olefin/Paraffin Separation. *Green Chem.* **2020**, *22* (16), 5369–5375. https://doi.org/10.1039/D0GC01769H.
(29) Zhang, Y.; Wang, Z.; Xu, X.; Gao, J.; Xu, D.; Zhang, L.; Wang, Y. Entrainers Selection and Vapour-Liquid Equilibrium Measurements for Separating

Azeotropic Mixtures (Ethanol + n-Hexane/Cyclohexane) by Extractive Distillation. *J. Chem. Thermodyn.* **2020**, *144*, 106070. https://doi.org/https://doi.org/10.1016/j.jct.2020.106070.

(30) Qi, J.; Qu, Y.; Zhou, M.; Su, Z.; Zhang, X.; Wei, R.; Xue, K.; Zhu, Z.; Meng, F.; Wang, Y. Phase Behavior and Molecular Insights on the Separation of Dimethyl Carbonate and Methanol Azeotrope by Extractive Distillation Using Deep Eutectic Solvents. *Sep. Purif. Technol.* **2023**, *305*, 122489. https://doi.org/https://doi.org/10.1016/j.seppur.2022.122489.

(31) Ma, Y.; Qu, Y.; Ji, Y.; Li, Y.; Wang, X.; Cui, P.; Zhu, Z.; Wang, Y. Structure-Activity Relationship and Experimental Study of Organic Solvents and Deep Eutectic Solvents in Separation of Cyclohexane-Ethyl Acetate. *J. Mol. Liq.* **2023**, *373*, 121263. https://doi.org/https://doi.org/10.1016/j.molliq.2023.121263.

(32) Jiang, H.; Xu, D.; Zhang, L.; Ma, Y.; Gao, J.; Wang, Y. Vapor–Liquid Phase Equilibrium for Separation of Isopropanol from Its Aqueous Solution by Choline Chloride-Based Deep Eutectic Solvent Selected by COSMO-SAC Model. *J. Chem. Eng. Data* **2019**, *64* (4), 1338–1348. https://doi.org/10.1021/acs.jced.8b00895.

(33) Gjineci, N.; Boli, E.; Tzani, A.; Detsi, A.; Voutsas, E. Separation of the Ethanol/Water Azeotropic Mixture Using Ionic Liquids and Deep Eutectic Solvents. *Fluid Phase Equilib.* **2016**, *424*, 1–7. https://doi.org/10.1016/j.fluid.2015.07.048.

(34) Sharma, B.; Singh, N.; Kushwaha, J. P. Ammonium-Based Deep Eutectic Solvent as Entrainer for Separation of Acetonitrile–Water Mixture by Extractive Distillation. *J. Mol. Liq.* **2019**, *285*, 185–193. https://doi.org/https://doi.org/10.1016/j.molliq.2019.04.089.

(35) Shang, X.; Ma, S.; Pan, Q.; Li, J.; Sun, Y.; Ji, K.; Sun, L. Process Analysis of Extractive Distillation for the Separation of Ethanol–Water Using Deep Eutectic Solvent as Entrainer. *Chem. Eng. Res. Des.* **2019**, *148*, 298–311. https://doi.org/https://doi.org/10.1016/j.cherd.2019.06.014.

(36) Bai, F.; Hua, C.; Bai, Y.; Ma, M. Design Optimization of Deep Eutectic Solvent Composition and Separation Performance of Cyclohexane and Benzene Mixtures with Extractive Distillation. *Processes*. 2021. https://doi.org/10.3390/pr9101706.

(37) Rodríguez, N. R.; González, A. S. B.; Tijssen, P. M. A.; Kroon, M. C. Low Transition Temperature Mixtures (LTTMs) as Novel Entrainers in Extractive Distillation. *Fluid Phase Equilib.* **2015**, *385*, 72–78. https://doi.org/https://doi.org/10.1016/j.fluid.2014.10.044.

(38) Qiu, X.; Qu, Y.; Zhou, M.; Liu, Y.; Zhu, Z.; Wang, Y.; Yang, J. Comparison of Deep Eutectic Solvents and Organic Solvent Effects on the Separation of Ternary Azeotropes by the Experimental Study and Molecular Simulation. *ACS Sustain. Chem. Eng.* **2021**, *9* (48), 16424–16436. https://doi.org/10.1021/acssuschemeng.1c06379.

(39) Zhao, D.; Liao, Y.; Zhang, Z. Toxicity of Ionic Liquids. *CLEAN – Soil, Air, Water* **2007**, *35* (1), 42–48. https://doi.org/https://doi.org/10.1002/clen.200600015.

(40) Costa, S. P. F.; Azevedo, A. M. O.; Pinto, P. C. A. G.; Saraiva, M. L. M. F. S. Environmental Impact of Ionic Liquids: Recent Advances in (Eco)Toxicology and (Bio)Degradability. *ChemSusChem* **2017**, *10* (11), 2321–2347. https://doi.org/https://doi.org/10.1002/cssc.201700261.

(41) Sharma, A.; Lee, B.-S.; Shin, H. Y. Assessing Suitability of Glycerol-Derived

Green Solvent for the Separation of n-Hexane + Ethanol Azeotropic Mixture, Accompanied by VLE Studies Using Machine Learning. *J. Mol. Liq.* **2025**, *423*, 127003. https://doi.org/https://doi.org/10.1016/j.molliq.2025.127003.

(42) Wang, Y.; Xu, H.; Yang, Q.; Wang, W.; Li, H.; Wang, Y.; Zhu, Z.; Li, X.; Song, X.; Cui, P. A Novel Intermediate Heat Exchange Intensified Extractive Pressure-Swing Distillation Process for Efficiently Separating n-Hexane-Tetrahydrofuran-Ethanol. *Chem. Eng. Sci.* **2024**, *300*, 120593. https://doi.org/https://doi.org/10.1016/j.ces.2024.120593.

(43) Rahayu, S. D.; Altway, S.; Tiwikrama, A. H.; Kuswandi, K. Isobaric Vapor–Liquid Equilibria for Separation of the n-Propanol and Water Azeotropic System with the Addition of a Choline Chloride–Ethylene Glycol-Based Deep Eutectic Solvent as an Entrainer. *J. Chem. Eng. Data* **2025**, *70* (1), 416–426. https://doi.org/10.1021/acs.jced.4c00511.

(44) Sander, A.; Petračić, A.; Rogošić, M.; Župan, M.; Frljak, L.; Cvetnić, M. Feasibility of Different Methods for Separating N-Hexane and Ethanol. *Separations*. 2024. https://doi.org/10.3390/separations11050151.

(45) Raverty, W. *Levoglucosenone: à la recherche de chimie perdue*. https://colloque.inrae.fr/explorebiomass/content/download/4041/41542/version/1/file/S5-Raverty.pdf (accessed 2022-12-10).

(46) Yu-Wu, Q. M.; Weiss-Hortala, E.; Barna, R.; Boucard, H.; Bulza, S. Glycerol and Bioglycerol Conversion in Supercritical Water for Hydrogen Production. *Environ. Technol.* **2012**, *33* (19), 2245–2255. https://doi.org/10.1080/09593330.2012.728738.

(47) CAMEO Chemicals. *Butyl butyrate*. https://cameochemicals.noaa.gov/chemical/10702 (accessed 2022-10-12).

(48) Gao, F.; Bai, R.; Ferlin, F.; Vaccaro, L.; Li, M.; Gu, Y. Replacement Strategies for Non-Green Dipolar Aprotic Solvents. *Green Chem.* **2020**, *22* (19), 6240–6257. https://doi.org/10.1039/D0GC02149K.

(49) Dai, Y.; van Spronsen, J.; Witkamp, G.-J.; Verpoorte, R.; Choi, Y. H. Natural Deep Eutectic Solvents as New Potential Media for Green Technology. *Anal. Chim. Acta* **2013**, *766*, 61–68. https://doi.org/https://doi.org/10.1016/j.aca.2012.12.019.

(50) Thomas, B.; Karl Hans, S. Knowledge Integrating System for the Selection of Solvents for Extractive and Azeotropic Distillation. *Comput. Chem. Eng.* **1994**, *18*, S25–S29. https://doi.org/https://doi.org/10.1016/0098-1354(94)80005-7.

(51) Brignole, E. A.; Bottini, S.; Gani, R. A Strategy for the Design and Selection of Solvents for Separation Processes. *Fluid Phase Equilib.* **1986**, *29*, 125–132. https://doi.org/https://doi.org/10.1016/0378-3812(86)85016-6.

(52) Chen, B.; Lei, Z.; Li, Q.; Li, C. Application of CAMD in Separating Hydrocarbons by Extractive Distillation. *AIChE J.* **2005**, *51* (12), 3114–3121. https://doi.org/https://doi.org/10.1002/aic.10562.

(53) Gani, R.; Brignole, E. A. Molecular Design of Solvents for Liquid Extraction Based on UNIFAC. *Fluid Phase Equilib.* **1983**, *13*, 331–340. https://doi.org/https://doi.org/10.1016/0378-3812(83)80104-6.

(54) Chai, S.; Song, Z.; Zhou, T.; Zhang, L.; Qi, Z. Computer-Aided Molecular Design of Solvents for Chemical Separation Processes. *Curr. Opin. Chem. Eng.* **2022**, *35*, 100732. https://doi.org/https://doi.org/10.1016/j.coche.2021.100732.

(55) Yang, X.; Song, H. Computer Aided Molecular Design of Solvents for Separation Processes. *Chem. Eng. Technol.* **2006**, *29* (1), 33–43.

https://doi.org/https://doi.org/10.1002/ceat.200500270.
(56) Brouwer, T.; Kersten, S. R. A.; Bargeman, G.; Schuur, B. Solvent Pre-Selection for Extractive Distillation Using Infinite Dilution Activity Coefficients and the Three-Component Margules Equation. *Sep. Purif. Technol.* **2021**, *276*, 119230. https://doi.org/https://doi.org/10.1016/j.seppur.2021.119230.
(57) Zhu, Z.; Ri, Y.; Li, M.; Jia, H.; Wang, Y.; Wang, Y. Extractive Distillation for Ethanol Dehydration Using Imidazolium-Based Ionic Liquids as Solvents. *Chem. Eng. Process. Process Intensif.* **2016**, *109*, 190–198. https://doi.org/10.1016/j.cep.2016.09.009.
(58) Pretel, E. J.; López, P. A.; Bottini, S. B.; Brignole, E. A. Computer-Aided Molecular Design of Solvents for Separation Processes. *AIChE J.* **1994**, *40* (8), 1349–1360. https://doi.org/https://doi.org/10.1002/aic.690400808.
(59) Bastos, J. C.; Soares, M. E.; Medina, A. G. Selection of Solvents for Extractive Distillation. A Data Bank for Activity Coefficients at Infinite Dilution. *Ind. Eng. Chem. Process Des. Dev.* **1985**, *24* (2), 420–426. https://doi.org/10.1021/i200029a035.
(60) Khan, A. S.; Ibrahim, T. H.; Rashid, Z.; Khamis, M. I.; Nancarrow, P.; Jabbar, N. A. COSMO-RS Based Screening of Ionic Liquids for Extraction of Phenolic Compounds from Aqueous Media. *J. Mol. Liq.* **2021**, *328*, 115387. https://doi.org/https://doi.org/10.1016/j.molliq.2021.115387.
(61) Jeon, Y.; Row, S. W.; Lee, G.; Park, S. S.; Seo, Y.-J.; Chu, Y. H.; Shul, Y.-G. Solvent Screening for the Separation of Ethylbenzene and P-Xylene by Extractive Distillation. *Korean J. Chem. Eng.* **2014**, *31* (10), 1824–1830. https://doi.org/10.1007/s11814-014-0115-2.
(62) Cignitti, S.; Rodriguez-Donis, I.; Abildskov, J.; You, X.; Shcherbakova, N.; Gerbaud, V. CAMD for Entrainer Screening of Extractive Distillation Process Based on New Thermodynamic Criteria. *Chem. Eng. Res. Des.* **2019**, *147*, 721–733. https://doi.org/https://doi.org/10.1016/j.cherd.2019.04.038.
(63) Gutiérrez, J. P.; Meindersma, G. W.; de Haan, A. B. COSMO-RS-Based Ionic-Liquid Selection for Extractive Distillation Processes. *Ind. Eng. Chem. Res.* **2012**, *51* (35), 11518–11529. https://doi.org/10.1021/ie301506n.
(64) Salleh, Z.; Wazeer, I.; Mulyono, S.; El-blidi, L.; Hashim, M. A.; Hadj-Kali, M. K. Efficient Removal of Benzene from Cyclohexane-Benzene Mixtures Using Deep Eutectic Solvents – COSMO-RS Screening and Experimental Validation. *J. Chem. Thermodyn.* **2017**, *104*, 33–44. https://doi.org/https://doi.org/10.1016/j.jct.2016.09.002.
(65) Cheng, H.; Liu, C.; Zhang, J.; Chen, L.; Zhang, B.; Qi, Z. Screening Deep Eutectic Solvents for Extractive Desulfurization of Fuel Based on COSMO-RS Model. *Chem. Eng. Process. - Process Intensif.* **2018**, *125*, 246–252. https://doi.org/https://doi.org/10.1016/j.cep.2018.02.006.
(66) Li, J.; Li, R.; Yang, J.; Li, S.; Zhang, Z.; Liu, H.; Ma, Z.; Sun, L. Biobased Solvents as Entrainers for Extractive Distillation in Isobutyl Acetate–Isobutanol Separation: Experimental Investigation, Toxicity Evaluation, and Mechanism Analysis. *J. Chem. Eng. Data* **2025**, *70* (11), 4648–4663. https://doi.org/10.1021/acs.jced.5c00514.
(67) Baek, S. H.; Kim, T. H.; Kang, J. W. An Entrainer Selection Method Based on Thermodynamic Considerations for the Purification of Methyl Benzoate via Extractive Distillation. *Sep. Purif. Technol.* **2025**, *375*, 133653.

https://doi.org/https://doi.org/10.1016/j.seppur.2025.133653.
(68) Li, F.; Li, Y.; Xiao, Y.; Zhang, Z.; Wang, Y.; Cai, W. Energy-Efficient Design of Extractive Distillation for Benzene–Cyclohexane–Cyclohexene Using Molecular Simulation and Multi-Objective Optimization. *Chem. Eng. Process. - Process Intensif.* **2026**, *220*, 110663. https://doi.org/https://doi.org/10.1016/j.cep.2025.110663.
(69) Zhan, G.; Shen, B.; Sun, H.; Chen, X. Extractive Distillation Approach to the Removal of Dimethyl Disulfide from Methyl Tert-Butyl Ether: Combined Computational Solvent Screening and Experimental Process Investigation. *Ind. Eng. Chem. Res.* **2018**, *57* (9), 3348–3358. https://doi.org/10.1021/acs.iecr.7b01766.
(70) Rodriguez-Donis, I.; Shcherbakova, N.; Parascandolo, E.; Abildskov, J.; Gerbaud, V. Entrainer Selection Using the Infinitely Sharp Split Method and Thermodynamic Criteria for Separating Binary Minimum-Boiling Azeotrope by Extractive Distillation. *Chem. Eng. Res. Des.* **2024**, *205*, 443–458. https://doi.org/https://doi.org/10.1016/j.cherd.2024.04.003.
(71) Sethi, S.; Zhang, X.; Sundmacher, K. Process-Driven Solvent Screening for Efficient Extractive Distillation Using Interpolative Rational Functions. *Chem. Eng. Sci.* **2025**, *301*, 120675. https://doi.org/https://doi.org/10.1016/j.ces.2024.120675.
(72) Cheng, Y.; Zhu, K.; Li, S.; Han, J.; Zhang, Z.; Li, M.; Ma, Y.; Gao, J. Economic, Environmental, Energy, Exergy (4E) and Inherent Safety Analysis of Hybrid Extractive-Heteroazeotropic Distillation for Sustainable Treatment of Crude n-Butanol Waste Liquor. *Process Saf. Environ. Prot.* **2025**, *193*, 1125–1138. https://doi.org/https://doi.org/10.1016/j.psep.2024.11.134.
(73) Xu, Z.; Wang, Y.; Li, J.; Wu, H.; Pan, J.; Ye, Q. Multi-Criteria Decision Analysis of Entrainers Screening on the Extractive Distillation Process for Separating Ternary Mixtures Based on Multi-Objective Optimization. *Chem. Eng. Res. Des.* **2025**, *218*, 376–387. https://doi.org/https://doi.org/10.1016/j.cherd.2025.04.041.
(74) Zhang, H.; Zhao, F.; Ma, Z.; Liu, X.; Cui, P.; Gao, J.; Wang, Y.; Zheng, S. Design and Optimization for the Separation of Cyclohexane-Isopropanol-Water Using Mixed Extractants with Thermal Integration Based on Molecular Mechanism. *Sep. Purif. Technol.* **2021**, *266*, 118541. https://doi.org/https://doi.org/10.1016/j.seppur.2021.118541.
(75) Brouwer, T.; Schuur, B. Comparison of Solvent-Based Affinity Separation Processes Using Cyrene and Sulfolane for Aromatic/Aliphatic Separations. *J. Chem. Technol. Biotechnol.* **2021**, *96* (9), 2630–2646. https://doi.org/https://doi.org/10.1002/jctb.6808.
(76) Minor, A.-J.; Hartanto, D.; de Haan, A. B. Assessment of Deep Eutectic Solvents for Alcohol-Water Separations by Extractive Distillation. In *The 12th international conference Distillation & Absorption 2022*; 2022.
(77) Quijada-Maldonado, E.; Meindersma, G. W.; de Haan, A. B. Pilot Plant Study on the Extractive Distillation of Toluene–Methylcyclohexane Mixtures Using NMP and the Ionic Liquid [Hmim][TCB] as Solvents. *Sep. Purif. Technol.* **2016**, *166*, 196–204. https://doi.org/https://doi.org/10.1016/j.seppur.2016.04.041.
(78) *Methylcyclohexane, 99% (CAS RN: 108-87-2)*; Sigma-Aldrich: Amsterdam, 2024. https://www.sigmaaldrich.com/NL/en/sds/sial/300306?userType=anonymous.
(79) *Toluene, 99.9% (CAS RN: 108-88-3)*; Sigma-Aldrich: Amsterdam, 2025.

https://www.sigmaaldrich.com/NL/en/sds/sial/244511?userType=anonymous.
(80) Hartanto, D.; Schuur, B.; Schuttevaer, T.; Kiss, A. A.; de Haan, A. B. Isobaric Vapor–Liquid Equilibrium of Methylcyclohexane + Toluene with Gamma-Valerolactone as a Biobased Entrainer and 1-Methylpyrrolidin-2-One as a Conventional Entrainer. *J. Chem. Eng. Data* **2025**, *70* (3), 1339−1351. https://doi.org/10.1021/acs.jced.4c00509.
(81) Caceres-Martinez, L. E.; Saavedra Lopez, J.; Dagle, R. A.; Gillespie, R.; Kenttämaa, H. I.; Kilaz, G. Influence of Blending Cycloalkanes on the Energy Content, Density, and Viscosity of Jet-A. *Fuel* **2024**, *358*, 129986. https://doi.org/https://doi.org/10.1016/j.fuel.2023.129986.
(82) Zou, J.; Zhang, J.; Lian, T.; Xu, Q.; Liu, B.; Wang, Z.; Yang, J.; Li, Y. Conformation-Dependent Low-Temperature Oxidation Chemistry of Methylcyclohexane: First Oxygen Addition and Chain-Branching. *Combust. Flame* **2022**, *243*, 111963. https://doi.org/https://doi.org/10.1016/j.combustflame.2021.111963.
(83) Meille, V.; Pitault, I. Liquid Organic Hydrogen Carriers or Organic Liquid Hydrides: 40 Years of History. *Reactions* **2021**, *2* (2), 94–101. https://doi.org/10.3390/reactions2020008.
(84) Wang, L.; Zhou, S.; Shi, M.; Jia, B.; Liu, H.; Li, Q. Liquid–Liquid Extraction of Cyclopentanone from Aqueous Solution with Methylcyclohexane or Propyl Acetate at Different Temperatures. *J. Chem. Eng. Data* **2018**, *63* (8), 2653–2659. https://doi.org/10.1021/acs.jced.7b01109.
(85) Bui, G.; Bhattacharya, A.; Kaario, O.; Vuorinen, V.; Tripathi, R.; Sarjovaara, T. On the Super Adiabatic Flame Temperature (SAFT) of Toluene Primary Reference Fuels. *Fuel* **2023**, *335*, 126989. https://doi.org/https://doi.org/10.1016/j.fuel.2022.126989.
(86) Lin, A.; Bagnato, G. Revolutionising Energy Storage: The Latest Breakthrough in Liquid Organic Hydrogen Carriers. *Int. J. Hydrogen Energy* **2024**, *63*, 315–329. https://doi.org/https://doi.org/10.1016/j.ijhydene.2024.03.146.
(87) Mu, X.; Ma, J.; Liu, F.; MengqinYao; He, L. The Solvent Extraction Is a Potential Choice to Recover Asphalt from Unconventional Oil Ores. *Arab. J. Chem.* **2023**, *16* (5), 104650. https://doi.org/https://doi.org/10.1016/j.arabjc.2023.104650.
(88) Sa, E. J.; Lee, B.-S.; Park, B. H. Extraction of Ethanol from Mixtures with N-Hexane by Deep Eutectic Solvents of Choline Chloride + Levulinic Acid, + Ethylene Glycol, or + Malonic Acid. *J. Mol. Liq.* **2020**, *316*, 113877. https://doi.org/https://doi.org/10.1016/j.molliq.2020.113877.
(89) Muhammed, N. S.; Gbadamosi, A. O.; Epelle, E. I.; Abdulrasheed, A. A.; Haq, B.; Patil, S.; Al-Shehri, D.; Kamal, M. S. Hydrogen Production, Transportation, Utilization, and Storage: Recent Advances towards Sustainable Energy. *J. Energy Storage* **2023**, *73*, 109207. https://doi.org/https://doi.org/10.1016/j.est.2023.109207.
(90) Kang, J.; He, S.; Zhou, W.; Shen, Z.; Li, Y.; Chen, M.; Zhang, Q.; Wang, Y. Single-Pass Transformation of Syngas into Ethanol with High Selectivity by Triple Tandem Catalysis. *Nat. Commun.* **2020**, *11* (1), 827. https://doi.org/10.1038/s41467-020-14672-8.
(91) Speight, J. G. Chapter 8 - Hydrocarbons from Synthesis Gas; Speight, J. G. B. T.-H. of I. H. P. (Second E., Ed.; Gulf Professional Publishing: Boston, 2020; pp 343–386. https://doi.org/https://doi.org/10.1016/B978-0-12-809923-0.00008-4.

(92) Sbihi, H. M.; Nehdi, I. A.; Mokbli, S.; Romdhani-Younes, M.; Al-Resayes, S. I. Hexane and Ethanol Extracted Seed Oils and Leaf Essential Compositions from Two Castor Plant (Ricinus Communis L.) Varieties. *Ind. Crops Prod.* **2018**, *122*, 174–181. https://doi.org/https://doi.org/10.1016/j.indcrop.2018.05.072.
(93) Richard W, B. *Separation of Organic Azeotropic Mixtures by Pervaporation*; United States, 1991. https://doi.org/10.2172/5926894.
(94) Bernd, A. K. Polyurethane-Imide Membranes and Their Use for the Separation of Aromatics from Non-Aromatics. US4929358A, 1989.
(95) Weissermel, K.; Arpe, H.-J. Aromatics — Production and Conversion. In *Industrial Organic Chemistry*; 2003; pp 313–336. https://doi.org/https://doi.org/10.1002/9783527619191.ch12.
(96) Pereiro, A. B.; Rodriguez, A. Purification of Hexane with Effective Extraction Using Ionic Liquid as Solvent. *Green Chem.* **2009**, *11* (3), 346–350. https://doi.org/10.1039/B814032D.
(97) Pereiro, A. B.; Rodríguez, A. Effective Extraction in Packed Column of Ethanol from the Azeotropic Mixture Ethanol+hexane with an Ionic Liquid as Solvent. *Chem. Eng. J.* **2009**, *153* (1), 80–85. https://doi.org/https://doi.org/10.1016/j.cej.2009.06.013.
(98) Ma, Y.; Xu, X.; Wen, G.; Xu, D.; Shi, P.; Wang, Y.; Gao, J. Separation of Azeotropes Hexane + Ethanol/1-Propanol by Ionic Liquid Extraction: Liquid–Liquid Phase Equilibrium Measurements and Thermodynamic Modeling. *J. Chem. Eng. Data* **2017**, *62* (12), 4296–4300. https://doi.org/10.1021/acs.jced.7b00643.
(99) J. Marwil, S. Separation of Hydrocarbon and Alcohol Azeotropic Mixtures by Distillation with Anhydrous Ammonia. US4437941A, 1984.
(100) Li, J.; Wang, M.; Huang, Y.; Luo, B.; Zhang, Y.; Yuan, Q. Separation of Binary Solvent Mixtures with Solvent Resistant Nanofiltration Membranes Part A: Investigation of Separation Performance. *RSC Adv.* **2014**, *4* (77), 40740–40747. https://doi.org/10.1039/C4RA04222K.

(*This page is intentionally left blank*)

# Chapter 2

## Systematic selection of biobased, greener organic, and natural deep eutectic solvents (NADESs) for azeotropic and close-boiling mixtures separation by extractive distillation

*Parts of this chapter have been published in:*
*Computer Aided Chemical Engineering 53, 1387-1392 (2024)*
*Journal of Chemical & Engineering Data, 70, 4091-4104, (2025)*

*and have been accepted in:*
*American Institute of Physics Conference Proceeding, (2026)*

## Abstract

Biobased and greener organic entrainers, along with natural deep eutectic solvents (NADESs) that possess high boiling points, good solvency, and environmentally friendly properties, are promising sustainable entrainer options for extractive distillation. This study developed a validated framework for systematically investigating greener entrainer candidates for the separation of a close-boiling mixture (methylcyclohexane–toluene) and an azeotropic mixture (n-hexane–ethanol), aiming to identify effective greener entrainers. A multi-stage selection methodology was employed. The initial screening focused on identifying greener entrainers based on their high-boiling properties, favorable solvency, and green aspects, followed by an integrated approach combining both predictive and experimental methods. Quantum chemical (COSMO-RS) and group contribution (UNIFAC, modified UNIFAC (Dortmund)) were utilized to predict key performance metrics, such as selectivity and relative volatility. Promising candidates were experimentally evaluated for miscibility and relative volatility, and the experimental relative volatility data were used to validate the predictive results. Additionally, the study examined the performance limits of NADESs in hydrocarbon separations and defined their more suitable application domain. The results show that the framework effectively identified several greener entrainers. Both predictive and experimental findings indicated that the evaluated greener entrainers exhibited comparable or improved selectivity and relative volatility compared to conventional organic entrainers, such as 1-methyl-2-pyrrolidinone (NMP). The predictive relative volatility values exhibited good agreement with the experimental results. Based on the miscibility and relative volatility measurements, gamma-valerolactone (GVL), 1-butylpyrrolidin-2-one (NBP), and dimethyl isosorbide (DMI) were identified as effective entrainers for the methylcyclohexane–toluene mixture, while NBP, DMI, and guaiacol were selected for the n-hexane–ethanol mixture. Several NADESs were also synthesized and characterized. However, their high polarity led to miscibility limitations with the hydrocarbon mixtures, preventing further experimental evaluation. Notably, predictive analyses indicated that certain NADESs demonstrated favorable selectivity for the ethanol-water mixture. Experimentally, they exhibited complete miscibility with ethanol, as a representation of a polar compound. This indicates their potential for polar mixture separations. Overall, the results confirm that the validated framework developed in this study provides a reliable and systematic approach for selecting effective greener entrainers for extractive distillation.

## 2.1. Introduction

To investigate greener entrainer candidates, a validated framework for systematic screening was established. This framework integrates green selection criteria for the initial screening and combines predictive and experimental approaches to evaluate separation performance. The established framework provides a systematic approach for identifying effective greener entrainers. To the best of our knowledge, no previous study has systematically integrated the evaluation of boiling point, potential solvency, and green aspects with key separation metrics, assessed using both COSMO-RS- and Group Contribution Methods (GCMs)-based calculations, alongside miscibility and relative volatility measurements. The initial selection of entrainers for the ED process was conducted by assessing high boiling-point properties and green aspects. Once greener entrainer candidates were selected, their separation performance metrics were evaluated using predictive models. COSMO-RS was employed to calculate, the activity coefficient, selectivity, and capacity at infinite dilution, as well as relative volatility at finite dilution. COSMO-RS calculations have emerged as powerful tools for screening potential entrainers for the ED process.[1–7] Additionally, UNIFAC and modified UNIFAC (Dortmund) were applied to estimate the relative volatility at finite dilution. GCMs, such as UNIFAC and modified UNIFAC (Dortmund), are also widely used as robust tools for entrainer selection in extractive distillation.[8–10] Selectivity and capacity were evaluated as selection parameters. It is important to examine the effectiveness of each parameter before designating one as the decisive criterion. The activity coefficient at infinite dilution provides insight into how the entrainer affects the relative volatility.[1,11,12] Relative volatility at finite dilution was measured to represent industrial separation conditions, validate predictions, and select the most suitable entrainers for each case study. The relative volatility was measured at a liquid mole fraction of methylcyclohexane of 0.5 for the methylcyclohexane-toluene mixture and a liquid mole fraction of n-hexane of 0.66 for the n-hexane-ethanol mixture. Prior to relative volatility measurement, the miscibility of the proposed greener entrainers was examined.

Selected NADESs were synthesized and characterized to evaluate their applicability limits for hydrocarbon separations. Their potential application domains were further examined through selectivity predictions for the ethanol-water mixture and miscibility tests with ethanol. The synthesized NADESs exhibited strong hydrogen-bonding networks and high polarity profiles, as described in Sigma (σ)-profile analysis Section. These characteristics can lead to poor miscibility with hydrocarbon mixtures, thereby restricting their applicability in such systems. In contrast, their high polarity and hydrogen-bonding ability are expected to promote favorable miscibility in polar mixtures, making these NADESs as potential candidates for separations involving polar-polar systems.

## 2.2. Separation parameters

Relative volatility $(\alpha)$, as defined in Eq. 1, is a key separation parameter in extractive distillation, where a higher value indicates an easier separation of component *i* from *j*.

$$\alpha_{ij} = \frac{y_i / x_i}{y_j / x_j} = \frac{\gamma_i p_i^{sat}}{\gamma_j p_j^{sat}} \quad 1)$$

In this expression, *x* and *y* represent the liquid- and vapor-phase mole fractions, respectively, while $\gamma$ is the activity coefficient in the liquid phase, and $p^{sat}$ is the saturated vapor pressure. The subscripts *i* and *j* denote the respective components. The relative volatility can be modified by altering the nonideal behaviour of the liquid phase, specifically by changing the ratio of activity coefficient through the addition of an entrainer. In the close-boiling or azeotropic mixtures, the ratio of saturated vapor pressures at a given temperature is essentially constant and close to unity. Under these conditions, the relative volatility simplifies to the ratio of activity coefficients, which is commonly referred to as selectivity ($S$), as shown in Eq. 2. Hence, for close-boiling or azeotropic mixtures, the relative volatility can be effectively represented by the selectivity.

$$S_{ij} = \frac{\gamma_i}{\gamma_j} \quad 2)$$

To evaluate the maximum effect of entrainers on mixture behavior, the infinite dilution method is often employed, which focuses on the solute-solvent interactions near the pure solvent limit. In this approach, each component of the mixture is treated as a solute, while the entrainer acts as a solvent. At infinite dilution, the solute is present at vanishingly small concentration in a solvent-rich phase. This means that interactions occur exclusively between the solute and entrainer, with negligible solute-solute interactions. This condition represents the maximum potential influence of the solvent on relative volatility. Furthermore, the concentration of the entrainer and the temperature affect both the activity coefficient and selectivity. Therefore, comparisons among different entrainer candidates should be performed under consistent entrainer concentrations and temperatures. The activity coefficient at infinite dilution ($\gamma^{\infty}$), which directly corresponds to the selectivity at infinite dilution ($S_{ij}^{\infty}$), as expressed in Eq. 3, serves as a reliable and effective parameter for evaluating and selecting suitable entrainers.[12,13]

$$S_{ij}^{\infty} = \frac{\gamma_i^{\infty}}{\gamma_j^{\infty}} \quad 3)$$

Entrainers exhibiting the highest selectivity are generally considered as the most promising candidates for separating close-boiling or azeotropic mixtures.[1,14,15] Selectivity directly influences key process design parameters, such as the reflux ratio, the number of stages, and the column diameter in the extractive distillation column. These parameters, in turn, determine the energy and water requirements, total annual cost (TAC), and potential $CO_2$ reduction in the extractive distillation processes. Higher selectivity enables operation with a smaller reflux ratio, fewer stages, and a thinner extractive distillation column. Collectively, these effects lead to reduced energy consumption and lower capital investment of the column, which are the main contributors to the cost of extractive distillation. Consequently, improvements in selectivity contribute not only to economic benefits but also to reduced $CO_2$ emissions and water consumption. As reported by Momoh, increasing selectivity consistently results in a decrease in TAC, with the minimum TAC achieved when the entrainer exhibits the highest selectivity.[16]

In addition to selectivity, capacity has been proposed as an additional assessment parameter for entrainer evaluation, typically serving as a secondary decision variable.[17] A higher capacity implies that a smaller amount of entrainer is required to achieve the desired separation, thereby reducing operating costs. The capacity of an entrainer at infinite dilution ($C_{j,entrainer}^{\infty}$) is defined in Eq. 4.

$$C_{j,entrainer}^{\infty} = \frac{1}{\gamma_j^{\infty}} \quad 4)$$

Furthermore, several researchers have introduced the performance index *(PI)* at infinite dilution as an integrated measure for entrainer selection.[5,6,18] The *PI* is calculated as the product of selectivity and capacity, as shown in Eq. 5, providing a straightforward method to combine both parameters into a single evaluation metric.

$$PI = S^{\infty} \times C^{\infty} \quad 5)$$

## 2.3. Modeling details

a. COSMO-RS simulation

The COnductor-like Screening MOdel for Realistic Solvents (COSMO-RS), developed by Eckert and Klamt,[19] was employed to predict thermophysical properties and phase behavior. COSMO-RS combines quantum chemical calculations with statistical thermodynamics to describes molecular interactions in

the liquid phase. A key advantage of COSMO-RS is the ability to predict molecular interactions without relying on group-contribution parameters or experimental data. All COSMO-RS calculations were performed using the COSMOthermX17 package (version C30_1705, COSMOLogic, Germany), which implements the COSMO-RS framework.[20] The software includes an extensive compound database; however, several of the new greener entrainers investigated in this study were not available. To overcome this limitation, new molecular COSMO files were generated. Each molecule was optimized using Turbomole (version 21.0.0, Biovia, Germany).[21] The density functional theory (DFT) optimization employed the Becke-Perdew (BP86) functional along with the resolution-of-identity (RI) approximation. This approach provides reliable molecular geometries and charge distributions at a reasonable computational cost. The basis set of triple-zeta valence plus polarization (TZVP) was applied to generate the COSMO surface charge density. The C30 cavity construction was adopted to define the molecular boundary surface for calculating screening charges. At infinite dilution, the activity coefficient, selectivity, and capacity were calculated at temperatures of 293.15 K and 400.15 K, representing atmospheric and typical extractive distillation temperatures, respectively. For NADESs simulations, a 1:1 molar ratio of constituent components was applied. Finally, the analysis of the σ-profile and σ-potential was carried out to elucidate the molecular interactions. In addition, and the relative volatility at finite dilution was also estimated within the COSMO-RS framework.

b. Group contribution methods (GCMs) simulation

GCMs apply a fundamentally different approach to calculating molecular interactions compared to COSMO-RS. GCMs are semi-empirical models that estimate activity coefficients based on functional group segments using empirically fitted binary interaction parameters between groups. These parameters are optimized from experimental VLE data or excess Gibbs energy correlations. The original UNIversal Quasichemical Functional-group Activity Coefficients (UNIFAC) method[22] and the modified UNIFAC (Dortmund)[23] were employed. Both models compute the activity coefficient of the component $i$ ($\gamma_i$) by combining the residual and combinatorial contributions, as illustrated in Eq. 6.

$$\ln \gamma_i = \ln \gamma_i^R + \ln \gamma_i^C \qquad 6)$$

where the residual and combinatorial activity coefficients are denoted by $\gamma_i^R$ and $\gamma_i^C$, respectively.

The residual contribution accounts for energetic interactions between functional groups and is expressed via Eqs. 7 and 8.

$$\ln \gamma_i^R = \sum_k v_k^{(i)} (\ln \Gamma_k - \ln \Gamma_k^{(i)}) \quad 7)$$

$$\ln \Gamma_k = Q_k \left[ 1 - \ln\left( \sum_m \theta_m \Psi_{mk} \right) - \sum_m \frac{\theta_m \Psi_{mk}}{\sum_n \theta_n \Psi_{nm}} \right] \quad 8)$$

where $\ln \Gamma_k$ represents the residual activity coefficient of group *k*, while $\ln \Gamma_k^{(i)}$ denotes the residual activity coefficient of group *k* when it is surrounded solely by molecule *i*. The term $v_k^{(i)}$ indicates the number of group *k* present in molecule *i,* while $Q_k$ refers to the van der Waals surface area parameter of group *k*. Additionally, $\theta_m$ represents the area fraction of group *m*. The term $\Psi_{mk}$ corresponds to the binary interaction parameter between group *m* and *k*. It is important to note that the formulation of these group interaction parameters in the residual contribution, and the volume fractions in the combinatorial contribution, differ between UNIFAC and modified UNIFAC (Dortmund) methods. In the original UNIFAC model, the group interaction parameter ($\Psi_{nm}$) is temperature-dependent via an empirical exponential function, as shown in Eq. 9.

$$\Psi_{nm} = \exp\left( \frac{-a_{nm}}{T} \right) \quad 9)$$

where $a_{nm}$ denotes the group binary interaction parameters, which is treated as temperature-independent in the original UNIFAC. In contrast, the modified UNIFAC (Dortmund) defines a more flexible temperature dependence by expressing $\Psi_{nm}$ as a function of three fitted group interaction coefficients $a_{nm}$, $b_{nm}$, and $c_{nm}$, as expressed in Eq. 10. These coefficients are fitted parameters for each group pair, while the resulting interaction term varies with temperature.

$$\Psi_{nm} = \exp\left( \frac{-a_{nm} + b_{nm} T + c_{nm} T^2}{T} \right) \quad 10)$$

The combinatorial contribution accounts for molecular size and shape effects. For the UNIFAC, this parameter is denoted in Eq. 11.

$$\ln \gamma_i^C = 1 - \phi_i + \ln \phi_i - 5q_i \left( 1 - \frac{\phi_i}{\theta_i} + \ln \frac{\phi_i}{\theta_i} \right) \quad 11)$$

where $\phi_i$ denotes the segment fraction, which is analogous to the volume fraction, while $q_i$ represents the van der Waals molecular surface area, and $\theta_i$ is the area fraction. The segment fraction is expressed by Eq. 12.

$$\phi_i = \frac{\sum_j v_k^{(i)} R_k}{\sum_j x_j \sum_j v_k^{(i)} R_k} \quad 12)$$

In the modified UNIFAC (Dortmund), a revised combinatorial expression is used, as given by Eq. 13, with the segment fraction redefined in Eq. 14.

$$\ln \gamma_i^C = 1 - \phi_i' + \ln \phi_i' - 5q_i \left( 1 - \frac{\phi_i}{\theta_i} + \ln \frac{\phi_i}{\theta_i} \right) \quad 13)$$

$$\phi_i' = \frac{\left( \sum_j v_k^{(i)} R_k \right)^{3/4}}{\sum_j x_j \left( \sum_j v_k^{(i)} R_k \right)^{3/4}} \quad 14)$$

Relative volatilities were subsequently calculated under isobaric condition at 100.0 kPa using Aspen Plus v.12. To obtain missing pure-component properties, the Aspen Property Constant Estimation System (PCES) was employed. This method estimates molecular properties from structural information, including atomic composition, bonding, and molecular connectivity.[24]

## 2.4. Experimental methods

### Materials

All purchased chemicals were used as received without further purification. The specifications of chemicals are provided in Table A1 in the Appendix.

### Experimental procedure

### Miscibility measurements

Entrainer-feed mixtures were prepared in sealed glass vials at specified E/Fs. The required quantities of an entrainer and the feed were accurately weighed using an analytical balance (Mettler Toledo AE200, USA) with an uncertainty of ±0.0001 g. The sealed vials were then placed in a thermostat uni-block vial holder mounted on a hot plate equipped with a magnetic stirrer (IKA RCT Basic, Germany). Each

mixture was stirred continuously for 15 minutes at the target temperature to ensure thorough mixing and heating. Afterward, the vials were allowed to settle briefly, and the phase behavior was immediately evaluated. Miscibility tests were conducted in duplicate to verify reproducibility. The results were assessed qualitatively by visual inspection, classifying each sample as either fully miscible (homogeneous liquid phase) or immiscible (heterogeneous liquid phase).

**Relative volatility measurements**

Relative volatility in this chapter, as well as vapor-liquid equilibrium (VLE) data in Chapters 3 and 4, were measured using a Fischer Labodest VLE602 ebulliometer, Germany. According to the manufacturer's specifications, the measurement uncertainties for temperature and pressure are within ±0.01 K and ±0.01 kPa, respectively. Temperature was measured using the built-in thermocouple integrated into the ebulliometer. The schematic diagram of the experimental setup was provided by Dias et al.[25] Mixtures and the entrainers were accurately prepared using a Mettler Toledo AE200 analytical balance (USA) with an uncertainty of 0.0001 g. For each experimental run, approximately 100 mL of the prepared mixture was introduced into the ebulliometer to ensure consistent liquid and vapor phase circulation in the setup. Vacuum conditions were established in a closed system using a Pfeiffer DUO 3 vacuum pump (Germany). The system pressure was maintained with a Burkert 2871 pressure controller (Germany) integrated with the i-Fischer Unicontrol VLE digital interface. The target pressure was set and kept constant throughout each experimental run. To ensure airtightness during the experiment, all sampling ports and vent outlets were tightly sealed. Each port was equipped with a cap fitted with a silicone rubber septum and a needle-valve stopcock to prevent contamination from atmospheric exposure. Equilibrium conditions were achieved when the temperature along with the pressure in the setup remained constant, within tolerances of 0.4 K and 0.1 kPa, respectively. The temperature stabilized after 30 minutes, and an additional 30 minutes was allowed before sampling to ensure that the equilibrium conditions were fully established. Therefore, the total duration of the experiment was 60 minutes. Selected VLE experiments were repeated under identical conditions to verify consistency in temperature, pressure, and composition measurement. These repetitions confirmed that equilibrium was reached, minimized systematic bias, and demonstrated the reproducibility of the equilibrium data. To maintain proper heating and temperature uniformity throughout the system, the setup utilized a heating rod immersed in the liquid chamber and a heating mantle surrounding the vapor chamber. Thermal insulation was applied to minimize heat loss from the setup. Simultaneously, continuous agitation was supplied by a magnetic stirrer to ensure thorough mixing of the liquid mixture. Additionally, the vapor generated

during boiling was condensed and returned to the liquid mixture chamber as reflux, further enhancing internal circulation and thermal homogeneity. These methods ensured a stable and uniform temperature within the system during the experiment. At equilibrium, around 0.1 mL of both the liquid phase and condensed vapor phase were sampled. Liquid samples were collected via a sampling valve. Vapor samples were obtained via syringe collection of condensed droplets. Each sample was immediately diluted in 1 mL analytical-grade acetone followed by GC analysis to determine the composition of the samples. This experimental approach aligns with established methodologies reported in previous studies.[8,9,26,27] Repeatability was verified by remeasuring selected data points in each investigated mixture under identical conditions. Furthermore, the VLE data for both binary mixtures were compared and validated against literature data. The comparisons are discussed in Chapters 3 and 4.

**Analysis method**

The composition analysis of the vapor and liquid phase samples was performed using a Thermo Scientific Trace 1300 gas chromatography (GC) (Switzerland). The GC was fitted with dual parallel ovens and an autosampler TriPlus 100 Liquid Samples. An Agilent DB-1MS capillary column (60 m length, 0.25 mm internal diameter, 0.25 μm film thickness) was employed for component separation. The minimum peak area detection threshold was set to 0.0001 to ensure accurate quantification of the key components. The injection system operated in Split/Splitless (SSL) mode, with a 1 μL injection volume. A temperature ramp was carried out in a multi-step mode: starting at 303.15 K, followed by the temperature increased at 10 K/min to 318.15 K, 5 K/min to 333.15 K, 2.5 K/min to 353.15 K, and 5 K/min to 368.15 K. A final rapid ramp of 50 K/min brought the temperature to 593.15 K. The full temperature ramp lasting approximately 21 minutes. Detection was achieved using a Flame Ionization Detector (FID) maintained at temperature of 713.15 K. The system operated with a helium carrier gas at 213.2 kPa, a column flow rate of 2 mL/min, a split flow of 300 mL/min (split ratio 150), an auxiliary hydrogen flow of 50 mL/min, helium makeup flow of 40 mL/min, and air flow of 350 mL/min.

Prior to sample analysis, calibration was performed using standard mixtures of known composition for each component within the mole fraction range of 0.000-1.000. The peak area fractions obtained from GC analysis were plotted against their corresponding mole fractions in the standard to construct calibration curves. This approach aligns with the established methodologies reported in the literature.[28–30] The mole fractions of each component in the unknown samples were determined by applying their GC area fractions to the regression equations derived from the calibration curves, which exhibited $R^2 > 0.9997$. Each sample was

analyzed in triplicate to minimize analytical variation. The final composition values were determined as the average from the three analysis results. For the VLE measurements, expanded combined uncertainties for liquid and vapor composition, pressure, and temperature were calculated in accordance with the NIST technical note and JCGM guideline.[31,32] Detailed uncertainty calculations are provided as supporting information for Chapters 3 and 4 in Appendix B, C, D, and E.

For the verification of the chemical purity, an Agilent DB-Wax capillary column was employed. This column has a length of 60 m, a diameter of 0.25 mm, and a film thickness of 0.25 μm. A 1 μL injection volume was utilized. A temperature ramp was applied, starting at 303.15 K. The temperature was initially increased at 10 K/min to 363.15 K, followed by a 5 K/min to 368.15 K. Subsequently, the temperature was elevated at 25 K/min to 473.15 K, and then further increased at 50 K/min to a final temperature of 523.15 K. Detection was carried out using a Thermal Conductivity Detector (TCD) maintained at 473.15 K. Helium serves as the carrier gas at a pressure of 213.2 kPa and a flow rate of 2 mL/min.

## 2.5.Results and discussion

### 2.5.1. Green entrainer selection

The greener entrainers investigated in this study were categorized into two groups: (i) biobased and greener organic entrainers and (ii) natural deep eutectic solvents (NADESs). The selected biobased and greener organic entrainers are listed in Table 1, while the evaluated NADESs are summarized in Table 2. The NADESs consist of combinations of hydrogen bond acceptor (HBA), such as choline chloride and amino acids, and hydrogen bond donor (HBD), such as sugar alcohols and organic acids. In addition, several common NADESs, such as choline chloride combined with triethylene glycol, glycerol, and D-isosorbide, were also examined. These entrainers were selected based on the key properties desirable for extractive distillation, including high boiling points, favorable solvency, low hazard, and environmentally benign characteristics. From a molecular perspective, the presence of electronegative atoms, such as oxygen (O) and nitrogen (N), in the proposed greener entrainers confers strong HBA capability. NADESs inherently contain both HBA (O and N) and HBD (H) functionalities, enabling the formation of extensive hydrogen-bonding networks. This dual capacity enhances molecular interactions and suggests strong potential for effective performance as entrainers. The polarity characteristics of these compounds, determined through σ-profile analysis, are further discussed in Sigma (σ)-profile analysis Section.

Tables 1 and 2 summarize the selected biobased and greener organic entrainers, and the NADESs components, along with boiling points and green

chemistry properties. For comparison, the conventional solvent NMP is also included in Table 1. The green evaluation criteria were based on the principles of safety, health, and environment (SHE) characteristics.[33] These included (i) the sustainability of raw materials or the alignment of solvent design in accordance with green chemistry principles. This ensures that the entrainers are derived from renewable sources or that the green chemistry principles are applied. Moreover, the following criteria with respect to safety and health are taken into account: (ii) flammability, reflecting a primary and immediate hazard that poses catastrophic risks in handling and manufacturing; (iii) acute oral toxicity, which reflects the potential for immediate lethal effects resulting from single-dose exposures, making it crucial for short-term safety assessments; and (iv) reproductive toxicity (reprotoxicity), specifically focusing on developmental toxicity. Reprotoxicity represents a critical hazard due to its long-term, irreversible effects, and the strict regulatory implications associated with reproductive toxicants.[34] These aspects capture both short-term and long-term hazard profiles. Together, these factors provide a comprehensive framework for evaluating the greenness of candidate entrainers.

Comparison with NMP highlights three major differentiating factors: reprotoxicity, boiling point, and regulatory status. All examined biobased and greener organic entrainers were identified as nonreprotoxic chemicals. Their no observed adverse effect level (NOAEL) values consistently higher than those of NMP. Higher NOAEL values indicate lower reprotoxicity, suggesting these entrainers are safer alternatives. Although specific NOAEL data for guaiacol are not available, its wide application as a flavoring agent in foods and as an ingredient or intermediate in pharmaceutical industries implies a relatively low toxicological concern under typical exposure conditions.[35] Additionally, all proposed biobased and greener organic entrainers exhibit higher boiling points than NMP. This indicates lower volatility and reduced risk during handling and operation. Similarly, the NADESs components displayed significantly higher boiling points than NMP, despite some individual constituents possessing lower values. The strong hydrogen-bonding interactions formed within NADESs significantly elevate their boiling points compared to those of their respective components. These strong interactions result in a markedly negligible vapor pressure, which minimize entrainer losses and emissions.[36] Among all compounds listed in Tables 1 and 2, only NMP is restricted under the REACH regulation due to its classification as a reproductive toxicant.[37]

**Table 1.** Boiling points and green chemistry properties of biobased and greener organic entrainers.

| Potential green solvents | $T_b$ (K) * | Green aspects | | | |
|---|---|---|---|---|---|
| | | **Biobased/ Sustainable materials/ designed according to green chemistry principle; Biodegradable** | **Flammability** | **Acute toxicity**: Oral $LD50_{rat}$ (mg/kg body weight/day)** | **Reprotoxicity***: NOAEL for developmental toxicity (mg/kg body weight/day)** |
| Glycerol carbonate[38,39] | 627.15 | Yes; Readily | Nonflammable | Nontoxic: >5000 | Nonreprotoxic: 2000 |
| Propylene carbonate[40,41] | 515.15 | Yes; Readily | Nonflammable | Nontoxic: >5000 | Nonreprotoxic: 10,100 |
| Ethylene carbonate[42,43] | 521.15 | Yes; Readily | Nonflammable | Nontoxic: 10,400 | Nonreprotoxic: >1000 |
| Diphenyl carbonate[44,45] | 575.15 | Yes; Readily | Nonflammable | Low toxic: 1500 | Nonreprotoxic: 1561 |
| N-Formylmorpholine[46,47] | 517.15 | Yes; Readily | Nonflammable | Nontoxic: 7314 | Nonreprotoxic: 1000 |
| Dimethyl isosorbide[48–52] | 508.15 | Yes; Readily | Nonflammable | Nontoxic: 6530 | Lowreprotoxic: 300 |
| 1-Butylpyrrolidin-2-one[53–56] | 514.15 | Yes; Inherently | Nonflammable | Moderate-low toxic: 300-2000 | Nonreprotoxic: >500 |
| Gamma-valerolactone[57–61] | 480.15 | Yes; Readily | Nonflammable | Nontoxic: 9249 | Nonreprotoxic: 1000 |
| Guaiacol[3562] | 479.15 | Yes; Readily | Nonflammable | Low toxic: 621-725 | N/A data; use in food and pharmaceutical |
| Methyl 5-(dimethylamino)-2-methyl-5-oxopentanoate (Polar Clean)[63] | 553.15 | Yes; Readily | Nonflammable | Nontoxic: 2000 | Nonreprotoxic: 1000 |
| NMP[64] | 475.15 | No; Readily | Nonflammable | Nontoxic: 4150 | Reprotoxic: 160 |

*At 101.13 kPa
**Lethal Dose for 50% of population (LD50)
***The No Observed Adverse Effect Level (NOAEL)
Higher value of NOAEL and LD50 means lower toxicity

**Table 2.** Boiling points and green chemistry properties of NADESs' compounds.

| Potential green solvents | $T_b$ (K) * | Green aspects | | | |
|---|---|---|---|---|---|
| | | **Biobased/ Sustainable materials/ designed according to green chemistry principle; Biodegradable** | **Flammability** | **Acute toxicity**: Oral $LD50_{rat}$ (mg/kg body weight/day)** | **Reprotoxicity***: NOAEL for developmental toxicity (mg/kg body weight/day)** |
| ***Hydrogen Bond Acceptor (HBA)*** | | | | | |
| ChCl[65,66] | 573.15 | Yes; Readily | Nonflammable | Nontoxic: >3500 | Nonreprotoxic: 4160 |
| Proline[67] | N/A, melting point at 473.15 (decomposes) | Yes; Readily | Nonflammable | Nontoxic: >5110 | Nonreprotoxic: has no observed effect on developmental toxicity |
| Betaine[68,69] | N/A, melting point at 578.15 (decomposes) | Yes; Readily | Nonflammable | Nontoxic: >11,179 | Nonreprotoxic: has no observed effect on developmental toxicity |
| β-alanine[70] | N/A, melting point at 470.15 (decomposes) | Yes; Readily | Nonflammable | Nontoxic: >5000 | Nonreprotoxic: 1000 |
| ***Hydrogen Bond Donor (HBD)*** | | | | | |
| Sorbitol[71–73] | N/A, melting point at 523.15 (decomposes) | Yes; Readily | Nonflammable | Nontoxic: >15,900 | Nonreprotoxic: has no observed effect on developmental toxicity |
| Xylitol[74,75] | 653.15 | Yes; Readily | Nonflammable | Nontoxic: 4000 | Nonreprotoxic: has no observed effect on developmental toxicity |
| Maltitol[76–78] | 546.15 | Yes; Readily | Nonflammable | Nontoxic: 24,370 | Nonreprotoxic: 4000 |
| Erythritol[76,79,80] | 603.15 | Yes; Readily | Nonflammable | Nontoxic: 13,100 | Nonreprotoxic: has no observed effect on developmental toxicity |
| Lactitol[81–83] | N/A, melting point at 408.15 | Yes; Readily | Nonflammable | Nontoxic: 30,000 | Nonreprotoxic: has no observed effect on developmental toxicity |
| Mannitol[84–86] | N/A, melting point at 441.15 | Yes; Readily | Nonflammable | Nontoxic: Use as a food ingredient | Nonreprotoxic: Use as a food ingredient |
| Ribitol[84,87] | N/A, melting point at 377.15 | Yes; Readily | Nonflammable | Nontoxic: 3500 | Use as a food ingredient |

| Potential green solvents | $T_b$ (K) * | Green aspects | | | |
|---|---|---|---|---|---|
| | | **Biobased/ Sustainable materials/ designed according to green chemistry principle; Biodegradable** | **Flammability** | **Acute toxicity**: Oral $LD50_{rat}$ (mg/kg body weight/day)** | **Reprotoxicity***: NOAEL for developmental toxicity (mg/kg body weight/day)** |
| Malic acid[88,89] | N/A, melting point at 508.15 (decomposes) | Yes; Readily | Nonflammable | Nontoxic: 3500 | Nonreprotoxic: 520 |
| Glycolic acid[90,91] | 373.15 | Yes; Readily | Nonflammable | Nontoxic: 5000 | Nonreprotoxic: 1640 |
| Glutaric acid[92,93] | 577.15 | Yes; Readily | Nonflammable | Nontoxic: 6000 | Nonreprotoxic: 1720 |
| Oxalic acid[94,95] | N/A, melting point at 433.15 (decomposes) | Yes; Readily | Nonflammable | Nontoxic: 375 | Nonreprotoxic: 450 |
| Triethylene glycol[96] | 559.15 | Yes; Readily | Nonflammable | Nontoxic: 18,080 | Nonreprotoxic: 565 |
| D-Isosorbide[97–99] | 645.15 | Yes; Readily | Nonflammable | Nontoxic: 2000 | Nonreprotoxic: has no observed effect on developmental toxicity |

*At 101.13 kPa
**Lethal Dose for 50% of population (LD50)
***The No Observed Adverse Effect Level (NOAEL)
Higher value of NOAEL and LD50 means lower toxicity

To provide a clearer overview of the screening procedure and the elimination of the candidates, Table 3 summarizes the full entrainer selection funnel. For each screening stage, the table reports the number candidates evaluated and eliminated.

**Table 3.** Overview of stepwise entrainer screening procedure and candidate reduction across selection stages for methylcyclohexane-toluene (MCH-TOL) and n-hexane-ethanol (HEX-ETH)

| Screening stage | Number of candidates entering stage | Number of candidates eliminated |
|---|---|---|
| Selectivity prediction | MCH-TOL: 61<br>HEX-ETH: 62 | MCH-TOL: 0<br>HEX-ETH: 0 |
| NADESs synthesis and evaluation | MCH-TOL: 61<br>HEX-ETH: 62 | MCH-TOL: 44<br>HEX-ETH: 44 |
| Miscibility test | MCH-TOL: 17<br>HEX-ETH: 18 | MCH-TOL: 12<br>HEX-ETH: 13 |
| Relative volatility (potential for VLE data measurement) | MCH-TOL: 5<br>HEX-ETH: 5 | MCH-TOL: 1<br>HEX-ETH: 1 |

| Screening stage | Number of candidates entering stage | Number of candidates eliminated |
|---|---|---|
| VLE measurements | MCH-TOL: 4<br>HEX-ETH: 4 | MCH-TOL: 0<br>HEX-ETH: 0 |
| Process performance comparison | MCH-TOL: 4<br>HEX-ETH: 4 | MCH-TOL: 0<br>HEX-ETH: 0 |
| Final entrainers | MCH-TOL: 4<br>HEX-ETH: 4 | |

### 2.5.2. Selectivity, capacity, and performance index evaluation

As outlined in Separation parameters Section, selectivity, capacity, and the performance index are key parameters for evaluating and selecting effective entrainer in extractive distillation. Each parameter, however, must be critically assessed before being used as a decisive selection criterion. The selectivity at infinite dilution and capacity at infinite dilution were predicted using COSMO-RS. Their respective trends are illustrated in Figures 1 and 2. For all NADESs simulations were performed at a 1:1 molar ratio between the HBA and HBD. This ratio is widely adopted in the literature because it effectively promotes hydrogen-bond formation and is commonly reported as an optimal composition for NADES formation.[100,101] From COSMO-RS perspective, the use of 1:1 ratio provides a simplified yet representative model for estimating intermolecular interactions and polarity effects. In practical applications, however, the optimal composition of NADESs can vary depending on the nature of HBD and HBA. Deviations from the 1:1 ratio primarily shift the overall polarity profile without altering the fundamental hydrogen-bonding characteristics. Thus, the 1:1 composition offers a consistent reference for comparative screening, while experimental optimization considering composition sensitivity remains essential for practical NADESs design and evaluation of their separation performances. The COSMO-RS predictions reveal an inverse relationship between selectivity and capacity for both mixtures studied. Higher selectivity corresponds to lower capacity, and vice versa. To address this trade-off, the PI, defined as the product of selectivity and capacity, was also evaluated.

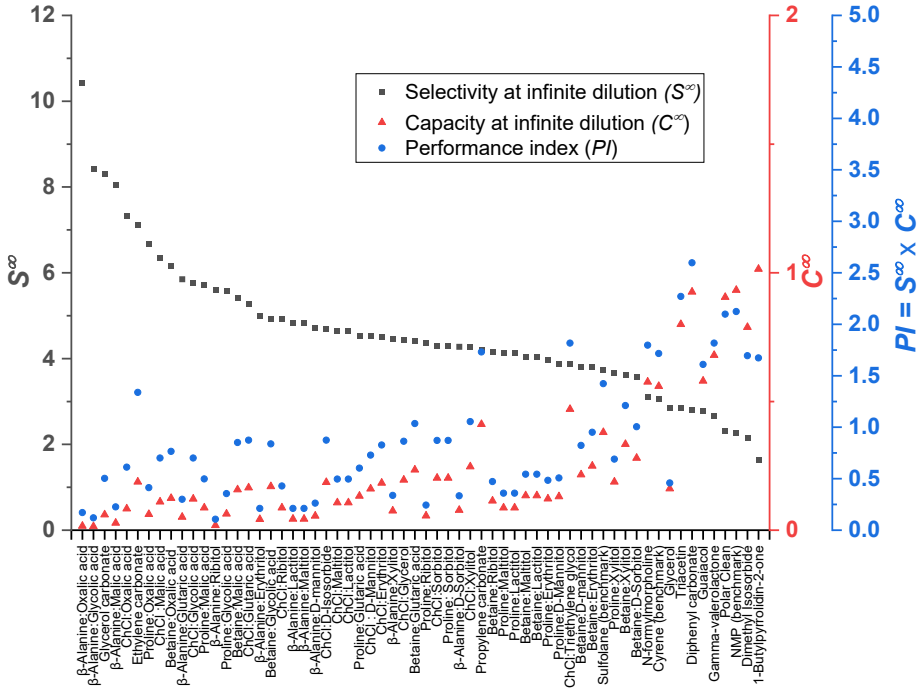


**Figure 1.** Selectivity, capacity, and performance index prediction of entrainers in the methylcyclohexane-toluene mixture at a temperature of 400.15 K.

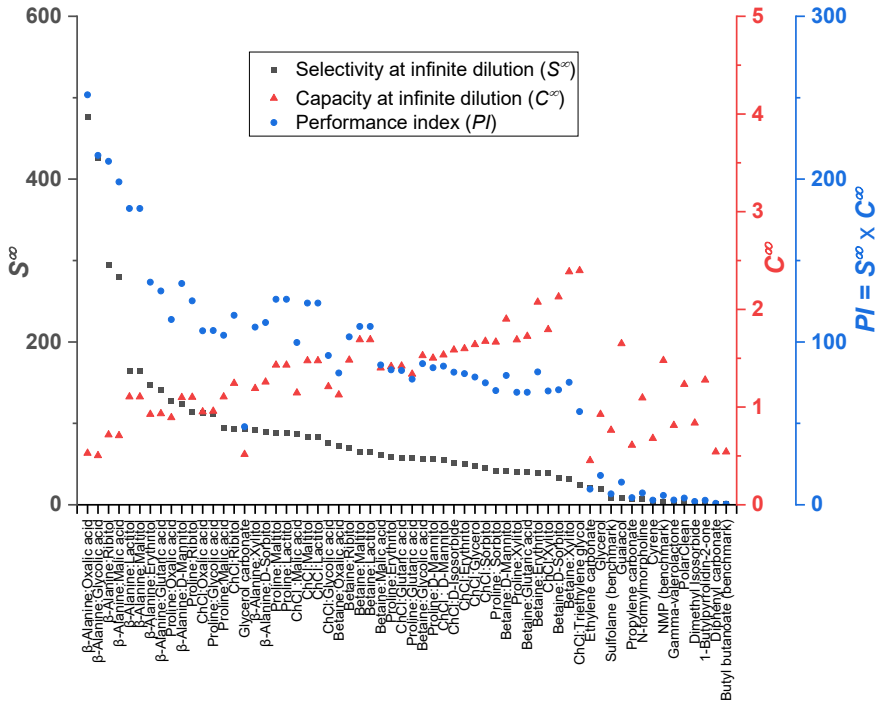


**Figure 2.** Selectivity, capacity, and performance index prediction of entrainers in the n-hexane-ethanol mixture at a temperature of 400.15 K.

Interestingly, the PI exhibited different behavior depending on the mixture studied. For the methylcyclohexane-toluene mixture, the PI trend followed that capacity, indicating that the PI is primarily influenced by capacity at lower selectivity values. Conversely, for the n-hexane-ethanol mixture, the PI correlated more strongly with selectivity, suggesting that when selectivity is dominant, it governs the PI trend. This demonstrates that the PI is a composite parameter whose behavior depends on the values selectivity. Consequently, the PI alone cannot serve as a universally decisive parameter since its trend can vary depending on the mixture and is easily affected by the selectivity value. The higher selectivity observed for the n-hexane-ethanol mixture compared to the methylcyclohexane-toluene mixture arises from stronger hydrogen bonding interaction between ethanol and the entrainers compared to toluene and the entrainers.

Overall, the results suggest that selectivity serves as the most decisive parameter, particularly in the preliminary stage of entrainer selection. Selectivity more accurately represents separation performance compared to capacity, as it directly reflects the entrainer's ability to alter relative volatility. This alteration enables easier separation of close-boiling or azeotropic mixtures. By contrast, capacity primarily indicates the amount of entrainer required in the process. A higher capacity reduces the entrainer circulation rate and reboiler duty in the entrainer recovery column, thereby lowering energy consumption. The trade-off between these two parameters lies in their respective impacts. Selectivity predominantly influences the size and energy consumption of the extractive distillation column, whereas capacity mainly affects the energy requirements of the entrainer recovery column. As the main column generally dominates capital and operating cost, improvement in selectivity translate directly into reduced TAC.[16] Therefore, selectivity exerts the most significant impact on process economics. This result aligns with previous study, which identified selectivity as the most reliable parameter for entrainer selection.[13–15] Since selectivity is derived directly from relative volatility, it provides a strong physical foundation for assessing entrainer performance. Accordingly, this study concludes that selectivity should be prioritized over capacity and the PI as the primary criterion for preliminary entrainer selection in extractive distillation. Process simulations incorporating varying selectivity values are nevertheless required to validate the relative importance of each parameter under practical operating conditions. A detailed discussion of this integration with process design is presented in Chapter 5.

### 2.5.3. Selectivity analysis

The interactions between solute and solvent, represented by the activity coefficient at infinite dilution, and derived selectivity at infinite dilution are strongly influenced by temperature. Two temperatures, 293.15 K and 400.15 K, were

evaluated. These temperatures represent the typical operating window of extractive distillation processes, which are generally operated from near ambient to elevated temperatures under low to atmospheric pressures. As shown in Figure 3 (methylcyclohexane–toluene mixture) and Figure 4 (n-hexane–ethanol mixture), selectivity decreases systematically with increasing temperature. This behavior arises due to higher temperatures weaken specific solute-entrainer interactions, thereby reducing liquid-phase nonideality. These results align with experimental observations reported in the literature, which demonstrated that the activity coefficient at infinite dilution decreases with increasing temperature.[102] While COSMO-RS reliably captures such qualitative trends within its temperature range, extrapolation far beyond this range may introduce uncertainty due to changes in molecular interaction strength, thereby affecting the predicted separation performance. Therefore, temperature of 400.15 K was selected as an upper-bound case to test selectivity at a high yet physically realistic process temperature.

In Figure 3, the activity coefficient at infinite dilution for toluene–entrainer are consistently lower than those for methylcyclohexane-entrainer. This indicates stronger entrainer-toluene interactions. Similarly, Figure 4 shows that the activity coefficient at infinite dilution for ethanol-entrainer are substantially lower than those for n-hexane–entrainer. This confirms that the entrainers exhibit stronger interactions with the polar component (ethanol) rather than the nonpolar component (n-hexane). As a result, the n-hexane-ethanol mixture exhibits significantly higher selectivity than the methylcyclohexane-toluene mixture, especially for NADESs, which possess pronounced polar characteristics. This contrast originates from the polarity difference between components. In the n-hexane-ethanol mixture, the polarity disparity between the nonpolar n-hexane and polar ethanol favors selective hydrogen-bonding interactions between ethanol and the entrainers, especially the NADESs, which provide both HBA and HBD sites. In contrast, both methylcyclohexane and toluene are essentially nonpolar, although toluene exhibits slightly higher polarizability due to its aromatic π-electron system. These polarity-driven effects explains the lower activity coefficient at infinite dilution for ethanol (Figure 4), compared to toluene (Figure 3).

In terms of separation performance, most biobased and greener organic entrainers, and all NADESs, demonstrated selectivity values comparable to or exceeding those of conventional and previously reported greener entrainers. Notably, NADESs consistently outperformed both biobased and greener organic entrainers, highlighting their strong potential as sustainable alternatives. Among them, only glycerol carbonate and ethylene carbonate achieved selectivity comparable to NADESs across both mixtures. A minimum selectivity threshold can be inferred from the VLE profiles discussed in Chapters 3 and 4. For the

methylcyclohexane-toluene mixture, a minimum selectivity of 1.6, as achieved by NBP, effectively remove the close-boiling behavior. For the n-hexane-ethanol mixture, a minimum selectivity of 2.1, also demonstrated by NBP, is sufficient to eliminate the azeotropic point. These values are therefore established as benchmark thresholds for evaluating entrainer performance in close-boiling and azeotropic mixtures, respectively.

Even though these greener entrainers exhibit selectivity equal to or higher than that of conventional solvents, they can be considered as fully promising candidates if they meet criteria, such as complete miscibility with the feed over the entire composition range, effectively eliminate close-boiling or azeotropic behavior, a significantly high boiling-point difference relative to the key components, and no formation of new azeotropes. Meeting these requirements enabling easy separation and recovery of the entrainers in the entrainer recovery column.

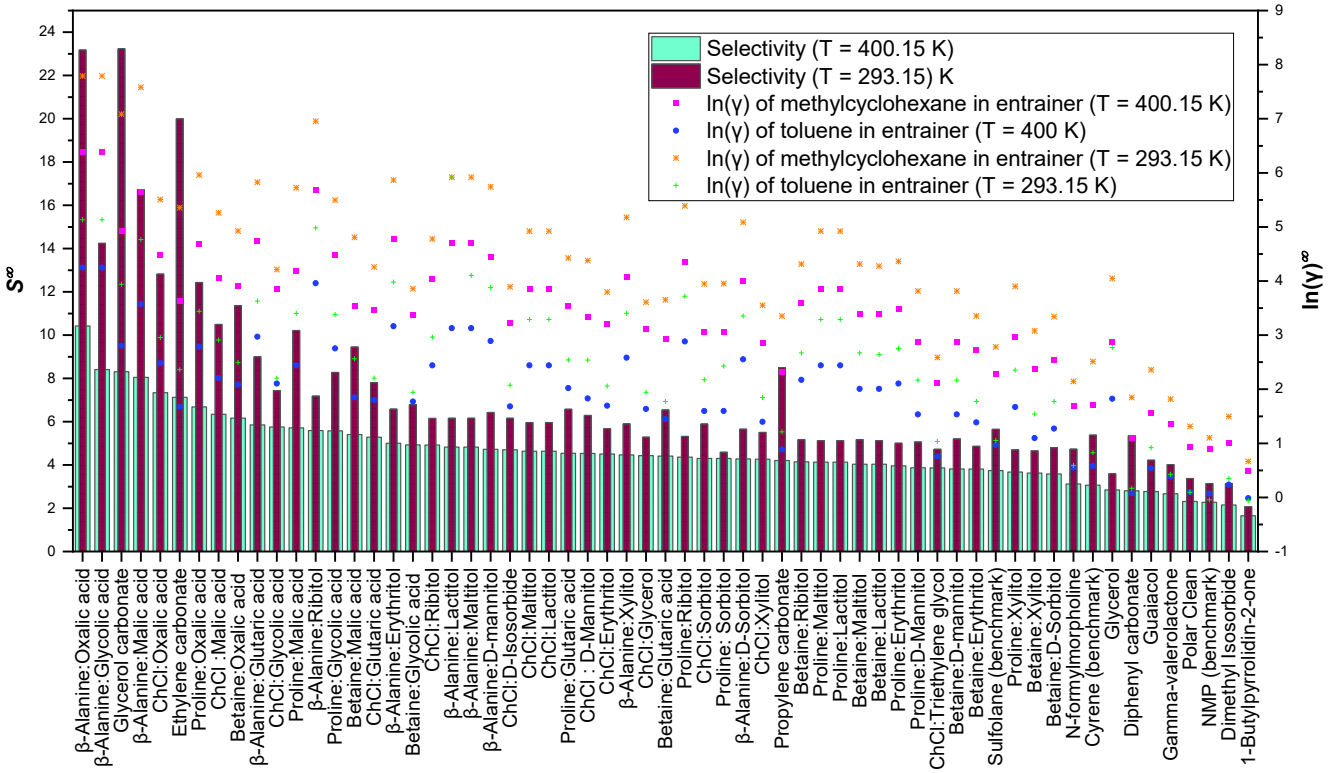


**Figure 3.** Selectivity prediction of entrainers at various temperatures for the methylcyclohexane-toluene mixture, along with ln(γ) at infinite dilution for both methylcyclohexane and toluene in the entrainer.

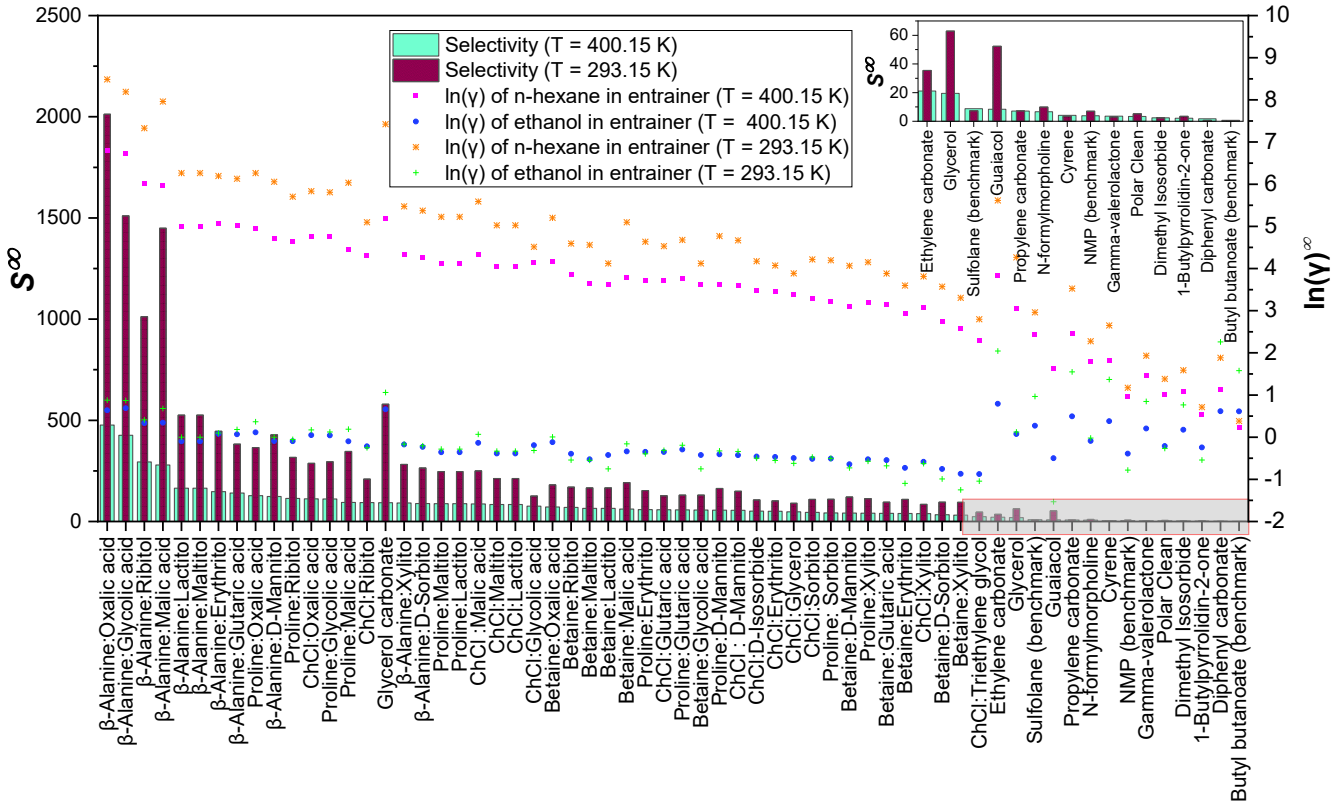


**Figure 4.** Selectivity prediction of entrainers at various temperatures for the n-hexane-ethanol mixture, along with ln(γ) at infinite dilution for both n-hexane and ethanol in the entrainer.

### 2.5.4. Sigma (σ)-profile analysis

The performance of entrainers can be qualitatively evaluated using the σ-profile generated by the COSMO-RS. The σ-profile represents the distribution of surface polarization of screening charge densities (σ) across a molecule surface. This provides insight into its polar and electronic surface characteristics. The probability distribution, p(σ), describes the amount of the molecular surface that falls within a specific σ interval. A screening charge density cutoff of ±0.0084 e/Å$^2$ is commonly applied as a threshold to determine whether a molecule possesses sufficient polarity to participate in hydrogen bonding.[103] In this context, a negative σ region corresponds to HBD capability, while a positive σ region indicates HBA ability. Larger deviations from zero reflect stronger donor or acceptor tendencies. The σ-profiles of methylcyclohexane, toluene, n-hexane, and ethanol are presented in Figure 5. Methylcyclohexane, toluene, and n-hexane exhibit σ-values largely confined within the nonpolar cutoff, classifying them as nonpolar molecules.

Methylcyclohexane and n-hexane exhibit narrow, nearly symmetric charge-density distributions centered around σ = 0 e/Å$^2$, confirming their strong nonpolar nature. Their dominant peaks occur near -0.001 e/Å$^2$ (arising from surface

hydrogen atoms carrying partial positive charge) and a smaller peak at +0.001 e/Å$^2$ (from carbon atoms with partial negative charge). It is vital to note that atoms bearing partial positive charge, such as hydrogen, contribute to negative σ values. On the other hand, atoms with partial negative charge, such as carbon, generate positive σ values. Since these peaks lie within the nonpolar cutoff region, both compounds exhibit negligible polarity and therefore prefer self-association over interaction with polar entrainers. Toluene displays a broader σ-profile compared to methylcyclohexane and n-hexane, although it remains primarily within nonpolar regions. Peaks at -0.005 e/Å$^2$ and +0.006 e/Å$^2$ correspond to the hydrogen atom on the methyl group and the aromatic ring (indicating donor tendency) and the π-electron cloud of the aromatic system (indicating acceptor tendency), respectively. These features suggest that toluene may interact modestly with polar entrainers, showing stronger interactions than methylcyclohexane. In contrast, ethanol demonstrates a distinctly broader σ-profile extending well beyond the ±0.0084 e/Å$^2$ cutoff, reflecting strong hydrogen-bonding capability. A prominent peak near -0.013 e/Å$^2$ corresponds to hydrogen, which carries a partial positive charge due to the high electronegativity of oxygen in the hydroxyl group. This property makes ethanol a strong HBD, as represented in the blue zone of the molecular profile. Conversely, a sharp peak around +0.017 e/Å$^2$ is attributed to the oxygen atom in the hydroxyl group. This atom has two lone pairs of electrons, confer strong HBA ability represented in the red zone. This dual donor-acceptor nature explains ethanol's higher polarity and its stronger interactions with entrainers compared to n-hexane.

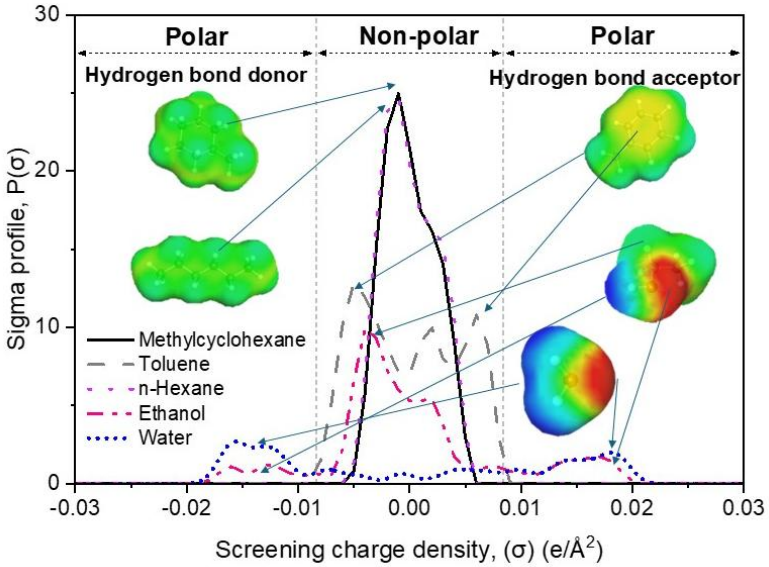


**Figure 5.** σ-profiles of methylcyclohexane, toluene, n-hexane, ethanol, and water.

For an effective separation of methylcyclohexane from toluene and n-hexane from ethanol, the entrainers should exhibit distinct peaks in both negative and positive regions of the σ-profile. In addition, they should show minimal surface distribution near 0 e/Å$^2$. A symmetric distribution with pronounced peaks away from zero implies strong HBD and HBA capabilities. This allows the entrainers to interact more effectively with the solute molecules. Such entrainers can form favorable interactions with the slightly polarized surface regions of toluene, as well the highly polar regions of ethanol. Consequently, this complementary polarity enhances the predicted selectivity of entrainers for both the methylcyclohexane-toluene and n-hexane-ethanol mixtures.

The σ-profiles of biobased and greener organic entrainers are presented in Figure 6. These entrainers exhibit substantial peaks in the positive region, suggesting strong HBA capability. Several entrainers, such as glycerol carbonate, glycerol, and guaiacol, also show peaks in the positive and negative region, indicating that they possess dual functionality as both HBA and HBD. These abilities provide greater flexibility in forming specific interactions with solutes. Importantly, the σ-profiles of these entrainers are comparable to those of benchmark entrainers, which similarly feature dominant peaks in the positive region. Thus, many biobased and greener organic entrainers show promising potential for selective interactions with toluene and ethanol, respectively. Figure 7 illustrates the σ-profiles of representative NADESs, selected to reflect high, medium, and low selectivity values across the dataset. Compared with biobased, greener organic, and benchmark entrainers, NADESs demonstrate broader and more intense peaks in both negative and positive polar regions. This behavior represents their enhanced HBD and HBA strength, arising from the synergistic hydrogen-bonding interactions between donor and acceptor components. As a result, NADESs are predicted to establish stronger and more versatile interactions with both toluene and ethanol. This characteristic explains why NADESs consistently demonstrate higher predicted selectivity values than most biobased, greener organic, and benchmark entrainers.

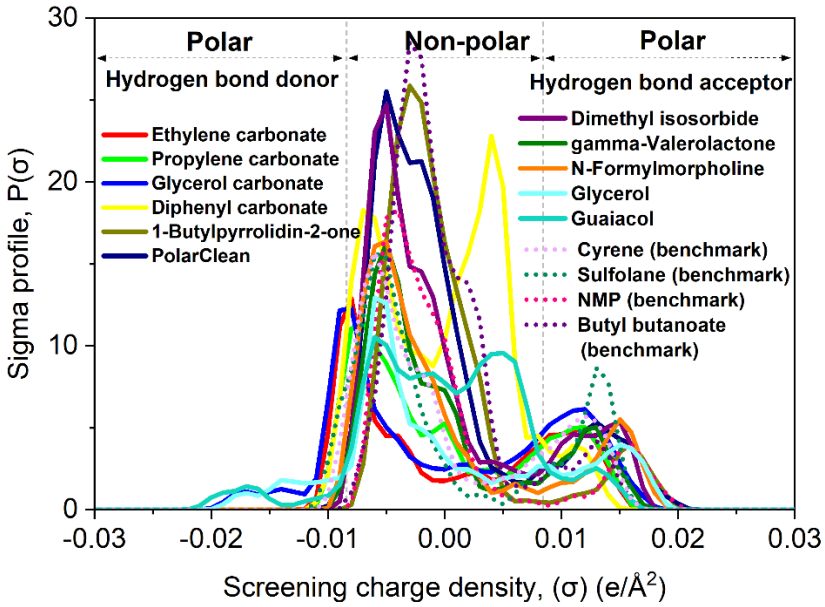


**Figure 6.** σ-profiles of biobased and greener organic entrainers.

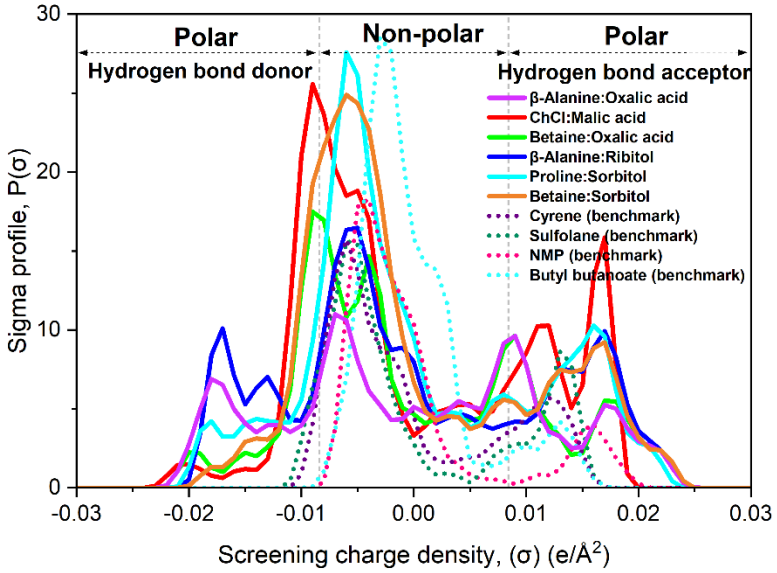


**Figure 7.** σ-profiles of the selected NADESs.

### 2.5.5. Sigma (σ)-potentials analysis

While σ-profiles describe the distribution of surface charge densities across a molecule, σ-potentials provide a complementary energetic perspective within the COSMO-RS framework. Specifically, σ-potentials quantify how favorably a molecule interacts with surfaces of different polarity. The σ-potentials represents

the chemical potential (μ (σ)) of a molecule when exposed to a virtual surface segment of polarity. Strong attractive interactions between molecules are reflected by lower (more negative) μ (σ) values, while strong repulsive behaviour is indicated by higher (more positive) values. As shown in Figures 8-10, the horizontal axis corresponds to surface polarity, with values beyond the cutoff ± 0.0084 e/Å$^2$ denoting regions capable of hydrogen-bonding. The negative region reflects an affinity toward HBD, while the positive region corresponds to affinity toward HBA.

As discussed in Sigma (σ)-profile analysis Section, toluene demonstrates a greater tendency to interact with polar compounds, such as entrainers, compared to methylcyclohexane. This trend is confirmed by the σ-potentials in Figure 8, where toluene exhibits lower σ-potential values in both polar regions, even though the values remain positive. This implies that toluene has a higher affinity for polar entrainers than methylcyclohexane. Similarly, n-hexane shows a σ-potential profile comparable to that of methylcyclohexane, with predominantly positive values This indicates that both hydrocarbons interact weakly with polar entrainers. In contrast, ethanol exhibits negative σ-potential values in both polar regions, consistent with its dual hydrogen bond-donor and acceptor capabilities. The more negative values in the negative σ region (HBD affinity) indicate ethanol interacts particularly strongly with donor sites. These results reinforce the σ-profile analysis, further explaining ethanol's stronger affinity for entrainers compared to n-hexane.

The σ-potential profiles of biobased and greener organic entrainers, along with benchmark entrainers, are shown in Figure 9. Most of these entrainers exhibit negative σ-potentials values in the negative region, indicating strong affinity toward HBD, while their σ-potential values in the positive region indicate weaker affinity toward HBA. Notably, glycerol carbonate, glycerol, and guaiacol exhibit negative σ-potential values in both regions, demonstrating dual affinity toward both HBD and HBA. This dual functionality enhances their versatility and effectiveness in forming specific solute-entrainer interactions. A similar trend is observed for the selected NADESs, as illustrated in Figure 10. Their σ-potential curves remain negative across both polar regions. This confirms strong affinity toward both HBD and HBA. This behavior reflects the synergistic hydrogen-bonding interactions between donor and acceptor components within the NADESs. These results complement the σ-profiles analysis and collectively indicate that all biobased, greener organic entrainers and NADESs demonstrate favorable separation performance, making them promising candidates for applications in extractive distillation.

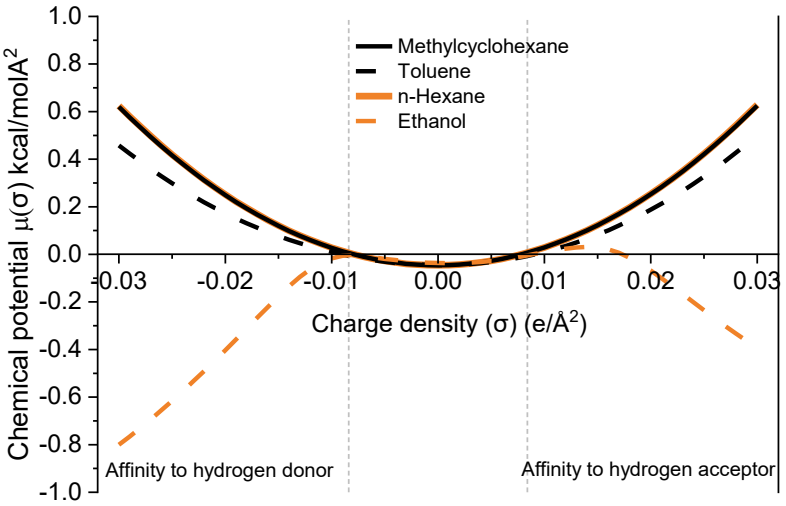


**Figure 8.** σ-potentials of methylcyclohexane, toluene, n-hexane, and ethanol.

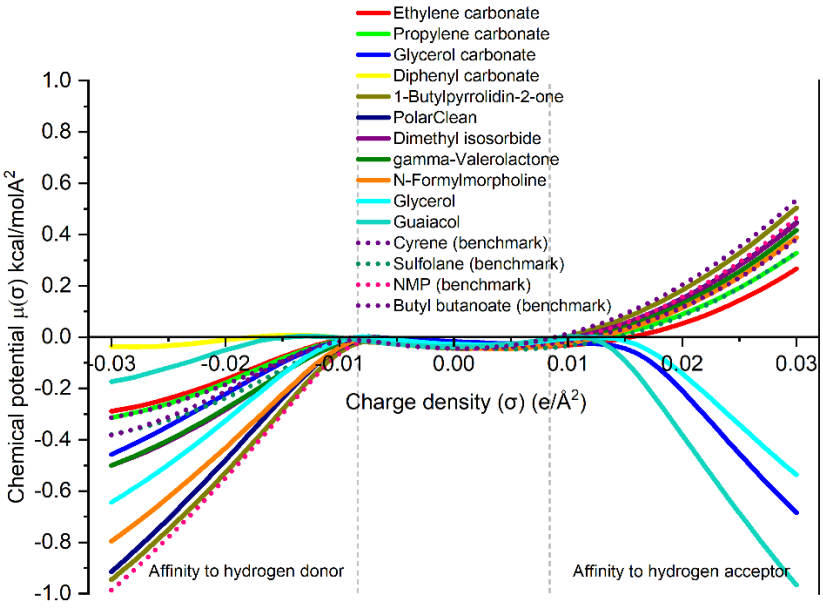


**Figure 9.** σ-potentials of biobased and greener organic entrainers.

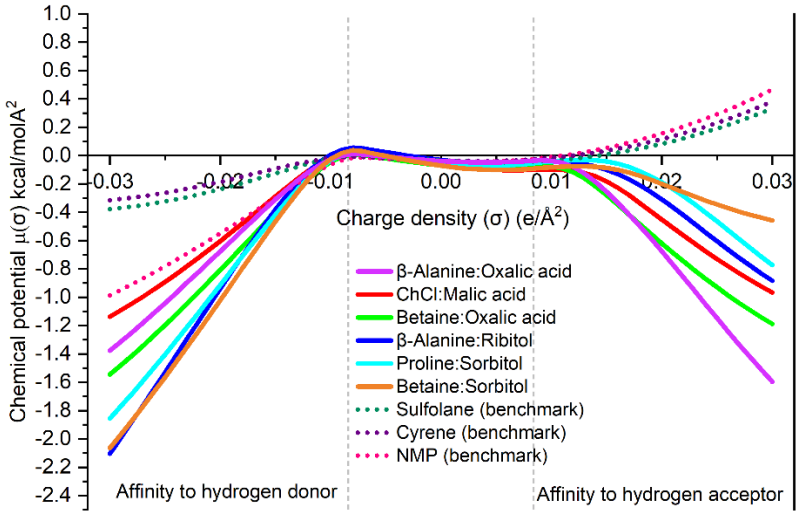


**Figure 10.** σ-potentials of selected NADESs.

### 2.5.6. Miscibility analysis

Prior to the relative volatility comparison of the predicted values with experimental data, the miscibility of biobased and greener organic entrainers, and NADESs was evaluated. Miscibility of entrainers in the mixture is an important property in extractive distillation. The entrainers must form a homogeneous liquid phase with the feed to ensure uniform distribution and effective molecular interactions with the target components. Homogeneous mixing enhances selectivity by facilitating solute-entrainer interactions. Conversely, phase separation (heterogeneous mixture) limit interactions to one phase, thereby reducing entrainer's effectiveness and overall separation performance. Additionally, ensuring a single liquid phase is essential for obtaining accurate VLE data, which is critical for process design. It also helps to mitigate potential operational issues in distillation columns, such as phase splitting on trays and reduced mass-transfer efficiency.

The miscibility of the entrainers was investigated at feed compositions representing critical separation conditions. For the methylcyclohexane (1) + toluene (2) mixture, the liquid mole fraction of methylcyclohexane was set at $x_1$ = 0.5. This corresponds to the midpoint of the close-boiling region. For the n-hexane (1) + ethanol (2) mixture, the liquid mole fraction of n-hexane was $x_1$ = 0.66, which corresponds to the azeotropic composition. These compositions were selected to assess entrainer miscibility under representative extractive distillation operating environments. Once miscibility was confirmed, relative volatility measurements

were performed. Miscibility tests were conducted at both atmospheric and elevated temperatures. For both mixtures, the atmospheric temperature of 293.15 was used to represent storage and handling conditions of the chemicals, and lower operating pressure of extractive distillation. While elevated temperatures representative of higher pressure of extractive distillation were 373.15 K the methylcyclohexane-toluene mixture and 343.15 K for the n-hexane–ethanol mixture. Moreover, miscibility was tested at varied E/F = 1–5, covering a wide yet practical range while ensuring reasonable entrainer usage. To confirm complete miscibility, tests were also conducted with pure feed compositions of methylcyclohexane and n-hexane ($x_1 = 1$), respectively. This ensures entrainer compatibility across the entire composition range, ensuring suitability for reliable VLE measurements.

Selected NADESs representing low, medium, and high predicted selectivity values were synthesized and tested. Synthesis and characterization details are provided in NADESs experiences Section. The miscibility results are summarized in Tables 4 and 5. As shown in Table 4, at $x_1 = 0.5$ and a temperature of 373.15 K, several entrainers formed homogeneous mixtures with the methylcyclohexane-toluene mixture. These include propylene carbonate, n-formylmorpholine (NFM), dimethyl isosorbide (DMI), 1-butylpyrrolidin-2-one (NBP), gamma-valerolactone (GVL), NMP, and guaiacol. However, other biobased and greener organic entrainers, as well as the tested NADESs, were immiscible. The miscible entrainers were subsequently selected for relative volatility measurements to evaluate their separation performance. These experimental results served as benchmarks for validating predictive results obtained from COSMO-RS, UNIFAC, and modified UNIFAC (Dortmund), as discussed in Relative volatility analysis Section.

As shown in Table 5, for the n-hexane–ethanol mixture at $x_1 = 0.66$ and 343.15 K, several entrainers including DMI, NBP, GVL, NMP, butyl butanoate, and guaiacol, were found to be miscible. However, other biobased and greener organic entrainers, as well as all NADESs, exhibited phase separation and thus formed heterogeneous mixtures. Polar Clean (methyl 5-(dimethylamino)-2-methyl-5-oxopentanoate) was excluded from testing due to limited commercial availability. All investigated NADESs exhibited heterogenous phase behavior in both mixtures, consistent with their high polarity. Their limited miscibility with hydrocarbon-rich mixtures highlights a fundamental constraint for their applications in nonpolar separations. This immiscibility arises from their strong polarity and extensive hydrogen-bonding, which are incompatible with nonpolar nature of hydrocarbon mixtures. Importantly, the proposed screening framework explicitly incorporates miscibility assessments as a key selection criterion. This enables clear distinction between suitable and unsuitable entrainers for specific separation targets. Consequently, the framework not only identifies promising

candidates but also systematically excludes those that are incompatible based on polarity mismatch. Furthermore, directing the application of NADESs and other immiscible biobased and greener entrainers toward polar separations, such as ethanol-water separation, would allow their intrinsic polarity and strong hydrogen-bonding characteristics to be utilized more effectively.

**Table 4.** The miscibility of entrainers in the methylcyclohexane-toluene mixture.

| Entrainer | E/F = 1 | | | | E/F = 2 | | | | E/F = 3 | | | | E/F = 4 | | | | E/F = 5 | | | |
|---|---|---|---|---|---|---|---|---|---|---|---|---|---|---|---|---|---|---|---|---|
| $T$ (K) | 293.15 | | 373.15 | | 293.15 | | 373.15 | | 293.15 | | 373.15 | | 293.15 | | 373.15 | | 293.15 | | 373.15 | |
| $x_1$ | 0.5 | 1 | 0.5 | 1 | 0.5 | 1 | 0.5 | 1 | 0.5 | 1 | 0.5 | 1 | 0.5 | 1 | 0.5 | 1 | 0.5 | 1 | 0.5 | 1 |
| Glycerol carbonate | ☒ | ☒ | ☒ | ☒ | ☒ | ☒ | ☒ | ☒ | ☒ | ☒ | ☒ | ☒ | ☒ | ☒ | ☒ | ☒ | ☒ | ☒ | ☒ | ☒ |
| Propylene carbonate | ☒ | ☒ | ☑ | ☒ | ☑ | ☒ | ☑ | ☒ | ☑ | ☒ | ☑ | ☒ | ☑ | ☒ | ☑ | ☒ | ☑ | ☒ | ☑ | ☒ |
| Ethylene carbonate | ☒ | ☒ | ☒ | ☒ | ☒ | ☒ | ☒ | ☒ | ☒ | ☒ | ☒ | ☒ | ☒ | ☒ | ☒ | ☒ | ☒ | ☒ | ☒ | ☒ |
| Diphenyl carbonate | ☒ | ☒ | ☒ | ☒ | ☒ | ☒ | ☒ | ☒ | ☒ | ☒ | ☒ | ☒ | ☒ | ☒ | ☒ | ☒ | ☒ | ☒ | ☒ | ☒ |
| N-Formylmorpholine | ☑ | ☒ | ☑ | ☒ | ☑ | ☒ | ☑ | ☒ | ☑ | ☒ | ☑ | ☒ | ☑ | ☒ | ☑ | ☒ | ☑ | ☒ | ☑ | ☒ |
| Dimethyl isosorbide | ☑ | ☑ | ☑ | ☑ | ☑ | ☑ | ☑ | ☑ | ☑ | ☑ | ☑ | ☑ | ☑ | ☑ | ☑ | ☑ | ☑ | ☑ | ☑ | ☑ |
| 1-Butylpyrrolidin-2-one | ☑ | ☑ | ☑ | ☑ | ☑ | ☑ | ☑ | ☑ | ☑ | ☑ | ☑ | ☑ | ☑ | ☑ | ☑ | ☑ | ☑ | ☑ | ☑ | ☑ |
| Gamma-valerolactone | ☑ | ☒ | ☑ | ☑ | ☑ | ☒ | ☑ | ☑ | ☑ | ☒ | ☑ | ☑ | ☑ | ☒ | ☑ | ☑ | ☑ | ☒ | ☑ | ☑ |
| NMP (benchmark) | ☑ | ☑ | ☑ | ☑ | ☑ | ☑ | ☑ | ☑ | ☑ | ☑ | ☑ | ☑ | ☑ | ☑ | ☑ | ☑ | ☑ | ☑ | ☑ | ☑ |
| Cyrene (benchmark) | ☒ | ☒ | ☒ | ☒ | ☒ | ☒ | ☒ | ☒ | ☒ | ☒ | ☒ | ☒ | ☒ | ☒ | ☒ | ☒ | ☒ | ☒ | ☒ | ☒ |
| Sulfolane (benchmark) | ☒ | ☒ | ☒ | ☒ | ☒ | ☒ | ☒ | ☒ | ☒ | ☒ | ☒ | ☒ | ☒ | ☒ | ☒ | ☒ | ☒ | ☒ | ☒ | ☒ |
| Guaiacol | ☒ | ☒ | ☑ | ☑ | ☒ | ☒ | ☑ | ☑ | ☒ | ☒ | ☑ | ☑ | ☒ | ☒ | ☑ | ☑ | ☒ | ☒ | ☑ | ☑ |
| ChCl–Malic acid (1:1) | ☒ | ☒ | ☒ | ☒ | ☒ | ☒ | ☒ | ☒ | ☒ | ☒ | ☒ | ☒ | ☒ | ☒ | ☒ | ☒ | ☒ | ☒ | ☒ | ☒ |
| ChCl–Oxalic acid (1:1) | ☒ | ☒ | ☒ | ☒ | ☒ | ☒ | ☒ | ☒ | ☒ | ☒ | ☒ | ☒ | ☒ | ☒ | ☒ | ☒ | ☒ | ☒ | ☒ | ☒ |
| Betaine–Malic acid (1:1) | ☒ | ☒ | ☒ | ☒ | ☒ | ☒ | ☒ | ☒ | ☒ | ☒ | ☒ | ☒ | ☒ | ☒ | ☒ | ☒ | ☒ | ☒ | ☒ | ☒ |
| Proline–Oxalic acid (1:1) | ☒ | ☒ | ☒ | ☒ | ☒ | ☒ | ☒ | ☒ | ☒ | ☒ | ☒ | ☒ | ☒ | ☒ | ☒ | ☒ | ☒ | ☒ | ☒ | ☒ |
| ChCl–Glutaric acid (1:1) | ☒ | ☒ | ☒ | ☒ | ☒ | ☒ | ☒ | ☒ | ☒ | ☒ | ☒ | ☒ | ☒ | ☒ | ☒ | ☒ | ☒ | ☒ | ☒ | ☒ |

☒: Immiscible
☑: Miscible

**Table 5.** The miscibility of entrainers in the n-hexane–ethanol mixture.

| Entrainer | E/F = 1 | | | | E/F = 2 | | | | E/F = 3 | | | | E/F = 4 | | | | E/F = 5 | | | |
|---|---|---|---|---|---|---|---|---|---|---|---|---|---|---|---|---|---|---|---|---|
| $T$ (K) | 293.15 | | 343.15 | | 293.15 | | 343.15 | | 293.15 | | 343.15 | | 293.15 | | 343.15 | | 293.15 | | 343.15 | |
| $x_1$ | 0.66 | 1 | 0.66 | 1 | 0.66 | 1 | 0.66 | 1 | 0.66 | 1 | 0.66 | 1 | 0.66 | 1 | 0.66 | 1 | 0.66 | 1 | 0.66 | 1 |
| Glycerol carbonate | ☒ | ☒ | ☒ | ☒ | ☒ | ☒ | ☒ | ☒ | ☒ | ☒ | ☒ | ☒ | ☒ | ☒ | ☒ | ☒ | ☒ | ☒ | ☒ | ☒ |
| Propylene carbonate | ☒ | ☒ | ☒ | ☒ | ☒ | ☒ | ☒ | ☒ | ☒ | ☒ | ☒ | ☒ | ☒ | ☒ | ☒ | ☒ | ☒ | ☒ | ☒ | ☒ |
| Ethylene carbonate | ☒ | ☒ | ☒ | ☒ | ☒ | ☒ | ☒ | ☒ | ☒ | ☒ | ☒ | ☒ | ☒ | ☒ | ☒ | ☒ | ☒ | ☒ | ☒ | ☒ |
| Diphenyl carbonate | ☒ | ☒ | ☒ | ☒ | ☒ | ☒ | ☒ | ☒ | ☒ | ☒ | ☒ | ☒ | ☒ | ☒ | ☒ | ☒ | ☒ | ☒ | ☒ | ☒ |
| N-Formylmorpholine | ☒ | ☒ | ☒ | ☒ | ☒ | ☒ | ☒ | ☒ | ☒ | ☒ | ☒ | ☒ | ☒ | ☒ | ☒ | ☒ | ☒ | ☒ | ☒ | ☒ |
| Dimethyl isosorbide | ☑ | ☒ | ☑ | ☑ | ☑ | ☑ | ☑ | ☑ | ☑ | ☑ | ☑ | ☑ | ☑ | ☑ | ☑ | ☑ | ☑ | ☑ | ☑ | ☑ |
| 1-Butylpyrrolidin-2-one | ☑ | ☑ | ☑ | ☑ | ☑ | ☑ | ☑ | ☑ | ☑ | ☑ | ☑ | ☑ | ☑ | ☑ | ☑ | ☑ | ☑ | ☑ | ☑ | ☑ |
| Gamma-valerolactone | ☒ | ☒ | ☑ | ☒ | ☑ | ☒ | ☑ | ☒ | ☑ | ☒ | ☑ | ☒ | ☑ | ☒ | ☑ | ☑ | ☑ | ☑ | ☑ | ☑ |
| NMP (benchmark) | ☒ | ☒ | ☑ | ☑ | ☑ | ☑ | ☑ | ☑ | ☑ | ☑ | ☑ | ☑ | ☑ | ☑ | ☑ | ☑ | ☑ | ☑ | ☑ | ☑ |
| Cyrene (benchmark) | ☒ | ☒ | ☒ | ☒ | ☒ | ☒ | ☒ | ☒ | ☒ | ☒ | ☒ | ☒ | ☒ | ☒ | ☒ | ☒ | ☒ | ☒ | ☒ | ☒ |
| Sulfolane (benchmark) | ☒ | ☒ | ☒ | ☒ | ☒ | ☒ | ☒ | ☒ | ☒ | ☒ | ☒ | ☒ | ☒ | ☒ | ☒ | ☒ | ☒ | ☒ | ☒ | ☒ |
| Butyl butanoate (benchmark) | ☑ | ☑ | ☑ | ☑ | ☑ | ☑ | ☑ | ☑ | ☑ | ☑ | ☑ | ☑ | ☑ | ☑ | ☑ | ☑ | ☑ | ☑ | ☑ | ☑ |

| Entrainer | | E/F = 1 | | | | E/F = 2 | | | | E/F = 3 | | | | E/F = 4 | | | | E/F = 5 | | | |
|---|---|---|---|---|---|---|---|---|---|---|---|---|---|---|---|---|---|---|---|---|---|
| | $T$ (K) | 293.15 | | 343.15 | | 293.15 | | 343.15 | | 293.15 | | 343.15 | | 293.15 | | 343.15 | | 293.15 | | 343.15 | |
| | $x_1$ | 0.66 | 1 | 0.66 | 1 | 0.66 | 1 | 0.66 | 1 | 0.66 | 1 | 0.66 | 1 | 0.66 | 1 | 0.66 | 1 | 0.66 | 1 | 0.66 | 1 |
| Guaiacol | | ☒ | ☒ | ☑ | ☑ | ☒ | ☒ | ☑ | ☑ | ☒ | ☒ | ☑ | ☑ | ☒ | ☒ | ☑ | ☑ | ☒ | ☒ | ☑ | ☑ |
| ChCl–Malic acid (1:1) | | ☒ | ☒ | ☒ | ☒ | ☒ | ☒ | ☒ | ☒ | ☒ | ☒ | ☒ | ☒ | ☒ | ☒ | ☒ | ☒ | ☒ | ☒ | ☒ | ☒ |
| ChCl–Oxalic acid (1:1) | | ☒ | ☒ | ☒ | ☒ | ☒ | ☒ | ☒ | ☒ | ☒ | ☒ | ☒ | ☒ | ☒ | ☒ | ☒ | ☒ | ☒ | ☒ | ☒ | ☒ |
| Betaine–Malic acid (1:1) | | ☒ | ☒ | ☒ | ☒ | ☒ | ☒ | ☒ | ☒ | ☒ | ☒ | ☒ | ☒ | ☒ | ☒ | ☒ | ☒ | ☒ | ☒ | ☒ | ☒ |
| Proline–Oxalic acid (1:1) | | ☒ | ☒ | ☒ | ☒ | ☒ | ☒ | ☒ | ☒ | ☒ | ☒ | ☒ | ☒ | ☒ | ☒ | ☒ | ☒ | ☒ | ☒ | ☒ | ☒ |
| ChCl–Glutaric acid (1:1) | | ☒ | ☒ | ☒ | ☒ | ☒ | ☒ | ☒ | ☒ | ☒ | ☒ | ☒ | ☒ | ☒ | ☒ | ☒ | ☒ | ☒ | ☒ | ☒ | ☒ |

☒: Immiscible
☑: Miscible

### 2.5.7. Relative volatility analysis

***Reliable predictions using GCMs***

Despite some limited miscibility observed experimentally for certain biobased and greener organic entrainers, and for the selected NADEs, the predictive models remain valuable for assessing the theoretical separation performance of screened entrainers. The relative volatility of component $i$ to $j$ ($\alpha_{ij}$), was calculated under conditions mimicking finite-dilution real solutions, providing for a better approximation of industrial operating environments. This provides a more realistic measure of entrainers performance. Figures 11 and 12 compare the predicted and experimental relative volatility values. In Figure 11, the experimental data for Cyrene and Sulfolane as benchmark entrainers were obtained from the literature.[9] In contrast, Figure 12 presents the results for butyl butanoate as a benchmark, whose experimental values was determined in this work since only predicted data were previously available.[104] Both UNIFAC and modified UNIFAC (Dortmund) models produced similar relative volatility trends, consistent with those predicted by COSMO-RS. The close agreement among these models increases confidence in the reliability of the predicted trends. Importantly, all evaluated biobased and greener organic entrainers enhanced the relative volatility to levels comparable with NMP. This suggests their capability to promote effective separation in both methylcyclohexane-toluene and n-hexane-ethanol mixtures. Based on these promising predictions, selected entrainers were advanced for experimental validation.

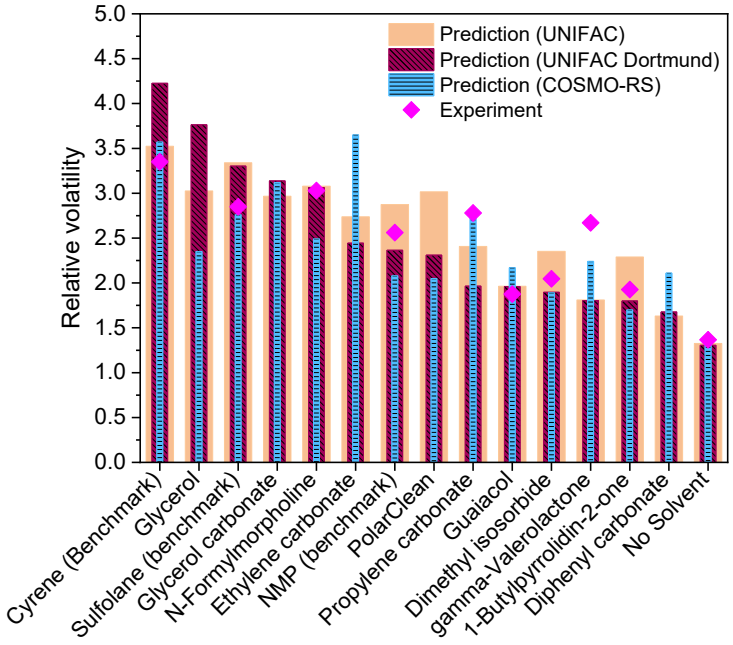


**Figure 11.** Relative volatility prediction and experiment results for methylcyclohexane (1) - toluene (2) ($x_1$ = 0.5, E/F = 1, P = 100.0 kPa). Cyrene and Sulfolane were referenced from existing literature.[9]

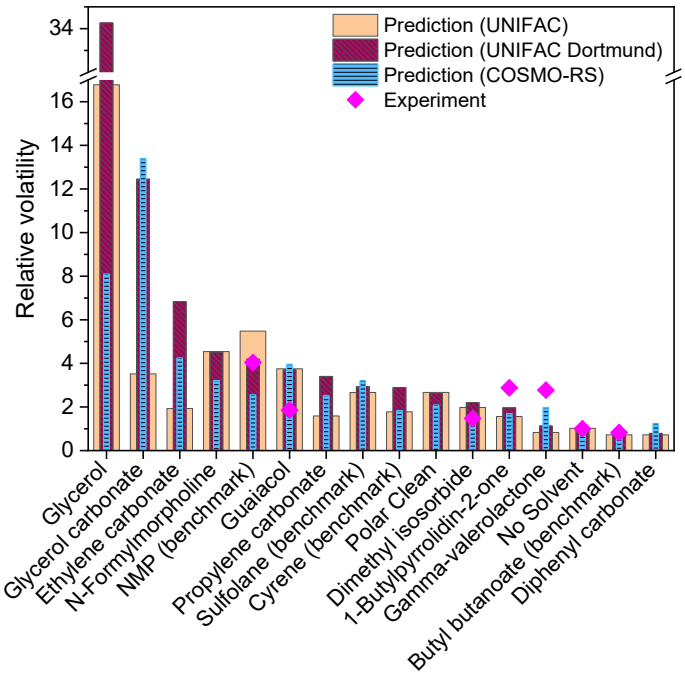


**Figure 12.** Relative volatility prediction and experiment results for n-hexane (1) - ethanol (2) ($x_1$ = 0.66; E/F = 1; P = 100.0 kPa). The experimental relative volatility data for butyl butanoate (benchmark) was obtained from this work.

Relative volatility experiments for NMP, GVL, NBP, and DMI in the methylcyclohexane–toluene mixture, as well as NMP, NBP, DMI, and guaiacol in the n-hexane–ethanol mixture, were conducted in duplicate to ensure reproducibility. These greener entrainers, along with NMP as the benchmark, were chosen because they formed homogeneous mixtures across the entire composition range of methylcyclohexane and n-hexane, respectively. Moreover, these entrainers provided promising relative volatility for separating close-boiling and azeotropic mixtures. Therefore, for further analysis, the complete VLE data for both mixtures with the presence of each entrainer were measured. The VLE data and their detailed discussion are provided in Chapters 3-4. The expanded standard uncertainties ($U$, $k$ = 2) For the relative volatility and VLE measurements were $U(x_1) = U(y_1) = 0.006$, $U(T) = 0.4$ K, and $U(P) = 0.23$ kPa. Although, Cyrene and Sulfolane were immiscible in this study, literature data for the methylcyclohexane–toluene mixture in their presence were included for comparison. However, these VLE data did not show a consistent profile, particularly in the methylcyclohexane-rich region, and were not subjected to thermodynamic consistency testing.[9]

The standard deviations of relative volatility measurements for NMP, GVL, NBP, and DMI in the methylcyclohexane–toluene mixture were 0.03, 0.01, 0.14, and 0.03, respectively. For the n-hexane–ethanol mixture, the corresponding standard deviations for NMP, NBP, DMI, and guaiacol were 0.15, 0.01, 0.01, and 0.02, respectively. These low deviations demonstrate the accuracy and repeatability of the relative volatility measurements obtained in this work. Model predictions were compared quantitatively using the average relative deviation (ARD) between predicted and experimental relative volatility values, as summarized in Table 6. COSMO-RS, UNIFAC, and modified UNIFAC (Dortmund) exhibit comparable ARD for both mixtures. For the methylcyclohexane-toluene mixture, the ARD values were 10.1 ± 2.0% for COSMO-RS, 12.3% ± 2.1 for modified UNIFAC (Dortmund), and 13.6 ± 3.1 % for UNIFAC. For the n-hexane-ethanol mixture, the ARD values were 32.4 ± 12.5 %, 43.3 ± 10.8 %, and 35.6 ± 11.6% for COSMO-RS, modified UNIFAC (Dortmund), and UNIFAC, respectively. The smaller ARD values for the methylcyclohexane–toluene mixture compared to those of the n-hexane–ethanol mixture arises from nonpolar–nonpolar components with similar structures. As discussed in Sigma (σ)-profile analysis Section, toluene's slightly higher polarizability allows the entrainer to interact more with toluene than methylcyclohexane, leading to mixture nonideality. Conversely, the n-hexane–ethanol mixture poses greater predictive challenges due to its polar–nonpolar components. Ethanol exhibits stronger interaction with the entrainer through strong hydrogen bonding, leading to high nonideality and thus higher ARD.

These results demonstrate that mixture nonideality significantly influences model performance, with larger deviations corresponding to stronger specific interactions. Overall, validation against experimental data for miscible entrainers showed good agreement, confirming that COSMO-RS and both UNIFAC models are reliable predictive tools for early-stage entrainer selection.

**Table 6.** The average relative deviations (ARD) for the relative volatility of the predictive models.

| Mixtures | ARD (%) ± SE[a,b] | | |
|---|---|---|---|
| | UNIFAC | modified UNIFAC (Dortmund) | COSMO-RS |
| Methylcyclohexane-toluene | 13.6 ± 3.1 | 12.3 ± 2.1 | 10.1 ± 2.0 |
| n-Hexane-ethanol | 35.6 ± 11.6 | 43.3 ± 10.8 | 32.4 ± 12.5 |

[a]ARD = $\frac{\sum_{i=1}^{N}\left|\frac{(\alpha_{ij})_{\text{model}}-(\alpha_{ij})_{\text{experimental}}}{(\alpha_{ij})_{\text{experimental}}}\right|}{N}$, where $(\alpha_{ij})$ is relative volatility component $i$ to $j$, and $N$ is the number of data point

[b]Standard Error (SE) = $\frac{\sqrt{\frac{\sum_{i=1}^{N}(D_i-\overline{D})^2}{N-1}}}{\sqrt{N}}$, where $D_i$ is the deviation of each entrainer, and $\overline{D}$ is the ARD.

### 2.5.8. Limited applicability of GCMs

Although GCMs are promising for predicting the relative volatility of the biobased and greener organic entrainer, their applicability remains limited for novel solvent classes such as NADESs. Both UNIFAC and modified UNIFAC (Dortmund) models depend on predefined group-contribution parameters, which are currently unavailable for many functional groups present in NADESs. Consequently, the separation performance of NADESs could not be predicted within this framework. This limitation underscores a fundamental challenge in applying group-contribution approaches to structurally complex and nonconventional solvents, where new parameterization or model extensions are required for accurate prediction.

### 2.5.9. NADESs experiences

**Synthesis of NADESs**

In this work, we initially attempted to prepare the NADESs using the vacuum evaporation method. Solid choline chloride (ChCl) and malic acid were mixed in a 1:1 molar ratio and dissolved in Milli-Q water. This ratio was chosen because it has been most commonly reported to yield stable DESs.[100,101] In addition, the molar ratios of 3:1 and 1:2 were selected for ChCl:Sorbitol as recommended in the literature.[105,106] The resulting solutions were subjected to a rotary evaporator (Buchi Rotavapor R-200, Switzerland) operated at 100 rpm, temperature of 313.15 K, and pressure of 10.0 kPa for 3-4 h. This process facilitated thorough mixing

and simultaneously removed water, yielding clear liquid NADESs at temperature of 298.15 K. This method has been reported previously in the literature.[107–109] However, it proved inefficient for preparing multiple NADESs simultaneously.

To overcome this limitation, an ultrasonic-assisted heating method adapted from Nguyen et al. (2020),[110] was adopted. This method involves preheating the components in an ultrasonic bath followed by mixing at the same temperature, enabling parallel synthesis with reduced time and energy consumption. The solid components were placed in sealed glass vials. To minimize moisture uptake, the vials flushed with nitrogen as an inert gas and immediately sealed. The mixture was first treated in an ultrasonic water bath (HBM Ultrasoon Reinigers, The Netherlands) at a temperature of 343.15 K for 3-3.5 h. Subsequently, the vials were transferred to a hot plate with a magnetic stirrer and maintained at the same temperature under continuous stirring until a clear, homogeneous liquid formed (approximately 1.5 h). The resulting NADESs were visually characterized to confirm homogeneity. The water content was determined by Karl Fischer (KF) titration using a Metrohm-787 KF Titrino 703 TiStand, Switzerland. All measurements were performed in triplicate, and the average values are reported.

## Results

### *Characterization of NADESs*

The selection of NADESs for synthesis was guided by the predicted selectivity values obtained from CORMO-RS, as shown in Figures 3 and 4. Candidates were chosen to represent high, medium, and low selectivity values. This ensures a comprehensive coverage of the selectivity spectrum. A balanced combination of HBD and HBA was also considered to provide adequate representation.

As summarized in Table 7 and depicted in Figure 13, several NADESs were successfully synthesized and remained clear, stable liquids at a temperature of 298.15 K for over three months. The formation of a clear, stable liquid is a reliable indicator of successful NADESs synthesis.[110–112] Their long-term liquid stability indicates the establishment of a strong hydrogen-bond network between components rather than a simple physical mixture, which would typically recrystallize over time. Thus, the sustained liquid stability confirms the successful formation of NADESs. Although visual observation and water-content measurement provide initial confirmation, detailed spectroscopic characterization, such as FTIR or NMR, is recommended in future work to verify hydrogen-bonding interactions. Due to time constraints, such analyses could not be performed in this study.

The NADESs that remained stable, homogeneous liquids at a room temperature included ChCl:Malic acid (1:1), ChCl:Oxalic acid (1:1), Betaine:Malic acid (1:1), Proline:Oxalic acid (1:1), and ChCl:Glutaric acid (1:1). Notably, ChCl:Malic acid (1:1) and Betaine:Malic acid (1:1) results were consistent with previous reports

employing the vacuum evaporating method.[105] These stable NADESs were subsequently examined for miscibility in close-boiling and azeotropic mixtures.

Some NADESs exhibited a yellowish coloration, particularly Proline:Malic acid (1:1) and Proline:Sorbitol (1:1). This discoloration is typically attributed to prolonged thermal exposure during heating-based synthesis.[112] Similar observations have been reported for amino acid and organic acid combinations, and for ChCl:Sulfonic acid.[113,114] The yellowish color may results from thermal degradation, side reactions, or the presence of impurities.[115] Therefore, these NADESs were excluded from further analyses of miscibility and water content to ensure that only stable, well-defined NADESs were evaluated. Other combinations, including ChCl:Sorbitol (1:2) and β-Alanine:Glutaric acid (1:1), remained solid at 298.15 K and became liquid only at 373.15 K. Similarly, Proline:Glutaric acid (1:1) remained solid even at 373.15 K, while Proline:Sorbitol (1:1) formed a yellowish, turbid solid at 298.15 K and a turbid liquid at 373.15 K. These NADESs were therefore excluded from further analysis of miscibility and water content, as described in Miscibility analysis Section. Other investigated NADESs were found to remain in a solid state. The inability to obtain clear-liquid NADESs under all tested conditions suggests that the eutectic point was not achieved. This is due to nonoptimal molar ratios or insufficient synthesis temperature. Increasing the synthesis temperature could, in principle, address this limitation. However, this approach poses a trade-off. Prolonged exposure to elevated temperatures can trigger decomposition, despite the pure components having higher decomposition temperatures.[116] Therefore, careful optimization of synthesis parameters, such as molar ratios, temperature, and preparation method, is essential to achieve stable and clear liquid NADESs.

The formation of turbid or gel-like NADESs can be attributed to the coexistence of multiple solid phases. These are affected by crystallization kinetics and polymorphic transitions, leading to metastable solids. NADESs exhibiting phase instability, turbidity or partial solidification are unsuitable for extractive distillation processes. Stable liquid behavior is crucial for consistent solvent-solute interactions and reliable vapor liquid equilibrium data. Solid and gel-like phases lead to ineffective interactions, poor mass transfer efficiency, and unreliable thermodynamic data. Furthermore, they can hinder column hydrodynamics, which may lead to fouling and reduced separation efficiency. Therefore, only NADESs that remain homogeneous, and stable liquids are considered viable entrainers for extractive distillation. Future studies should explore alternative synthesis strategies to optimize molar ratios and minimize thermal degradation while ensuring the eutectic point is reached. These refinements will broaden the range of NADESs available for evaluation as greener entrainers.

**Table 7.** Visual characterization of the resulting NADESs.

| NADESs | Visual characteristics | |
|---|---|---|
| | ***T* = 298.15 K** | ***T* = 373.15 K** |
| ChCl:Malic acid (1:1) | transparent, clear liquid, less viscous | transparent, clear liquid, less viscous |
| ChCl:Oxalic acid (1:1) | transparent, clear liquid, less viscous | transparent, clear liquid, less viscous |
| Betaine:Malic acid (1:1) | transparent, clear liquid, less viscous | transparent, clear liquid, less viscous |
| Proline:Oxalic acid (1:1) | transparent, clear liquid, viscous | transparent, clear liquid, less viscous |
| ChCl:Glutaric acid (1:1) | transparent, clear liquid, less viscous | transparent, clear liquid, less viscous |
| Proline:Malic acid (1:1) | yellowish, transparent, clear solid/gel | yellowish, transparent, clear liquid, viscous, some crystallite |
| β-Alanine:Glutaric acid (1:1) | turbid solid/gel | transparent, clear liquid, viscous |
| ChCl:Sorbitol (1:2) | transparent, clear solid/gel | transparent, clear liquid |
| Proline:Glutaric acid (1:1) | turbid solid/gel | transparent, clear liquid, viscous, some crystallite |
| Proline:Sorbitol (1:1) | yellowish-transparent, turbid solid/gel | yellowish-transparent, turbid liquid, viscous |
| Proline:Maltitol (1:1) | clear solid/gel | clear solid/gel, viscous |
| ChCl:Maltitol (1:1) | turbid solid/gel | turbid liquid, viscous |
| β-Alanine:Sorbitol (1:1) | white solid | white solid |
| ChCl:Sorbitol (3:1) | white solid | white solid |
| β-Alanine:Oxalic acid (1:1) | white solid | white solid |
| Betaine:Glutaric acid (1:1) | white solid | white solid |
| Betaine:Oxalic acid (1:1) | white solid | white solid |
| Betaine:Sorbitol (1:1) | white solid | white solid |
| β-Alanine:Maltitol (1:1) | white solid | white solid |
| β-Alanine:Ribitol (1:1) | white solid | white solid |
| Proline:Ribitol (1:1) | yellow solid | yellow solid |

(*T* = 298.15 K) ChCl:Malic acid (1:1)

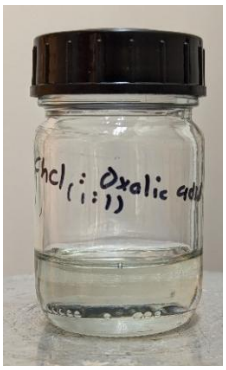

(*T* = 298.15 K) ChCl:Oxalic acid (1:1)

(*T* = 298.15 K) Betaine:Malic acid (1:1)

(*T* = 298.15 K) Proline:Oxalic acid (1:1)

(*T* = 298.15 K ChCl:Glutaric acid (1:1)

(*T* = 298.15 K) Proline:Malic acid (1:1)

(*T* = 298.15 K)

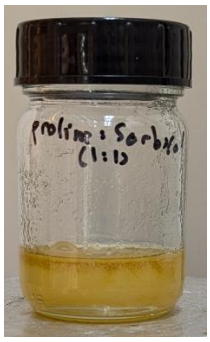

(*T* = 373.15 K) Proline:Sorbitol (1:1)

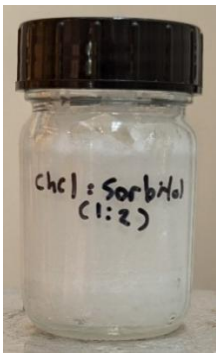

(*T* =298.15 K)

(*T* = 373.15 K) ChCl:Sorbitol (1:2)

(*T* = 298.15 K)

(*T* = 373.15 K) β-Alanine:Glutaric acid (1:1)

(*T* = 298.15 K)

(*T* = 373.15 K) Proline:Glutaric acid (1:1)

**Figure 13.** Pictures of various NADESs.

***Water content***

The water content of the selected NADESs was analyzed to determine its potential influence on miscibility behavior. As shown in Table 8, the synthesized NADESs exhibited relatively low water contents, ranging from 0.13 to 0.19 wt%. These values align well with those reported in the literature, which described that NADESs, particularly those composed of hygroscopic components, such as ChCl and amino acids, typically contain between 0.04 and 5.4 wt% water.[113,117] Such agreement confirms that the small amounts of water present in the prepared NADESs is typical and acceptable for their intended application. Importantly, these findings indicate that the observed immiscibility of the NADESs with the investigated mixtures cannot be attributed to excess water but rather reflects the inherent polarity property of the NADESs themselves. Furthermore, previous studies have shown that water content below 1 wt% do not disrupt the eutectic behavior or hydrogen-bonding network of NADESs.[115] Thus, the hydrogen-bonded structure of the synthesized NADESs can be assumed to remain intact. Consequently, their phase behavior in the tested mixtures arises primarily from polarity mismatch between the NADESs and the hydrocarbon-rich mixture, rather than from the presence of water impurities.

**Table 8.** Water content of the resulting NADESs.

| NADESs | Water content (wt%) |
|---|---|
| ChCl:Malic acid (1:1) | 0.13 |
| ChCl:Oxalic acid (1:1) | 0.19 |
| Betaine:Malic acid (1:1) | 0.14 |
| Proline:Oxalic acid (1:1) | 0.15 |
| ChCl:Glutaric acid (1:1) | 0.13 |

**Potential use of NADESs in polar organic solvent.**

Despite the fact that the synthesized NADESs were unsuitable for application in the investigated hydrocarbon-rich mixtures, further study was conducted on a representative polar-polar system, the ethanol-water mixture, to further demonstrate the predictive capability of the developed framework beyond hydrocarbon systems. This mixture was evaluated using the same workflow; however, the analysis was limited to selectivity at infinite dilution predicted by COSMO-RS and the miscibility assessment of the selected NADESs. As the main focus of this work is on hydrocarbon separations, experimental validation, such as relative volatility and VLE measurements, was not performed and is recommended for future research. Nevertheless, this preliminary screening effectively identifies suitable NADESs and confirms the broader applicability of the framework to polar separation systems.

Figure 14 shows that several NADESs exhibit promising selectivity to eliminate the azeotropic point in the ethanol-water mixture. As described in Selectivity analysis Section, the minimum selectivity threshold for azeotropic mixtures was set to 2.1. Among tested NADESs, ChCl: Oxalic acid (1:1), ChCl:Malic acid (1:1), and ChCl:Glutaric acid (1:1) achieved selectivity values equal to or higher than this threshold. This confirms their potential as effective entrainers. In contrast, Proline:Oxalic acid (1:1) and Betaine:Malic acid (1:1) demonstrated selectivity values below 2.1 and were therefore excluded from subsequent miscibility analysis. The activity coefficient at infinite dilution for the water-NADESs were lower than those for ethanol-NADESs. This indicates that the NADESs have stronger interaction with water than with ethanol. As illustrated in Figure 5, water possesses a more polar σ-profile than ethanol, resulting in stronger interactions with NADESs.

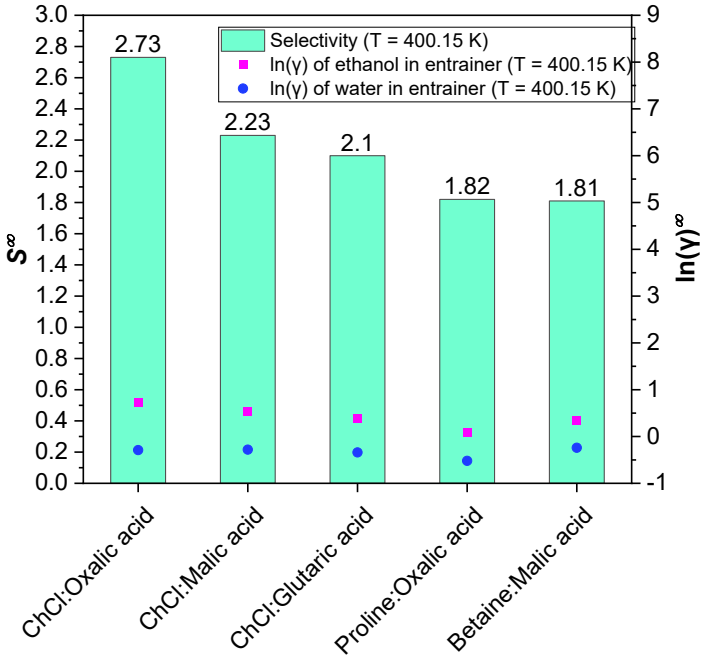


**Figure 14.** Selectivity prediction of selected NADESs at temperature of 400.15 K for the ethanol-water mixture, along with ln(γ) at infinite dilution for both ethanol and water in the NADESs.

Table 9 presents the miscibility results of the selected NADESs in ethanol at an E/F = 1. At 293.15 K, ChCl:Oxalic acid (1:1) and ChCl:Glutaric acid (1:1) formed heterogeneous mixtures with ethanol. However, when the temperature was increased to 343.15 K, all tested NADESs become fully miscible, indicating their strong potential for application as entrainers in polar-polar separations. The observed immiscibility at lower temperatures can be attributed to the strong self-interactions through extensive hydrogen bonding, which limits their interaction

with other molecules. At elevated temperatures, increased thermal motion enhances molecular disorder, weakens cohesive self-interactions within the NADESs, and facilitates intermolecular interactions with ethanol. This explains the observed temperature-dependent transition from heterogeneous to homogeneous mixtures. Together, the selectivity predictions and miscibility results demonstrate the strength of the developed framework to not only systematically excludes NADESs unsuitable for nonpolar separations but also effectively identifies promising candidates for polar-polar systems. This highlights the versatility of the approach across different mixture types.

**Table 9.** The miscibility of NADESs in ethanol.

| NADESs | E/F = 1 | | |
|---|---|---|---|
| | 293.15 K | 343.15 K | 373.15 K |
| ChCl:Malic acid (1:1) | ☑ | ☑ | ☑ |
| ChCl:Oxalic acid (1:1) | ☒ | ☑ | ☑ |
| ChCl:Glutaric acid (1:1) | ☒ | ☑ | ☑ |

☒: Immiscible
☑: Miscible

## 2.6. Conclusions

Potential biobased and greener organic entrainers, together with NADESs, were effectively identified based on their high-boiling characteristics, favorable solvency, and green chemistry attributes. Among the evaluated parameters, selectivity was established as a preferred preliminary screening parameter than capacity and performance index, as it directly reflects separation performance. Nevertheless, process simulations remain essential to determine which of those parameters should be prioritized when selecting entrainers.

COSMO-RS predictions revealed that all NADESs exhibited higher selectivity than the benchmark entrainer NMP in both close-boiling and azeotropic mixtures. Similarly, most biobased and greener organic entrainers demonstrated selectivity values comparable to or higher than those of NMP, confirming their potential as greener alternatives. Miscibility tests showed that several biobased and greener organic entrainers formed homogeneous mixtures across the relevant composition ranges, making them suitable for further evaluation. In contrast, some entrainers, along with all tested NADESs, were immiscible in methylcyclohexane- and n-hexane-rich regions. This immiscibility restricts their applicability in hydrocarbon separations and excludes them from relative-volatility measurements.

The relative volatility of the selected greener entrainers was assessed using predictive models (COSMO-RS, UNIFAC, and modified UNIFAC (Dortmund))

and validated experimentally. The results demonstrated favorable agreement between predicted and experimental data. This confirm the reliability of these models for early stage entrainer screening. These models demonstrated comparable predictive capability. Additionally, the prediction accuracy for the methylcyclohexane-toluene is better to that of the n-hexane-ethanol mixture. Collectively, predictive and experimental results indicated that several biobased and greener organic entrainers are promising replacements for conventional solvents, such as NMP, in the separation of close-boiling and azeotropic mixtures.

With respect to NADESs, several were successfully synthesized as clear, stable liquids at room temperature with low water content, confirming their stability and suitability. However, others remained solid under similar conditions, suggesting that their eutectic points were not achieved. This highlights the need for further optimization of synthesis conditions, including molar ratios, preparation temperatures, and alternative preparation methods. Although NADESs demonstrated high predicted selectivity, their strong polarity rendered them incompatible with nonpolar hydrocarbon mixtures. This characteristic limits their applications in such systems. However, predictive results showed that selected NADESs possess high selectivity toward the ethanol-water mixture. In addition, their complete miscibility with ethanol highlights their potential as entrainers for polar-polar mixture separations. These findings suggest that NADESs are promising candidates for separating polar azeotropes, such as ethanol-water. The intrinsic polarity of NADESs, combined with their dual HBD-HBA characteristics, merits further investigation for polar separation applications.

Overall, the validated framework developed in this study, integrating sustainability assessment, COSMO-RS predictions, UNIFAC-based modeling, miscibility evaluation, and experimental validation, proved to be a robust and systematic approach for selecting sustainable entrainers. Moreover, the framework demonstrated flexibility for application to both nonpolar and polar mixtures. Based on this framework, the effective entrainers identified for subsequent VLE measurement were GVL, NBP, DMI, and NMP for the methylcyclohexane-toluene mixture, and NBP, guaiacol, DMI, and NMP for the n-hexane-ethanol mixture. The corresponding VLE data and detailed discussions are presented in Chapters 3 and 4, while comprehensive process performance evaluations are provided in Chapter 5.

## References


(1) Gutiérrez, J. P.; Meindersma, G. W.; de Haan, A. B. COSMO-RS-Based Ionic-Liquid Selection for Extractive Distillation Processes. *Ind. Eng. Chem. Res.* **2012**, *51* (35), 11518–11529. https://doi.org/10.1021/ie301506n.

(2) Malik, H.; Khan, H. W.; Hassan Shah, M. U.; Ahmad, M. I.; Khan, I.; Al-Kahtani, A. A.; Sillanpää, M. Screening of Ionic Liquids as Green Entrainers for Ethanol Water Separation by Extractive Distillation: COSMO-RS Prediction and Aspen plus Simulation. *Chemosphere* **2022**, 136901. https://doi.org/https://doi.org/10.1016/j.chemosphere.2022.136901.

(3) Zhan, G.; Shen, B.; Sun, H.; Chen, X. Extractive Distillation Approach to the Removal of Dimethyl Disulfide from Methyl Tert-Butyl Ether: Combined Computational Solvent Screening and Experimental Process Investigation. *Ind. Eng. Chem. Res.* **2018**, *57* (9), 3348–3358. https://doi.org/10.1021/acs.iecr.7b01766.

(4) Jeon, Y.; Row, S. W.; Lee, G.; Park, S. S.; Seo, Y.-J.; Chu, Y. H.; Shul, Y.-G. Solvent Screening for the Separation of Ethylbenzene and P-Xylene by Extractive Distillation. *Korean J. Chem. Eng.* **2014**, *31* (10), 1824–1830. https://doi.org/10.1007/s11814-014-0115-2.

(5) Jiang, H.; Xu, D.; Zhang, L.; Ma, Y.; Gao, J.; Wang, Y. Vapor–Liquid Phase Equilibrium for Separation of Isopropanol from Its Aqueous Solution by Choline Chloride-Based Deep Eutectic Solvent Selected by COSMO-SAC Model. *J. Chem. Eng. Data* **2019**, *64* (4), 1338–1348. https://doi.org/10.1021/acs.jced.8b00895.

(6) Salleh, Z.; Wazeer, I.; Mulyono, S.; El-blidi, L.; Hashim, M. A.; Hadj-Kali, M. K. Efficient Removal of Benzene from Cyclohexane-Benzene Mixtures Using Deep Eutectic Solvents – COSMO-RS Screening and Experimental Validation. *J. Chem. Thermodyn.* **2017**, *104*, 33–44. https://doi.org/https://doi.org/10.1016/j.jct.2016.09.002.

(7) Cheng, H.; Liu, C.; Zhang, J.; Chen, L.; Zhang, B.; Qi, Z. Screening Deep Eutectic Solvents for Extractive Desulfurization of Fuel Based on COSMO-RS Model. *Chem. Eng. Process. - Process Intensif.* **2018**, *125*, 246–252. https://doi.org/https://doi.org/10.1016/j.cep.2018.02.006.

(8) Brouwer, T.; Schuur, B. Biobased Entrainer Screening for Extractive Distillation of Acetone and Diisopropyl Ether. *Sep. Purif. Technol.* **2021**, *270*, 118749. https://doi.org/https://doi.org/10.1016/j.seppur.2021.118749.

(9) Brouwer, T.; Schuur, B. Bio-Based Solvents as Entrainers for Extractive Distillation in Aromatic/Aliphatic and Olefin/Paraffin Separation. *Green Chem.* **2020**, *22* (16), 5369–5375. https://doi.org/10.1039/D0GC01769H.

(10) He, S.; Fan, W.; Huang, H.; Gao, J.; Xu, D.; Ma, Y.; Zhang, L.; Wang, Y. Separation of the Azeotropic Mixture Methanol and Toluene Using Extractive Distillation: Entrainer Determination, Vapor–Liquid Equilibrium Measurement, and Modeling. *ACS Omega* **2021**, *6* (50), 34736–34743. https://doi.org/10.1021/acsomega.1c05164.

(11) Lei, Z.; Li, C.; Chen, B. Extractive Distillation: A Review. *Sep. Purif. Rev.* **2003**, *32* (2), 121–213. https://doi.org/10.1081/SPM-120026627.

(12) Bastos, J. C.; Soares, M. E.; Medina, A. G. Selection of Solvents for Extractive Distillation. A Data Bank for Activity Coefficients at Infinite Dilution. *Ind. Eng. Chem. Process Des. Dev.* **1985**, *24* (2), 420–426.

https://doi.org/10.1021/i200029a035.
(13) Krummen, M.; Gruber, D.; Gmehling, J. Measurement of Activity Coefficients at Infinite Dilution in Solvent Mixtures Using the Dilutor Technique. *Ind. Eng. Chem. Res.* **2000**, *39* (6), 2114–2123. https://doi.org/10.1021/ie990830p.
(14) Jiménez, L.; Costa-López, J. Solvent Selection for a Reactive and Extractive Distillation Process by Headspace Gas Chromatography. *Sep. Sci. Technol.* **2003**, *38* (1), 21–37. https://doi.org/10.1081/SS-120016696.
(15) Kyle, B. G.; Leng, D. E. Solvent Selection for Extractive Distillation. *Ind. Eng. Chem.* **1965**, *57* (2), 43–48. https://doi.org/10.1021/ie50662a007.
(16) Momoh, S. O. Assessing the Accuracy of Selectivity as a Basis for Solvent Screening in Extractive Distillation Processes. *Sep. Sci. Technol.* **1991**, *26* (5), 729–742. https://doi.org/10.1080/01496399108049911.
(17) Kossack, S.; Kraemer, K.; Gani, R.; Marquardt, W. A Systematic Synthesis Framework for Extractive Distillation Processes. *Chem. Eng. Res. Des.* **2008**, *86* (7), 781–792. https://doi.org/https://doi.org/10.1016/j.cherd.2008.01.008.
(18) Zhou, Y.; Xu, D.; Zhang, L.; Ma, Y.; Ma, X.; Gao, J.; Wang, Y. Separation of Thioglycolic Acid from Its Aqueous Solution by Ionic Liquids: Ionic Liquids Selection by the COSMO-SAC Model and Liquid-Liquid Phase Equilibrium. *J. Chem. Thermodyn.* **2018**, *118*, 263–273. https://doi.org/https://doi.org/10.1016/j.jct.2017.12.007.
(19) Eckert, F.; Klamt, A.; Gmbh, C.; Kg, C.; Leverkusen, D.-. Fast Solvent Screening via Quantum Chemistry : COSMO-RS Approach. *AIChE J.* **2002**, *48* (2), 369–385.
(20) Dassault Systemes. COSMOtherm, Version C30, Release 17.05. COSMOlogic GmbH & Co. KG 2012. http://www.cosmologic.de.
(21) Dassault Systemes. Turbomole, Version 7.1.1. 2012. https://cosmologic.de/.
(22) Fredenslund, A.; Jones, R. L.; Prausnitz, J. M. Group-Contribution Estimation of Activity Coefficients in Nonideal Liquid Mixtures. *AIChE J.* **1975**, *21* (6), 1086–1099. https://doi.org/https://doi.org/10.1002/aic.690210607.
(23) Weidlich, U.; Gmehling, J. A Modified UNIFAC Model. 1. Prediction of VLE, HE, and .Gamma..Infin. *Ind. Eng. Chem. Res.* **1987**, *26* (7), 1372–1381. https://doi.org/10.1021/ie00067a018.
(24) *Aspen Plus Software, Version 12.0*; Aspen Technology, Inc., 2020.
(25) Dias, T. P. V. B.; Fonseca, L. A. A. P.; Ruiz, M. C.; Batista, F. R. M.; Batista, E. A. C.; Meirelles, A. J. A. Vapor–Liquid Equilibrium of Mixtures Containing the Following Higher Alcohols: 2-Propanol, 2-Methyl-1-Propanol, and 3-Methyl-1-Butanol. *J. Chem. Eng. Data* **2014**, *59* (3), 659–665. https://doi.org/10.1021/je400581e.
(26) Hartanto, D.; Schuur, B.; Schuttevaer, T.; Kiss, A. A.; de Haan, A. B. Isobaric Vapor–Liquid Equilibrium of Methylcyclohexane + Toluene with Gamma-Valerolactone as a Biobased Entrainer and 1-Methylpyrrolidin-2-One as a Conventional Entrainer. *J. Chem. Eng. Data* **2025**, *70* (3), 1339−1351. https://doi.org/10.1021/acs.jced.4c00509.
(27) Keestra, H.; Brouwer, T.; Schuur, B.; Lange, J.-P. Entrainer Selection for the Extractive Distillation of Acrylic Acid and Propionic Acid. *Chem. Eng. Res. Des.* **2023**, *192*, 653–663. https://doi.org/https://doi.org/10.1016/j.cherd.2023.02.049.
(28) Hartanto, D.; Gupta, B. S.; Taha, M.; Lee, M.-J. Isobaric Vapour–Liquid Equilibrium of (Tert-Butanol+water) System with Biological Buffer TRIS at 101.3kPa. *J. Chem. Thermodyn.* **2016**, *98*, 159–164.

https://doi.org/10.1016/j.jct.2016.03.013.
(29) Morales-Díaz, C.; Cartes, M.; Mejía, A. Measurements and Correlation of Isobaric Vapor–Liquid Equilibria and the Isothermal Surface Tension of the Methyl Butyrate + Dibutyl Ether Binary Mixture. *J. Chem. Eng. Data* **2024**, *69* (11), 3975–3981. https://doi.org/10.1021/acs.jced.4c00386.
(30) Hernandez, A.; Morales, M.; Cartes, M.; Mejía, A. Experimental Determination of Selected Thermophysical Properties of the 2-Methylfuran + Ethanol Binary Mixture. *J. Chem. Eng. Data* **2025**. https://doi.org/10.1021/acs.jced.5c00429.
(31) Taylor, Barry N; Kuyatt, C. E. NIST Technical Note 1297 Guidelines for Evaluating and Expressing the Uncertainty of NIST Measurement Results. *Technology* **1994**.
(32) *Evaluation of Measurement Data — Guide to the Expression of Uncertainty in Measurement*; Working Group 1 of the Joint Committee for Guides in Metrology (JCGM/WG 1); 2008. https://www.bipm.org/documents/20126/2071204/JCGM_100_2008_E.pdf.
(33) Gao, F.; Bai, R.; Ferlin, F.; Vaccaro, L.; Li, M.; Gu, Y. Replacement Strategies for Non-Green Dipolar Aprotic Solvents. *Green Chem.* **2020**, *22* (19), 6240–6257. https://doi.org/10.1039/D0GC02149K.
(34) European Chemical Agency. *Harmonised classification and labelling (CLH)*. https://echa.europa.eu/regulations/clp/harmonised-classification-and-labelling? (accessed 2025-09-25).
(35) Severini, A.; Ferrari, C.; Marchetti, A.; Vizza, F.; Bonechi, M.; Innocenti, M.; Lagostina, V.; Salvadori, E.; Chiesa, M.; Roncaglia, F.; Fontanesi, C. Electrochemical Oxidation of Guaiacol as a Sacrificial Anodic Process Producing Fine Chemical Derivative, for Hydrogen Production via Electrolysis. *Int. J. Hydrogen Energy* **2025**, *124*, 345–354. https://doi.org/https://doi.org/10.1016/j.ijhydene.2025.03.439.
(36) Yeow, A. T. H.; Hayyan, A.; Hayyan, M.; Usman Mohd Junaidi, M.; Saleh, J.; Jefrey Basirun, W.; Roslan Mohd Nor, M.; Al Abdulmonem, W.; Zulhaziman M. Salleh, M.; Mohamed Zuki, F.; Diana Hamid, M. A Comprehensive Review on the Physicochemical Properties of Deep Eutectic Solvents. *Results Chem.* **2024**, *7*, 101378. https://doi.org/https://doi.org/10.1016/j.rechem.2024.101378.
(37) Commission Regulation of European Union. *The European Parliament and of the Council Concerning the Registration, Evaluation, Authorisation and Restriction of Chemicals (REACH) as Regards 1-Methyl-2-Pyrrolidone*; 2018. https://eur-lex.europa.eu/eli/reg/2018/588/oj/eng?utm.com.
(38) European Chemical Agency. *4-hydroxymethyl-1,3-dioxolan-2-one*. https://chem.echa.europa.eu/100.012.032/overview?searchText=4-hydroxymethyl-1,3-dioxolan-2-one (accessed 2025-09-23).
(39) Morales Cepeda, A. B.; Macclesh del Pino, L. A.; Ramos Galvan, C. E.; González Pedraza, E. J.; Aguilera Vazquez, L. Synthesis of Glycerol Carbonate from Glycerin with CaCO3 in a Batch Reactor. *Des. Monomers Polym.* **2022**, *25* (1), 25–31. https://doi.org/10.1080/15685551.2022.2037215.
(40) European Chemical Agency. *Propylene carbonate*. https://chem.echa.europa.eu/100.003.248/overview?searchText=Propylene carbonate (accessed 2025-09-23).
(41) Aouissi, A.; Aldhayan, D.; Abduh, N. A. Y.; Kahtani, A. Al. Propylene Carbonate Synthesis from Propylene Oxide and CO2 over Ga-Silicate-1 Catalyst. **2020**, *9* (1),

440–450. https://doi.org/doi:10.1515/gps-2020-0048.
(42) European Chemical Agency. *Ethylene carbonate*. 2018. https://chem.echa.europa.eu/100.002.283/overview?searchText=Ethylene carbonate (accessed 2025-09-23).
(43) Ng, W. L.; Er, Z. X.; Chandrakumar, D.; Loy, A. C. M.; Vongsvivut, J.; Bhattacharya, S. Sustainable Route of Ethylene Carbonate Production via CO2 Carboxylation: Process Development, Process Integration, and Economic Analysis. *ACS Sustain. Chem. Eng.* **2024**, *12* (51), 18320–18334. https://doi.org/10.1021/acssuschemeng.4c06519.
(44) European Chemical Agency. *Diphenyl carbonate*. https://chem.echa.europa.eu/100.002.733/overview?searchText=Diphenyl carbonate (accessed 2025-09-24).
(45) Wang, S.; Jiang, N.; Peng, J.; Yang, P.; Cui, C.; Niu, H.; Zhang, Q.; Wang, J. Efficient Synthesis of Diphenyl Carbonate from CO2, Phenol, and Carbon Tetrachloride under Mild Conditions. *ACS Sustain. Chem. Eng.* **2022**, *10* (38), 12689–12697. https://doi.org/10.1021/acssuschemeng.2c03400.
(46) European Chemical Agency. *N-Formylmorpholine*. https://chem.echa.europa.eu/100.022.291/overview?searchText=N-Formylmorpholine (accessed 2025-09-24).
(47) Schmid, L.; Schneider, M. S.; Engel, D.; Baiker, A. Formylation with "Supercritical" CO2: Efficient Ruthenium-Catalyzed Synthesis of N-Formylmorpholine. *Catal. Letters* **2003**, *88* (3), 105–113. https://doi.org/10.1023/A:1024009722078.
(48) Ma, Y.; Qu, Y.; Ji, Y.; Li, Y.; Wang, X.; Cui, P.; Zhu, Z.; Wang, Y. Structure-Activity Relationship and Experimental Study of Organic Solvents and Deep Eutectic Solvents in Separation of Cyclohexane-Ethyl Acetate. *J. Mol. Liq.* **2023**, *373*, 121263. https://doi.org/https://doi.org/10.1016/j.molliq.2023.121263.
(49) Sharma, B.; Singh, N.; Kushwaha, J. P. Ammonium-Based Deep Eutectic Solvent as Entrainer for Separation of Acetonitrile–Water Mixture by Extractive Distillation. *J. Mol. Liq.* **2019**, *285*, 185–193. https://doi.org/https://doi.org/10.1016/j.molliq.2019.04.089.
(50) European Chemical Agency. *1,4:3,6-dianhydro-2,5-di-O-methyl-D-glucitol*. https://chem.echa.europa.eu/100.023.782/overview?searchText=1,4:3,6-dianhydro-2,5-di-O-methyl-D-gluc (accessed 2025-07-03).
(51) *Dimethyl isosorbide; U.S. Environmental Protection Agency*. https://comptox.epa.gov/dashboard/chemical/genotoxicity/DTXSID201019399 (accessed 2025-08-27).
(52) *Public Report, Arlasolve DMI*; The National Industrial Chemicals Notification and Assessment Scheme (NICNAS); 2004. https://www.industrialchemicals.gov.au/sites/default/files/STD1052 Public Report PDF.pdf.
(53) European Chemical Agency. *1-butylpyrrolidin-2-one*. https://chem.echa.europa.eu/100.020.399/overview?searchText=1-butylpyrrolidin-2-one (accessed 2025-09-23).
(54) *Public Report, 2-Pyrrolidinone, 1-Butyl-*; 2020. https://www.industrialchemicals.gov.au/sites/default/files/STD1698 public report %5B780 KB%5D.pdf.
(55) Jiang, X.; Yong, W. F.; Gao, J.; Shao, D.-D.; Sun, S.-P. Understanding the Role

of Substrates on Thin Film Composite Membranes: A Green Solvent Approach with TamiSolve® NxG. *J. Memb. Sci.* **2021**, *635*, 119530. https://doi.org/https://doi.org/10.1016/j.memsci.2021.119530.

(56) Sigma-Aldrich. *The Future is Greener Solvents*. https://www.sigmaaldrich.com/NL/en/campaigns/biorenewable-solvents?srsltid=AfmBOopKiYMS66bYBcB7PpBmYEKoCbYz6oCzDgdRuzXu4VKkCzwLjIk6 (accessed 2025-09-24).

(57) Strappaveccia, G.; Luciani, L.; Bartollini, E.; Marrocchi, A.; Pizzo, F.; Vaccaro, L. γ-Valerolactone as an Alternative Biomass-Derived Medium for the Sonogashira Reaction. *Green Chem.* **2015**, *17* (2), 1071–1076. https://doi.org/10.1039/C4GC01728E.

(58) Ye, L.; Han, Y.; Feng, J.; Lu, X. A Review about GVL Production from Lignocellulose: Focusing on the Full Components Utilization. *Ind. Crops Prod.* **2020**, *144*, 112031. https://doi.org/https://doi.org/10.1016/j.indcrop.2019.112031.

(59) Api, A. M.; Belmonte, F.; Belsito, D.; Biserta, S.; Botelho, D.; Bruze, M.; Burton, G. A.; Buschmann, J.; Cancellieri, M. A.; Dagli, M. L.; Date, M.; Dekant, W.; Deodhar, C.; Fryer, A. D.; Gadhia, S.; Jones, L.; Joshi, K.; Lapczynski, A.; Lavelle, M.; Liebler, D. C.; Na, M.; O'Brien, D.; Patel, A.; Penning, T. M.; Ritacco, G.; Rodriguez-Ropero, F.; Romine, J.; Sadekar, N.; Salvito, D.; Schultz, T. W.; Sipes, I. G.; Sullivan, G.; Thakkar, Y.; Tokura, Y.; Tsang, S. RIFM Fragrance Ingredient Safety Assessment, γ-Valerolactone, CAS Registry Number 108-29-2. *Food Chem. Toxicol.* **2019**, *134*, 110950. https://doi.org/https://doi.org/10.1016/j.fct.2019.110950.

(60) European Chemical Agency. *γ-valerolactone*. https://chem.echa.europa.eu/100.003.245/overview?searchText=γ-valerolactone (accessed 2025-09-23).

(61) Huerta-Rosas, B.; Coronel-Muñoz, M.; Quiroz-Ramírez, J. J.; Cáceres-Barrera, C. R.; Contreras-Zarazúa, G.; Segovia-Hernández, J. G.; Sánchez-Ramírez, E. Intensified Alternative for Sustainable Gamma-Valerolactone Production from Levulinic Acid. *Chem. Eng. Res. Des.* **2025**, *217*, 38–48. https://doi.org/https://doi.org/10.1016/j.cherd.2025.03.023.

(62) European Chemical Agency. *Guaiacol*. https://chem.echa.europa.eu/100.001.786/overview?searchText=guaiacol (accessed 2025-07-03).

(63) European Chemical Agency. *Methyl 5-(dimethylamino)-2-methyl-5-oxopentanoate*. https://chem.echa.europa.eu/100.148.956/overview?searchText=Methyl 5-(dimethylamino)-2-methyl-5-oxop (accessed 2025-09-24).

(64) *Opinion on N-Methyl-2-Pyrrolidone (NMP)*; Scientific Committee on Consumer Safety, European Union; 2011. https://ec.europa.eu/health/scientific_committees/consumer_safety/docs/sccs_o_050.pdf.

(65) Hansen, B. B.; Spittle, S.; Chen, B.; Poe, D.; Zhang, Y.; Klein, J. M.; Horton, A.; Adhikari, L.; Zelovich, T.; Doherty, B. W.; Gurkan, B.; Maginn, E. J.; Ragauskas, A.; Dadmun, M.; Zawodzinski, T. A.; Baker, G. A.; Tuckerman, M. E.; Savinell, R. F.; Sangoro, J. R. Deep Eutectic Solvents: A Review of Fundamentals and Applications. *Chem. Rev.* **2021**, *121* (3), 1232–1285. https://doi.org/10.1021/acs.chemrev.0c00385.

(66) European Chemical Agency. *Choline chloride*. https://chem.echa.europa.eu/100.000.596/overview?searchText=Choline chloride (accessed 2025-09-24).
(67) European Chemical Agency. *Proline*. https://chem.echa.europa.eu/100.005.185/overview?searchText=Proline (accessed 2025-09-24).
(68) European Chemical Agency. *Betaine*. https://chem.echa.europa.eu/100.003.174/overview?searchText=Betaine (accessed 2025-09-24).
(69) NIST Chemistry WebBook. *Betaine*. https://webbook.nist.gov/cgi/cbook.cgi?ID=C590476&Mask=80&utm.com (accessed 2025-09-24).
(70) European Chemical Agency. *β-alanine*. https://chem.echa.europa.eu/100.003.215/overview?searchText=β-alanine (accessed 2025-09-24).
(71) Schwarz, E. M.; Grundstein, V. V; Ievins, A. F. Thermal Investigation of Polyols. *J. Therm. Anal.* **1972**, *4* (3), 331–337. https://doi.org/10.1007/BF01911695.
(72) PubChem. *Sorbitol*. https://pubchem.ncbi.nlm.nih.gov/compound/Sorbitol (accessed 2025-09-24).
(73) (CONTAM), E. P. on C. in the F. C. Scientific Opinion on the Evaluation of the Substances Currently on the List in the Annex to Commission Directive 96/3/EC as Acceptable Previous Cargoes for Edible Fats and Oils – Part II of III. *EFSA J.* **2012**, *10* (5), 2703. https://doi.org/https://doi.org/10.2903/j.efsa.2012.2703.
(74) Umai, D.; Kayalvizhi, R.; Kumar, V.; Jacob, S. Xylitol: Bioproduction and Applications-A Review. *Front. Sustain.* **2022**, *Volume 3-*. https://doi.org/10.3389/frsus.2022.826190.
(75) European Chemical Agency. *Xylitol*. https://chem.echa.europa.eu/100.001.626/overview?searchText=Xylitol (accessed 2025-09-25).
(76) Gatidou, G.; Vazaiou, N.; Thomaidis, N. S.; Stasinakis, A. S. Biodegradability Assessment of Food Additives Using OECD 301F Respirometric Test. *Chemosphere* **2020**, *241*, 125071. https://doi.org/https://doi.org/10.1016/j.chemosphere.2019.125071.
(77) Suckling, J.; Brussino, G.; Koukouna, E.; Misailidis, N.; Koulouris, A.; Petrides, D.; Morse, S.; Raats, M.; Scholten, J.; Westbroek, C.; Halford, J. C. G.; Harrold, J. A.; Raben, A.; Murphy, R. Environmental Life Cycle Assessment of Producing Sorbitol and Maltitol from Wheat Starch Using Process Simulation: The SWEET Project. *J. Clean. Prod.* **2025**, *494*, 144985. https://doi.org/https://doi.org/10.1016/j.jclepro.2025.144985.
(78) European Chemical Agency. *Maltitol*. https://chem.echa.europa.eu/100.008.699/overview?searchText=Maltitol (accessed 2025-09-25).
(79) European Chemical Agency. *Erythritol*. https://chem.echa.europa.eu/100.005.217/overview?searchText=Erythritol (accessed 2025-09-25).
(80) (FAF), E. P. on F. A. and F.; Younes, M.; Aquilina, G.; Castle, L.; Degen, G.; Engel, K.-H.; Fowler, P. J.; Frutos Fernandez, M. J.; Fürst, P.; Gundert-Remy, U.; Gürtler, R.; Husøy, T.; Manco, M.; Mennes, W.; Moldeus, P.; Passamonti, S.;

Shah, R.; Waalkens-Berendsen, I.; Wright, M.; Batke, M.; Boon, P.; Bruzell, E.; Chipman, J.; Crebelli, R.; FitzGerald, R.; Fortes, C.; Halldorsson, T.; LeBlanc, J.-C.; Lindtner, O.; Mortensen, A.; Ntzani, E.; Wallace, H.; Barmaz, S.; Civitella, C.; D'Angelo, L.; Lodi, F.; Laganaro, M.; Rincon, A. M.; Smeraldi, C.; Tard, A. Re-Evaluation of Erythritol (E 968) as a Food Additive. *EFSA J.* **2023**, *21* (12), e8430. https://doi.org/https://doi.org/10.2903/j.efsa.2023.8430.

(81) Martínez-Monteagudo, S. I.; Enteshari, M.; Metzger, L. Lactitol: Production, Properties, and Applications. *Trends Food Sci. Technol.* **2019**, *83*, 181–191. https://doi.org/https://doi.org/10.1016/j.tifs.2018.11.020.

(82) Selvasekaran, P.; Chidambaram, R. Advances in Formulation for the Production of Low-Fat, Fat-Free, Low-Sugar, and Sugar-Free Chocolates: An Overview of the Past Decade. *Trends Food Sci. Technol.* **2021**, *113*, 315–334. https://doi.org/https://doi.org/10.1016/j.tifs.2021.05.008.

(83) NINOMIYA, H.; KONDO, J.; IDE, Y.; YAMASHITA, Y.; NISHIKAWA, K.; KISHIDA, K.; WATANABE, M.; SUMI, N. REPRODUCTIVE AND DEVELOPMENTAL TOXICITY STUDIES OF LACTITOL (NS-4) (1): Fertility Study in Rats by Oral Administration. *J. Toxicol. Sci.* **1994**, *19* (SupplementIII), 429–439. https://doi.org/10.2131/jts.19.SupplementIII_429.

(84) Liu, L.; Redden, H.; Alper, H. S. Frontiers of Yeast Metabolic Engineering: Diversifying beyond Ethanol and Saccharomyces. *Curr. Opin. Biotechnol.* **2013**, *24* (6), 1023–1030. https://doi.org/https://doi.org/10.1016/j.copbio.2013.03.005.

(85) National Center for Biotechnology Information. *PubChem Compound Summary for CID 6251, Mannitol*. https://pubchem.ncbi.nlm.nih.gov/compound/Mannitol (accessed 2022-09-28).

(86) Wisselink, H. W.; Weusthuis, R. A.; Eggink, G.; Hugenholtz, J.; Grobben, G. J. Mannitol Production by Lactic Acid Bacteria: A Review. *Int. Dairy J.* **2002**, *12* (2), 151–161. https://doi.org/https://doi.org/10.1016/S0958-6946(01)00153-4.

(87) *Ribitol*. https://www.thegoodscentscompany.com/data/rw1216341.html (accessed 2025-09-25).

(88) European Chemical Agency. *Malic acid*. https://chem.echa.europa.eu/100.027.293/overview?searchText=malic acid (accessed 2025-09-25).

(89) Wu, N.; Wang, W.; Zhu, J. Progress on Production of Malic Acid and Succinic Acid by Industrially-Important Engineered Microorganisms. *J. Biotechnol.* **2025**, *400*, 8–19. https://doi.org/https://doi.org/10.1016/j.jbiotec.2025.02.001.

(90) *Priority Existing Chemical Assesment Report No.12, Glycolic Acid*; 2000. https://www.industrialchemicals.gov.au/sites/default/files/PEC12-Glycolic-acid.pdf.

(91) *Glycolic acid*. https://echa.europa.eu/registration-dossier/-/registered-dossier/14561/7/9/1 (accessed 2025-09-25).

(92) European Chemical Agency. *Glutaric acid*. https://chem.echa.europa.eu/100.003.471/overview?searchText=Glutaric acid (accessed 2025-09-25).

(93) *Glutaric Acid, 99% (CAS RN: 110-94-1)*; 2024. https://www.sigmaaldrich.com/NL/en/sds/aldrich/g3407?userType=anonymous.

(94) European Chemical Agency. *Oxalic acid*. 2022. https://chem.echa.europa.eu/100.005.123/overview?searchText=oxalic acid (accessed 2025-09-25).

(95) Werpy, T.; Petersen, G. *Top Value Added Chemicals from Biomass Volume I—Results of Screening for Potential Candidates from Sugars and Synthesis Gas*; Golden, CO (United States), 2004. https://docs.nrel.gov/docs/fy04osti/35523.pdf.
(96) European Chemical Agency. *2,2'-(ethylenedioxy)diethanol*. https://chem.echa.europa.eu/100.003.594/overview?searchText=112-27-6 (accessed 2025-09-25).
(97) Rose, M.; Palkovits, R. Isosorbide as a Renewable Platform Chemical for Versatile Applications—Quo Vadis? *ChemSusChem* **2012**, *5* (1), 167–176. https://doi.org/https://doi.org/10.1002/cssc.201100580.
(98) *Isosorbide*. https://www.chemsrc.com/en/cas/652-67-5_1150157.html (accessed 2025-09-25).
(99) *Isosorbide, (CAS RN: 652-67-5)*; 2022. https://www.sigmaaldrich.com/NL/en/sds/usp/1352008?userType=anonymous.
(100) Liu, Y.; Friesen, J. B.; McAlpine, J. B.; Lankin, D. C.; Chen, S.-N.; Pauli, G. F. Natural Deep Eutectic Solvents: Properties, Applications, and Perspectives. *J. Nat. Prod.* **2018**, *81* (3), 679–690. https://doi.org/10.1021/acs.jnatprod.7b00945.
(101) Fajar, A. T. N.; Hanada, T.; Hartono, A. D.; Goto, M. Estimating the Phase Diagrams of Deep Eutectic Solvents within an Extensive Chemical Space. *Commun. Chem.* **2024**, *7* (1), 27. https://doi.org/10.1038/s42004-024-01116-3.
(102) Nkosi, N.; Tumba, K.; Ramsuroop, S. Activity Coefficients at Infinite Dilution of Various Solutes in Tetrapropylammonium Bromide + 1,6-Hexanediol Deep Eutectic Solvent. *J. Chem. Eng. Data* **2018**, *63* (12), 4502–4512. https://doi.org/10.1021/acs.jced.8b00600.
(103) Mullins, E.; Oldland, R.; Liu, Y. A.; Wang, S.; Sandler, S. I.; Chen, C.-C.; Zwolak, M.; Seavey, K. C. Sigma-Profile Database for Using COSMO-Based Thermodynamic Methods. *Ind. Eng. Chem. Res.* **2006**, *45* (12), 4389–4415. https://doi.org/10.1021/ie060370h.
(104) Zhang, Y.; Wang, Z.; Xu, X.; Gao, J.; Xu, D.; Zhang, L.; Wang, Y. Entrainers Selection and Vapour-Liquid Equilibrium Measurements for Separating Azeotropic Mixtures (Ethanol + n-Hexane/Cyclohexane) by Extractive Distillation. *J. Chem. Thermodyn.* **2020**, *144*, 106070. https://doi.org/https://doi.org/10.1016/j.jct.2020.106070.
(105) Dai, Y.; van Spronsen, J.; Witkamp, G.-J.; Verpoorte, R.; Choi, Y. H. Natural Deep Eutectic Solvents as New Potential Media for Green Technology. *Anal. Chim. Acta* **2013**, *766*, 61–68. https://doi.org/https://doi.org/10.1016/j.aca.2012.12.019.
(106) Chakravorty, P.; Das, A. B. Impact of Choline Choride and Sugar Natural Deep Eutectic Solvents on Structure and Functionality of Treebean (Parkia Timoriana) Seed Protein. *Sci. Rep.* **2025**, *15* (1), 3701. https://doi.org/10.1038/s41598-025-87890-z.
(107) Wikene, K. O.; Bruzell, E.; Tønnesen, H. H. Characterization and Antimicrobial Phototoxicity of Curcumin Dissolved in Natural Deep Eutectic Solvents. *Eur. J. Pharm. Sci.* **2015**, *80*, 26–32. https://doi.org/https://doi.org/10.1016/j.ejps.2015.09.013.
(108) Liu, Y.; Garzon, J.; Friesen, J. B.; Zhang, Y.; McAlpine, J. B.; Lankin, D. C.; Chen, S.-N.; Pauli, G. F. Countercurrent Assisted Quantitative Recovery of Metabolites from Plant-Associated Natural Deep Eutectic Solvents. *Fitoterapia* **2016**, *112*, 30–37. https://doi.org/https://doi.org/10.1016/j.fitote.2016.04.019.
(109) Li, D. Natural Deep Eutectic Solvents in Phytonutrient Extraction and Other

Applications. *Front. Plant Sci.* **2022**, *Volume 13*.
(110) Nguyen, H. V. D.; De Vries, R.; Stoyanov, S. D. Natural Deep Eutectics as a "Green" Cellulose Cosolvent. *ACS Sustain. Chem. Eng.* **2020**, *8* (37), 14166–14178. https://doi.org/10.1021/acssuschemeng.0c04982.
(111) Santana, A. P. R.; Andrade, D. F.; Mora-Vargas, J. A.; Amaral, C. D. B.; Oliveira, A.; Gonzalez, M. H. Natural Deep Eutectic Solvents for Sample Preparation Prior to Elemental Analysis by Plasma-Based Techniques. *Talanta* **2019**, *199*, 361–369. https://doi.org/https://doi.org/10.1016/j.talanta.2019.02.083.
(112) Farooq, M. Q.; Abbasi, N. M.; Anderson, J. L. Deep Eutectic Solvents in Separations: Methods of Preparation, Polarity, and Applications in Extractions and Capillary Electrochromatography. *J. Chromatogr. A* **2020**, *1633*, 461613. https://doi.org/https://doi.org/10.1016/j.chroma.2020.461613.
(113) Altamash, T.; Nasser, M. S.; Elhamarnah, Y.; Magzoub, M.; Ullah, R.; Qiblawey, H.; Aparicio, S.; Atilhan, M. Gas Solubility and Rheological Behavior Study of Betaine and Alanine Based Natural Deep Eutectic Solvents (NADES). *J. Mol. Liq.* **2018**, *256*, 286–295. https://doi.org/https://doi.org/10.1016/j.molliq.2018.02.049.
(114) Hasibuan, D. R.; Manurung, R.; Iriany; Siregar, A. G. A. Application of Choline Chloride-Based Deep Eutectic Solvent (DES) as Catalyst for Glycerolysis of Palm Fatty Acid Distillate (PFAD) and Glycerol. *Case Stud. Chem. Environ. Eng.* **2025**, *11*, 101205. https://doi.org/https://doi.org/10.1016/j.cscee.2025.101205.
(115) Richter, J.; Pietsch, T.; Elsner, N.; Ruck, M. Critical Investigation of Betaine Hydrochloride-Based Deep Eutectic Solvent for Ionometallurgical Metal Production. *ChemistryOpen* **2023**, *12* (8), e202300114. https://doi.org/https://doi.org/10.1002/open.202300114.
(116) Jangir, A. K.; Bhawna; Verma, G.; Pandey, S.; Kuperkar, K. Design and Thermophysical Characterization of Betaine Hydrochloride-Based Deep Eutectic Solvents as a New Platform for CO2 Capture. *New J. Chem.* **2022**, *46* (11), 5332–5345. https://doi.org/10.1039/D1NJ05373F.
(117) Gajardo-Parra, N. F.; Lubben, M. J.; Winnert, J. M.; Leiva, Á.; Brennecke, J. F.; Canales, R. I. Physicochemical Properties of Choline Chloride-Based Deep Eutectic Solvents and Excess Properties of Their Pseudo-Binary Mixtures with 1-Butanol. *J. Chem. Thermodyn.* **2019**, *133*, 272–284. https://doi.org/https://doi.org/10.1016/j.jct.2019.02.010.

# Chapter 3

## Vapor-liquid equilibrium data of the methylcyclohexane-toluene mixture with the presence of entrainers

Chapter 3 provides vapor-liquid equilibrium (VLE) data for the close-boiling methylcyclohexane-toluene mixture in the presence of the biobased and greener entrainer, as well as benchmark entrainer NMP. This chapter contains two main sections, as follows:

3.1 VLE data of methylcyclohexane-toluene with gamma-valerolactone and 1-methylpyrrolidin-2-one.

3.2 VLE data of methylcyclohexane-toluene with dimethyl isosorbide and 1-butylpyrrolidin-2-one.

*This chapter has been published in:*
*Journal of Chemical & Engineering Data, 70 (3),1339-1351, (2025)*
*Industrial & Engineering Chemistry Research 64 (38), 18927-18937, (2025)*

## 3.1 VLE data of methylcyclohexane-toluene with gamma-valerolactone and 1-methylpyrrolidin-2-one


### Abstract

The isobaric vapor-liquid equilibrium (VLE) data of the binary mixture of methylcyclohexane (1) + toluene (2) at 101.3 kPa; the pseudo-ternary mixture of methylcyclohexane (1) + toluene (2) + gamma-valerolactone (GVL) (3) with entrainer-to-feed ratio (E/F) = 1 (mass basis) at 50, 80, and 100 kPa, and E/F = 2 and 3 at 100 kPa; and the pseudo-ternary mixture of methylcyclohexane (1) + toluene (2) + 1-methylpyrrolidin-2-one (NMP) (3) with E/F = 1 at 100 kPa were measured using a Fischer Labodest VLE602 ebulliometer. The reliability of the experimental VLE data was tested and confirmed by Van Ness and Fredenslund thermodynamic consistency tests. The experimental results indicate that the presence of GVL and NMP increases the relative volatility of methylcyclohexane to toluene, therefore, both entrainers remove a close-boiling behavior in the mixture. Non-Random Two Liquid (NRTL) and Universal Quasi Chemical (UNIQUAC) thermodynamic models were applied in the experimental data correlation to obtain the optimum binary interaction parameters. For the mixture involving GVL, the experimental VLE data were accurately correlated by NRTL and UNIQUAC. However, NRTL has more accurate results compared to UNIQUAC. For the mixture containing NMP, both the UNIQUAC and NRTL models show favorable regression results.

### 3.1.1. Introduction

GVL can be readily produced from lignocellulosic biomass and possesses crucial characteristics that make it a viable bio-based substitute for restricted conventional organic entrainers due to its environmentally friendly properties such as biodegradability, non-toxicity, and sustainability.[1,2] Moreover, GVL offers favorable properties, including a liquid phase at room temperature, good polarity and hydrogen bond acceptor capability (K-T parameters: polarizability ($\pi^*$) = 0.83, hydrogen bond acceptor ($\beta$) = 0.6, and hydrogen bond donor ($\alpha$) = 0.20), high boiling point (480.15 K at 101.3 kPa), high decomposition temperatures (873.15 K at pressure of 170 kPa), good chemical stability, and low vapor pressure (2.67 kPa at 370.4 K), making it a well-suited entrainer for extractive distillation.[3–8]

Vapor-liquid equilibrium (VLE) is essential as thermodynamic data for designing and optimizing extractive distillation. However, there is no existing VLE data in the literature on the mixture of methylcyclohexane and toluene using GVL as a bio-based entrainer and NMP as a conventional organic entrainer. The VLE data for the methylcyclohexane-toluene with the addition of morpholine as an entrainer was provided by Coca and Pis[9]. Brower and Schuur[10] studied the VLE data of methylcyclohexane-toluene with Cyrene™ as an entrainer. The effect of some ionic liquids as entrainers on methylcyclohexane-toluene VLE data behavior was investigated by Liebert et al[11]. Gutierrez et al[12] reported the NMP effect at molar ratios of 0.1 and 0.3 on the relative volatility of methylcyclohexane to toluene; however, the publication did not provide complete VLE data. Other researchers reported the separation of methylcyclohexane and toluene mixture using extractive distillation in either a pilot plant or a process simulation evaluation. Quijada-Maldonado et al[13] studied the use of ILs and NMP as effective entrainers to separate methylcyclohexane from toluene in the pilot plant extractive distillation. Anwani and Shirsat[14] also simulated the use of phenol as an entrainer in the extractive distillation process for separating methylcyclohexane and toluene. Some other conventional organic entrainers, such as acetophenone, methyl n-amyl ketone, cyclohexanone, *o*-cresol, dimethylformamide (DMF), propylene glycol, furfural, phenol, and aniline, have been evaluated using process simulation for the separation of methylcyclohexane-toluene by extractive distillation.[15]

In this study, GVL was evaluated for the first time as a bio-based entrainer for the methylcyclohexane and toluene separation by extractive distillation. The evaluation was conducted by measuring the VLE data. The VLE data of methylcyclohexane and toluene with NMP as an entrainer was investigated as a benchmark. The consistency of the VLE data was tested using Van Ness[16] and Fredenslund[17] to confirm the reliability of the data. Furthermore, the experimental VLE data were correlated with activity coefficient thermodynamic models such as

NRTL[18] and UNIQUAC[19] to obtain the optimum binary parameters for the investigated system.

### 3.1.2. Methods

#### Chemicals

All chemicals were purchased from commercial suppliers. Gas chromatography (GC) was utilized to check the purity level of the chemicals. All chemicals were used as received without performing any additional purifications since no detectable impurities were found. The detailed chemical specifications, such as name, CAS registry number, molecular weight, boiling point, density, suppliers, purity, and purity analysis method, are presented in Table 1.

**Table 1.** The specification of chemicals

| chemicals | CAS registry number | molecular weight (g/mol) | $T_{boiling}$ (K)[a,b] | density (g/cm$^3$)[a,c] | suppliers | purity (mass fraction)[a] | purity analysis method | purification method |
|---|---|---|---|---|---|---|---|---|
| methylcyclohexane | 108-87-2 | 98.19 | 374.15 | 0.770 | Sigma-Aldrich | ≥0.990 | GC[d] | none |
| toluene | 108-88-3 | 92.14 | 383.15 | 0.865 | Sigma-Aldrich | 0.999 | GC[d] | none |
| gamma-valerolactone | 108-29-2 | 100.12 | 479.15 | 1.052 | Sigma-Aldrich | ≥0.999 | GC[d] | none |
| 1-methylpyrrolidin-2-one | 872-50-4 | 99.13 | 475.15 | 1.028 | Sigma-Aldrich | ≥0.995 | GC[d] | none |
| acetone | 67-64-1 | 58.08 | 329.15 | 0.791 | Merck | ≥0.998 | GC[d] | none |

[a]specified by the suppliers
[b]at pressure of 101.3 kPa
[c]at temperature of 298.15 and pressure of 101.3 kPa
[d]GC (Gas Chromatography)

#### Experimental procedures and analytical methods

The detailed experimental procedures and analytical methods for the VLE data measurements are provided in Chapter 2. The standard uncertainty calculations for temperature, pressure, and liquid and vapor composition were based on NIST Technical Note 1297[20] and Joint Committee for Guides in Metrology (JCGM)[21], which are listed in Eqs. B1-B6 in Appendix B. The standard uncertainties are provided in the VLE data tabulation in Results and Discussion Section.

### 3.1.3. Results and discussion

#### Experimental Results

The VLE data for the binary mixture of methylcyclohexane and toluene was measured at a pressure of 101.3 kPa. The experimental values consist of the mole fraction of methylcyclohexane in a liquid phase ($x_1$) and a vapor phase ($y_1$),

equilibrium temperature ($T$), the activity coefficient of methylcyclohexane ($\gamma_1$) and toluene ($\gamma_2$), and the relative volatility of methylcyclohexane to toluene ($\alpha_{12}$), which are tabulated in Table 2.

**Table 2.** VLE data for methylcyclohexane (1) + toluene (2) at 101.3 kPa[a,b]

| $T$/K | $x_1$ | $y_1$ | $\gamma_1$ | $\gamma_2$ | $\alpha_{12}$ |
|---|---|---|---|---|---|
| 383.87 | 0.000 | 0.000 | - | 1.000 | - |
| 382.50 | 0.046 | 0.078 | 1.344 | 1.004 | 1.76 |
| 381.50 | 0.095 | 0.146 | 1.243 | 1.009 | 1.62 |
| 379.87 | 0.188 | 0.273 | 1.230 | 1.003 | 1.62 |
| 378.43 | 0.297 | 0.386 | 1.145 | 1.021 | 1.49 |
| 377.45 | 0.396 | 0.476 | 1.088 | 1.044 | 1.39 |
| 376.42 | 0.498 | 0.571 | 1.066 | 1.063 | 1.34 |
| 375.60 | 0.595 | 0.655 | 1.049 | 1.083 | 1.29 |
| 375.03 | 0.705 | 0.743 | 1.021 | 1.125 | 1.21 |
| 374.62 | 0.800 | 0.823 | 1.007 | 1.160 | 1.16 |
| 374.16 | 0.906 | 0.915 | 1.002 | 1.199 | 1.12 |
| 373.92 | 1.000 | 1.000 | 1.000 | - | - |

[a] $T$ is the equilibrium temperature; $x_1$ is a liquid-phase mole fraction of methylcyclohexane; $y_1$ is a vapor-phase mole fraction of methylcyclohexane; $\gamma_1$ is the activity coefficient of methylcyclohexane; $\gamma_2$ is the activity coefficient of toluene; $\alpha_{12}$ is the relative volatility of methylcyclohexane to toluene.

[b] Expanded combined uncertainties $U$ with $k = 2$ are $U(T) = 0.2$ K, $U(P) = 0.20$ kPa, and $U(x_1) = U(y_1) = 0.006$.

Ideal gas behavior was assumed to be applicable because the VLE data of the binary mixture were investigated at atmospheric pressure. The activity coefficient of the component $i$ ($\gamma_i$) in the binary mixture as a representation of the non-ideal behavior of the compound in the mixture was calculated using Eq. 1:

$$\gamma_i = \frac{y_i P}{x_i P_i^{sat}} \qquad 1)$$

where $x_i$ and $y_i$ are a liquid-phase and a vapor-phase mole fraction of the component $i$, respectively, $P$ is the total pressure in the system, and $P_i^{sat}$ is the saturated vapor pressure of the component $i$. The saturated vapor pressure of the component $i$ ($P_i^{sat}$) was calculated using the extended Antoine parameters taken from the Aspen Plus physical property databank listed in Table 3.

**Table 3.** The parameters of the extended Antoine equation[a, b]

| Compound | $A_1$ | $A_2$ | $A_3$ | $A_4$ | $A_5$ | $10^6 A_6$ | $A_7$ | $A_8$ | $A_9$ |
|---|---|---|---|---|---|---|---|---|---|
| methylcyclohexane | 85.776 | -7080.8 | 0 | 0 | -10.695 | 8.14 | 2.0 | 146.58 | 572.1 |
| toluene | 70.037 | -6729.8 | 0 | 0 | -8.179 | 5.30 | 2.0 | 178.18 | 591.8 |

[a]Taken from the Aspen Plus physical property databank; $A_1$, $A_2$, $A_3$, $A_4$, $A_5$, $A_6$, $A_7$, $A_8$, and $A_9$ are Extended Antoine constants.

[b]Extended Antoine equation:

$\ln(P^s) = A_1 + A_2/(T + A_3) + A_4 T + A_5 \ln T + A_6 T^{A_7}$ for $A_8 < T < A_9$, where $P^s$ is in kPa and $T$ in K.

The relative volatility of methylcyclohexane to toluene ($\alpha_{12}$) in the binary mixture was defined by Eq. 2:

$$\alpha_{12} = \frac{y_1 / x_1}{y_2 / x_2} \qquad 2)$$

The experimental results were compared with the VLE data from the literature.[9,22] The graphical comparison of the VLE data is depicted in Figure 1.

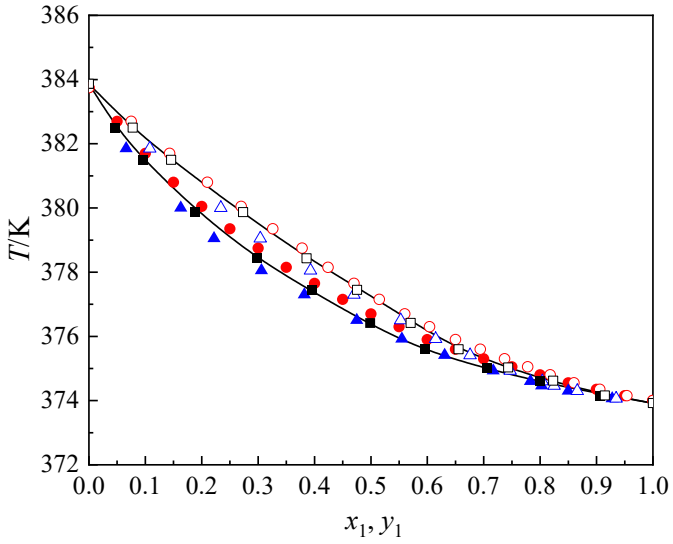


**Figure 1.** *T-xy* diagram for methylcyclohexane (1) + toluene (2) at 101.3 kPa: (■), liquid-phase and (□), vapor-phase from this work; (●), liquid-phase and (○), vapor-phase from literature[22]; (▲), liquid-phase; (Δ), vapor-phase from literature[9], and (—), correlated by NRTL.

The results indicate that the VLE data obtained in this study are in a better agreement with the VLE data reported by Coca and Pis[9] than those by Quiggle and Fenske[22]. The equilibrium temperature provided by Quiggle and Fenske is slightly

higher than ours and that of Coca and Pis. In addition, the *x*-*y* diagram is presented in Figure B1. The vapor pressure of methylcyclohexane and toluene was measured and compared with literature values.[23,24] The results show that the vapor pressure from this work aligns well with the literature data, as provided in Figures B2 and B3. These results confirmed the reliability of the experimental apparatus and method. Moreover, the VLE data of the binary mixture from this work are consistent according to the Van Ness and Fredenslund thermodynamic consistency tests. A more detailed description of the thermodynamic consistency test is provided in the below section. The VLE data of the binary mixture at 53.3 kPa was taken from literature[25], as shown in Figure 2. Figures 2 and B1 also show that a reduced pressure at 53.3 kPa did not significantly change the close-boiling behavior of the mixture. This data, along with the VLE data of the binary mixture at 101.3 kPa obtained from this work, were used for the regression analysis.

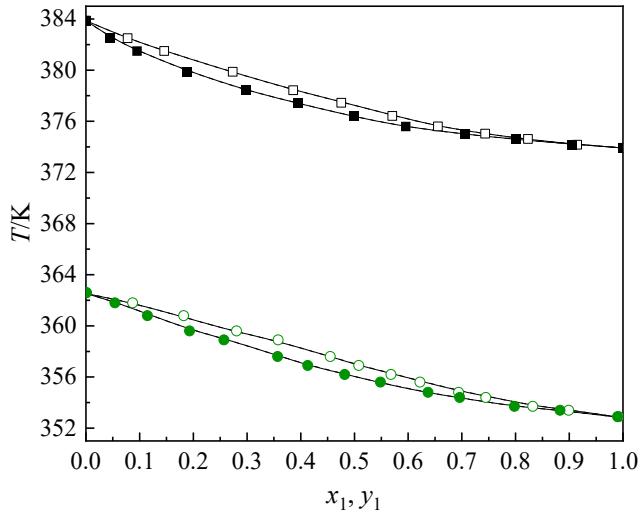


**Figure 2.** *T*-*xy* diagram for methylcyclohexane (1) + toluene (2) at 53.3 and 101.3 kPa: (●), liquid-phase and (○), vapor-phase at 53.3 kPa from literature[25], (■), liquid-phase and (□), vapor-phase at 101.3 kPa from this work; (—), correlated by NRTL; and (- - -), UNIQUAC.

The apparatus was further utilized to measure the vapor-liquid equilibrium for the pseudo-ternary mixture of methylcyclohexane (1) + toluene (2) + GVL (3) with the entrainer-to-feed ratio (E/F) = 1 at pressures of 50, 80, and 100 kPa, respectively. The E/F describes the mass-based ratio of the entrainer added to the binary mixture, which is expressed as the mass of the entrainer divided by the mass of the binary mixture. The experimental VLE data for the pseudo-ternary mixture are provided in Table 4, where $x_1'$ and $y_1'$ represent the mole fractions of methylcyclohexane in the liquid and vapor phases on an entrainer-free basis, respectively. $x_1$, $x_2$, and $x_3$ denote the mole fractions of methylcyclohexane,

toluene, and GVL in the liquid phase, respectively. $y_1$, $y_2$, and $y_3$ indicate the mole fractions of methylcyclohexane, toluene, and GVL in the vapor phase, respectively. Moreover, the VLE data of the pseudo-ternary mixture containing GVL with E/F = 2 and E/F = 3 at a pressure of 100 kPa were investigated, with the results listed in Table 5.

**Table 4.** VLE data for methylcyclohexane (1) + toluene (2) + gamma-valerolactone (3) with E/F = 1 (mass basis) and pressures at 50, 80, and 100 kPa[a,b]

| *T*/K | $x_1'$ | $x_1$ | $x_2$ | $x_3$ | $y_1'$ | $y_1$ | $y_2$ | $y_3$ | $\gamma_1$ | $\gamma_2$ | $\alpha_{12}$ |
|---|---|---|---|---|---|---|---|---|---|---|---|
| | | | | | *50 kPa* | | | | | | |
| 372.75 | 0.000 | 0.000 | 0.523 | 0.477 | 0.000 | 0.000 | 0.994 | 0.006 | - | 1.299 | - |
| 368.43 | 0.080 | 0.041 | 0.477 | 0.482 | 0.233 | 0.232 | 0.763 | 0.005 | 3.262 | 1.250 | 3.50 |
| 365.26 | 0.184 | 0.098 | 0.434 | 0.468 | 0.404 | 0.402 | 0.595 | 0.003 | 2.598 | 1.182 | 3.00 |
| 362.38 | 0.283 | 0.147 | 0.374 | 0.479 | 0.534 | 0.530 | 0.463 | 0.007 | 2.491 | 1.172 | 2.91 |
| 359.90 | 0.377 | 0.194 | 0.320 | 0.486 | 0.647 | 0.643 | 0.350 | 0.007 | 2.467 | 1.126 | 3.03 |
| 358.07 | 0.474 | 0.241 | 0.267 | 0.492 | 0.746 | 0.742 | 0.252 | 0.006 | 2.425 | 1.034 | 3.26 |
| 356.84 | 0.586 | 0.306 | 0.216 | 0.478 | 0.804 | 0.799 | 0.194 | 0.007 | 2.138 | 1.027 | 2.90 |
| 355.79 | 0.687 | 0.348 | 0.158 | 0.494 | 0.862 | 0.856 | 0.137 | 0.007 | 2.082 | 1.023 | 2.83 |
| 354.83 | 0.801 | 0.416 | 0.104 | 0.480 | 0.915 | 0.909 | 0.084 | 0.007 | 1.907 | 0.988 | 2.68 |
| 354.14 | 0.897 | 0.443 | 0.050 | 0.507 | 0.964 | 0.962 | 0.036 | 0.002 | 1.936 | 0.895 | 3.06 |
| 353.84 | 1.000 | 0.508 | 0.000 | 0.492 | 1.000 | 0.998 | 0.000 | 0.002 | 1.771 | - | - |
| | | | | | *80 kPa* | | | | | | |
| 388.60 | 0.000 | 0.000 | 0.519 | 0.481 | 0.000 | 0.000 | 0.989 | 0.011 | - | 1.318 | - |
| 384.56 | 0.082 | 0.043 | 0.475 | 0.482 | 0.215 | 0.213 | 0.777 | 0.010 | 2.922 | 1.266 | 3.05 |
| 381.29 | 0.181 | 0.095 | 0.433 | 0.472 | 0.384 | 0.383 | 0.607 | 0.010 | 2.596 | 1.192 | 2.82 |
| 378.71 | 0.281 | 0.146 | 0.373 | 0.481 | 0.512 | 0.506 | 0.482 | 0.012 | 2.392 | 1.185 | 2.68 |
| 376.52 | 0.367 | 0.183 | 0.316 | 0.501 | 0.619 | 0.612 | 0.376 | 0.012 | 2.451 | 1.163 | 2.80 |
| 374.08 | 0.475 | 0.240 | 0.265 | 0.495 | 0.713 | 0.706 | 0.283 | 0.011 | 2.308 | 1.126 | 2.75 |
| 372.07 | 0.576 | 0.292 | 0.214 | 0.494 | 0.784 | 0.777 | 0.214 | 0.009 | 2.212 | 1.114 | 2.67 |
| 370.73 | 0.673 | 0.339 | 0.164 | 0.497 | 0.848 | 0.838 | 0.151 | 0.011 | 2.135 | 1.069 | 2.70 |
| 369.29 | 0.783 | 0.397 | 0.110 | 0.493 | 0.909 | 0.900 | 0.091 | 0.009 | 2.041 | 1.002 | 2.76 |
| 368.53 | 0.897 | 0.444 | 0.051 | 0.505 | 0.960 | 0.948 | 0.040 | 0.012 | 1.965 | 0.966 | 2.74 |
| 367.71 | 1.000 | 0.501 | 0.000 | 0.499 | 1.000 | 0.988 | 0.000 | 0.012 | 1.856 | - | - |
| | | | | | *100 kPa* | | | | | | |
| 396.48 | 0.000 | 0.000 | 0.521 | 0.479 | 0.000 | 0.000 | 0.983 | 0.017 | - | 1.318 | - |
| 392.70 | 0.082 | 0.042 | 0.470 | 0.488 | 0.205 | 0.202 | 0.783 | 0.015 | 2.878 | 1.287 | 2.88 |
| 389.67 | 0.180 | 0.095 | 0.431 | 0.474 | 0.374 | 0.369 | 0.617 | 0.014 | 2.496 | 1.202 | 2.72 |
| 387.03 | 0.275 | 0.142 | 0.374 | 0.484 | 0.497 | 0.491 | 0.496 | 0.013 | 2.390 | 1.198 | 2.60 |
| 384.45 | 0.383 | 0.199 | 0.321 | 0.480 | 0.610 | 0.603 | 0.386 | 0.011 | 2.242 | 1.166 | 2.52 |
| 382.24 | 0.468 | 0.230 | 0.262 | 0.508 | 0.701 | 0.691 | 0.295 | 0.014 | 2.357 | 1.164 | 2.66 |
| 380.75 | 0.581 | 0.295 | 0.213 | 0.492 | 0.772 | 0.761 | 0.225 | 0.014 | 2.107 | 1.137 | 2.44 |

| $T$/K | $x_1$' | $x_1$ | $x_2$ | $x_3$ | $y_1$' | $y_1$ | $y_2$ | $y_3$ | $\gamma_1$ | $\gamma_2$ | $\alpha_{12}$ |
|---|---|---|---|---|---|---|---|---|---|---|---|
| 379.72 | 0.666 | 0.334 | 0.167 | 0.499 | 0.842 | 0.830 | 0.156 | 0.014 | 2.086 | 1.038 | 2.67 |
| 378.43 | 0.790 | 0.388 | 0.103 | 0.509 | 0.902 | 0.889 | 0.096 | 0.015 | 1.993 | 1.082 | 2.45 |
| 377.63 | 0.893 | 0.452 | 0.054 | 0.494 | 0.956 | 0.943 | 0.044 | 0.013 | 1.854 | 0.963 | 2.57 |
| 377.27 | 1.000 | 0.503 | 0.000 | 0.497 | 1.000 | 0.985 | 0.000 | 0.015 | 1.758 | - | - |

[a] $T$ is the equilibrium temperature; $x_1$' is a liquid-phase mole fraction of methylcyclohexane on a GVL-free basis; $x_1$, $x_2$, and $x_3$ are liquid-phase mole fractions of methylcyclohexane, toluene, and GVL, respectively; $y_1$' is a vapor-phase mole fraction of methylcyclohexane on a GVL-free basis; $y_1$, $y_2$, and $y_3$ are vapor-phase mole fractions of methylcyclohexane, toluene, and GVL, respectively; $\gamma_1$ is the activity coefficient of methylcyclohexane; $\gamma_2$ is the activity coefficient of toluene; $\alpha_{12}$ is the relative volatility of methylcyclohexane to toluene.

[b] Expanded combined uncertainties $U$ with $k = 2$ are $U(T) = 0.4$ K, $U(P) = 0.23$ kPa, and $U(x_1) = U(y_1) = 0.006$.

**Table 5.** VLE data for methylcyclohexane (1) + toluene (2) + gamma-valerolactone (3) with E/F = 2 and 3 (mass basis) and pressure at 100 kPa[a,b]

| $T$/K | $x_1$' | $x_1$ | $x_2$ | $x_3$ | $y_1$' | $y_1$ | $y_2$ | $y_3$ | $\gamma_1$ | $\gamma_2$ | $\alpha_{12}$ |
|---|---|---|---|---|---|---|---|---|---|---|---|
| | | | | | *E/F =2* | | | | | | |
| 405.28 | 0.000 | 0.000 | 0.346 | 0.654 | 0.000 | 0.000 | 0.970 | 0.030 | - | 1.560 | - |
| 399.63 | 0.078 | 0.027 | 0.323 | 0.650 | 0.204 | 0.198 | 0.774 | 0.028 | 3.701 | 1.540 | 3.01 |
| 396.20 | 0.152 | 0.053 | 0.296 | 0.651 | 0.329 | 0.319 | 0.649 | 0.032 | 3.301 | 1.543 | 2.75 |
| 392.31 | 0.268 | 0.094 | 0.258 | 0.648 | 0.518 | 0.508 | 0.472 | 0.020 | 3.268 | 1.426 | 2.95 |
| 389.01 | 0.370 | 0.129 | 0.219 | 0.652 | 0.657 | 0.643 | 0.336 | 0.021 | 3.277 | 1.311 | 3.26 |
| 386.78 | 0.455 | 0.155 | 0.185 | 0.660 | 0.718 | 0.702 | 0.276 | 0.022 | 3.152 | 1.356 | 3.04 |
| 384.48 | 0.567 | 0.190 | 0.145 | 0.665 | 0.799 | 0.785 | 0.197 | 0.018 | 3.054 | 1.318 | 3.03 |
| 382.62 | 0.677 | 0.228 | 0.109 | 0.663 | 0.867 | 0.852 | 0.131 | 0.017 | 2.902 | 1.229 | 3.11 |
| 381.33 | 0.769 | 0.257 | 0.077 | 0.666 | 0.918 | 0.901 | 0.081 | 0.018 | 2.819 | 1.112 | 3.34 |
| 379.77 | 0.890 | 0.296 | 0.036 | 0.668 | 0.967 | 0.953 | 0.032 | 0.015 | 2.700 | 0.992 | 3.62 |
| 378.84 | 1.000 | 0.340 | 0.000 | 0.660 | 1.000 | 0.986 | 0.000 | 0.014 | 2.493 | - | - |
| | | | | | *E/F =3* | | | | | | |
| 417.51 | 0.000 | 0.000 | 0.270 | 0.730 | 0.000 | 0.000 | 0.949 | 0.051 | - | 1.453 | - |
| 414.94 | 0.063 | 0.017 | 0.250 | 0.733 | 0.149 | 0.142 | 0.808 | 0.050 | 2.935 | 1.422 | 2.61 |
| 412.08 | 0.108 | 0.030 | 0.248 | 0.722 | 0.301 | 0.288 | 0.670 | 0.042 | 3.634 | 1.272 | 3.54 |
| 408.02 | 0.237 | 0.064 | 0.207 | 0.729 | 0.446 | 0.428 | 0.531 | 0.041 | 2.771 | 1.334 | 2.60 |
| 403.72 | 0.330 | 0.086 | 0.176 | 0.738 | 0.565 | 0.548 | 0.421 | 0.031 | 2.919 | 1.386 | 2.65 |
| 400.48 | 0.436 | 0.114 | 0.147 | 0.739 | 0.670 | 0.653 | 0.322 | 0.025 | 2.832 | 1.378 | 2.62 |
| 395.46 | 0.567 | 0.146 | 0.111 | 0.743 | 0.814 | 0.794 | 0.181 | 0.025 | 3.041 | 1.168 | 3.35 |
| 391.68 | 0.671 | 0.171 | 0.084 | 0.745 | 0.872 | 0.860 | 0.125 | 0.015 | 3.087 | 1.182 | 3.35 |
| 388.62 | 0.779 | 0.200 | 0.057 | 0.743 | 0.924 | 0.906 | 0.074 | 0.020 | 3.006 | 1.120 | 3.45 |
| 385.51 | 0.893 | 0.222 | 0.027 | 0.751 | 0.973 | 0.955 | 0.026 | 0.019 | 3.094 | 0.922 | 4.38 |
| 384.58 | 1.000 | 0.254 | 0.000 | 0.746 | 1.000 | 0.981 | 0.000 | 0.019 | 2.849 | - | - |

[a] $T$ is the equilibrium temperature; $x_1$' is a liquid-phase mole fraction of methylcyclohexane on a GVL-free basis; $x_1$, $x_2$, and $x_3$ are liquid-phase mole fractions of methylcyclohexane, toluene, and GVL, respectively; $y_1$' is a vapor-phase mole fraction of methylcyclohexane on a GVL-free basis; $y_1$, $y_2$, and $y_3$ are vapor-phase mole fractions of methylcyclohexane, toluene, and GVL, respectively; $\gamma_1$ is the activity coefficient of methylcyclohexane; $\gamma_2$ is the activity coefficient of toluene; $\alpha_{12}$ is the relative volatility of methylcyclohexane to toluene.

[b] Expanded combined uncertainties $U$ with $k = 2$ are $U(T) = 0.4$ K, $U(P) = 0.23$ kPa, and $U(x_1) = U(y_1) = 0.006$.

We also investigated the VLE for the pseudo-ternary mixture of methylcyclohexane (1) + toluene (2) containing NMP (3) with E/F = 1 at a pressure of 100 kPa as a benchmark entrainer. The VLE data are provided as a pseudo-ternary mixture in Table 6. The VLE measurements for pseudo-ternary systems were performed at 100 kPa rather than 101.3 kPa due to the ambience pressure in our laboratory varying between 100 and 101.3 kPa. Therefore, the pressure of 100 kPa was selected as it allows more accurate control of the pressure within the setup. In both pseudo-ternary mixtures, one liquid phase is observed throughout the entire composition range of methylcyclohexane at all investigated E/Fs and temperature ranges.

**Table 6.** VLE data for methylcyclohexane (1) + toluene (2) + 1-methylpyrrolidin-2-one (3) with E/F = 1 (mass basis) and pressure at 100 kPa[a,b]

| $T$/K | $x_1$' | $x_1$ | $x_2$ | $x_3$ | $y_1$' | $y_1$ | $y_2$ | $y_3$ | $\gamma_1$ | $\gamma_2$ | $\alpha_{12}$ |
|---|---|---|---|---|---|---|---|---|---|---|---|
| 399.15 | 0.000 | 0.000 | 0.513 | 0.487 | 0.000 | 0.000 | 0.986 | 0.014 | - | 1.251 | - |
| 395.29 | 0.091 | 0.050 | 0.487 | 0.463 | 0.216 | 0.213 | 0.773 | 0.014 | 2.418 | 1.142 | 2.74 |
| 393.85 | 0.133 | 0.070 | 0.452 | 0.478 | 0.297 | 0.294 | 0.695 | 0.011 | 2.438 | 1.152 | 2.75 |
| 392.62 | 0.179 | 0.096 | 0.438 | 0.466 | 0.377 | 0.373 | 0.616 | 0.011 | 2.323 | 1.089 | 2.78 |
| 391.02 | 0.232 | 0.124 | 0.407 | 0.469 | 0.447 | 0.439 | 0.543 | 0.018 | 2.205 | 1.079 | 2.67 |
| 389.79 | 0.280 | 0.148 | 0.376 | 0.476 | 0.510 | 0.507 | 0.486 | 0.007 | 2.205 | 1.083 | 2.68 |
| 388.43 | 0.329 | 0.175 | 0.353 | 0.472 | 0.561 | 0.555 | 0.435 | 0.010 | 2.111 | 1.070 | 2.60 |
| 387.30 | 0.372 | 0.193 | 0.322 | 0.485 | 0.617 | 0.611 | 0.380 | 0.009 | 2.169 | 1.058 | 2.71 |
| 386.36 | 0.421 | 0.219 | 0.296 | 0.485 | 0.656 | 0.648 | 0.340 | 0.012 | 2.084 | 1.056 | 2.62 |
| 385.43 | 0.482 | 0.251 | 0.265 | 0.484 | 0.707 | 0.700 | 0.290 | 0.010 | 2.012 | 1.032 | 2.60 |
| 384.52 | 0.527 | 0.272 | 0.240 | 0.488 | 0.742 | 0.735 | 0.255 | 0.010 | 1.994 | 1.030 | 2.59 |
| 383.83 | 0.588 | 0.311 | 0.214 | 0.475 | 0.781 | 0.776 | 0.217 | 0.007 | 1.873 | 1.005 | 2.50 |
| 383.23 | 0.629 | 0.323 | 0.185 | 0.492 | 0.812 | 0.798 | 0.189 | 0.013 | 1.889 | 1.024 | 2.55 |
| 382.34 | 0.692 | 0.360 | 0.156 | 0.484 | 0.851 | 0.836 | 0.146 | 0.018 | 1.817 | 0.967 | 2.56 |
| 381.33 | 0.793 | 0.414 | 0.103 | 0.483 | 0.904 | 0.892 | 0.094 | 0.014 | 1.732 | 0.964 | 2.47 |
| 380.48 | 0.893 | 0.465 | 0.051 | 0.484 | 0.954 | 0.940 | 0.045 | 0.015 | 1.664 | 0.956 | 2.51 |
| 379.52 | 1.000 | 0.506 | 0.000 | 0.494 | 1.000 | 0.986 | 0.000 | 0.014 | 1.646 | - | - |

[a] $T$ is the equilibrium temperature; $x_1$' is a liquid-phase mole fraction of methylcyclohexane on an NMP-free basis; $x_1$, $x_2$, and $x_3$ are liquid-phase mole fractions of methylcyclohexane, toluene, and

NMP, respectively; $y_1$' is a vapor-phase mole fraction of methylcyclohexane on a NMP-free basis; $y_1$, $y_2$, and $y_3$ are vapor-phase mole fractions of methylcyclohexane, toluene, and NMP, respectively; $\gamma_1$ is the activity coefficient of methylcyclohexane; $\gamma_2$ is the activity coefficient of toluene; $\alpha_{12}$ is the relative volatility of methylcyclohexane to toluene.
[b]Expanded combined uncertainties $U$ with $k$ = 2 are $U(T)$ = 0.4 K, $U(P)$ = 0.23 kPa, and $U(x_1)$ = $U(y_1)$ = 0.006.

The non-ideality of the substance in the liquid phase for the pseudo-ternary mixture, as indicated by the activity coefficient of the component $i$ ($\gamma_i$), was determined using Eq. 1 with consideration of the ideal gas applied in the system since the VLE data were measured at the atmospheric and vacuum pressures. For the pseudo-ternary mixture, the relative volatility of methylcyclohexane to toluene ($\alpha_{12}$) was determined by Eq. 3.

$$\alpha_{12} = \frac{y_1'/x_1'}{y_2'/x_2'} \qquad 3)$$

where $x_1$' and $x_2$' denote the liquid-phase mole fractions of methylcyclohexane and toluene on an entrainer-free basis, respectively. $y_1$' and $y_2$' represent the vapor-phase mole fractions of methylcyclohexane and toluene on an entrainer-free basis, respectively.

As observed in Figure 3, reducing the pressure in the VLE significantly reduces the equilibrium temperature since the reduced pressure will decrease the boiling point of each compound.

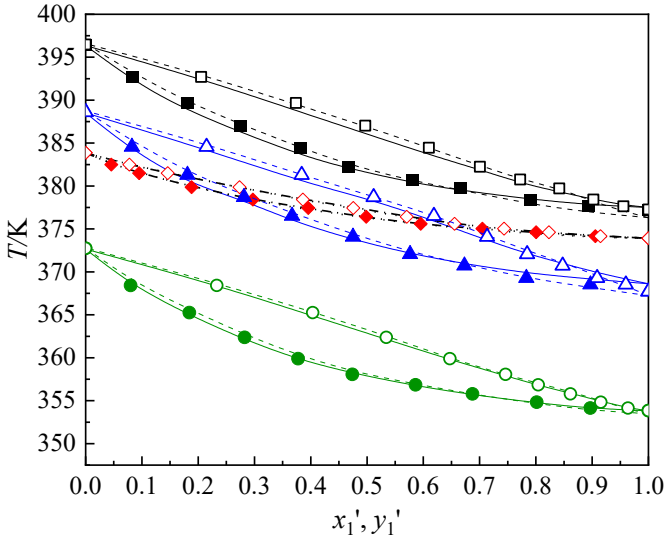


**Figure 3.** *T-x'y'* diagram for methylcyclohexane (1) + toluene (2) + gamma-valerolactone (3) with E/F = 1: (■), $x_1'$ and (□), $y_1'$ experimental at 100 kPa; (♦), $x_1$ and (◊), $y_1$ experimental at 101.3 kPa (no entrainer); (▲), $x_1'$ and (Δ), $y_1'$ experimental at 80 kPa; (●), $x_1'$ and (○), $y_1'$ experimental at 50 kPa; (—), correlated

by NRTL; and (- - -), UNIQUAC: black, blue, and green line for the pressure of 100 kPa, 80 kPa, and 50 kPa, respectively; and correlated by (-··-), NRTL; and (·· ··), UNIQUAC for no entrainer.

Figure 4 indicates that increasing the amount of GVL with the E/F ratio at 2 and 3, while maintaining the pressure constant at 100 kPa leads to an increase in the equilibrium temperature. The addition of a higher amount of GVL to the mixture results in a higher equilibrium temperature. GVL exhibits a higher affinity for toluene, resulting in reduced vaporization of toluene. As a result, a higher temperature is required to achieve vaporization for equilibrium, thereby raising the overall equilibrium temperature.

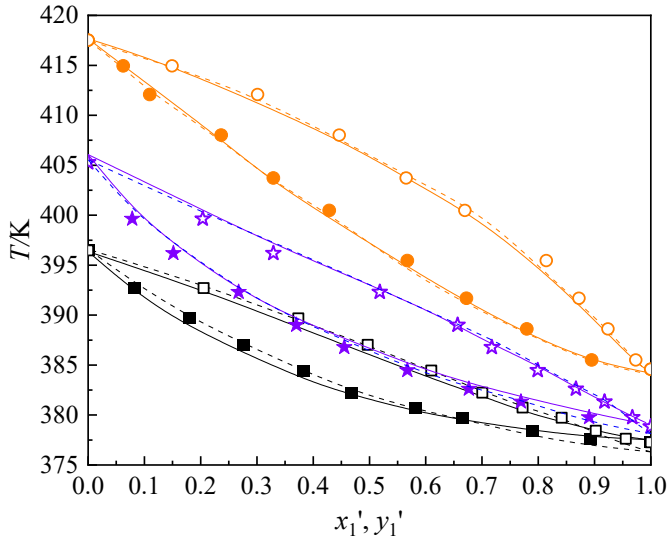


**Figure 4.** *T*-*x*'*y*' diagram for methylcyclohexane (1) + toluene (2) + gamma-valerolactone (3) at 100 kPa with E/F = 1: (■), $x_1'$ and (□), $y_1'$ experimental; E/F = 2: (★), $x_1'$ and (☆), $y_1'$ experimental; E/F = 3: (●), $x_1'$ and (○), $y_1'$ experimental; (—), correlated by NRTL; and (- - -), UNIQUAC: black, purple, and orange line for E/F = 1, 2, and 3, respectively.

Figures 5 and 6 are used to visually demonstrate the influence of GVL on the separation of the mixture by presenting *x*'-*y*' diagrams. The presence of GVL induces a significant rise in the relative volatility of methylcyclohexane to toluene compared to the mixture without GVL. Thus, the close-boiling behavior in the methylcyclohexane-toluene mixture was successfully eliminated.

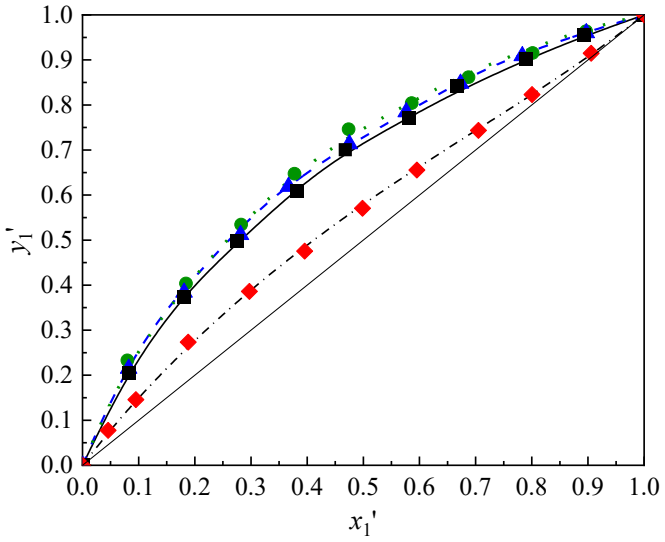


**Figure 5.** *x*'-*y*' diagram for methylcyclohexane (1) + toluene (2) + gamma-valerolactone (3) with E/F = 1 : (■), experimental at 100 kPa; (▲), 80 kPa; (●), 50 kPa; (♦), no entrainer at 101.3 kPa; (—), correlated by NRTL at 100 kPa; (- - -), 80 kPa; and (····), 50 kPa; and (-·-), correlated by NRTL for no entrainer.

The introduction of GVL into the mixture resulted in a change in the non-ideality behavior of the mixture. It is confirmed by the increase in the activity coefficients of methylcyclohexane ($\gamma_1$) and toluene ($\gamma_2$), as listed in Tables 4 and 5, compared to the activity coefficients in the binary mixture depicted in Table 2. The increase in relative volatility can be attributed to the stronger molecular interaction between GVL and toluene, as opposed to the GVL and methylcyclohexane interaction. This is mainly because GVL is a polar entrainer, while toluene is comparatively less non-polar than methylcyclohexane. Consequently, GVL is expected to have more affinity towards toluene compared to methylcyclohexane. Accordingly, the interaction between methylcyclohexane and toluene can be minimized.

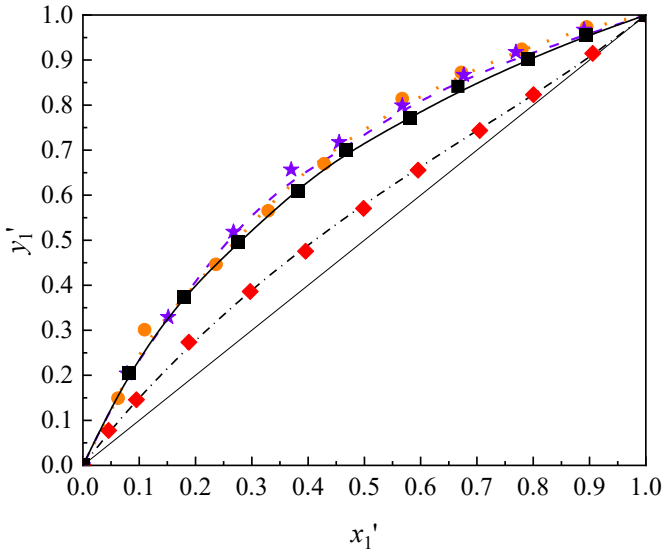


**Figure 6.** *x*'-*y*' diagram for methylcyclohexane (1) + toluene (2) + gamma-valerolactone (3) at 100 kPa: E/F = 1: (■); E/F = 2: (★); E/F = 3: (●); (♦), no entrainer at 101.3 kPa; correlated by NRTL for E/F = 1: (—); E/F = 2: (- - -); E/F = 3: (····); and (-··-), correlated by NRTL for no entrainer.

The results in Tables 4 and 5 show that the presence of GVL in the mixture provides lower activity coefficients for toluene ($\gamma_2$) compared to methylcyclohexane ($\gamma_1$). This implies that GVL has a stronger interaction with toluene than does methylcyclohexane. As a result, methylcyclohexane has a higher vaporization efficiency, allowing it easier to separate from the mixture. An investigation was conducted to examine the impact of pressure on relative volatility. Figure 5 illustrates that reducing the pressure from 100 to 80 and 50 kPa leads to an increase in relative volatility. The reduction in pressure will amplify the non-ideality of the mixture, thus leading to an increase in relative volatility. Nevertheless, the rise in relative volatility is merely modest. It can be observed that interactions between GVL and toluene do not significantly increase when the pressure is dropped to 80 and 50 kPa. This study also investigated the effect of the amount of GVL on the relative volatility, as depicted in Figure 6. Similarly to the pressure effect, increasing the E/F ratio to 2 and 3 has a slight effect on enhancing the relative volatility. This indicates that increasing the amount of GVL in E/F ratios 2 and 3 did not result in a significant increase in the interaction between GVL and toluene compared to that observed in E/F = 1.

Introducing NMP to the methylcyclohexane-toluene mixture with E/F = 1 at a pressure of 100 kPa induces an increase in the equilibrium temperature compared to the binary mixture, as shown in Figure 7.

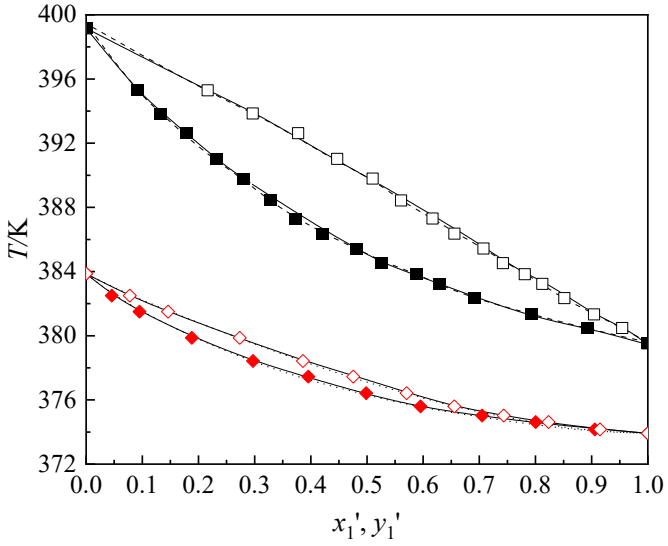


**Figure 7**. *T- x'y'* diagram for methylcyclohexane (1) + toluene (2) + 1-methylpyrrolidin-2-one (3) at 100 kPa and E/F = 1: (■), $x_1'$; (□), $y_1'$ experimental; (♦), $x_1$ and (◊), $y_1$ experimental at 101.3 kPa (no entrainer); (—), correlated by NRTL; and (- - -), UNIQUAC.

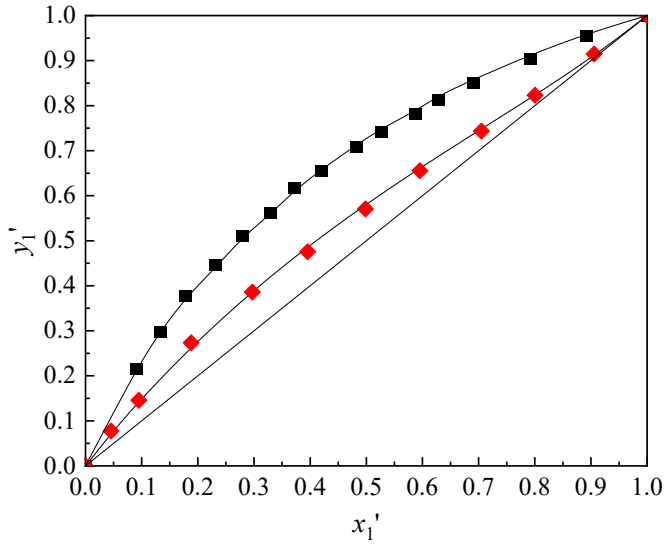


**Figure 8.** *x'-y'* diagram for methylcyclohexane (1) + toluene (2) + 1-methylpyrrolidin-2-one (3) at 100 kPa: (■), E/F = 1; (♦), no entrainer at 101.3 kPa; (—), correlated by NRTL.

The interaction between NMP with toluene decreases the toluene vaporization. Consequently, an increased temperature must be attained to reach the equilibrium, thus elevating the entire equilibrium temperature. Figure 8 demonstrates that NMP effectively enhanced the relative volatility of methylcyclohexane to toluene, resulting in the elimination of a close-boiling behavior.

This can be described as NMP acting as a polar entrainer that exhibits more interaction with toluene than with methylcyclohexane. According to Table 6, the presence of NMP in the mixture induces this non-ideal behavior, which is confirmed by the increased activity coefficients for both methylcyclohexane ($\gamma_1$) and toluene ($\gamma_2$) compared to the activity coefficients in their binary mixture, which are presented in Table 2. The addition of NMP to the mixture produces lower activity coefficients of toluene ($\gamma_2$) than methylcyclohexane ($\gamma_1$), indicating that NMP has more interaction with toluene than those with methylcyclohexane. As a result, the interaction between toluene and methylcyclohexane decreases, leading to a more facile vaporization of methylcyclohexane. This implies that easier separation of methylcyclohexane from toluene will be attained. The binary endpoints of our works were compared with the data from the literature, as presented in Figures B4-B7. Overall, the experimental data from our study align well with the literature values.[26–30] For the toluene (1) + gamma-valerolactone (2), Figure B4 indicates that the experimental data from this work are in good agreement with the literature values[26]. At a pressure of 100 kPa, the vapor phase composition of toluene is slightly higher than the values reported in the literature[26]. In the case of the toluene (1) + 1-methylpyrrolidin-2-one (2) mixture, the VLE data from this work align closely with the VLE data from Zaretskii et al[28] and show a slightly higher vapor phase composition of toluene compared to the data from Gupta et al[27], as illustrated in Figure B5. For the 1-methylpyrrolidin-2-one (1) + toluene (2) and 1-methylpyrrolidin-2-one (1) + methylcyclohexane (2) mixtures, the phase boundary pressures observed in this study are consistent with the trend outlined in the literature.[29,30] This is further supported by the phase boundary pressure profile, as illustrated in Figures B6 and B7, predicted by the UNIQUAC-Hayden O'Connell (HOC) model from Aspen Plus since the experimental data for the investigated temperature are unavailable in the existing literature.

In addition, the relative volatility performance of GVL was compared against that of NMP and sulfolane, which acted as benchmark entrainers. The comparison was performed at a mole fraction of methylcyclohexane of 0.5, an E/F = 1, and a pressure of 100 kPa. The relative volatility of the mixture with no entrainer and with the addition of GVL and NMP entrainers, respectively, was obtained from this work. While the relative volatility with the addition of sulfolane entrainer was taken from literature[10]. As illustrated in Figure 9, GVL outperforms both benchmark entrainers in terms of relative volatility performance. Thus, GVL shows great potential and serves as an effective bio-based entrainer to substitute NMP or sulfolane in the separation of methylcyclohexane from toluene.

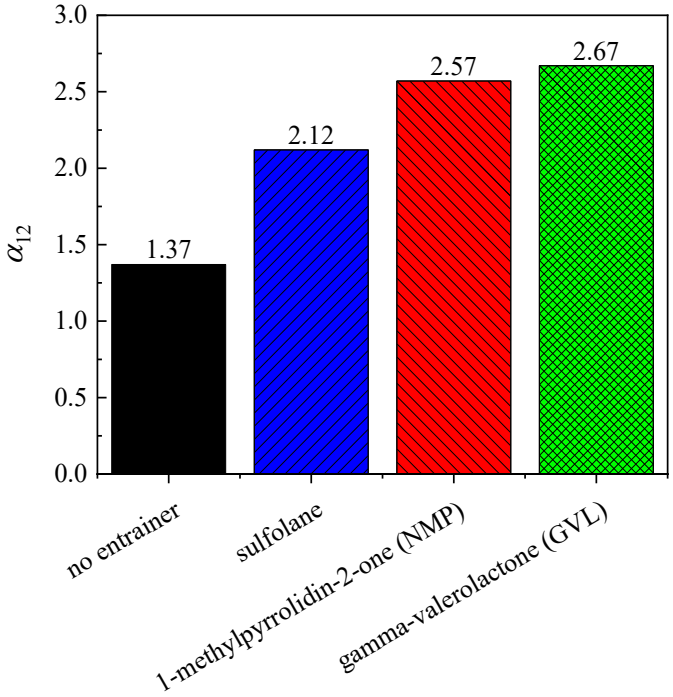


**Figure 9.** Relative volatility of methylcyclohexane (1) + toluene (2) ($\alpha_{12}$) with no entrainer, and with entrainers of sulfolane and 1-methylpyrrolidin-2-one as benchmark entrainers, and gamma-valerolactone as a bio-based entrainer at $x_1'$ = 0.5, E/F = 1, and a pressure of 100 kPa. The experiment was conducted in duplo, and the deviation of the relative volatility was 0.02. The relative volatility data for sulfolane was taken from literature.[10]

**Thermodynamic consistency test**

The reliability of the VLE data for both binary and pseudo-ternary mixtures was tested using the Van Ness[16], which is based on the Gibbs-Duhem equation. The Van Ness test is expressed in Eqs. 4 and 5.

$$\Delta P = \frac{1}{n_p} \times \sum_{i=1}^{n_p} \Delta P_i = \frac{1}{n_p} \times \sum_{i=1}^{n_p} 100 \left| \frac{P_i^{cal} - P_i^{\exp}}{P_i^{\exp}} \right| \quad 4)$$

$$\Delta y = \frac{1}{n_p} \times \sum_{i=1}^{n_p} \Delta y_i = \frac{1}{n_p} \times \sum_{i=1}^{n_p} 100 \left| y_i^{cal} - y_i^{\exp} \right| \quad 5)$$

where $n_p$ is the number of experimental data points, $P$ stands for pressure, $y$ denotes a vapor-phase mole fraction, and the superscripts *cal* and *exp* represent the calculated value from the model and the experimental value, respectively. The calculated value for this test was obtained from the NRTL correlation. The experimental data point is considered to meet the Van Ness test criteria and is therefore considered consistent if the values are $\Delta P < 1$ and $\Delta y < 1$. According to Table 7, the VLE data for the investigated binary and pseudo-ternary mixtures have the values of $\Delta P$ and $\Delta y$ are less than 1. Moreover, the residual distribution

of $\ln(\gamma_1/\gamma_2)$ should behave randomly to satisfy the Van Ness test. The residual distribution of $\ln(\gamma_1/\gamma_2)$ for each mixture, as shown in Figures B8, B9, and B10, confirms their random distribution. The results indicate that the VLE data from our work are thermodynamically consistent.

The VLE data also tested according to the criterion from Fredenslund[17] which compared the experimental and calculated values of vapor-phase mole fraction, as provided in Eq. 6.

$$\frac{1}{n_p}\left\{\sum_{i=1}^{n_p}\left|y_{i,\exp}-y_{i,cal}\right|\right\}\leq 0.01 \qquad 6)$$

Based on the Fredenslund's criterion, the VLE data is considered consistent if the average absolute value of the vapor-phase mole fraction between the experimental and calculated values is less than 0.01. For the binary mixture of methylcyclohexane (1) + toluene (2) at 101.3 kPa, the Legendre polynomial equation in Fredenslund's test was used to calculate the excess Gibbs energy, as shown in Eqs. 7 and 8.

$$\frac{g^E}{RT}=x_1(1-x_1)\sum_{k=1}^{n}a_kL_k(x_1) \qquad 7)$$

where

$$L_k(x_1)=[(2k-1)(2x_1-1)L_{k-1}(x_1)-(k-1)L_{k-2}(x_1)]/k \qquad 8)$$

The method uses the objective function (*OF*) as depicted in Eq. 9.

$$OF=\sum_{i=1}^{N}(P_i^{calc}-P_i^{\exp})^2 \qquad 9)$$

where the number of the data is signified by *N*; the calculated and experimental values for the pressure are represented as $P^{cal}$ and $P^{exp}$, respectively. The obtained excess Gibbs energy allows for the calculation of the activity coefficient and the vapor-phase mole fraction. For the pseudo-ternary mixtures, the calculated value of vapor-phase mole fraction was obtained from the NRTL correlation. The NRTL model incorporates temperature-dependent binary interaction parameters that provide a more accurate description for the VLE data containing an entrainer, wherein the liquid mixture exhibits non-ideal behavior. Conversely, the Legendre polynomial equation and its parameters are mathematical approximations that do not explicitly consider the interaction among the components in a complex mixture. This prevents the equation from accurately describing the pseudo-ternary mixture that exhibits non-ideal behavior. Thus, in the pseudo-ternary mixtures, the NRTL model is selected as it can more precisely represent the excess Gibbs energy to predict the vapor-phase mole fraction compared to the Legendre polynomial equation. As suggested by Wisniak[31], the criterion from Fredenslund should be complemented by a residual distribution analysis between the experimental and

calculated values of vapor-phase mole fraction or other variables, such as pressure, which should be random and close to the value of zero.[31–33] The use of Fredenslund's criterion utilizing the calculated values of vapor-phase mole fraction obtained from the activity coefficient model, such as NRTL, complemented by residual distribution analysis as a thermodynamic consistency test, has been implemented in existing literature.[32–34] In this work, the criterion from Fredenslund along with additional criteria proposed by Wisniak[31], was employed to evaluate the reliability of the VLE data for the pseudo-ternary mixtures. These criteria provide an adequate framework for examining thermodynamic consistency. Table 7 shows that the experimental VLE data of the investigated mixtures passed the thermodynamic consistency test since the average absolute deviation of the vapor-phase mole fraction is less than 0.01. Figure B11 and Figures B12 and B13, respectively, present the residual plots of vapor-phase mole fractions for the binary mixture and the pseudo-ternary mixtures. It indicates that the values are less than 0.01 in all composition ranges.

**Table 7.** Results of thermodynamic consistency tests[a,b]

| Mixture | Van Ness | | Fredenslund | | Results |
|---|---|---|---|---|---|
| | $\Delta y$ | $\Delta P$ | AAD $y$ | AAD $P$ (kPa) | |
| methylcyclohexane (1) + toluene (2) | 0.3 | 0.6 | 0.003 | 0.56 | Consistent |
| methylcyclohexane (1) + toluene (2) + GVL (3) | 0.6 | 0.9 | 0.006 | 0.92 | Consistent |
| methylcyclohexane (1) + toluene (2) + NMP (3) | 0.3 | 0.2 | 0.003 | 0.23 | Consistent |

[a] $\Delta y = \frac{1}{n_p} \times \sum_{i=1}^{n_p} \Delta y_i = \frac{1}{n_p} \times \sum_{i=1}^{n_p} 100 \left| y_i^{cal} - y_i^{\exp} \right| < 1;$

$\Delta P = \frac{1}{n_p} \times \sum_{i=1}^{n_p} \Delta P_i = \frac{1}{n_p} \times \sum_{i=1}^{n_p} 100 \left| \frac{P_i^{cal} - P_i^{\exp}}{P_i^{\exp}} \right| < 1$

[b] AAD $y = \frac{1}{n_p} \left\{ \sum_{i=1}^{n_p} \left| y_{i,\exp} - y_{i,cal} \right| \right\} \leq 0.01;$ AAD $P = \frac{1}{n_p} \left\{ \sum_{i=1}^{n_p} \left| P_{i,\exp} - P_{i,cal} \right| \right\}$

Moreover, the residual distribution and the average absolute deviation of the calculated and measured pressure are random and close to zero, respectively. The graphical representation of the pressure residual distribution can be seen in Figures B14, B15, and B16. These results indicate that the experimental value of VLE data for the investigated mixtures is reliable.

**Correlation for the VLE data**

Two thermodynamic models, namely NRTL and UNIQUAC, were chosen to correlate the VLE data. These thermodynamic models often provide a good agreement with the experimental data, making them favored choices among researchers for correlating the VLE data containing entrainers.[35–41] The NRTL formula is provided in Eq. 10 as follows:

$$\ln \gamma_i = \frac{\sum_{j=1}^{n_c} x_j \tau_{ji} G_{ji}}{\sum_{k=1}^{n_c} x_k G_{ki}} + \sum_{j=1}^{n_c} \frac{x_j G_{ij}}{\sum_{k=1}^{N} x_k G_{kj}} \left( \tau_{ij} - \frac{\sum_{m=1}^{n_c} x_m \tau_{mj} G_{mj}}{\sum_{k=1}^{n_c} x_k G_{kj}} \right) \quad 10)$$

Where $\gamma_i$ and $n_c$ is the activity coefficient of component *i* and the number of components, respectively. The parameters in the NRTL model are formulated in Eq. 11, as follows:

$$G_{ij} = \exp(-C_{ij}\tau_{ij});\ \tau_{ij} = A_{ij} + B_{ij}/T;\ \tau_{ii} = 0;\ G_{ii} = 1 \quad 11)$$

Where $C_{ij}$ represents the non-randomness constant in the binary component interaction of *ij*.

For the UNIQUAC model, the formula is expressed by Eq. 12.

$$\ln \gamma_i = \ln \frac{\Phi_i}{x_i} + \frac{z}{2} q_i \ln \frac{\theta_i}{\Phi_i} + l_i - \frac{\Phi_i}{x_i} \sum_{j=1}^{n_c} x_j l_j - q_i \ln\left(\sum_{j=1}^{n_c} \theta_j \tau_{ji}\right) + q_i - q_i \sum_{j=1}^{n_c} \frac{\theta_j \tau_{ij}}{\sum_{k=1}^{n_c} \theta_k \tau_{kj}} \quad 12)$$

Where $\theta_i$ and $\Phi_i$ indicate the average of area and volume fractions of component *i*, respectively; $r_i$ and $q_i$ correspond to the parameters of volume and surface area of component *i*, respectively; and *z* denotes the number of lattice coordination. The parameters $r_i$ and $q_i$ are retrieved from the Aspen Plus physical property databank and provided in Table 8. The parameters in the UNIQUAC model are expressed in Eq. 13.

**Table 8.** Parameters of pure components for $r_i$ and $q_i$ in UNIQUAC model[a,b]

| component | $r_i$ | $q_j$ |
|---|---|---|
| methylcyclohexane | 4.64 | 3.55 |
| toluene | 3.92 | 2.97 |
| gamma-valerolactone | 3.71 | 3.04 |
| 1-methylpyrrolidin-2-one | 3.98 | 3.20 |

[a] $r_i$ is the volume parameter of component *i*; $q_i$ is the surface area parameter of component *i*.

[b]Taken from the Aspen Plus physical property databank.

$$\tau_{ij} = \exp\left(A_{ij} + B_{ij}/T\right);\ \ l_i = \frac{z}{2}(r_i - q_i) - (r_i - 1);\ \ \Phi_i = \frac{r_i x_i}{\sum_{j=1}^{n_c} r_j x_j};\ \ \theta_i = \frac{x_i q_i}{\sum_{j=1}^{n_c} x_j q_j};\ \ z = 10 \qquad 13)$$

The binary interaction parameters (BIPs) for the methylcyclohexane-toluene pair were determined from the regression of the VLE data for the binary mixture of methylcyclohexane and toluene at two different pressures: 101.3 kPa (this work) and 53.3 kPa (literature[25]). These BIPs are subsequently employed in the regression of pseudo-ternary mixtures of methylcyclohexane and toluene with the addition of GVL and NMP, respectively, in which the VLE data for methylcyclohexane (1) + toluene (2) + GVL (3) was measured from 50 to 100 kPa. Thus, the regression was performed on the binary mixture under both normal and low pressures in order to encompass the temperature range within the investigated pseudo-ternary mixture of methylcyclohexane (1) + toluene (2) + GVL (3). In the NRTL model, the non-randomness parameter ($C_{ij}$) for the binary and pseudo-ternary mixtures regression were assigned a value of 0.3. The algorithm with the maximum likelihood concept proposed by Britt and Luecke[42] was employed to minimize the objective function in order to determine the BIPs. The objective function (*OF*) formula is shown in Eq. 14.

$$OF = \sum_{k=1}^{n_p} \left\{ \left| \frac{P_k^{cal} - P_k^{\exp}}{\sigma_P} \right|^2 + \left| \frac{T_k^{cal} - T_k^{\exp}}{\sigma_T} \right|^2 + \left| \frac{x_{1,k}^{cal} - x_{1,k}^{\exp}}{\sigma_x} \right|^2 + \left| \frac{y_{1,k}^{cal} - y_{1,k}^{\exp}}{\sigma_y} \right|^2 \right\} \qquad 14)$$

Where $n_p$ represents the number of data points and $\sigma$ defines the standard deviation of the data. The optimal values of the BIPs for all pairs in the NRTL and UNIQUAC models are reported in Table 9.

**Table 9.** Binary interaction parameters of the NRTL and UNIQUAC models for methylcyclohexane (1) + toluene (2) + gamma-valerolactone (3) and methylcyclohexane (1) + toluene (2) + 1-methylpyrrolidin-2-one (3)[a]

| *i* component | *j* component | $A_{ij}$ | $A_{ji}$ | $B_{ij}$/K | $B_{ji}$/K | $C_{ij}$ |
|---|---|---|---|---|---|---|
| | | NRTL[b] | | | | |
| [d]methylcyclohexane (1) | toluene (2) | -1.018 | 2.709 | 792.083 | -1248.381 | 0.30 |
| methylcyclohexane (1) | gamma-valerolactone (2) | 3.396 | -8.614 | -672.438 | 3617.877 | 0.30 |
| toluene (1) | gamma-valerolactone (2) | 0.208 | -1.592 | 5066.002 | 703.426 | 0.30 |
| methylcyclohexane (1) | 1-methylpyrrolidin-2-one (2) | -3.548 | 4.113 | 1979.856 | 394.855 | 0.30 |
| toluene (1) | 1-methylpyrrolidin-2-one (2) | 13.533 | 13.858 | -5223.890 | -3020.539 | 0.30 |

| *i* component | *j* component | $A_{ij}$ | $A_{ji}$ | $B_{ij}$/K | $B_{ji}$/K | $C_{ij}$ |
|---|---|---|---|---|---|---|
| | | UNIQUAC[c] | | | | |
| [d]methylcyclohexane (1) | toluene (2) | 0.324 | -0.769 | -363.296 | 446.877 | - |
| methylcyclohexane (1) | gamma-valerolactone (2) | -1.991 | 1.183 | 341.007 | -387.553 | - |
| toluene (1) | gamma-valerolactone (2) | -1.219 | 0.318 | 155.438 | -15.592 | - |
| methylcyclohexane (1) | 1-methylpyrrolidin-2-one (2) | 8.904 | -14.505 | -3571.259 | 5452.163 | - |
| toluene (1) | 1-methylpyrrolidin-2-one (2) | -0.647 | -5.553 | 403.434 | 1791.435 | - |

[a]$A_{ij}$, $A_{ji}$, $B_{ij}$, and $B_{ji}$ are unsymmetrical parameters; $C_{ij}$ is the non-randomness constant.

[b]NRTL Model: $\tau_{ij} = A_{ij} + B_{ij} / T$

[c]UNIQUAC Model: $\tau_{ij} = \exp\left(A_{ij} + B_{ij} / T\right)$

[d]The binary interaction parameters of methylcyclohexane (1) – toluene (2) pair were obtained from the correlation based on the combination of the binary VLE data measured in this work and literature[25].

The average absolute deviation between the experimental and regression values is provided in Table 10. Both models give a satisfactory fit to the experimental data for the regression of the binary mixture of methylcyclohexane (1) + toluene (2), as illustrated in Figure 2. This is also confirmed by the small deviation between the experimental and regression results presented in Table 10.

**Table 10.** Average absolute deviation (AAD) from the correlated results using NRTL and UNIQUAC models[a]

| | AAD[b] | | | |
|---|---|---|---|---|
| | *T*/K | *P*/kPa | $x_1$' | $y_1$ |
| methylcyclohexane (1) + toluene (2) | | | | |
| NRTL | 0.02 | 0.56 | 0.003 | 0.003 |
| UNIQUAC | 0.03 | 0.45 | 0.004 | 0.004 |
| methylcyclohexane (1) + toluene (2) + gamma-valerolactone (3) | | | | |
| NRTL | 0.36 | 0.92 | 0.002 | 0.006 |
| UNIQUAC | 0.31 | 2.13 | 0.003 | 0.009 |
| methylcyclohexane (1) + toluene (2) + 1-methylpyrrolidin-2-one (3) | | | | |
| NRTL | 0.07 | 0.23 | 0.001 | 0.003 |
| UNIQUAC | 0.09 | 0.31 | 0.001 | 0.001 |

[a]*T* is the temperature; *P* is the pressure; $x_1$' is a liquid-phase mole fraction of methylcyclohexane on an entrainer-free basis; $y_1$ is a vapor-phase mole fraction of methylcyclohexane.

[b]Average absolute deviation (AAD) $\Delta M = \frac{1}{n}\sum\left|M_{\exp} - M_{cal}\right|$, where *n* is total of data points; *M* denotes for *T*, *P*, $x_1$', and $y_1$, respectively.

For the pseudo-ternary mixture of methylcyclohexane (1) + toluene (2) + GVL (3), the VLE data with E/F = 1 at the pressures of 50, 80, and 100 kPa and E/F = 2 and 3 at the pressure of 100 kPa were correlated together as one regression in order to achieve more accurate BIPs to represent the experimental VLE data. The NRTL and UNIQUAC models provided satisfactorily results. However, the NRTL model performed better than the UNIQUAC model in representing the experimental VLE data for the regression of the pseudo-ternary mixture comprising GVL, as indicated by the smaller average absolute deviation listed in Table 10. Moreover, the graphical depiction in Figures 3 and 4 illustrate that the correlation results obtained from the NRTL model exhibit a better agreement with the experimental data compared to the regression results obtained from the UNIQUAC model. This suggests that the NRTL model provides a good quantitative correlation in the pseudo-ternary mixture of methylcyclohexane and toluene containing GVL. Hence, the NRTL model can be employed for modeling the extractive distillation process for the pseudo-ternary mixture of methylcyclohexane and toluene with the GVL as an entrainer. Figures 5 and 6 display the *x*'-*y*' diagram, where only the regression result from the NRTL model is provided and compared with the experimental value with a good agreement.

In the regression of pseudo-ternary mixtures of methylcyclohexane and toluene containing NMP, the NRTL and UNIQUAC models both yield good regression results. The NRTL model yields a slightly better accuracy for correlating the experimental data compared to the UNIQUAC model, as shown by the average absolute deviation listed in Table 10 and represented by Figure 7. However, the deviation between the NRTL and UNIQUAC models is not significant. Therefore, both models are recommended to be applied for process modeling in extractive distillation. The NRTL regression results are further deployed to show an *x*'-*y*' diagram between the experimental and regression values for a mixture of methylcyclohexane and toluene with the addition of NMP, as illustrated in Figure 8.

## References


(1) Ye, L.; Han, Y.; Feng, J.; Lu, X. A Review about GVL Production from Lignocellulose: Focusing on the Full Components Utilization. *Ind. Crops Prod.* **2020**, *144*, 112031. https://doi.org/https://doi.org/10.1016/j.indcrop.2019.112031.

(2) Strappaveccia, G.; Luciani, L.; Bartollini, E.; Marrocchi, A.; Pizzo, F.; Vaccaro, L. γ-Valerolactone as an Alternative Biomass-Derived Medium for the Sonogashira Reaction. *Green Chem.* **2015**, *17* (2), 1071–1076. https://doi.org/10.1039/C4GC01728E.

(3) Duereh, A.; Sato, Y.; Smith, R. L. J.; Inomata, H. Methodology for Replacing Dipolar Aprotic Solvents Used in API Processing with Safe Hydrogen-Bond Donor and Acceptor Solvent-Pair Mixtures. *Org. Process Res. Dev.* **2017**, *21* (1),

114–124. https://doi.org/10.1021/acs.oprd.6b00401.
(4) Havasi, D.; Mizsey, P.; Mika, L. T. Vapor–Liquid Equilibrium Study of the Gamma-Valerolactone–Water Binary System. *J. Chem. Eng. Data* **2016**, *61* (4), 1502–1508. https://doi.org/10.1021/acs.jced.5b00849.
(5) Stull, D. R. Vapor Pressure of Pure Substances. Organic and Inorganic Compounds. *Ind. Eng. Chem.* **1947**, *39* (4), 517–550. https://doi.org/10.1021/ie50448a022.
(6) Alonso, D. M.; Wettstein, S. G.; Dumesic, J. A. Gamma-Valerolactone, a Sustainable Platform Molecule Derived from Lignocellulosic Biomass. *Green Chem.* **2013**, *15* (3), 584–595. https://doi.org/10.1039/C3GC37065H.
(7) Wong, C. Y. Y.; Choi, A. W.-T.; Lui, M. Y.; Fridrich, B.; Horváth, A. K.; Mika, L. T.; Horváth, I. T. Stability of Gamma-Valerolactone under Neutral, Acidic, and Basic Conditions. *Struct. Chem.* **2017**, *28* (2), 423–429. https://doi.org/10.1007/s11224-016-0887-6.
(8) De Bruycker, R.; Carstensen, H.-H.; Simmie, J. M.; Van Geem, K. M.; Marin, G. B. Experimental and Computational Study of the Initial Decomposition of Gamma-Valerolactone. *Proc. Combust. Inst.* **2015**, *35* (1), 515–523. https://doi.org/https://doi.org/10.1016/j.proci.2014.04.001.
(9) Coca, J.; Pis, J. J. Effect of Morpholine on the Vapor-Liquid Equilibrium of the System Methylcyclohexane-Toluene. *J. Chem. Eng. Data* **1979**, *24* (2), 103–105. https://doi.org/10.1021/je60081a017.
(10) Brouwer, T.; Schuur, B. Bio-Based Solvents as Entrainers for Extractive Distillation in Aromatic/Aliphatic and Olefin/Paraffin Separation. *Green Chem.* **2020**, *22* (16), 5369–5375. https://doi.org/10.1039/D0GC01769H.
(11) Liebert, V.; Nebig, S.; Gmehling, J. Experimental and Predicted Phase Equilibria and Excess Properties for Systems with Ionic Liquids. *Fluid Phase Equilib.* **2008**, *268* (1), 14–20. https://doi.org/https://doi.org/10.1016/j.fluid.2008.03.011.
(12) Gutierrez, J. P.; Meindersma, W.; de Haan, A. B. Ionic Liquid Selection and Performance Evaluation for The Separation Of Methylcyclohexane/Toluene by Extractive Distillation. In *Distillation absorption 2010 : conference proceedings*; Technische Universiteit Eindhoven: Eindhoven, 2010.
(13) Quijada-Maldonado, E.; Meindersma, G. W.; de Haan, A. B. Pilot Plant Study on the Extractive Distillation of Toluene–Methylcyclohexane Mixtures Using NMP and the Ionic Liquid [Hmim][TCB] as Solvents. *Sep. Purif. Technol.* **2016**, *166*, 196–204. https://doi.org/https://doi.org/10.1016/j.seppur.2016.04.041.
(14) Anwani, S. S.; Shirsat, S. P. Extractive Distillation Simulation for the Separation of Methylcyclohexane and Toluene Mixture with Phenol as an Extractor Using Chemcad. In *Novel Water Treatment and Separation Methods: Simulation of Chemical Processes*; Bhanvase, B. A., Ugwekar, R. P., Mankar, R. B., Eds.; Apple Academic Press, Taylor & Francis Group: New York, 2017. https://doi.org/https://doi.org/10.1201/9781315225395.
(15) Tiverios, P. G.; Van Brunt, V. Extractive Distillation Solvent Characterization and Shortcut Design Procedure for Methylcyclohexane−Toluene Mixtures. *Ind. Eng. Chem. Res.* **2000**, *39* (6), 1614–1623. https://doi.org/10.1021/ie990654k.
(16) Van Ness, H. C. Thermodynamics in the Treatment of Vapor/Liquid Equilibrium (VLE) Data. **1995**, *67* (6), 859–872. https://doi.org/doi:10.1351/pac199567060859.
(17) Fredenslund, A. *Vapor-Liquid Equilibria Using UNIFAC: A Group-Contribution*

*Method*; Elsevier, 1977.
(18) Renon, H.; Prausnitz, J. Local Compositions in Thermodynamic Excess Functions for Liquid Mixtures. *AIChE J.* **1968**, *14* (1), 135–144. https://doi.org/10.1002/aic.690140124.
(19) Abrams, D. S.; Prausnitz, J. M. Statistical Thermodynamics of Liquid Mixtures: A New Expression for the Excess Gibbs Energy of Partly or Completely Miscible Systems. *AIChE J.* **1975**, *21* (1), 116–128. https://doi.org/https://doi.org/10.1002/aic.690210115.
(20) Taylor, Barry N; Kuyatt, C. E. NIST Technical Note 1297 Guidelines for Evaluating and Expressing the Uncertainty of NIST Measurement Results. *Technology* **1994**.
(21) *Evaluation of Measurement Data — Guide to the Expression of Uncertainty in Measurement*; Working Group 1 of the Joint Committee for Guides in Metrology (JCGM/WG 1); 2008. https://www.bipm.org/documents/20126/2071204/JCGM_100_2008_E.pdf.
(22) Quiggle, D.; Fenske, M. R. Vapor—Liquid Equilibria of Methylcyclohexane—Toluene Mixtures. *J. Am. Chem. Soc.* **1937**, *59* (10), 1829–1832. https://doi.org/10.1021/ja01289a012.
(23) Yaws, C. L.; H.C., Y. To Estimate Vapor Pressure Easily. Antoine Coefficients Relate Vapor Pressure to Temperature for Almost 700 Major Organic Compounds. *Hydrocarb. Process.* **1989**, *68* (10), 65–68.
(24) Willingham, C. B.; Taylor, W. J.; Pignocco, J. M.; Rossini, F. D. Vapor Pressures and Boiling Points of Some Paraffin, Alkylcyclopentane, Alkylcyclohexane, and Alkylbenzene Hydrocarbons. *J. Res. Natl. Bur. Stand. (1934).* **1945**, *35* (3), 219–244.
(25) Weber, J. H. Vapor-Liquid Equilibria for System Methylcyclohexane-Toluene at Subatmospheric Pressures. *Ind. Eng. Chem.* **1955**, *47* (3), 454–457. https://doi.org/10.1021/ie50543a036.
(26) Al-Lami, M.; Havasi, D.; Koczka, K.; Mika, L. T. Isobaric Vapor–Liquid Equilibria for Binary Mixtures of Gamma-Valerolactone + Toluene. *J. Chem. Eng. Data* **2021**, *66* (1), 568–574. https://doi.org/10.1021/acs.jced.0c00791.
(27) Gupta, S. K.; Rawat, B. S. Isobaric Binary and Ternary Vapor-Liquid Equilibria of N-Methylpyrrolidone with Water and Toluene at 760 MmHg. *J. Chem. Eng. Data* **1992**, *37* (2), 139–140. https://doi.org/10.1021/je00006a001.
(28) Zaretskii, M. I.; Kogan, V. B.; Kononov, N. F.; MiroshniChenko, A. A.; Usyushkina, I. V; Podolyak, V. G. Liquid—Vapor Equilibrium in Systems Formed by Aromatic Hydrocarbons and Thiophene with Some Polar Solvents. *J. Appl. Chem. USSR* **1974**, *47* (9), 2142–2145.
(29) Gierycz, P.; Rogalski, M.; Malanowski, S. Vapour—Liquid Equilibria in Binary Systems Formed by N-Methylpyrrolidone with Hydrocarbons and Hydroxyl Derivatives. *Fluid Phase Equilib.* **1985**, *22* (1), 107–122. https://doi.org/https://doi.org/10.1016/0378-3812(85)87014-X.
(30) Linek, J.; Wichterle, I.; Marsh, K. N. Vapor−Liquid Equilibria for N-Methyl-2-Pyrrolidone + Benzene, +Toluene, +Heptane, and +Methylcyclohexane. *J. Chem. Eng. Data* **1996**, *41* (6), 1212–1218. https://doi.org/10.1021/je9601826.
(31) Wisniak, J.; Ortega, J.; Fernández, L. A Fresh Look at the Thermodynamic Consistency of Vapour-Liquid Equilibria Data. *J. Chem. Thermodyn.* **2017**, *105*, 385–395. https://doi.org/https://doi.org/10.1016/j.jct.2016.10.038.

(32) Huo, B.; Qiu, X.; Zhang, H.; Zhang, Y.; Yang, J.; Zhu, Z.; Wang, Y.; Gao, J. Isobaric Vapor–Liquid Equilibrium of Isoamyl Alcohol, Cyclohexane, n-Hexane, and the n-Heptane + Isoamyl Butyrate Binary System at 101.3 KPa. *J. Chem. Eng. Data* **2021**, *66* (12), 4476–4483. https://doi.org/10.1021/acs.jced.1c00555.
(33) Zhou, M.; Hu, R.; Qiu, Z.; Jiao, M.; Zhu, Z.; Wang, Y.; Cui, P.; Yang, J. Isobaric Vapor–Liquid Equilibrium of Ethyl Acetate + 1-Hexanol, Methanol + 1-Hexanol, and n-Heptane + Cyclohexanol Binary System at 101.3 KPa. *J. Chem. Eng. Data* **2023**, *68* (8), 2014–2022. https://doi.org/10.1021/acs.jced.3c00245.
(34) Wang, L.; Zhao, H.; Han, L.; Wang, Y.; Xin, J. Isobaric Vapor–Liquid Equilibrium of Binary Mixtures of 2-Methylpentanedioic Acid Dimethyl Ester and Dimethyl Adipate at 101.3, 50.0, 30.0, and 10.0 KPa. *J. Chem. Eng. Data* **2024**, *69* (4), 1613–1620. https://doi.org/10.1021/acs.jced.3c00665.
(35) Li, F.; Li, M.; Guo, J.; Hu, X.; Zhu, J.; Li, Q.; Zhao, H. Isobaric Vapor–Liquid Equilibrium Experiment of N-Propanol and N-Propyl Acetate at 101.3 KPa. *J. Chem. Eng. Data* **2023**, *68* (2), 358–365. https://doi.org/10.1021/acs.jced.2c00609.
(36) Cao, M.; Tian, H.; Li, M. Vapor–Liquid Equilibrium Data Determination and Model Correlation for 1-Octene + 1,4-Dioxane, 2-Octanol + 1,4-Dioxane, 1-Octene + Isophorone, and 2-Octanol + Isophorone Systems at 101.3 KPa. *J. Chem. Eng. Data* **2023**, *68* (9), 2275–2282. https://doi.org/10.1021/acs.jced.3c00136.
(37) Lei, Z.; Arlt, W.; Wasserscheid, P. Selection of Entrainers in the 1-Hexene/n-Hexane System with a Limited Solubility. *Fluid Phase Equilib.* **2007**, *260* (1), 29–35. https://doi.org/https://doi.org/10.1016/j.fluid.2006.06.009.
(38) Zhang, Z.; Zhang, Z.; Dong, B.; Chen, J.; Xin, H.; Zhang, Q. Vapor-Liquid Equilibrium Experiment and Model Prediction for Separating Ethyl Propionate and Ethanol Using Ionic Liquids with Acetate Anion. *J. Mol. Liq.* **2020**, *318*, 113688. https://doi.org/https://doi.org/10.1016/j.molliq.2020.113688.
(39) Yang, C.; Zeng, H.; Yin, X.; Ma, S.; Sun, F.; Li, Y.; Li, J. Measurement of (Vapor+liquid) Equilibrium for the Systems {methanol+dimethyl Carbonate} and {methanol+dimethyl Carbonate+tetramethylammonium Bicarbonate} at P=(34.43, 67.74)KPa. *J. Chem. Thermodyn.* **2012**, *53*, 158–166. https://doi.org/https://doi.org/10.1016/j.jct.2012.05.002.
(40) Zhang, Y.; Wang, Z.; Xu, X.; Gao, J.; Xu, D.; Zhang, L.; Wang, Y. Entrainers Selection and Vapour-Liquid Equilibrium Measurements for Separating Azeotropic Mixtures (Ethanol + n-Hexane/Cyclohexane) by Extractive Distillation. *J. Chem. Thermodyn.* **2020**, *144*, 106070. https://doi.org/https://doi.org/10.1016/j.jct.2020.106070.
(41) He, S.; Fan, W.; Huang, H.; Gao, J.; Xu, D.; Ma, Y.; Zhang, L.; Wang, Y. Separation of the Azeotropic Mixture Methanol and Toluene Using Extractive Distillation: Entrainer Determination, Vapor–Liquid Equilibrium Measurement, and Modeling. *ACS Omega* **2021**, *6* (50), 34736–34743. https://doi.org/10.1021/acsomega.1c05164.
(42) Britt, H. I.; Luecke, R. H. The Estimation of Parameters in Nonlinear, Implicit Models. *Technometrics* **1973**, *15* (2), 233–247. https://doi.org/10.2307/1266984.

## 3.2. VLE data of methylcyclohexane-toluene with dimethyl isosorbide and 1-butylpyrrolidin-2-one


### Abstract

In this work, dimethyl isosorbide (DMI) and 1-butylpyrrolidin-2-one (NBP), as bio-based and greener organic solvents, were used for the first time as entrainers in extractive distillation to separate a close–boiling mixture of methylcyclohexane–toluene. Vapor–liquid equilibrium (VLE) data were collected for pseudo–ternary mixtures consisting of methylcyclohexane and toluene with the presence of DMI and NBP at various entrainer-to-feed ratios (E/F) and pressures. The VLE measurements were conducted using a Fischer Labodest VLE602 ebulliometer, and the thermodynamic consistency of the data was verified using the Van Ness test. Both DMI and NBP were found to increase the relative volatility of methylcyclohexane to toluene, successfully eliminating close–boiling behaviour. Compared to benchmark entrainers, both outperformed NMP and sulfolane in certain conditions. In comparison with other green entrainers, DMI and NBP showed similar performance to gamma-valerolactone (GVL) and Cyrene under specific conditions. The VLE data were accurately correlated using the nonrandom two-liquid (NRTL) model.


.

### 3.2.1. Introduction

Despite the increasing emphasis on green solvents, certain promising greener alternative entrainers are dimethyl isosorbide (DMI) as a biobased solvent and 1-butylpyrrolidin-2-one (NBP), also known as TamiSolve® NxG, as a greener organic solvent. These solvents remain largely unexplored as entrainers in extractive distillation. The absence of the experimental VLE data and BIPs for the methylcyclohexane and toluene in the presence of DMI and NBP limits the development of accurate and reliable extractive distillation processes. Given their potential as greener entrainers, employing these solvents could lead to more sustainable and greener extractive distillation. This work aims to fill this important VLE data and the knowledge gap.

Our previous study indicated that both solvents show favorable relative volatility for separating methylcyclohexane from toluene. This is based on prediction results obtained from group contributions methods and unimolecular quantum chemical calculations.[1] Regarding the greener properties, DMI can be readily synthesized from isosorbide, which is the product derived from sorbitol. DMI can also be directly produced from d-sorbitol.[2] Sorbitol, as one of the sugar alcohols, can naturally be found in fruits and plants.[3] In addition, it is commercially manufactured through hydrogenation of glucose or sucrose.[4] DMI exhibits environmentally favorable characteristics, including nontoxicity, biodegradability, high–water solubility, and sustainability.[5] DMI was also listed among the top ten biobased solvents.[6] The toxicity of DMI is significantly lower than that of NMP. The acute oral toxicity values in rats, expressed as LD50 (Lethal Dose for 50% of population), are 6530.8 mg/kg body weight for DMI and 4150 mg/kg body weight for NMP. A higher LD50 value indicates lower toxicity. Additionally, DMI is categorized as very slightly irritating to skin and eyes and nonirritating to ears. Some reports have also shown that DMI is nongenotoxic, as it was found not to be mutagenic to both mammalian cells and bacteria. Furthermore, DMI is classified as nonreprotoxic, with no observed harmful effects on maternal health and embryo–fetal development.[7–10]

Furthermore, DMI possesses advantageous properties, such as noncorrosive, nonflammable, a high boiling point ($T_b$= 513.15 K at 101.3 kPa), low vapor pressure (0.11 kPa at 293.15 K), and a high decomposition temperature (>513.15 K).[8,11] DMI has a higher hydrogen bonding potential (Hansen Solubility Parameters (HSPs) for hydrogen bonding ($\delta_h$) = 7.5 $MPa^{1/2}$) compared to NMP ($\delta_h$ = 7.2 $MPa^{1/2}$),[12,13] which makes it a promising entrainer candidate for extractive distillation. NBP is another highly promising environmentally friendly entrainer. NBP is a high-boiling point organic and polar aprotic solvent ($T_b$ = 514.15 K at 101.3 kPa) with good thermal and chemical stability (temperature decomposition is above 514.15 K), high–water solubility, low vapor pressure (0.013 kPa at 298.15

K), and is a noncorrosive solvent.[14,15] NBP has promising polarity (HSPs for polarity ($\delta_P$) = 8.2 $MPa^{1/2}$), which is slightly lower compared to the polarity of NMP ($\delta_P$ = 12.3 $MPa^{1/2}$).[13,14] According to the European Chemical Agency (ECHA) and Economic Co-operation and Development (OECD) test method, NBP is classified as an inherently biodegradable solvent with low hazard potential and nonmutagenic properties and does not have reprotoxicity[16,17] as conventional solvents, such as NMP, which is categorized as a reprotoxic solvent reported by OECD.[18] NBP demonstrates lower toxicity on fetal development compared to NMP, as evidenced by its higher value of No Observed Adverse Effect Level (NOAEL) for over 500 mg/kg body weight/day, in contrast to NMP's NOAEL of 160 mg/kg body weight/day.[9,19] These NOAEL values represent the highest dose of substance that does not cause any harmful effects on fetal development. This indicates that a higher NOAEL value reflects lower toxicity. Therefore, NBP can be considered a greener solvent than NMP. In spite of these advantages of DMI and NBP over conventional solvents, they have not been examined for use as entrainers in extractive distillation processes through VLE data measurements. Therefore, DMI and NBP were selected as entrainers in this study.

In addition, effective design of extractive distillation requires reliable VLE data as a thermodynamic package. Despite its importance, there is currently no available VLE data for the methylcyclohexane and toluene mixture in the presence of the entrainers DMI and NBP, respectively. Recently, researchers have examined VLE data of a methylcyclohexane and toluene mixture with the addition of entrainers, such as sulfolane, Cyrene™,[20] morpholine,[21] gamma-valerolactone (GVL), 1-methylpyrrolidin-2-one,[22] and ionic liquid 1-hexyl-3-methyl-imidazolium bis(trifluoromethylsulfonyl)imide.[23] Several studies for the separation of a methylcyclohexane and toluene mixture using extractive distillation through process simulation and a pilot plant have been conducted using entrainers, such as ionic liquid of 1-hexyl-3-methylimidazolium tetracyanoborate ([hmim][TCB]) and NMP,[24] ionic liquids of 1-hexyl-3-methylimidazolium tetracyanoborate and 1-butyl-3-methylimidazolium tetracyanoborate, NMP,[25] and phenol.[26] In addition, Tiverios and Van Brunt evaluated extractive distillation through process simulation to separate methylcyclohexane from toluene using some entrainers, such as propylene glycol, aniline, methyl n-amyl ketone, phenol, dimethylformamide (DMF), acetophenone, *o*-cresol, furfural, and cyclohexane.[27]

This work aimed to assess the effectiveness of DMI and NBP as entrainers in the separation of methylcyclohexane from toluene using extractive distillation. This was achieved by performing VLE data measurements for the pseudo–ternary mixtures of methylcyclohexane and toluene in the presence of DMI and NBP. The relative volatility performance of DMI and NBP was compared to that of NMP and sulfolane as benchmark entrainers and GVL and Cyrene as alternative green

entrainers. The reliability of the VLE data was evaluated using the Van Ness thermodynamic consistency test.[28] Moreover, the NRTL model was implemented for the VLE data correlation in order to determine the optimum binary interaction parameters (BIPs) for the studied mixtures.

### 3.2.2. Experimental methods

#### Chemicals

Chemicals used in this study were acquired from commercial companies. The purity of the chemicals was determined using gas chromatography (GC). All chemicals were used in their original form without undergoing any further purifying procedures, as no notable contaminants were found. Table 1 provides a detailed specification of chemicals.

**Table 1.** Material specifications

| chemicals | CAS number | molecular weight (g/mol) | $T_{boiling}$ (K)[a,b] | density (g/cm$^3$)[a,c] | companies | purity (mass fraction)[a] | method of purity analysis | method of purification |
|---|---|---|---|---|---|---|---|---|
| methylcyclohexane | 108-87-2 | 98.19 | 374.15 | 0.770 | Sigma-Aldrich | ≥0.990 | GC[d] | none |
| toluene | 108-88-3 | 92.14 | 383.15 | 0.865 | Sigma-Aldrich | 0.999 | GC[d] | none |
| dimethyl isosorbide | 5306-85-4 | 174.19 | 513.15 | 1.167 | Sigma-Aldrich | ≥0.990 | GC[d] | none |
| 1-butylpyrrolidin-2-one | 3470-98-2 | 141.21 | 514.15 | 0.960 | BioPSX | 0.995 | GC[d] | none |
| acetone | 67-64-1 | 58.08 | 329.15 | 0.791 | Merck | ≥0.998 | GC[d] | none |

[a]Specified by the companies

[b]At 101.3 kPa

[c]At 298.15 K and 101.3 kPa

[d]Gas chromatography (GC)

#### Experimental procedures and analytical methods

The detailed experimental procedures and analytical methods for the VLE data measurements are provided in Chapter 2. The Joint Committee for Guides in Metrology (JCGM)[29] and the NIST Technical Note 1297[30] were used as a basis for the calculation of the standard uncertainty for a liquid– and a vapor–phase composition as well as for temperature and pressure. The detailed standard uncertainty calculations are described in Appendix C (Eqs. C1-C3). Each table of the VLE data in Supporting Information includes the standard uncertainty values.

### 3.2.3 Results and discussion

**Experimental results**

The reliability of the apparatus and methods employed in this study has been confirmed in our previous work.[22] As depicted in Figure C1, the VLE data for the binary mixture of methylcyclohexane and toluene at lower pressures of 26.7 and 53.3 kPa acquired from literature[31] were used together with the VLE data at 101.3 kPa from our prior work[22] to obtain the BIPs of the methylcyclohexane–toluene pair. In addition, Figure C2 shows that the profile of close–boiling in the binary mixture of methylcyclohexane and toluene remains unaltered when the pressure is reduced from 101.3 kPa to 53.3 and 26.7 kPa.

In this work, the VLE data were measured for the pseudo–ternary mixtures of methylcyclohexane and toluene with entrainers of dimethyl isosorbide (DMI) and 1-butylpyrrolidin-2-one (NBP), respectively. For each pseudo–ternary mixture, entrainer-to-feed ratio (E/F) = 1 at pressures of 10.0 and 100.0 kPa and E/F = 3 at a pressure of 10.0 kPa were investigated. E/F quantifies as the mass ratio of the entrainer introduced to the binary mixture, calculated as the entrainer's mass divided by the binary mixture's mass. The VLE measurement was conducted at a pressure of 100.0 kPa instead of 101.3 kPa because the pressure in our laboratory fluctuated from 100.0 to 101.3 kPa. Consequently, a pressure of 100.0 kPa was selected as it facilitated more precise pressure control in the setup. A pressure of 10.0 kPa was selected to obtain higher relative volatility in the pseudo–ternary mixtures. The experimental results for the pseudo–ternary mixture of methylcyclohexane and toluene involving DMI entrainer with E/F = 1 at pressures of 10.0 and 100.0 kPa are depicted in Table 2, while those with E/F = 3 at a pressure of 10.0 kPa are provided in Table 3. The mole fraction of methylcyclohexane in a liquid phase on an excluded-entrainer basis and in a vapor phase was expressed by $x_1$' and $y_1$, respectively. The mole fractions in the liquid phase for methylcyclohexane, toluene, and entrainer are represented as $x_1$, $x_2$, and $x_3$, respectively. In the vapor phase, the mole fractions for methylcyclohexane, toluene, and entrainer are denoted as $y_1$, $y_2$, and $y_3$, respectively. While the temperature at equilibrium, the activity coefficient of methylcyclohexane, the activity coefficient of toluene, and the relative volatility of methylcyclohexane to toluene are expressed by $T$, $\gamma_1$, $\gamma_2$, and $\alpha_{12}$, respectively. As the entrainer was not observed in the vapor phase, its vapor–phase mole fraction is considered less than 0.0005. Therefore, in Tables 2-5, the corresponding values ($y_3$) are reported as 0.000 for clarity and consistency.

**Table 2.** Experimental VLE data for methylcyclohexane (1) + toluene (2) + dimethyl isosorbide (3) at E/F = 1 and pressure of 10.0 and 100.0 kPa[a,b,c]

| *T*/K | $x_1'$ | $x_1$ | $x_2$ | $x_3$ | $y_1$ | $y_2$ | $y_3$ | $\gamma_1$ | $\gamma_2$ | $\alpha_{12}$ |
|---|---|---|---|---|---|---|---|---|---|---|
| ***10.0 kPa*** | | | | | | | | | | |
| 331.98 | 0.000 | 0.000 | 0.651 | 0.349 | 0.000 | 1.000 | 0.000 | - | 0.871 | - |
| 329.37 | 0.056 | 0.037 | 0.616 | 0.347 | 0.148 | 0.852 | 0.000 | 1.695 | 0.872 | 2.93 |
| 327.19 | 0.111 | 0.072 | 0.573 | 0.355 | 0.273 | 0.727 | 0.000 | 1.752 | 0.874 | 3.01 |
| 325.37 | 0.175 | 0.113 | 0.531 | 0.356 | 0.385 | 0.615 | 0.000 | 1.687 | 0.861 | 2.95 |
| 324.06 | 0.233 | 0.149 | 0.487 | 0.364 | 0.470 | 0.530 | 0.000 | 1.645 | 0.855 | 2.92 |
| 322.70 | 0.305 | 0.196 | 0.442 | 0.362 | 0.559 | 0.441 | 0.000 | 1.572 | 0.829 | 2.89 |
| 321.65 | 0.360 | 0.228 | 0.402 | 0.370 | 0.620 | 0.380 | 0.000 | 1.562 | 0.823 | 2.90 |
| 320.22 | 0.485 | 0.316 | 0.331 | 0.353 | 0.715 | 0.285 | 0.000 | 1.378 | 0.796 | 2.67 |
| 319.10 | 0.578 | 0.365 | 0.262 | 0.373 | 0.787 | 0.213 | 0.000 | 1.375 | 0.790 | 2.70 |
| 318.35 | 0.657 | 0.422 | 0.217 | 0.361 | 0.832 | 0.168 | 0.000 | 1.297 | 0.776 | 2.60 |
| 317.83 | 0.725 | 0.478 | 0.178 | 0.344 | 0.870 | 0.130 | 0.000 | 1.223 | 0.751 | 2.54 |
| 317.22 | 0.797 | 0.499 | 0.124 | 0.377 | 0.908 | 0.092 | 0.000 | 1.255 | 0.781 | 2.53 |
| 316.76 | 0.867 | 0.557 | 0.082 | 0.361 | 0.942 | 0.058 | 0.000 | 1.188 | 0.760 | 2.49 |
| 316.43 | 0.942 | 0.608 | 0.035 | 0.357 | 0.977 | 0.023 | 0.000 | 1.145 | 0.715 | 2.65 |
| 316.12 | 1.000 | 0.633 | 0.000 | 0.367 | 1.000 | 0.000 | 0.000 | 1.140 | - | 2.93 |
| ***100.0 kPa*** | | | | | | | | | | |
| 396.48 | 0.000 | 0.000 | 0.652 | 0.348 | 0.000 | 1.000 | 0.000 | - | 1.071 | - |
| 394.21 | 0.059 | 0.040 | 0.616 | 0.344 | 0.122 | 0.878 | 0.000 | 1.756 | 1.057 | 2.20 |
| 392.21 | 0.121 | 0.080 | 0.572 | 0.348 | 0.227 | 0.773 | 0.000 | 1.716 | 1.058 | 2.13 |
| 390.77 | 0.189 | 0.125 | 0.532 | 0.343 | 0.323 | 0.677 | 0.000 | 1.626 | 1.035 | 2.05 |
| 389.37 | 0.247 | 0.159 | 0.481 | 0.360 | 0.412 | 0.588 | 0.000 | 1.687 | 1.034 | 2.13 |
| 388.17 | 0.318 | 0.206 | 0.439 | 0.355 | 0.485 | 0.515 | 0.000 | 1.580 | 1.026 | 2.02 |
| 387.02 | 0.380 | 0.244 | 0.394 | 0.362 | 0.556 | 0.444 | 0.000 | 1.576 | 1.019 | 2.04 |
| 385.87 | 0.457 | 0.298 | 0.349 | 0.353 | 0.635 | 0.365 | 0.000 | 1.519 | 0.975 | 2.07 |
| 384.64 | 0.558 | 0.357 | 0.278 | 0.365 | 0.733 | 0.267 | 0.000 | 1.512 | 0.926 | 2.17 |
| 383.76 | 0.659 | 0.422 | 0.214 | 0.364 | 0.792 | 0.208 | 0.000 | 1.415 | 0.959 | 1.98 |
| 383.21 | 0.726 | 0.460 | 0.171 | 0.369 | 0.837 | 0.163 | 0.000 | 1.392 | 0.955 | 1.94 |
| 382.67 | 0.799 | 0.509 | 0.125 | 0.366 | 0.881 | 0.119 | 0.000 | 1.342 | 0.973 | 1.86 |
| 382.16 | 0.869 | 0.554 | 0.080 | 0.366 | 0.923 | 0.077 | 0.000 | 1.310 | 0.997 | 1.81 |
| 381.66 | 0.943 | 0.618 | 0.034 | 0.348 | 0.968 | 0.032 | 0.000 | 1.248 | 0.997 | 1.80 |
| 381.41 | 1.000 | 0.639 | 0.000 | 0.361 | 1.000 | 0.000 | 0.000 | 1.255 | - | - |

[a]Where equilibrium temperature is denoted as $T$; the mole fractions of methylcyclohexane (DMI-free basis), toluene, and DMI in the liquid phase are represented as $x_1'$ $x_2$, $x_3$, respectively; the mole fractions of methylcyclohexane, toluene, and DMI in the vapor phase are expressed as $y_1$, $y_2$, $y_3$, respectively; the activity coefficient of methylcyclohexane is indicated as $\gamma_1$; the activity coefficient of toluene is signified as $\gamma_2$; the relative volatility of methylcyclohexane to toluene is shown as $\alpha_{12}$; and the entrainer-to-feed ratio in a mass basis is depicted as E/F.

[b]Expanded combined uncertainties $U$ with $k = 2$: $U(T) = 0.4$ K, $U(P) = 0.23$ kPa, and $U(x_1) = U(y_1) = 0.006$.

[c]$y_3$ values are less than 0.0005.

**Table 3.** Experimental VLE data for methylcyclohexane (1) + toluene (2) + dimethyl isosorbide (3) at E/F = 3 and pressure of 10.0 kPa[a,b,c]

| $T$/K | $x_1$' | $x_1$ | $x_2$ | $x_3$ | $y_1$ | $y_2$ | $y_3$ | $\gamma_1$ | $\gamma_2$ | $\alpha_{12}$ |
|---|---|---|---|---|---|---|---|---|---|---|
| 341.95 | 0.000 | 0.000 | 0.385 | 0.615 | 0.000 | 1.000 | 0.000 | - | 1.003 | - |
| 337.45 | 0.127 | 0.049 | 0.333 | 0.618 | 0.206 | 0.794 | 0.000 | 1.322 | 1.091 | 1.80 |
| 333.65 | 0.246 | 0.074 | 0.307 | 0.619 | 0.381 | 0.619 | 0.000 | 1.860 | 1.070 | 1.88 |
| 330.05 | 0.354 | 0.137 | 0.242 | 0.621 | 0.528 | 0.472 | 0.000 | 1.593 | 1.195 | 2.04 |
| 327.65 | 0.453 | 0.150 | 0.229 | 0.621 | 0.619 | 0.381 | 0.000 | 1.870 | 1.125 | 1.89 |
| 324.45 | 0.577 | 0.218 | 0.159 | 0.623 | 0.745 | 0.255 | 0.000 | 1.755 | 1.239 | 2.02 |
| 322.05 | 0.665 | 0.230 | 0.146 | 0.624 | 0.817 | 0.183 | 0.000 | 2.008 | 1.072 | 2.26 |
| 319.55 | 0.771 | 0.292 | 0.081 | 0.627 | 0.894 | 0.106 | 0.000 | 1.916 | 1.248 | 2.38 |
| 318.55 | 0.819 | 0.287 | 0.084 | 0.629 | 0.930 | 0.070 | 0.000 | 2.113 | 0.830 | 2.95 |
| 317.55 | 0.929 | 0.340 | 0.029 | 0.631 | 0.978 | 0.022 | 0.000 | 1.955 | 0.790 | 3.39 |
| 317.35 | 1.000 | 0.366 | 0.000 | 0.634 | 1.000 | 0.000 | 0.000 | 1.873 | - | - |

[a]Where equilibrium temperature is denoted as $T$; the mole fractions of methylcyclohexane (DMI-free basis), toluene, and DMI in the liquid phase are represented as $x_1$' $x_2$, $x_3$, respectively; the mole fractions of methylcyclohexane, toluene, and DMI in the vapor phase are expressed as $y_1$, $y_2$, $y_3$, respectively; the activity coefficient of methylcyclohexane is indicated as $\gamma_1$; the activity coefficient of toluene is signified as $\gamma_2$; the relative volatility of methylcyclohexane to toluene is shown as $\alpha_{12}$; and the entrainer-to-feed ratio in a mass basis is depicted as E/F.

[b]Expanded combined uncertainties $U$ with $k$ = 2: $U(T)$ = 0.4 K, $U(P)$ = 0.23 kPa, and $U(x_1) = U(y_1)$ = 0.006.

[c]$y_3$ values are less than 0.0005.

The activity coefficient of component $i$ in the pseudo–ternary mixtures, which is denoted as $\gamma_i$, was used to evaluate the nonideality of the component in the liquid phase as shown in Eq. 1. The ideal gas considered occurred in the mixture since the VLE data were experimentally conducted at vacuum and atmospheric pressure.

$$\gamma_i = \frac{y_i P}{x_i P_i^{sat}} \quad 1)$$

where $i$ stands for component $i$, $x$ represents the mole fraction in the liquid phase, $y$ indicates the mole fraction in the vapor phase, and $P$ and $P_i^{sat}$ denote the total pressure and the saturated vapor pressure for component $i$, respectively. The extended Antoine and the NIST Wagner25 equations with their corresponding parameters obtained from the physical properties of the Aspen Plus database were utilized to calculate the saturated vapor pressure of the component $i$ ($P_i^{sat}$), as shown in Table 4. The extended Antoine equation was used for methylcyclohexane, toluene, and NBP, while the NIST Wagner25 equation was used for DMI, as no extended Antoine parameters were available for DMI.

**Table 4.** The extended Antoine and the NIST Wagner25 parameters[a]

| Compound | Extended Antoine[b] | | | | | | | | |
|---|---|---|---|---|---|---|---|---|---|
| | $A_1$ | $A_2$ | $A_3$ | $A_4$ | $A_5$ | $A_6$ | $A_7$ | $A_8$ | $A_9$ |
| methylcyclohexane | 85.776 | -7080.8 | 0 | 0 | -10.695 | $8.14 \times 10^{-6}$ | 2.0 | 146.58 | 572.10 |
| toluene | 70.037 | -6729.8 | 0 | 0 | -8.179 | $5.30 \times 10^{-6}$ | 2.0 | 178.18 | 591.75 |
| 1-butylpyrrolidin-2-one | 44.387 | -7118.4 | 0 | 0 | -4.101 | $1.39 \times 10^{-18}$ | 6.0 | 496.64 | 756.51 |
| | NIST Wagner25[c] | | | | | | | | |
| | $A_1$ | $A_2$ | $A_3$ | $A_4$ | $ln\ P_{ci}$ | $T_{ci}$ | $T_{lower}$ | $T_{upper}$ | |
| dimethyl isosorbide | -8.552 | 2.397 | -4.204 | -3.911 | 8.041 | 688 | 220 | 688 | |

[a]The extended Antoine and the NIST Wagner25 parameters were taken from the physical property databank of Aspen Plus.32

[b]Equation of the extended Antoine:

$\ln(P^s) = A_1 + A_2/(T + A_3) + A_4 T + A_5 \ln T + A_6 T^{A_7}$ for $A_8 \le T \le A_9$, where $P^s$ is in kPa and $T$ in K.

[c]Equation of the NIST Wagner25:

$$\ln(P^s) = \ln P_{ci} + \frac{A_1(1-T_{ri}) + A_2(1-T_{ri})^{1.5} + A_3(1-T_{ri})^{2.5} + A_4(1-T_{ri})^5}{T_{ri}} \text{ for } T_{lower} \le T \le T_{upper},$$

where $P^s$ is in kPa, $T$ in K, and $T_{ri}=T/T_{ci}$

In order to assess the separation performance of the entrainer in the pseudo–ternary mixture, the relative volatility of methylcyclohexane to toluene ($\alpha_{12}$) was evaluated using Eq 2.

$$\alpha_{12} = \frac{y_1 / x_1'}{y_2 / x_2'} \qquad 2)$$

where $x_1'$ and $x_2'$ denote mole fractions of methylcyclohexane and toluene on an excluded-entrainer basis in the liquid phase.

Tables 5 and 6 present the experimental VLE data for the pseudo-ternary mixture of methylcyclohexane and toluene with the addition of NBP as an entrainer, with E/F = 1 at 10.0 and 100.0 kPa and with E/F = 3 at 10.0 kPa, respectively. The introduction of DMI into the mixture has similar effects to those observed with the addition of NBP.

**Table 5.** Experimental VLE data for methylcyclohexane (1) + toluene (2) + 1-butylpyrrolidin-2-one (3) at E/F = 1 and pressure of 10.0 and 100.0 kPa[a,b,c]

| $T$/K | $x_1$' | $x_1$ | $x_2$ | $x_3$ | $y_1$ | $y_2$ | $y_3$ | $\gamma_1$ | $\gamma_2$ | $\alpha_{12}$ |
|---|---|---|---|---|---|---|---|---|---|---|
| | | | | | ***10.0 kPa*** | | | | | |
| 334.92 | 0.000 | 0.000 | 0.604 | 0.396 | 0.000 | 1.000 | 0.000 | - | 0.836 | - |
| 332.85 | 0.056 | 0.034 | 0.569 | 0.397 | 0.148 | 0.852 | 0.000 | 1.618 | 0.820 | 2.91 |
| 331.75 | 0.087 | 0.053 | 0.545 | 0.402 | 0.212 | 0.788 | 0.000 | 1.549 | 0.828 | 2.80 |
| 329.29 | 0.181 | 0.108 | 0.486 | 0.406 | 0.373 | 0.627 | 0.000 | 1.468 | 0.816 | 2.68 |
| 327.58 | 0.235 | 0.141 | 0.454 | 0.405 | 0.463 | 0.537 | 0.000 | 1.493 | 0.802 | 2.81 |
| 326.38 | 0.282 | 0.169 | 0.425 | 0.406 | 0.534 | 0.466 | 0.000 | 1.504 | 0.781 | 2.91 |
| 325.32 | 0.339 | 0.200 | 0.386 | 0.414 | 0.595 | 0.405 | 0.000 | 1.475 | 0.782 | 2.86 |
| 323.77 | 0.427 | 0.257 | 0.341 | 0.402 | 0.680 | 0.320 | 0.000 | 1.396 | 0.746 | 2.85 |
| 322.12 | 0.556 | 0.330 | 0.260 | 0.410 | 0.774 | 0.226 | 0.000 | 1.322 | 0.742 | 2.73 |
| 321.81 | 0.575 | 0.339 | 0.247 | 0.414 | 0.796 | 0.204 | 0.000 | 1.340 | 0.715 | 2.88 |
| 320.52 | 0.704 | 0.410 | 0.169 | 0.421 | 0.865 | 0.135 | 0.000 | 1.268 | 0.732 | 2.69 |
| 319.70 | 0.785 | 0.467 | 0.124 | 0.409 | 0.908 | 0.092 | 0.000 | 1.209 | 0.705 | 2.69 |
| 319.06 | 0.862 | 0.515 | 0.079 | 0.406 | 0.944 | 0.056 | 0.000 | 1.171 | 0.689 | 2.71 |
| 318.53 | 0.931 | 0.532 | 0.036 | 0.432 | 0.976 | 0.024 | 0.000 | 1.197 | 0.676 | 2.95 |
| 317.92 | 1.000 | 0.589 | 0.000 | 0.411 | 1.000 | 0.000 | 0.000 | 1.136 | - | - |
| | | | | | ***100.0 kPa*** | | | | | |
| 399.34 | 0.000 | 0.000 | 0.606 | 0.394 | 0.000 | 1.000 | 0.000 | - | 1.069 | - |
| 397.36 | 0.060 | 0.036 | 0.566 | 0.398 | 0.119 | 0.881 | 0.000 | 1.760 | 1.062 | 2.12 |
| 395.48 | 0.120 | 0.072 | 0.525 | 0.403 | 0.228 | 0.772 | 0.000 | 1.772 | 1.054 | 2.16 |
| 394.01 | 0.185 | 0.112 | 0.489 | 0.399 | 0.317 | 0.683 | 0.000 | 1.638 | 1.042 | 2.05 |
| 392.44 | 0.249 | 0.151 | 0.450 | 0.399 | 0.409 | 0.591 | 0.000 | 1.632 | 1.021 | 2.09 |
| 391.17 | 0.322 | 0.194 | 0.405 | 0.401 | 0.485 | 0.515 | 0.000 | 1.554 | 1.024 | 1.98 |
| 390.09 | 0.385 | 0.233 | 0.368 | 0.399 | 0.552 | 0.448 | 0.000 | 1.515 | 1.009 | 1.97 |
| 388.81 | 0.455 | 0.273 | 0.323 | 0.404 | 0.618 | 0.382 | 0.000 | 1.495 | 1.016 | 1.94 |
| 386.46 | 0.594 | 0.358 | 0.240 | 0.402 | 0.734 | 0.266 | 0.000 | 1.439 | 1.017 | 1.88 |
| 385.43 | 0.663 | 0.400 | 0.199 | 0.401 | 0.788 | 0.212 | 0.000 | 1.420 | 1.006 | 1.89 |
| 384.38 | 0.733 | 0.434 | 0.154 | 0.412 | 0.843 | 0.157 | 0.000 | 1.440 | 0.990 | 1.96 |
| 383.55 | 0.801 | 0.475 | 0.114 | 0.411 | 0.883 | 0.117 | 0.000 | 1.409 | 1.018 | 1.88 |
| 382.69 | 0.872 | 0.515 | 0.073 | 0.412 | 0.929 | 0.071 | 0.000 | 1.398 | 1.004 | 1.92 |
| 382.20 | 0.942 | 0.556 | 0.031 | 0.413 | 0.969 | 0.031 | 0.000 | 1.369 | 1.040 | 1.91 |
| 381.98 | 1.000 | 0.588 | 0.000 | 0.412 | 1.000 | 0.000 | 0.000 | 1.344 | - | - |

[a]Where equilibrium temperature is denoted as $T$; the mole fractions of methylcyclohexane (NBP-free basis), toluene, and NBP in the liquid phase are represented as $x_1$' $x_2$, $x_3$, respectively; the mole fractions of methylcyclohexane, toluene, and NBP in the vapor phase are expressed as $y_1$, $y_2$, $y_3$, respectively; the activity coefficient of methylcyclohexane is indicated as $\gamma_1$; the activity coefficient of toluene is signified as $\gamma_2$; the relative volatility of methylcyclohexane to toluene is shown as $\alpha_{12}$; and the entrainer-to-feed ratio in a mass basis is depicted as E/F.

[b]Expanded combined uncertainties $U$ with $k$ = 2: $U(T)$ = 0.4 K, $U(P)$ = 0.23 kPa, and $U(x_1) = U(y_1)$ = 0.006.

[c]$y_3$ values are less than 0.0005.

**Table 6.** Experimental VLE data for methylcyclohexane (1) + toluene (2) + 1-butylpyrrolidin-2-one (3) at E/F = 3 and pressure of 10.0 kPa[a,b,c]

| $T$/K | $x_1'$ | $x_1$ | $x_2$ | $x_3$ | $y_1$ | $y_2$ | $y_3$ | $\gamma_1$ | $\gamma_2$ | $\alpha_{12}$ |
|---|---|---|---|---|---|---|---|---|---|---|
| 349.65 | 0.000 | 0.000 | 0.337 | 0.663 | 0.000 | 1.000 | 0.000 | - | 0.866 | - |
| 345.55 | 0.121 | 0.042 | 0.293 | 0.665 | 0.201 | 0.799 | 0.000 | 1.134 | 0.922 | 1.83 |
| 342.35 | 0.248 | 0.076 | 0.255 | 0.669 | 0.344 | 0.656 | 0.000 | 1.198 | 0.978 | 1.59 |
| 338.95 | 0.366 | 0.124 | 0.210 | 0.666 | 0.502 | 0.498 | 0.000 | 1.206 | 1.026 | 1.74 |
| 336.85 | 0.455 | 0.141 | 0.196 | 0.663 | 0.601 | 0.399 | 0.000 | 1.369 | 0.956 | 1.81 |
| 333.85 | 0.577 | 0.188 | 0.132 | 0.680 | 0.743 | 0.257 | 0.000 | 1.417 | 1.024 | 2.13 |
| 332.65 | 0.616 | 0.204 | 0.121 | 0.675 | 0.787 | 0.213 | 0.000 | 1.445 | 0.974 | 2.30 |
| 329.55 | 0.764 | 0.252 | 0.073 | 0.675 | 0.874 | 0.126 | 0.000 | 1.461 | 1.080 | 2.15 |
| 328.25 | 0.818 | 0.275 | 0.052 | 0.673 | 0.916 | 0.084 | 0.000 | 1.475 | 1.063 | 2.44 |
| 326.25 | 0.944 | 0.310 | 0.016 | 0.674 | 0.972 | 0.028 | 0.000 | 1.500 | 1.269 | 2.02 |
| 325.45 | 1.000 | 0.324 | 0.000 | 0.676 | 1.000 | 0.000 | 0.000 | 1.536 | - | - |

[a]Where equilibrium temperature is denoted as $T$; the mole fractions of methylcyclohexane (NBP-free basis), toluene, and NBP in the liquid phase are represented as $x_1'$ $x_2$, $x_3$, respectively; the mole fractions of methylcyclohexane, toluene, and NBP in the vapor phase are expressed as $y_1$, $y_2$, $y_3$, respectively; the activity coefficient of methylcyclohexane is indicated as $\gamma_1$; the activity coefficient of toluene is signified as $\gamma_2$; the relative volatility of methylcyclohexane to toluene is shown as $\alpha_{12}$; and the entrainer-to-feed ratio in a mass basis is depicted as E/F.

[b]Expanded combined uncertainties $U$ with $k$ = 2: $U(T)$ = 0.4 K, $U(P)$ = 0.23 kPa, and $U(x_1)$ = $U(y_1)$ = 0.006.

[c]$y_3$ values are less than 0.0005.

Figures 1 and 2 illustrate that adding DMI and NBP, respectively, at a pressure of 100.0 kPa with E/F = 1 increases the equilibrium temperature compared to the mixture without DMI and NBP.

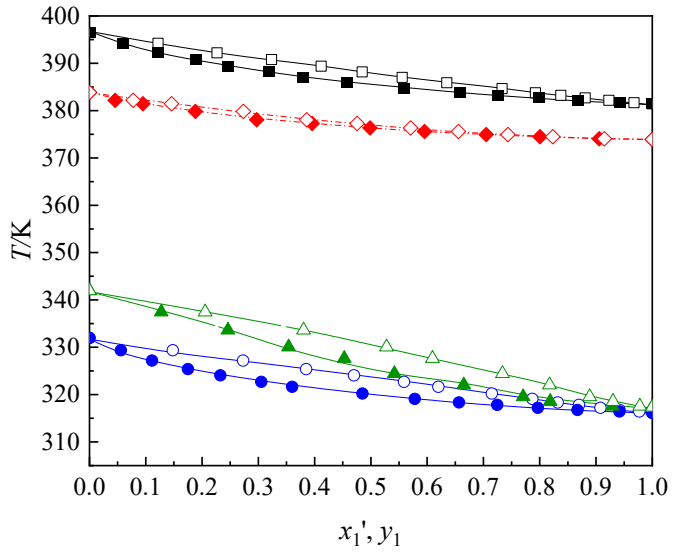


**Figure 1.** $T$–$x_1'$–$y_1$ diagrams of methylcyclohexane (1) + toluene (2) + dimethyl isosorbide (3), experimental for E/F = 1: (■), $x_1'$ and (□), $y_1$ at 100.0 kPa; (●), $x_1'$

and (○), $y_1$ at 10.0 kPa; E/F = 3: (▲), $x_1'$ and (△), $y_1$ at 10.0 kPa; No entrainer: (♦), $x_1$ and (◊), $y_1$ at 101.3 kPa[22]; and correlated by NRTL: (—), black and blue line for E/F 1 at 100.0 and 10.0 kPa, respectively; green line for E/F 3 at 10.0 kPa; and (- · -), red line for no entrainer.

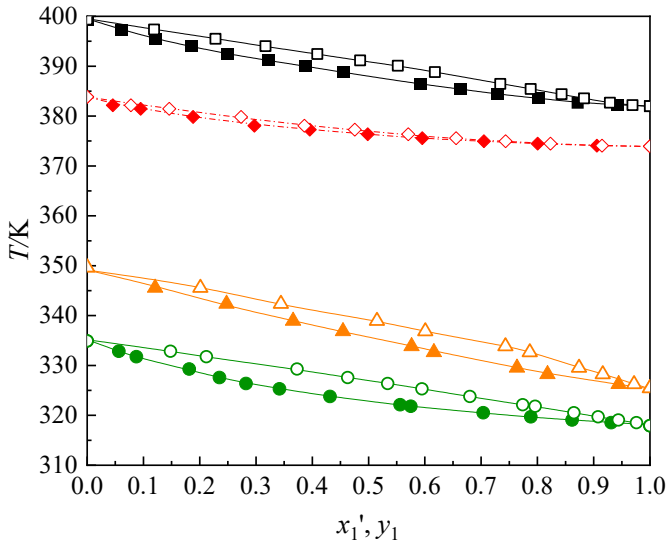


**Figure 2.** $T$–$x_1'$–$y_1$ diagrams of methylcyclohexane (1) + toluene (2) + 1-butylpyrrolidin-2-one (3), experimental for E/F = 1: (■), $x_1'$ and (□), $y_1$ at 100.0 kPa; (●), $x_1'$ and (○), $y_1$ at 10.0 kPa; E/F = 3: (▲), $x_1'$ and (△), $y_1$ at 10.0 kPa; No entrainer: (♦), $x_1$ and (◊), $y_1$ at 101.3 kPa[22]; and correlated by NRTL, (—), black and green line for E/F 1 at 100.0 and 10.0 kPa, respectively, orange line for E/F 3 at 10.0 kPa; and (- · -), red line for no entrainer.

The presence of DMI and NBP demonstrates attraction towards toluene, leading to a decrease toluene vaporization. As a result, an elevated temperature must be achieved to vaporize the mixture and attain the equilibrium condition. At E/F = 1, lowering the pressure from 100.0 to 10.0 kPa significantly reduces the equilibrium temperature. This occurs because reduced pressure lowers the boiling point of the components, enabling them to vaporize at lower temperature. Therefore, the temperature needed to achieve the equilibrium temperature is decreased. At the pressure of 10.0 kPa, the addition of DMI and NBP, respectively, with E/F = 3 to the mixture shifts the equilibrium temperature higher than the addition of DMI and NBP with E/F = 1. Introducing larger amounts of DMI and NBP results in these entrainers predominating the liquid composition. This considerably reduces the vaporization of both methylcyclohexane and toluene. Consequently, a higher temperature is required to vaporize both components and establish equilibrium, leading to an increase in the equilibrium temperature.

Graphical representations of *y*–*x*' diagrams in Figures 3 and 4 illustrate the impact of DMI and NBP, respectively, on the methylcyclohexane–toluene separation. The addition of DMI and NBP to the mixture provides a significant increase in the relative volatility of methylcyclohexane in comparison to the mixture excluding these biobased and greener entrainers. As a result, the close-boiling profile is effectively removed from the methylcyclohexane–toluene mixture.

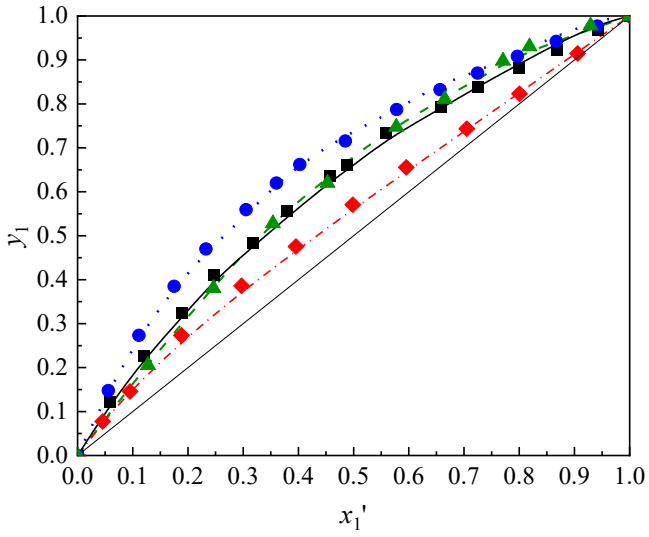


**Figure 3.** $y_1$–$x_1'$ diagrams of methylcyclohexane (1) + toluene (2) + dimethyl isosorbide (3), experimental for E/F = 1: (■), at 100.0 kPa; and (●), at 10.0 kPa; E/F = 3: (▲) at 10.0 kPa; no entrainer: (♦), at 101.3 kPa[22]; and correlated by NRTL: (—), black line for E/F 1 at 100.0 kPa; and (····), blue line for E/F =1 at 10.0 kPa; (- - -), green line for E/F = 3 at 10.0 kPa; and (-··-), red line for no entrainer at 101.3 kPa.

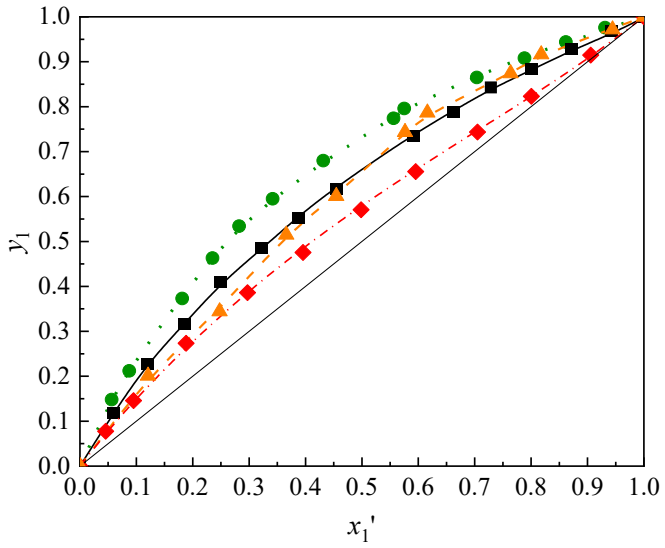


**Figure 4.** $y_1$–$x_1'$ diagrams of methylcyclohexane (1) + toluene (2) + 1-butylpyrrolidin-2-one (3), experimental for E/F = 1: (■), at 100.0 kPa; and (●), at 10.0 kPa; E/F = 3: (▲), at 10.0 kPa; no entrainer: (♦), at 101.3 kPa[22]; and correlated by NRTL: (—), black line for E/F = 1 at 100.0 kPa; and (····), green line for E/F = 1 at 10.0 kPa; (- - -), orange line for E/F = 3 at 10.0 kPa; and (-·-), red line for no entrainer at 101.3 kPa.

The presence of DMI and NBP in the methylcyclohexane–toluene mixture contributed to the change in nonideal characteristics. In contrast to the molecular interactions between the DMI and the NBP with methylcyclohexane, the interactions between the DMI and the NBP with toluene molecules are responsible for producing a higher relative volatility in the mixture. This is primarily because DMI and NBP act as polar entrainers, while toluene has a lower degree of nonpolarity in comparison to methylcyclohexane. Hence, DMI and NBP exhibit a higher affinity for toluene compared to methylcyclohexane. As a result, the addition of DMI and NBP can provide a minimum molecular interaction between methylcyclohexane and toluene. The data shown in Tables 2 and 3 for the DMI and Tables 5 and 6 for the NBP indicate that the introduction of DMI and NBP to the mixture leads to a higher activity coefficient of methylcyclohexane ($\gamma_1$) than toluene ($\gamma_2$). It can be inferred that DMI and NBP possess a more pronounced affinity for toluene compared to methylcyclohexane. Therefore, methylcyclohexane becomes more volatile, facilitating its separation from the mixture. The current work also examined the influence of pressure on relative volatility. Figures 3 and 4 confirm that reducing the pressure from 100.0 to 10.0 kPa at an E/F = 1 induces an elevated relative volatility. As shown in Table 2 and 3 for the DMI and the NBP, respectively, the activity coefficients of toluene ($\gamma_2$)

at 10.0 kPa are lower compared to those at 100.0 kPa. This indicates the interaction between the DMI and the NBP with toluene, is stronger at 10.0 kPa compared to that at 100.0 kPa. These stronger interactions make it easier for methylcyclohexane to evaporate, and therefore, significant increases in relative volatility can be achieved.

Furthermore, this work also studied the quantity impact of DMI and NBP on the relative volatility of the mixture. DMI and NBP with E/F = 3 were introduced to the mixture. The addition of entrainers at high E/F is reliable in industrial applications, particularly because entrainers are recycled within extractive distillation process. Therefore, the entrainer consumption over time remain stable, requiring only a small amount of make–up entrainer, rather than significant fresh entrainer input during continues operation. Previous studies have also employed high E/F to achieve the desired separation performance.[27,33–38] In the separation of a methylcyclohexane–toluene mixture, the E/F values commonly used vary within the range of 0.7 to 18.8. For example, the E/F value for morpholine is 0.7,[21] ILs values between 3 and 18.8,[23,25]. Additionally, some other organic entrainers, including acetophenone, methyl n-amyl ketone, cyclohexanone, *o*-cresol, dimethylformamide, phenol, propylene glycol, cyclohexane, and furfural, have E/F values ranging from 2.5 to 4.2.[27] At E/F = 1, the reduction in pressure from 100.0 to 10.0 kPa resulted in a significant increase in relative volatility. Hence, the VLE measurement with the addition of DMI and NBP with E/F = 3 were performed at 10.0 kPa. Figures 3 and 4, however, illustrate that using a higher quantity of DMI and NBP, with E/F = 3 at 10.0 kPa decreases the relative volatility compared to that at E/F = 1 and at 10.0 kPa. An increase in DMI and NBP quantity with E/F = 3 at 10.0 kPa leads to a higher equilibrium temperature in comparison to that at E/F = 1. This can be attributed to the increased temperature at E/F = 3, as already illustrated in Figures 1 and 2, which reduces the nonideality of the mixture. Table 3 shows that the activity coefficient of toluene at 10.0 kPa for E/F = 3 is higher than that at E/F = 1, as indicated in Table 2. This suggests a weaker interaction between the DMI and toluene at a higher equilibrium temperature. A similar trend is observed for the NBP, as presented in Table 6, where the activity coefficient of toluene at 10.0 kPa for E/F = 3 is higher than that for E/F = 1, as shown in Table 5. Therefore, at higher E/F ratios, the relative volatility of the mixture decreases again due to the weaker interactions between entrainers and toluene. Consequently, the effectiveness of the methylcyclohexane–toluene separation is reduced. Furthermore, the molecular interactions between methylcyclohexane, toluene, and the entrainers have been studied in our previous work using COSMO–RS for unimolecular quantum chemical calculations.[1]

Additionally, the entrainers' effect on the separation of methylcyclohexane from toluene was compared as *y*–*x*' diagrams in Figure 5. It reveals that the addition

of DMI and NBP, with E/F = 1 at 10.0 kPa, to the mixture results in a similar relative volatility performance to remove a close–boiling profile. The performance of both entrainers at E/F = 1 and 10.0 kPa in terms of relative volatility is slightly higher than that of the conventional entrainer of 1-methylpyrrolidin-2-one (NMP) at E/F = 1 and 100.0 kPa in all methylcyclohexane composition ranges. This confirms their potential to replace the currently used NMP with more environmentally friendly greener entrainers provided that the right operating conditions are selected. In addition, in the methylcyclohexane–rich region, both entrainers at E/F = 1 and 10.0 kPa show significantly higher relative volatility performance than sulfolane, the other conventional entrainer, at E/F = 1 and 100.0 kPa. Moreover, the relative volatility for the pseudo–ternary mixture methylcyclohexane (1) to toluene (2), in the presence of DMI and NBP at $x_1' = 0.5$ and E/F = 1, was compared with other green entrainers, such as GVL and Cyrene. Figure 6 illustrates that both DMI and NBP, at E/F = 1 and 10.0 kPa, demonstrate similar relative volatility to that of GVL and Cyrene at E/F = 1 and 100.0 kPa. These results show that, based on the relative volatility comparison, both DMI and NBP demonstrate noteworthy potential and could act as excellent biobased and greener organic entrainers, providing an alternative to NMP and sulfolane for the separation of methylcyclohexane from toluene via extractive distillation.

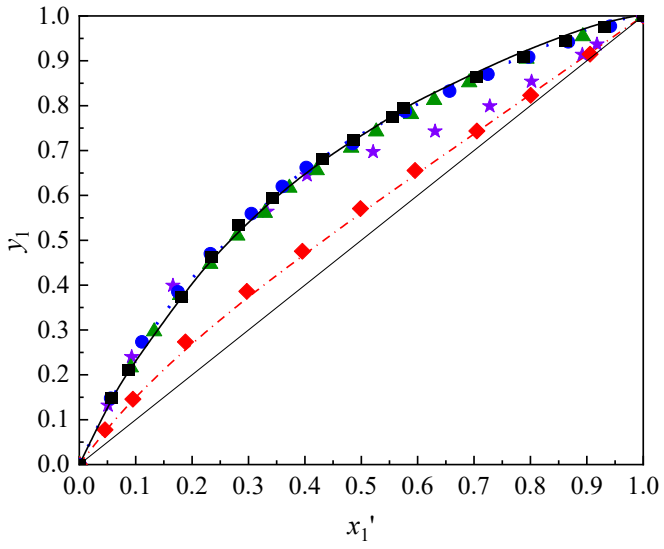


**Figure 5.** $y_1$–$x_1'$ diagrams for the comparison of dimethyl isosorbide, 1-butylpyrrolidin-2-one, 1-methylpyrrolidin-2-one, and sulfolane in the methylcyclohexane (1) + toluene (2) mixture, (●), dimethyl isosorbide with E/F = 1 at 10.0 kPa; (■), 1-butylpyrrolidin-2-one with E/F = 1 at 10.0 kPa; (▲), 1-methylpyrrolidin-2-one with E/F = 1 at 100.0 kPa (entrainer–free based in the vapor phase mole fraction)[22]; (★), sulfolane with E/F = 1 at

100.0 kPa[20]; no entrainer: (♦), at 101.3 kPa[22]; and correlated by NRTL: (···· ), blue line for dimethyl isosorbide with E/F = 1 at 10.0 kPa; and (—), black line for 1-butylpyrrolidin-2-one with E/F = 1 at 10.0 kPa; and (- · -), red line for no entrainer at 101.3 kPa.

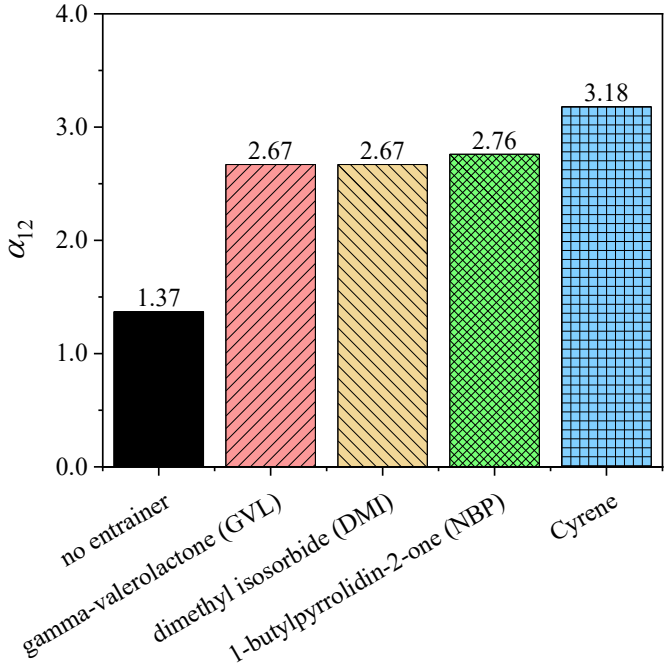


**Figure 6.** The comparison of the relative volatility ($\alpha_{12}$) for the methylcyclohexane (1) to toluene (2) at $x_1' = 0.5$, E/F = 1: with no entrainer and with the presence of biobased entrainers DMI, Cyrene, and GVL, and a greener entrainer NBP. Cyrene and GVL were evaluated at 100.0 kPa, while DMI and NBP were provided at 10.0 kPa. Experimental works were performed in duplicate, with a relative volatility deviation of 0.07. Data for Cyrene were sourced from literature,[20] while the binary mixture with no entrainer and with GVL was taken from our previous study.[22]

## Thermodynamic consistency test

The Van Ness thermodynamic consistency test[28] was performed to verify the consistency of the experimental VLE data for pseudo–ternary mixtures of methylcyclohexane and toluene containing DMI and NBP. The Van Ness consistency test was calculated using Eqs. 3 and 4.

$$\Delta P = \frac{1}{n_p} \times \sum_{i=1}^{n_p} \Delta P_i = \frac{1}{n_p} \times \sum_{i=1}^{n_p} 100 \left| \frac{P_i^{cal} - P_i^{\exp}}{P_i^{\exp}} \right| \qquad 3)$$

$$\Delta y = \frac{1}{n_p} \times \sum_{i=1}^{n_p} \Delta y_i = \frac{1}{n_p} \times \sum_{i=1}^{n_p} 100 \left| y_i^{cal} - y_i^{\exp} \right| \quad 4)$$

where $P$ stands for pressure, $y$ for the mole fraction in the vapor phase, $n_p$ for the experimental data points, *cal* for the calculated values obtained from the correlation using the NRTL thermodynamic model, and *exp* for the experimental values. The experimental VLE data complies with the criteria of the Van Ness test if both values of $\Delta P$ and $\Delta y$ are less than 1 and are thus regarded as consistent. In this work, the experimental VLE data for both pseudo–ternary mixtures satisfy the Van Ness test and are therefore considered consistent data, as the $\Delta P$ and $\Delta y$ values are below 1, as depicted in Table 3.

**Table 3.** Thermodynamic consistency test

| Mixture | $\Delta y^a$ | $\Delta P^b$ | Test Results |
|---|---|---|---|
| methylcyclohexane (1) + toluene (2) + DMI (3) | 0.4 | 0.5 | Passed |
| methylcyclohexane (1) + toluene (2) + NBP (3) | 0.1 | 0.5 | Passed |

[a] $\Delta y = \frac{1}{n_p} \times \sum_{i=1}^{n_p} \Delta y_i = \frac{1}{n_p} \times \sum_{i=1}^{n_p} 100 \left| y_i^{cal} - y_i^{\exp} \right| < 1$

[b] $\Delta P = \frac{1}{n_p} \times \sum_{i=1}^{n_p} \Delta P_i = \frac{1}{n_p} \times \sum_{i=1}^{n_p} 100 \left| \frac{P_i^{cal} - P_i^{\exp}}{P_i^{\exp}} \right| < 1$

In addition, the residual distribution of $\ln(\gamma_1 / \gamma_2)$ is required to demonstrate randomness to comply with the Van Ness test.[39] In this study, the residual distributions of $\ln(\gamma_1 / \gamma_2)$ for DMI and NBP are illustrated in Figures C3-C5 and C6-C8, respectively, indicating their randomness. These results confirm that the VLE data measured in this study are consistent.

## Data correlation

The NRTL thermodynamic model was employed for the VLE data correlation. The NRTL model frequently shows good results in the VLE data correlation for both binary and pseudo–ternary systems involving entrainers.[22,40–46] Additionally, our previous work showed that the NRTL model demonstrates better correlation than the UNIQUAC model.[22] The equation for the NRTL model is shown in Eq. 5.

$$\ln \gamma_i = \frac{\sum_{j=1}^{n_c} x_j \tau_{ji} G_{ji}}{\sum_{k=1}^{n_c} x_k G_{ki}} + \sum_{j=1}^{n_c} \frac{x_j G_{ij}}{\sum_{k=1}^{N} x_k G_{kj}} \left( \tau_{ij} - \frac{\sum_{m=1}^{n_c} x_m \tau_{mj} G_{mj}}{\sum_{k=1}^{n_c} x_k G_{kj}} \right) \quad 5)$$

In Eq. 5, $\gamma_i$ denotes the activity coefficient of component *i* and $n_c$ represents the number of components. Furthermore, the parameters used in the NRTL model are defined in Eqs. 6, 7, 8, and 9.

$$G_{ij} = \exp(-C_{ij}\tau_{ij}) \quad 6)$$

$$\tau_{ij} = A_{ij} + B_{ij} / T \quad 7)$$

$$\tau_{ii} = 0 \quad 8)$$

$$G_{ii} = 1 \quad 9)$$

where $C_{ij}$ is the nonrandomness constant in the binary interaction of components *ij*.

For the methylcyclohexane–toluene pair, the BIPs were regressed from the experimental VLE data for the binary mixture of methylcyclohexane and toluene at pressures of 101.3, 53.3, and 26.7 kPa. The experimental VLE data at 101.3 kPa was obtained from our previous work,[22] while at 53.3 and 26.7 kPa were obtained from literature.[31] The VLE data from these pressures were calculated together in a single correlation. The obtained BIPs are afterwards used to perform the correlation for the pseudo–ternary mixtures of methylcyclohexane–toluene–DMI and methylcyclohexane–toluene–NBP, where the VLE for these systems was measured from 10.0 to 100.0 kPa. Therefore, the correlation for the binary mixture was conducted at normal and low pressure in order to approach the temperature range of the measured VLE data of both pseudo–ternary mixtures. In the binary mixture correlation, the parameter of the nonrandomness ($C_{ij}$) for the NRTL model was selected with the value of 0.3. On the other hand, for the correlation of the pseudo–ternary mixtures, this parameter was not defined by a specific value to provide flexibility in the correlation, which yields more accurate results. We initially examined the correlation of the pseudo–ternary mixtures by fixing the value at 0.3 for the methylcyclohexane–entrainer and toluene–entrainer pairs. However, the results were unsatisfactory. In strongly nonideal systems, this value can deviate from 0.3 to more accurately represent the system. Therefore, we decided to regress this parameter in order to achieve better correlation results. Furthermore, the parameters $A_{ij}$ and $A_{ji}$ were included in the regression rather than fixing them to 0. This method yielded more precise results. The maximum likelihood approach provided by Britt and Luecke,[47] as shown in Eq. 10, was adopted for minimizing the objective function (*OF*) to obtain the BIPs.

$$OF = \sum_{k=1}^{n_p} \left\{ \left| \frac{P_k^{cal} - P_k^{\exp}}{\sigma_P} \right|^2 + \left| \frac{T_k^{cal} - T_k^{\exp}}{\sigma_T} \right|^2 + \left| \frac{x_{1,k}^{cal} - x_{1,k}^{\exp}}{\sigma_x} \right|^2 + \left| \frac{y_{1,k}^{cal} - y_{1,k}^{\exp}}{\sigma_y} \right|^2 \right\} \quad 10)$$

Let $n_p$ and $\sigma$ denote the quantity of data points and the data standard deviation, respectively. The optimized BIP values for each pair are presented in Table 4. While the values of the root–mean–square deviation obtained from the comparison between the experiment results and the correlation values are provided in Table 5.

**Table 4.** Values of binary interaction parameters for the NRTL[a,b]

| *i* component | *j* component | $A_{ij}$ | $A_{ji}$ | $B_{ij}$/K | $B_{ji}$/K | $C_{ij}$ |
|---|---|---|---|---|---|---|
| [c]methylcyclohexane (1) | toluene (2) | -0.523 | -0.811 | -55.064 | 736.883 | 0.30 |
| methylcyclohexane (1) | dimethyl isosorbide (3) | 3.745 | 13.580 | -1626.755 | -2771.820 | 0.11 |
| toluene (2) | dimethyl isosorbide (3) | 5.206 | -1.493 | -2769.191 | 3938.608 | 0.11 |
| methylcyclohexane (1) | 1-butylpyrrolidin-2-one (3) | 3.751 | 4.791 | -2538.214 | 347.731 | 0.03 |
| toluene (2) | 1-butylpyrrolidin-2-one (3) | 6.496 | -13.495 | -3624.621 | 7959.587 | 0.10 |

[a]Unsymmetrical parameters denoted as $A_{ij}$, $A_{ji}$, $B_{ij}$, and $B_{ji}$; the nonrandomness constant represented as $C_{ij}$.

[b]NRTL: $\tau_{ij} = A_{ij} + B_{ij} / T$

[c]Experimental VLE data for a binary system of methylcyclohexane (1) and toluene (2) at 101.3 kPa from our previous work[22] and at 26.7 and 53.3 kPa from reference[31] were combined and used to obtain the BIPs of methylcyclohexane and toluene pair.

**Table 5.** Root–Mean–Square Deviation (RMSD) of the NRTL model[a]

| | RMSD[b] | | | |
|---|---|---|---|---|
| | *T*/K | *P*/kPa | $x_1$' | $y_1$ |
| methylcyclohexane (1) + toluene (2) | 0.02 | 0.31 | 0.005 | 0.005 |
| methylcyclohexane (1) + toluene (2) + dimethyl isosorbide (3) | 0.24 | 0.36 | 0.001 | 0.005 |
| methylcyclohexane (1) + toluene (2) + 1-butylpyrrolidin-2-one (3) | 0.15 | 0.36 | 0.001 | 0.002 |

[a]Temperature (*T*); pressure (*P*); mole fraction of methylcyclohexane in the liquid phase on an entrainer–free basis ($x_1$'); mole fraction of methylcyclohexane in the vapor phase ($y_1$).

[b]RMSD: $\Delta M = \sqrt{\frac{1}{n}\sum_{i=1}^{n}\left(M_{\exp} - M_{cal}\right)^2}$, where *n* represents the total number of data points; *M* stands for *T*, *P*, $x_1$', and $y_1$, respectively.

The correlation results from the NRTL model align well with the experimental data for the binary mixture of methylcyclohexane–toluene, as indicated in Figures C1 and C2. The NRTL model also provides good correlation results when implemented for the pseudo–ternary mixture of methylcyclohexane–toluene–DMI, as shown in Figures 1 and 3. Moreover, the model demonstrates satisfactory correlation for the pseudo–ternary mixture of methylcyclohexane–toluene–NBP, as depicted in Figures 2 and 4. The experimental VLE data for each pseudo–ternary mixture with E/F = 1 at 10.0 and 100.0 kPa and E/F = 3 at 10.0 kPa were regressed as a single correlation to attain more accurate BIPs that precisely describe the VLE data, encompassing various entrainer to feed ratios and pressures. The minimum RMSD in Table 5 also indicated a good correlation of the NRTL model. Therefore, the NRTL models along with the obtained optimum BIPs, are reliable for modeling the extractive distillation for separating methylcyclohexane from toluene using entrainer DMI and NBP, respectively.

## References


(1) Hartanto, D.; Schuur, B.; Kiss, A. A.; de Haan, A. B. Effective Selection of Green Organics and Natural Deep Eutectic Solvents as Advanced Entrainers by COSMO-RS and Group Contributions Methods for Enhanced Design of Extractive Distillation. In *Computer Aided Chemical Engineering*; Manenti, F., Reklaitis, G. V. B. T.-C. A. C. E., Eds.; Elsevier, 2024; Vol. 53, pp 1387–1392. https://doi.org/https://doi.org/10.1016/B978-0-443-28824-1.50232-5.

(2) Aricò, F.; Aldoshin, A. S.; Tundo, P. One-Pot Preparation of Dimethyl Isosorbide from d-Sorbitol via Dimethyl Carbonate Chemistry. *ChemSusChem* **2017**, *10* (1), 53–57. https://doi.org/https://doi.org/10.1002/cssc.201601382.

(3) Zarour, K.; Vieco, N.; Pérez-Ramos, A.; Nácher-Vázquez, M.; Mohedano, M. L.; López, P. Chapter 4 - Food Ingredients Synthesized by Lactic Acid Bacteria. In *Handbook of Food Bioengineering*; Holban, A. M., Grumezescu, A. M. B. T.-M. P. of F. I. and A., Eds.; Academic Press, 2017; pp 89–124. https://doi.org/https://doi.org/10.1016/B978-0-12-811520-6.00004-0.

(4) Grembecka, M. Sugar Alcohols—Their Role in the Modern World of Sweeteners: A Review. *Eur. Food Res. Technol.* **2015**, *241* (1), 1–14. https://doi.org/10.1007/s00217-015-2437-7.

(5) Xie, W.; Li, T.; Tiraferri, A.; Drioli, E.; Figoli, A.; Crittenden, J. C.; Liu, B. Toward the Next Generation of Sustainable Membranes from Green Chemistry Principles. *ACS Sustain. Chem. Eng.* **2021**, *9* (1), 50–75. https://doi.org/10.1021/acssuschemeng.0c07119.

(6) Bozell, J. J.; Petersen, G. R. Technology Development for the Production of Biobased Products from Biorefinery Carbohydrates—the US Department of Energy's "Top 10" Revisited. *Green Chem.* **2010**, *12* (4), 539–554. https://doi.org/10.1039/B922014C.

(7) *Public Report, Arlasolve DMI*; The National Industrial Chemicals Notification and Assessment Scheme (NICNAS); 2004. https://www.industrialchemicals.gov.au/sites/default/files/STD1052 Public Report PDF.pdf.

(8) European Chemical Agency. *1,4:3,6-dianhydro-2,5-di-O-methyl-D-glucitol*. https://chem.echa.europa.eu/100.023.782/overview?searchText=1,4:3,6-dianhydro-2,5-di-O-methyl-D-gluc (accessed 2025-07-03).

(9) *Opinion on N-Methyl-2-Pyrrolidone (NMP)*; Scientific Committee on Consumer Safety, European Union; 2011. https://ec.europa.eu/health/scientific_committees/consumer_safety/docs/sccs_o_050.pdf.

(10) *Dimethyl isosorbide; U.S. Environmental Protection Agency*. https://comptox.epa.gov/dashboard/chemical/genotoxicity/DTXSID201019399 (accessed 2025-08-27).

(11) Annatelli, M.; Dalla Torre, D.; Musolino, M.; Aricò, F. Dimethyl Isosorbide via Organocatalyst N-Methyl Pyrrolidine: Scaling up, Purification and Concurrent Reaction Pathways. *Catal. Sci. Technol.* **2021**, *11* (10), 3411–3421. https://doi.org/10.1039/D1CY00465D.

(12) Benazzouz, A.; Moity, L.; Pierlot, C.; Sergent, M.; Molinier, V.; Aubry, J.-M. Selection of a Greener Set of Solvents Evenly Spread in the Hansen Space by Space-Filling Design. *Ind. Eng. Chem. Res.* **2013**, *52* (47), 16585–16597. https://doi.org/10.1021/ie402410w.

(13) Buken, O.; Mancini, K.; Sarkar, A. A Sustainable Approach to Cathode Delamination Using a Green Solvent. *RSC Adv.* **2021**, *11* (44), 27356–27368. https://doi.org/10.1039/D1RA04922D.
(14) Eastman. *TamiSolve NxG*. https://www.eastman.com/Pages/ProductHome.aspx?product=71103844&pn=TamiSolve+NxG.
(15) *SDS TamiSolve® NxG-PS No. 150000112709 (CAS RN: 3470-98-2)*; Eastman: Tennessee, 2020. https://ws.eastman.com/ProductCatalogApps/PageControllers/MSDSShow_PC.aspx.
(16) European Chemical Agency. *1-butylpyrrolidin-2-one*. https://chem.echa.europa.eu/100.020.399/overview?searchText=1-butylpyrrolidin-2-one (accessed 2025-09-23).
(17) Sherwood, J.; Parker, H. L.; Moonen, K.; Farmer, T. J.; Hunt, A. J. N-Butylpyrrolidinone as a Dipolar Aprotic Solvent for Organic Synthesis. *Green Chem.* **2016**, *18* (14), 3990–3996. https://doi.org/10.1039/C6GC00932H.
(18) *Economic Valuation in 1-Methyl-2-Pyrrolidone (NMP) Regulation*; OECD Environment Working Papers; 131; 2018. https://doi.org/https://doi.org/10.1787/ef67fa08-en.
(19) *Public Report, 2-Pyrrolidinone, 1-Butyl-*; 2020. https://www.industrialchemicals.gov.au/sites/default/files/STD1698 public report %5B780 KB%5D.pdf.
(20) Brouwer, T.; Schuur, B. Bio-Based Solvents as Entrainers for Extractive Distillation in Aromatic/Aliphatic and Olefin/Paraffin Separation. *Green Chem.* **2020**, *22* (16), 5369–5375. https://doi.org/10.1039/D0GC01769H.
(21) Coca, J.; Pis, J. J. Effect of Morpholine on the Vapor-Liquid Equilibrium of the System Methylcyclohexane-Toluene. *J. Chem. Eng. Data* **1979**, *24* (2), 103–105. https://doi.org/10.1021/je60081a017.
(22) Hartanto, D.; Schuur, B.; Schuttevaer, T.; Kiss, A. A.; de Haan, A. B. Isobaric Vapor–Liquid Equilibrium of Methylcyclohexane + Toluene with Gamma-Valerolactone as a Biobased Entrainer and 1-Methylpyrrolidin-2-One as a Conventional Entrainer. *J. Chem. Eng. Data* **2025**, *70* (3), 1339−1351. https://doi.org/10.1021/acs.jced.4c00509.
(23) Liebert, V.; Nebig, S.; Gmehling, J. Experimental and Predicted Phase Equilibria and Excess Properties for Systems with Ionic Liquids. *Fluid Phase Equilib.* **2008**, *268* (1), 14–20. https://doi.org/https://doi.org/10.1016/j.fluid.2008.03.011.
(24) Quijada-Maldonado, E.; Meindersma, G. W.; de Haan, A. B. Pilot Plant Study on the Extractive Distillation of Toluene–Methylcyclohexane Mixtures Using NMP and the Ionic Liquid [Hmim][TCB] as Solvents. *Sep. Purif. Technol.* **2016**, *166*, 196–204. https://doi.org/https://doi.org/10.1016/j.seppur.2016.04.041.
(25) Gutierrez, J. P.; Meindersma, W.; de Haan, A. B. Ionic Liquid Selection and Performance Evaluation for The Separation Of Methylcyclohexane/Toluene by Extractive Distillation. In *Distillation absorption 2010 : conference proceedings*; Technische Universiteit Eindhoven: Eindhoven, 2010.
(26) Anwani, S. S.; Shirsat, S. P. Extractive Distillation Simulation for the Separation of Methylcyclohexane and Toluene Mixture with Phenol as an Extractor Using Chemcad. In *Novel Water Treatment and Separation Methods: Simulation of Chemical Processes*; Bhanvase, B. A., Ugwekar, R. P., Mankar, R. B., Eds.; Apple

Academic Press, Taylor & Francis Group: New York, 2017. https://doi.org/https://doi.org/10.1201/9781315225395.
(27) Tiverios, P. G.; Van Brunt, V. Extractive Distillation Solvent Characterization and Shortcut Design Procedure for Methylcyclohexane−Toluene Mixtures. *Ind. Eng. Chem. Res.* **2000**, *39* (6), 1614–1623. https://doi.org/10.1021/ie990654k.
(28) Van Ness, H. C. Thermodynamics in the Treatment of Vapor/Liquid Equilibrium (VLE) Data. **1995**, *67* (6), 859–872. https://doi.org/doi:10.1351/pac199567060859.
(29) *Evaluation of Measurement Data — Guide to the Expression of Uncertainty in Measurement*; Working Group 1 of the Joint Committee for Guides in Metrology (JCGM/WG 1); 2008. https://www.bipm.org/documents/20126/2071204/JCGM_100_2008_E.pdf.
(30) Taylor, Barry N; Kuyatt, C. E. NIST Technical Note 1297 Guidelines for Evaluating and Expressing the Uncertainty of NIST Measurement Results. *Technology* **1994**.
(31) Weber, J. H. Vapor-Liquid Equilibria for System Methylcyclohexane-Toluene at Subatmospheric Pressures. *Ind. Eng. Chem.* **1955**, *47* (3), 454–457. https://doi.org/10.1021/ie50543a036.
(32) *Aspen Plus Software, Version 12.0*; Aspen Technology, Inc., 2020.
(33) Seiler, M.; Jork, C.; Kavarnou, A.; Arlt, W.; Hirsch, R. Separation of Azeotropic Mixtures Using Hyperbranched Polymers or Ionic Liquids. *AIChE J.* **2004**, *50* (10), 2439–2454. https://doi.org/https://doi.org/10.1002/aic.10249.
(34) Gutiérrez, J. P.; Meindersma, G. W.; de Haan, A. B. COSMO-RS-Based Ionic-Liquid Selection for Extractive Distillation Processes. *Ind. Eng. Chem. Res.* **2012**, *51* (35), 11518–11529. https://doi.org/10.1021/ie301506n.
(35) Meindersma, G. W.; Quijada-Maldonado, E.; Jongmans, M. T. G.; Hernandez, J. P. G.; Schuur, B.; de Haan, A. B. Extractive Distillation with Ionic Liquids: Pilot Plant Experiments and Conceptual Process Design BT - Ionic Liquids for Better Separation Processes; Rodríguez, H., Ed.; Springer Berlin Heidelberg: Berlin, Heidelberg, 2016; pp 11–38. https://doi.org/10.1007/978-3-662-48520-0_2.
(36) Gerbaud, V.; Rodriguez-Donis Molecular Sciences and Chemical Engineering, I. B. T.-R. M. in C. Advances in Extractive Distillation☆; Elsevier, 2019. https://doi.org/https://doi.org/10.1016/B978-0-12-409547-2.05949-7.
(37) Kiss, A. A. Distillation: Extractive Distillation. *Ref. Modul. Chem. Mol. Sci. Chem. Eng.* **2013**, 1–11.
(38) Botía, D. C.; Riveros, D. C.; Ortiz, P.; Gil, I. D.; Sánchez, O. F. Vapor−Liquid Equilibrium in Extractive Distillation of the Acetone/Methanol System Using Water as Entrainer and Pressure Reduction. *Ind. Eng. Chem. Res.* **2010**, *49* (13), 6176–6183. https://doi.org/10.1021/ie901702h.
(39) Wisniak, J.; Ortega, J.; Fernández, L. A Fresh Look at the Thermodynamic Consistency of Vapour-Liquid Equilibria Data. *J. Chem. Thermodyn.* **2017**, *105*, 385–395. https://doi.org/https://doi.org/10.1016/j.jct.2016.10.038.
(40) Li, F.; Li, M.; Guo, J.; Hu, X.; Zhu, J.; Li, Q.; Zhao, H. Isobaric Vapor–Liquid Equilibrium Experiment of N-Propanol and N-Propyl Acetate at 101.3 KPa. *J. Chem. Eng. Data* **2023**, *68* (2), 358–365. https://doi.org/10.1021/acs.jced.2c00609.
(41) Cao, M.; Tian, H.; Li, M. Vapor–Liquid Equilibrium Data Determination and Model Correlation for 1-Octene + 1,4-Dioxane, 2-Octanol + 1,4-Dioxane, 1-

Octene + Isophorone, and 2-Octanol + Isophorone Systems at 101.3 KPa. *J. Chem. Eng. Data* **2023**, *68* (9), 2275–2282. https://doi.org/10.1021/acs.jced.3c00136.
(42) Lei, Z.; Arlt, W.; Wasserscheid, P. Selection of Entrainers in the 1-Hexene/n-Hexane System with a Limited Solubility. *Fluid Phase Equilib.* **2007**, *260* (1), 29–35. https://doi.org/https://doi.org/10.1016/j.fluid.2006.06.009.
(43) Zhang, Z.; Zhang, Z.; Dong, B.; Chen, J.; Xin, H.; Zhang, Q. Vapor-Liquid Equilibrium Experiment and Model Prediction for Separating Ethyl Propionate and Ethanol Using Ionic Liquids with Acetate Anion. *J. Mol. Liq.* **2020**, *318*, 113688. https://doi.org/https://doi.org/10.1016/j.molliq.2020.113688.
(44) Yang, C.; Zeng, H.; Yin, X.; Ma, S.; Sun, F.; Li, Y.; Li, J. Measurement of (Vapor+liquid) Equilibrium for the Systems {methanol+dimethyl Carbonate} and {methanol+dimethyl Carbonate+tetramethylammonium Bicarbonate} at P=(34.43, 67.74)KPa. *J. Chem. Thermodyn.* **2012**, *53*, 158–166. https://doi.org/https://doi.org/10.1016/j.jct.2012.05.002.
(45) Zhang, Y.; Wang, Z.; Xu, X.; Gao, J.; Xu, D.; Zhang, L.; Wang, Y. Entrainers Selection and Vapour-Liquid Equilibrium Measurements for Separating Azeotropic Mixtures (Ethanol + n-Hexane/Cyclohexane) by Extractive Distillation. *J. Chem. Thermodyn.* **2020**, *144*, 106070. https://doi.org/https://doi.org/10.1016/j.jct.2020.106070.
(46) He, S.; Fan, W.; Huang, H.; Gao, J.; Xu, D.; Ma, Y.; Zhang, L.; Wang, Y. Separation of the Azeotropic Mixture Methanol and Toluene Using Extractive Distillation: Entrainer Determination, Vapor–Liquid Equilibrium Measurement, and Modeling. *ACS Omega* **2021**, *6* (50), 34736–34743. https://doi.org/10.1021/acsomega.1c05164.
(47) Britt, H. I.; Luecke, R. H. The Estimation of Parameters in Nonlinear, Implicit Models. *Technometrics* **1973**, *15* (2), 233–247. https://doi.org/10.2307/1266984.

## 3.3. Conclusions of Sections 3.1 and 3.2

In this Chapter 3, isobaric VLE data were measured using a Fischer Labodest VLE602 ebulliometer for the binary mixture of methylcyclohexane (1) + toluene (2) and the pseudo-ternary mixtures of methylcyclohexane (1) + toluene (2) containing the greener entrainers of GVL, DMI, NBP, and NMP, along with benchmark entrainer NMP. All experimental VLE data were thermodynamically consistent, having successfully passed the thermodynamic consistency tests, confirming the reliability of the data.

The results demonstrate that the addition of these entrainers significantly increases the relative volatility of methylcyclohexane to toluene and effectively removes close-boiling behavior. For all investigated mixtures, reducing the pressure increases relative volatility. Increasing E/F generally improves separation performance, although the enhancement becomes less pronounced or may even decrease at higher entrainer concentrations. Among the investigated entrainers, GVL exhibits the best separation performance compared to other greener entrainers of DMI and NBP as well as conventional entrainers, such as NMP and sulfolane. With the addition of GVL, reducing the pressure yields a slight increase in the relative volatility of methylcyclohexane to toluene. A similar behavior occurs when the amount of GVL added to the mixture increases; the relative volatility is also enhanced, but only modestly. For DMI and NBP, decreasing the pressure from 100.0 to 10.0 kPa at E/F = 1 leads to a significant increase in relative volatility. However, increasing the amount of DMI and NBP to E/F = 3 at 10.0 kPa resulted in a decrease in relative volatility compared to those with E/F = 1 at 10.0 kPa. The relative volatility performance of DMI and NBP was compared at E/F = 1 and 10.0 kPa. Both DMI and NBP demonstrate a comparable relative volatility performance to remove a close–boiling behavior. Moreover, both DMI and NBP at E/F = 1 and 10.0 kPa exhibit a slightly higher relative volatility than NMP at E/F = 1 and 100.0 kPa in all composition ranges of methylcyclohexane. Notably, they show higher relative volatility than sulfolane at E/F = 1 and 100.0 kPa in the methylcyclohexane–rich region. In comparison with other green entrainers, DMI and NBP at E/F = 1 and 10.0 kPa have comparable relative volatility to GVL and Cyrene at E/F = 1 and 100.0 kPa. These results highlight the strong potential of GVL, DMI, and NBP as effective biobased and greener alternatives to conventional entrainers for the separation of methylcyclohexane from toluene through extractive distillation.

The data correlation was implemented to acquire the optimized binary interaction parameters. The NRTL and UNIQUAC models were employed to establish correlations for the VLE data of binary and pseudo-ternary mixtures. Both models accurately fit the VLE data of the binary methylcyclohexane-toluene mixture. For the pseudo-ternary mixture containing GVL, the NRTL model

demonstrates better agreement with the experimental values than the UNIQUAC model, whereas for the mixture with NMP, both models provided accurate correlations. For the mixture containing DMI and NBP, the NRTL model also demonstrates good agreement with the experimental data. The regression results provide optimized binary interaction parameters for each component pair.

Overall, the VLE data and optimized binary interaction parameters provide a reliable thermodynamic basis for modelling and simulation of extractive distillation processes for methylcyclohexane-toluene separation. Process simulations for evaluating the ED performance for each entrainer, considering economic and sustainability metrics, are discussed in Chapter 5.

(*This page is intentionally left blank*)

# Chapter 4

## Vapor-liquid equilibrium data of the n-hexane-ethanol mixture with the presence of entrainers

Chapter 4 discusses vapor-liquid equilibrium (VLE) data for the azeotropic n-hexane-ethanol mixture in the presence of the biobased, greener, and benchmark entrainers. This chapter contains two sections:

4.1 VLE data of n-hexane-ethanol with 1-butylpyrrolidin-2-one and 1-methylpyrrolidin-2-one.

4.2 VLE data of n-hexane-ethanol with dimethyl isosorbide and guaiacol.

*This chapter has been published in:*
*Journal of Chemical & Engineering Data 70 (10), 4091-4104, (2025)*
*Fluid Phase Equilibria 605, 114694, (2026)*

## 4.1 VLE data of hexane-ethanol with 1-butylpyrrolidin-2-one and 1-methylpyrrolidin-2-one


### Abstract

Green solvents have emerged as promising green entrainers to substitute conventional entrainers in extractive distillation to separate azeotropic mixtures. However, the limited availability of the thermodynamic data for green solvent-containing mixtures continues to hinder their practical implementation in this process. This study reports the first experimental vapor-liquid equilibrium (VLE) data for the n-hexane + ethanol azeotropic system containing the greener entrainer 1-butylpyrrolidin-2-one (NBP) alongside the benchmark entrainer 1-methylpyrrolidin-2-one (NMP). Using a Fischer Labodest VLE602 ebulliometer, VLE measurements were performed at pressures of 50.0-100.0 kPa and various entrainer-to-feed ratios (E/F). The reliability of the reported VLE data was tested and confirmed using the Van Ness thermodynamic consistency test. The results show that NBP enhances relative volatility and effectively eliminates the azeotrope, performing comparably to the benchmark entrainer NMP. The Non-Random Two Liquid (NRTL) model was utilized to regress the investigated VLE data and determine the optimum binary interaction parameters (BIPs). As a result, the NRTL model demonstrates a good agreement with the experimental data. This thermodynamic modeling confirms the data's reliability and suitability for process design, highlighting NBP's potential as an environmentally friendly alternative entrainer in extractive distillation.

### 4.1.1. Introduction

In the separation of n-hexane-ethanol, current research has reported several potential entrainers, particularly focusing on the VLE data for the binary mixture of n-hexane with butyl propanoate and butyl butanoate, respectively,[1] along with VLE data for the binary mixture of ethanol with butyl propanoate and butyl butanoate.[2] In these studies, however, only binary VLE data were provided and no VLE data were provided for the pseudo-ternary mixture of n-hexane-ethanol containing butyl propanoate and butyl butanoate as entrainers. In addition, ionic liquids, including cations such as 1-ethyl-3-methyl-imidazolium [EMIM], 1-butyl-3-methyl-imidazolium [BMIM], and 1-hexyl-3-methyl-imidazolium [HMIM] combined with hydrogen sulfate [$HSO_4$], have been studied for n-hexane-ethanol separation.[3] Furthermore, the high cost of ionic liquids compared to conventional solvents poses challenges for their industrial application. Extractive distillation experiments using a simple round bottom flask have also been reported using deep eutectic solvents (DESs), such as choline chloride-glycerol, menthol-decanoic acid, and menthol-dodecanoic acid.[4] However, choline chloride-glycerol based DES faces miscibility issues, and the maximum purity of n-hexane obtained using these DESs with mass fraction of 0.05 was only 0.87 mas fraction. Additionally, Wang et al. investigated the impact of conventional solvents such as dimethyl sulfoxide, 1,2-propanediol, 1,3-propanediol, ethylene glycol, dimethylformamide, dimethylacetamide, and NMP on the relative volatility of n-hexane-ethanol mixture.[5] This publication provided only predicted results without complete experimental VLE data.

According to the prediction results using unimolecular quantum chemical calculation and group contribution methods from our previous work, NBP demonstrated a comparable relative volatility to NMP.[6] Furthermore, NBP is classified by the European Chemical Agency as a non-toxic and non-reprotoxic solvent, making it a safer alternative to conventional solvents.[7] In contrast, NMP is deemed as a toxic chemical. The No Observed Adverse Effect Level (NOAEL) for developmental toxicity exceeds 500 mg/kg body weight/day for NBP, in contrast to 160 mg/kg body weight/day for NMP.[8,9] As NOAEL values define the maximum dose at which there are no harmful effects on fetal development. A higher NOAEL indicates lower toxicity. This suggests that NBP has lower fetal development toxicity than NMP. In addition, NBP complies with the principles of green chemistry by employing biobased and economically viable glutamic acid as a renewable feedstock. Its synthesis pathway minimizes environmental impact by generating near-zero waste throughout the process.[10]

From a technical standpoint, NBP possesses a high boiling point (514.15 K at a pressure of 101.3 kPa), which is higher than NMP (475.15 K at a pressure of 101.3 kPa), favorable thermal stability, good polarity (Hansen solubility

parameters, ($\delta_P$) = 8.2 $MPa^{1/2}$, which is comparable to those of NMP with $\delta_P$ = 12.3 $MPa^{1/2}$. Additionally, NBP has a lower vapor pressure of 0.013 kPa at a temperature of 298.15 K, compared to NMP's vapor pressure of 0.044 kPa at the same temperature. These properties are advantageous for use in extractive distillation.[11–14]

Therefore, the present study evaluates for the first time the performance of NBP as a greener entrainer for separating the azeotropic mixture n-hexane-ethanol by measuring the VLE data for the n-hexane-ethanol mixture containing NBP. For comparative purposes, the VLE data for n-hexane-ethanol mixture in the presence of NMP as a benchmark entrainer was measured as NMP has been proven effective in commercial separation processes, offers less expensive solvent, and possesses good solvency properties, including high polarity and thermal stability.[15] NMP is already produced on a large scale. According to the European Chemical Agency, the production and import of NMP in Europe is from 10,000 to 100,000 tons per year.[16] This indicates that, despite some restrictions, NMP remains widely used in various industrial applications, such as lithium battery industries, membrane fabrications, pharmaceutical industries, and coal and oil exploration.[15] Furthermore, NMP is commonly employed in process separation, particularly as an entrainer in extractive distillation.[17–19]

The VLE data were tested for thermodynamic consistency using the Van Ness method.[20] To further assess the applicability of NBP, the NRTL activity coefficient model was employed to regress the experimental data and determine optimum BIPs.[21] Accurate experimental VLE data and optimum BIPs obtained from thermodynamic modeling serve as a critical foundation for the effective design and optimization of extractive distillation processes.

## 4.1.2. Experimental methods

The following sections outline the chemical information, the experimental setup and procedures, as well as the analytical methods employed.

**Chemicals**

The chemicals used in this work were procured from commercial suppliers. Their purity was assessed using gas chromatography (GC). All chemicals were employed in their original state without any additional purification processes, as no significant contaminants were identified. Table 1 presents the detailed information of the chemicals used.

**Table 1.** The Technical information of the chemicals

| chemicals | CAS No. | molecular weight (g/mol) | Boiling point (K)[a,b] | density ($g/cm^3$)[a,c] | commercial suppliers | purity (in a mass fraction)[a] | analysis method | purification |
|---|---|---|---|---|---|---|---|---|
| n-hexane | 110-54-3 | 86.18 | 342.15 | 0.660 | Merck | ≥0.990 | GC[d] | none |
| ethanol | 64-17-5 | 46.07 | 351.44 | 0.790 | Merck | ≥0.999 | GC[d] | none |
| 1-butylpyrrolidin-2-one | 3470-98-2 | 141.21 | 514.15 | 0.960 | BioPSX | 0.995 | GC[d] | none |
| 1-methylpyrrolidin-2-one | 872-50-4 | 99.13 | 475.15 | 1.028 | Sigma-Aldrich | ≥0.995 | GC[d] | none |
| acetone | 67-64-1 | 58.08 | 329.15 | 0.791 | Merck | ≥0.998 | GC[d] | none |

[a]specified by the commercial suppliers

[b]at pressure of 101.3 kPa

[c]at temperature of 298.15 and pressure of 101.3 kPa

[d]GC (gas chromatography)

**Experimental setup and procedures**

Experimental and analytical methods for the VLE data measurements are described in Chapter 2. In addition, expanded combined uncertainties for liquid and vapor composition, pressure, and temperature were calculated in accordance with the NIST technical note and JCGM guideline,[27,28] as detailed in Eqs. D1-D6 in the Appendix. The uncertainty values are reported alongside the VLE data in Results and discussions Section. In addition, the expanded combined uncertainties for vapor pressure measurements for n-hexane and ethanol were calculated using Eqs. D7 and D8 and presented in Table D1 in the Appendix.

## 4.1.3. Results and discussion

**Experimental Results**

In this study, isobaric VLE data for the binary mixture of n-hexane and ethanol at 101.3 kPa were measured. The results of the VLE data are presented in Table 2. The liquid phase and vapor phase mole fraction of n-hexane are denoted as $x_1$ and $y_1$, respectively. While the equilibrium temperature is represented as $T$, and the activity coefficient for n-hexane and ethanol are indicated as $\gamma_1$ and $\gamma_2$, respectively. Additionally, the relative volatility of n-hexane to ethanol is denoted as $\alpha_{12}$.

**Table 2.** VLE data for hexane (1) + ethanol (2) at 101.3 kPa[a,b]

| $T$/K | $x_1$ | $y_1$ | $\gamma_1$ | $\gamma_2$ | $\alpha_{12}$ |
|---|---|---|---|---|---|
| 351.55 | 0.000 | 0.000 | | 1.000 | |
| 347.18 | 0.015 | 0.144 | 8.161 | 1.031 | 11.05 |
| 345.39 | 0.021 | 0.197 | 8.490 | 1.046 | 11.53 |
| 340.46 | 0.064 | 0.381 | 6.248 | 1.035 | 9.05 |
| 338.61 | 0.092 | 0.451 | 5.416 | 1.026 | 8.08 |
| 336.82 | 0.116 | 0.497 | 5.025 | 1.043 | 7.52 |
| 335.90 | 0.132 | 0.529 | 4.847 | 1.035 | 7.39 |
| 335.35 | 0.141 | 0.548 | 4.790 | 1.028 | 7.40 |
| 334.26 | 0.162 | 0.567 | 4.461 | 1.060 | 6.77 |
| 332.51 | 0.252 | 0.606 | 3.247 | 1.169 | 4.56 |
| 331.39 | 0.577 | 0.645 | 1.568 | 1.958 | 1.33 |
| 331.26 | 0.687 | 0.654 | 1.341 | 2.597 | 0.86 |
| 331.52 | 0.802 | 0.665 | 1.159 | 3.922 | 0.49 |
| 332.35 | 0.895 | 0.708 | 1.075 | 6.218 | 0.28 |
| 334.07 | 0.958 | 0.765 | 1.025 | 11.598 | 0.14 |
| 336.10 | 0.978 | 0.843 | 1.036 | 13.378 | 0.12 |
| 339.32 | 0.990 | 0.939 | 1.028 | 10.275 | 0.15 |
| 342.15 | 1.000 | 1.000 | 1.000 | | |

[a] $T$: equilibrium temperature; $x_1$ and $y_1$: mole fraction of n-hexane in the liquid and vapor-phases, respectively; $\gamma_1$ and $\gamma_2$: activity coefficient of n-hexane and ethanol, respectively; $\alpha_{12}$: relative volatility of n-hexane to ethanol.
[b] Expanded combined uncertainties ($U$ with $k$ = 2): $U(T)$ = 0.20 K, $U(P)$ = 0.20 kPa, and $U(x_1) = U(y_1)$ = 0.006.

To quantify the deviation from ideal solution behavior, Eq. 1 was used to determine the activity coefficient of component $i$ in the binary mixture ($\gamma_i$).

$$\gamma_i = \frac{y_i P}{x_i P_i^{sat}} \qquad 1)$$

For component $i$, the liquid-phase mole fraction is denoted as $x_i$, while the vapor-phase mole fraction is defined as $y_i$. The total pressure of the system and saturated vapor pressure of component $i$ are expressed as $P$ and $P_i^{sat}$, respectively. The constant of the extended Antoine and its equation retrieved from the physical properties databank of the Aspen Plus, is provided in Table 3 and was utilized to calculate the saturated vapor pressure for component $i$. As the VLE data measurements for the binary mixture were conducted at atmospheric and lower pressures, ideal gas behavior was assumed.

**Table 3.** The constant of the extended Antoine[a, b]

| Components | $A_1$ | $A_2$ | $A_3$ | $A_4$ | $A_5$ | $10^6A_6$ | $A_7$ | $A_8$ | $A_9$ |
|---|---|---|---|---|---|---|---|---|---|
| n-hexane | 97.742 | -6995.5 | 0 | 0 | -12.702 | 12.381 | 2 | 177.83 | 507.6 |
| ethanol | 66.396 | -7122.3 | 0 | 0 | -7.142 | 2.8853 | 2 | 159.05 | 514.0 |

[a]Extended Antoine constants: $A_1$, $A_2$, $A_3$, $A_4$, $A_5$, $A_6$, $A_7$, $A_8$, and $A_9$ (physical property databank of Aspen Plus)
[b]Extended Antoine:
$\ln(P^{sat}) = A_1 + A_2/(T + A_3) + A_4T + A_5 \ln T + A_6T^{A_7}$ for $A_8 < T < A_9$, where $P^{sat}$ is in kPa and $T$ in K.

The relative volatility for the binary mixture of n-hexane (1) and ethanol (2) ($\alpha_{12}$) is expressed in Eq. 2:

$$\alpha_{12} = \frac{y_1 / x_1}{y_2 / x_2} \qquad 2)$$

To validate our method and setup, we compared the VLE data for the binary mixture of n-hexane and ethanol measured at 101.3 kPa from our work with the data from existing literature. The $T$-$x_1$-$y_1$ diagram, as illustrated in Figure 1, and the $x_1$-$y_1$ diagram, as shown in Figure D1, shows that our VLE data are consistent with those reported by Sinor and Weber,[29] as well as Ortega and Espiau.[30]

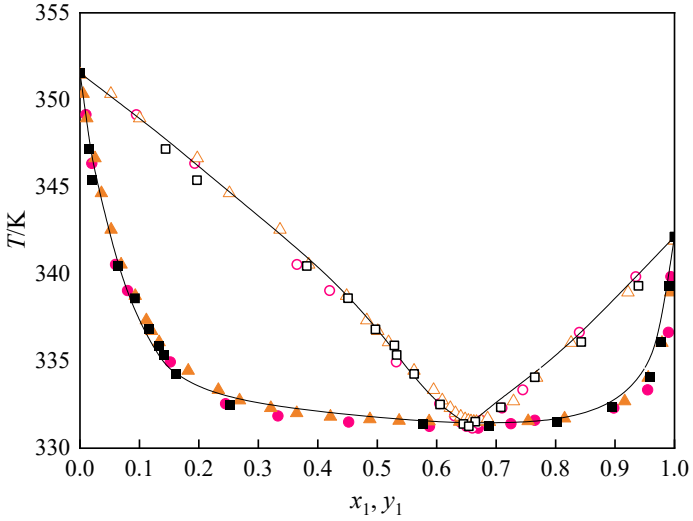


**Figure 1.** $T$-$x_1$-$y_1$ diagram of n-hexane (1) + ethanol (2) at 101.3 kPa: (■), experimental liquid- and (□), vapor-phase from this work; (●), experimental liquid- and (○), vapor-phase from literature (Sinor and Weber, 1960)[29]; (▲), experimental liquid- and ; (Δ), vapor-phase from literature (Ortega and Espiau, 2003)[30]; and (—), regressed with the NRTL model.

Additionally, we measured the pure component vapor pressure for n-hexane and ethanol and compared our results with values from existing literature. The vapor pressure values for n-hexane and ethanol obtained from our experiments closely match those reported by Williamham et al.[31] and Kretschmer and Wiebe,[32] as shown in Figures D2 and D3 and tabulated in Table D1. This alignment confirms both the accuracy of our experimental setup and the reliability of the methods. The VLE data was verified for the thermodynamic consistency using the method proposed by Van Ness,[20] which confirmed their consistency. A discussion of this consistency test is presented in Thermodynamic consistency test Section. Furthermore, the effect of reduced pressure on the relative volatility of n-hexane to ethanol was investigated at pressures of 61.3 and 101.3 kPa. The VLE data for the binary mixture at a reduced pressure of 61.3 kPa were taken from the literature.[30] Figures 2 and D1 indicate that lowering the pressure to 61.3 kPa exerted a negligible effect on the azeotropic behavior of the mixture. The relative volatility is only slightly increased, and the azeotropic point remains in the mixture, shifting just slightly towards the n-hexane-rich region. These literature data, combined with the VLE data at 101.3 from this study, were utilized for the regression.

The setup and methods were then employed to measure the VLE data for the pseudo-ternary mixture of n-hexane and ethanol with the entrainers NBP and NMP, respectively. The amount of entrainer added to the mixture on a mass basis is defined by the E/F. The VLE data for the pseudo-ternary mixture of n-hexane (1) + ethanol (2) + NBP (3) was measured at E/F = 1, under pressures of 50.0, 80.0, and 100.0 kPa. In addition, measurements were conducted at the different E/F values of 2 and 3 at a pressure of 100.0 kPa. The collected VLE data for this pseudo-ternary mixture are presented in Tables 4 and 5, where the liquid phase and the vapor phase mole fraction of n-hexane, on an entrainer-free basis, are denoted as $x_1'$ and $y_1'$, respectively. The liquid and vapor phase mole fractions of n-hexane, ethanol, and the entrainer are expressed as $x_1$, $x_2$, and $x_3$, and $y_1$, $y_2$, and $y_3$, respectively. The equilibrium temperature is represented as $T$, the activity coefficients of n-hexane and ethanol are denoted as $\gamma_1$ and $\gamma_2$, and the relative volatility of n-hexane to ethanol is defined as $\alpha_{12}$. As no entrainer was detected in the vapor phase, the values of $y_3$ are considered to be smaller than 0.0005. Therefore, the values of $y_1'$ are equal to $y_1$.

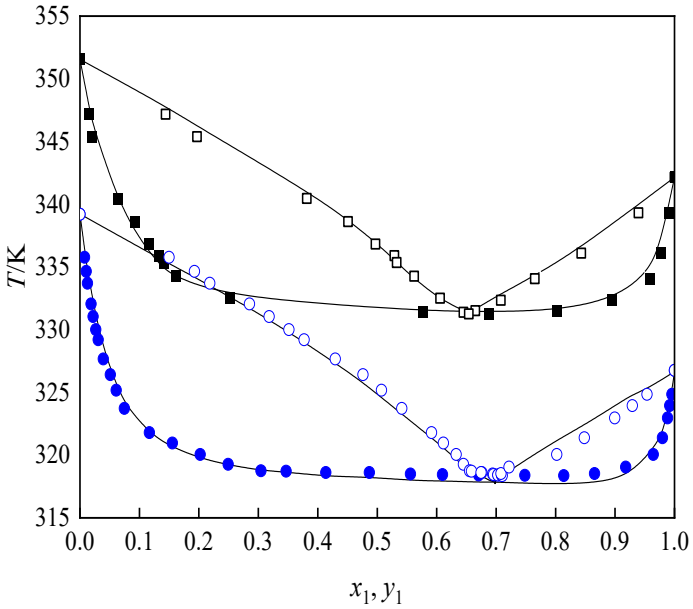


**Figure 2.** $T$-$x_1$-$y_1$ diagram of n-hexane (1) + ethanol (2) at pressures of 61.3 and 101.3 kPa: (●), experimental liquid- and (○), vapor-phase at 61.3 kPa from literature (Ortega and Espiau, 2003)[30]; (■), experimental liquid- and (□), vapor-phase at 101.3 kPa from this work; and (—), regressed with the NRTL model.

**Table 4.** VLE data for hexane (1) + ethanol (2) + 1-butylpyrrolidin-2-one (3) with mass-based E/F = 1 and various pressures at 50.0, 80.0, and 100.0 kPa[a,b,c]

| $T$/K | $x_1$' | $x_1$ | $x_2$ | $x_3$ | $y_1$' | $y_1$ | $y_2$ | $y_3$ | $\gamma_1$ | $\gamma_2$ | $\alpha_{12}$ |
|---|---|---|---|---|---|---|---|---|---|---|---|
| ***50.0 kPa*** | | | | | | | | | | | |
| 342.20 | 0.000 | 0.000 | 0.754 | 0.246 | 0.000 | 0.000 | 1.000 | 0.000 | | 0.954 | |
| 333.50 | 0.096 | 0.071 | 0.668 | 0.261 | 0.399 | 0.399 | 0.601 | 0.000 | 3.633 | 0.941 | 6.26 |
| 332.04 | 0.114 | 0.084 | 0.652 | 0.264 | 0.451 | 0.451 | 0.549 | 0.000 | 3.659 | 0.941 | 6.42 |
| 325.59 | 0.231 | 0.166 | 0.552 | 0.282 | 0.681 | 0.681 | 0.319 | 0.000 | 3.465 | 0.869 | 7.10 |
| 323.71 | 0.287 | 0.224 | 0.486 | 0.290 | 0.730 | 0.730 | 0.270 | 0.000 | 2.942 | 0.914 | 6.70 |
| 321.64 | 0.474 | 0.310 | 0.374 | 0.316 | 0.805 | 0.805 | 0.195 | 0.000 | 2.526 | 0.946 | 4.58 |
| 321.72 | 0.621 | 0.413 | 0.252 | 0.335 | 0.867 | 0.867 | 0.133 | 0.000 | 2.035 | 0.956 | 3.98 |
| 322.05 | 0.691 | 0.450 | 0.207 | 0.343 | 0.881 | 0.881 | 0.119 | 0.000 | 1.878 | 1.021 | 3.31 |
| 323.14 | 0.799 | 0.516 | 0.127 | 0.357 | 0.928 | 0.928 | 0.072 | 0.000 | 1.656 | 0.961 | 3.24 |
| 323.90 | 0.908 | 0.569 | 0.062 | 0.369 | 0.964 | 0.964 | 0.036 | 0.000 | 1.520 | 0.955 | 2.68 |
| 325.29 | 1.000 | 0.621 | 0.000 | 0.379 | 1.000 | 1.000 | 0.000 | 0.000 | 1.376 | | |
| ***80.0 kPa*** | | | | | | | | | | | |
| 353.50 | 0.000 | 0.000 | 0.754 | 0.246 | 0.000 | 0.000 | 1.000 | 0.000 | | 0.967 | |
| 346.58 | 0.094 | 0.070 | 0.669 | 0.261 | 0.408 | 0.408 | 0.592 | 0.000 | 3.999 | 0.849 | 6.62 |
| 346.01 | 0.107 | 0.079 | 0.658 | 0.263 | 0.413 | 0.413 | 0.587 | 0.000 | 3.648 | 0.876 | 5.89 |
| 341.35 | 0.204 | 0.148 | 0.575 | 0.277 | 0.613 | 0.613 | 0.387 | 0.000 | 3.334 | 0.802 | 6.17 |
| 339.96 | 0.242 | 0.174 | 0.543 | 0.283 | 0.654 | 0.654 | 0.346 | 0.000 | 3.150 | 0.807 | 5.91 |

| *T*/K | $x_1'$ | $x_1$ | $x_2$ | $x_3$ | $y_1'$ | $y_1$ | $y_2$ | $y_3$ | $\gamma_1$ | $\gamma_2$ | $\alpha_{12}$ |
|---|---|---|---|---|---|---|---|---|---|---|---|
| 335.70 | 0.467 | 0.320 | 0.365 | 0.315 | 0.768 | 0.768 | 0.232 | 0.000 | 2.305 | 0.966 | 3.77 |
| 334.99 | 0.643 | 0.427 | 0.236 | 0.337 | 0.843 | 0.843 | 0.157 | 0.000 | 1.943 | 1.042 | 2.99 |
| 335.34 | 0.683 | 0.449 | 0.209 | 0.342 | 0.857 | 0.857 | 0.143 | 0.000 | 1.855 | 1.059 | 2.78 |
| 336.67 | 0.788 | 0.509 | 0.136 | 0.355 | 0.908 | 0.908 | 0.092 | 0.000 | 1.661 | 0.991 | 2.64 |
| 337.94 | 0.903 | 0.572 | 0.060 | 0.368 | 0.957 | 0.957 | 0.043 | 0.000 | 1.497 | 0.993 | 2.39 |
| 339.58 | 1.000 | 0.621 | 0.000 | 0.379 | 1.000 | 1.000 | 0.000 | 0.000 | 1.367 | | |
| ***100.0 kPa*** | | | | | | | | | | | |
| 359.46 | 0.000 | 0.000 | 0.754 | 0.246 | 0.000 | 0.000 | 1.000 | 0.000 | | 0.963 | |
| 350.71 | 0.090 | 0.067 | 0.673 | 0.260 | 0.365 | 0.365 | 0.635 | 0.000 | 4.116 | 0.959 | 5.83 |
| 349.81 | 0.112 | 0.082 | 0.654 | 0.264 | 0.396 | 0.396 | 0.604 | 0.000 | 3.732 | 0.973 | 5.21 |
| 345.10 | 0.203 | 0.146 | 0.577 | 0.277 | 0.586 | 0.586 | 0.414 | 0.000 | 3.590 | 0.914 | 5.58 |
| 342.45 | 0.366 | 0.255 | 0.445 | 0.301 | 0.709 | 0.709 | 0.291 | 0.000 | 2.699 | 0.930 | 4.24 |
| 341.86 | 0.443 | 0.305 | 0.384 | 0.311 | 0.748 | 0.748 | 0.252 | 0.000 | 2.421 | 0.959 | 3.73 |
| 342.24 | 0.645 | 0.427 | 0.235 | 0.338 | 0.833 | 0.833 | 0.167 | 0.000 | 1.904 | 1.017 | 2.75 |
| 342.56 | 0.691 | 0.447 | 0.210 | 0.343 | 0.842 | 0.842 | 0.158 | 0.000 | 1.821 | 1.065 | 2.39 |
| 343.77 | 0.795 | 0.513 | 0.131 | 0.356 | 0.900 | 0.900 | 0.100 | 0.000 | 1.634 | 1.033 | 2.31 |
| 345.05 | 0.904 | 0.571 | 0.061 | 0.368 | 0.954 | 0.954 | 0.046 | 0.000 | 1.495 | 0.974 | 2.20 |
| 347.02 | 1.000 | 0.621 | 0.000 | 0.379 | 1.000 | 1.000 | 0.000 | 0.000 | 1.358 | | |

[a] *T*: equilibrium temperature; $x_1'$: mole fraction of n-hexane in the liquid phase (NBP-free basis); $y_1'$: mole fraction of n-hexane in the vapor phase (NBP-free basis); $x_1$, $x_2$, and $x_3$: mole fractions of n-hexane, ethanol, and NBP in the liquid phase, respectively; $y_1$, $y_2$, and $y_3$: mole fractions of n-hexane, ethanol, and NBP in the vapor phase; $\gamma_1$ and $\gamma_2$: activity coefficient of n-hexane and ethanol, respectively: $\alpha_{12}$: relative volatility of n-hexane to ethanol.

[b] Expanded combined uncertainties ($U$ with $k$ = 2): $U(T)$ = 0.40 K, $U(P)$ = 0.23 kPa, and $U(x_1)$ = $U(y_1)$ = 0.006.

[c] $y_3$ values are less than 0.0005.

**Table 5.** VLE data for hexane (1) + ethanol (2) + 1-butylpyrrolidin-2-one (3) at pressure of 100.0 kPa with mass-based E/F = 2 and 3[a,b,c]

| *T*/K | $x_1'$ | $x_1$ | $x_2$ | $x_3$ | $y_1'$ | $y_1$ | $y_2$ | $y_3$ | $\gamma_1$ | $\gamma_2$ | $\alpha_{12}$ |
|---|---|---|---|---|---|---|---|---|---|---|---|
| ***E/F = 2*** | | | | | | | | | | | |
| 369.53 | 0.000 | 0.000 | 0.605 | 0.395 | 0.000 | 0.000 | 1.000 | 0.000 | | 0.834 | |
| 361.33 | 0.082 | 0.048 | 0.540 | 0.412 | 0.275 | 0.275 | 0.725 | 0.000 | 3.201 | 0.910 | 4.22 |
| 353.98 | 0.157 | 0.090 | 0.484 | 0.426 | 0.539 | 0.539 | 0.461 | 0.000 | 4.112 | 0.851 | 6.31 |
| 351.20 | 0.224 | 0.126 | 0.436 | 0.438 | 0.624 | 0.624 | 0.376 | 0.000 | 3.692 | 0.859 | 5.75 |
| 349.31 | 0.355 | 0.191 | 0.348 | 0.461 | 0.734 | 0.734 | 0.266 | 0.000 | 3.025 | 0.824 | 5.01 |
| 348.97 | 0.477 | 0.248 | 0.272 | 0.480 | 0.801 | 0.801 | 0.199 | 0.000 | 2.570 | 0.796 | 4.42 |
| 349.14 | 0.659 | 0.326 | 0.167 | 0.507 | 0.878 | 0.878 | 0.122 | 0.000 | 2.133 | 0.791 | 3.71 |
| 349.41 | 0.808 | 0.399 | 0.074 | 0.527 | 0.947 | 0.947 | 0.053 | 0.000 | 1.863 | 0.771 | 4.20 |
| 350.10 | 0.913 | 0.423 | 0.037 | 0.540 | 0.972 | 0.972 | 0.028 | 0.000 | 1.768 | 0.797 | 3.26 |
| 350.93 | 1.000 | 0.450 | 0.000 | 0.550 | 1.000 | 1.000 | 0.000 | 0.000 | 1.668 | | |

| *T*/K | $x_1'$ | $x_1$ | $x_2$ | $x_3$ | $y_1'$ | $y_1$ | $y_2$ | $y_3$ | $\gamma_1$ | $\gamma_2$ | $\alpha_{12}$ |
|---|---|---|---|---|---|---|---|---|---|---|---|
| ***E/F = 3*** | | | | | | | | | | | |
| 380.85 | 0.000 | 0.000 | 0.505 | 0.495 | 0.000 | 0.000 | 1.000 | 0.000 | | 0.682 | |
| 375.24 | 0.091 | 0.044 | 0.442 | 0.514 | 0.257 | 0.257 | 0.743 | 0.000 | 2.252 | 0.698 | 3.45 |
| 372.51 | 0.142 | 0.068 | 0.408 | 0.524 | 0.459 | 0.459 | 0.541 | 0.000 | 2.819 | 0.603 | 5.12 |
| 369.28 | 0.224 | 0.123 | 0.338 | 0.539 | 0.616 | 0.616 | 0.384 | 0.000 | 2.266 | 0.579 | 5.57 |
| 367.74 | 0.289 | 0.133 | 0.316 | 0.551 | 0.648 | 0.648 | 0.352 | 0.000 | 2.296 | 0.598 | 4.52 |
| 365.12 | 0.413 | 0.177 | 0.252 | 0.571 | 0.742 | 0.742 | 0.258 | 0.000 | 2.116 | 0.604 | 4.10 |
| 363.01 | 0.625 | 0.249 | 0.149 | 0.602 | 0.869 | 0.869 | 0.131 | 0.000 | 1.866 | 0.560 | 3.97 |
| 362.28 | 0.705 | 0.274 | 0.114 | 0.612 | 0.903 | 0.903 | 0.097 | 0.000 | 1.796 | 0.557 | 3.90 |
| 361.95 | 0.803 | 0.302 | 0.074 | 0.624 | 0.941 | 0.941 | 0.059 | 0.000 | 1.717 | 0.524 | 3.95 |
| 362.00 | 0.913 | 0.331 | 0.032 | 0.637 | 0.975 | 0.975 | 0.025 | 0.000 | 1.616 | 0.524 | 3.66 |
| 362.19 | 1.000 | 0.353 | 0.000 | 0.647 | 1.000 | 1.000 | 0.000 | 0.000 | 1.547 | | |

[a] $T$: equilibrium temperature; $x_1'$: mole fraction of n-hexane in the liquid phase (NBP-free basis); $y_1'$: mole fraction of n-hexane in the vapor phase (NBP-free basis); $x_1$, $x_2$, and $x_3$: mole fractions of n-hexane, ethanol, and NBP in the liquid phase, respectively; $y_1$, $y_2$, and $y_3$: mole fractions of n-hexane, ethanol, and NBP in the vapor phase; $\gamma_1$ and $\gamma_2$: activity coefficient of n-hexane and ethanol, respectively: $\alpha_{12}$: relative volatility of n-hexane to ethanol.
[b] Expanded combined uncertainties ($U$ with $k$ = 2): $U(T)$ = 0.40 K, $U(P)$ = 0.23 kPa, and $U(x_1)$ = $U(y_1)$ = 0.006.
[c] $y_3$ values are less than 0.0005.

In addition, the VLE data for the pseudo-ternary mixture of n-hexane (1) and ethanol (2), with the benchmark entrainer of NMP, were measured at the E/F = 1 and a pressure of 100.0 kPa. The results of the VLE data are shown in Table 6. The VLE data for both pseudo-ternary mixtures were preferably measured at 100.0 kPa instead of at 101.3 kPa since the laboratory pressure vary with the range of 100.0 and 101.3 kPa. Hence, measurements conducted at 100.0 kPa provide more precise control to the pressure in the setup. The introduction of NBP and NMP into the n-hexane and ethanol mixture at all composition ranges studied under the specified E/Fs and pressures resulted in a homogenous mixture instead of a heterogenous one, confirming that VLE data measurements can be conducted successfully. For the pseudo-ternary mixture, the activity coefficient of component $i$ ($\gamma_i$), which represents non-ideal behavior in the liquid phase, was calculated similarly to that of the binary mixture as shown in Eq 1. Ideal gas behavior was assumed to occur in these mixtures since the VLE data were measured at low pressures (atmospheric and vacuum).

**Table 6.** VLE data for n-hexane (1) + ethanol (2) + 1-methylpyrrolidin-2-one (3) with with mass-based E/F = 1 and and pressure at 100.0 kPa[a,b,c]

| $T$/K | $x_1$' | $x_1$ | $x_2$ | $x_3$ | $y_1$' | $y_1$ | $y_2$ | $y_3$ | $\gamma_1$ | $\gamma_2$ | $\alpha_{12}$ |
|---|---|---|---|---|---|---|---|---|---|---|---|
| 362.49 | 0.000 | 0.000 | 0.683 | 0.317 | 0.000 | 0.000 | 1.000 | 0.000 | | 0.951 | |
| 354.18 | 0.067 | 0.044 | 0.626 | 0.330 | 0.255 | 0.255 | 0.745 | 0.000 | 3.926 | 1.056 | 4.77 |
| 350.65 | 0.096 | 0.064 | 0.601 | 0.335 | 0.438 | 0.438 | 0.562 | 0.000 | 5.181 | 0.952 | 7.33 |
| 344.98 | 0.145 | 0.095 | 0.561 | 0.344 | 0.601 | 0.601 | 0.399 | 0.000 | 5.676 | 0.909 | 8.92 |
| 344.01 | 0.159 | 0.104 | 0.550 | 0.346 | 0.637 | 0.637 | 0.363 | 0.000 | 5.667 | 0.880 | 9.30 |
| 341.71 | 0.240 | 0.154 | 0.486 | 0.360 | 0.724 | 0.724 | 0.276 | 0.000 | 4.674 | 0.833 | 8.32 |
| 340.12 | 0.350 | 0.218 | 0.404 | 0.378 | 0.781 | 0.781 | 0.219 | 0.000 | 3.735 | 0.850 | 6.63 |
| 339.99 | 0.465 | 0.282 | 0.323 | 0.395 | 0.819 | 0.819 | 0.181 | 0.000 | 3.044 | 0.884 | 5.21 |
| 340.29 | 0.610 | 0.358 | 0.226 | 0.416 | 0.882 | 0.882 | 0.118 | 0.000 | 2.556 | 0.816 | 4.78 |
| 340.82 | 0.683 | 0.393 | 0.181 | 0.426 | 0.899 | 0.899 | 0.101 | 0.000 | 2.337 | 0.846 | 4.15 |
| 341.87 | 0.780 | 0.441 | 0.120 | 0.439 | 0.931 | 0.931 | 0.069 | 0.000 | 2.087 | 0.833 | 3.82 |
| 343.29 | 0.886 | 0.488 | 0.060 | 0.452 | 0.964 | 0.964 | 0.036 | 0.000 | 1.867 | 0.827 | 3.41 |
| 344.12 | 0.956 | 0.518 | 0.022 | 0.460 | 0.983 | 0.983 | 0.017 | 0.000 | 1.749 | 0.987 | 2.73 |
| 344.77 | 1.000 | 0.535 | 0.000 | 0.465 | 1.000 | 1.000 | 0.000 | 0.000 | 1.688 | | |

[a] $T$: equilibrium temperature; $x_1$': mole fraction of n-hexane in the liquid phase (NMP-free basis); $y_1$': mole fraction of n-hexane in the vapor phase (NMP-free basis); $x_1$, $x_2$, and $x_3$: mole fractions of n-hexane, ethanol, and NMP in the liquid phase, respectively; $y_1$, $y_2$, and $y_3$: mole fractions of n-hexane, ethanol, and NMP in the vapor phase; $\gamma_1$ and $\gamma_2$: activity coefficient of n-hexane and ethanol, respectively: $\alpha_{12}$: relative volatility of n-hexane to ethanol.

[b] Expanded combined uncertainties ($U$ with $k$ = 2): $U(T)$ = 0.40 K, $U(P)$ = 0.23 kPa, and $U(x_1)$ = $U(y_1)$ = 0.006.

[c] $y_3$ values are less than 0.0005.

Eq. 3 was used to calculate the relative volatility of n-hexane to ethanol ($\alpha_{12}$) in the pseudo-ternary mixture of n-hexane (1) and ethanol (2) with the presence of NBP and NMP, respectively. The equation employs $x_1$' and $x_2$', which represent the liquid phase mole fraction of n-hexane and ethanol on an excluded-entrainer basis, as well as $y_1$ and $y_2$, which denote the vapor phase mole fraction of n-hexane and ethanol.

$$\alpha_{12} = \frac{y_1 / x_1'}{y_2 / x_2'} \qquad 3)$$

The trends observed in the VLE data shown in Table 2, which presents a binary mixture, and Tables 4-6, which depict pseudo-ternary mixtures, provide the following key points: the shifting of the equilibrium temperature, the increasing relative volatility, and the elimination of azeotropes when entrainers are added to the mixtures. These trends are further illustrated in Figures 3-8.

Figure 3 illustrates the effect of a reducing the pressure from 100.0 kPa to 80.0 and then to 50.0 kPa on the VLE behavior. The results indicate that decreasing the pressure lowers the equilibrium temperature of the mixture.

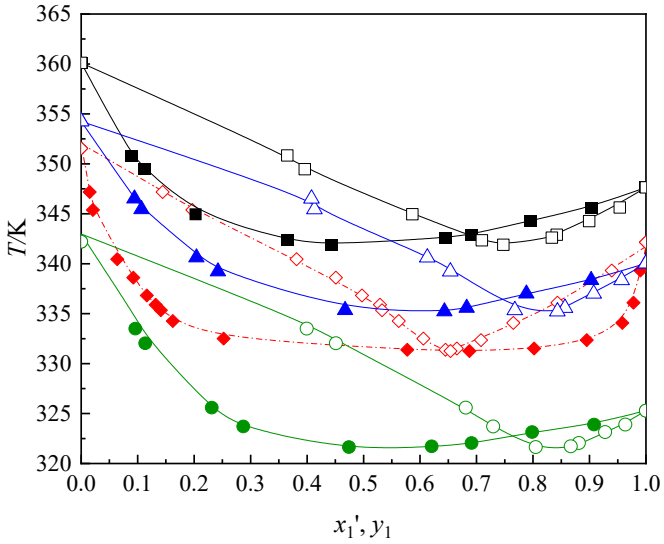


**Figure 3.** *T*- $x_1$'-$y_1$ diagram of n-hexane (1) + ethanol (2) + 1-butylpyrrolidin-2-one (3) for the experimental data with E/F = 1: (■), $x_1$' and (□), $y_1$ at 100.0 kPa; (▲), $x_1$' and (Δ), $y_1$ at 80.0 kPa; (●), $x_1$' and (○), $y_1$ at 50.0 kPa; and (♦), $x_1$ and (◊), $y_1$ for the binary mixture at 101.3 kPa. Regressed with the NRTL model: (—), 100.0 kPa (black); 80.0 kPa (blue); 50.0 kPa (green); and (_ . _), binary mixture at 101.3 kPa (red).

This occurs because the boiling point of each component in the mixture decreases at lower pressures, resulting in a decrease of the equilibrium temperature within the setup. When E/F = 1 is applied at these pressures, a minimum temperature occurs in the mixture. However, this minimum temperature is not indicative of azeotropic behavior, as the $y_1$ value does not equal the $x_1$' value at this temperature. Throughout the three pressures tested, the $y_1$ values consistently exceed the $x_1$' values across the entire range of n-hexane compositions, confirming the absence of azeotropic behavior. The minimum temperature phenomenon in this system is driven by strong positive deviations from ideality (primarily due to differences in polarity and hydrogen bonding, which lead to repulsive mixing effects, increasing the activity coefficients), boiling point depression (when the combined vapor pressure of the mixture exceeds that of the pure components due to non-ideal mixing), ternary interactions (addition of NBP modifies the binary interactions between n-hexane and ethanol), and pressure dependence (at lower pressures the boiling points of all components decrease, but the relative volatility shifts can amplify non-ideality, leading to a more pronounced minimum temperature effect). The combination of these phenomena leads to an effective increase in total vapor pressure and thus a lower boiling point at certain compositions, even in the

absence of an azeotropic. The phenomena of minimum temperature occurring when the azeotropic point is absent have also been reported in studies involving mixtures of water and acetonitrile with the addition of entrainers such as ethylene glycol[33] and dimethyl sulfoxide,[34] mixtures of methyl propionate and ethanol with ionic liquids,[35] as well as in the mixture of 2-butanone and ethanol in the presence of ionic liquids.[36,37]

The effect of the amount of entrainer in the mixture on the equilibrium temperature was investigated. As illustrated in Figure 4, when the mass of the NBP is increased from E/F = 1 to 2 and 3 at a constant pressure of 100.0 kPa, the equilibrium temperature also increases compared to that without the entrainer.

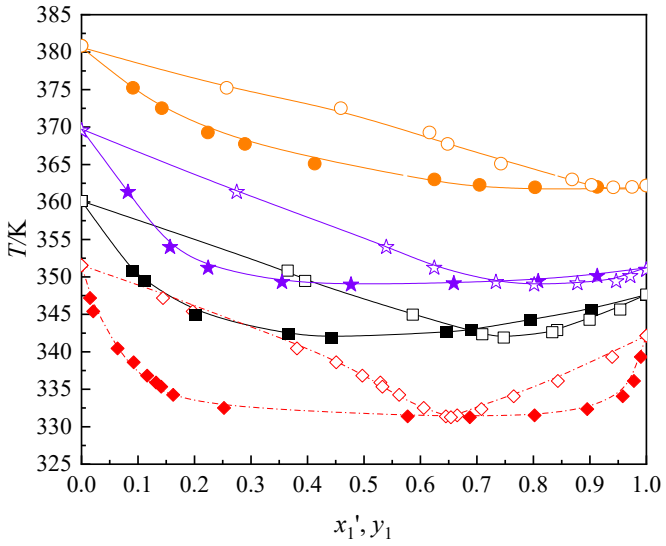


**Figure 4.** *T*- $x_1$'-$y_1$ diagram of n-hexane (1) + ethanol (2) + 1-butylpyrrolidin-2-one (3) for the experimental data at pressure of 100.0 kPa: (■), $x_1$' and (□), $y_1$ for E/F = 1; (★), $x_1$' and (☆), $y_1$ for E/F = 2; (●), $x_1$' and (○), $y_1$ for E/F = 3; and (♦), $x_1$ and (◊), $y_1$ for the binary mixture (E/F = 0) at 101.3 kPa. Regressed with the NRTL model: (—), E/F = 1 (black); E/F =2 (purple); E/F = 3 (orange); and (_ . _), binary mixture at 101.3 kPa (red).

The addition of a larger mass of NBP in the mixture causes the entrainer to dominate the liquid composition. Furthermore, NBP has a stronger interaction with ethanol. The stronger interaction is mainly due to hydrogen bonding between the hydroxyl group of ethanol, which acts as a hydrogen bond donor, and the carbonyl group of the pyrrolidone ring in NBP, which serves as a hydrogen bond acceptor. In contrast, the interaction with n-hexane is governed by weaker van der Walls forces due to the nonpolar nature of n-hexane. These two causes lead to a decrease in the vaporization of both the n-hexane and ethanol. As a result, an elevated temperature is needed to evaporate n-hexane and

ethanol in order to achieve the equilibrium conditions, resulting in an increase in the equilibrium temperature of the mixture. Figure 4 also indicates that the minimum temperature occurs at E/Fs = 1 and 2, even though the azeotropic point is already removed, as demonstrated in Figure 6. However, the minimum temperature nearly disappears at E/F = 3.

The effect of the presence of NBP on breaking the azeotropic behavior in a mixture of n-hexane and ethanol is demonstrated in the $x_1$'-$y_1$ diagrams shown in Figures 5 and 6. The addition of NBP to this mixture alters its non-ideal behavior by modifying the molecular interactions between the components. Ethanol is a polar component, while n-hexane is non-polar. Due to its polar nature, NBP interacts more favorably with ethanol than with n-hexane. This preferential interaction effectively reduces the interaction between n-hexane and ethanol, leading to an increase in relative volatility and eliminating the azeotropic behavior. As a result, n-hexane can be separated more efficiently from ethanol. Tables 4 and 5 show that the introduction of NBP results in a lower activity coefficient for ethanol ($\gamma_2$) compared to n-hexane ($\gamma_1$). This signifies that NBP interacts more strongly with ethanol than with n-hexane. Consequently, the volatility of n-hexane increases, allowing it to be more easily separated from ethanol.

In this study, the pressure effect on the relative volatility was investigated. As shown in Figure 5, the addition of NBP with an E/F = 1 at various pressures of 100.0, 80.0, and 50.0 kPa, respectively, was found to increase the relative volatility of n-hexane to ethanol, effectively removing the azeotropic point.

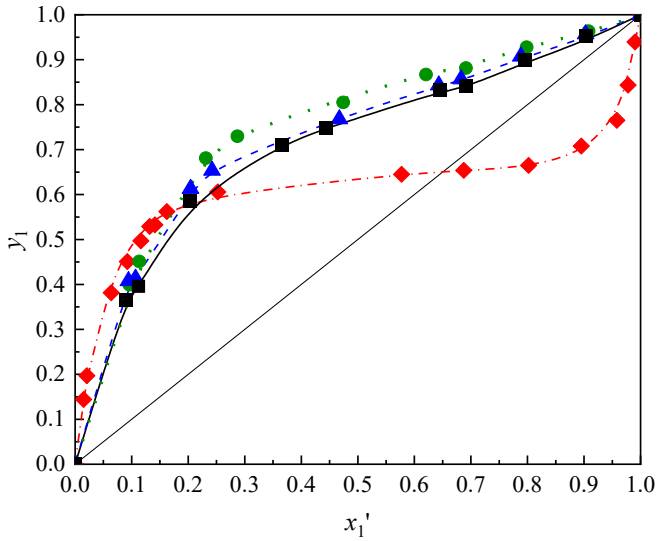


**Figure 5.** $x_1$'-$y_1$ diagram of n-hexane (1) + ethanol (2) + 1-butylpyrrolidin-2-one (3) for the experimental data with E/F = 1: (■), at 100.0 kPa; (▲), at 80.0 kPa; (●), at 50.0 kPa; and (♦), binary mixture at 101.3 kPa. Regressed with the NRTL

model: (—), 100.0 kPa; (- - -), 80.0 kPa; (····), 50.0 kPa; and (_ . _), binary mixture at 101.3 kPa.

As the pressure decreases from 100.0 kPa to 80.0 kPa and 50.0 kPa, the relative volatility of n-hexane to ethanol increases. Lower pressure result in a lower equilibrium temperature, which elevates the non-ideality of the mixture and contributes to the increased relative volatility. However, when pressure is reduced to 80.0 and 50.0 kPa, the increase in the relative volatility levels off, as the interaction between NBP and ethanol tend not to considerably increase at these lower pressures. This is confirmed in Table 4, which shows that the activity coefficient of ethanol ($\gamma_2$) slightly decreases when the pressure is lowered from 100.0 to 80.0 and 50.0 kPa.

This work also examined the effect of NBP concentration on the relative volatility. Similar to the influence of pressure, Figure 6 shows that increasing the E/F from 1 to 2 and 3 results only in a modest increase of the relative volatility. Furthermore, the relative volatility remains unchanged when E/F was increased from 2 to 3. As detailed in Table 5, increasing the amount of NBP enhances the interaction between NBP and ethanol, which is confirmed by the decrease in the activity coefficient of ethanol ($\gamma_2$). However, the non-ideality of n-hexane decreases with an increase in the amount of NBP as the activity coefficient of n-hexane ($\gamma_1$) decrease. This corresponds to the significant rise in equilibrium temperature. The combination of both effects contribute to the overall slight increase in relative volatility.

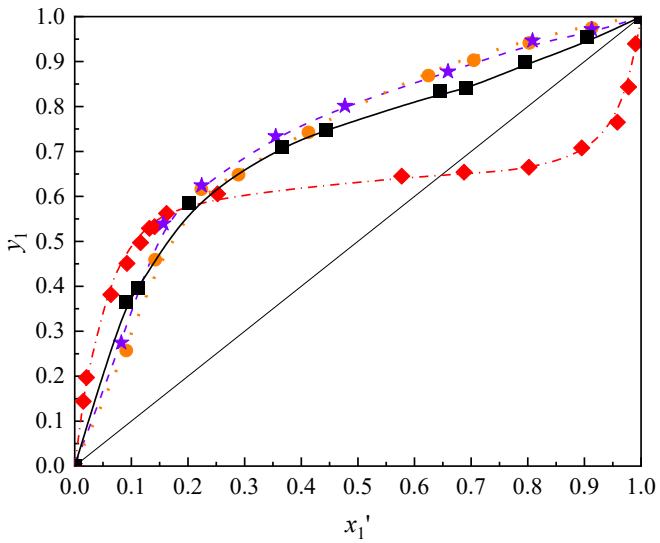


**Figure 6.** $x_1'$-$y_1$ diagram of n-hexane (1) + ethanol (2) + 1-butylpyrrolidin-2-one (3) for the experimental data at pressure of 100.0 kPa: (■), E/F = 1; (★), E/F = 2; (●), E/F = 3; and (♦), binary mixture at 101.3 kPa**.** Regressed with the NRTL

model: (—), E/F = 1; (- -), E/F =2; (····), E/F = 3; and (_ . _), binary mixture at 101.3 kPa.

NMP as a benchmark entrainer was also evaluated in this work. It was added to an azeotropic mixture of n-hexane and ethanol with an E/F = 1 and a pressure of 100.0 kPa. As depicted in Figure 7, the introduction of NMP leads to an elevated equilibrium temperature when compared to binary mixture without entrainer, a trend similar to that observed with the addition of NBP. NMP has a higher boiling point than both n-hexane and ethanol, and it becomes the dominant component in the liquid phase, when NMP is added with an E/F = 1. Additionally, NMP exhibits stronger interaction with ethanol. These situations result in reduced vaporization of the mixture, thus requiring a higher temperature to reach equilibrium.

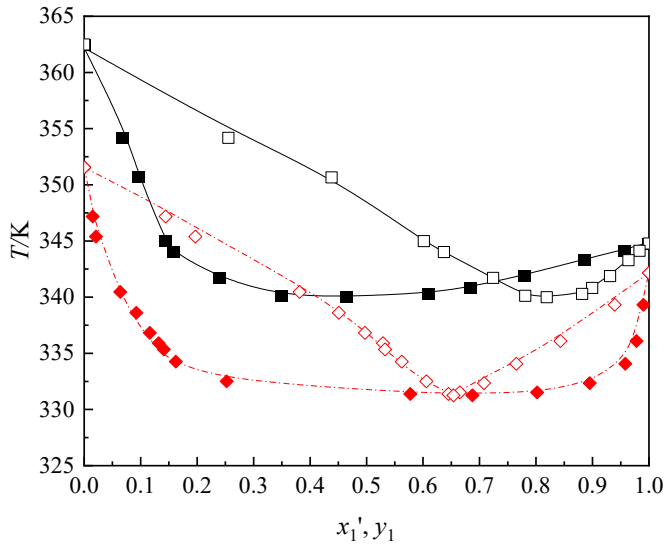


**Figure 7.** *T*- $x_1$'-$y_1$ diagram of n-hexane (1) + ethanol (2) + 1-methylpyrrolidin-2-one (3) for the experimental data with E/F =1: (■), $x_1$' and (□), $y_1$ at 100.0 kPa; and (♦), $x_1$ and (◊), $y_1$ for the binary mixture at 101.3 kPa. Regressed with the NRTL model: (—), 100.0 kPa (black); and (_ . _), binary mixture at 101.3 kPa (red).

As shown in Figure 8, the presence of NMP in the mixture effectively elevates the relative volatility and eliminates the azeotropic point. Similar to NBP, as a polar entrainer, NMP is more likely to interact with a polar component than a non-polar one. Hence, NMP has a stronger interaction with ethanol compared to n-hexane. This is indicated in Table 6, where the activity coefficient of ethanol ($\gamma_2$) is lower than that of n-hexane ($\gamma_1$). The stronger interaction between NMP and

ethanol weakens the original interaction between n-hexane and ethanol, resulting in the easier vaporization of n-hexane. This promotes a more effective separation of n-hexane from toluene. In our previous work, we examined molecular interactions using unimolecular quantum chemical calculations (COSMO-RS) to better understand the polar roles of the NBP and NMP. The results indicated that both NBP and NMP, as polar compounds, exhibited stronger interaction with the compounds that have more polar behavior.[6] Additionally, we compared the binary endpoints of the VLE data for n-hexane–NMP from our study with existing literature, as illustrated in Figure D4. The data from our work demonstrates good agreement with the literature data,[38,39] confirming the reliability of our results.

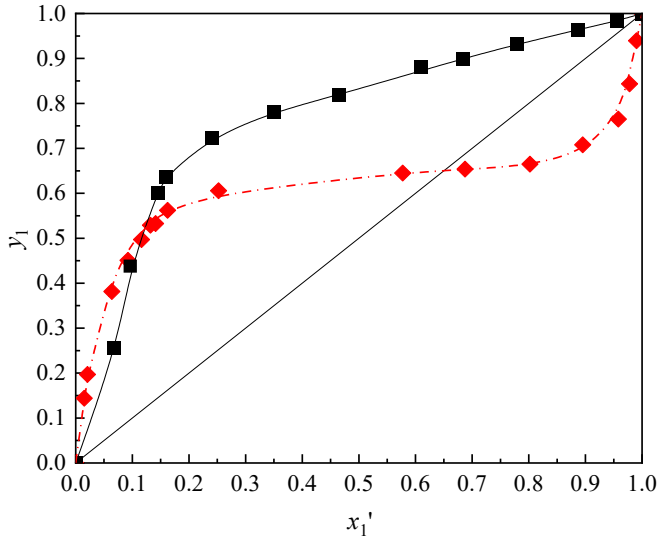


**Figure 8.** $x_1'$-$y_1$ diagram of n-hexane (1) + ethanol (2) + 1-methylpyrrolidin-2-one (3) for the experimental data: (■), E/F =1 at 100.0 kPa; and (♦), binary mixture at 101.3 kPa. Regressed with the NRTL model: (—), E/F =1 at 100.0 kPa; and (_ . _), binary mixture at 101.3 kPa.

These VLE results are fundamental for designing extractive distillation processes. However, their direct application to real extractive distillation column has inherent limitations. This is because the VLE data do not consider the mass transfer resistance that occurs at the vapor-liquid interfaces in actual column. Moreover, while the entrainer concentration in the VLE is assumed to be uniform, in a real extractive distillation column, the entrainer concentration varies stage by stage. Therefore, while promising, the translation of these VLE data to full-scale operations require further validation through rigorous process simulation or pilot-scale experiments.

To compare the performance of NBP and NMP in increasing relative volatility, we analyzed the relative volatility of NBP under various E/Fs and

pressures with NMP at E/F = 1 and a pressure of 100.0 kPa, specifically at the azeotropic point, where the mole fraction of n-hexane on an entrainer free-basis is $x_1' = 0.66$. In the binary mixture, the relative volatility at the azeotropic point is 1, meaning the mole fraction n-hexane in the liquid phase is equal to that in the vapor phase. Figure 9 shows that the NBP with an E/F 1 and a pressure of 50.0 kPa, as well as NBP with E/Fs 2 and 3 at pressure of 100.0 kPa, exhibits comparable relative volatility to NMP with an E/F = 1 at a pressure of 100.0 kPa.

At E/F = 1 and a pressure of 100.0 kPa, NMP demonstrates a higher relative volatility compared to NBP. This indicates a stronger interaction between NMP and ethanol as the activity coefficient of ethanol ($\gamma_2$) is lower, as shown in Table 6, compared to that in NBP in Table 4. This facilitates easier separation of n-hexane. When NBP is applied at E/F = 1 and at a reduced pressure of 50.0 kPa or at higher E/Fs of 2 and 3 at 100.0 kPa, its relative volatility become comparable, which is slightly lower than that of NMP. The lower pressure decrease equilibrium temperature, enhances the interaction between NBP and ethanol and increases the non-ideality of the mixture, both of which favor separation of n-hexane from ethanol. Similarly, increasing the E/F strengthens the interaction between NBP and ethanol, as shown in Table 5, further increases relative volatility. A slightly lower relative volatility can result in a higher number of stages and reflux ratio required in an extractive distillation column, contributing to increased energy consumption. However, operating at lower pressures can reduce the reboiler temperature, which in turn decreases the energy requirements.

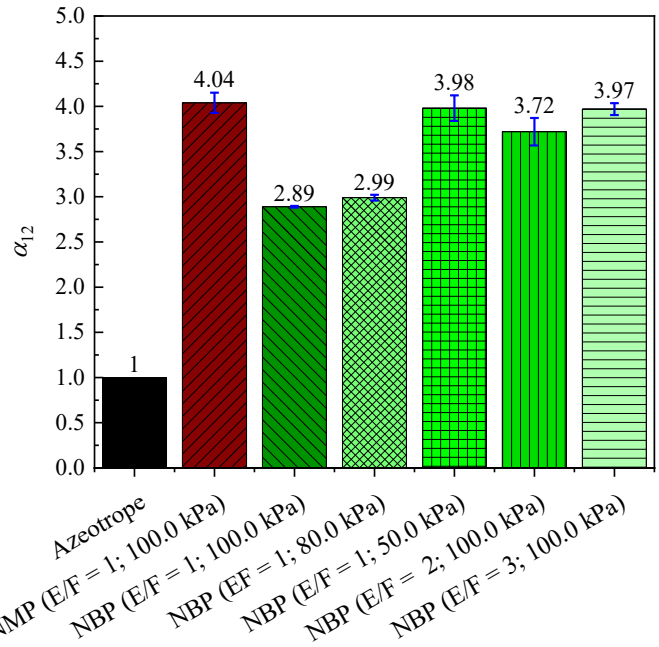


**Figure 9.** Relative volatility of n-hexane (1) to ethanol (2) ($\alpha_{12}$) containing entrainer of NMP at E/F =1 and a pressure of 100.0 kPa and NBP at various E/Fs

and pressures. The relative volatility was measured at an azeotropic point (mole fraction of n-hexane on an entrainer free-basis; $x_1' = 0.66$).

Furthermore, NBP has a higher boiling point than NMP, which provides higher thermal stability and can minimize entrainer loss in extractive distillation. Environmentally, NBP is categorized as non-toxic, biodegradable, and free from reproductive toxicity. These relative volatility, thermal and environmental benefits highlight the promising performance of NBP, as a greener entrainer, presenting a viable alternative to NMP, as a conventional entrainer, for separating n-hexane from ethanol via extractive distillation. This suggests that utilizing NBP as a greener entrainer could contribute to the development of more sustainable and green extractive distillation processes.

## Thermodynamic consistency test

The consistency of the investigated VLE data was evaluated using the Van Ness thermodynamic consistency test.[20]

$$\Delta P = \frac{1}{n_p} \times \sum_{i=1}^{n_p} \Delta P_i = \frac{1}{n_p} \times \sum_{i=1}^{n_p} 100 \left| \frac{P_i^{cal} - P_i^{\exp}}{P_i^{\exp}} \right| \quad 4)$$

$$\Delta y = \frac{1}{n_p} \times \sum_{i=1}^{n_p} \Delta y_i = \frac{1}{n_p} \times \sum_{i=1}^{n_p} 100 \left| y_i^{cal} - y_i^{\exp} \right| \quad 5)$$

This test ensures the reliability of the VLE data. The Van Ness method is mathematically represented in Eqs. 4 and 5, where the pressure, the number of data, and mole fraction in vapor-phase are denoted as $n_p$, $P$, and $y$, respectively. Moreover, the values calculated from the NRTL model and those obtained from experimental work are represented as *cal* and *exp*, respectively. According to the Van Ness method, a data set is classified as consistent if both $\Delta P$ and $\Delta y$ values are less than 1. As presented in Table 7, the values for $\Delta P$ and $\Delta y$ for the studied binary mixture and the pseudo-ternary mixtures fall below this threshold.

**Table 7.** Thermodynamic consistency test results

| Mixture | $\Delta y^a$ | $\Delta P^b$ | Results |
|---|---|---|---|
| n-hexane (1) + ethanol (2) | 0.6 | 0.4 | passed |
| n-hexane (1) + ethanol (2) + NBP (3) | 0.5 | 0.8 | Passed |
| n-hexane (1) + ethanol (2) + NMP (3) | 0.4 | 0.8 | passed |

[a] $\Delta y = \frac{1}{n_p} \times \sum_{i=1}^{n_p} \Delta y_i = \frac{1}{n_p} \times \sum_{i=1}^{n_p} 100 \left| y_i^{cal} - y_i^{\exp} \right| < 1$

$$^{b}\Delta P = \frac{1}{n_p} \times \sum_{i=1}^{n_p} \Delta P_i = \frac{1}{n_p} \times \sum_{i=1}^{n_p} 100 \left| \frac{P_i^{cal} - P_i^{\exp}}{P_i^{\exp}} \right| < 1$$

The detailed values of $\Delta P$ and $\Delta y$ for the investigated mixtures are provided in Tables D2-D4. Furthermore, the $\ln(\gamma_1 / \gamma_2)$ residual distribution must demonstrate random behavior to satisfy the Van Ness criteria. As shown in Figures D5 – D7, the results of the $\ln(\gamma_1 / \gamma_2)$ residual distribution verifies this randomness. These findings affirm the thermodynamic consistency of the VLE data obtained in this study.

## VLE data correlation

The investigated VLE data was regressed to obtain the optimum BIPs. In this regression, NRTL as a widely adopted thermodynamic model, was employed. This model is well-regarded for its ability to accurately represent the mixture involving entrainers, often yielding excellent agreement with experimental results.[1,40–45] Furthermore, our previous study demonstrated that the NRTL model exhibits more accurate correlation results than the UNIQUAC model.[23] The NRTL model is expressed in Eq. 6.

$$\ln \gamma_i = \frac{\sum_{j=1}^{n_c} x_j \tau_{ji} G_{ji}}{\sum_{k=1}^{n_c} x_k G_{ki}} + \sum_{j=1}^{n_c} \frac{x_j G_{ij}}{\sum_{k=1}^{N} x_k G_{kj}} \left( \tau_{ij} - \frac{\sum_{m=1}^{n_c} x_m \tau_{mj} G_{mj}}{\sum_{k=1}^{n_c} x_k G_{kj}} \right) \quad 6)$$

Where the activity coefficient for component *i* is expressed as $\gamma_i$ and the total number of the components is denoted as $n_c$. In this model, the parameters are explained as outlined in Eq. 7, where $C_{ij}$ indicates the constant of non-randomness in the binary interaction for the component *i-j*.

$$G_{ij} = \exp(-C_{ij}\tau_{ij});\ \tau_{ij} = A_{ij} + B_{ij}/T;\ G_{ii} = 1;\ \tau_{ii} = 0 \quad 7)$$

The BIPs for the n-hexane and ethanol pair were obtained by regressing the VLE data of the binary mixture of n-hexane and ethanol at pressures of 61.3 and 101.3 kPa. The VLE data at 61.3 kPa was retrieved from the literature,[30] while the data at 101.3 kPa was obtained from this work. These VLE data sets were simultaneously regressed to determine the optimum BIPs for the n-hexane and ethanol pair. The resulting BIPs were then applied to regress the VLE data of the pseudo-ternary mixture of n-hexane and ethanol containing NBP and NMP, respectively. As the experimental VLE data for n-hexane and ethanol with the presence of NBP were collected over a pressure range of 50.0 to 100.0 kPa, the regression of the binary mixture was conducted using data from both

atmospheric and reduced pressure to ensure that the BIPs for n-hexane and ethanol pair accurately captured the temperature range relevant to this pseudo-ternary mixture. For the binary mixture of n-hexane-ethanol regression, the non-randomness parameter of the NRTL model ($C_{ij}$) was fixed at a value of 0.47. In contrast, for the pseudo-ternary mixture regression, $C_{ij}$ was treated as an adjustable parameter rather than being fixed. This approach provides greater flexibility, leading to improved regression accuracy. Initially, we attempted to correlate the pseudo-ternary mixture data using a fixed value of 0.3. Unfortunately, this approach did not yield satisfactory results due to the strong non-ideal behavior of the system, which caused the value to deviate from 0.3. We then evaluated a fixed value of 0.2, but this also resulted in inaccurate correlation since it only represented the n-hexane–entrainer pair, and not the ethanol–entrainer pair. Moreover, we assessed a fixed value of 0.47; however, this value did not adequately represent the n-hexane–entrainer or ethanol–entrainer pairs, as it was primarily applicable to the pair of nonpolar- strongly self-associated substances. Therefore, the correlation results were not in good agreement with the experimental data when using fixed values. As a result, we opted to regress this parameter for both n-hexane–entrainer and ethanol–entrainer pairs to obtain a more accurate correlation. In addition, the $A_{ij}$ and $A_{ji}$ parameters were involved as adjustable variables in the regression, as this enhanced the correlation results. In the regression, the optimization of BIPs was obtained by minimizing the objective function (*OF*) of using the maximum likelihood-based algorithm developed by Britt and Luecke.[46] The formulation of the objective function is presented in Eq. 8.

$$OF = \sum_{k=1}^{n_p} \left\{ \left| \frac{P_k^{cal} - P_k^{\exp}}{\sigma_P} \right|^2 + \left| \frac{T_k^{cal} - T_k^{\exp}}{\sigma_T} \right|^2 + \left| \frac{x_{1,k}^{cal} - x_{1,k}^{\exp}}{\sigma_x} \right|^2 + \left| \frac{y_{1,k}^{cal} - y_{1,k}^{\exp}}{\sigma_y} \right|^2 \right\} \quad 8)$$

Here the total number of data points is defined by $n_p$ and the standard deviation is represented by $\sigma$. The optimum BIPs for all component pairs obtained from the regression are summarized in Table 8.

**Table 8.** NRTL binary interaction parameters for hexane (1) + ethanol (2) + 1-butylpyrrolidin-2-one (3) and hexane (1) + ethanol (2) + 1-methylpyrrolidin-2-one (3)[a,b]

| *i* component | *j* component | $A_{ij}$ | $A_{ji}$ | $B_{ij}$/K | $B_{ji}$/K | $C_{ij}$ |
|---|---|---|---|---|---|---|
| [c]n-hexane (1) | ethanol (2) | -10.342 | -3.854 | 4120.934 | 1829.392 | 0.47 |
| n-hexane (1) | 1-butylpyrrolidin-2-one (3) | 1.748 | -13.206 | -581.379 | 5130.115 | 0.05 |
| ethanol (2) | 1-butylpyrrolidin-2-one (3) | 22.377 | -1.069 | -5518.982 | -133.055 | 0.45 |
| n-hexane (1) | 1-methylpyrrolidin-2-one (3) | -20.689 | 413.501 | 7863.726 | 9869.500 | 0.03 |
| ethanol (2) | 1-methylpyrrolidin-2-one (3) | 19.225 | 5.003 | -5179.301 | -2561.179 | 0.30 |

[a] $A_{ij}$, $A_{ji}$, $B_{ij}$, and $B_{ji}$: asymmetric parameters; $C_{ij}$: the constant of non-randomness.

[b] NRTL Model: $\tau_{ij} = A_{ij} + B_{ij} / T$

[c] The BIPs for the hexane (1) – ethanol (2) pair were derived from the correlation of the VLE data at 101.3 kPa from this work combined with the VLE data at 61.3 kPa from literature.[30]

The regression result from the NRTL model accurately represent the experimental data for both the binary mixture of n-hexane and ethanol and the pseudo-ternary mixtures of n-hexane and ethanol with the addition of NBP and NMP, respectively. For the pseudo-ternary mixture containing NBP, the VLE data at all E/Fs and pressures were regressed together to obtain the BIPs, which accurately describe the system over a wide range of entrainer compositions and various pressures. Figure 2 shows the regression results for the binary mixture, while Figures 3 and 4 illustrate the results for the pseudo-ternary mixture with the presence of NBP, and Figure 7 demonstrates the results for the mixture containing NMP. The good agreements observed are further confirmed by the low values of the root-mean-square deviations for each mixture, as listed in Table 9. The residual plots of liquid and vapor mole fraction, and temperature are listed in Figures D8-D16. These results confirm that the NRTL model, along with the optimum BIPs, can be reliably applied for the process simulation of extractive distillation to separate the azeotropic mixture of n-hexane and ethanol using the greener entrainer NBP as well as the benchmark entrainer NMP.

**Table 9.** Root-Mean-Square Deviation (RMSD)[a]

| | RMSD[b] | | | |
|---|---|---|---|---|
| | *T*/K | *P*/kPa | $x_1$' | $y_1$ |
| n-hexane (1) + ethanol (2) | 0.38 | 0.5 | 0.003 | 0.007 |
| n-hexane (1) + ethanol (2) + 1-butylpyrrolidin-2-one (3) | 0.32 | 0.6 | 0.003 | 0.007 |
| n-hexane (1) + ethanol (2) + 1-methylpyrrolidin-2-one (3) | 0.12 | 0.9 | 0.003 | 0.009 |

[a] *T*: temperature, *P*: pressure; $x_1$': mole fraction of n-hexane in the liquid phase (entrainer-free basis), $y_1$: mole fraction of n-hexane in the vapor phase.

[b]RMSD: $\Delta M = \sqrt{\frac{1}{n}\sum_{i=1}^{n}\left(M_{\exp} - M_{cal}\right)^2}$, where $n$ denotes the number of data points;

$M$ corresponding to $T$, $P$, $x_1$', and $y_1$, respectively.

## References


(1) Zhang, Y.; Wang, Z.; Xu, X.; Gao, J.; Xu, D.; Zhang, L.; Wang, Y. Entrainers Selection and Vapour-Liquid Equilibrium Measurements for Separating Azeotropic Mixtures (Ethanol + n-Hexane/Cyclohexane) by Extractive Distillation. *J. Chem. Thermodyn.* **2020**, *144*, 106070. https://doi.org/https://doi.org/10.1016/j.jct.2020.106070.

(2) Gonzalez, E.; Ortega, J. Densities and Isobaric Vapor-Liquid Equilibria of Butyl Esters (Methanoate to Butanoate) with Ethanol at 101.32 KPa. *J. Chem. Eng. Data* **1995**, *40* (6), 1178–1183. https://doi.org/10.1021/je00022a004.

(3) Wang, Y.; Hu, R.; Liu, W.; Zhu, Z.; Wang, Y.; Yang, J.; Qi, J.; Cui, P. Separation of Ethanol/n-Hexane Azeotrope by Imidazolium Ionic Liquids: Experimental Study and Mechanism Analysis. *Sep. Purif. Technol.* **2025**, *357*, 130063. https://doi.org/https://doi.org/10.1016/j.seppur.2024.130063.

(4) Sander, A.; Petračić, A.; Rogošić, M.; Župan, M.; Frljak, L.; Cvetnić, M. Feasibility of Different Methods for Separating N-Hexane and Ethanol. *Separations*. 2024. https://doi.org/10.3390/separations11050151.

(5) Wang, Y.; Xu, H.; Yang, Q.; Wang, W.; Li, H.; Wang, Y.; Zhu, Z.; Li, X.; Song, X.; Cui, P. A Novel Intermediate Heat Exchange Intensified Extractive Pressure-Swing Distillation Process for Efficiently Separating n-Hexane-Tetrahydrofuran-Ethanol. *Chem. Eng. Sci.* **2024**, *300*, 120593. https://doi.org/https://doi.org/10.1016/j.ces.2024.120593.

(6) Hartanto, D.; Schuur, B.; Kiss, A. A.; de Haan, A. B. Effective Selection of Green Organics and Natural Deep Eutectic Solvents as Advanced Entrainers by COSMO-RS and Group Contributions Methods for Enhanced Design of Extractive Distillation. In *Computer Aided Chemical Engineering*; Manenti, F., Reklaitis, G. V. B. T.-C. A. C. E., Eds.; Elsevier, 2024; Vol. 53, pp 1387–1392. https://doi.org/https://doi.org/10.1016/B978-0-443-28824-1.50232-5.

(7) European Chemical Agency. *1-butylpyrrolidin-2-one*. https://chem.echa.europa.eu/100.020.399/overview?searchText=1-butylpyrrolidin-2-one (accessed 2025-09-23).

(8) *Public Report, 2-Pyrrolidinone, 1-Butyl-*; 2020. https://www.industrialchemicals.gov.au/sites/default/files/STD1698 public report %5B780 KB%5D.pdf.

(9) *Opinion on N-Methyl-2-Pyrrolidone (NMP)*; Scientific Committee on Consumer Safety, European Union; 2011. https://ec.europa.eu/health/scientific_committees/consumer_safety/docs/sccs_o_050.pdf.

(10) Jiang, X.; Yong, W. F.; Gao, J.; Shao, D.-D.; Sun, S.-P. Understanding the Role of Substrates on Thin Film Composite Membranes: A Green Solvent Approach with TamiSolve® NxG. *J. Memb. Sci.* **2021**, *635*, 119530. https://doi.org/https://doi.org/10.1016/j.memsci.2021.119530.
(11) Buken, O.; Mancini, K.; Sarkar, A. A Sustainable Approach to Cathode Delamination Using a Green Solvent. *RSC Adv.* **2021**, *11* (44), 27356–27368. https://doi.org/10.1039/D1RA04922D.
(12) Eastman. *TamiSolve NxG*. https://www.eastman.com/Pages/ProductHome.aspx?product=71103844&pn=TamiSolve+NxG.
(13) *SDS TamiSolve® NxG-PS No. 150000112709 (CAS RN: 3470-98-2)*; Eastman: Tennessee, 2020. https://ws.eastman.com/ProductCatalogApps/PageControllers/MSDSShow_PC.aspx.
(14) Palczewska-Tulińska, M.; Oracz, P. Vapor Pressures of 1-Methyl-2-Pyrrolidone, 1-Methyl-Azepan-2-One, and 1,2-Epoxy-3-Chloropropane. *J. Chem. Eng. Data* **2007**, *52* (6), 2468–2471. https://doi.org/10.1021/je700398k.
(15) Li, N.; Han, X.; Lv, H.; Jin, Y.; Yu, J. Biodegradation of N-Methyl-2-Pyrrolidone (NMP) in Wastewater: A Review of Current Knowledge and Future Perspectives. *J. Clean. Prod.* **2025**, *486*, 144452. https://doi.org/https://doi.org/10.1016/j.jclepro.2024.144452.
(16) European Chemical Agency. *1-methyl-2-pyrrolidone*. https://chem.echa.europa.eu/100.011.662/overview?searchText=1-methyl-2-pyrrolidone (accessed 2025-08-04).
(17) Tian, X.; Wang, R.; Wang, H.; Li, C.; Liu, J. Energy-Saving Extractive Distillation Processes Design and Optimization for the Separation of Ethyl Acetate and n-Heptane Azeotrope. *Fuel* **2025**, *379*, 132974. https://doi.org/https://doi.org/10.1016/j.fuel.2024.132974.
(18) Zhang, J.; Pan, C.; Ren, C.; Li, C.; Di, S.; Jiang, S.; Huang, Q.; Gao, N.; Wang, N.; Chang, K.; Kong, L.; Wang, Z.; Hu, Y.; Liu, Z.; Guo, X. Exploration of Energy-Saving Processes for the Separation of Tetrahydrofuran/Methanol/Water: From Separation Mechanism to Experimental Validation. *Fuel* **2025**, *388*, 134498. https://doi.org/https://doi.org/10.1016/j.fuel.2025.134498.
(19) Zhang, R.; Xu, Z.; Li, J.; Pan, J.; Wang, H.; Dai, T.; Ye, Q. Sustainable Process Design and Multiobjective Optimization for Separation of N-Heptane/Tert-Butyl Acetate by Extractive Distillation: From Separation Mechanism to Experimental. *Ind. Eng. Chem. Res.* **2025**, *64* (12), 6676–6691. https://doi.org/10.1021/acs.iecr.4c04569.
(20) Van Ness, H. C. Thermodynamics in the Treatment of Vapor/Liquid Equilibrium (VLE) Data. **1995**, *67* (6), 859–872. https://doi.org/doi:10.1351/pac199567060859.
(21) Renon, H.; Prausnitz, J. Local Compositions in Thermodynamic Excess Functions for Liquid Mixtures. *AIChE J.* **1968**, *14* (1), 135–144. https://doi.org/10.1002/aic.690140124.
(22) Dias, T. P. V. B.; Fonseca, L. A. A. P.; Ruiz, M. C.; Batista, F. R. M.; Batista, E. A. C.; Meirelles, A. J. A. Vapor–Liquid Equilibrium of Mixtures Containing the Following Higher Alcohols: 2-Propanol, 2-Methyl-1-Propanol, and 3-Methyl-1-Butanol. *J. Chem. Eng. Data* **2014**, *59* (3), 659–665.

https://doi.org/10.1021/je400581e.
(23) Hartanto, D.; Schuur, B.; Schuttevaer, T.; Kiss, A. A.; de Haan, A. B. Isobaric Vapor–Liquid Equilibrium of Methylcyclohexane + Toluene with Gamma-Valerolactone as a Biobased Entrainer and 1-Methylpyrrolidin-2-One as a Conventional Entrainer. *J. Chem. Eng. Data* **2025**, *70* (3), 1339−1351. https://doi.org/10.1021/acs.jced.4c00509.
(24) Keestra, H.; Brouwer, T.; Schuur, B.; Lange, J.-P. Entrainer Selection for the Extractive Distillation of Acrylic Acid and Propionic Acid. *Chem. Eng. Res. Des.* **2023**, *192*, 653–663. https://doi.org/https://doi.org/10.1016/j.cherd.2023.02.049.
(25) Brouwer, T.; Schuur, B. Bio-Based Solvents as Entrainers for Extractive Distillation in Aromatic/Aliphatic and Olefin/Paraffin Separation. *Green Chem.* **2020**, *22* (16), 5369–5375. https://doi.org/10.1039/D0GC01769H.
(26) Brouwer, T.; Schuur, B. Biobased Entrainer Screening for Extractive Distillation of Acetone and Diisopropyl Ether. *Sep. Purif. Technol.* **2021**, *270*, 118749. https://doi.org/https://doi.org/10.1016/j.seppur.2021.118749.
(27) Taylor, Barry N; Kuyatt, C. E. NIST Technical Note 1297 Guidelines for Evaluating and Expressing the Uncertainty of NIST Measurement Results. *Technology* **1994**.
(28) *Evaluation of Measurement Data — Guide to the Expression of Uncertainty in Measurement*; Working Group 1 of the Joint Committee for Guides in Metrology (JCGM/WG 1); 2008. https://www.bipm.org/documents/20126/2071204/JCGM_100_2008_E.pdf.
(29) Sinor, J. E.; Weber, J. H. Vapor-Liquid Equilibria at Atmospheric Pressure. Systems Containing Ethyl Alcohol, n-Hexane, Benzene, and Methylcyclopentane. *J. Chem. Eng. Data* **1960**, *5* (3), 243–247. https://doi.org/10.1021/je60007a003.
(30) Ortega, J.; Espiau, F. A New Correlation Method for Vapor−Liquid Equilibria and Excess Enthalpies for Nonideal Solutions Using a Genetic Algorithm. Application to Ethanol + an n-Alkane Mixtures. *Ind. Eng. Chem. Res.* **2003**, *42* (20), 4978–4992. https://doi.org/10.1021/ie030327j.
(31) Williamham, C. B. .; Taylor, W. J. .; Pignocco, J. M. .; Rossini, F. D. Vapor Pressures and Boiling Points of Some Paraffin, Alkylcyclopentane, Alkylcyclohexane, and Alkylbenzene Hydrocarbons. *J. Res. Natl. Bur. Stand. (1934).* **1945**, *35* (3), 219–244. https://doi.org/https://doi.org/10.6028/jres.035.009.
(32) Kretschmer, C. B.; Wiebe, R. Liquid-Vapor Equilibrium of Ethanol--Toluene Solutions. *J. Am. Chem. Soc.* **1949**, *71* (5), 1793–1797. https://doi.org/10.1021/ja01173a076.
(33) Zhang, L.; Shen, D.; Zhang, Z.; Wu, X. Experimental Measurement and Modeling of Vapor–Liquid Equilibrium for the Ternary System Water + Acetonitrile + Ethylene Glycol. *J. Chem. Eng. Data* **2017**, *62* (5), 1725–1731. https://doi.org/10.1021/acs.jced.7b00178.
(34) Zhang, Z.; Lv, M.; Huang, D.; Jia, P.; Sun, D.; Li, W. Isobaric Vapor–Liquid Equilibrium for the Extractive Distillation of Acetonitrile + Water Mixtures Using Dimethyl Sulfoxide at 101.3 KPa. *J. Chem. Eng. Data* **2013**, *58* (12), 3364–3369. https://doi.org/10.1021/je400531a.
(35) Zhu, J.; Sun, Y.; Chen, Y.; Wu, N.; Shi, R.; Ren, Z.; Li, Q.; Zhao, H. Isobaric Vapor–Liquid Equilibrium Experiments of Methyl Propionate + Ethanol with

Different Ionic Liquids at 101.3 KPa. *J. Chem. Eng. Data* **2025**, *70* (1), 427–438. https://doi.org/10.1021/acs.jced.4c00517.

(36) Li, W.; Chen, X.; Yin, H.; Li, L.; Zhang, T. Isobaric Vapor–Liquid Equilibrium for 2-Butanone + Ethanol System Containing Different Ionic Liquids at 101.3 KPa. *J. Chem. Eng. Data* **2018**, *63* (2), 380–388. https://doi.org/10.1021/acs.jced.7b00783.

(37) Li, W.; Li, L.; Zhang, L.; Li, H.; Zhang, T. Isobaric Vapor-Liquid Equilibrium for 2-Butanone + Ethanol + Phosphate-Based Ionic Liquids at 101.3 KPa. *Fluid Phase Equilib.* **2018**, *456*, 57–64. https://doi.org/https://doi.org/10.1016/j.fluid.2017.10.001.

(38) Blanco, B.; Beltrán, S.; Cabezas, J. L.; Coca, J. Phase Equilibria of Binary Systems Formed by Hydrocarbons from Petroleum Fractions and the Solvents N-Methylpyrrolidone and N,N-Dimethylformamide. 1. Isobaric Vapor−Liquid Equilibria. *J. Chem. Eng. Data* **1997**, *42* (5), 938–942. https://doi.org/10.1021/je970059u.

(39) Li, M.; Yu, Y.; Zhang, L.; Li, J.; Song, Y. Isobaric Binary and Ternary Vapor–Liquid Equilibrium for the Mixture of n-Hexane, Methylcyclopentane and N-Methylpyrrolidone. *J. Solution Chem.* **2021**, *50* (9), 1258–1284. https://doi.org/10.1007/s10953-021-01116-0.

(40) Li, F.; Li, M.; Guo, J.; Hu, X.; Zhu, J.; Li, Q.; Zhao, H. Isobaric Vapor–Liquid Equilibrium Experiment of N-Propanol and N-Propyl Acetate at 101.3 KPa. *J. Chem. Eng. Data* **2023**, *68* (2), 358–365. https://doi.org/10.1021/acs.jced.2c00609.

(41) Cao, M.; Tian, H.; Li, M. Vapor–Liquid Equilibrium Data Determination and Model Correlation for 1-Octene + 1,4-Dioxane, 2-Octanol + 1,4-Dioxane, 1-Octene + Isophorone, and 2-Octanol + Isophorone Systems at 101.3 KPa. *J. Chem. Eng. Data* **2023**, *68* (9), 2275–2282. https://doi.org/10.1021/acs.jced.3c00136.

(42) Lei, Z.; Arlt, W.; Wasserscheid, P. Selection of Entrainers in the 1-Hexene/n-Hexane System with a Limited Solubility. *Fluid Phase Equilib.* **2007**, *260* (1), 29–35. https://doi.org/https://doi.org/10.1016/j.fluid.2006.06.009.

(43) Zhang, Z.; Zhang, Z.; Dong, B.; Chen, J.; Xin, H.; Zhang, Q. Vapor-Liquid Equilibrium Experiment and Model Prediction for Separating Ethyl Propionate and Ethanol Using Ionic Liquids with Acetate Anion. *J. Mol. Liq.* **2020**, *318*, 113688. https://doi.org/https://doi.org/10.1016/j.molliq.2020.113688.

(44) Yang, C.; Zeng, H.; Yin, X.; Ma, S.; Sun, F.; Li, Y.; Li, J. Measurement of (Vapor+liquid) Equilibrium for the Systems {methanol+dimethyl Carbonate} and {methanol+dimethyl Carbonate+tetramethylammonium Bicarbonate} at P=(34.43, 67.74)KPa. *J. Chem. Thermodyn.* **2012**, *53*, 158–166. https://doi.org/https://doi.org/10.1016/j.jct.2012.05.002.

(45) He, S.; Fan, W.; Huang, H.; Gao, J.; Xu, D.; Ma, Y.; Zhang, L.; Wang, Y. Separation of the Azeotropic Mixture Methanol and Toluene Using Extractive Distillation: Entrainer Determination, Vapor–Liquid Equilibrium Measurement, and Modeling. *ACS Omega* **2021**, *6* (50), 34736–34743. https://doi.org/10.1021/acsomega.1c05164.

(46) Britt, H. I.; Luecke, R. H. The Estimation of Parameters in Nonlinear, Implicit Models. *Technometrics* **1973**, *15* (2), 233–247. https://doi.org/10.2307/1266984.

## 4.2 VLE data of hexane-ethanol with 1-butylpyrrolidin-2-one and 1-methylpyrrolidin-2-one


### Abstract

In extractive distillation for the separation of azeotropic mixtures, eco-friendly solvents have demonstrated potential as greener alternatives to conventional entrainers. However, the absence of thermodynamic data for mixtures that include green solvents presents a significant hurdle to their practical application. This work explores, for the first time, vapor-liquid equilibrium (VLE) data for the azeotropic mixture of n-hexane and ethanol in the presence of the biobased entrainers guaiacol and dimethyl isosorbide (DMI). The VLE measurements were conducted using a Fischer Labodest VLE 502 ebulliometer with varying pressures and entrainer-to-feed ratios (E/Fs). The VLE data met the criteria of the Van Ness method and thereby pass the thermodynamic consistency test. The results confirm that the relative volatility of n-hexane to ethanol is increased by the addition of guaiacol and DMI to the mixture. Moreover, the azeotrope has been successfully removed. The VLE data were well regressed using the Non-Random Two Liquid (NRTL) thermodynamic model, which provided accurate binary interaction parameters (BIPs). The thermodynamic modeling verifies the reliability of the experimental data and its relevance for effective process design, emphasizing the viability of guaiacol and DMI as biobased entrainers for more sustainable and greener extractive distillation.

### 4.2.1. Introduction

Guaiacol and DMI are not classified as reprotoxic like NMP and exhibit substantially higher NOAEL (No Observed Adverse Effect Level) for DMI reflecting their lower developmental toxicity and better regulatory profile. NOAEL is the highest dose of exposure at which no adverse developmental effects are observed. A higher NOAEL value therefore indicates lower toxicity and, consequently, better chemical safety and greenness. Both are biodegradable and derived from renewable feedstocks, whereas NMP is petrochemical-based. These features provide a clear health and sustainability advantage, even if the thermodynamic separation performance is somewhat lower. Guaiacol is a non-reprotoxic chemical. Although no specific data on its developmental toxicity is available, its widespread use in the food, beverage, and pharmaceutical industries suggests that guaiacol presents a low reprotoxicity. DMI is also classified as low in reprotoxicity, with a NOAEL for developmental toxicity of 300 mg/kg body weight/day. Moreover, DMI has been recognized as one of the top ten biobased platform chemicals. [1–6] On the contrary, NMP is a reprotoxic solvent with the NOAEL of 160 mg/kg body weight/day.[7] This makes NMP unsuitable for industrial applications. Additionally, guaiacol ($T_b$=478.20 K) and DMI ($T_b$=513.15 K) were selected as they exhibit significantly higher boiling points than other biobased solvents, such as furfural ($T_b$=435.15 K), and provide better miscibility in hydrocarbons compared to glycerol derivatives.

Compared to NMP, these solvents have higher boiling points and comparable polarity, as indicated by Hansen Solubility Parameters (HSPs). [1,8–11] Detailed information regarding their boiling point and HSPs is provided in Table E1. These properties make both entrainers advantageous for use in extractive distillation. Moreover, there are no experimental VLE data and BIPs available for n-hexane and ethanol with these solvents, which poses challenges for developing the process design. Thus, this research aims to fill that knowledge gap by providing the first VLE data for the n-hexane and ethanol mixture containing guaiacol and DMI.

Given their promising solvent characteristics, guaiacol and DMI were selected for the VLE experimental in this study to assess their effectiveness in breaking the n-hexane – ethanol azeotrope. To ensure the reliability of the VLE data, thermodynamic consistency was verified using the Van Ness test.[12] Following this, data regression was performed to obtain the optimum BIPs using the NRTL model.[13] These results provide a robust thermodynamic foundation for the design and optimization of more eco-efficient extractive distillation involving guaiacol and DMI as green entrainers.

## 4.2.2. Experiments and methods

The subsequent sections provide the details of the chemical specifications, experimental apparatus, and methodology, along with the analytical techniques applied in this study.

**Materials**

All chemicals used in this study were obtained from commercial sources, and their purity was determined using gas chromatography (GC). The water content of hygroscopic compounds was measured using Karl Fischer (KF) titration (Metrohm-787 KF Titrino 703 TiStand, Switzerland). Due to the absence of substantial impurities, the chemicals were used as received without further purification. A detailed specification of these chemicals is summarized in Table 1.

**Table 1.** The detailed specification of the chemicals

| chemicals | CAS-No | MW (g/mol) | $T_{boiling}$ (K)[a,b] | density ($g/cm^3$)[a,c] | sources | purity (in a mass fraction)[a] | Water content (%)[d] | purity analysis | additional purification |
|---|---|---|---|---|---|---|---|---|---|
| n-hexane | 110-54-3 | 86.18 | 342.15 | 0.660 | Merck | ≥0.990 | - | GC[e] | none |
| ethanol | 64-17-5 | 46.07 | 351.44 | 0.790 | Merck | ≥0.999 | 0.04 | GC[e] | none |
| guaiacol | 90-05-1 | 124.14 | 478.20 | 1.129 | Acros Organics | ≥0.990 | 0.07 | GC[e] | none |
| dimethyl isosorbide | 5306-85-4 | 174.20 | 513.15 | 1.167 | Sigma-Aldrich | ≥0.990 | 0.09 | GC[e] | none |
| acetone | 67-64-1 | 58.08 | 329.15 | 0.791 | Merck | ≥0.998 | 0.05 | GC[e] | none |

[a]specified by the suppliers; [b]pressure:101.3 kPa; [c]temperature: 298.15 and pressure: 101.3 kPa; [d]KF (Karl Fischer titration); [e]GC (gas chromatography)

**Experimental details and procedures**

Methodology for the VLE data measurements and GC analysis is provided in Chapter 2. The standard uncertainties for pressure, temperature, and phase compositions were quantified following the methodologies outlined in the guidelines from NIST and JCGM, [14,15] with equations provided in the Appendix (Eqs. E1-E3). These uncertainty values are included with the VLE data presented in Results and discussion Section.

## 4.2.3. Results and discussion

**Experimental results**

Our previous studies have verified the reliability of both the setup and methods applied in this work.[16,17] The present study assessed the introduction of biobased entrainers guaiacol and DMI to the n-hexane and ethanol mixtures. The experimental VLE data for pseudo-ternary mixtures of n-hexane and ethanol involving guaiacol and DMI were measured. Each pseudo-ternary mixture was investigated at an E/F of 1 under the pressures of 50.0 kPa and 100.0 kPa and at an

E/F of 3 at a pressure of 50.0 kPa. The E/F represents the amount of the entrainer introduced to the azeotropic mixture, which is defined as the mass of the entrainer divided by the mass of the azeotropic mixture. In all composition ranges of n-hexane examined under specified E/Fs and pressures, the presence of guaiacol and DMI in the n-hexane and ethanol mixture exhibit homogeneous mixtures, indicating that VLE measurements were feasible. Moreover, given that the laboratory pressure varied between 100 and 101.3 kPa, the experiments were conducted at 100.0 kPa in a closed vacuum system because it provided a more accurate pressure regulation in the setup.

The experimental VLE data for the pseudo-ternary mixture of n-hexane and toluene with guaiacol are provided in Table 2, while the data for the mixture with DMI are shown in Table 4. In these tables, $x_1'$ and $y_1'$ represent the entrainer-free mole fraction of liquid and vapor phases for n-hexane. The $x_1$, $x_2$, and $x_3$ denote the mole fractions of the liquid phase for n-hexane, ethanol, and entrainer, respectively, while $y_1$, $y_2$, and $y_3$ represent the mole fractions of the vapor phase for n-hexane, ethanol, and entrainer, respectively. The $T$, $\gamma_1$, $\gamma_2$, and $\alpha_{12}$ express the equilibrium temperature, the activity coefficient of n-hexane, the activity coefficient of ethanol, and the relative volatility of n-hexane to toluene, respectively. Since the absence of detectable entrainer in the vapor phase, $y_3$ is considered to be below 0.0005. Consequently, $y_1'$ is regarded as equivalent to $y_1$. This threshold corresponds to the value that does not alter the activity coefficient or relative volatilities within the experimental uncertainty. To ensure consistency in reporting, the $y_3$ values are presented as 0.000 in Tables 2 and 4.

**Table 2.** Experimental VLE data for pseudo-ternary mixture of n-hexane (1) + ethanol (2) + guaiacol (3)[a,b,c]

| $T$/K | $x_1'$ | $x_1$ | $x_2$ | $x_3$ | $y_1'$ | $y_1$ | $y_2$ | $y_3$ | $\gamma_1$ | $\gamma_2$ | $\alpha_{12}$ |
|---|---|---|---|---|---|---|---|---|---|---|---|
| ***E/F = 1; 100.0 kPa*** | | | | | | | | | | | |
| 358.65 | 0.000 | 0.000 | 0.729 | 0.271 | 0.000 | 0.000 | 1.000 | 0.000 | | 1.026 | |
| 353.05 | 0.028 | 0.020 | 0.704 | 0.276 | 0.176 | 0.176 | 0.824 | 0.000 | 6.150 | 1.084 | 7.47 |
| 345.55 | 0.107 | 0.076 | 0.635 | 0.289 | 0.451 | 0.451 | 0.549 | 0.000 | 5.220 | 1.082 | 6.85 |
| 342.05 | 0.133 | 0.094 | 0.614 | 0.292 | 0.556 | 0.556 | 0.444 | 0.000 | 5.820 | 1.048 | 8.19 |
| 339.85 | 0.197 | 0.137 | 0.560 | 0.303 | 0.636 | 0.636 | 0.364 | 0.000 | 4.886 | 1.031 | 7.15 |
| 338.85 | 0.236 | 0.163 | 0.528 | 0.309 | 0.681 | 0.681 | 0.319 | 0.000 | 4.537 | 1.003 | 6.91 |
| 338.25 | 0.277 | 0.190 | 0.495 | 0.315 | 0.700 | 0.700 | 0.300 | 0.000 | 4.087 | 1.029 | 6.11 |
| 337.85 | 0.372 | 0.250 | 0.420 | 0.330 | 0.709 | 0.709 | 0.291 | 0.000 | 3.174 | 1.200 | 4.10 |
| 337.65 | 0.437 | 0.290 | 0.371 | 0.339 | 0.736 | 0.736 | 0.264 | 0.000 | 2.866 | 1.242 | 3.58 |
| 337.65 | 0.586 | 0.376 | 0.265 | 0.359 | 0.753 | 0.753 | 0.247 | 0.000 | 2.260 | 1.629 | 2.15 |
| 337.55 | 0.640 | 0.406 | 0.228 | 0.366 | 0.776 | 0.776 | 0.224 | 0.000 | 2.166 | 1.720 | 1.95 |
| 337.95 | 0.689 | 0.432 | 0.195 | 0.373 | 0.807 | 0.807 | 0.193 | 0.000 | 2.086 | 1.706 | 1.88 |
| 340.55 | 0.840 | 0.512 | 0.097 | 0.391 | 0.893 | 0.893 | 0.107 | 0.000 | 1.796 | 1.698 | 1.60 |
| 344.85 | 0.916 | 0.549 | 0.051 | 0.400 | 0.948 | 0.948 | 0.052 | 0.000 | 1.555 | 1.312 | 1.69 |
| 348.25 | 1.000 | 0.590 | 0.000 | 0.410 | 1.000 | 1.000 | 0.000 | 0.000 | 1.377 | | |
| ***E/F = 1; 50.0 kPa*** | | | | | | | | | | | |
| 341.05 | 0.000 | 0.000 | 0.729 | 0.271 | 0.000 | 0.000 | 1.000 | 0.000 | | 1.035 | |
| 334.35 | 0.027 | 0.019 | 0.705 | 0.276 | 0.238 | 0.238 | 0.762 | 0.000 | 7.706 | 1.089 | 11.40 |

| $T$/K | $x_1$' | $x_1$ | $x_2$ | $x_3$ | $y_1$' | $y_1$ | $y_2$ | $y_3$ | $\gamma_1$ | $\gamma_2$ | $\alpha_{12}$ |
|---|---|---|---|---|---|---|---|---|---|---|---|
| 325.05 | 0.113 | 0.080 | 0.630 | 0.290 | 0.560 | 0.560 | 0.440 | 0.000 | 6.015 | 1.078 | 10.00 |
| 322.15 | 0.140 | 0.099 | 0.607 | 0.294 | 0.654 | 0.654 | 0.346 | 0.000 | 6.329 | 1.009 | 11.65 |
| 320.05 | 0.214 | 0.148 | 0.546 | 0.306 | 0.722 | 0.722 | 0.278 | 0.000 | 5.017 | 0.998 | 9.58 |
| 318.75 | 0.270 | 0.185 | 0.500 | 0.315 | 0.749 | 0.749 | 0.251 | 0.000 | 4.370 | 1.049 | 8.07 |
| 318.25 | 0.342 | 0.231 | 0.444 | 0.325 | 0.770 | 0.770 | 0.230 | 0.000 | 3.675 | 1.110 | 6.45 |
| 318.25 | 0.421 | 0.279 | 0.384 | 0.337 | 0.795 | 0.795 | 0.205 | 0.000 | 3.134 | 1.146 | 5.33 |
| 318.15 | 0.424 | 0.281 | 0.382 | 0.337 | 0.791 | 0.791 | 0.209 | 0.000 | 3.108 | 1.180 | 5.14 |
| 318.15 | 0.442 | 0.292 | 0.369 | 0.339 | 0.803 | 0.803 | 0.197 | 0.000 | 3.041 | 1.154 | 5.14 |
| 318.55 | 0.588 | 0.377 | 0.264 | 0.359 | 0.833 | 0.833 | 0.167 | 0.000 | 2.408 | 1.340 | 3.49 |
| 318.95 | 0.618 | 0.394 | 0.243 | 0.363 | 0.849 | 0.849 | 0.151 | 0.000 | 2.314 | 1.288 | 3.47 |
| 320.05 | 0.740 | 0.459 | 0.162 | 0.379 | 0.899 | 0.899 | 0.101 | 0.000 | 2.016 | 1.233 | 3.12 |
| 320.85 | 0.806 | 0.494 | 0.119 | 0.387 | 0.910 | 0.910 | 0.090 | 0.000 | 1.843 | 1.430 | 2.43 |
| 322.55 | 0.901 | 0.542 | 0.060 | 0.398 | 0.952 | 0.952 | 0.048 | 0.000 | 1.654 | 1.402 | 2.18 |
| 325.35 | 1.000 | 0.590 | 0.000 | 0.410 | 1.000 | 1.000 | 0.000 | 0.000 | 1.444 | | |
| ***E/F = 3; 50.0 kPa*** | | | | | | | | | | | |
| 349.55 | 0.000 | 0.000 | 0.473 | 0.527 | 0.000 | 0.000 | 1.000 | 0.000 | | 1.125 | |
| 341.55 | 0.108 | 0.049 | 0.402 | 0.549 | 0.250 | 0.250 | 0.750 | 0.000 | 2.559 | 1.378 | 2.75 |
| 335.65 | 0.170 | 0.074 | 0.365 | 0.561 | 0.510 | 0.510 | 0.490 | 0.000 | 4.121 | 1.280 | 5.10 |
| 329.95 | 0.314 | 0.130 | 0.284 | 0.586 | 0.709 | 0.709 | 0.291 | 0.000 | 3.979 | 1.258 | 5.32 |
| 326.45 | 0.394 | 0.158 | 0.243 | 0.599 | 0.780 | 0.780 | 0.220 | 0.000 | 4.046 | 1.311 | 5.45 |
| 324.45 | 0.588 | 0.219 | 0.153 | 0.628 | 0.836 | 0.836 | 0.164 | 0.000 | 3.355 | 1.697 | 3.57 |
| 324.25 | 0.630 | 0.231 | 0.136 | 0.633 | 0.859 | 0.859 | 0.141 | 0.000 | 3.290 | 1.666 | 3.58 |
| 323.95 | 0.793 | 0.275 | 0.072 | 0.653 | 0.904 | 0.904 | 0.096 | 0.000 | 2.943 | 2.171 | 2.46 |
| 324.35 | 0.837 | 0.286 | 0.056 | 0.658 | 0.926 | 0.926 | 0.074 | 0.000 | 2.857 | 2.122 | 2.43 |
| 325.45 | 0.940 | 0.311 | 0.020 | 0.669 | 0.968 | 0.968 | 0.032 | 0.000 | 2.646 | 2.433 | 1.92 |
| 326.95 | 1.000 | 0.324 | 0.000 | 0.676 | 1.000 | 1.000 | 0.000 | 0.000 | 2.485 | | |

[a]equilibrium temperature ($T$); mole fraction of liquid phase for n-hexane (guaiacol-free basis) ($x_1$'); mole fraction of vapor phase for n-hexane (guaiacol-free basis) ($y_1$'); mole fractions of liquid phase for n-hexane, ethanol, and guaiacol ($x_1$, $x_2$, and $x_3$); mole fractions of liquid phase for n-hexane, ethanol, and guaiacol ($y_1$, $y_2$, and $y_3$); activity coefficient of n-hexane and ethanol ($\gamma_1$ and $\gamma_2$); and relative volatility of n-hexane to ethanol ($\alpha_{12}$).

[b]Expanded combined uncertainties ($U$) with $k$ = 2 for $U(T)$ is 0.20 K, $U(P)$ is 0.2 kPa, and $U(x_1)$ and $U(y_1)$ are 0.006.

[c]$y_3$ are lower than 0.0005

Eq. 1 defines the activity coefficient ($\gamma_i$), which was utilized to evaluate the non-ideal behavior of component $i$ in the liquid phase of the pseudo-ternary mixtures. The vapor phase was treated as ideal, which is justified by the vacuum and atmospheric operating pressures under which the VLE experiments were conducted.

$$\gamma_i = \frac{y_i P}{x_i P_i^{sat}} \qquad 1)$$

In this equation, $x_i$ and $y_i$ correspond to the mole fractions of component $i$ in the liquid and vapor phase, respectively. $P$ and $P_i^{sat}$ refer to the total pressure in the system and the saturated vapor pressure of component $i$, respectively. The saturated vapor pressure was determined using equations and parameters from

the extended Antoine and the NIST Wagner 25, which are taken from the Aspen Plus physical properties database. For n-hexane, ethanol, and guaiacol, the extended Antoine equation was employed. For DMI, the NIST Wagner 25 equation was applied since no data was available for the extended Antoine equation. The equations and their parameters are provided in Table 3.

**Table 3.** The equation and parameters of the extended Antoine and the NIST Wagner 25[a]

| Compounds | The extended Antoine [b] | | | | | | | | |
|---|---|---|---|---|---|---|---|---|---|
| | $A_1$ | $A_2$ | $A_3$ | $A_4$ | $A_5$ | $10^6A_6$ | $A_7$ | $A_8$ | $A_9$ |
| n-hexane | 97.742 | -6995.5 | 0 | 0 | -12.702 | 12.381 | 2 | 177.83 | 507.6 |
| ethanol | 66.396 | -7122.3 | 0 | 0 | -7.142 | 2.885 | 2 | 159.05 | 514.0 |
| guaiacol | 244.642 | -17453.0 | 0 | 0 | -33.723 | 19.843 | 2 | 31.5 | 423.9 |
| | The NIST Wagner25[c] | | | | | | | | |
| | $A_1$ | $A_2$ | $A_3$ | $A_4$ | $ln\ P_{ci}$ | $T_{ci}$ | $T_{lower}$ | $T_{upper}$ | |
| dimethyl isosorbide | -8.552 | 2.397 | -4.204 | -3.911 | 8.041 | 688 | 220 | 688 | |

[a]Parameters of the extended Antoine and the NIST Wagner25 were retrieved from the Aspen Plus physical property databank.

[b]Equation (the extended Antoine):

$\ln(P^{sat}) = A_1 + A_2/(T + A_3) + A_4T + A_5 \ln T + A_6T^{A_7}$ for $A_8 < T < A_9$, where $P^{sat}$ is in kPa and $T$ in K.

[c]Equation (the NIST Wagner25):

$$\ln(P^s) = \ln P_{ci} + \frac{A_1(1-T_{ri}) + A_2(1-T_{ri})^{1.5} + A_3(1-T_{ri})^{2.5} + A_4(1-T_{ri})^5}{T_{ri}} \text{ for } T_{lower} \le T \le T_{upper},$$

where $P^s$ is in kPa, $T$ in K, and $T_{ri}=T/T_{ci}$

Separation performance of the entrainer was examined using the relative volatility equation, as shown in Eq. 2.

$$\alpha_{12} = \frac{y_1 / x_1'}{y_2 / x_2'} \qquad 2)$$

In this equation, the relative volatility of n-hexane to ethanol is represented by $\alpha_{12}$, mole fractions of liquid phase for n-hexane and ethanol on an entrainer-free basis are denoted as $x_1'$ and $x_2'$, and mole fractions of vapor phase for n-hexane and ethanol are defined as $y_1$ and $y_2$. The VLE data in Tables 2 and 4 highlight important trends, including altered equilibrium temperatures, enhanced relative volatilities, and the removal of azeotropic constraints when entrainers are added to the mixture. These effects are visually depicted in Figures 1-4.

**Table 4.** Experimental VLE data for pseudo-ternary mixture of n-hexane (1) + ethanol (2) + dimethyl isosorbide (3) [a,b,c]

| *T*/K | $x_1'$ | $x_1$ | $x_2$ | $x_3$ | $y_1'$ | $y_1$ | $y_2$ | $y_3$ | $\gamma_1$ | $\gamma_2$ | $\alpha_{12}$ |
|---|---|---|---|---|---|---|---|---|---|---|---|
| ***E/F = 1; 100.0 kPa*** | | | | | | | | | | | |
| 357.05 | 0.000 | 0.000 | 0.791 | 0.209 | 0.000 | 0.000 | 1.000 | 0.000 | | 1.006 | |
| 350.85 | 0.051 | 0.040 | 0.744 | 0.216 | 0.195 | 0.195 | 0.805 | 0.000 | 3.668 | 1.095 | 4.51 |
| 346.25 | 0.109 | 0.084 | 0.691 | 0.225 | 0.364 | 0.364 | 0.636 | 0.000 | 3.726 | 1.119 | 4.69 |
| 339.85 | 0.209 | 0.160 | 0.602 | 0.238 | 0.605 | 0.605 | 0.395 | 0.000 | 3.989 | 1.042 | 5.78 |
| 337.95 | 0.370 | 0.275 | 0.466 | 0.259 | 0.680 | 0.680 | 0.320 | 0.000 | 2.766 | 1.184 | 3.61 |
| 337.05 | 0.516 | 0.373 | 0.350 | 0.277 | 0.719 | 0.719 | 0.281 | 0.000 | 2.216 | 1.440 | 2.40 |
| 337.15 | 0.569 | 0.408 | 0.309 | 0.283 | 0.733 | 0.733 | 0.267 | 0.000 | 2.062 | 1.541 | 2.08 |
| 337.35 | 0.701 | 0.492 | 0.210 | 0.298 | 0.775 | 0.775 | 0.225 | 0.000 | 1.797 | 1.894 | 1.47 |
| 339.45 | 0.835 | 0.573 | 0.114 | 0.313 | 0.835 | 0.835 | 0.165 | 0.000 | 1.553 | 2.344 | 1.00 |
| 341.15 | 0.878 | 0.598 | 0.084 | 0.318 | 0.868 | 0.868 | 0.132 | 0.000 | 1.467 | 2.347 | 0.91 |
| 344.45 | 0.967 | 0.650 | 0.022 | 0.328 | 0.963 | 0.963 | 0.037 | 0.000 | 1.350 | 2.186 | 0.89 |
| 347.25 | 1.000 | 0.669 | 0.000 | 0.331 | 1.000 | 1.000 | 0.000 | 0.000 | 1.252 | | |
| ***E/F = 1; 50.0 kPa*** | | | | | | | | | | | |
| 339.25 | 0.000 | 0.000 | 0.791 | 0.209 | 0.000 | 0.000 | 1.000 | 0.000 | | 1.030 | |
| 332.25 | 0.064 | 0.050 | 0.732 | 0.218 | 0.253 | 0.253 | 0.747 | 0.000 | 3.394 | 1.131 | 4.94 |
| 326.15 | 0.120 | 0.093 | 0.681 | 0.226 | 0.478 | 0.478 | 0.522 | 0.000 | 4.276 | 1.123 | 6.69 |
| 319.95 | 0.237 | 0.180 | 0.579 | 0.241 | 0.683 | 0.683 | 0.317 | 0.000 | 3.938 | 1.080 | 6.94 |
| 318.45 | 0.366 | 0.270 | 0.471 | 0.259 | 0.727 | 0.727 | 0.273 | 0.000 | 2.940 | 1.231 | 4.62 |
| 317.65 | 0.516 | 0.373 | 0.350 | 0.277 | 0.770 | 0.770 | 0.230 | 0.000 | 2.328 | 1.449 | 3.15 |
| 317.75 | 0.615 | 0.438 | 0.273 | 0.289 | 0.780 | 0.780 | 0.220 | 0.000 | 1.999 | 1.770 | 2.22 |
| 318.05 | 0.690 | 0.484 | 0.218 | 0.298 | 0.812 | 0.812 | 0.188 | 0.000 | 1.860 | 1.864 | 1.95 |
| 319.25 | 0.839 | 0.575 | 0.111 | 0.314 | 0.860 | 0.860 | 0.140 | 0.000 | 1.587 | 2.581 | 1.18 |
| 320.25 | 0.881 | 0.600 | 0.082 | 0.318 | 0.879 | 0.879 | 0.121 | 0.000 | 1.500 | 2.862 | 0.99 |
| 322.65 | 0.962 | 0.648 | 0.025 | 0.327 | 0.961 | 0.961 | 0.039 | 0.000 | 1.392 | 2.672 | 0.99 |
| 324.85 | 1.000 | 0.669 | 0.000 | 0.331 | 1.000 | 1.000 | 0.000 | 0.000 | 1.297 | | |
| ***E/F = 3; 50.0 kPa*** | | | | | | | | | | | |
| 346.05 | 0.000 | 0.000 | 0.558 | 0.442 | 0.000 | 0.000 | 1.000 | 0.000 | | 1.099 | |
| 341.85 | 0.046 | 0.025 | 0.523 | 0.452 | 0.099 | 0.099 | 0.901 | 0.000 | 1.953 | 1.257 | 2.30 |
| 336.75 | 0.116 | 0.062 | 0.472 | 0.466 | 0.252 | 0.252 | 0.748 | 0.000 | 2.360 | 1.439 | 2.56 |
| 329.85 | 0.243 | 0.124 | 0.386 | 0.490 | 0.587 | 0.587 | 0.413 | 0.000 | 3.458 | 1.322 | 4.43 |
| 325.85 | 0.358 | 0.176 | 0.314 | 0.510 | 0.717 | 0.717 | 0.283 | 0.000 | 3.417 | 1.340 | 4.53 |
| 323.45 | 0.561 | 0.257 | 0.201 | 0.542 | 0.802 | 0.802 | 0.198 | 0.000 | 2.844 | 1.636 | 3.17 |
| 323.45 | 0.645 | 0.288 | 0.159 | 0.553 | 0.844 | 0.844 | 0.156 | 0.000 | 2.671 | 1.641 | 2.97 |
| 323.45 | 0.694 | 0.305 | 0.134 | 0.561 | 0.867 | 0.867 | 0.133 | 0.000 | 2.590 | 1.641 | 2.88 |
| 324.45 | 0.861 | 0.360 | 0.059 | 0.581 | 0.925 | 0.925 | 0.075 | 0.000 | 2.261 | 2.025 | 1.99 |
| 324.85 | 0.914 | 0.377 | 0.035 | 0.588 | 0.958 | 0.958 | 0.042 | 0.000 | 2.204 | 1.862 | 2.14 |
| 327.35 | 1.000 | 0.403 | 0.000 | 0.597 | 1.000 | 1.000 | 0.000 | 0.000 | 1.975 | | |

[a] equilibrium temperature ($T$); mole fraction of liquid phase for n-hexane (DMI-free basis) ($x_1'$); mole fraction of vapor phase for n-hexane (DMI-free basis) ($y_1'$); mole fractions of liquid phase for n-hexane, ethanol, and DMI ($x_1$, $x_2$, and $x_3$); mole fractions of liquid phase for n-hexane, ethanol, and DMI ($y_1$, $y_2$, and $y_3$); activity coefficient of n-hexane and ethanol ($\gamma_1$ and $\gamma_2$); and relative volatility of n-hexane to ethanol ($\alpha_{12}$).

[b] Expanded combined uncertainties ($U$) with $k = 2$ for $U(T)$ is 0.20 K, $U(P)$ is 0.2 kPa, and $U(x_1)$ and $U(y_1)$ are 0.006.

[c] $y_3$ are lower than 0.0005

Figures 1 and 2 illustrate that the presence of guaiacol in the n-hexane and ethanol mixture exhibits a comparable effect to that of DMI. Both entrainers increase the equilibrium temperature when added at an E/F of 1 and at a pressure of 100.0 kPa, compared to the binary mixture without an entrainer. Guaiacol and

DMI demonstrate an affinity for ethanol, which reduces the vaporization of ethanol. Moreover, the addition of a high boiling point entrainer in the mixture, with an E/F of 1 (or 50% mass of the total liquid composition), significantly affects the boiling point of the mixture. As a result, these two factors contribute to an increase in the equilibrium temperature. The effects of reduced pressure were also investigated. Lowering the pressure from 100.0 to 50.0 kPa while maintaining a constant E/F of 1 lead to a significant decrease in the equilibrium temperature. This is because each component has a lower boiling point under reduced pressure, requiring less heat to achieve equilibrium.

At the pressure of 50.0 kPa, increasing the amount of guaiacol and DMI to an E/F of 3 results in a higher equilibrium temperature compared to an E/F of 1. This is attributed to the entrainers becoming the major constituents of the liquid phase. Moreover, it reduces the vaporization of both n-hexane and ethanol, thereby elevating the equilibrium temperature. A minimum temperature is observed at all investigated E/Fs and pressures with the addition of guaiacol. However, this does not correspond to the presence of an azeotropic point, as the vapor phase composition of n-hexane consistently remains higher than its liquid phase composition. Similarly, in the presence of DMI, the minimum temperature does not indicate an azeotrope either. At an E/F of 3 and a pressure of 50.0 kPa, the vapor phase composition of n-hexane always exceeds that of the liquid phase. Furthermore, although an azeotrope occurs at an E/F of 1 and pressures of 50 and 100 kPa, the composition of this azeotrope differs from the composition at which the minimum temperature is observed. The occurrence of the minimum temperature in this system is predominantly governed by strong positive deviations from ideal behavior. These deviations are mainly associated with polarity differences and hydrogen-bonding effects that induce repulsive mixing, increasing activity coefficients. This phenomenon is accompanied by a depression of the boiling point, in which the total vapor pressure of the mixture surpasses that of pure components because of non-ideal interactions. Other contributing phenomena include ternary molecular interactions, where the introduction of guaiacol and DMI alters the n-hexane and ethanol binary interactions. Additionally, pressure dependence, where reduced pressure lowers the boiling points of all compounds, while changes in relative volatility accentuate non-ideality. Collectively, these phenomena elevate the total vapor pressure at specific compositions, resulting in a minimum boiling temperature, even if the azeotrope is significantly shifted or completely removed. This minimum temperature behavior is consistent with our previous studies of the n-hexane and ethanol mixture when 1-butylpyrrolidin-2-one (NBP) and NMP were used as entrainers.[17] This finding also aligns with the reported azeotropic mixtures from literature, such as those involving ethanol and methyl propionate and ethanol and 2-butanone with the addition of various ionic liquids as entrainers,[18–20] as well

as acetonitrile-water mixture with the presence of dimethyl sulfoxide and ethylene glycol.[21,22]

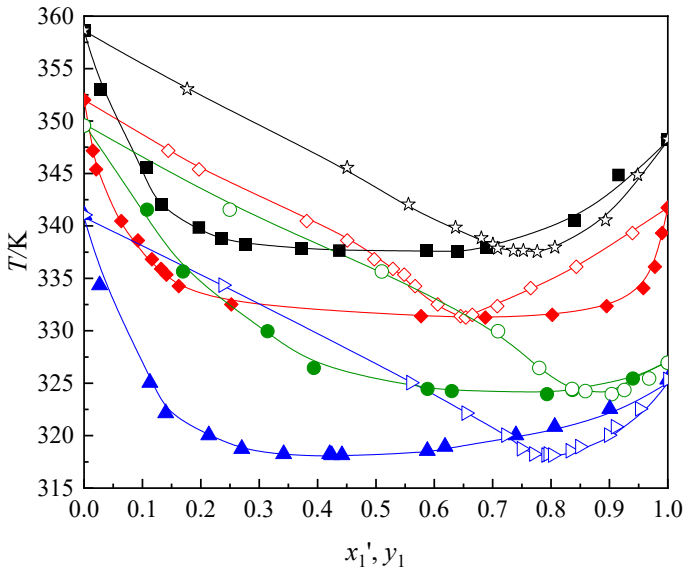


**Figure 1.** $x_1$'-$y_1$-$T$ profiles for n-hexane (1) + ethanol (2) + guaiacol (3). Experimental data with an E/F of 1: (■), $x_1$' and (☆), $y_1$ at 100.0 kPa; and (▲), $x_1$' and (▷), $y_1$ at 50.0 kPa; with an E/F of 3: (●), $x_1$' and (○), $y_1$ at 50.0 kPa; and binary mixture: (♦), $x_1$ and (◊), $y_1$ at 101.3 kPa. Correlated results from the NRTL model (—): with an E/F of 1, 100.0 kPa (black); and 50.0 kPa (blue); with an E/F of 3, 50.0 kPa (green); and (- · -), binary mixture at 101.3 kPa (red). The binary mixture were taken from our previous work.[17] Note: $x_1$ and $y_1$ denote the entrainer-free mole fractions of n-hexane in the liquid and vapor phases, respectively, as defined in Tables 2 and 4.

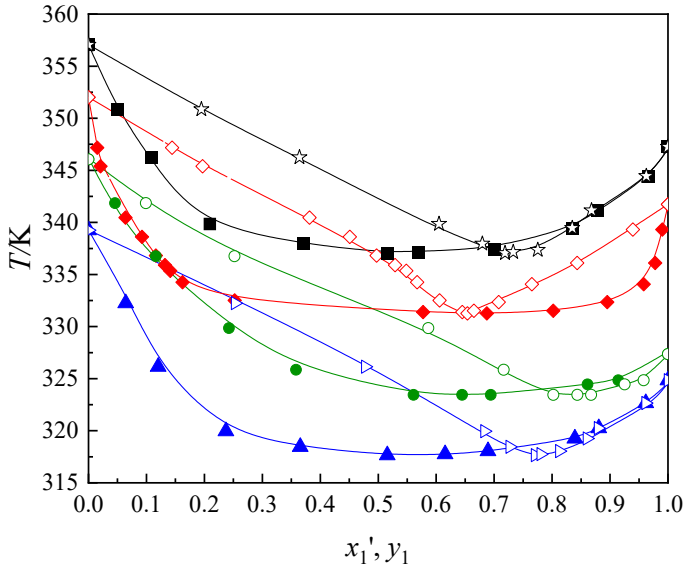


**Figure 2.** $x_1$'-$y_1$-$T$ profiles for n-hexane (1) + ethanol (2) + dimethyl isosorbide (3). Experimental data with an E/F of 1: (■), $x_1$' and (☆), $y_1$ at 100.0 kPa; and (▲), $x_1$' and (▷), $y_1$ at 50.0 kPa; E/F of 3: (●), $x_1$' and (○), $y_1$ at 50.0 kPa; and binary mixture: (♦), $x_1$ and (◊), $y_1$ at 101.3 kPa. Correlated results from the NRTL model (—): with an E/F of 1, 100.0 kPa (black); and 50.0 kPa (blue); with an E/F of 3, 50.0 kPa (green); and (-··-), binary mixture at 101.3 kPa (red). The binary mixture were taken from our previous work.[17].Note: $x_1$ and $y_1$ denote the entrainer-free mole fractions of n-hexane in the liquid and vapor phases, respectively, as defined in Tables 2 and 4.

In Figures 1 and 2, the VLE curves are plotted in terms of the entrainer-free mole fractions $x_1$' and $y_1$. At high entrainer loadings, the strong non-ideal behavior and the re-normalization to an entrainer-free basis can lead to pronounced curvature of the $x_1$'-$y_1$ profiles and to sections where the projected vapor curve appears below the projected liquid curve in the 2D representation. This effect is purely geometric and does not indicate a violation of phase-equilibrium conditions, as confirmed by the Van Ness consistency test (Table 5) and the random distribution of residuals of of the $\ln(\gamma_1/\gamma_2)$. Data points that visually overlap at high $x_1$' (particularly in Figure 2) correspond to measurements at very similar compositions and temperatures; they were retained to demonstrate measurement reproducibility.

The $x_1$'-$y_1$ profiles, shown in Figures 3-4, highlight how the presence of guaiacol and DMI contributes to the elimination of the azeotropic point in the n-hexane and ethanol mixture. The initial azeotropic composition was $x_1 = 0.660$.[17] The addition of guaiacol and DMI to the mixture modifies its non-ideal thermodynamic behavior by affecting the molecular interactions of its components. Since ethanol is polar and n-hexane is non-polar, both guaiacol and DMI, which are polar components,

demonstrate stronger interactions toward polar ethanol compared to non-polar n-hexane. This selective affinity weakens the ethanol and n-hexane interactions, thereby enhancing the relative volatility and removing the azeotropic point, which facilitates a more effective separation of n-hexane from ethanol. The pronounced affinity between ethanol and both guaiacol and DMI can be attributed to specific hydrogen-bonding interactions, wherein the hydroxyl group in ethanol acts as a hydrogen bond donor to the phenolic hydroxyl and ether oxygen in guaiacol, which serve as hydrogen bond acceptors. Similarly, the interactions of ethanol and DMI involve the hydroxyl group of ethanol bonding with ether oxygen in DMI. On the other hand, n-hexane, as a nonpolar compound, exhibits weaker van der Waals interactions with guaiacol and DMI.

With the addition of guaiacol, the VLE data presented in Table 2 shows that the activity coefficient of n-hexane ($\gamma_1$) is larger than that of ethanol ($\gamma_2$) across all compositions of n-hexane for the investigated E/Fs and pressures. This indicates a stronger molecular affinity between guaiacol and ethanol than between guaiacol and n-hexane, which enhances the volatility of n-hexane and effectively removes the azeotropic point. Notably, the azeotropic point has already been removed in the presence of guaiacol at an E/F of 1 and a pressure of 100.0 kPa. Additionally, this work studied the effect of lowering the pressure from 100.0 to 50.0 kPa at an E/F of 1 on relative volatility. Table 2 illustrates that the values of $\gamma_2$ at 50.0 kPa are overall smaller than at 100.0 kPa. This indicates that at a reduced pressure, the guaiacol and ethanol interaction is stronger. This enhanced interaction facilitates the easier separation of n-hexane, and therefore the relative volatility at a reduced pressure is significantly increased, as shown in Figure 3.

This study further investigated the effect of the guaiacol amount added to the mixture. The addition of guaiacol to the mixture with an E/F of 3 was evaluated. Given that a significant increase in relative volatility is observed when the pressure is reduced from 100.0 to 50.0 kPa at an E/F of 1, the VLE measurements at an E/F of 3 were conducted at a pressure of 50.0 kPa to examine whether a further increase in guaiacol amount would amplify the separation of n-hexane from ethanol. As shown in Figure 3, however, when the amount of the guaiacol is increased from an E/F of 1 to an E/F of 3 at a pressure of 50.0 kPa, the relative volatility remains unchanged. This behavior is attributed to the tendency of guaiacol, when presented in higher amounts, to interact not only with ethanol but also with itself. Although the interaction between guaiacol and ethanol is still present, as indicated by the $\gamma_2$ values being smaller than $\gamma_1$ across all n-hexane compositions, the self-interaction of guaiacol prevents the interaction between guaiacol and ethanol from being as effective as at an E/F of 1 and a pressure of 50.0 kPa. Consequently, the interaction strength between guaiacol and ethanol at an E/F of 3 is diminished compared to at an E/F of 1, under the same pressure of 50.0 kPa. This reduced interaction reflected

by the higher values of $\gamma_2$ at an E/F of 3 compared to that at an E/F of 1 at the same pressure. Conversely, the non-ideality of n-hexane increases when a larger amount of guaiacol is added to the mixture. This can be explained by the fact that n-hexane, a non-polar compound, exhibits an easier tendency to evaporate when the liquid mixture is dominated by the polar guaiacol composition. This is indicated by the higher values of $\gamma_1$ at an E/F of 3 compared to an E/F of 1 at the same pressure of 50.0 kPa. At this pressure, although the $\gamma_1$ values increase, increasing the E/F from 1 to 3 does not lead to an increase in relative volatility, as this is accompanied by an increase in $\gamma_2$.

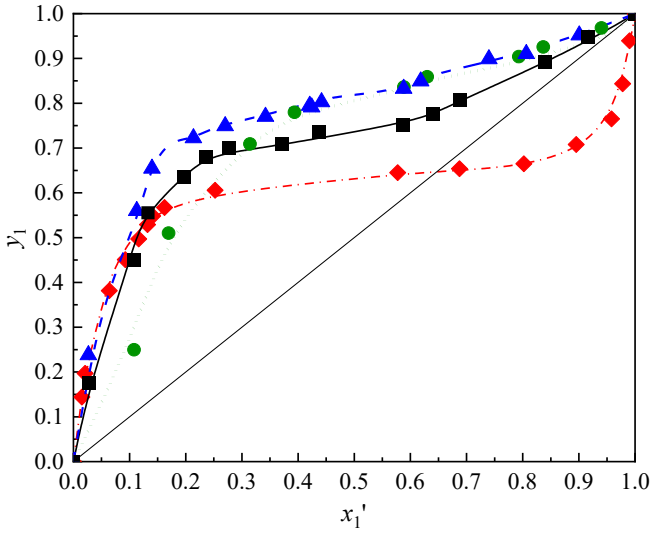


**Figure 3.** $x_1'$-$y_1$ profiles for n-hexane (1) + ethanol (2) + guaiacol (3). Experimental data with an E/F of 1: (■), at 100.0 kPa; and (▲), at 50.0 kPa; E/F of 3: (●), at 50.0 kPa; and (♦), binary mixture at 101.3 kPa. Correlated results from the NRTL model with an E/F of 1: (—), at 100.0 kPa (black); and (- - -), 50.0 kPa (blue); with an E/F of 3: (····), 50.0 kPa (green); and (-·-), binary mixture at 101.3 kPa (red). The binary mixture were taken from our previous work.[17]

Unlike with the presence of guaiacol, where $\gamma_2$ values are consistently smaller than $\gamma_1$ across all investigated E/Fs and pressures throughout all n-hexane compositions, the presence of DMI shows a distinct behavior. As presented in Table 4, the VLE data with the addition of DMI demonstrate that $\gamma_2$ values are smaller than $\gamma_1$ at the entire composition of n-hexane only at an E/F of 3 and a pressure of 50.0 kPa. This shows stronger molecular interactions between DMI and ethanol than between DMI and n-hexane. As a result, the relative volatility is significantly enhanced, allowing the azeotrope to be effectively removed under these conditions, as illustrated in Figure 4. However, when DMI is added to the mixture at an E/F of

1 and pressures of 50.0 and 100.0 kPa, the $\gamma_2$ values, particularly, in the n-hexane-rich region, are higher than $\gamma_1$. This indicates insufficient interactions between DMI and ethanol in this region. As a result, although DMI can increase relative volatility, it does not completely remove the azeotrope but shifts its composition from the original azeotropic point at $x_1 = 0.660$ toward the n-hexane-rich region.

Figure 4 presents that reducing the pressure from 100.0 to 50.0 kPa when DMI is added at an E/F of 1 does not significantly increase the relative volatility in the n-hexane-rich region, and the azeotrope remains present in the mixture. In contrast, when a larger quantity of DMI is added at an E/F of 3 and operated at a pressure of 50.0 kPa, the relative volatility can be significantly increased, and the azeotropic point is effectively eliminated. The different behaviors between guaiacol and DMI can be attributed to their polarity properties. DMI exhibits lower polarity than guaiacol, as reflected by its lower HSPs values, listed in Table E1. This lower polarity characteristic reduces the potential of self-interaction between molecules of DMI compared to that of guaiacol. Therefore, adding a larger amount of DMI at a low pressure still allows for effective interactions between DMI and ethanol. Our earlier research applied unimolecular quantum chemical calculations through COSMO-RS to investigate the interaction tendencies of polar entrainers. It was observed that these entrainers form stronger interactions with molecules possessing greater polar characteristics.[23]

Notably, guaiacol at an E/F of 1 and a pressure of 100.0 kPa is already effective at removing the azeotrope, while DMI requires higher E/F and lower operating pressure to achieve the same result. This indicates that guaiacol demonstrates better separation performance than DMI in the separation of n-hexane and ethanol. Additionally, Figures 3 and 4 confirm that the azeotropic point is completely eliminated under all conditions studied involving guaiacol.

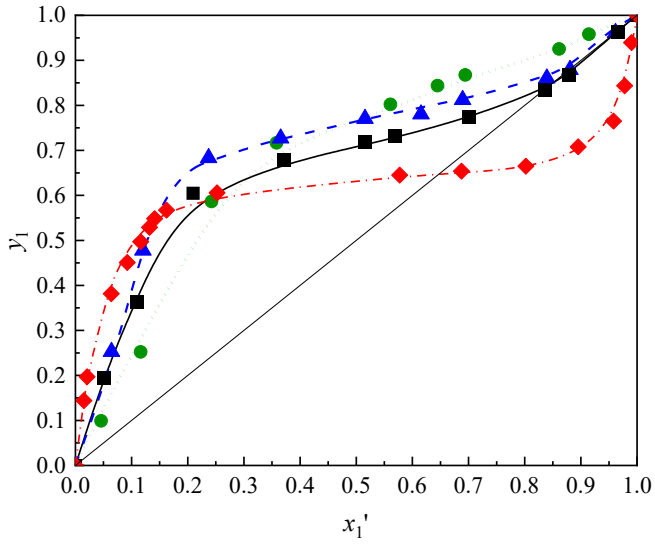


**Figure 4.** $x_1$'-$y_1$ profiles for n-hexane (1) + ethanol (2) + dimethyl isosorbide (3). Experimental data with an E/F of 1: (■), at 100.0 kPa; and (▲), at 50.0 kPa; with an E/F of 3: (●), at 50.0 kPa; and (♦), binary mixture at 101.3 kPa. Correlated results from the NRTL model with E/F of 1: (—), at 100.0 kPa (black); and (- - -), 50.0 kPa (blue); with an E/F of 3: (····), 50.0 kPa (green); and (-·-), binary mixture at 101.3 kPa (red). The binary mixture were taken from our previous work.[17]

For DMI, complete azeotrope removal occurs at an E/F of 3 and a pressure of 50 kPa. This is achieved despite the minimum temperature present in the mixture, as shown in Figure 1 and 2. The composition dependence of the activity coefficients $\gamma_1$ and $\gamma_2$ is illustrated in Figures E1-E4, which show $\gamma_i$ versus entrainer-free mole fraction of n-hexane for all investigated EF values and pressures. These plots highlight the pronounced positive deviations from ideality and confirm the stronger non-ideality of n-hexane compared to ethanol in the presence of both guaiacol and DMI. The corresponding excess Gibbs free energy ($G^E/RT$) as a function of composition is presented in Figures E5–E6. The asymmetric $G^E$ curves are consistent with the selective interactions between the entrainers and ethanol and provide direct insight into the thermodynamic basis for the observed shifts and removal of the azeotropic point.

A comparative assessment of guaiacol and DMI as biobased entrainers and NMP as a benchmark entrainer was conducted to evaluate how these entrainers effectively separate n-hexane from ethanol, particularly with respect to their ability to enhance the relative volatility. Figure 5 shows that, in the n-hexane-rich region at 50.0 kPa, guaiacol at EF = 1 and DMI at EF = 3 provide relative volatilities that are 13–17% lower than those achieved with NMP at EF = 1 and 100.0 kPa.

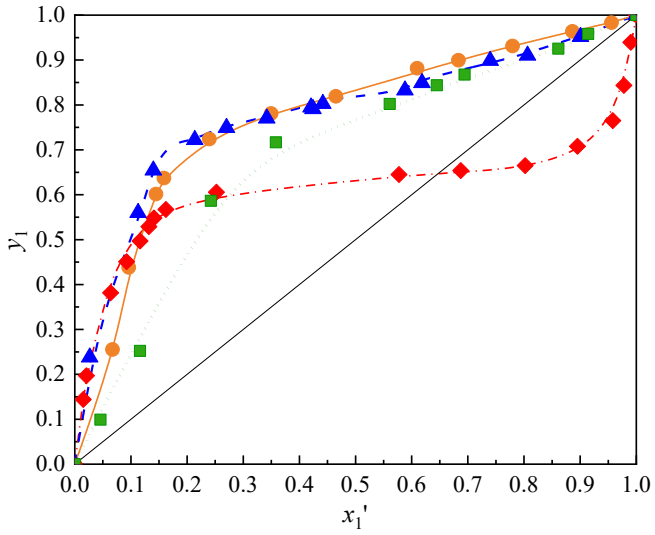


**Figure 5.** $x_1$'-$y_1$ profiles for the comparison of the biobased entrainers guaiacol and DMI with the benchmark entrainer NMP in the n-hexane and ethanol mixture: (▲), guaiacol with an E/F of 1 at 50.0 kPa; (■), DMI with an E/F of 3 at 50.0 kPa; (●), NMP with an E/F of 1 at 100.0 kPa; (♦), the binary mixture at 101.3 kPa, and regressed by NRTL: (- - -), blue line for guaiacol; (····), green line for DMI; (—), orange line for NMP; and (-··-), red line for the binary mixture. The binary mixture were taken from our previous work.[17]

This lower relative volatility would translate into a higher minimum number of theoretical stages and/or higher reflux ratios in an extractive distillation column, increasing energy demand compared to a process using NMP. However, when these thermodynamic differences are considered together with the markedly lower toxicity, biobased origin, and absence of strict regulatory constraints for guaiacol and DMI, these entrainers, under suitable operating conditions, remain attractive candidates for greener process designs. Their performance is comparable to that of other green entrainers, such as NBP and selected ionic liquids, while avoiding the handling and miscibility challenges encountered with ionic liquids and deep eutectic solvents in this particular system.

In extractive distillation, a lower relative volatility at the same pressure and entrainer fraction generally increases the minimum number of theoretical stages and the energy demand through higher reflux ratios. Thus, the 13–17% lower relative volatilities observed for guaiacol and DMI compared to NMP and NBP suggest that, at otherwise identical design assumptions, an extractive distillation column using guaiacol or DMI would require more separation effort. A detailed process simulation and optimization, including column configuration, heat integration, and entrainer recovery, is therefore needed to quantify the trade-off between increased energy consumption and the benefits arising from lower toxicity and improved

sustainability of guaiacol and DMI. Such analysis is beyond the scope of the present thermodynamic data study but represents an important direction for future work.

A direct comparison with our previous work on NBP and NMP as entrainers for n-hexane + ethanol[17] and a selected imidazolium ionic liquid [24] and glycerol-based deep eutectic solvents[25] is summarized in Figure 6. At the azeotropic composition and 100.0 kPa, NMP at EF = 1 yields the highest relative volatility among the green entrainers considered. At 50.0 kPa and E/F = 1, NBP exhibit the highest relative volatility between the green entrainers. Under the same pressure, guaiacol at EF = 1 and DMI at EF = 3 exhibit relative volatilities that are only 13–17% lower than those of NBP, while still achieving complete removal of the azeotrope (guaiacol) or a strong shift with eventual removal (DMI at EF = 3). In contrast, the benchmark solvent NMP at 100.0 kPa and EF = 1 provides slightly higher relative volatilities but at the expense of significantly higher toxicity and regulatory restrictions. Thus, guaiacol and DMI bridge the gap between the high separation efficiency of NBP/NMP and the stricter safety requirements of modern solvent selection.

As summarized in Figure 6, guaiacol at EF = 1 and 50.0 kPa and DMI at EF = 3 and 50.0 kPa provide relative volatilities only slightly lower than those of NBP and a selected imidazolium ionic liquid, but markedly higher than those reported for glycerol-based deep eutectic solvents in the n-hexane + ethanol system. In addition, recent studies on DES entrainers for other azeotropic mixtures confirm that DESs often suffer from limited entrainer loading due to viscosity and miscibility constraints, which restrict the achievable relative volatility. This highlights that performance parity with NBP and ionic liquids, combined with superior practicality and greenness, is more relevant than achieving the highest absolute relative volatility.

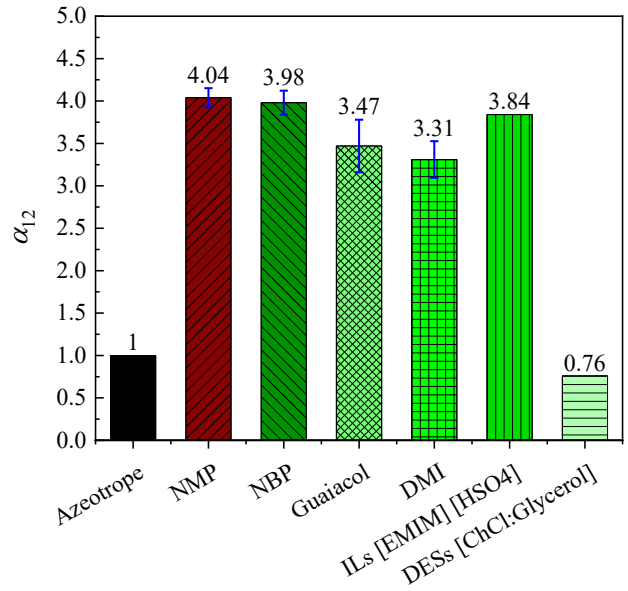


**Figure 6.** Comparison for the relative volatility of n-hexane (1) to ethanol (2) ($\alpha_{12}$) in the presence of conventional entrainer NMP (E/F = 1; 100.0 kPa) and various biobased and greener entrainers: NBP (E/F = 1; 50.0 kPa)[17]; guaiacol (E/F of 1; 50.0 kPa); DMI (E/F of 3; 50.0 kPa); 1-ethyl-3-methyl-imidazolium hydrogen sulfate [EMIM] [$HSO_4$] IL (E/F of 0.4; 101.3 kPa)[24]; ChCl:Glycerol (1:3) DES (E/F of 0.3, 328.15 K)[25]. All measurements were performed at the azeotropic composition.

Despite guaiacol and DMI exhibit slightly lower relative volatility compared to other entrainers, which could increase column stages and higher reflux ratios in extractive distillation, they still show practical potential as green entrainers in this process as both of them effectively increase the relative volatility and eliminate the azeotrope. While relative volatility is an important factor affecting separation efficiency, the values observed for guaiacol and DMI remain competitive for industrial applications, allowing for effective separation under optimized operating conditions. Importantly, both guaiacol and DMI are biobased entrainers that offer significant environmental advantages, such as non-toxic, biodegradable, and a renewable bio-based origin. In addition, guaiacol and DMI exhibit higher boiling points than NMP and do not experience the miscibility issues as ILs and DESs, when applied at high concentrations. These benefits make them attractive as entrainers in the context of sustainable process development. These characteristics compensate for their slightly reduced relative volatility compared to the benchmark entrainer, especially when considering the growing emphasis on greener solvents in regulatory and industrial frameworks. The results highlight the promising performance of guaiacol and DMI as biobased entrainers, positioning them as viable replacements for conventional entrainer NMP toward achieving greener and more sustainable extractive distillation processes.

While the favorable thermodynamic and separation performance of guaiacol and DMI establish them as promising green entrainers, it is important to note that these evaluations are primarily based on VLE data. Although these data provide an essential thermodynamic foundation for the effective design of extractive distillation processes. Their translation to real column design involves certain constraints. Specifically, these data do not incorporate the mass transfer resistance present at the vapor-liquid interfaces under actual operating conditions in a real column. Additionally, they assume a uniform entrainer concentration, which deviates from the reality where entrainer concentrations vary between different stages of the column. Therefore, to confirm their suitability for real-world extractive distillation applications, further validation of these entrainers is required. This should include rigorous process simulation or experimental validation of extractive distillation processes at the pilot-plant scale. In addition, a comprehensive assessment of total annual costs and sustainability should be conducted to ensure both economic and environmental feasibility.

**Thermodynamic consistency test**

The thermodynamic consistency test was performed to confirm the reliability of the VLE data. In this work, the Van Ness method, expressed in Eqs. 3 and 4, was employed.[12]

$$\Delta P = \frac{1}{n_p} \times \sum_{i=1}^{n_p} \Delta P_i = \frac{1}{n_p} \times \sum_{i=1}^{n_p} 100 \left| \frac{P_i^{cal} - P_i^{\exp}}{P_i^{\exp}} \right| \quad 3)$$

$$\Delta y = \frac{1}{n_p} \times \sum_{i=1}^{n_p} \Delta y_i = \frac{1}{n_p} \times \sum_{i=1}^{n_p} 100 \left| y_i^{cal} - y_i^{\exp} \right| \quad 4)$$

In these equations, $n_p$ represents the number of data points, $y$ is the vapor phase mole fraction, and $P$ is the pressure. The term *cal* refers to the values calculated using the NRTL model, while *exp* refers to the values obtained from the experimental work. Under the criteria from the Van Ness method, the VLE data are regarded as thermodynamically consistent when the values for both $\Delta P$ and $\Delta y$ are below 1. Table 5 illustrates that the values for $\Delta P$ and $\Delta y$ for each pseudo-ternary mixture comply with this requirement. Additional details regarding the $\Delta P$ and $\Delta y$ values can be found in Tables E2-E3. Furthermore, the Van Ness test also requires that the residual distribution of the $\ln(\gamma_1 / \gamma_2)$ exhibits a random pattern. Figures E7-E8 demonstrate that the residual distribution behaves randomly, providing further confirmation of the thermodynamic consistency of the investigated VLE data. In the original work of Van Ness, Legendre polynomials were suggested as a convenient flexible representation for the VLE data. In the present work, the NRTL

model was instead used as the correlation function in the Van Ness test because NRTL is specifically developed for non-ideal and azeotropic mixtures and is widely applied for systems containing entrainers. Using NRTL at this stage also ensures consistency with the subsequent regression of the same VLE data. The small values of $\Delta y$ and $\Delta P$ (Table 5) and the random distribution of residuals (Figures E7-E8) confirm that the NRTL model is sufficiently flexible for the consistency test.

**Table 5.** Results of the thermodynamic consistency test

| Mixtures | $\Delta y^a$ | $\Delta P^b$ | Results |
|---|---|---|---|
| n-hexane (1) + ethanol (2) + guaiacol (3) | 0.5 | 0.8 | Passed |
| n-hexane (1) + ethanol (2) + DMI (3) | 0.5 | 0.9 | Passed |

$$^a \Delta y = \frac{1}{n_p} \times \sum_{i=1}^{n_p} \Delta y_i = \frac{1}{n_p} \times \sum_{i=1}^{n_p} 100 \left| y_i^{cal} - y_i^{\exp} \right| < 1$$

$$^b \Delta P = \frac{1}{n_p} \times \sum_{i=1}^{n_p} \Delta P_i = \frac{1}{n_p} \times \sum_{i=1}^{n_p} 100 \left| \frac{P_i^{cal} - P_i^{\exp}}{P_i^{\exp}} \right| < 1$$

**Regression of the VLE data**

To determine the optimum BIPs, the VLE data were regressed using the NRTL model. Among the available excess-Gibbs-energy models, NRTL was selected because it is particularly suitable for strongly non-ideal mixtures with specific interactions, including systems with entrainers where local-composition effects are significant. Its application for the pseudo-ternary mixture with the presence of entrainer frequently results in strong correlations with the experimental data.[26–32] Previous work on pseudo-ternary mixtures of n-hexane and ethanol with NBP and NMP has demonstrated that NRTL correlates such systems accurately.[17] Moreover, we have previously reported that the NRTL model outperforms the UNIQUAC model based on their correlation results in the pseudo-ternary mixture that contains entrainers, particularly for methylcyclohexane – toluene with the presence of entrainer NMP and gamma-valerolactone.[16] For completeness, limited trial regressions with the Wilson and UNIQUAC models were performed for selected data sets. These models led to larger RMSDs in temperature and compositions than NRTL, confirming that NRTL provides the best compromise between accuracy and parameter parsimony for the present pseudo-ternary mixtures. The equation for the model is outlined in Eq. 5.

$$\ln \gamma_i = \frac{\sum_{j=1}^{n_c} x_j \tau_{ji} G_{ji}}{\sum_{k=1}^{n_c} x_k G_{ki}} + \sum_{j=1}^{n_c} \frac{x_j G_{ij}}{\sum_{k=1}^{N} x_k G_{kj}} \left( \tau_{ij} - \frac{\sum_{m=1}^{n_c} x_m \tau_{mj} G_{mj}}{\sum_{k=1}^{n_c} x_k G_{kj}} \right) \quad 5)$$

In the NRTL model equation, $\gamma_i$ indicates the activity coefficient of the component *i*, and $n_c$ defines the total number of components. In addition, the parameters associated with this model are described in Eq. 6. The non-randomness constant for the binary pair interaction (*i-j*) in this model is denoted by $C_{ij}$ .

$$G_{ij} = \exp(-C_{ij}\tau_{ij}); \ \tau_{ij} = A_{ij} + B_{ij}/T; G_{ii} = 1; \ \tau_{ii} = 0 \quad 6)$$

For the n-hexane and ethanol pair, the BIPs were obtained from our previous study[17], which accurately represents the temperature range relevant to the VLE data in this work. For the n-hexane and ethanol binary mixture, the non-randomness constant was set at 0.47. On the other hand, this value was allowed to vary in the regression of the pseudo-ternary n-hexane-ethanol-guaiacol mixture, offering enhanced flexibility and leading to improved accuracy of the regression. However, for the mixture of n-hexane-ethanol-dimethyl isosorbide, the non-randomness constant was fixed at 0.30, as this provided better regression results. The Britt and Luecke method was used as a maximum likelihood-based algorithm to minimize the objective function (*OF*) in the regression, allowing determination of optimum BIPs.[33] The *OF* equation is presented in Eq. 7. In this equation, $n_p$ indicates the total number of data points, while $\sigma$ refers to the standard deviations. Table 6 provides the optimum BIPs for the component pairs determined from the regression.

$$OF = \sum_{k=1}^{n_p} \left\{ \left| \frac{P_k^{cal} - P_k^{\exp}}{\sigma_P} \right|^2 + \left| \frac{T_k^{cal} - T_k^{\exp}}{\sigma_T} \right|^2 + \left| \frac{x_{1,k}^{cal} - x_{1,k}^{\exp}}{\sigma_x} \right|^2 + \left| \frac{y_{1,k}^{cal} - y_{1,k}^{\exp}}{\sigma_y} \right|^2 \right\} \quad 7)$$

**Table 6.** Binary interaction parameters from the NRTL model for pseudo-ternary mixtures of n-hexane (1) + ethanol (2) with the biobased entrainers guaiacol (3) and dimethyl isosorbide (3)[a,b]

| *i* component | *j* component | $A_{ij}$ | $A_{ji}$ | $B_{ij}$/K | $B_{ji}$/K | $C_{ij}$ |
|---|---|---|---|---|---|---|
| [c]n-hexane (1) | ethanol (2) | -10.342 | -3.854 | 4120.934 | 1829.392 | 0.47 |
| n-hexane (1) | guaiacol (3) | 24.967 | -14.786 | -7227.525 | 4793.393 | 0.26 |
| ethanol (2) | guaiacol (3) | 11.866 | -4.250 | -1934.061 | 1244.481 | 0.55 |
| n-hexane (1) | dimethyl isosorbide (3) | 11.988 | -12.067 | -2984.570 | 3932.560 | 0.30 |
| ethanol (2) | dimethyl isosorbide (3) | 11.537 | -11.680 | -3369.973 | 3639.305 | 0.30 |

[a] $A_{ij}$, $A_{ji}$, $B_{ij}$, and $B_{ji}$ are asymmetric parameters; $C_{ij}$ is the non-randomness constant.

[b] NRTL: $\tau_{ij} = A_{ij} + B_{ij} / T$

[c] The BIPs for the hexane (1) – ethanol (2) were obtained from our previous work.[17]

The NRTL regression results demonstrated a strong agreement with the experimental VLE data for pseudo-ternary mixtures of n-hexane and ethanol containing guaiacol and DMI, respectively. The regression was conducted in a single regression for the VLE data across all E/Fs and pressures, resulting in BIPs that effectively capture the system's behavior across various compositions of the entrainer and pressures. The regression results for the n-hexane and ethanol mixture using guaiacol as an entrainer are presented in Figure 1, while Figure 2 illustrates the results with DMI as an entrainer. Moreover, Table 7 shows the root-mean-square deviations, confirming a strong correlation between the regressed values and the experimental data. Figures E9-E14 provide detailed residual plots for the mole fractions of both the liquid and vapor phases, as well as the temperature. These results affirm the reliability of the NRTL model and its associated BIPs for designing effective extractive distillation processes through a process simulation to separate the n-hexane and ethanol mixture using the biobased entrainers guaiacol and DMI.

**Table 7.** Root-Mean-Square Deviations (RMSD)[a]

| | RMSD[b] | | | |
|---|---|---|---|---|
| | *T*/K | *P*/kPa | $x_1$' | $y_1$ |
| n-hexane (1) + ethanol (2) + guaiacol (3) | 0.38 | 0.6 | 0.006 | 0.007 |
| n-hexane (1) + ethanol (2) + dimethyl isosorbide (3) | 0.52 | 0.8 | 0.007 | 0.007 |

[a] *T* is a temperature, *P* is a pressure; $x_1$' is the mole fraction of liquid phase for n-hexane (entrainer-free basis), $y_1$: mole fraction of vapor phase for n-hexane.

[b] RMSD: $\Delta M = \sqrt{\frac{1}{n}\sum_{i=1}^{n}\left(M_{\exp} - M_{cal}\right)^2}$, where *n* represent the number of data points; *M* describes *T*, *P*, $x_1$', and $y_1$, respectively.

## References


(1) European Chemical Agency. *1,4:3,6-dianhydro-2,5-di-O-methyl-D-glucitol*. https://chem.echa.europa.eu/100.023.782/overview?searchText=1,4:3,6-dianhydro-2,5-di-O-methyl-D-gluc (accessed 2025-07-03).

(2) Severini, A.; Ferrari, C.; Marchetti, A.; Vizza, F.; Bonechi, M.; Innocenti, M.; Lagostina, V.; Salvadori, E.; Chiesa, M.; Roncaglia, F.; Fontanesi, C. Electrochemical Oxidation of Guaiacol as a Sacrificial Anodic Process Producing Fine Chemical Derivative, for Hydrogen Production via Electrolysis. *Int. J. Hydrogen Energy* **2025**, *124*, 345–354. https://doi.org/https://doi.org/10.1016/j.ijhydene.2025.03.439.

(3) van der Maas, K.; Weinland, D. H.; van Putten, R.-J.; Wang, B.; Gruter, G.-J. M. Catalyst Free PET and PEF Polyesters Using a New Traceless Oxalate Chain Extender. *Green Chem.* **2024**, *26* (22), 11182–11195. https://doi.org/10.1039/D4GC02791D.

(4) European Chemical Agency. *Guaiacol*. https://chem.echa.europa.eu/100.001.786/overview?searchText=guaiacol (accessed 2025-07-03).

(5) Bozell, J. J.; Petersen, G. R. Technology Development for the Production of Biobased Products from Biorefinery Carbohydrates—the US Department of Energy's "Top 10" Revisited. *Green Chem.* **2010**, *12* (4), 539–554. https://doi.org/10.1039/B922014C.

(6) Gao, F.; Bai, R.; Ferlin, F.; Vaccaro, L.; Li, M.; Gu, Y. Replacement Strategies for Non-Green Dipolar Aprotic Solvents. *Green Chem.* **2020**, *22* (19), 6240–6257. https://doi.org/10.1039/D0GC02149K.

(7) *Public Report, 2-Pyrrolidinone, 1-Butyl-*; 2020. https://www.industrialchemicals.gov.au/sites/default/files/STD1698 public report %5B780 KB%5D.pdf.

(8) Weast, R. C. .; Grasselli, J. G. *Handbook of Data on Organic Compounds*, 2nd Editon.; CRC Press, Inc.: Boca Raton, FL, 1989.

(9) Kim, H.; Vinueza, N. R.; Kelley, S. S.; Park, S. Correlation between Solubility Parameters and Recovery of Phenolic Compounds from Fast Pyrolysis Bio-Oil by Diesel Extraction. *Carbon Resour. Convers.* **2018**, *1* (3), 238–244. https://doi.org/https://doi.org/10.1016/j.crcon.2018.08.004.

(10) Benazzouz, A.; Moity, L.; Pierlot, C.; Sergent, M.; Molinier, V.; Aubry, J.-M. Selection of a Greener Set of Solvents Evenly Spread in the Hansen Space by Space-Filling Design. *Ind. Eng. Chem. Res.* **2013**, *52* (47), 16585–16597. https://doi.org/10.1021/ie402410w.

(11) Buken, O.; Mancini, K.; Sarkar, A. A Sustainable Approach to Cathode Delamination Using a Green Solvent. *RSC Adv.* **2021**, *11* (44), 27356–27368. https://doi.org/10.1039/D1RA04922D.

(12) Van Ness, H. C. Thermodynamics in the Treatment of Vapor/Liquid Equilibrium (VLE) Data. **1995**, *67* (6), 859–872. https://doi.org/doi:10.1351/pac199567060859.

(13) Renon, H.; Prausnitz, J. Local Compositions in Thermodynamic Excess Functions for Liquid Mixtures. *AIChE J.* **1968**, *14* (1), 135–144. https://doi.org/10.1002/aic.690140124.

(14) Taylor, Barry N; Kuyatt, C. E. NIST Technical Note 1297 Guidelines for Evaluating and Expressing the Uncertainty of NIST Measurement Results. *Technology* **1994**.

(15) *Evaluation of Measurement Data — Guide to the Expression of Uncertainty in*

*Measurement*; Working Group 1 of the Joint Committee for Guides in Metrology (JCGM/WG 1); 2008. https://www.bipm.org/documents/20126/2071204/JCGM_100_2008_E.pdf.
(16) Hartanto, D.; Schuur, B.; Schuttevaer, T.; Kiss, A. A.; de Haan, A. B. Isobaric Vapor–Liquid Equilibrium of Methylcyclohexane + Toluene with Gamma-Valerolactone as a Biobased Entrainer and 1-Methylpyrrolidin-2-One as a Conventional Entrainer. *J. Chem. Eng. Data* **2025**, *70* (3), 1339−1351. https://doi.org/10.1021/acs.jced.4c00509.
(17) Hartanto, D.; Schuur, B.; A. Kiss, A.; de Haan, A. B. Isobaric Vapor-Liquid Equilibrium of the Azeotropic Mixture n-Hexane + Ethanol with 1-Butylpyrrolidin-2-One as a Greener Entrainer and 1-Methylpyrrolidin-2-One as a Benchmark Entrainer. *J. Chem. Eng. Data* **2025**, *70* (10), 4091−4104.
(18) Zhu, J.; Sun, Y.; Chen, Y.; Wu, N.; Shi, R.; Ren, Z.; Li, Q.; Zhao, H. Isobaric Vapor–Liquid Equilibrium Experiments of Methyl Propionate + Ethanol with Different Ionic Liquids at 101.3 KPa. *J. Chem. Eng. Data* **2025**, *70* (1), 427–438. https://doi.org/10.1021/acs.jced.4c00517.
(19) Li, W.; Chen, X.; Yin, H.; Li, L.; Zhang, T. Isobaric Vapor–Liquid Equilibrium for 2-Butanone + Ethanol System Containing Different Ionic Liquids at 101.3 KPa. *J. Chem. Eng. Data* **2018**, *63* (2), 380–388. https://doi.org/10.1021/acs.jced.7b00783.
(20) Li, W.; Li, L.; Zhang, L.; Li, H.; Zhang, T. Isobaric Vapor-Liquid Equilibrium for 2-Butanone + Ethanol + Phosphate-Based Ionic Liquids at 101.3 KPa. *Fluid Phase Equilib.* **2018**, *456*, 57–64. https://doi.org/https://doi.org/10.1016/j.fluid.2017.10.001.
(21) Zhang, Z.; Lv, M.; Huang, D.; Jia, P.; Sun, D.; Li, W. Isobaric Vapor–Liquid Equilibrium for the Extractive Distillation of Acetonitrile + Water Mixtures Using Dimethyl Sulfoxide at 101.3 KPa. *J. Chem. Eng. Data* **2013**, *58* (12), 3364–3369. https://doi.org/10.1021/je400531a.
(22) Zhang, L.; Shen, D.; Zhang, Z.; Wu, X. Experimental Measurement and Modeling of Vapor–Liquid Equilibrium for the Ternary System Water + Acetonitrile + Ethylene Glycol. *J. Chem. Eng. Data* **2017**, *62* (5), 1725–1731. https://doi.org/10.1021/acs.jced.7b00178.
(23) Hartanto, D.; Schuur, B.; Kiss, A. A.; de Haan, A. B. Effective Selection of Green Organics and Natural Deep Eutectic Solvents as Advanced Entrainers by COSMO-RS and Group Contributions Methods for Enhanced Design of Extractive Distillation. In *Computer Aided Chemical Engineering*; Manenti, F., Reklaitis, G. V. B. T.-C. A. C. E., Eds.; Elsevier, 2024; Vol. 53, pp 1387–1392. https://doi.org/https://doi.org/10.1016/B978-0-443-28824-1.50232-5.
(24) Wang, Y.; Hu, R.; Liu, W.; Zhu, Z.; Wang, Y.; Yang, J.; Qi, J.; Cui, P. Separation of Ethanol/n-Hexane Azeotrope by Imidazolium Ionic Liquids: Experimental Study and Mechanism Analysis. *Sep. Purif. Technol.* **2025**, *357*, 130063. https://doi.org/https://doi.org/10.1016/j.seppur.2024.130063.
(25) Sharma, A.; Lee, B.-S.; Shin, H. Y. Assessing Suitability of Glycerol-Derived Green Solvent for the Separation of n-Hexane + Ethanol Azeotropic Mixture, Accompanied by VLE Studies Using Machine Learning. *J. Mol. Liq.* **2025**, *423*, 127003. https://doi.org/https://doi.org/10.1016/j.molliq.2025.127003.
(26) Li, F.; Li, M.; Guo, J.; Hu, X.; Zhu, J.; Li, Q.; Zhao, H. Isobaric Vapor–Liquid Equilibrium Experiment of N-Propanol and N-Propyl Acetate at 101.3 KPa. *J. Chem. Eng. Data* **2023**, *68* (2), 358–365. https://doi.org/10.1021/acs.jced.2c00609.

(27) Cao, M.; Tian, H.; Li, M. Vapor–Liquid Equilibrium Data Determination and Model Correlation for 1-Octene + 1,4-Dioxane, 2-Octanol + 1,4-Dioxane, 1-Octene + Isophorone, and 2-Octanol + Isophorone Systems at 101.3 KPa. *J. Chem. Eng. Data* **2023**, *68* (9), 2275–2282. https://doi.org/10.1021/acs.jced.3c00136.
(28) Lei, Z.; Arlt, W.; Wasserscheid, P. Selection of Entrainers in the 1-Hexene/n-Hexane System with a Limited Solubility. *Fluid Phase Equilib.* **2007**, *260* (1), 29–35. https://doi.org/https://doi.org/10.1016/j.fluid.2006.06.009.
(29) Zhang, Z.; Zhang, Z.; Dong, B.; Chen, J.; Xin, H.; Zhang, Q. Vapor-Liquid Equilibrium Experiment and Model Prediction for Separating Ethyl Propionate and Ethanol Using Ionic Liquids with Acetate Anion. *J. Mol. Liq.* **2020**, *318*, 113688. https://doi.org/https://doi.org/10.1016/j.molliq.2020.113688.
(30) Yang, C.; Zeng, H.; Yin, X.; Ma, S.; Sun, F.; Li, Y.; Li, J. Measurement of (Vapor+liquid) Equilibrium for the Systems {methanol+dimethyl Carbonate} and {methanol+dimethyl Carbonate+tetramethylammonium Bicarbonate} at P=(34.43, 67.74)KPa. *J. Chem. Thermodyn.* **2012**, *53*, 158–166. https://doi.org/https://doi.org/10.1016/j.jct.2012.05.002.
(31) Zhang, Y.; Wang, Z.; Xu, X.; Gao, J.; Xu, D.; Zhang, L.; Wang, Y. Entrainers Selection and Vapour-Liquid Equilibrium Measurements for Separating Azeotropic Mixtures (Ethanol + n-Hexane/Cyclohexane) by Extractive Distillation. *J. Chem. Thermodyn.* **2020**, *144*, 106070. https://doi.org/https://doi.org/10.1016/j.jct.2020.106070.
(32) He, S.; Fan, W.; Huang, H.; Gao, J.; Xu, D.; Ma, Y.; Zhang, L.; Wang, Y. Separation of the Azeotropic Mixture Methanol and Toluene Using Extractive Distillation: Entrainer Determination, Vapor–Liquid Equilibrium Measurement, and Modeling. *ACS Omega* **2021**, *6* (50), 34736–34743. https://doi.org/10.1021/acsomega.1c05164.
(33) Britt, H. I.; Luecke, R. H. The Estimation of Parameters in Nonlinear, Implicit Models. *Technometrics* **1973**, *15* (2), 233–247. https://doi.org/10.2307/1266984.

## 4.3. Conclusions of Sections 4.1 and 4.2

In this Chapter 4, the VLE data were measured for the binary n-hexane-ethanol mixture as well as the pseudo-mixtures of n-hexane-ethanol containing greener entrainers of NBP, guaiacol, and DMI and the benchmark entrainer of NMP. A Fischer Labodest VLE602 ebulliometer was employed. All measured data were found to be consistent as they passed the thermodynamic consistency test, indicating that the VLE data provided in this work are accurate and reliable.

The results show that the introduction of these green and benchmark entrainers enhances the relative volatility of n-hexane to ethanol and effectively eliminates the azeotropic point. For the mixture containing NBP, introducing NBP into the mixture at lower pressures leads to a slight increase in the relative volatility of n-hexane to ethanol. However, as the amount of the NBP is increased from an E/F of 1 to 2 and 3 at 100.0 kPa, the relative volatility increases further, although the relative volatility for E/F of 2 and 3 are similar. Furthermore, the relative volatility comparison of NBP and NMP reveals that NBP at E/F = 1 and 50.0 kPa and E/F = 2 and 3 at 100.0 kPa demonstrate a comparable performance to NMP at E/F = 1 and 100.0 kPa.

The addition of biobased entrainers guaiacol and DMI also enhances relative volatility and effectively eliminates the azeotrope. Introducing guaiacol to the n-hexane and ethanol mixture at an E/F of 1 and pressures of 50.0 and 100.0 kPa, as well as an E/F of 3 and a pressure of 50.0 kPa, effectively removes the azeotrope behavior. When DMI was added at an E/F of 1 and pressures of 50.0 and 100.0 kPa, the azeotropic point shifted significantly toward the n-hexane-rich region compared to the original azeotropic composition at $x_1 = 0.66$. However, the azeotrope is not completely eliminated. The azeotropic point is successfully removed when DMI was added at E/F of 3 and a pressure of 50 kPa. Therefore, the operating conditions must be adjusted to suit this region, ensuring a thermodynamically feasible separation. Consequently, the process simulations were limited to conditions that achieved complete azeotrope elimination. Compared to NBP and NMP, guaiacol and DMI show somewhat lower relative volatilities but still provide effective azeotrope removal under optimal conditions. Guaiacol performs similarly to NBP at reduced pressure and moderate entrainer loadings, whereas DMI requires a higher EF but benefits from good miscibility. These differences, together with the improved toxicological and sustainability profile of guaiacol and DMI, highlight the role of these solvents as competitive green alternatives to both NBP and NMP. In addition, at optimal operating conditions, guaiacol and DMI exhibit relative volatility performance comparable to the other greener entrainers, such as NBP and IL, and demonstrate better relative volatility than DES. These results emphasize the potential of NBP, guaiacol and DMI as greener alternative entrainers to NMP for greener extractive distillation processes in the separation of n-hexane and ethanol.

Furthermore, the NRTL model was employed to regress the VLE data, resulting in a good fit between the regressed values and the experimental data. As a result, optimum BIPs were successfully determined. The NRTL model and its parameters provide a reliable thermodynamic basis for the process design of an extractive distillation process utilizing greener entrainers, NBP, guaiacol and DMI, to separate n-hexane and ethanol. Process simulations for the extractive distillation of n-hexane and ethanol mixture, with the presence of NBP, guaiacol and DMI to examine their economic viability and environmental sustainability under real-world column conditions are provided in Chapter 5.

(*This page is intentionally left blank*)

# Chapter 5

## Eco-efficient extractive distillation processes using biobased and greener entrainers for the separation of azeotropic and close-boiling mixtures

*This chapter has been submitted to:*
*Separation and Purification Technology*

## Abstract

Extractive distillation (ED) is a well-established method for separating azeotropic and close-boiling mixtures. However, the use of conventional entrainers, such as 1-methyl-2-pyrrolidone (NMP), has raised safety and environmental concerns. The use of biobased and greener solvents as sustainable entrainers for the industrial interest separations of an azeotropic mixture (n-hexane-ethanol) and a close-boiling mixture (methylcyclohexane-toluene) using ED was investigated. Rigorous process simulations were performed using Aspen Plus V14 to evaluate the performance of ED.

A multi-stage entrainer selection framework was applied, integrating computational predictions, experimental validation, and process-level assessment, to identify effective greener entrainers. A comprehensive assessment for the economic and sustainability performances was conducted, including total annual cost (TAC), energy intensity, $CO_2$ emissions, and water consumption. Sensitivity analyses were further performed to evaluate the effect of recycled entrainer purity, payback period, and entrainer price on the TAC was evaluated.

The results indicate that all investigated greener entrainers achieve economic and sustainability performances that are comparable to or better than those of NMP, while offering substantially lower toxicity. For both mixtures, greener entrainer-based ED processes show similar or improved economic and sustainability performance compared to NMP-based processes. Moreover, these greener entrainers exhibited nontoxic characteristics, indicating that they are not only cost-effective but also offer promising sustainability performance for industrial implementation. Sensitivity analysis confirms that entrainer ranking remains robust under variations in entrainer purity constraint and payback periods, whereas entrainer price significantly affects economic competitiveness.

As supporting analyses, the reliability of commonly used screening metrics (selectivity and capacity at infinite dilution), and predictive thermodynamic models (COSMO-RS/COSMO-SAC) and UNIFAC) was examined. Selectivity showed better agreement with TAC trends than capacity, particularly for the non-associating methylcyclohexane-toluene mixture, whereas both metrics were less reliable for the associating n-hexane-ethanol mixture. Furthermore, Predictive models of UNIFAC and COSMO-based yielded TAC deviations below 31% and 32%, respectively, compared with NRTL-based simulations, indicating their suitability for early-stage entrainer screening for the system without predicted abnormal phase behavior. However, it is limited in applicability for strongly associating mixtures unless validated by experimental data.

## 5.1. Introduction and problem statement

Driven by sustainability goals, the chemical process industries are implementing extensive efforts to apply more sustainable processes. These efforts focus on improving energy efficiency, reducing greenhouse gas emissions, particularly $CO_2$, lowering water consumption, and maintaining cost competitiveness while producing high-purity chemicals. One of the vital processes is separation, which requires intensive energy and cost. This process leads to more than 50% of the total energy consumption and cost of the processes.[1,2] Distillation is the most widely used separation technology since it provides many advantages, including effectiveness for large-scale and complex separations, suitable for wide operational ranges of feed flow rates and compositions, operational efficiency and control, and the ability to produce high-purity chemicals with an array of industrial requirements.[3,4] However, this technology is not effective for challenging separations, such as azeotropic and close-boiling mixtures. To overcome these limitations, extractive distillation (ED) has emerged as a widely selected technology, which proves to be more effective and feasible than other methods for various industrial applications.[5,6]

The azeotropic mixture of n-hexane (HEX) and ethanol (ETH) and the close-boiling mixture of methylcyclohexane (MCH) and toluene (TOL) are of significant industrial interest and are required to be separated to obtain high-purity products that meet industrial standards. In extractive distillation, an entrainer is required to alter the relative volatility of the mixture since an entrainer interacts with one of the components to facilitate the separation of the targeted components. Currently, the conventional entrainer 1-methyl-2-pyrrolidone, also known as NMP, is widely used. However, its high toxicity, especially reproductive toxicity, has led to its restriction by REACH and EPA regulations.[7,8] Thus, it is important to identify greener and safer alternatives to NMP. According to the relative volatility measurements, miscibility tests, and vapor-liquid equilibrium (VLE) experiments discussed in Chapters 2-4, several biobased and greener entrainers have been selected to effectively enhance the relative volatility and remove the azeotropic and close-boiling behaviors. These include guaiacol, dimethyl isosorbide (DMI), and 1-butylpyrrolidin-2-one (NBP) for the separation of the azeotropic HEX-ETH mixture and gamma-valerolactone (GVL), DMI, and NBP for the separation of the close-boiling methylcyclohexane MCH-TOL mixture. NMP was used as a benchmark entrainer in both mixtures.

Currently, there is no study that systematically compares the process performance of biobased or greener organic entrainers in extractive distillation, especially for the HEX-ETH and MCH-TOL mixtures. Existing studies on ED can be classified into three categories, each leaving a critical gap.

First, some studies evaluated the ED process comparison using alternative entrainers, such as ionic liquids (ILs) and conventional solvents in several mixtures. However, they do not examine the biobased or greener organic solvents. For example, Li et al.,[9] Liu et al.[10] and Ayuso et al.[11] evaluated ILs and conventional solvents, while Ghuge et al.[12] and Simasatitkul et al.[13] assessed common organic entrainers. In addition, Minor et al.[14] and Yin et al.[15] studied the process performance comparison for the ED with different deep eutectic solvents in comparison with the conventional solvent ethylene glycol. While these works offer valuable contributions at the process level, they do not assess biobased or greener organic entrainers and benchmark them against NMP. This limitation motivates Objective 1, which is to compare ED process performances among selected greener entrainers and a benchmark entrainer by using economic and multi-criteria sustainability assessment.

Second, previous studies mostly rely on thermodynamic screening indicators such as selectivity, capacity, or performance index but do not critically assess their reliability in predicting process-level performance.[16–21] Momoh examined the correlation between selectivity and TAC across different mixtures, concluding that the selectivity cannot correlate well with TAC.[22] While Kossack et al. examine the reliability of selectivity and performance index on TAC. They found that the performance index exhibits better results compared to selectivity to represent TAC in process performance. However, the comparison with capacity is not evaluated.[23] A systematic accuracy comparison between selection and capacity for the correlation with TAC in various mixtures and entrainers remains lacking. Consequently, which effective metrics should be selected for early-stage entrainer screening is still unclear. This knowledge gap addressed in Objective 2, which evaluates selectivity and capacity as screening metrics by directly correlating them with the TAC results.

Third, the implementation of predictive thermodynamic models for entrainer screening has not been rigorously benchmarked against experiment-based models, such as NRTL, in a process design context. Marcos et al.[24] and Ferro et al.[25] utilized COSMO-based models in the process simulation for evaluating ED process performance. Taylor et al. compared the use of COSMO-RS with UNIQUAC and UNIFAC for the evaluation of ED column profiles.[26] However, the comparison for ED process performances obtained from prediction-based models, such as COSMO-based models and UNIFAC, with experiment-based model NRTL are not available. As a result, the applicability and limitations of predictive models for early-stage entrainer screening remain insufficiently validated. This gap underpins Objective 3, which quantitatively examines the accuracy of predictive models through comparison with the experiment-based model in ED process performances.

To address these gaps as well as go beyond finding greener alternative entrainers to NMP through process performance comparisons, specific frameworks were developed for the greener entrainer selection methodology that bridges molecular-level screening metrics with process-level performance evaluation while also linking prediction-based and experiment-based model process simulations. The proposed frameworks advance the existing entrainer selection guide by evaluating screening metrics through their correlation with the TAC. Moreover, the frameworks extend conventional ED process comparison studies by benchmarking process performance calculated from prediction-based models against an experiment-based model. Specifically, the methodology systematically links predictive selection metrics (selectivity and capacity at infinite dilution calculated using COSMO-RS) to TAC values obtained from optimized ED simulations employing experiment-based NRTL model. In addition, the approach further establishes the applicability of predictive thermodynamic models for early-stage entrainer screening and process design by comparing TAC of ED calculated using COSMO-based model (COSMO-RS/COSMO-SAC) and UNIFAC model against the experiment-based NRTL model.

ED represents the separation for the azeotropic (HEX-ETH) and the close-boiling (MCH-TOL) mixtures using biobased and greener entrainers, with performance compared to the conventional entrainer NMP was evaluated. Process economics are represented by TAC while sustainability expressed with toxicity, energy intensity, $CO_2$ emissions, and water consumption. The economic evaluation aims to define the reliability of the ED process, while the objective of sustainability evaluation is to identify the viability and potential human and ecological hazards associated with selected entrainers as well as to support the selection of greener alternatives with lower risk profiles. The effect of recycled entrainer purity, payback period, and entrainer make-up cost on TAC was investigated. Furthermore, the influence of the solvent price ratio of green solvent to NMP on the TAC ratio of green solvent to NMP was evaluated. The specific workflow was implemented to evaluate the effectiveness of predicted selectivity and capacity at infinite dilution as early-stage entrainer selection parameters by correlating their predictions with optimized TAC results. Finally, the accuracy of predictive models was assessed by comparing their ED process performances with those of the experiment-based NRTL model to assess their effectiveness for early-stage entrainer screening. While predictive models are evaluated, this study also tests the potential limitations for the system involving strongly associating systems, as illustrated by non-physical azeotrope predicted for the ethanol-DMI system.

## 5.2. Process simulation

### 5.2.1. Process description

The schematic diagrams of the ED process for the azeotropic mixture of HEX-ETH and the close-boiling mixture of MCH-TOL are illustrated in Figures 1 and 2, respectively. The ED process consists of two distillation columns arranged in series: an extractive distillation column (EDC) and an entrainer regeneration column (ERC). The ED conventional configuration was selected to enable consistent comparison for entrainers under a single industrially representative baseline flowsheet. Introducing additional degrees of freedom, such as partial condensation or multiple feed/entrainer introduction strategies, can change internal vapor-liquid traffic and controllability, but it would also confound the interpretation of performance differences by blending entrainer effects with configuration effects. However, process intensification could further improve both economic and sustainability performances. The feed mixture and the entrainer stream are introduced at specific stages of the first column (EDC). The main separation work occurs in the extractive section, below the entrainer feed stage and above the feed stage. In this section, the entrainer as a polar compound possesses more interaction with a more polar compound, and therefore it can induce significant non-ideality of the mixture, leading to increased relative volatility within the extractive section. In the EDC, the light component is separated as the distillate, while the heavier component remains in the bottom column together with the entrainer. This mixture is subsequently fed to the second column (ERC). Within the ERC, the heavier component originating from the EDC is distilled to the top column, while the entrainer is separated and recovered in the bottom stream. Prior to recycling and reintroducing into the EDC, the recovered entrainer is used to preheat the fresh feed through heat integration using a heat exchanger (HE). The implementation of heat integration reduces the reboiler duty in the EDC. For instance, in the case of MCH-TOL using the entrainer NMP, applying heat integration leads to 5.2% reduction in reboiler duty. Specifically, the reboiler duty with heat integration is 1264 kW, compared to 1330 kW when heat integration is not used. An additional cooler is employed to reduce the temperature of the entrainer stream exiting the HE, after which the recycled entrainer is fed into the EDC. A small amount of make-up entrainer is added to compensate for entrainer loss during the process.

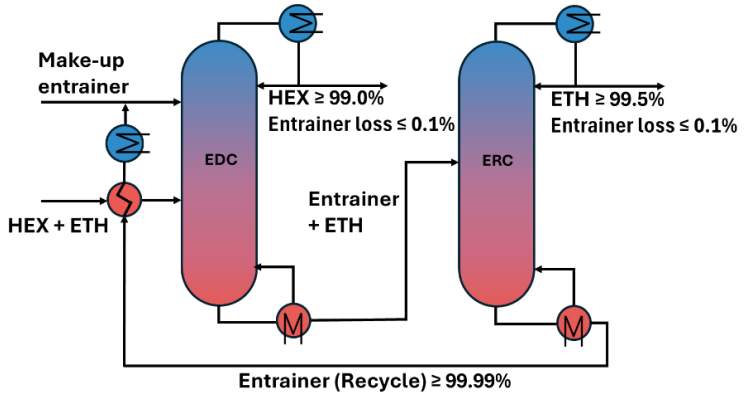


**Figure 1.** Schematic diagram of extractive distillation and the purity constrains for the n-hexane (HEX) – ethanol (ETH) mixture.

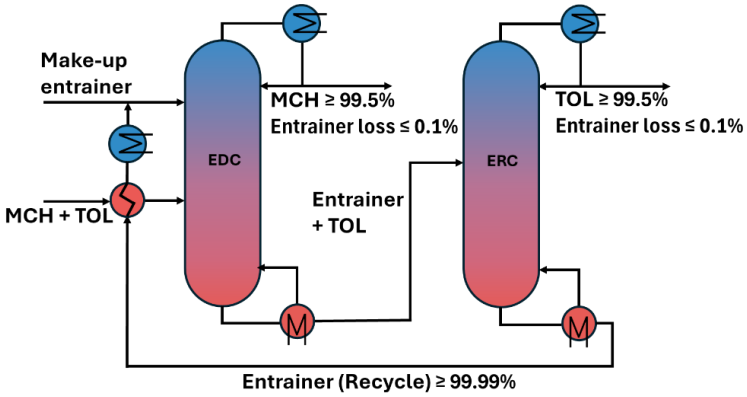


**Figure 2.** Schematic diagram of extractive distillation and the purity constrains for the methylcyclohexane (MCH) – toluene (TOL) mixture.

### 5.2.2. Simulation approaches

Aspen Plus V14 was used to simulate the ED process. The RadFrac block was employed to accurately model both the EDC and ERC. An experiment-based NRTL model was used to evaluate the ED. Binary interaction parameters (BIPs) obtained from the experimental VLE studies described in Chapters 3 and 4 were employed. The detailed BIPs are listed in Tables F1 and F2. For the n-hexane-ethanol-NMP mixture and the methylcyclohexane-toluene mixture in the presence of GVL and NBP, the BIPs were re-regressed, as the updated parameters provided more accurate results, indicated by the successful convergence of the process simulations, in contrast to the original BIPs reported in Chapters 3 and 4. The use of the original BIPs led to simulation non-convergence, preventing the attainment of optimal ED results. To resolve this issue, the BIPs were re-regressed by adjusting the weighting of the experimental datasets, assigning higher weights to datasets with a larger number of data points. This approach improved the

regression accuracy by reducing the root mean square deviation (RMSD), as shown in Table 1, enabling converged process simulations within the investigated operating conditions, with reliable ED results.

**Table 1.** Comparison of root mean square deviation (RMSD) for original and updated BIPs

| Mixture | *T*/K | | *P*/kPa | | $x_1$ | | $y_1$ | |
|---|---|---|---|---|---|---|---|---|
| | Old | New | Old | New | Old | New | Old | New |
| HEX-ETH-NMP | 0.12 | 0.10 | 0.9 | 0.5 | 0.003 | 0.002 | 0.009 | 0.005 |
| MCH-TOL-GVL | 0.36 | 0.20 | 0.9 | 0.4 | 0.002 | 0.002 | 0.006 | 0.003 |
| MCH-TOL-NBP | 0.15 | 0.10 | 0.4 | 0.4 | 0.001 | 0.001 | 0.002 | 0.001 |

To verify the reliability of the BIPs, the predicted VLE diagrams were compared with experimental data. The results indicate that all BIPs accurately predict the VLE behavior for both mixtures, as shown in Figures F1 and F2. The predicted VLE outcomes exhibit trends that align with the experimental data for all entrainers in both mixtures. This consistency is demonstrated by the disappearance of the azeotropic point in the HEX-ETH mixture and the elimination of close-boiling behavior in the MCH-TOL mixture, as seen in both prediction and experiment results. Additionally, similar patterns were observed for relative volatility in both mixtures, highlighting the alignment of the predicted results with the experimental data.

The fresh feed of HEX-ETH and MCH-TOL, with a flow rate of 100 kmol/h, was introduced into the middle to lower sections of the EDC to ensure effective contact with the entrainer. A feed flow rate of 100 kmol/h represents a moderately scaled continuous process basis commonly adopted in ED process design studies.[15,27–30] This basis provides numerical stability in rigorous simulations. Furthermore, this study focuses on normalized performance metrics and comparative trends, which are expected to be independent of throughput under steady-state operation. This ensures that comparisons of economic and sustainability performance among entrainers are not biased by scale effects. The feed composition for HEX and ETH was set at 0.6 and 0.4 mole fractions, respectively, to represent the composition just before the azeotropic point (0.660).[31] For the MCH and TOL mixture, the compositions were 0.7 and 0.3 mole fractions, respectively. This composition falls within the composition range for which ED effectively separates MCH-TOL.[32] However, because MCH-TOL is a close-boiling mixture without an azeotropic composition that uniquely constraints the feed selection, this composition was adopted as a representative assumed feed for comparative evaluation purposes. The entrainer was introduced between stages of 3 to 8 to ensure that it remained in the liquid phase across the column, providing effective enrichment at all stages while minimizing entrainer loss. The pressures

of both EDC and ERC were allowed to vary to balance the increase in relative volatility and energy requirements while maintaining product purity, regaining entrainer purity, and minimizing entrainer loss. The entrainer increases the relative volatility of the mixtures. Therefore, the azeotropic and close-boiling mixtures can be removed, and high-purity of HEX, ETH, MCH and TOL can be achieved.

## 5.3. Process optimization

The optimization goal is to define the parameter values that minimize a signed objective function while maintaining the constraints.[33] The optimization process was conducted by first evaluating integer variables using sensitivity analysis. Subsequently, non-integer variables were optimized using the bound optimization quadratic approximation (BOBYQA) method in Aspen Plus.[34,35] BOBYQA was selected due to its ability to effectively optimize various unit operations, such as distillation.[36,37] Sensitivity analysis was performed for integer variables associated with both columns. For the EDC, the number of stages, feed stages, and entrainer feed stages were evaluated. For the ERC, the number of stages and feed stages were involved. Convergence was achieved when the relative difference in the reboiler duty, as the objective function, fell below $10^{-4}$ between consecutive iterations. This criterion was complemented by the stabilization of decision variables within a tolerance of $10^{-4}$. Additionally, a maximum evaluation limit of 1000 was implemented to ensure numerical robustness. The initial operating pressure of both EDC and ERC was set to 100 kPa for both mixtures. Initial estimates values of the reflux ratio, number of theoretical stages, and the feed stage location were determined using Fenske-Underwood-Gilliland-Kirkbride (FUGK) method.[38–41]

For the MCH-TOL mixture, the initial value of reflux ratio, number of theoretical stages, and the feed stage were 1.7, 33, and 19 respectively. Correspondingly, for the HEX-ETH mixture, the initial reflux ratio, number of theoretical stages, and feed stage were 1.1, 36, and 19, respectively. For both mixtures, the initial entrainer feed location was defined at stage of 3. The minimization of energy requirements was set as the objective function, represented by the reboiler duty (Qreb) for both the EDC and ERC. Reboiler duty was chosen as it represents the major energy requirements of the ED process, and it directly impacts the TAC. Therefore, lowering Qreb leads to a decrease in TAC. Moreover, the use of Qreb as an objective function has been widely implemented in distillation process simulation.[30,37,42–44] The constraints used are product purity, entrainer loss in the top stream of both the EDC and ERC, and entrainer purity in the bottom stream of the ERC. For the HEX-ETH mixture, the purity of HEX and ETH was set to ≥ 99.0 (%wt) and ≥ 99.5 (%wt), respectively. For the MCH-TOL mixture, the purity of both MCH and TOL was set to ≥ 99.5 (%wt). These purity

levels were selected to align with industrial specifications.[45–49] Entrainer loss in the top stream of the EDC and ERC for both mixtures was limited to ≤0.1 (%wt). This value was selected to prevent the entrainer loss as minimum as possible. The entrainer purity in the ERC bottom stream was set to ≥ 99.99 (%wt). This constraint ensures that the recycled entrainer maintains similar performance to the fresh entrainer and prevent accumulation of light components in the entrainer loop. This accumulation could potentially gradually dilute the effective entrainer strength in extractive distillation column. In addition, this entrainer purity is considered to be in the plateau region, where an entrainer purity above 99.9% achieves the desired product purity. Beyond this point, increasing the purity of the entrainer results in negligible improvements in product purity. In this region, extractive column performance become relatively insensitive to an increase of purity of the entrainer. Figure F3 illustrates the sensitivity of recycled entrainer purity on the product purity. These constraints are also shown in Figures 1 and 2. For the optimization, the variables and their corresponding lower and upper bounds, as listed in Table 2, were adjusted to meet the desired constraints. The E/F bound was constrained between 50 and 300 kmol/hr to capture the region where relative volatility enhancement is significant while avoiding thermodynamically and hydraulically unfavorable regimes. The lower bound (50 kmol/hr) prevents operation under insufficient entrainer concentration in the extractive section. This limits activity coefficient modification, resulting in an inadequate increase of relative volatility to effectively separate an azeotrope or close-boiling mixture. Conversely, the upper bound (300 kmol/hr) limits excessive solvent circulation that could result in column flooding and high reboiler duties and condenser load. High E/F can over-dilute the mixture, yielding a marginal increase in relative volatility. Additionally, these E/F are within the range of practical feasibility that is typically used in ED.[50–53] The pressure range of 30-100 kPa reflects utility and temperature-feasibility bottlenecks. At pressures below 30 kPa, although relative volatility may increase, the overhead temperature can fall below practical cooling limits, require refrigeration and significantly increase operating costs. At pressures above 100 kPa, higher bottom temperatures demand higher steam grades and increase reboiler duty. Therefore, the selected pressure range provides a compromise between improved relative volatility and feasible condenser and reboiler operation. Reflux ratios between 0.1 and 5 were selected to ensure convergence and operability while spanning the range required to achieve high-purity specifications without imposing excessive energy consumption. In addition, this range aligns with the values generally considered practical for ED operations.[50–53]

**Table 2** Variables and their bound for the optimization

| Variable | Lower bound | Upper bound |
|---|---|---|
| Entrainer flowrate (kmol/hr) | 50 | 300 |
| Pressure at EDC (kPa) | 30 | 100 |
| Reflux ratio at EDC | 0.1 | 5 |
| Pressure at ERC (kPa) | 30 | 100 |
| Reflux ratio at ERC | 0.1 | 5 |

## 5.4. Process performance assessments

Process performance assessments were performed to quantitatively evaluate the economic and sustainability performances of each entrainer in ED processes.

### 5.4.1. Economic assessment

TAC serves as the principal metric for assessing the economic viability of a chemical process. It is determined from the set of design and operating parameters that meet the specified process constraints. The estimation approach was first introduced by Douglas (1988),[54] who defined TAC as the sum of the annualized capital and operating costs. TAC is calculated by using the equation providing in Table F3. Total Capital Cost (TCC) includes the costs associated with the distillation column, plates, and heat exchangers, with a Marshall & Swift (M&S) cost index of 1773.4 (2021). Since the capital cost equations are applied identically across all cases, changes in the most updated cost basis would uniformly scale the TAC values and thus would not affect the comparative ranking of entrainers. Total Operating Cost (TOC) represents the costs of steam and cooling water. A three-year payback period was adopted as it represents a practical compromise between economic realism and design simplicity. This value enables meaningful comparison of process alternatives without requiring detailed cash-flow analysis. The detailed equations for the equipment cost calculations are provided in Table F4. In this calculation, the price of the entrainer was not included, as the entrainer will be recycled and reused, with only a small amount of make-up entrainer required during the ED process. Therefore, fresh entrainer is only required at the beginning of the process. This calculation method is widely used in ED process evaluations, as it provides a robust approach to assess the economic performance of ED.[55,56]

A sensitivity analysis was performed by comparing TAC obtained from simulations with entrainer purity constraints of ≥ 99.99 (%wt) and ≥ 99.90 (%wt) to evaluate changes in TAC and the comparative ranking of the entrainers. In addition, a sensitivity analysis of the payback period on the TAC was conducted to assess whether variations in the payback period influence the relative economic ranking of the entrainers in both mixtures. Although solvent price was not considered for the TAC evaluation in this work, solvent prices for the green entrainers corresponding to 1, 3, 5, 7, and 10 times the price of NMP were

subsequently incorporated to examine their impact on the TAC. Furthermore, the contribution of make-up costs to the overall TAC was evaluated.

### 5.4.2. Sustainability evaluation

The environmental impact of the ED processes was evaluated using sustainability parameters. These include the toxicity of entrainers, energy intensity, greenhouse gas (GHG) emissions, particularly $CO_2$ emissions, and water consumption.[57,58] Lower values for these parameters correspond to improved sustainability of the processes.

*Toxicity of the entrainers*

The toxicity of the entrainers was evaluated using the Safety, Health, and Environment (SHE) indicators. The methods outlined in the CHEM21 Solvent Selection Guide to complement the process sustainability assessment to complement the process sustainability assessment.[59] Toxicological and ecotoxicological data were collected from the European Chemical Agency (ECHA) REACH database.[60] Safety was assessed based on flash points, which indicate flammable risk. Health hazards were evaluated by considering hazard statements related to carcinogenic, mutagenic, and/or reprotoxic (CMR) effects. Single-target organ toxicity (STOT), acute toxicity, and potential for irritation were also considered. Environmental risk was quantified with Predicted No-Effect Concentration (PNEC) values for fresh water, air, and soil. The scoring system from the CHEM21 Selection Guide was applied, where higher scores reflect a greater potential hazard. Entrainers with low aggregate SHE scores were considered safer and more environmentally benign.

*Energy intensity*

Energy intensity refers to the total energy required in the ED process, measured in kWh/kg. It is primarily determined by the total reboiler duties of the EDC and ERC per kg of products. The reboiler duty represents the primary energy demand in ED process. To evaluate energy intensity, thermal energy was used for calculations. Energy intensity formula is listed in Table F3. Additionally, the products are the high-purity chemicals obtained in the top stream of EDC and ERC. For instance, in the separation of HEX-ETH, n-hexane and ethanol are the resulting products. Similarly, in the separation of MCH-TOL, the products are methylcyclohexane and toluene.

*Greenhouse gas (GHG) emissions*

Greenhouse gas emissions quantify the equivalent mass of $CO_2$ released due to thermal consumption processes. The calculation of $CO_2$ emissions, using equation proposed by Gadalla et al. (Table F3).[61] This calculation accounts for the quality of the fuel through its net heating value, carbon content, the molar ratio of $CO_2$ to carbon, and the amount of fuel consumed. This method is widely used for the calculation of $CO_2$ emissions.[56,61–63]

*Water consumption*
Water consumption in ED process is expressed in $m^3$ per kg of products. It includes cooling water for the condenser in both EDC and ERC, cooling water for the cooler, and water used as steam in the reboiler for both EDC and ERC.

## 5.5.Separation metric assessment

Selectivity and capacity at infinite dilution were predicted using COSMOTherm X17 software, as explained in Chapter 2. Selectivity is defined as the ratio of the activity coefficients of components *i* and *j*, which represents the ease with which component *i* can be separated from component *j*. Capacity denotes the amount of solvent needed to perform the separation while achieving the desired purity. Infinite dilution is the effective calculation method to capture the maximum capability separation of an entrainer. Under infinite dilution conditions, the entrainer acts as the dominant solvent, and each component of the mixture is considered as a trace solute. Therefore, at a minimal concentration of solute, the intermolecular interactions occur exclusively between the solute and the solvents, with negligible solute-solute interactions. The selectivity and capacity profiles were compared with the TAC obtained from the ED process simulation.

## 5.6. Predictive model evaluation

For the UNIFAC method, all compounds were selected from the Aspen physical property database, except for NBP, which is not included. Therefore, NBP was implemented using a user-defined method by specifying its molecular structure and functional groups. The pure-component properties of NBP were evaluated by the NIST-TDE integrated in Aspen Plus. For DMI, the compound is available in the Aspen database. However, its molecular structure is explicitly defined and was therefore entered manually.

To perform the simulation using COSMO-based calculation, the COSMO-SAC model was employed. To define the COSMO-SAC model, sigma profiles and molecular volume were required for the simulation. These properties were calculated using COSMOTherm X17 software. The obtained sigma profiles were input into Aspen Plus as sigma profile parameters, called SGPRF1 - SGPRF5. The molecular volume was entered into Aspen Plus under the volume parameter, referred to as CSACVL. It should be noted uncertainties may arise from both UNIFAC and COSMO-based calculation, for example manually defining molecular structures and functional group assignments introduces additional uncertainty in UNIFAC predictions. Additionally, although COSMO-based method does not rely on fitted parameters from experimental data, uncertainties may arise from the underlying quantum chemical calculations, including

conformer selection, surface charge distribution, and the treatment of hydrogen bonding. These uncertainties contribute to deviations in predicted phase behavior and process performance. Therefore, the relative volatility, as represented by *x-y* diagram, calculated from UNIFAC and COSMO-based were compared to NRTL. As shown in Figures F4 and F5 for both HEX-ETH and MCH-TOL mixtures, the *x-y* profiles obtained from UNIFAC and COSMO-based methods exhibit reliable results when compared to the NRTL results.

## 5.7. Results and discussion

### 5.7.1. ED results for the HEX-ETH and MCH-TOL mixtures

Prior to assessing the greener entrainers, the process simulation method was validated by comparing this work with the literature.[64] For this comparison, the ED process for the separation of MCH-TOL with the conventional entrainer NMP was evaluated. This system was selected, as it is available in literature as benchmark simulation. Identical process design and operating conditions were adopted. These include column pressures and key constraints, such as the purity of the top products, entrainer loss in the EDC and ERC, and purity of the recycled entrainer, were set similarly to ensure a fair comparison. For the simulation, the BIPs were obtained from the previous experimental work,[65] while for the benchmark simulation, the BIPs were obtained from the literature.[64] As shown in Table 3, the simulated results indicate good agreement with the literature, mean that the simulation approach is reliable. Comparable key design parameters, product and entrainer purity constraints, and energy intensity are observed, with only minor differences. In this work, ED comprises 32 numbers of stages, slightly higher compared to the 30 numbers of stages reported in the literature. E/F is slightly higher in this study (1.53) than in literature (1.37). While the reflux ratio in this work is lower (1.57) than in the literature (1.70). Despite these minor differences, the energy intensity in this work (0.28 kW/kg products) is identical to that reported in the literature (0.29 kW/kg products).

Process simulations and comparisons with different greener entrainers were conducted. The process simulation was adjusted by adding heat integration. The pressures in both the EDC and ERC were optimized to meet product purity constraints while maintaining low reboiler duty. Additionally, the purity of the recycled entrainer was set to ≥0.9999 (wt%) to ensure its performance remained comparable to that of the fresh entrainer. Tables 4 and 5 provide the key design metrics and performance indicators for both mixtures.

**Table 3.** Comparison of key design parameters for the ED processes in separating the methylcyclohexane-toluene mixture using NMP as an entrainer from our work and existing literature

| Key design variables | This Work | | Literature[64] | |
|---|---|---|---|---|
| | **EDC** | **ERC** | **EDC** | **ERC** |
| Operating pressure (kPa) | 100 | 40 | 100 | 40 |
| Number of stages | 32 | 13 | 30 | 14 |
| Feed stages | 19 | 9 | 19 | 9 |
| Entrainer feed stages | 8 | - | 7 | - |
| Reflux ratio | 1.57 | 0.44 | 1.70 | 0.41 |
| Entrainer-to-feed-ratio | 1.53 | - | 1.37 | - |
| ***Top Product (mole fraction)*** | | | | |
| Methylcyclohexane | 0.9953 | 0.0039 | 0.995 | 0.0019 |
| Toluene | 0.0001 | 0.9958 | 0.001 | 0.9976 |
| NMP | 0.0046 | 0.0004 | 0.004 | 0.0004 |
| ***Bottom Product (mole fraction)*** | | | | |
| Methylcyclohexane | 0.0012 | <0.0001 | 0.001 | <0.0001 |
| Toluene | 0.2976 | 0.0009 | 0.337 | 0.0007 |
| NMP | 0.7012 | 0.9991 | 0.662 | 0.9993 |
| **Energy intensity (kW/kg products)** | **0.28** | | **0.29** | |

Additionally, based on a column design perspective, the optimized solutions fall within acceptable range of the hydraulic limits. The maximum flooding levels in the ED column range from approximately between 65 to 75% for all entrainers. This indicates that the columns operate safely below flooding conditions while ensuring effective contact between vapor and liquid. Furthermore, the resulting column diameter are similar across all entrainers, ranging between 1.1 – 1.4 m for both mixtures. Therefore, the differences in TAC are primarily driven by energy requirements rather than hydraulic constraints.

As shown in Table 4, all investigated entrainers effectively separate the HEX-ETH azeotrope while meeting the required constraints. EDC for all entrainers produces high-purity n-hexane in the distillate, with a mass fraction higher than 0.99, suggests that each entrainer effectively breaks the azeotrope. In the ERC, ethanol is recovered at purities 0.998 for all entrainers. This confirms minimal entrainer contamination in the distillate and effective entrainer recovery, which remains consistently below 0.001. In the bottom stream of the ERC, the purity of the recycled entrainer reaches 0.9999 mass fraction for all cases, supporting high entrainer recyclability.

**Table 4.** Comparison of process performance among entrainers in the n-hexane-ethanol mixture

| Key design parameters | NMP | | Guaiacol | | DMI | | NBP | |
|---|---|---|---|---|---|---|---|---|
| | EDC | ERC | EDC | ERC | EDC | ERC | EDC | ERC |
| ***column*** | | | | | | | | |
| Operating pressure (kPa) | 54 | 42 | 61 | 30 | 41 | 33 | 34 | 37 |
| Number of stages | 37 | 10 | 40 | 12 | 40 | 12 | 39 | 9 |
| Feed stages | 19 | 3 | 19 | 8 | 20 | 5 | 19 | 5 |
| Entrainer feed stages | 4 | - | 3 | - | 4 | - | 4 | - |
| Molar reflux ratio | 0.50 | 0.80 | 0.56 | 1.08 | 0.43 | 0.60 | 0.19 | 0.20 |
| Entrainer-to-feed-ratio (mass-based) | 1.53 | - | 1.72 | - | 2.75 | - | 1.85 | - |
| ***stream*** | | | | | | | | |
| ***Top Product*** | | | | | | | | |
| Temperature (K) | 322.78 | 330.78 | 323.03 | 322.40 | 310.91 | 325.14 | 307.58 | 327.88 |
| Flowrate (kg/h) | 5172.2 | 1840.6 | 5199.9 | 1813.7 | 5214.8 | 1796.0 | 5222.5 | 1790.1 |
| Composition (mass fraction): | | | | | | | | |
| Hexane | 0.9985 | 0.0014 | 0.9929 | 0.0000 | 0.9915 | 0.0000 | 0.9901 | 0.0000 |
| Ethanol | 0.0014 | 0.9981 | 0.0071 | 0.9995 | 0.0084 | 0.9995 | 0.0099 | 0.9999 |
| Entrainer | 0.0001 | 0.0005 | 0.0000 | 0.0008 | 0.0001 | 0.0005 | 0.0001 | 0.0001 |
| ***Bottom Product*** | | | | | | | | |
| Temperature | 378.15 | 451.03 | 391.99 | 444.34 | 391.28 | 440.91 | 381.82 | 482.79 |
| Flowrate (kg/h) | 12563.0 | 10722.3 | 13910.2 | 12096.5 | 21086.6 | 19189.8 | 13623.3 | 12975.3 |
| Composition (mass fraction): | | | | | | | | |
| Hexane | 0.0000 | 0.0000 | 0.0005 | 0.0000 | 0.0000 | 0.0000 | 0.0000 | 0.0000 |
| Ethanol | 0.1466 | 0.0001 | 0.1298 | 0.0001 | 0.0853 | 0.0001 | 0.1213 | 0.0001 |
| Entrainer | 0.8534 | 0.9999 | 0.8696 | 0.9999 | 0.9147 | 0.9999 | 0.8787 | 0.9999 |
| ***heat duty*** | | | | | | | | |
| Condenser (kW) | -731 | -817 | -797 | -935 | -752 | -819 | -639 | -527 |
| Reboiler (kW) | 940 | 1336 | 1441 | 1086 | 1710 | 943 | 1076 | 1237 |

Optimization of the operating pressure in the EDC and ERC showed that all entrainers performed effectively under sub-atmospheric conditions. This operating pressure provides favorable separations while maintaining low energy requirements in the reboiler duty. For the EDC, the number of stages across all entrainers remained similar, requiring 37 stages for NMP, 40 stages for guaiacol and DMI, and 39 stages for NBP. The entrainer feed was introduced below the top of the column. NMP, guaiacol, DMI, and NBP had entrainer feed stages at 4, 3, 4, and 4, respectively. The placement at these stages is to minimize the entrainer loss in the top product and to ensure that the entrainer can have maximum interaction with the feed. The feed was introduced near the lower-middle section of the EDC, at stages 19, 19, 20, and 19 for NMP, guaiacol, DMI, and NBP, respectively. Therefore, the separation of the mixtures can be achieved effectively.

Both the reflux ratio and entrainer-to-feed ratio (E/F) varied among the entrainers, which reflects their capabilities to alter the HEX-ETH relative volatility. The reflux ratio defines the amount of condensed liquid in the top product that is recycled back to the column to increase separation efficiency. The observed reflux ratios were moderate for NMP (0.50), guaiacol (0.56), DMI

(0.43), and NBP (0.19). The E/F ratio, which determines the amount of entrainer required to alter the relative volatility, showed more pronounced differences. NMP required the smallest E/F of 1.53, followed by guaiacol (1.72), NBP (1.85), and DMI (2.75). The slightly higher E/F for NBP compared to guaiacol is attributed to its lower molar reflux ratio, which requires more entrainer to remove the azeotrope. Both the molar reflux ratio and E/F influence the reboiler duty by determining the internal vapor-liquid circulation in the column. A larger reflux ratio increases the liquid returning from the condenser, thereby increasing the vapor flow required from the reboiler. However, as the entrainer is a heavy component in ED, it dominates the bottom of the column; therefore, the E/F typically exerts a stronger effect on reboiler duty. Higher E/F significantly enhances the circulation of the high-boiling entrainer in the stripping section. This leads to larger flow rates in the bottom and substantially increases reboiler duties. These trends result in NMP having the lowest reboiler duty (940 kW), followed by NBP (1076 kW), guaiacol (1441 kW), and DMI (1710 kW). This ordering aligns with the experimental relative volatilities discussed in Chapter 2,[66] as shown in Figure F6a, and the VLE data in Chapter 4,[31,67] where NMP provided the highest relative volatility, followed by NBP, guaiacol, and DMI.

For the close-boiling MCH-TOL separation, as listed in Table 5, all entrainers demonstrate favorable performance, effectively separating the close-boiling mixture and fulfilling the constraints. EDC employing the studied entrainers yields methylcyclohexane with a purity above 0.995 (mass fraction). All investigated entrainers effectively remove the close-boiling behavior. The toluene in the top product of the ERC exhibited a mass fraction of purity higher than 0.995, highlighting successful separation of ethanol and entrainer. Furthermore, the entrainer is effectively recovered in the bottom stream, with a purity of 0.9999 mass fraction for all entrainers. The optimization in this system is similar to that for the HEX-ETH separation. The pressures in the EDC and ERC were operated below atmospheric. This condition provides more effective separation and keeps reboiler duties low. For effective separation, the number of stages for GVL and NMP are 36, while for DMI and NBP are 35. The entrainer was fed at stages lower than the top column. The selected stages are 7, 8, 7, and 3 for GVL, NMP, DMI, and NBP, respectively. This configuration prevents entrainer loss and ensures maximum contact with the close-boiling mixture for effective separation. The close-boiling mixture was introduced at the lower-middle section of the EDC at stages 21, 19, 22, and 22 for GVL, NMP, DMI, and NBP, respectively. For the reflux ratio GVL, NMP, DMI, and NBP show values of 2.1, 3.5, 2.1, and 1.6, respectively. The E/F for each entrainer is 1.14, 1.60, 2.97, and 2.25, respectively. The reboiler duties for each entrainer are 1719 kW for GVL, 1746 kW for NMP, 1747 kW for DMI, and 2279 kW for NBP. This

rank is aligned with the measured relative volatilities described in Chapters 2 and 3.[65,66,68] Furthermore, the profile of relative volatility in correlation with energy intensity is shown in Figure F6b. The coefficient of Spearman rank correlation (ρ) shown in Figure F6 indicates a negative monotonic relationship between relative volatility and energy intensity, with ρ = -1 for both mixtures. However, due to small sample size (n = 4), the correlation is not statistically significant (p-value = 0.083). This suggest that the observed trend should be interpreted cautiously, despite its strong directional consistency.

**Table 5.** Comparison of process performance among entrainers in the methylcyclohexane-toluene mixture

| Key design parameters | NMP | | GVL | | DMI | | NBP | |
|---|---|---|---|---|---|---|---|---|
| | EDC | ERC | EDC | ERC | EDC | ERC | EDC | ERC |
| ***column*** | | | | | | | | |
| Operating pressure (kPa) | 88 | 35 | 80 | 31 | 86 | 31 | 92 | 34 |
| Number of stages | 36 | 13 | 36 | 13 | 35 | 12 | 35 | 11 |
| Feed stages | 19 | 9 | 21 | 7 | 22 | 8 | 22 | 6 |
| Entrainer feed stages | 8 | - | 7 | - | 7 | - | 3 | - |
| Reflux ratio | 3.5 | 0.4 | 2.1 | 0.6 | 2.1 | 0.3 | 1.6 | 0.4 |
| Entrainer-to-feed ratio (mass-based) | 1.60 | - | 1.14 | - | 2.97 | - | 2.25 | - |
| ***stream*** | | | | | | | | |
| ***Top Product (mole fraction)*** | | | | | | | | |
| Temperature (K) | 368.87 | 350.20 | 364.50 | 346.61 | 368.03 | 346.74 | 370.46 | 349.24 |
| Flowrate (kg/h) | 2936.5 | 6467.0 | 2956.8 | 6439.8 | 2914.8 | 6478.9 | 2946.9 | 6448.4 |
| Composition (mass fraction): | | | | | | | | |
| Methylcyclohexane | 0.9974 | 0.0026 | 0.9958 | 0.0002 | 0.9994 | 0.0050 | 0.9974 | 0.0009 |
| Toluene | 0.0001 | 0.9971 | 0.0038 | 0.9998 | 0.0002 | 0.9950 | 0.0019 | 0.9991 |
| Entrainer | 0.0026 | 0.0003 | 0.0004 | 0.0004 | 0.0006 | 0.0000 | 0.0007 | 0.0000 |
| ***Bottom Product (mole fraction)*** | | | | | | | | |
| Temperature (K) | 398.9 | 350.2 | 398.2 | 444.0 | 389.6 | 419.0 | 427.1 | 480.9 |
| Flowrate (kg/h) | 21503.5 | 15036.5 | 17189.8 | 10750.0 | 34352.1 | 27873.2 | 27610.3 | 21161.9 |
| Composition (mass fraction): | | | | | | | | |
| Methylcyclohexane | 0.0008 | 0.0000 | 0.0001 | 0.0001 | 0.0009 | 0.0000 | 0.0002 | 0.0000 |
| Toluene | 0.2999 | 0.0001 | 0.3746 | 0.0000 | 0.1877 | 0.0001 | 0.2334 | 0.0001 |
| Entrainer | 0.6993 | 0.9999 | 0.6254 | 0.9999 | 0.8113 | 0.9999 | 0.7664 | 0.9999 |
| ***heat duty*** | | | | | | | | |
| Condenser (kW) | -1176 | -989 | -822 | -1113 | -805 | -934 | -527 | -937 |
| Reboiler (kW) | 1746 | 1340 | 1719 | 1190 | 1747 | 1472 | 2279 | 1422 |

### i) Economic evaluation

An economic evaluation was performed by comparing the TAC for the ED using biobased and greener entrainers against conventional entrainer NMP. Figure 3 shows the TCC, TOC, and TAC for each entrainer. For the HEX-ETH mixture, as illustrated in Figure 3a, the TAC for all three greener entrainers (NBP, guaiacol, and DMI) are comparable to that of NMP. In the case of the close-boiling MCH-TOL mixture, as shown in Figure 3b, the biobased solvent GVL presents the most economically attractive option for replacing NMP, as it demonstrates a lower TAC than NMP. Additionally, DMI and NBP, as biobased and greener organic solvents,

can also serve as alternatives since they demonstrate TAC values comparable to that of NMP. Overall, these greener entrainers are economically viable alternatives to NMP for both azeotropic and close-boiling separations using extractive distillation.

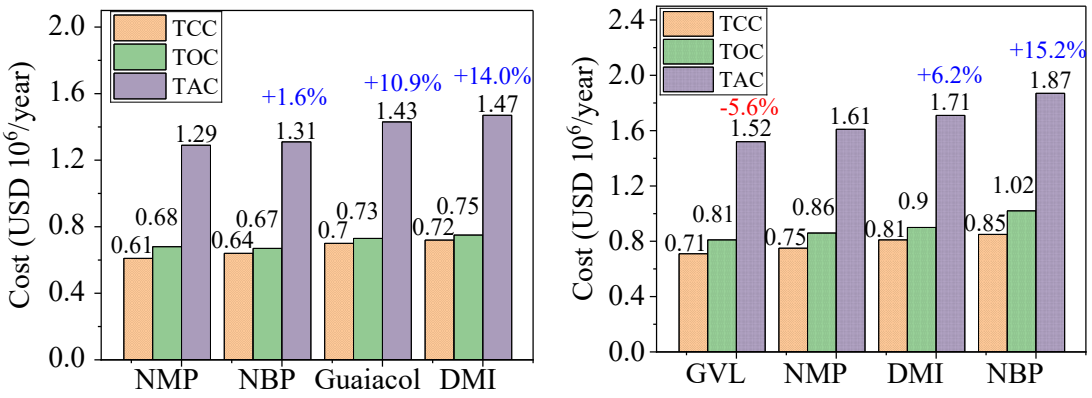


**Figure 3.** Economic evaluation (total annual cost (TAC), total capital cost (TCC) and total operating cost (TOC): a) n-hexane-ethanol mixture and b) methylcyclohexane-toluene mixture.

***Sensitivity analysis***

a) Effect of recycled entrainer purity on the TAC.

The recycled entrainer purity in the bottom stream of ERC strongly influences the energy consumptions and, consequently, the TAC. To assess this effect, the recycled entrainer purity requirement was relaxed from 99.99% to 99.9%. Reducing the purity constraint results in a noticeable decrease in TAC. Relaxing the entrainer purity constraint shifts the operating point away from the pinch region. This effect increases the composition driving force between the liquid and vapor phase, which enables the separation to be achieved with lower energy requirement, as shown in Figure F7. Therefore, lower the constraint decrease reboiler duty as well as TAC. Across both mixtures, TAC reductions range from approximately 1-9% for the n-hexane-ethanol mixture (as illustrated in Figure 4) and 11-24% for the methylcyclohexane-toluene mixture (Figure F8). The relative ranking of entrainers remains largely unchanged, with only minor shifts observed in closely performing cases. The overall economic competitiveness of the greener entrainers relative to NMP is therefore preserved under relaxed purity constraints.

From an industrial perspective, these results indicate that the purity requirements of the recycled entrainer should be carefully balanced against economic considerations, as purities above 99.99% may not be required in practical operation. A purity level around 99.9% appears sufficient to maintain process performance while reducing operational costs. While changes in purity constraints can slightly affect entrainer ranking, the impact is not economically penalizing, as the greener entrainers continue to exhibit TAC values comparable to the conventional entrainer NMP.

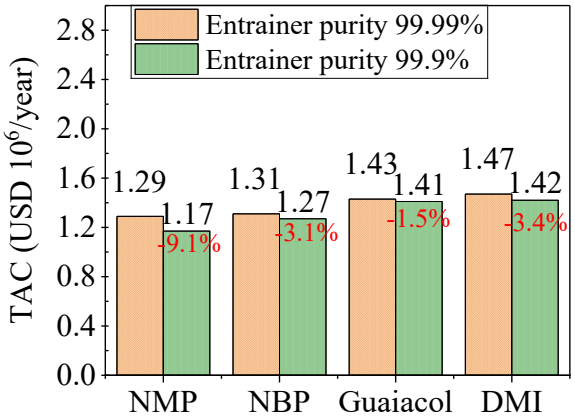


**Figure 4.** Sensitivity analysis of the entrainer purity on the total annual cost (TAC) for the n-hexane-ethanol mixture .

b) Effect of payback period on the TAC.

Sensitivity analysis of the payback period on the TAC for each entrainer in both HEX-ETH and MCH-TOL mixtures shows that increasing the assumed payback period from 3 to 5, 7, and 10 years lead to a decrease in TAC, as illustrated in Figures 5 for HEX-ETH and F9 for MCH-TOL. This trend arises from the reduced annualized CAPEX as the same capital cost is distributed over a longer recovery period. Furthermore, the relative ranking of the entrainers remains unchanged even though the payback period is extended to 10 years. This indicates that the economic comparison among entrainers is robust with respect to the assumed payback period.

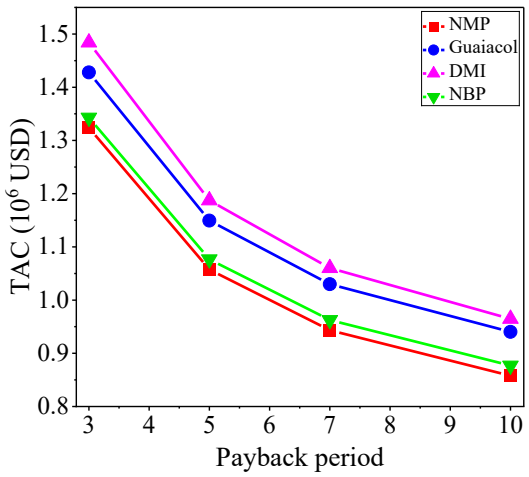


**Figure 5.** Sensitivity analysis of payback period vs TAC for the HEX-ETH mixture.

c) Effect of solvent price ratio (green solvent/NMP) on TAC ratio (green solvent/NMP).

To evaluate the impact of solvent price on the TAC of green solvent-based process relative to TAC of NMP-based process, Figure 6 illustrate the sensitivity of TAC in the n-hexane-ethanol mixture to increasing solvent price ratios of 1 to 3, 5, 7, and 10. Increasing the solvent price leads to increase in TAC for the green-based process in both mixtures. In the HEX-ETH mixture, NBP was selected as the green entrainer with the highest relative volatility, while DMI represents the greener entrainer with the lowest relative volatility. For the MCH-TOL mixture (Figure F10), GVL is green entrainer with the highest relative volatility, and NBP reflects the lowest relative volatility. All TAC values were calculated assuming a payback period of 3 years.

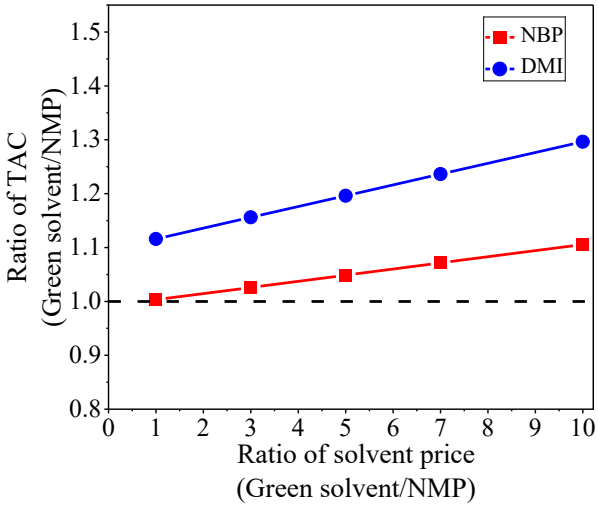


**Figure 6.** Sensitivity analysis of solvent price ratio (green solvent/NMP) vs TAC ratio (green solvent/NMP) for the HEX-ETH mixture.

d) Effect of entrainer make-up cost on the TAC.

To assess whether entrainer make-up cost has a significant impact on the TAC, ED processes were evaluated with and without inclusion of the entrainer make-up cost. For each mixture, green entrainers with the highest and lowest relative volatility were selected. In the HEX-ETH, NBP and DMI correspond to the highest and lowest relative volatility, respectively. For MCH-TOL, GVL and NBP denote the highest and lowest relative volatility, respectively. When the green solvent price is comparable to that of NMP, the contribution of entrainer make-up cost to TAC is relatively minor in both mixtures for all entrainers. However, as the green solvent price increases relative to NMP, the entrainer make-up cost becomes increasingly significant. This leads to a larger deviation between TAC values calculated with and without entrainer make-up, as shown in Figure 7 for the HEX-ETH mixture and Figure F11 for the MCH-TOL

mixture. In the HEX-ETH mixture, the deviation in TAC due to inclusion of entrainer make-up is more pronounced for DMI than NBP. This behavior is attributed to the slightly higher entrainer make-up requirement associated with DMI (1.34 kg/hr) compared to NBP (0.46 kg/hr), which amplifies the impact of solvent price in OPEX. Similarly, in the MCH-TOL mixture, NBP exhibits slightly larger deviation in TAC compared to GVL, as the entrainer make-up flowrate required for NBP (1.93 kg/hr) is slightly higher than GVL (1.39 kg/hr). These results indicate that the significance of entrainer make-up cost on TAC depends on both the solvent price and the magnitude of the required make-up flowrate.

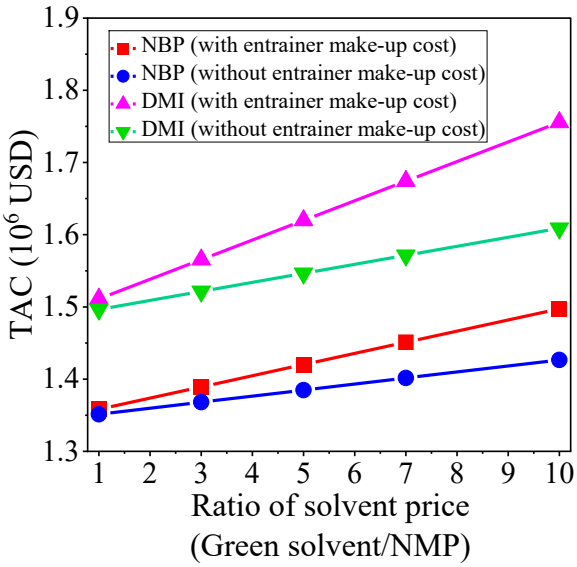


**Figure 7.** Sensitivity analysis for solvent price ratio (green solvent/NMP) with and without make up entrainer cost vs TAC for the HEX-ETH mixture.

**ii) Sustainability evaluation**

The sustainability assessment was performed by integrating both substance-inherent and process-related indicators. Substance-inherent indicator include toxicity, while process-related indicators comprised energy intensity, $CO_2$ emissions, and water consumption associated with the extractive distillation process. These indicators collectively capture intrinsic solvent safety, represented by toxicity. They also reflect operational sustainability through energy and water use, and potential $CO_2$ emissions.

i) Toxicity

Table 6 summarizes the toxicity evaluation based on safety, health, and environmental (SHE) metrics derived from hazard classifications by the CHEM21 Solvent Selection Guide. The final toxicity classification for each entrainer was

determined based on the combined scores of these metrics. The safety metric was assessed using flash point values. According to this guide, all investigated greener entrainers, including NMP, were scored 1, as their flash points exceeded 60 °C. This indicates a low flammability risk and compliance with standard safety criteria. However, a comprehensive toxicity evaluation also requires consideration of health and environmental impacts. For the health metric, all greener entrainers exhibit no CMR classifications. In contrast, NMP was identified as reprotoxic (H360D), resulting in a score of 9, the highest among the evaluated solvents. According to the scoring criteria, any indicator with a score exceeding 8 classifies the substance as hazardous, confirming the significant toxicological concern associated with NMP. None of the evaluated entrainers exhibited STOT. All entrainers except DMI showed low irritation effects corresponding to a score of 2, while DMI, with no reported irritation potential, received a score of 1. The environmental metric was evaluated using PNEC, which represents the maximum concentration of a chemical that is not expected to cause adverse effects on air, aquatic life, or soil organisms. Higher PNEC values indicate lower environmental toxicity. GVL was scored a 3, as no hazards were identified for any environmental metric, and no ozone-depleting potential was reported. Guaiacol and DMI also received scores of 3, since no PNEC data were available under REACH registration and no ozone layer hazards were identified. For reference, water was assigned a baseline score of 1 for this metric. NBP exhibited low ecological impact, with PNEC values of 4 mg/L for freshwater and 1.68 mg/L for soil, resulting in a score of 4. In contrast, NMP showed substantially lower PNEC values (0.25 mg/L for freshwater and 0.07 mg/L for soil). This corresponds to a score of 7, signifying considerable environmental risk. Taking it together, the results of SHE assessments clearly demonstrate that all evaluated greener entrainers exhibit favorable SHE profiles, fulfilling the criteria for sustainable entrainers. Conversely, NMP, as the conventional benchmark entrainer, is not recommended due to its reprotoxicity and hazard potential to freshwater and soil ecosystems.

**Table 6.** Safety, health, and environment profile of entrainers[a,b]

| Entrainers | Safety | | Health | | | | | Environment PNEC value (mg/L)[c] | | | | Status |
|---|---|---|---|---|---|---|---|---|---|---|---|---|
| | Flash point (°C) | Score | carcinogen, mutagen or reprotoxic (score) | single target organ toxicity (score) | Acute toxicity | Irritation (score) | Score | Fresh water | Air | Soil | Score | |
| NMP | 91 | 1 | H360D (9) | No | No | H315 (2) H319 (2) H335 (2) | 9 | 0.25 | No | 0.07 | 7 | No |
| GVL | 97 | 1 | No | No | No | H315 (2) H319 (2) | 2 | No | No | No | 3 | Yes |
| NBP | 108 | 1 | No | No | H302 (2) | H315 (2) H319 (2) | 2 | 4 | No | 1.68 | 4 | Yes |
| Guaiacol | 90 | 1 | No | No | H302 (2) | H315 (2) H319 (2) | 2 | N/A | N/A | N/A | 3 | Yes |
| DMI | 116 | 1 | No | No | No | No | 1 | N/A | N/A | N/A | 3 | Yes |

[a]at 101.3 kPa; No: No hazard identified; N/A: Not available information under REACH
[b]data obtained from https://chem.echa.europa.eu
[c]Predicted No-Effect Concentration (PNEC)

ii) Energy intensity

As shown in Figure 8, both the HEX-ETH and MCH-TOL mixtures exhibit distinct energy intensity profiles across the tested entrainers. For the HEX-ETH mixture, the biobased and greener entrainers achieve energy intensity comparable to NMP. NMP shows the lowest energy intensity, with a value of 0.32 kWh/kg of products. NBP demonstrates comparable performance, with an energy intensity of 0.33 kWh/kg of products. The other greener entrainers, guaiacol and DMI, exhibit slightly higher energy intensity of 0.36 and 0.38 kWh/kg of products, respectively, compared to NMP. For the MCH-TOL mixture, GVL achieves the lowest energy intensity of 0.31 kWh/kg of products, lower than that of NMP (0.33 kWh/kg of products). While DMI and NBP exhibit energy intensity of 0.34 and 0.39 kWh/kg of products. Additionally, for the investigated mixtures, minimization of reboiler duty was found to directly correlate with minimization of TAC. This behavior arises since operating cost dominates the TAC, while capital cost difference among entrainers is relatively small within the optimized design space. Figure F12 provides a correlation of the reboiler duty to the TAC. It shows that lower reboiler duty exhibits lower TAC.

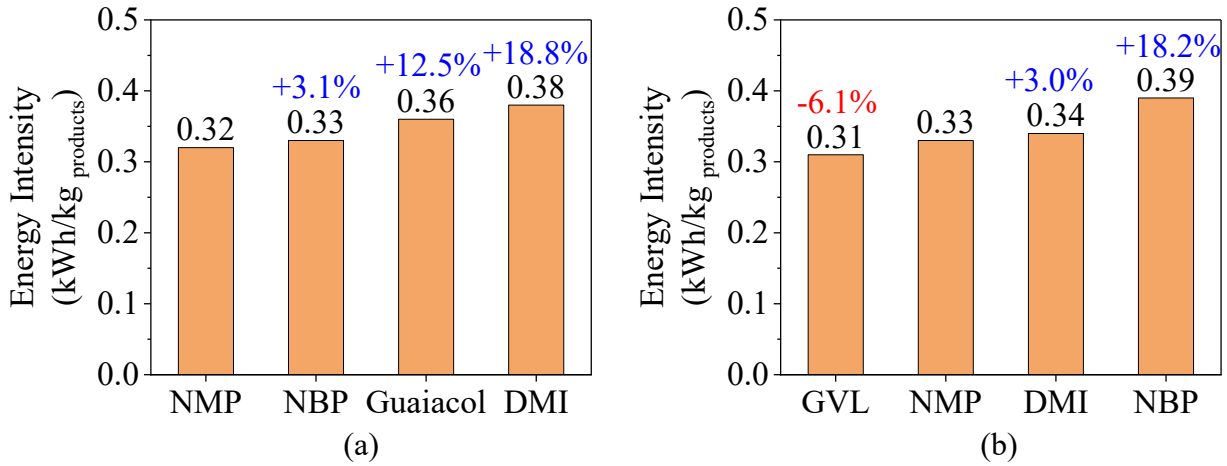


**Figure 8.** Energy intensity of extractive distillation processes for each entrainer: a) n-hexane-ethanol mixture and b) methylcyclohexane-toluene mixture.

iii) $CO_2$ emissions

In sustainability assessment within the chemical industry, $CO_2$ emissions are a crucial indicator.[69,70] $CO_2$ emissions were evaluated by comparing each entrainer in ED processes. $CO_2$ emissions were calculated based on the fuel consumption of the reboilers in both the EDC and ERC, as reboiler duty represents the main energy requirements in ED. Consequently, the primary source of $CO_2$ emissions originates from reboiler fuel combustion. As shown in Figure 9a, for the HEX-ETH mixture separation using natural gas as a reboiler fuel, the $CO_2$ emissions of NBP, guaiacol, and DMI are comparable to that of NMP. For the MCH-TOL mixture, as illustrated in Figure 9b, $CO_2$ emissions of GVL is lower than NMP, while DMI and NBP are

comparable to those of NMP. The $CO_2$ emission trends observed for both mixtures are consistent with the energy intensity profiles shown in Figure 8. Overall, the results demonstrate that biobased and greener entrainers provide $CO_2$ emissions lower and comparable to those of the conventional entrainer NMP, indicating that ED processes using these entrainers are environmentally viable.

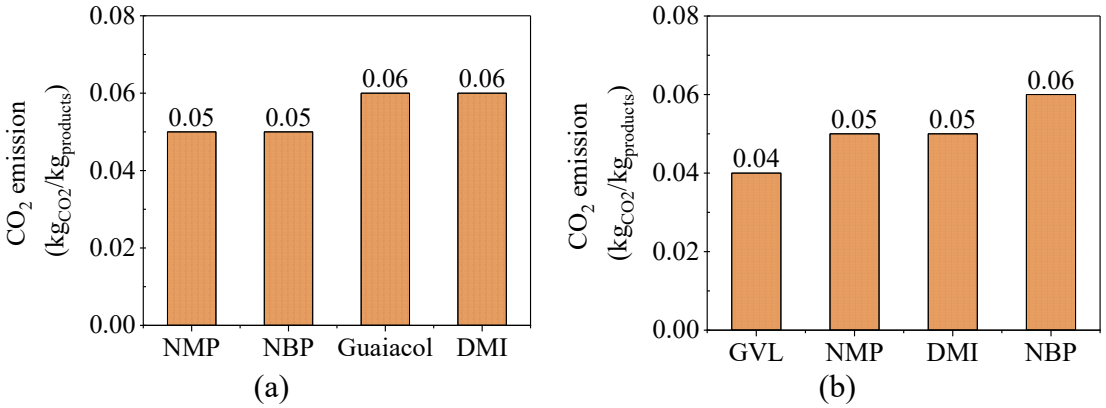


**Figure 9.** $CO_2$ emission of ED for each entrainer using natural gas as a reboiler fuel: a) n-hexane-ethanol mixture and b) methylcyclohexane-toluene mixture.

iv) Water consumption

Water consumption in ED processes is another important metric for sustainability evaluation.[71] As shown in Figure 10a, the water consumption of NBP, DMI, and guaiacol is comparable with NMP for the HEX-ETH separation. For the MCH-TOL mixture, as illustrated in Figure 10b, GVL and DMI demonstrate water consumption comparable to NMP, while NBP exhibits a slightly higher value. These results indicate that all investigated biobased and greener entrainers demonstrate water consumption levels comparable to those of the conventional entrainer, confirming their feasibility for use in ED processes from a water sustainability perspective. The sustainability evaluation results indicate that substituting a hazardous entrainer with greener alternatives demonstrates significantly lower toxicity than NMP. Moreover, it maintains efficiency in process energy, $CO_2$ emissions, and water consumption, which are essential for industrial implementation.

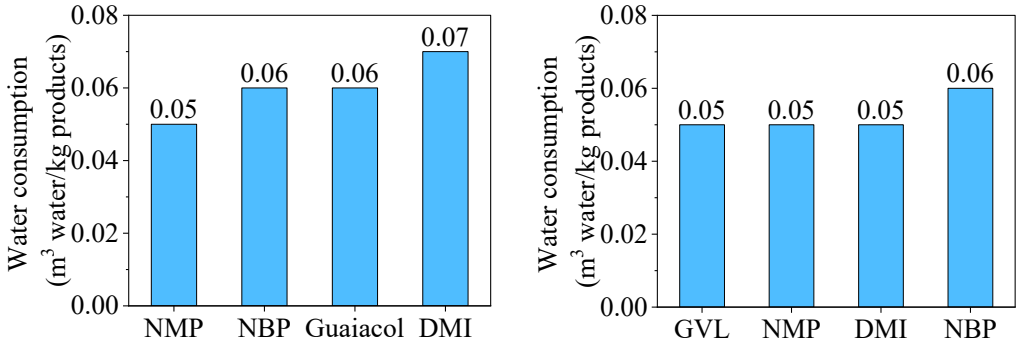


**Figure 10.** Water consumption of ED for each entrainer a) n-hexane-ethanol mixture and b) methylcyclohexane-toluene mixture.

### iii) Distillation drivers for TAC and sustainability

The evaluation of the economic and sustainability performance is closely driven by key operating parameters of ED, such as E/F, pressure, and reflux ratio. A summary of the key design parameters for each entrainer in both mixtures is provided in Tables 7 and 8. Overall, higher E/F values lead to an increase in the reboiler duty of the column, as this results in higher liquid circulation. This higher heat demand subsequently increase both energy requirements and TAC, since energy contributes a major operating costs in ED. In addition, these factors impact sustainability performances, including energy intensity, $CO_2$ emissions and water requirement. For instance, in the HEX-ETH mixture, as shown in Table 7, NMP exhibits the lowest E/F among other entrainers at similar pressure and reflux ratio conditions. As a result, NMP demonstrates the lowest TAC and sustainability performances. In the MCH-TOL mixture, Table 8 shows that GVL outperforms NMP, as GVL demonstrates the lowest E/F under comparable pressure and reflux ratio conditions. Consequently, GVL also exhibit the lowest TAC and sustainability performances. Additionally, the pressure the ED column using each entrainer in both mixtures is comparable to each other. This means that the required condenser utility, using water, is also comparable. Therefore, the water requirements remain similar across these systems.

**Table 7.** Summary of the ED key parameters for the n-hexane-ethanol mixture

| Key parameters | NMP | NBP | Guaiacol | DMI |
|---|---|---|---|---|
| Pressure (kPa) | 54 | 61 | 41 | 34 |
| E/F | 1.53 | 1.85 | 1.72 | 2.75 |
| Reflux ratio | 0.50 | 0.56 | 0.43 | 0.19 |
| TAC (USD $10^6$/year) | 1.29 | 1.31 | 1.43 | 1.47 |
| Energy intensity ($kWh/kg_{products}$) | 0.32 | 0.33 | 0.36 | 0.38 |
| $CO_2$ emissions ($kg_{CO2}/kg_{products}$) | 0.05 | 0.05 | 0.06 | 0.06 |
| Water requirements ($m^3_{water}/kg_{products}$) | 0.05 | 0.06 | 0.06 | 0.07 |

**Table 8.** Summary of the ED key parameters for the methylcyclohexane-toluene mixture

| Key parameters | NMP | GVL | DMI | NBP |
|---|---|---|---|---|
| Pressure (kPa) | 88 | 80 | 86 | 92 |
| E/F | 1.60 | 1.14 | 2.97 | 2.25 |
| Reflux ratio | 3.5 | 2.1 | 2.1 | 1.6 |
| TAC (USD $10^6$/year) | 1.61 | 1.52 | 1.71 | 1.70 |
| Energy intensity ($kWh/kg_{products}$) | 0.33 | 0.31 | 0.34 | 0.39 |
| $CO_2$ emissions ($kg_{CO2}/kg_{products}$) | 0.04 | 0.05 | 0.05 | 0.06 |
| Water requirements ($m^3_{water}/kg_{products}$) | 0.05 | 0.05 | 0.05 | 0.06 |

### 5.7.2. Use and limits of predictive tools for ED entrainer screening

**Separation metrics assessment**

The suitability of predictive selectivity and capacity at infinite dilution from COSMO-RS as screening parameters was evaluated by correlating them with TAC obtained from process simulations. This evaluation is essential because selectivity and capacity exhibit well-known opposing trends, as discussed in Chapter 2.[66] Therefore, it is vital to identify which parameter serves as a more effective decision parameter. Correlation plot with $R^2$ values between selectivity or capacity at infinite dilution against normalized TAC was used to evaluate the accuracy of predictive metrics to capture TAC. Rank correlation coefficient proposed by Spearman was utilized to identify ranking consistency.[72] As shown in Figures 11 and 12, for the HEX-ETH mixture, both selectivity and capacity exhibits weak correlation with TAC as well as weak ranking consistency. This indicates that neither metric reliably represents economic performance in associating mixture characterized by strong hydrogen bonding. Infinite-dilution data only assess the behavior of solutes at very lean concentrations. In contrast, ED columns operate at finite solute concentrations on most trays. As illustrated in Figure F13, the local composition profile shows that the compositions of ethanol and hexane in the presence of an entrainer vary significantly along the column. This strong dependence on composition explains why infinite-dilution-based selectivity fails to accurately predict TAC, particularly for the HEX-ETH mixture. As a result, composition-dependent-interactions, especially hydrogen bonding in associating systems such as HEX-ETH, are not sufficiently captured by infinite-dilution data. This discrepancy leads to a poor correlation with TAC. In contrast, for the non-associating MCH-TOL mixture, selectivity strongly correlates with TAC, following the expected trend of higher selectivity leading to lower TAC, consistent with literature finding.[22] Capacity, however, shows an opposite and less reliable trend. Moreover, capacity demonstrates weak ranking consistency with TAC, suggesting that it is not an appropriate screening parameter. In contrast, selectivity exhibits strong ranking consistency, indicating that selectivity is a more reliable screening metric for MCH-TOL mixture.

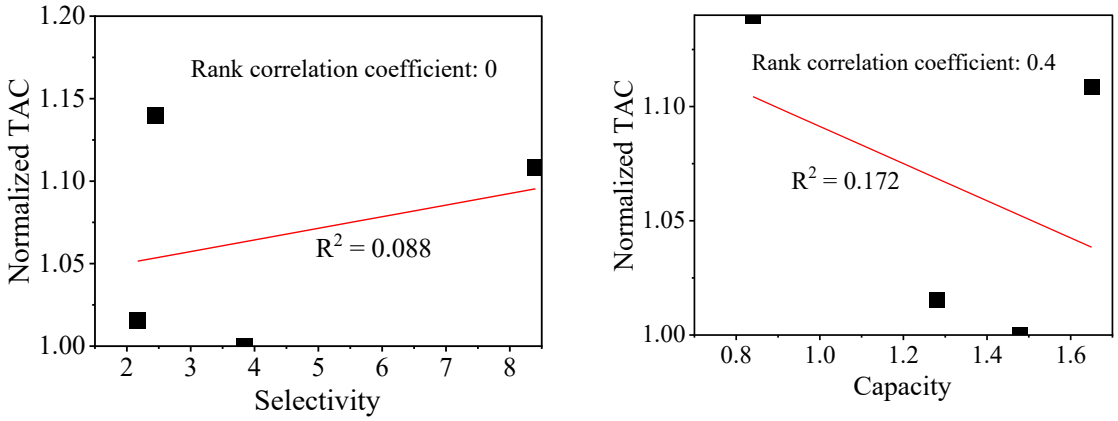


(a) (b)

**Figure 11.** Comparison of separation metrics with TAC in the HEX-ETH mixture: a) predicted selectivity vs TAC, and b) predicted capacity vs TAC.

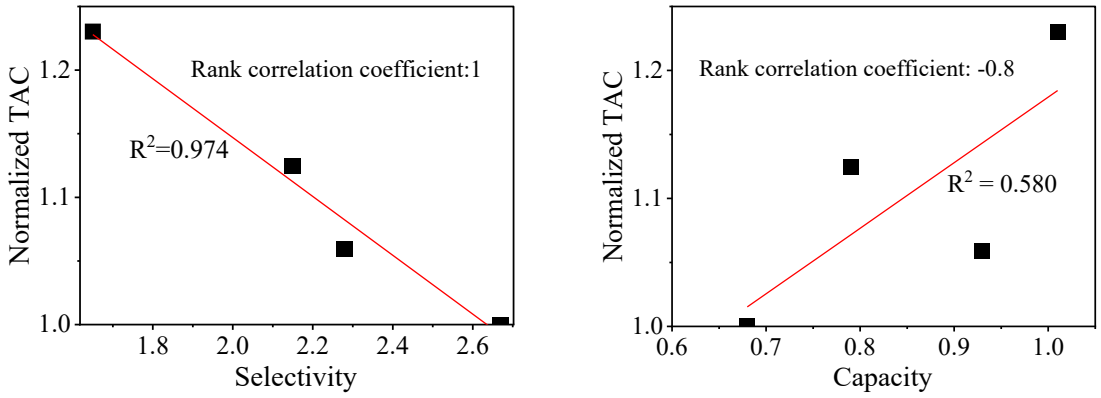


(a) (b)

**Figure 12.** Comparison of separation metrics with TAC in the MCH-TOL mixture: a) predicted selectivity vs TAC, and b) predicted capacity vs TAC.

**Predictive model evaluation in process simulation**

To quantitatively assess predictive thermodynamic model performance, evaluation metrics were defined: (i) average relative deviations ± standard deviations for TAC, and (ii) ranking accuracy to the NRTL benchmark. Overall, predictive models in both mixtures shows satisfactory agreement with NRTL. UNIFAC model exhibiting slightly lower average relative deviations than COSMO-based model, as listed in Table 9.

**Table 9.** The average relative deviation (ARD) for the TAC of the predictive models

| Mixtures | ARD (%) ± SE[a,b] | |
|---|---|---|
| | COSMO-based | UNIFAC |
| n-Hexane-ethanol | -17.7 ± 7.7 | -12.0 ± 3.5 |
| Methylcyclohexane-toluene | -12.0 ± 18.1 | -2.5 ± 10.1 |

[a]ARD (%) = $\frac{1}{N}\sum_{i=1}^{N}\left|\frac{(\alpha_{ij})_{\text{model}}-(\alpha_{ij})_{\text{experimental}}}{(\alpha_{ij})_{\text{experimental}}}\right|\times 100$

where ($\alpha_{ij}$) is relative volatility component i to j, and N is the number of data point

[b]Standard Error (SE) = $\frac{\sqrt{\frac{\sum_{i=1}^{N}(D_i-\overline{D})^2}{N-1}}}{\sqrt{N}}$, where Di is the deviation of each entrainer, and $\overline{D}$ is the ARD.

A detailed TAC comparison is provided in Figure 13. Most deviations falling within the acceptable uncertainty typically associated with conceptual process estimates of 20-50%,[73] with the largest deviation for UNIFAC and COSMO-based models are 31% and 32%, respectively. Therefore, the deviation for both models is acceptable for early-stage entrainer screening. Although the ranking of each entrainer is slightly change in both mixtures, the overall performance trends remain largely consistent. Predictive performance is strongly system-dependent that both models perform better for nonpolar MCH-TOL mixture, while larger deviations occur for strongly associating HEX-ETH mixture. Additionally, it is crucial to highlight a possible limitation of the predictive model approach, as it directly affects the convergence and reliability of the corresponding simulation. The COSMO-based model failed to converge for the ethanol-DMI mixture due to the prediction of a nonphysical azeotrope at an ethanol liquid phase composition of approximately 0.2, where the relative volatility approaches unity ($\alpha = 1$), as shown in Figure F14. As a result, the ethanol-DMI case cannot be interpreted as a normal quantitative TAC devation. Rather, it represents a qualitative failure in feasibility prediction. In contrast, NRTL calculations indicate no azeotropic condition across the entire composition range, with relative volatility $\neq 1$. The nonphysical azeotrope predicted by COSMO-based model introduces an artificial thermodynamic pinch in the ERC. This eliminates the continuous composition path required to drive the separation toward the desired composition, thereby preventing convergence of the ED simulation. Therefore, although predictive thermodynamic models can be potentially applied for the early-stage entrainer

screening, experimental data remains essential for final entrainer selection and reliable process development.

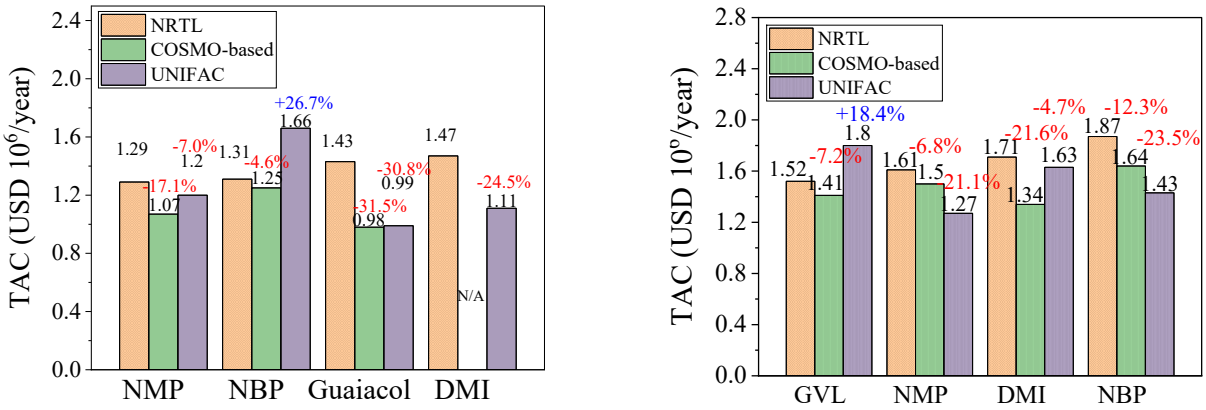


**Figure 13.** Comparison of TAC calculated using NRTL, COSMO-based, and UNIFAC models for: a) n-hexane-ethanol mixture; b) the methylcyclohexane-toluene mixture. COSMO-RS for DMI in the n-hexane-ethanol could not be performed as azeotrope for DMI-ethanol has appeared in the ERC.

## 5.8. Conclusions

The present work demonstrates that the process performances of biobased and greener entrainers in extractive distillation can be comparable to, or better than, those of the conventional entrainer NMP. The investigated greener entrainers effectively separate components in both azeotropic and close-boiling mixtures. Commercially relevant product purities were achieved, including n-hexane (>99.0 %wt) and ethanol (>99.5 %wt) for the azeotropic separation, as well as methylcyclohexane (>99.5 %wt) and toluene (>99.5 %wt) for the close-boiling mixture separation, confirming the technical feasibility of the investigated alternatives.

From an economic and sustainability perspective, the greener entrainers show competitive performance relative to NMP. In the azeotropic separation of n-hexane-ethanol, NBP, guaiacol, and DMI exhibit comparable economic and sustainability performances to NMP, with remarkably lower toxicity. For the separation of the close-boiling methylcyclohexane-toluene, GVL outperforms NMP economically and sustainably, while DMI and NBP remain comparable. These results indicate that the studied greener entrainers are not only technically feasible but also economically and environmentally viable, supporting the transition toward more eco-efficient extractive distillation.

Sensitivity analysis confirm the robustness of entrainer ranking. Reducing entrainer purity constraints and extending the payback period from 3 to 10 years

decrease TAC without altering the relative ranking of the entrainers. In contrast, increasing entrainer price leads to higher TAC for greener-based processes. Entrainer make-up costs remain minor when green entrainer prices are comparable to NMP but become increasingly significant at higher prices ratios.

Supporting analyses highlight limitations of common screening metrics and predictive models. Selectivity and capacity at infinite dilution calculated using COSMO-RS cannot adequately reflect the TAC behavior in the associating HEX-ETH mixture. Nevertheless, selectivity proves to be a reliable screening parameter for the non-associating MCH-TOL mixture, whereas capacity is not recommended. Predictive thermodynamic models (UNIFAC and COSMO-based) yield acceptable TAC deviations of less than 31% and 32%, respectively, compared to the experiment-based NRTL model, demonstrating suitability for early-stage entrainer screening. Nevertheless, predictive models may generate nonphysical azeotrope behavior in strongly associating mixture and therefore require experimental validation prior to detailed process design and scale-up.

The conclusion of this chapter should also be interpreted within several practical limitations. The optimization was performed using fixed feed compositions, whereas industrial feed compositions may vary and potentially influence separation performance and entrainer ranking. In addition, the simulations were based on theoretical equilibrium stages and therefore did not account for practical column non-idealities such as finite tray efficiency, entrainer maldistribution and foaming.

Overall, this study confirm that greener entrainers can deliver competitive economic and sustainability performances in extractive distillation. Importantly, the validated framework developed in this study provides a reliable and effective method that bridges molecular modelling, experimental study, and process-level evaluation for systematic entrainer screening and ED process design for azeotropic and close-boiling mixture separations.

## References


(1) de Haan, A. B.; Eral, H. B.; Schuur, B. *Industrial Separation Processes*; De Gruyter, 2025. https://doi.org/doi:10.1515/9783111063812.

(2) Chavez Velasco, J. A.; Tawarmalani, M.; Agrawal, R. Systematic Analysis Reveals Thermal Separations Are Not Necessarily Most Energy Intensive. *Joule* **2021**, *5* (2), 330–343. https://doi.org/https://doi.org/10.1016/j.joule.2020.12.002.

(3) Kiss, A. A.; Lange, J.-P.; Schuur, B.; Brilman, D. W. F.; van der Ham, A. G. J.; Kersten, S. R. A. Separation Technology–Making a Difference in Biorefineries. *Biomass and Bioenergy* **2016**, *95*, 296–309. https://doi.org/https://doi.org/10.1016/j.biombioe.2016.05.021.

(4) Kooijman, H. A.; Sorensen, E. Recent Advances and Future Perspectives on More Sustainable and Energy Efficient Distillation Processes. *Chem. Eng. Res. Des.* **2022**, *188*, 473–482. https://doi.org/https://doi.org/10.1016/j.cherd.2022.10.005.

(5) Gerbaud, V.; Rodriguez-Donis, I. Chapter 6 - Extractive Distillation; Górak, A., Olujić, Ž. B. T.-D., Eds.; Academic Press: Boston, 2014; pp 201–245. https://doi.org/https://doi.org/10.1016/B978-0-12-386878-7.00006-1.

(6) Zhu, J.; Sun, Y.; Chen, Y.; Wu, N.; Shi, R.; Ren, Z.; Li, Q.; Zhao, H. Isobaric Vapor–Liquid Equilibrium Experiments of Methyl Propionate + Ethanol with Different Ionic Liquids at 101.3 KPa. *J. Chem. Eng. Data* **2025**, *70* (1), 427–438. https://doi.org/10.1021/acs.jced.4c00517.

(7) Sherwood, J.; Farmer, T. J.; Clark, J. H. Catalyst: Possible Consequences of the N-Methyl Pyrrolidone REACH Restriction. *Chem* **2018**, *4* (9), 2010–2012. https://doi.org/https://doi.org/10.1016/j.chempr.2018.08.035.

(8) Kirman, C. R.; Sonawane, B. R.; Seed, J. G.; Azu, N. O.; Barranco, W. T.; Hamilton, W. R.; Stedeford, T. J.; Hays, S. M. An Evaluation of Reproductive Toxicity Studies and Data Interpretation of N-Methylpyrrolidone for Risk Assessment: An Expert Panel Review. *Regul. Toxicol. Pharmacol.* **2023**, *138*, 105337. https://doi.org/https://doi.org/10.1016/j.yrtph.2023.105337.

(9) Li, J.; Li, T.; Peng, C.; Liu, H. Extractive Distillation with Ionic Liquid Entrainers for the Separation of Acetonitrile and Water. *Ind. Eng. Chem. Res.* **2019**, *58* (14), 5602–5612. https://doi.org/10.1021/acs.iecr.8b05907.

(10) Liu, J.; Yin, Y.; Dai, S.; Liu, B.; Wang, Q. Mechanistic Analysis and Process Simulation of Ethyl Acetate-Ethanol Separation by Complex Solvent Extractive Distillation. *ACS Omega* **2024**, *9* (24), 26596–26606. https://doi.org/10.1021/acsomega.4c03270.

(11) Ayuso, M.; Navarro, P.; Moya, C.; Moreno, D.; Palomar, J.; García, J.; Rodríguez, F. Extractive Distillation with Ionic Liquids To Separate Benzene, Toluene, and Xylene from Pyrolysis Gasoline: Process Design and Techno-Economic Comparison with the Morphylane Process. *Ind. Eng. Chem. Res.* **2022**, *61* (6), 2511–2523. https://doi.org/10.1021/acs.iecr.1c04363.

(12) Ghuge, P. D.; Mali, N. A.; Joshi, S. S. Comparative Analysis of Extractive and Pressure Swing Distillation for Separation of THF-Water Separation. *Comput. Chem. Eng.* **2017**, *103*, 188–200. https://doi.org/https://doi.org/10.1016/j.compchemeng.2017.03.019.

(13) Simasatitkul, L.; Kaewwisetkul, P.; Arpornwichanop, A. Techno-Economic Assessment of Extractive Distillation for Tert-Butyl Alcohol Recovery in Fuel Additive Production. *Chem. Eng. Process. Process Intensif.* **2017**, *122*, 161–171.

https://doi.org/https://doi.org/10.1016/j.cep.2017.10.004.
(14) Minor, A.-J.; Hartanto, D.; de Haan, A. B. Assessment of Deep Eutectic Solvents for Alcohol-Water Separations by Extractive Distillation. In *The 12th international conference Distillation & Absorption 2022*; 2022.
(15) Yin, L.; Hu, Y.; Li, Y.; Jiang, S.; Gao, N. Extractive Distillation Using Salt-Based Deep Eutectic Solvent as Entrainer for Separating Acetonitrile-Water Mixture. *J. Mol. Liq.* **2024**, *414*, 126120. https://doi.org/https://doi.org/10.1016/j.molliq.2024.126120.
(16) Malik, H.; Khan, H. W.; Hassan Shah, M. U.; Ahmad, M. I.; Khan, I.; Al-Kahtani, A. A.; Sillanpää, M. Screening of Ionic Liquids as Green Entrainers for Ethanol Water Separation by Extractive Distillation: COSMO-RS Prediction and Aspen plus Simulation. *Chemosphere* **2023**, *311*, 136901. https://doi.org/https://doi.org/10.1016/j.chemosphere.2022.136901.
(17) Li, J.; Li, R.; Yang, J.; Li, S.; Zhang, Z.; Liu, H.; Ma, Z.; Sun, L. Biobased Solvents as Entrainers for Extractive Distillation in Isobutyl Acetate–Isobutanol Separation: Experimental Investigation, Toxicity Evaluation, and Mechanism Analysis. *J. Chem. Eng. Data* **2025**, *70* (11), 4648–4663. https://doi.org/10.1021/acs.jced.5c00514.
(18) Gomes, J. P.; Silva, R.; Nunes, C. P.; Barbosa, D. Towards Sustainable Industrial Processes: A Preselection Method for Screening Green Solvents in the 1,3-Butadiene Extractive Distillation Process. *Sustainability*. 2025. https://doi.org/10.3390/su17083285.
(19) Manyoni, L.; Kabane, B.; Redhi, G. G. Deep Eutectic Solvent as a Possible Entrainer for Industrial Separation Problems: Pre-Screening Tool for Solvent Selection. *Fluid Phase Equilib.* **2022**, *553*, 113266. https://doi.org/https://doi.org/10.1016/j.fluid.2021.113266.
(20) Bai, F.; Hua, C.; Li, J. Separation of Benzene-Cyclohexane Azeotropes Via Extractive Distillation Using Deep Eutectic Solvents as Entrainers. *Processes* . 2021. https://doi.org/10.3390/pr9020336.
(21) Khan, A. S.; Ibrahim, T. H.; Rashid, Z.; Khamis, M. I.; Nancarrow, P.; Jabbar, N. A. COSMO-RS Based Screening of Ionic Liquids for Extraction of Phenolic Compounds from Aqueous Media. *J. Mol. Liq.* **2021**, *328*, 115387. https://doi.org/https://doi.org/10.1016/j.molliq.2021.115387.
(22) Momoh, S. O. Assessing the Accuracy of Selectivity as a Basis for Solvent Screening in Extractive Distillation Processes. *Sep. Sci. Technol.* **1991**, *26* (5), 729–742. https://doi.org/10.1080/01496399108049911.
(23) Kossack, S.; Kraemer, K.; Gani, R.; Marquardt, W. A Systematic Synthesis Framework for Extractive Distillation Processes. *Chem. Eng. Res. Des.* **2008**, *86* (7), 781–792. https://doi.org/https://doi.org/10.1016/j.cherd.2008.01.008.
(24) Larriba, M.; de Riva, J.; Navarro, P.; Moreno, D.; Delgado-Mellado, N.; García, J.; Ferro, V. R.; Rodríguez, F.; Palomar, J. COSMO-Based/Aspen Plus Process Simulation of the Aromatic Extraction from Pyrolysis Gasoline Using the {[4empy][NTf2] + [Emim][DCA]} Ionic Liquid Mixture. *Sep. Purif. Technol.* **2018**, *190*, 211–227. https://doi.org/https://doi.org/10.1016/j.seppur.2017.08.062.
(25) Ferro, V. R.; Moya, C.; Moreno, D.; Santiago, R.; de Riva, J.; Pedrosa, G.; Larriba, M.; Diaz, I.; Palomar, J. Enterprise Ionic Liquids Database (ILUAM) for Use in Aspen ONE Programs Suite with COSMO-Based Property Methods. *Ind. Eng. Chem. Res.* **2018**, *57* (3), 980–989. https://doi.org/10.1021/acs.iecr.7b04031.

(26) Taylor, R. .; Koojiman H.A.; Klamt, A. .; Eckert, F. Distillation Simulation with COSMO-RS. In *Distillation & Absorption Conference*; Baden-Baden, 2002.
(27) Yin, L.; Li, Y.; Hu, Y.; Wang, J.; Xue, Y.; Duan, W.; He, Y.; Tang, S.; Fu, T. Energy-Saving Extractive Distillation Using Salt-Based DESs as an Entrainer for Separating 2-Propanol and Water Mixture. *J. Water Process Eng.* **2025**, *72*, 107433. https://doi.org/https://doi.org/10.1016/j.jwpe.2025.107433.
(28) Zhang, Z.; Wang, J.; Zhu, K.; Li, S.; Li, M.; Fan, X.; Gao, J. An Efficient Heat-Pump Extractive Distillation Process for Recovering Lower Alcohols from Bioethanol Fusel Oil. *Chem. Eng. Process. - Process Intensif.* **2025**, *213*, 110291. https://doi.org/https://doi.org/10.1016/j.cep.2025.110291.
(29) Hu, N.; Zhang, J.; Yuan, S.; Zhang, Y.; Li, Q. Design of Extractive Distillation Considering the Effect of Feed Components on the Separation of Multiazeotropic Systems. *Ind. Eng. Chem. Res.* **2025**, *64* (16), 8442–8451. https://doi.org/10.1021/acs.iecr.5c00689.
(30) Cruz Valdez, J. A.; Patiño-Herrera, R.; Avilés Martínez, A.; Pérez, E. Separation of the Cyclohexane-Benzene Mixture by the Extractive Distillation Process Using Ethylene Glycol as a Solvent. *Chem. Eng. Process. - Process Intensif.* **2024**, *196*, 109686. https://doi.org/https://doi.org/10.1016/j.cep.2024.109686.
(31) Hartanto, D.; Schuur, B.; A. Kiss, A.; de Haan, A. B. Isobaric Vapor-Liquid Equilibrium of the Azeotropic Mixture n-Hexane + Ethanol with 1-Butylpyrrolidin-2-One as a Greener Entrainer and 1-Methylpyrrolidin-2-One as a Benchmark Entrainer. *J. Chem. Eng. Data* **2025**, *70* (10), 4091−4104.
(32) Brouwer, T.; Schuur, B. Comparison of Solvent-Based Affinity Separation Processes Using Cyrene and Sulfolane for Aromatic/Aliphatic Separations. *J. Chem. Technol. Biotechnol.* **2021**, *96* (9), 2630–2646. https://doi.org/https://doi.org/10.1002/jctb.6808.
(33) Liang, S.; Cao, Y.; Liu, X.; Li, X.; Zhao, Y.; Wang, Y.; Wang, Y. Insight into Pressure-Swing Distillation from Azeotropic Phenomenon to Dynamic Control. *Chem. Eng. Res. Des.* **2017**, *117*, 318–335. https://doi.org/https://doi.org/10.1016/j.cherd.2016.10.040.
(34) *Aspen Plus Software, Version 12.0*; Aspen Technology, Inc., 2020.
(35) Powell, M. J. D. *The BOBYQA Algorithm for Bound Constrained Optimization without Derivatives, Report No. DAMTP 2009/NA06*; 2009.
(36) Negrellos-Ortiz, I.; Flores-Tlacuahuac, A.; Gutiérrez-Limón, M. A. Dynamic Optimization of a Cryogenic Air Separation Unit Using a Derivative-Free Optimization Approach. *Comput. Chem. Eng.* **2018**, *109*, 1–8. https://doi.org/https://doi.org/10.1016/j.compchemeng.2017.10.020.
(37) da Silva, J. O.; de Farias Gonçalves, R. C.; Brito, K. D.; Ramos, W. B.; Brito, R. P. Rigorous Energetic Analysis of the Pressure-Swing Distillation Process. *Chem. Eng. Res. Des.* **2022**, *186*, 556–567. https://doi.org/https://doi.org/10.1016/j.cherd.2022.08.032.
(38) Gilliland, E. R. Multicomponent Rectification Estimation of the Number of Theoretical Plates as a Function of the Reflux Ratio. *Ind. Eng. Chem.* **1940**, *32* (9), 1220–1223. https://doi.org/10.1021/ie50369a035.
(39) Fenske, M. R. Fractionation of Straight-Run Pennsylvania Gasoline. *Ind. Eng. Chem.* **1932**, *24* (5), 482–485. https://doi.org/10.1021/ie50269a003.
(40) Underwood, A. J. V. Fractional Distillation of Multicomponent Mixtures. *Ind. Eng. Chem.* **1949**, *41* (12), 2844–2847. https://doi.org/10.1021/ie50480a044.

(41) Eduljee, H. E. Equations Replace Gilliland Plot. *Hydrocarb. Process.* **1975**, *54* (9), 120–122.
(42) Huang, X.; Jin, Y.; Fang, C.; Yang, W.; Li, Z.; Tian, Y. Process Simulation and Optimization of Extractive Distillation for Separating Isopropanol-Ethanol from IBE Fermentation Broth as a Gasoline Additive. *Ind. Crops Prod.* **2025**, *236*, 121853. https://doi.org/https://doi.org/10.1016/j.indcrop.2025.121853.
(43) Liu, L.; Zhu, L.; Sun, L.; Zhu, M.; Liu, G. Simulation and Optimization of Different Pressure Thermally Coupled Distillation for Separating a Close-Boiling Mixture of n-Butanol and Iso-Butanol. *Appl. Petrochemical Res.* **2017**, *7* (2), 143–150. https://doi.org/10.1007/s13203-017-0186-1.
(44) Teh, I. A. X.; Lee, H.-Y.; Kong, Z. Y.; Aqsha, A.; Sunarso, J. An Improved and Extended Approach to Design Heat-Integrated Side-Stream Reactive Distillation. *Chem. Eng. Res. Des.* **2025**, *221*, 81–96. https://doi.org/https://doi.org/10.1016/j.cherd.2025.07.045.
(45) Liaoning Yugeng Chemical Co. Ltd. *n-Hexane*. http://www.yfhexane.com/product_detail_en/17.html (accessed 2025-12-19).
(46) JunYuan Petroleum Group. *n-Hexane*. https://junyuanpetroleumgroup.com/product/hexane/ (accessed 2025-12-19).
(47) FUJIFILM Wako Pure Chemical Corporation. *Ethanol*. https://labchem-wako.fujifilm.com/europe/product/detail/W01W0105-0045.html (accessed 2025-12-19).
(48) Penpet Petrochemical Trading GmBH. *Methylcyclohexane*; Hamburg, 2022. https://www.penpet.com/fileadmin/user_upload/Produkte/Methylcyclohexan/English/Methylcyclohexane-product-no-16398.pdf.
(49) Japanese Industrial Standards. *Toluene, JIS K 8680:2006*; 2006.
(50) Coca, J.; Pis, J. J. Effect of Morpholine on the Vapor-Liquid Equilibrium of the System Methylcyclohexane-Toluene. *J. Chem. Eng. Data* **1979**, *24* (2), 103–105. https://doi.org/10.1021/je60081a017.
(51) Liebert, V.; Nebig, S.; Gmehling, J. Experimental and Predicted Phase Equilibria and Excess Properties for Systems with Ionic Liquids. *Fluid Phase Equilib.* **2008**, *268* (1), 14–20. https://doi.org/https://doi.org/10.1016/j.fluid.2008.03.011.
(52) Gutierrez, J. P.; Meindersma, W.; de Haan, A. B. Ionic Liquid Selection and Performance Evaluation for The Separation Of Methylcyclohexane/Toluene by Extractive Distillation. In *Distillation absorption 2010 : conference proceedings*; Technische Universiteit Eindhoven: Eindhoven, 2010.
(53) Tiverios, P. G.; Van Brunt, V. Extractive Distillation Solvent Characterization and Shortcut Design Procedure for Methylcyclohexane−Toluene Mixtures. *Ind. Eng. Chem. Res.* **2000**, *39* (6), 1614–1623. https://doi.org/10.1021/ie990654k.
(54) Douglas, J. *Conceptual Design of Chemical Process*; McGraw-Hill: New York, 1988.
(55) Zhang, X.; Li, X.; Li, G.; Zhu, Z.; Wang, Y.; Xu, D. Determination of an Optimum Entrainer for Extractive Distillation Based on an Isovolatility Curve at Different Pressures. *Sep. Purif. Technol.* **2018**, *201*, 79–95. https://doi.org/https://doi.org/10.1016/j.seppur.2018.03.007.
(56) Chandra, A. K.; Patraşcu, I.; Bîldea, C. S.; Kiss, A. A. Eco-Efficient Separation of Mono- and Dichloroacetic Acid by Thermally Coupled Extractive Distillation. *Chem. Eng. Technol.* **2020**, *43* (12), 2403–2417. https://doi.org/https://doi.org/10.1002/ceat.202000232.

(57) Beaver, E.; Schwarz, J. M.; Beloff, B. R. Use Sustainability Metrics to Guide Decision-Making. *Chem. Eng. Prog.* **2002**, *98*, 58–63.
(58) Institution of Chemical Engineers. *The Sustainability Metrics: Sustainable Development Progress Metrics Recommended for Use in the Process Industries*; Rugby, 2010. https://www.icheme.org/media/16021/sustainability-metrics.pdf.
(59) Prat, D.; Wells, A.; Hayler, J.; Sneddon, H.; McElroy, C. R.; Abou-Shehada, S.; Dunn, P. J. CHEM21 Selection Guide of Classical- and Less Classical-Solvents. *Green Chem.* **2016**, *18* (1), 288–296. https://doi.org/10.1039/C5GC01008J.
(60) European Chemical Agency. *ECHA Chemicals database*. https://chem.echa.europa.eu/ (accessed 2025-11-06).
(61) Xu, Z.; Wang, Y.; Li, J.; Wu, H.; Pan, J.; Ye, Q. Multi-Objective Optimization and Performance Evaluation for the Recovery of Isopropanol and Benzene from Effluent via Side-Stream Extractive Distillation with Intermediate Reboiler Processes. *Sep. Purif. Technol.* **2025**, *358*, 130338. https://doi.org/https://doi.org/10.1016/j.seppur.2024.130338.
(62) Wang, Y.; Wang, S.; Shan, B.; Ma, Y.; Xu, Q.; Wang, Y.; Cui, P.; Zhang, F. Sustainable Process Design and Multi-Objective Optimization of Efficient and Energy-Saving Separation of Xylene Isomers via Extractive Distillation Based on Double Extractants. *Sep. Purif. Technol.* **2025**, *354*, 128899. https://doi.org/https://doi.org/10.1016/j.seppur.2024.128899.
(63) Tian, X.; Wang, R.; Wang, H.; Li, C.; Liu, J. Energy-Saving Extractive Distillation Processes Design and Optimization for the Separation of Ethyl Acetate and n-Heptane Azeotrope. *Fuel* **2025**, *379*, 132974. https://doi.org/https://doi.org/10.1016/j.fuel.2024.132974.
(64) Gutierrez Hernandez, J. P. Extractive Distillation with Ionic Liquids as Solvents : Selection and Conceptual Process Design, Technische Universiteit Eindhoven, 2013. https://doi.org/10.6100/IR751728.
(65) Hartanto, D.; Schuur, B.; Schuttevaer, T.; Kiss, A. A.; de Haan, A. B. Isobaric Vapor–Liquid Equilibrium of Methylcyclohexane + Toluene with Gamma-Valerolactone as a Biobased Entrainer and 1-Methylpyrrolidin-2-One as a Conventional Entrainer. *J. Chem. Eng. Data* **2025**, *70* (3), 1339−1351. https://doi.org/10.1021/acs.jced.4c00509.
(66) Hartanto, D.; Schuur, B.; Kiss, A. A.; de Haan, A. B. Effective Selection of Green Organics and Natural Deep Eutectic Solvents as Advanced Entrainers by COSMO-RS and Group Contributions Methods for Enhanced Design of Extractive Distillation. In *Computer Aided Chemical Engineering*; Manenti, F., Reklaitis, G. V. B. T.-C. A. C. E., Eds.; Elsevier, 2024; Vol. 53, pp 1387–1392. https://doi.org/https://doi.org/10.1016/B978-0-443-28824-1.50232-5.
(67) Hartanto, D.; Schuur, B.; Kiss, A. A.; de Haan, A. B. Vapor-Liquid Equilibrium for the Separation of the n-Hexane + Ethanol Azeotropic Mixture with Biobased Entrainers Guaiacol and Dimethyl Isosorbide. *Fluid Phase Equilib.* **2026**, *605*, 114694. https://doi.org/https://doi.org/10.1016/j.fluid.2026.114694.
(68) Hartanto, D.; Schuur, B.; Ammerlaan, M.; Kiss, A. A.; de Haan, A. B. Vapor–Liquid Equilibrium for the Separation of the Close-Boiling Mixture Methylcyclohexane–Toluene with Dimethyl Isosorbide as a Biobased Entrainer and 1-Butylpyrrolidin-2-One as a Greener Entrainer. *Ind. Eng. Chem. Res.* **2025**, *64* (38), 18927–18937. https://doi.org/10.1021/acs.iecr.5c01616.
(69) Blum, C.; Zeschmar-Lahl, B.; Heidbüchel, E.; Stolzenberg, H. C.; Kümmerer, K.;

Becker, A.; Friege, H. Metrics Are the Key: Development of Criteria and Indicators for Measuring Sustainability in International Chemicals Management. *RSC Sustain.* **2025**, *3* (10), 4724–4745. https://doi.org/10.1039/D5SU00135H.
(70) Blömer, J.; Maga, D.; Röttgen, J.; Wu, Z.; Hiebel, M.; Eilebrecht, S.; Jentsch, S.; Eggers, N. Assessment of Chemical Products and Processes: Green Metrics and Life Cycle Assessment – A Comparison. *Chemie Ing. Tech.* **2024**, *96* (5), 561–574. https://doi.org/https://doi.org/10.1002/cite.202300229.
(71) Wang, F.; Wang, S.; Li, Z.; You, H.; Aviso, K. B.; Tan, R. R.; Jia, X. Water Footprint Sustainability Assessment for the Chemical Sector at the Regional Level. *Resour. Conserv. Recycl.* **2019**, *142*, 69–77. https://doi.org/https://doi.org/10.1016/j.resconrec.2018.11.009.
(72) Spearman, C. The Proof and Measurement of Association between Two Things. *Am. J. Psychol.* **1904**, *15* (1), 72–101. https://doi.org/10.2307/1412159.
(73) Harmsen, J.; de Haan, A. B.; Swinkels, P. L. J. *Product and Process Design: Driving Sustainable Innovation*; De Gruyter: Berlin, Boston, 2024. https://doi.org/doi:10.1515/9783110782127.

(*This page is intentionally left blank*)

# Chapter 6

## Conclusions and future outlook

## 6.1. Conclusions

In this work, greener entrainer were screened using a multi-stage selection method to identify potential candidates for extractive distillation (ED). The screening results identified GVL, NBP, and DMI as promising candidates, alongside the benchmark entrainer NMP, for separating the close-boiling methylcyclohexane-toluene mixture. For the azeotropic mixture of n-hexane-ethanol, the selected greener entrainers included NBP, guaiacol, and DMI, along with NMP. Reliable vapor-liquid equilibrium (VLE) data were measured to provide a robust thermodynamic basis and optimum binary interaction parameters for effective ED process design, as well as to confirm the separation performance of the selected entrainers. All measured data passed the thermodynamic consistency test, indicating their reliability. The results demonstrated that these entrainers significantly increased relative volatility and effectively removed the close-boiling and azeotropic behavior. Finally, the ED process performances of the selected greener entrainers were evaluated and compared against the benchmark entrainer NMP to determine their suitability as alternatives to NMP based on economic and multiple-sustainability metrics. The findings revealed that the selected greener entrainers achieved comparable or outperform economic and sustainability performance, while exhibiting significantly lower toxicity compared to NMP. Predictive tools for ED were examined concerning their use and limitations. These tools are reliable for use in early-stage entrainer screening and preliminary ED design. However, for the detailed process design, experimental data is required.

Overall, the framework effectively identified greener entrainers that are technically feasible, economically viable, and environmentally preferable for separating both the close-boiling methylcyclohexane-toluene mixture and the azeotropic n-hexane-ethanol mixture.

## 6.2. Future outlook

The predictive model based on quantum chemical calculation (COSMO-RS) and group contribution methods (UNIFAC and modified UNIFAC-Dortmund) proved reliable for the early-stage screening of greener entrainers. However, the prediction of NADESs cannot currently be performed using UNIFAC and modified UNIFAC-Dortmund, as the required parameters and methodological framework for representing NADESs are not yet available. Therefore, future work should focus on developing suitable functional group parameters for NADESs through new VLE data

measurements and establishing robust methodological approaches for implementing NADESs in UNIFAC-based models.

Several NADESs, including ChCl–Malic acid (1:1), ChCl–Oxalic acid (1:1), Betaine–Malic acid (1:1), Proline–Oxalic acid (1:1), and ChCl–Glutaric acid (1:1), were successfully synthesized. Unfortunately, these NADESs formed heterogeneous mixtures with the investigated nonpolar systems, limiting their applicability for such separations. To address this miscibility challenge, a potential direction for future research is the use of mixed greener entrainers. Combining these NADESs with greener entrainers, such as GVL, DMI, NBP, or guaiacol at appropriate concentrations, may enable synergistic effects that improve separation performance while maintaining complete miscibility in nonpolar systems. In contrast, these NADESs exhibited homogeneous mixtures in the polar system of the ethanol-water mixture, and showed favorable separation based on predictive selectivity results. Further experimental studies are therefore recommended to measure relative volatility and VLE data for the ethanol-water mixtures containing these NADESs. Subsequent process simulation works could then be performed to evaluate their economic and sustainability performance relative to the benchmark entrainer. In addition, the applicability of these NADESs could be explored for other polar mixture separations.

Regarding process design and simulations, this study employed conventional ED process configuration. Future research could explore process intensification strategies, such as integrating heat pumps or applying a dividing-wall column in the ED system, to further reduce energy consumption and operational costs. Sensitivity of process performance and entrainer ranking to feed composition variations could be conducted, as it can more represent industrial practices where feed composition may vary. Moreover, for the detailed design, the practical non-idealities of the column, including tray efficiency, entrainer maldistribution, and foaming should be considered to be included in the process design. These approaches could be particularly promising when applied to the best-performing greener entrainers identified in this work, for example, GVL the methylcyclohexane-toluene separation and NBP for the n-hexane-ethanol separation. According to the process simulation results, methylcyclohexane-toluene-GVL and n-hexane-ethanol-NBP, along with NMP, are the readiest for pilot-scale ED experiments. For the NBP and DMI in the methylcyclohexane-toluene mixture, and guaiacol and DMI in the n-hexane-ethanol mixture, are suggested as secondary options for the pilot-scale evaluation.

This can validate the practical applicability of the proposed greener entrainers compared to conventional entrainer. Such studies would provide valuable insights into operational stability, entrainer recovery, and long-term performance under industrially relevant conditions.

# Appendix

## Appendix A

**Table A1** The chemical specification.

| Chemical | Source | Purity (wt%) | Molecular structure |
|---|---|---|---|
| Methylcyclohexane | Merck | >99% | 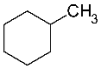 |
| Toluene | Merck | >99% |  |
| n-Hexane | Merck | ≥99% | 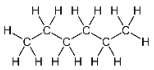 |
| Ethanol | Merck | ≤100% | 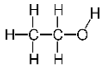 |
| Sulfolane | Merck | ≥99% |  |
| N-Formylmorpholine | Thermo scientific | ≥99% |  |
| Propylene carbonate | Sigma-Aldrich | ≥99.7% | 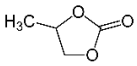 |
| Glycerol carbonate | TCI | >90.0% | 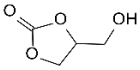 |
| Diethyl carbonate | Sigma-Aldrich | 99% | 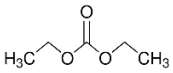 |
| Ethylene carbonate | Thermo scientific | >99% |  |
| Diphenyl carbonate | Sigma-Aldrich | 99% | 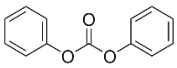 |
| Dimethyl isosorbide | Sigma-Aldrich | ≥99% |  |
| 1-Butylpyrrolidin-2-one | BioPSX | 99.5% | 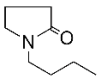 |
| gamma-Valerolactone | Sigma-Aldrich | ≥99.9% | 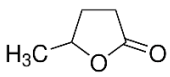 |
| Butyl butanoate | Sigma-Aldrich | 98% | 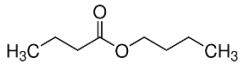 |
| 1-Methyl-2-pyrrolidinone | Sigma-Aldrich | 99% |  |

| Chemical | Source | Purity (wt%) | Molecular structure |
|---|---|---|---|
| Choline chloride | VWR | 99% | 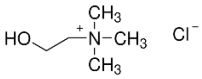 |
| β-Alanine | VWR | 99% | 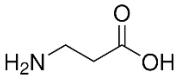 |
| L-Proline | VWR | ≥99% | 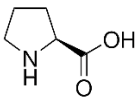 |
| DL-Malic acid | VWR | ≥99% | 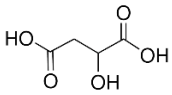 |
| Oxalic acid | Merck | 99% | 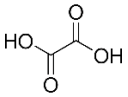 |
| Glutaric acid | Merck | ≥99% | 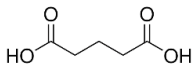 |
| Adonitol | Merck | ≥99% | 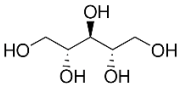 |
| Maltitol | VWR | 97% | 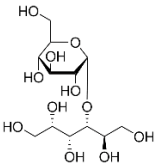 |
| D-Sorbitol | Merck | ≥99% | 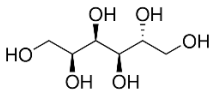 |
| Cyrene | Circa | 99% |  |
| Guaiacol | Across Organics | >99% | 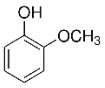 |
| Acetone | Merck | ≥ 99.8 % | 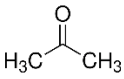 |

## Appendix B

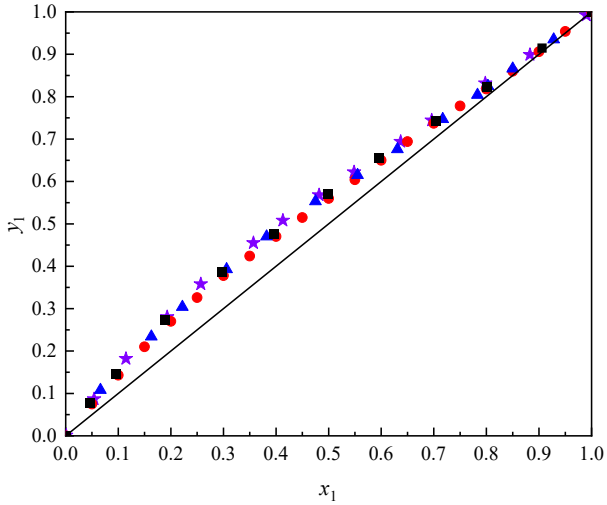


**Figure B1.** *x-y* diagram for methylcyclohexane (1) + toluene (2) at 101.3 kPa: (■), this work; (●), literature (Quiggle and Fenske[1]); (▲), literature (Coca and Pis[2]); and at 53.3 kPa: (★), literature (Weber[3]).

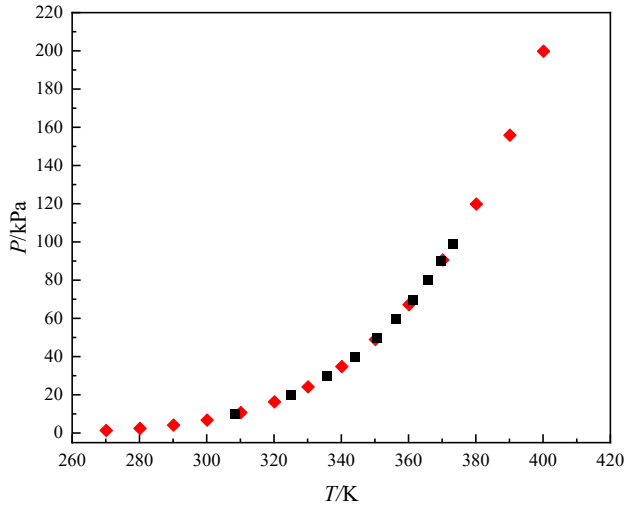


**Figure B2.** Vapor pressure measurement of methylcyclohexane (■), this work; (♦), literature (Yaws and Yang)[4].

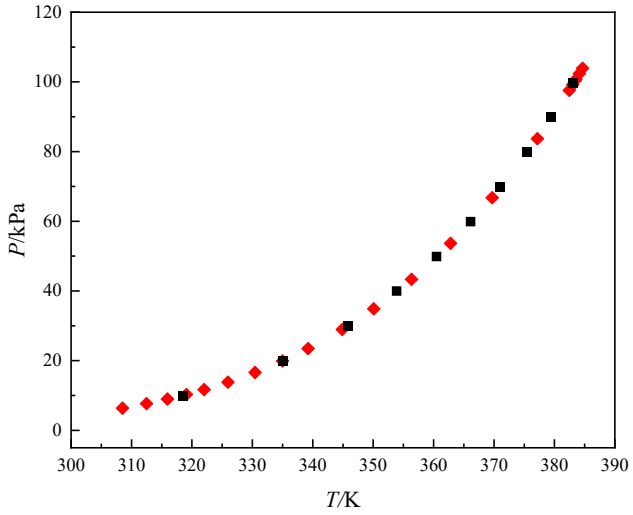


**Figure B3.** Vapor pressure measurement of toluene (■), this work; (♦), literature (Willingham et al.[5])

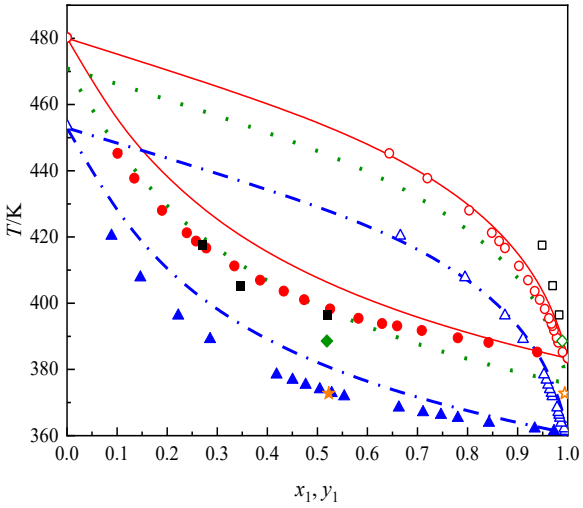


**Figure B4.** *T-xy* diagram for toluene (1) + gamma-valerolactone (2), experimental from this work: (■), $x_1$ and (□), $y_1$ at 100 kPa; (♦), $x_1$ and (◊), $y_1$ at 80 kPa (★), $x_1$ and (☆), $y_1$ at 50 kPa; experimental from literature (Al-Lami et al[6]): (●), $x_1$ and (○), $y_1$ at 101.3 kPa; (▲), $x_1$ and (Δ), $y_1$ at 50.7 kPa; UNIQUAC-HOC prediction: (—), at 100 kPa; (- -), at 80 kPa, and (- · -), at 50 kPa.

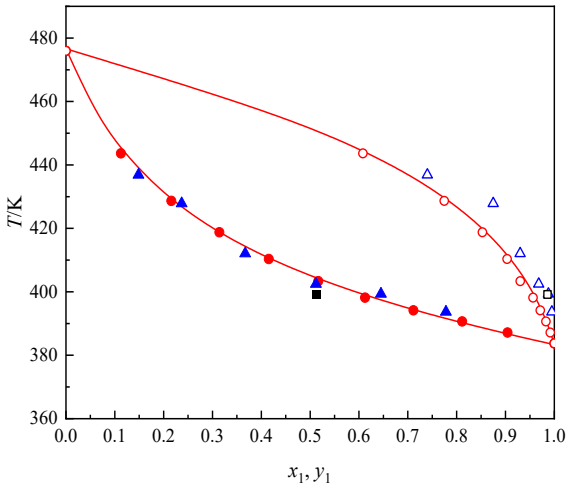


**Figure B5.** *T-xy* diagram for toluene (1) + 1-methylpyrrolidin-2-one (2), experimental from this work: (■), $x_1$ and (□), $y_1$ at 100 kPa; experimental from literatures: (●), $x_1$ and (○), $y_1$ at 101.3 kPa (Gupta et al[7]); (▲), $x_1$ and (Δ), $y_1$ at 101.3 kPa (Zaretskii et al[8]); UNIQUAC-HOC prediction: (—), at 100 kPa.

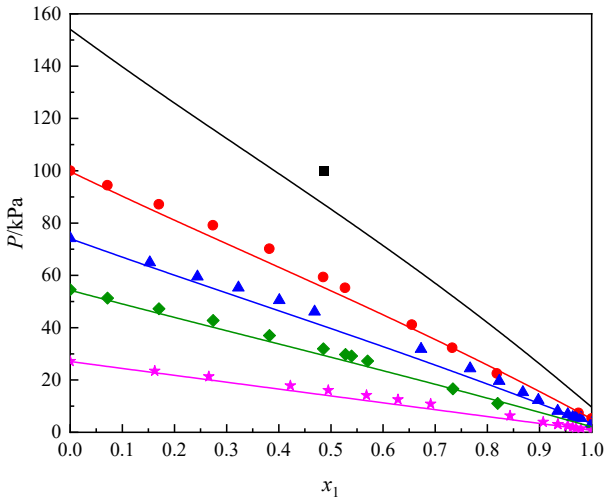


**Figure B6.** *x-P* diagram for 1-methylpyrrolidin-2-one (1) + toluene (2): this work, (■), at 399.15 K; literature (Gierycz et al[9]), (●), at 383.35 K, and (♦), at 363.25 K; literature (Linek et al[10]), (▲), at 373.15 K, and (★), at 343.15 K; UNIQUAC-HOC prediction: (—), black line for 399.15 K, red line for 383.15 K, blue line for 373.15 K, green line for 363.25 K, and magenta line for 343.15 K.

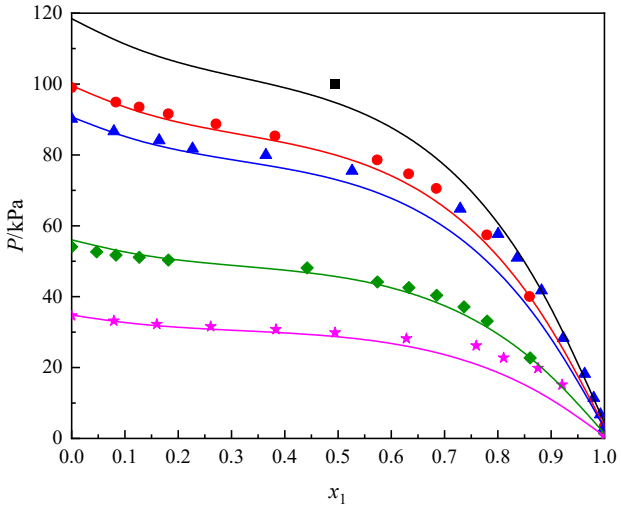


**Figure B7.** *x-P* diagram for 1-methylpyrrolidin-2-one (1) + methylcyclohexane (2): this work, (■), at 379.52 K; literature (Gierycz et al[9]), (●), at 373.25 K, and (♦), at 354.15 K; literature (Linek et al[10]), (▲), at 370.00 K, and (★), at 340.00 K; UNIQUAC-HOC prediction: (—), black line for 379.52 K, red line for 373.25 K, blue line for 370.00 K, green line for 354.15 K, and magenta line for 340.00 K.

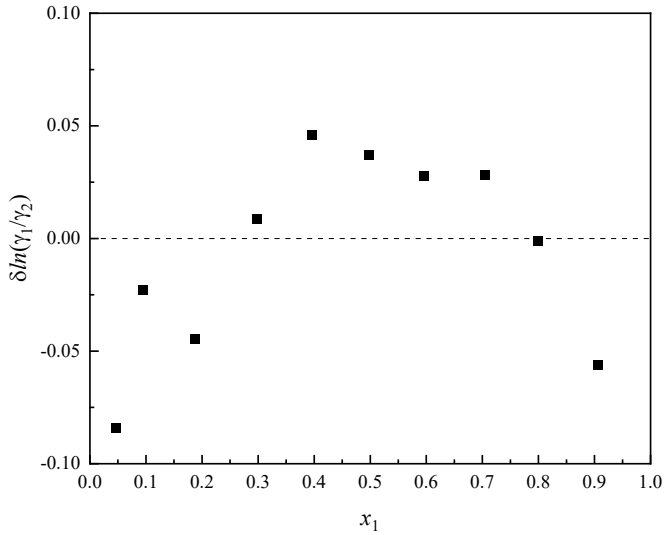


**Figure B8.** Residual distribution of $\ln(\gamma_1 / \gamma_2)$ for methylcyclohexane (1) + toluene (2) at 101.3 kPa.

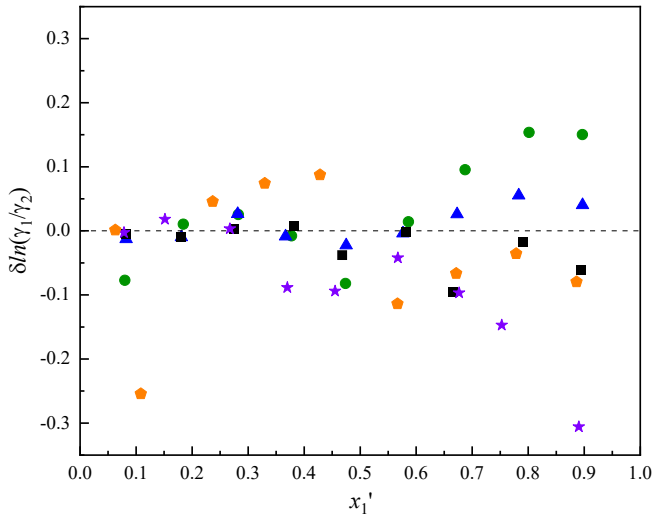


**Figure B9.** Residual distribution of $\ln(\gamma_1 / \gamma_2)$ for methylcyclohexane (1) + toluene (2) + gamma-valerolactone (3) with E/F = 1: (■) at 100 kPa; (▲), 80 kPa; (●), 50 kPa, and with E/F = 2: (★), and E/F = 3: (⬟) at 100 kPa.

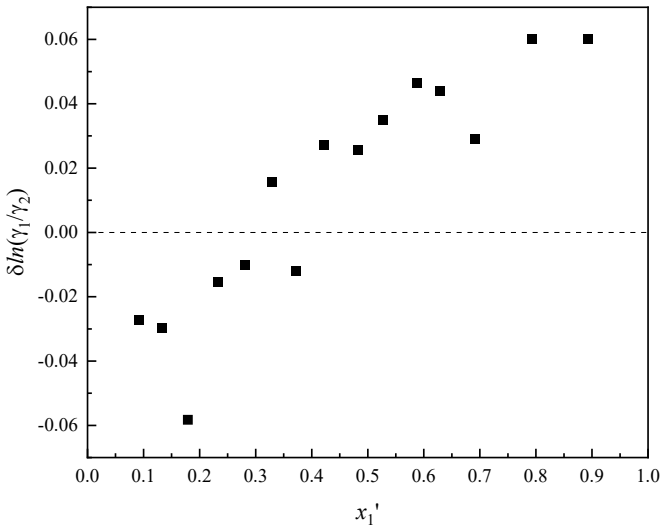


**Figure B10.** Residual distribution of $\ln(\gamma_1 / \gamma_2)$ for methylcyclohexane (1) + toluene (2) + 1-methylpyrrolidin-2-one (3) with E/F = 1 at 100 kPa.

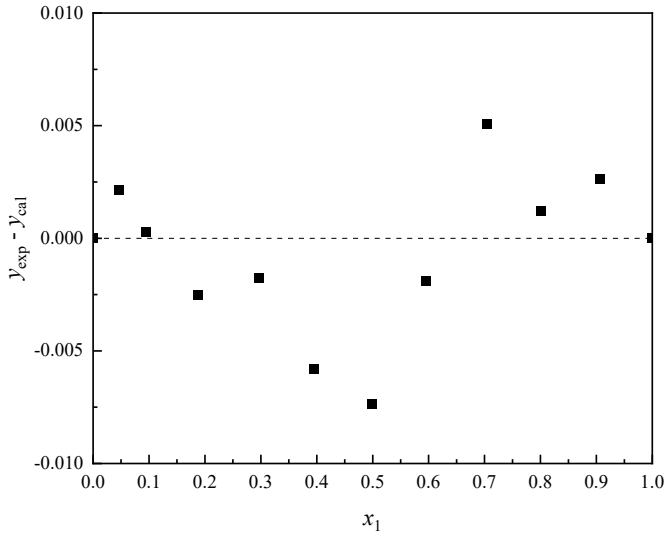


**Figure B11.** Residual plots of vapor composition for methylcyclohexane (1) + toluene (2) at 101.3 kPa.

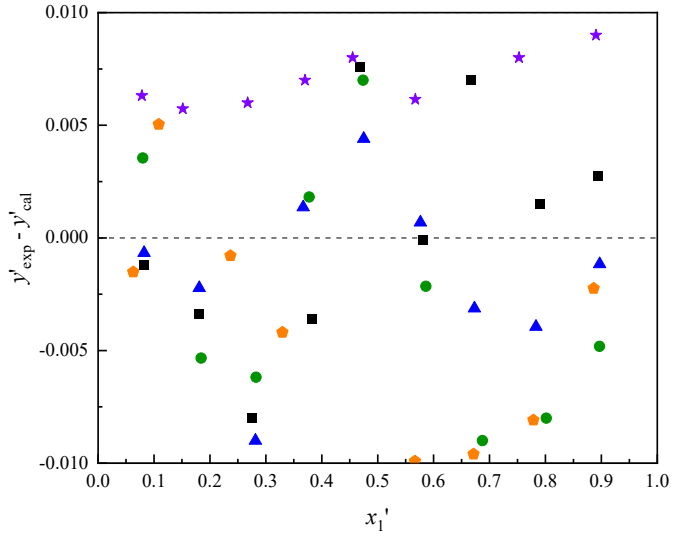


**Figure B12.** Residual plots of vapor composition for methylcyclohexane (1) + toluene (2) + gamma-valerolactone (3) with E/F = 1: (■) at 100 kPa; (▲), 80 kPa; (●), 50 kPa, and with E/F = 2: (★), and E/F = 3: (⬟) at 100 kPa.

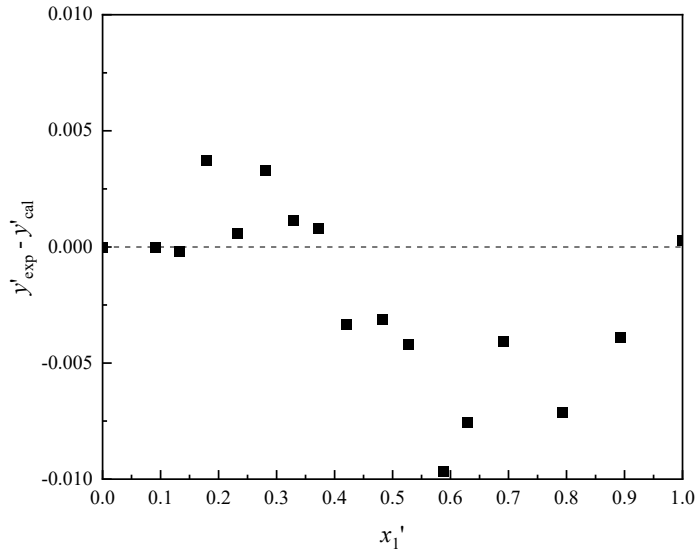


**Figure B13.** Residual plots of vapor composition for methylcyclohexane (1) + toluene (2) + 1-methylpyrrolidin-2-one (3) with E/F = 1 at 100 kPa.

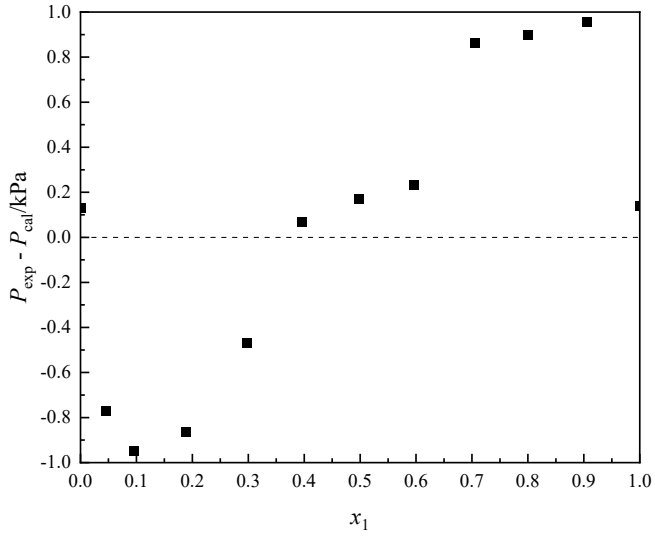


**Figure B14.** Residual plots of pressure (kPa) for methylcyclohexane (1) + toluene (2) at 101.3 kPa.

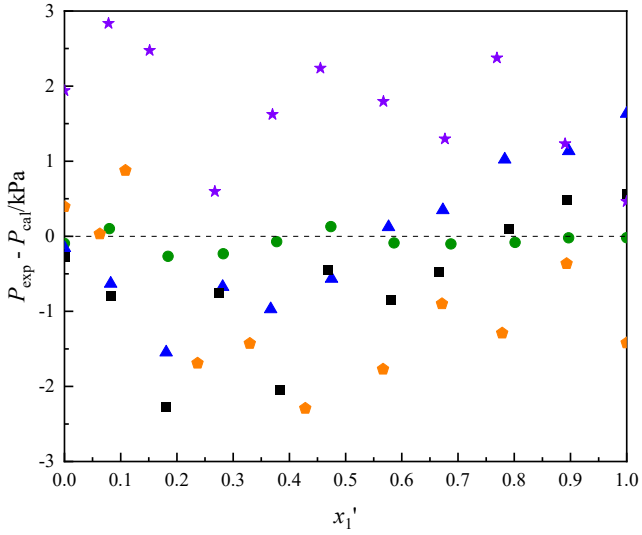


**Figure B15.** Residual plots of pressure (kPa) for methylcyclohexane (1) + toluene (2) + gamma-valerolactone (3) with E/F = 1: (■) at 100 kPa; (▲), 80 kPa; (●), 50 kPa, and with E/F = 2: (★), and E/F = 3: (⬟) at 100 kPa.

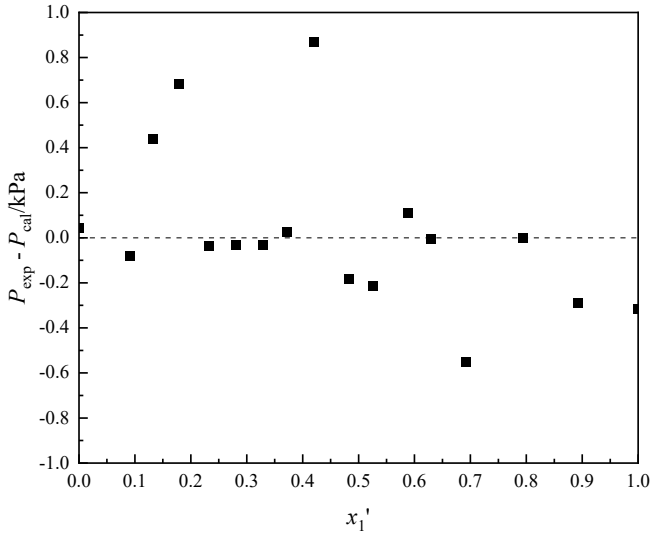


**Figure B16.** Residual plots of pressure (kPa) for methylcyclohexane (1) + toluene (2) + 1-methylpyrrolidin-2-one (3) with E/F = 1 at 100 kPa.

## Uncertainty Calculations

The expanded combined uncertainties were calculated based on the Guide to the Expression of Uncertainty in Measurement, ISO, October 1993, which had been updated in 2008[11].

The expanded combined uncertainties calculation for binary mixture:

$$u_c(T) = \pm\sqrt{u^2(T_{fluctuation}) + u^2(T_{device\ specification})} \quad \text{B1)}$$

$$= \pm\sqrt{u^2(\frac{T_{fluctuation\ observed}}{\sqrt{n_T}}) + u^2(T_{device\ specification})}$$

$$= \pm\sqrt{u^2(\frac{0.05}{\sqrt{4}}) + 0.01^2}$$

$$= \pm\sqrt{0.025^2 + 0.01^2}$$

$$= 0.1\text{K}$$

$U(T)$ =>> 0.2K (level of confident 0.95 ($k$ = 2)

$n_T$ represents the number of observations made for the reading value of $T$ in 15 minutes prior to sample collection.

$$u_c(P) = \pm\sqrt{u^2(P_{fluctuation}) + u^2(P_{device\ specification})} \quad \text{B2)}$$

$$= \pm\sqrt{u^2(\frac{P_{fluctuation\ observed}}{\sqrt{n_P}}) + u^2(P_{device\ specification})}$$

$$= \pm\sqrt{u^2(\frac{0.05}{\sqrt{4}}) + 0.01^2}$$

$$= \pm\sqrt{0.025^2 + 0.01^2}$$

$$= 0.10\ \text{kPa}$$

$U(P)$ =>> 0.20 kPa (level of confident 0.95 ($k$ = 2)

$n_P$ represents the number of observations made for the reading value of $P$ in 15 minutes prior to sample collection.

$$u_c(x) = u_c(y) = \pm\sqrt{u^2(x_{repetition}) + u^2(x_{analytical\ balance}) + u^2(x_{GC})} \quad \text{B3)}$$

$$= \pm\sqrt{0.0001^2 + 0.0001^2 + 0.0027^2}$$

$$= 0.003$$

$U(x) = U(y)$ =>> 0.006 (level of confident 0.95 ($k$ = 2)

The expanded combined uncertainties calculation for pseudo-ternary mixtures:

$$u_c(T) = \pm\sqrt{u^2(T_{fluctuation}) + u^2(T_{device\ specification})} \quad \text{B4)}$$

$$= \pm\sqrt{u^2(\frac{T_{fluctuation\ observed}}{\sqrt{n_T}}) + u^2(T_{device\ specification})}$$

$$= \pm\sqrt{u^2(\frac{0.4}{\sqrt{4}}) + 0.01^2}$$

$$= \pm\sqrt{0.2^2 + 0.01^2}$$

$$= 0.2\text{K}$$

$U(T)$ =>> 0.4K (level of confident 0.95 ($k$ = 2)

$n_T$ represents the number of observations made for the reading value of $T$ in 15 minutes prior to sample collection.

$$u_c(P) = \pm\sqrt{u^2(P_{fluctuation}) + u^2(P_{device\ specification})} \quad \text{B5)}$$

$$= \pm\sqrt{u^2(\frac{P_{fluctuation\ observed}}{\sqrt{n_P}}) + u^2(P_{device\ specification})}$$

$$= \pm\sqrt{u^2(\frac{0.12}{\sqrt{4}}) + 0.01^2}$$

$$= \pm\sqrt{0.06^2 + 0.01^2}$$

$$= 0.11\ \text{kPa}$$

$U(P)$ =>> 0.23 kPa (level of confident 0.95 ($k$ = 2)

$n_P$ represents the number of observations made for the reading value of $P$ in 15 minutes prior to sample collection.

$$u_c(x) = u_c(y) = \pm\sqrt{u^2(x_{repetition}) + u^2(x_{analytical\ balance}) + u^2(x_{GC})} \quad \text{B6)}$$

$$= \pm\sqrt{0.0001^2 + 0.0001^2 + 0.0027^2}$$

$$= 0.003$$

$U(x) = U(y)$ =>> 0.006 (level of confident 0.95 ($k$ = 2)

**References**


(1) Quiggle, D.; Fenske, M. R. Vapor—Liquid Equilibria of Methylcyclohexane—Toluene Mixtures. *J. Am. Chem. Soc.* **1937**, *59* (10), 1829–1832. https://doi.org/10.1021/ja01289a012.

(2) Coca, J.; Pis, J. J. Effect of Morpholine on the Vapor-Liquid Equilibrium of the System Methylcyclohexane-Toluene. *J. Chem. Eng. Data* **1979**, *24* (2), 103–105. https://doi.org/10.1021/je60081a017.

(3) Weber, J. H. Vapor-Liquid Equilibria for System Methylcyclohexane-Toluene at Subatmospheric Pressures. *Ind. Eng. Chem.* **1955**, *47* (3), 454–457. https://doi.org/10.1021/ie50543a036.

(4) Yaws, C. L.; H.C., Y. To Estimate Vapor Pressure Easily. Antoine Coefficients Relate Vapor Pressure to Temperature for Almost 700 Major Organic Compounds. *Hydrocarb. Process.* **1989**, *68* (10), 65–68.

(5) Willingham, C. B.; Taylor, W. J.; Pignocco, J. M.; Rossini, F. D. Vapor Pressures and Boiling Points of Some Paraffin, Alkylcyclopentane, Alkylcyclohexane, and Alkylbenzene Hydrocarbons. *J. Res. Natl. Bur. Stand. (1934).* **1945**, *35* (3), 219–244.

(6) Al-Lami, M.; Havasi, D.; Koczka, K.; Mika, L. T. Isobaric Vapor–Liquid Equilibria for Binary Mixtures of Gamma-Valerolactone + Toluene. *J. Chem. Eng. Data* **2021**, *66* (1), 568–574. https://doi.org/10.1021/acs.jced.0c00791.

(7) Gupta, S. K.; Rawat, B. S. Isobaric Binary and Ternary Vapor-Liquid Equilibria of N-Methylpyrrolidone with Water and Toluene at 760 MmHg. *J. Chem. Eng. Data* **1992**, *37* (2), 139–140. https://doi.org/10.1021/je00006a001.

(8) Zaretskii, M. I.; Kogan, V. B.; Kononov, N. F.; MiroshniChenko, A. A.; Usyushkina, I. V; Podolyak, V. G. Liquid—Vapor Equilibrium in Systems Formed by Aromatic Hydrocarbons and Thiophene with Some Polar Solvents. *J. Appl. Chem. USSR* **1974**, *47* (9), 2142–2145.

(9) Gierycz, P.; Rogalski, M.; Malanowski, S. Vapour—Liquid Equilibria in Binary Systems Formed by N-Methylpyrrolidone with Hydrocarbons and Hydroxyl Derivatives. *Fluid Phase Equilib.* **1985**, *22* (1), 107–122. https://doi.org/https://doi.org/10.1016/0378-3812(85)87014-X.

(10) Linek, J.; Wichterle, I.; Marsh, K. N. Vapor−Liquid Equilibria for N-Methyl-2-Pyrrolidone + Benzene, +Toluene, +Heptane, and +Methylcyclohexane. *J. Chem. Eng. Data* **1996**, *41* (6), 1212–1218. https://doi.org/10.1021/je9601826.

(11) Working Group 1 of the Joint Committee for Guides in Metrology (JCGM/WG 1). Evaluation of Measurement Data — Guide to the Expression of Uncertainty in Measurement. *Int. Organ. Stand. Geneva ISBN* **2008**, *50* (September), 134.

## Appendix C

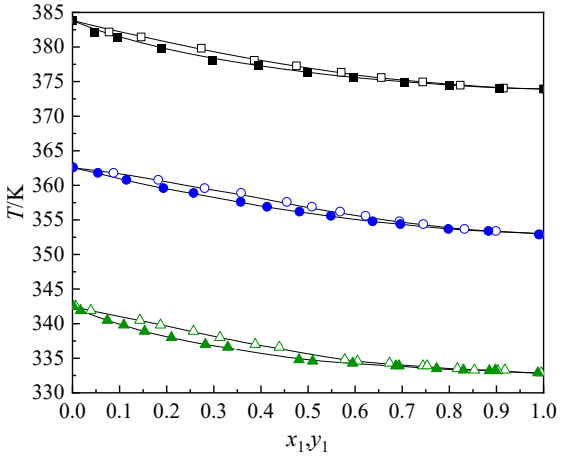


**Figure C1.** $T$–$x_1$–$y_1$ diagrams of methylcyclohexane (1) + toluene (2): experimental (▲), liquid- and (Δ), vapor-phase at 26.7 kPa from literature[1]; (●), liquid- and (○), vapor-phase at 53.3 kPa from literature[1]; (■), liquid- and (□), vapor-phase at 101.3 kPa from our previous study[2]; and (—), correlated by NRTL.

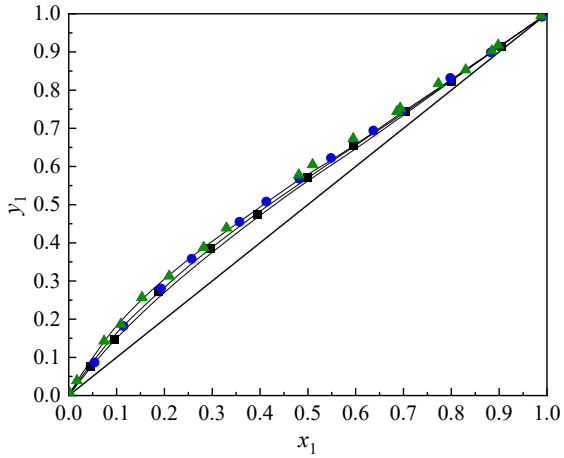


**Figure C2.** $y_1$–$x_1$ diagrams of methylcyclohexane (1) + toluene (2): experimental (▲), at 26.7 kPa and (●), at 53.3 kPa from literature[1]; (■), at 101.3 kPa from our previous study[2]; and (—), correlated by NRTL.

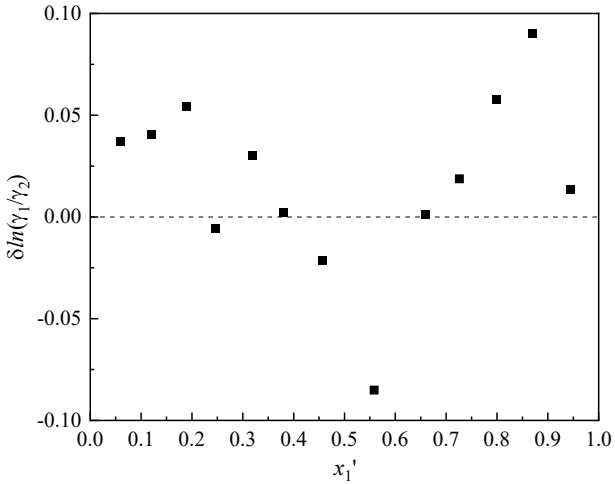


**Figure C3.** Residual distribution of $\ln(\gamma_1 / \gamma_2)$ for methylcyclohexane (1) + toluene (2) + dimethyl isosorbide (3) with E/F = 1 at 100.0 kPa.

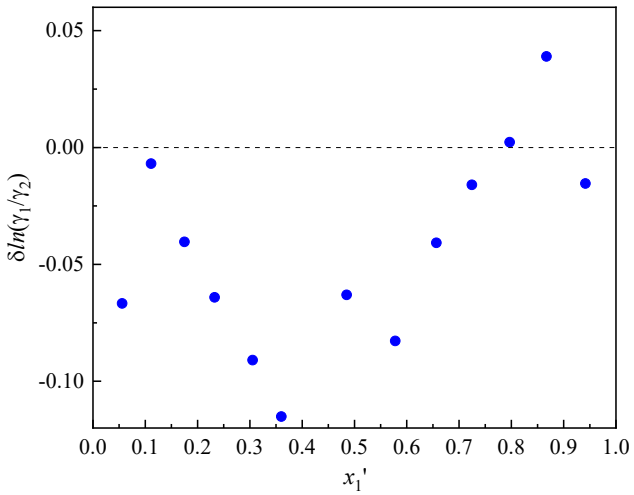


**Figure C4.** Residual distribution of $\ln(\gamma_1 / \gamma_2)$ for methylcyclohexane (1) + toluene (2) + dimethyl isosorbide (3) with E/F = 1 at 10.0 kPa.

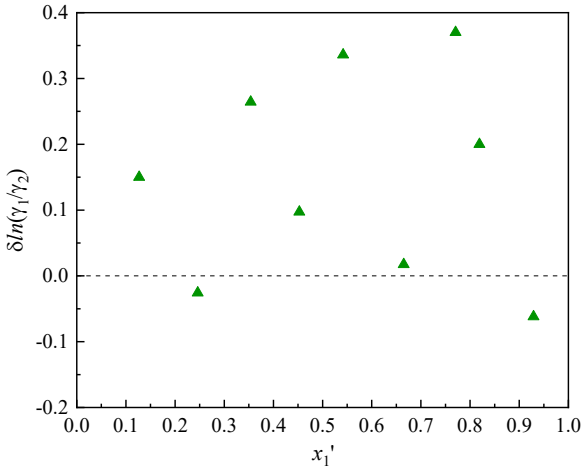


**Figure C5.** Residual distribution of $\ln(\gamma_1 / \gamma_2)$ for methylcyclohexane (1) + toluene (2) + dimethyl isosorbide (3) with E/F = 3 at 10.0 kPa.

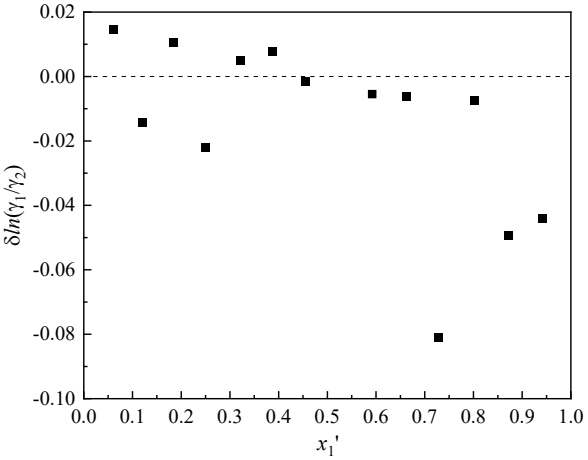


**Figure C6.** Residual distribution of $\ln(\gamma_1 / \gamma_2)$ for methylcyclohexane (1) + toluene (2) + 1-butylpyrrolidin-2-one (3) with E/F = 1 at 100.0 kPa.

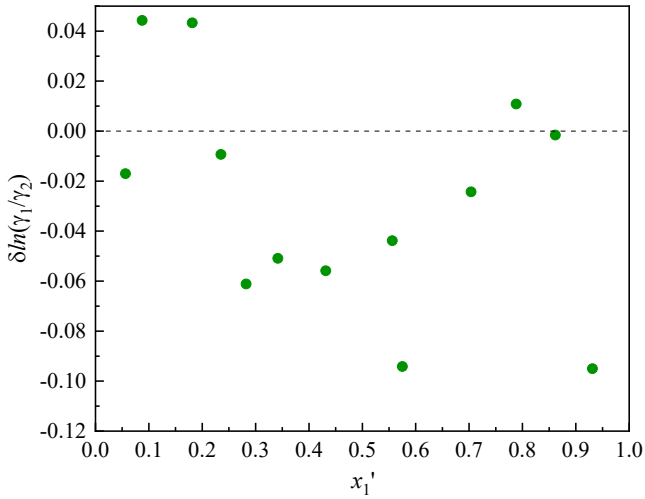


**Figure C7.** Residual distribution of $\ln(\gamma_1 / \gamma_2)$ for methylcyclohexane (1) + toluene (2) + 1-butylpyrrolidin-2-one (3) with E/F = 1 at 10.0 kPa.

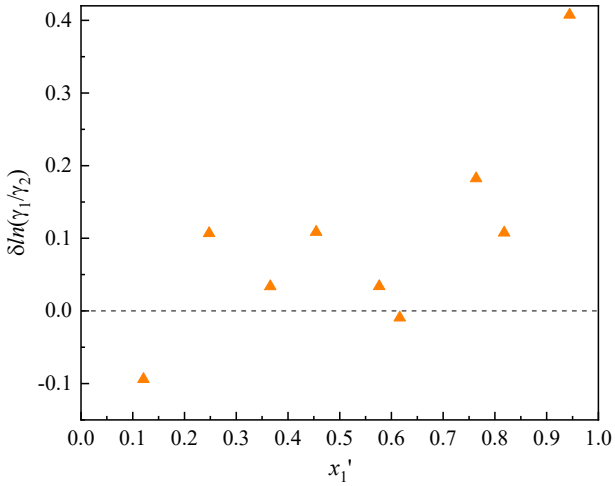


**Figure C8.** Residual distribution of $\ln(\gamma_1 / \gamma_2)$ for methylcyclohexane (1) + toluene (2) + 1-butylpyrrolidin-2-one (3) with E/F = 3 at 10.0 kPa.

**Calculations for the Uncertainty**

The expanded combined uncertainties for pseudo-ternary mixtures were obtained from the calculation according to the Guide to the Expression of Uncertainty in Measurement, ISO, October 1993, and updated in 2008[3], as follows:

$$u_c(T) = \pm\sqrt{u^2(T_{fluctuation}) + u^2(T_{device\ specification})} \quad \text{C1)}$$

$$= \pm\sqrt{u^2(\frac{T_{fluctuation\ observed}}{\sqrt{n_T}}) + u^2(T_{device\ specification})}$$

$$= \pm\sqrt{u^2(\frac{0.4}{\sqrt{4}}) + 0.01^2}$$

$$= \pm\sqrt{0.2^2 + 0.01^2}$$

$$= 0.2\text{K}$$

$U(T)$ =>> 0.4K (level of confident 0.95 ($k$ = 2)

$n_T$ represents the number of observations made for the reading value of $T$ in 15 minutes prior to sample collection.

$$u_c(P) = \pm\sqrt{u^2(P_{fluctuation}) + u^2(P_{device\ specification})} \quad \text{C2)}$$

$$= \pm\sqrt{u^2(\frac{P_{fluctuation\ observed}}{\sqrt{n_P}}) + u^2(P_{device\ specification})}$$

$$= \pm\sqrt{u^2(\frac{0.12}{\sqrt{4}}) + 0.01^2}$$

$$= \pm\sqrt{0.06^2 + 0.01^2}$$

$$= 0.11\ \text{kPa}$$

$U(P)$ =>> 0.23 kPa (level of confident 0.95 ($k$ = 2)

$n_P$ represents the number of observations made for the reading value of $P$ in 15 minutes prior to sample collection.

$$u_c(x) = u_c(y) = \pm\sqrt{u^2(x_{repetition}) + u^2(x_{analytical\ balance}) + u^2(x_{GC})} \quad \text{C3)}$$

$$= \pm\sqrt{0.0001^2 + 0.0001^2 + 0.0027^2}$$

$$= 0.003$$

$U(x) = U(y)$ =>> 0.006 (level of confident 0.95 ($k$ = 2)

**References**


(1) Weber, J. H. Vapor-Liquid Equilibria for System Methylcyclohexane-Toluene at Subatmospheric Pressures. *Ind. Eng. Chem.* **1955**, *47* (3), 454–457. https://doi.org/10.1021/ie50543a036.

(2) Hartanto, D.; Schuur, B.; Schuttevaer, T.; Kiss, A. A.; de Haan, A. B. Isobaric Vapor–Liquid Equilibrium of Methylcyclohexane + Toluene with Gamma-Valerolactone as a Biobased Entrainer and 1-Methylpyrrolidin-2-One as a Conventional Entrainer. *J. Chem. Eng. Data* **2025**, *70* (3), 1339−1351. https://doi.org/10.1021/acs.jced.4c00509.

(3) Working Group 1 of the Joint Committee for Guides in Metrology (JCGM/WG 1). Evaluation of Measurement Data — Guide to the Expression of Uncertainty in Measurement. *Int. Organ. Stand. Geneva ISBN* **2008**, *50* (September), 134.

## Appendix D

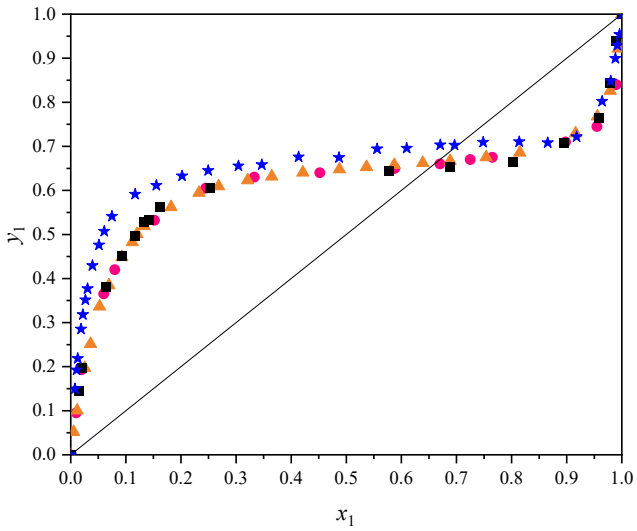


**Figure D1.** $x_1$-$y_1$ diagram for n-hexane (1) + ethanol (2) at 101.3 kPa: (■), this work; (●), literature (Sinor and Weber, 1960)[1]; (▲), literature (Ortega and Espiau, 2003)[2]; and at 61.3 kPa: (★), literature (Ortega and Espiau, 2003)[2].

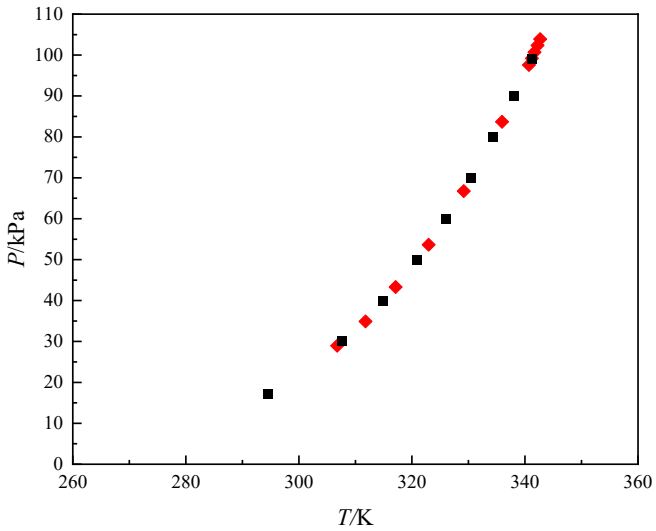


**Figure D2.** Vapor pressure for pure component of n-hexane: (■), this work; (♦), literature (Williamham et al.)[3].

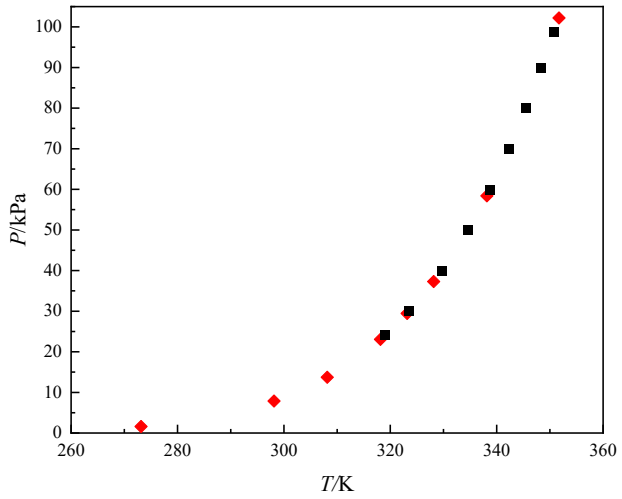


**Figure D3.** Vapor pressure for pure component of ethanol: (■), this work; (♦), literature (Kretschmer and Wiebe).[4]

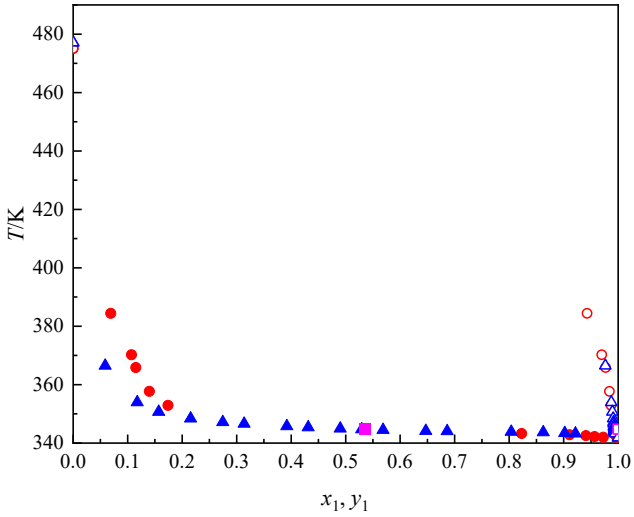


**Figure D4.** *T*- $x_1$-$y_1$ diagram of n-hexane (1) + NMP (2), experimental from this work (■), $x_1$ and (□), $y_1$ at 100.0 kPa; experimental from literatures: (●), $x_1$ and (○), $y_1$ at 101.3 kPa (Blanco et al[5]); and (▲), $x_1$ and (Δ), $y_1$ at 101.3 kPa (Li et al[6]).

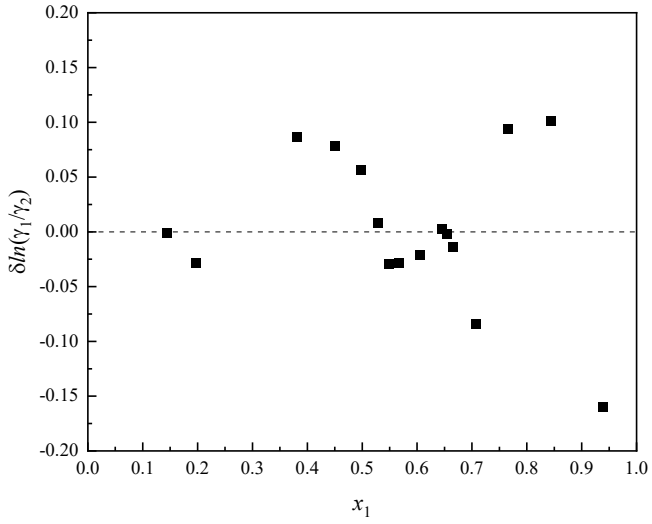


**Figure D5.** Residual distribution ( $\delta$ ) of $\ln(\gamma_1 / \gamma_2)$ for n-hexane (1) + ethanol (2) at 101.3 kPa.

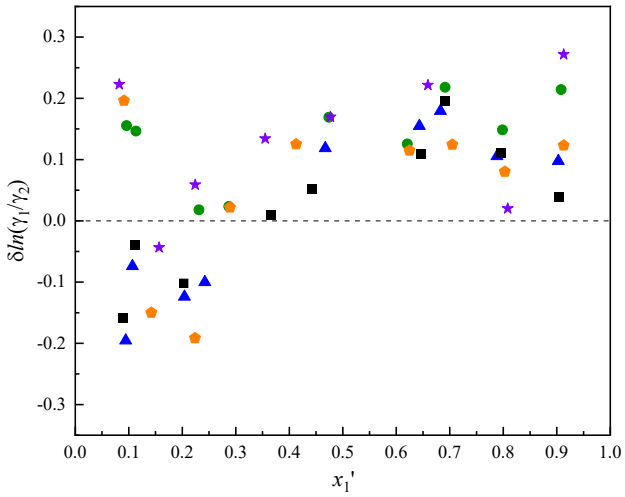


**Figure D6.** Residual distribution ( $\delta$ ) of $\ln(\gamma_1 / \gamma_2)$ for n-hexane (1) + ethanol (2) + 1-butylpyrrolidin-2-one (3) with E/F = 1: (■) at 100.0 kPa; (▲), 80.0 kPa; (●), 50.0 kPa, and with E/F = 2: (★), and E/F = 3: (⬟) at 100.0 kPa.

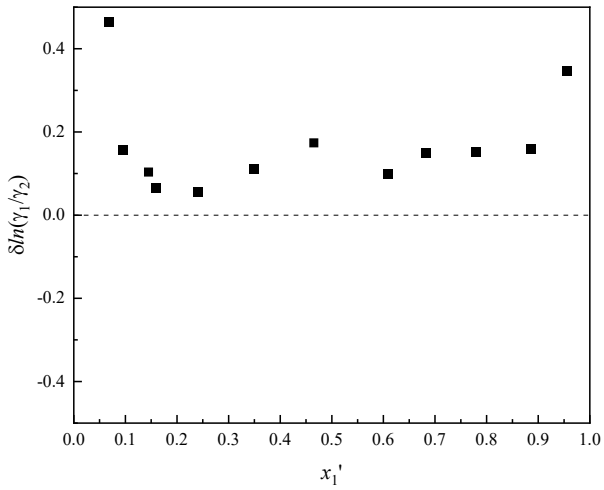


**Figure D7.** Residual distribution ( $\delta$ ) of $\ln(\gamma_1 / \gamma_2)$ for n-hexane (1) + ethanol (2) + 1-methylpyrrolidin-2-one (3) with E/F = 1 at 100.0 kPa.

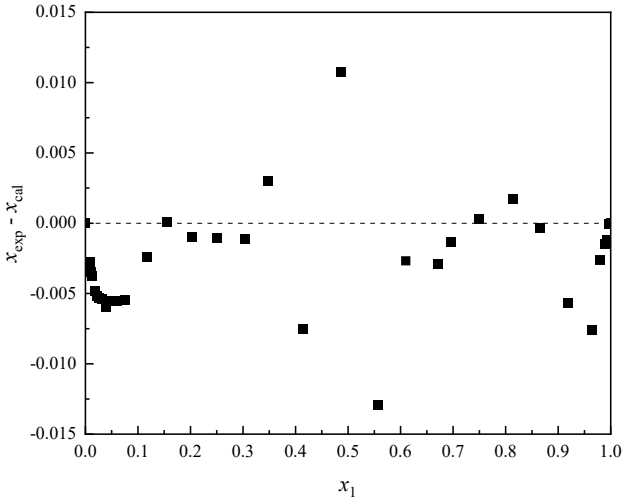


**Figure D8.** Residual plots of liquid composition for n-hexane (1) + ethanol (2) at 101.3 kPa.

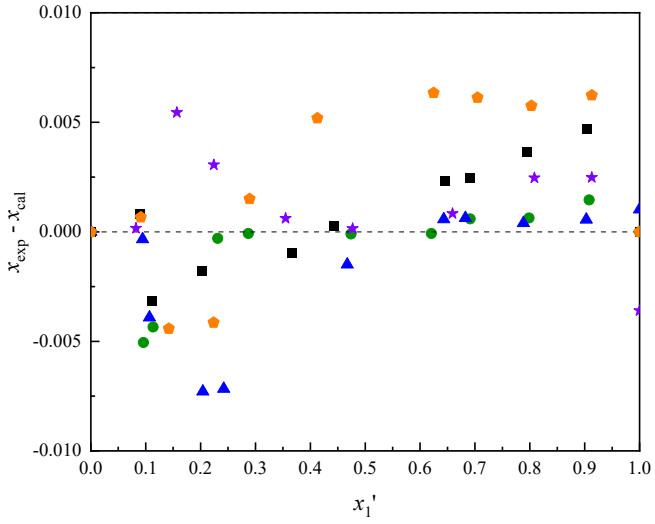


**Figure D9.** Residual plots of liquid composition for n-hexane (1) + ethanol (2) + 1-butylpyrrolidin-2-one (3) with E/F = 1: (■) at 100.0 kPa; (▲), 80.0 kPa; (●), 50.0 kPa, and with E/F = 2: (★), and E/F = 3: (⬟) at 100.0 kPa.

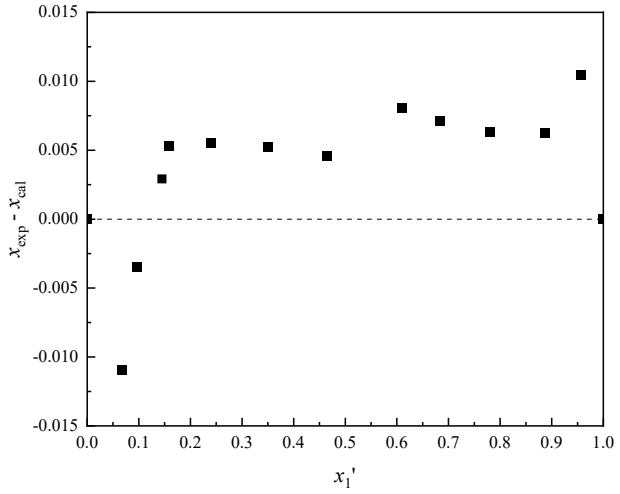


**Figure D10.** Residual plots of liquid composition for n-hexane (1) + ethanol (2) + 1-methylpyrrolidin-2-one (3) with E/F = 1 at 100.0 kPa.

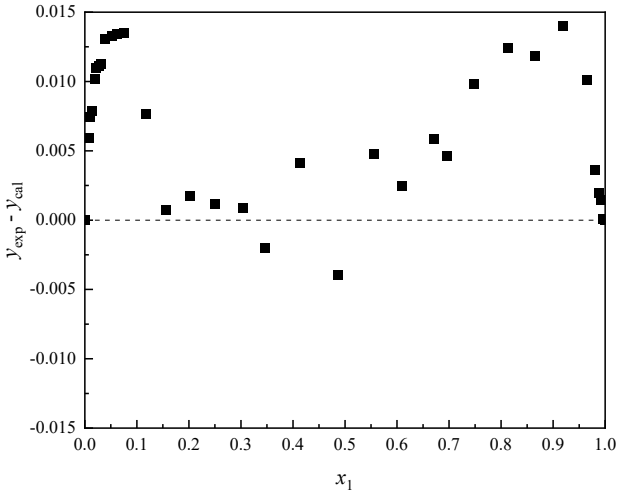


**Figure D11.** Residual plots of vapor composition for n-hexane (1) + ethanol (2) at 101.3 kPa.

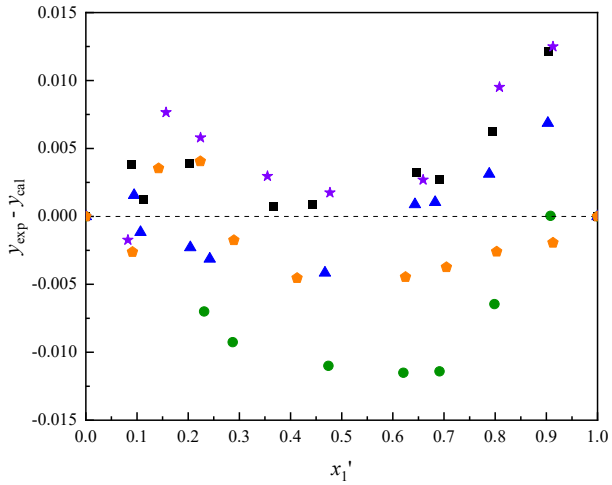


**Figure D12.** Residual plots of vapor composition for n-hexane (1) + ethanol (2) + 1-butylpyrrolidin-2-one (3) with E/F = 1: (■) at 100.0 kPa; (▲), 80.0 kPa; (●), 50.0 kPa, and with E/F = 2: (★), and E/F = 3: (⬟) at 100.0 kPa.

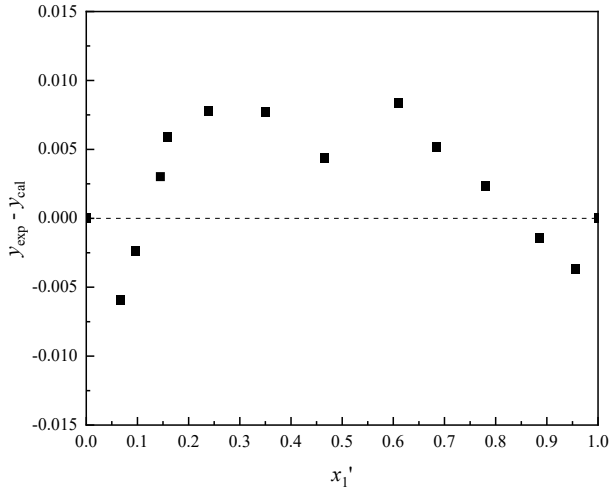


**Figure D13.** Residual plots of vapor composition for n-hexane (1) + ethanol (2) + 1-methylpyrrolidin-2-one (3) with E/F = 1 at 100.0 kPa.

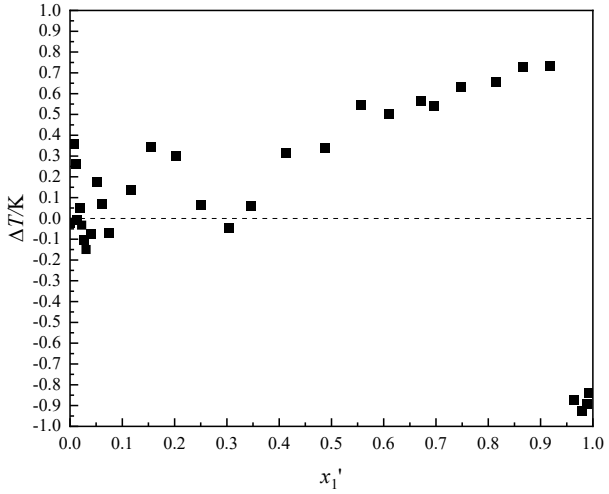


**Figure D14.** Residual plots of temperature for n-hexane (1) + ethanol (2) at 101.3 kPa.

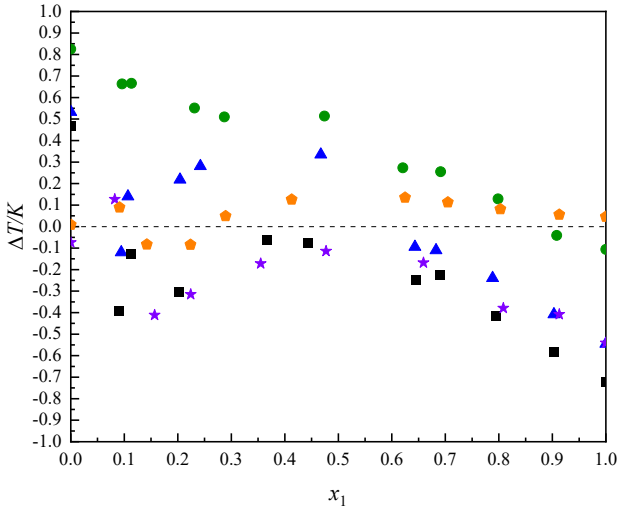


**Figure D15.** Residual plots of temperature for n-hexane (1) + ethanol (2) + 1-butylpyrrolidin-2-one (3) with E/F = 1: (■) at 100.0 kPa; (▲), 80.0 kPa; (●), 50.0 kPa, and with E/F = 2: (★), and E/F = 3: (⬟) at 100.0 kPa.

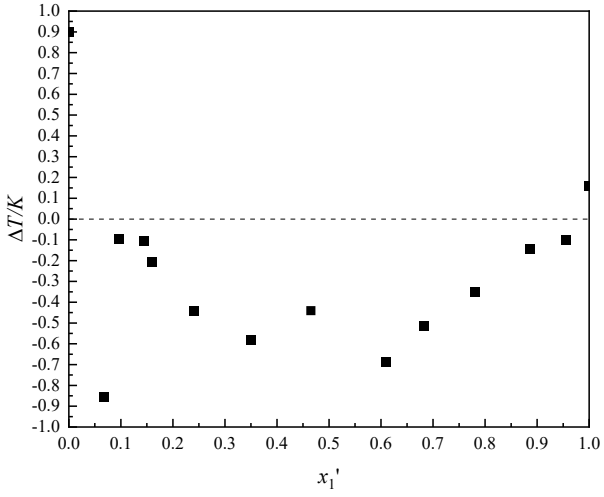


**Figure D16.** Residual plots of temperature for n-hexane (1) + ethanol (2) + 1-methylpyrrolidin-2-one (3) with E/F = 1 at 100.0 kPa.

**Table D1.** Vapor pressure for the pure component of n-hexane and ethanol[a].

| n-Hexane | | Ethanol | |
|---|---|---|---|
| *T*/K | *P*/kPa | *T*/K | *P*/kPa |
| 294.49 | 17.14 | 319.03 | 24.07 |
| 307.63 | 30.00 | 323.53 | 29.99 |
| 314.94 | 39.99 | 329.62 | 39.99 |
| 320.91 | 49.94 | 334.55 | 49.96 |
| 325.99 | 59.96 | 338.70 | 59.96 |
| 330.42 | 69.90 | 342.30 | 69.94 |
| 334.42 | 79.90 | 345.52 | 79.99 |
| 338.02 | 89.91 | 348.39 | 89.91 |
| 340.94 | 98.99 | 350.77 | 98.75 |

[a]Expanded combined uncertainties ($U$ with $k = 2$):
$U(T) = 0.20$ K, $U(P) = 0.20$ kPa

**Table D2.** The values of $\Delta P$ and $\Delta y$ for n-hexane (1) + ethanol (2) at 101.3 kPa.

| $x_1$ | $100\left\|y_i^{cal} - y_i^{\exp}\right\|$ | $100\left\|\frac{P_i^{cal} - P_i^{\exp}}{P_i^{\exp}}\right\|$ |
|---|---|---|
| 0.000 | 0.0 | 0.0 |
| 0.015 | 0.1 | 0.5 |
| 0.021 | 0.2 | 1.1 |
| 0.064 | 1.0 | 1.0 |
| 0.092 | 1.4 | 1.3 |
| 0.116 | 1.2 | 0.9 |
| 0.132 | 0.3 | 0.3 |
| 0.141 | 0.4 | 0.1 |
| 0.162 | 0.6 | 0.2 |
| 0.252 | 0.5 | 0.3 |
| 0.577 | 0.0 | 0.0 |
| 0.687 | 0.1 | 0.1 |
| 0.802 | 0.3 | 0.2 |
| 0.895 | 1.4 | 0.2 |
| 0.958 | 0.9 | 1.5 |
| 0.978 | 0.5 | 2.0 |
| 0.990 | 0.2 | 1.8 |
| 1.000 | 0.0 | 0.0 |
| average | **0.6** | **0.4** |

**Table D3.** The values of $\Delta P$ and $\Delta y$ for n-hexane (1) + ethanol (2) + 1-butylpyrrolidin-2-one (3).

| $x_1$ | $100\left\|y_i^{cal}-y_i^{\exp}\right\|$ | $100\left\|\frac{P_i^{cal}-P_i^{\exp}}{P_i^{\exp}}\right\|$ | $x_1$ | $100\left\|y_i^{cal}-y_i^{\exp}\right\|$ | $100\left\|\frac{P_i^{cal}-P_i^{\exp}}{P_i^{\exp}}\right\|$ |
|---|---|---|---|---|---|
| ***E/F = 1; 50.0 kPa*** | | | ***E/F = 2; 100 kPa*** | | |
| 0.000 | 0.0 | 1.4 | 0.000 | 0.0 | 0.1 |
| 0.096 | 2.1 | 2.3 | 0.082 | 0.2 | 1.9 |
| 0.114 | 2.2 | 1.7 | 0.157 | 0.8 | 2.7 |
| 0.231 | 2.1 | 0.9 | 0.224 | 0.6 | 2.4 |
| 0.287 | 1.9 | 1.3 | 0.355 | 0.3 | 1.5 |
| 0.474 | 2.0 | 0.9 | 0.477 | 0.2 | 0.8 |
| 0.621 | 1.2 | 0.8 | 0.659 | 0.3 | 0.2 |
| 0.691 | 1.1 | 0.5 | 0.808 | 1.0 | 0.6 |
| 0.799 | 0.6 | 0.3 | 0.913 | 1.2 | 0.3 |
| 0.908 | 0.0 | 0.3 | 1.000 | 0.0 | 0.2 |
| 1.000 | 0.0 | 0.0 | | | |
| ***E/F = 1; 80.0 kPa*** | | | ***E/F = 3; 100 kPa*** | | |
| 0.000 | 0.0 | 1.5 | 0.000 | 0.0 | 0.2 |
| 0.096 | 0.2 | 1.2 | 0.091 | 0.3 | 1.6 |
| 0.114 | 0.1 | 2.4 | 0.142 | 0.4 | 1.3 |
| 0.231 | 0.2 | 0.7 | 0.224 | 0.4 | 1.5 |
| 0.287 | 0.3 | 0.5 | 0.289 | 0.2 | 0.1 |
| 0.474 | 0.4 | 0.4 | 0.413 | 0.5 | 0.4 |
| 0.621 | 0.1 | 0.1 | 0.625 | 0.4 | 0.5 |
| 0.691 | 0.1 | 0.1 | 0.705 | 0.4 | 0.4 |
| 0.799 | 0.3 | 0.4 | 0.803 | 0.3 | 0.3 |
| 0.908 | 0.7 | 0.4 | 0.913 | 0.2 | 0.4 |
| 1.000 | 0.0 | 0.9 | 1.000 | 0.0 | 0.4 |
| ***E/F = 1; 100.0 kPa*** | | | average | **0.5** | **0.8** |
| 0.000 | 0.0 | 1.7 | | | |
| 0.090 | 0.4 | 0.4 | | | |
| 0.112 | 0.1 | 1.6 | | | |
| 0.203 | 0.4 | 1.0 | | | |
| 0.366 | 0.1 | 0.3 | | | |
| 0.443 | 0.1 | 0.1 | | | |
| 0.645 | 0.3 | 0.4 | | | |
| 0.691 | 0.3 | 0.8 | | | |
| 0.795 | 0.6 | 0.7 | | | |
| 0.904 | 1.2 | 0.4 | | | |
| 1.000 | 0.0 | 1.1 | | | |

**Table D4.** The values of $\Delta P$ and $\Delta y$ for n-hexane (1) + ethanol (2) + 1-methylpyrrolidin-2-one (3) with E/F = 1 at 100.0 kPa.

| $x_1$ | $100\left\|y_i^{cal} - y_i^{\exp}\right\|$ | $100\left\|\frac{P_i^{cal} - P_i^{\exp}}{P_i^{\exp}}\right\|$ |
|---|---|---|
| 0.000 | 0.0 | 0.3 |
| 0.067 | 0.4 | 0.3 |
| 0.096 | 0.1 | 0.0 |
| 0.145 | 0.2 | 0.3 |
| 0.159 | 0.5 | 0.6 |
| 0.240 | 0.8 | 1.0 |
| 0.350 | 0.4 | 0.6 |
| 0.465 | 0.8 | 1.0 |
| 0.610 | 0.8 | 1.1 |
| 0.683 | 0.6 | 0.9 |
| 0.780 | 0.3 | 0.5 |
| 0.886 | 0.2 | 0.5 |
| 0.956 | 0.6 | 2.3 |
| 1.000 | 0.0 | 1.5 |
| average | **0.4** | **0.8** |

## Uncertainty Calculations

The Guide to the Expression of Uncertainty in Measurement, ISO, October 1993, with an updated in 2008[7], was used to determine the expanded combined uncertainties.

The calculation of the expanded combined uncertainties for binary mixture:

$$u_c(T) = \pm\sqrt{u^2(T_{fluctuation}) + u^2(T_{device\ specification})} \quad \text{D1)}$$

$$= \pm\sqrt{u^2(\frac{T_{fluctuation\ observed}}{\sqrt{n_T}}) + u^2(T_{device\ specification})}$$

$$= \pm\sqrt{u^2(\frac{0.05}{\sqrt{4}}) + 0.01^2}$$

$$= \pm\sqrt{0.025^2 + 0.01^2}$$

$$= 0.10\,\mathrm{K}$$

$$U(T) \Rightarrow\Rightarrow 0.20\,\mathrm{K} \text{ (confidence level 0.95 } (k = 2))$$

$n_T$ is the number of readings recorded for the value of $T$ within 15 minutes prior to sample collection.

$$u_c(P) = \pm\sqrt{u^2(P_{fluctuation}) + u^2(P_{device\ specification})} \quad \text{D2)}$$

$$= \pm\sqrt{u^2(\frac{P_{fluctuation\ observed}}{\sqrt{n_P}}) + u^2(P_{device\ specification})}$$

$$= \pm\sqrt{u^2(\frac{0.05}{\sqrt{4}}) + 0.01^2}$$

$$= \pm\sqrt{0.025^2 + 0.01^2}$$

$$= 0.10 \text{ kPa}$$

$$U(P) \Rightarrow\Rightarrow 0.20 \text{ kPa (confidence level 0.95 } (k = 2))$$

$n_P$ is the number of readings recorded for the value of $P$ within 15 minutes prior to sample collection.

$$u_c(x) = u_c(y) = \pm\sqrt{u^2(x_{repetition}) + u^2(x_{analytical\ balance}) + u^2(x_{GC})} \quad \text{D3)}$$

$$= \pm\sqrt{0.0001^2 + 0.0001^2 + 0.0027^2}$$

$$= 0.003$$

$$U(x) = U(y) \Rightarrow\Rightarrow 0.006 \text{ (confidence level 0.95 } (k = 2))$$

The calculation of the expanded combined uncertainties for the pseudo-ternary mixtures:

D4)

$$u_c(T) = \pm\sqrt{u^2(T_{fluctuation}) + u^2(T_{device\ specification})}$$
$$= \pm\sqrt{u^2(\frac{T_{fluctuation\ observed}}{\sqrt{n_T}}) + u^2(T_{device\ specification})}$$
$$= \pm\sqrt{u^2(\frac{0.4}{\sqrt{4}}) + 0.01^2}$$
$$= \pm\sqrt{0.2^2 + 0.01^2}$$
$$= 0.20\,\mathrm{K}$$
$$U(T) \text{ =>> } 0.40\,\mathrm{K} \text{ (confidence level 0.95 } (k = 2))$$

$n_T$ is the number of readings recorded for the value of $T$ within 15 minutes prior to sample collection.

D5)

$$u_c(P) = \pm\sqrt{u^2(P_{fluctuation}) + u^2(P_{device\ specification})}$$
$$= \pm\sqrt{u^2(\frac{P_{fluctuation\ observed}}{\sqrt{n_P}}) + u^2(P_{device\ specification})}$$
$$= \pm\sqrt{u^2(\frac{0.12}{\sqrt{4}}) + 0.01^2}$$
$$= \pm\sqrt{0.06^2 + 0.01^2}$$
$$= 0.11 \text{ kPa}$$
$$U(P) \text{ =>> } 0.23 \text{ kPa (confidence level 0.95 } (k = 2))$$

is the number of readings recorded for the value of $P$ within 15 minutes prior to sample collection.

D6)

$$u_c(x) = u_c(y) = \pm\sqrt{u^2(x_{repetition}) + u^2(x_{analytical\ balance}) + u^2(x_{GC})}$$
$$= \pm\sqrt{0.0001^2 + 0.0001^2 + 0.0027^2}$$
$$= 0.003$$
$$U(x) = U(y) \text{ =>> } 0.006 \text{ (confidence level 0.95 } (k = 2))$$

The calculation of the expanded combined uncertainties for vapor pressure measurements of pure n-hexane and ethanol:

$$
\begin{aligned}
u_c(T) &= \pm\sqrt{u^2(T_{fluctuation}) + u^2(T_{device\ specification})} \\
&= \pm\sqrt{u^2(\frac{T_{fluctuation\ observed}}{\sqrt{n_T}}) + u^2(T_{device\ specification})} \\
&= \pm\sqrt{u^2(\frac{0.05}{\sqrt{4}}) + 0.01^2} \\
&= \pm\sqrt{0.025^2 + 0.01^2} \\
&= 0.10\,\mathrm{K} \\
U(T) &=>> 0.20\,\mathrm{K}\ \text{(confidence level 0.95 (}k = 2\text{))}
\end{aligned}
\qquad \text{D7)}
$$

$n_T$ is the number of readings recorded for the value of $T$ within 15 minutes prior to data collection.

$$
\begin{aligned}
u_c(P) &= \pm\sqrt{u^2(P_{fluctuation}) + u^2(P_{device\ specification})} \\
&= \pm\sqrt{u^2(\frac{P_{fluctuation\ observed}}{\sqrt{n_P}}) + u^2(P_{device\ specification})} \\
&= \pm\sqrt{u^2(\frac{0.02}{\sqrt{4}}) + 0.01^2} \\
&= \pm\sqrt{0.025^2 + 0.01^2} \\
&= 0.10\ \mathrm{kPa} \\
U(P) &=>> 0.20\ \mathrm{kPa}\ \text{(confidence level 0.95 (}k = 2\text{))}
\end{aligned}
\qquad \text{D8)}
$$

$n_P$ is the number of readings recorded for the value of $P$ within 15 minutes prior to data collection.

**References**


(1) Sinor, J. E.; Weber, J. H. Vapor-Liquid Equilibria at Atmospheric Pressure. Systems Containing Ethyl Alcohol, n-Hexane, Benzene, and Methylcyclopentane. *J. Chem. Eng. Data* **1960**, *5* (3), 243–247. https://doi.org/10.1021/je60007a003.

(2) Ortega, J.; Espiau, F. A New Correlation Method for Vapor−Liquid Equilibria and Excess Enthalpies for Nonideal Solutions Using a Genetic Algorithm. Application to Ethanol + an n-Alkane Mixtures. *Ind. Eng. Chem. Res.* **2003**, *42* (20), 4978–4992. https://doi.org/10.1021/ie030327j.

(3) Williamham, C. B. .; Taylor, W. J. .; Pignocco, J. M. .; Rossini, F. D. Vapor

Pressures and Boiling Points of Some Paraffin, Alkylcyclopentane, Alkylcyclohexane, and Alkylbenzene Hydrocarbons. *J. Res. Natl. Bur. Stand. (1934).* **1945**, *35* (3), 219–244. https://doi.org/https://doi.org/10.6028/jres.035.009.

(4) Kretschmer, C. B.; Wiebe, R. Liquid-Vapor Equilibrium of Ethanol--Toluene Solutions. *J. Am. Chem. Soc.* **1949**, *71* (5), 1793–1797. https://doi.org/10.1021/ja01173a076.

(5) Blanco, B.; Beltrán, S.; Cabezas, J. L.; Coca, J. Phase Equilibria of Binary Systems Formed by Hydrocarbons from Petroleum Fractions and the Solvents N-Methylpyrrolidone and N,N-Dimethylformamide. 1. Isobaric Vapor−Liquid Equilibria. *J. Chem. Eng. Data* **1997**, *42* (5), 938–942. https://doi.org/10.1021/je970059u.

(6) Li, M.; Yu, Y.; Zhang, L.; Li, J.; Song, Y. Isobaric Binary and Ternary Vapor–Liquid Equilibrium for the Mixture of n-Hexane, Methylcyclopentane and N-Methylpyrrolidone. *J. Solution Chem.* **2021**, *50* (9), 1258–1284. https://doi.org/10.1007/s10953-021-01116-0.

(7) Working Group 1 of the Joint Committee for Guides in Metrology (JCGM/WG 1). Evaluation of Measurement Data — Guide to the Expression of Uncertainty in Measurement. *Int. Organ. Stand. Geneva ISBN* **2008**, *50* (September), 134.

## Appendix E

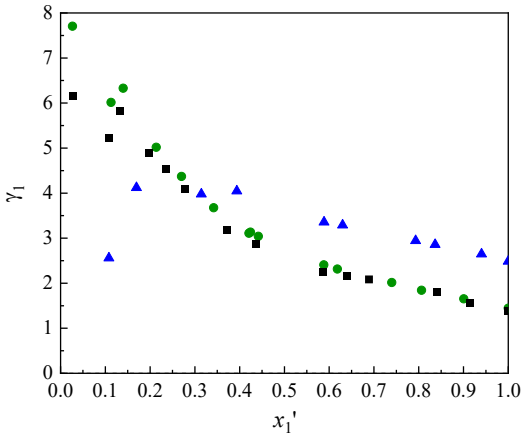


**Figure E1.** Activity coefficients of n-hexane ($\gamma_1$) versus entrainer-free basis liquid mole fraction of n-hexane ($x_1'$) for n-hexane (1) + ethanol (2) + guaiacol (3) with an E/F = 1: (■) at 100.0 kPa; and (●), 50.0 kPa, and an E/F = 3: (▲) at 50.0 kPa.

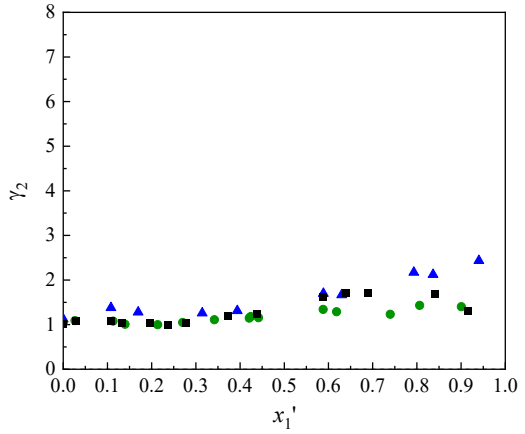


**Figure E2.** Activity coefficients of ethanol ($\gamma_2$) versus entrainer-free basis liquid mole fraction of n-hexane ($x_1'$) for n-hexane (1) + ethanol (2) + guaiacol (3) with an E/F = 1: (■) at 100.0 kPa; and (●), 50.0 kPa, and an E/F = 3: (▲) at 50.0 kPa.

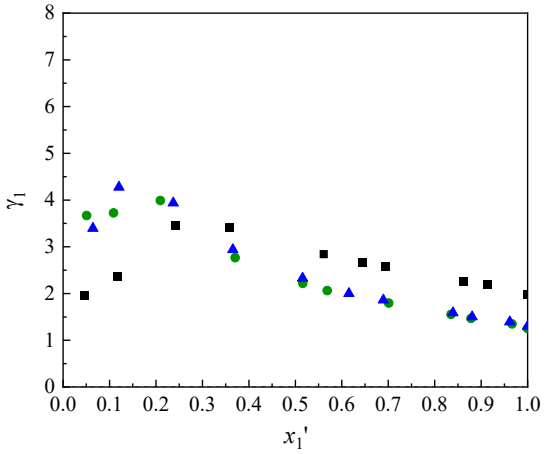


**Figure E3.** Activity coefficients of n-hexane ($\gamma_1$) versus entrainer-free basis liquid mole fraction of n-hexane ($x_1'$) for n-hexane (1) + ethanol (2) + DMI (3) with an E/F = 1: (■) at 100.0 kPa; and (●), 50.0 kPa, and an E/F = 3: (▲) at 50.0 kPa.

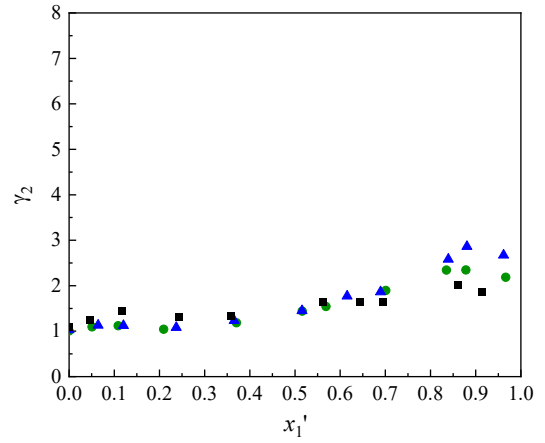


**Figure E4.** Activity coefficients of ethanol ($\gamma_2$) versus entrainer-free basis liquid mole fraction of n-hexane ($x_1'$) for n-hexane (1) + ethanol (2) + DMI (3) with an E/F = 1: (■) at 100.0 kPa; and (●), 50.0 kPa, and an E/F = 3: (▲) at 50.0 kPa.

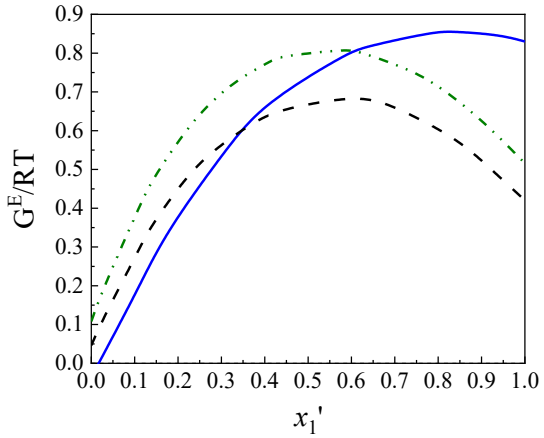


**Figure E5.** Excess Gibbs free energy ($G^E/RT$) versus liquid mole fraction of n-hexane ($x_1$') calculated from NRTL parameters for n-hexane (1) + ethanol (2) + guaiacol (3) with an E/F = 1: (black dashed line) at 100.0 kPa; and (green dash-dot line), 50.0 kPa, and an E/F = 3: (blue line) at 50.0 kPa.

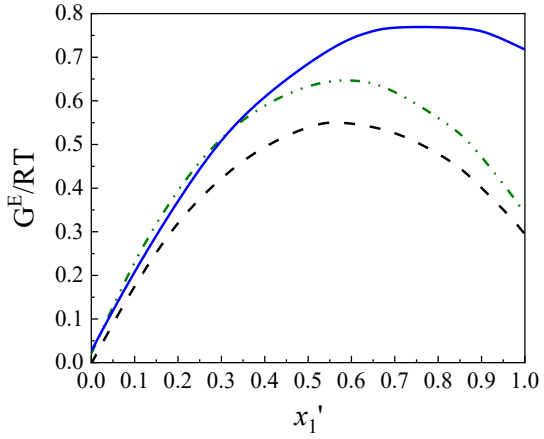


**Figure E6.** Excess Gibbs free energy ($G^E/RT$) versus liquid mole fraction of n-hexane ($x_1$') calculated from NRTL parameters for n-hexane (1) + ethanol (2) + DMI (3) with an E/F = 1: (black dashed line) at 100.0 kPa; and (green dash-dot line), 50.0 kPa, and an E/F = 3: (blue line) at 50.0 kPa.

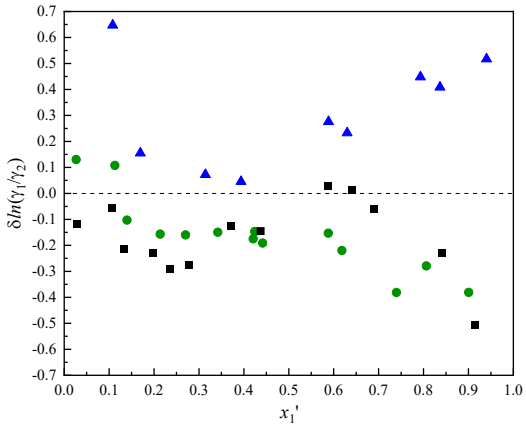


**Figure E7.** Residual distribution ( $\delta$ ) of $\ln(\gamma_1 / \gamma_2)$ for n-hexane (1) + ethanol (2) + guaiacol (3) with an E/F = 1: (■) at 100.0 kPa; and (●), 50.0 kPa, and an E/F = 3: (▲) at 50.0 kPa.

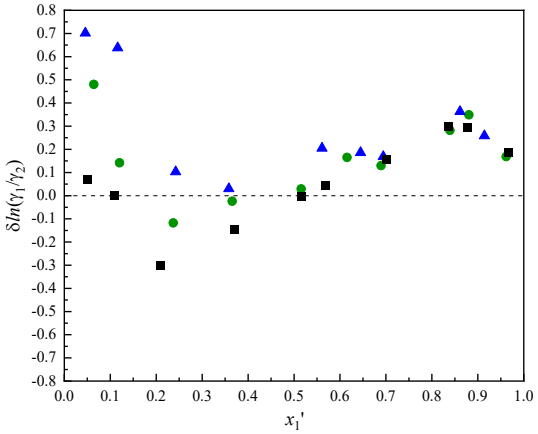


**Figure E8.** Residual distribution ( $\delta$ ) of $\ln(\gamma_1 / \gamma_2)$ for n-hexane (1) + ethanol (2) + DMI (3) with an E/F = 1: (■) at 100.0 kPa; and (●), 50.0 kPa, and an E/F = 3: (▲) at 50.0 kPa.

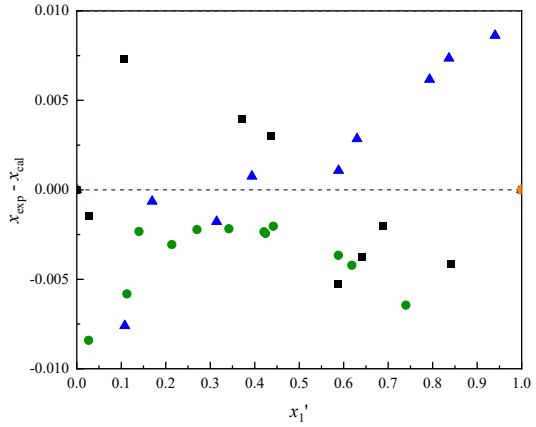


**Figure E9.** Residual plots of liquid composition for n-hexane (1) + ethanol (2) + guaiacol (3) with an E/F = 1: (■) at 100.0 kPa; and (●), 50.0 kPa, and an E/F = 3: (▲) at 50.0 kPa.

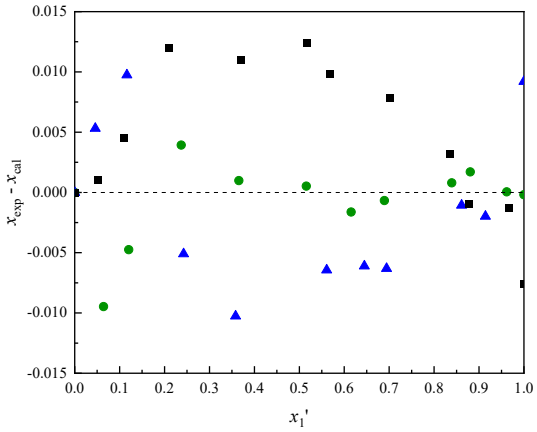


**Figure E10.** Residual plots of liquid composition for n-hexane (1) + ethanol (2) + DMI (3) with an E/F = 1: (■) at 100.0 kPa; and (●), 50.0 kPa, and an E/F = 3: (▲) at 50.0 kPa.

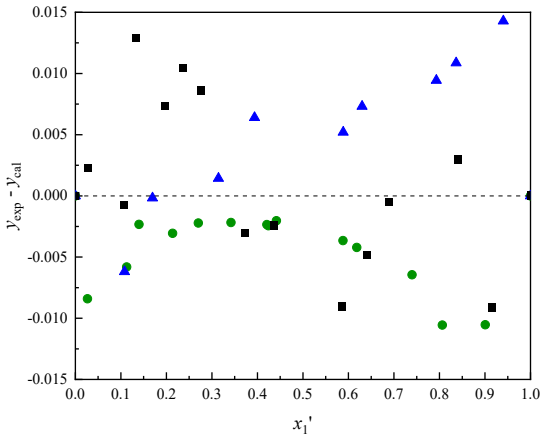


**Figure E11.** Residual plots of vapor composition for n-hexane (1) + ethanol (2) + guaiacol (3) with an E/F = 1: (■) at 100.0 kPa; and (●), 50.0 kPa, and an E/F = 3: (▲) at 50.0 kPa.

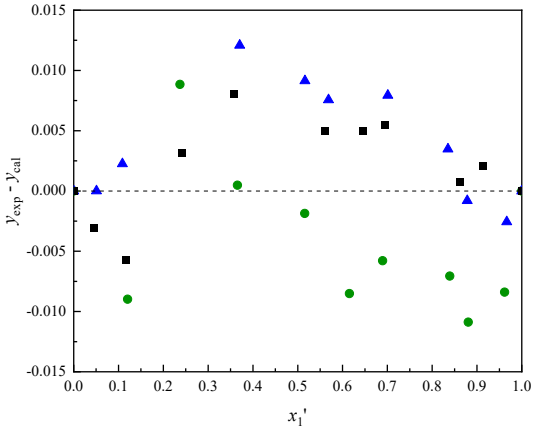


**Figure E12.** Residual plots of vapor composition for n-hexane (1) + ethanol (2) + DMI (3) with an E/F = 1: (■) at 100.0 kPa; and (●), 50.0 kPa, and an E/F = 3: (▲) at 50.0 kPa.

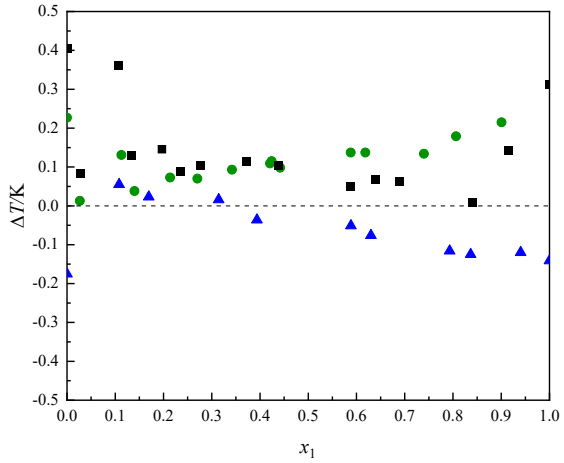


**Figure E13.** Residual plots of temperature for n-hexane (1) + ethanol (2) + guaiacol (3) with an E/F = 1: (■) at 100.0 kPa; and (●), 50.0 kPa, and an E/F = 3: (▲) at 50.0 kPa.

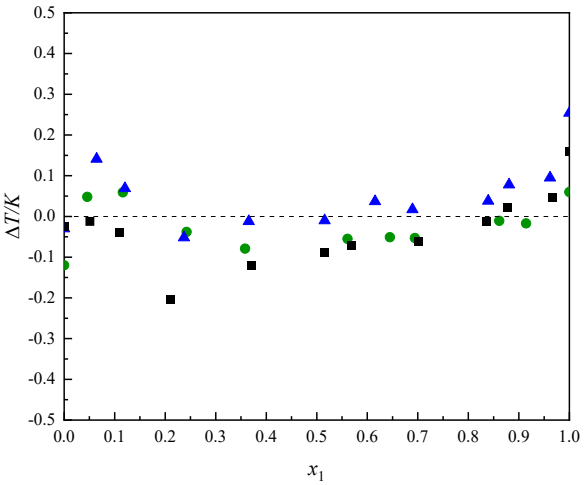


**Figure E14.** Residual plots of temperature for n-hexane (1) + ethanol (2) + DMI (3) with an E/F = 1: (■) at 100.0 kPa; and (●), 50.0 kPa, and an E/F = 3: (▲) at 50.0 kPa.

**Table E1.** Properties of the chemicals

| Chemical | $T_{\text{boiling point}}$ (K) | Hansen Solubility Parameters ($MPa^{1/2}$) | | | Ref. |
|---|---|---|---|---|---|
| | | $\delta_D$ | $\delta_P$ | $\delta_H$ | |
| Guaiacol | 478.20 | 18.0 | 8.2 | 13.3 | [1,2] |
| Dimethyl isosorbide (DMI) | 513.15 | 17.6 | 7.1 | 7.5 | [3,4] |
| 1-Methylpyrrolidin-2-one (NMP) | 475.15 | 18.0 | 12.3 | 7.2 | [1,5] |

$\delta_D$:Dispersion
$\delta_P$:Polarity
$\delta_H$:Hydrogen bonding

**Table E2.** The values of $\Delta P$ and $\Delta y$ for n-hexane (1) + ethanol (2) + guaiacol (3)

| $x_1$ | $100\left\|y_i^{cal}-y_i^{\exp}\right\|$ | $100\left\|\frac{P_i^{cal}-P_i^{\exp}}{P_i^{\exp}}\right\|$ | $x_1$ | $100\left\|y_i^{cal}-y_i^{\exp}\right\|$ | $100\left\|\frac{P_i^{cal}-P_i^{\exp}}{P_i^{\exp}}\right\|$ |
|---|---|---|---|---|---|
| ***E/F = 1; 100.0 kPa*** | | | ***E/F = 3; 50.0 kPa*** | | |
| 0.000 | 0.0 | 0.9 | 0.000 | 0.0 | 1.1 |
| 0.028 | 0.2 | 0.8 | 0.108 | 0.6 | 1.9 |
| 0.107 | 0.1 | 0.1 | 0.170 | 0.0 | 0.0 |
| 0.133 | 1.3 | 1.4 | 0.314 | 0.1 | 0.3 |
| 0.197 | 0.7 | 0.7 | 0.394 | 0.6 | 1.3 |
| 0.236 | 1.0 | 0.9 | 0.588 | 0.5 | 1.0 |
| 0.277 | 0.9 | 0.7 | 0.630 | 0.7 | 1.3 |
| 0.372 | 0.3 | 0.3 | 0.793 | 0.9 | 1.5 |
| 0.437 | 0.2 | 0.2 | 0.837 | 1.1 | 1.6 |
| 0.586 | 0.9 | 0.8 | 0.940 | 1.4 | 1.5 |
| 0.640 | 0.5 | 0.4 | 1.000 | 0.0 | 1.5 |
| 0.689 | 0.0 | 0.0 | average | **0.5** | **0.8** |
| 0.840 | 0.3 | 0.2 | | | |
| 0.916 | 0.9 | 0.9 | | | |
| 1.000 | 0.0 | 1.6 | | | |
| ***E/F = 1; 50.0 kPa*** | | | | | |
| 0.000 | 0.0 | 1.5 | | | |
| 0.027 | 0.4 | 1.1 | | | |
| 0.113 | 1.9 | 0.3 | | | |
| 0.140 | 0.6 | 0.7 | | | |
| 0.214 | 0.7 | 0.7 | | | |
| 0.270 | 0.4 | 0.4 | | | |
| 0.342 | 0.5 | 0.4 | | | |
| 0.421 | 0.5 | 0.4 | | | |
| 0.424 | 0.5 | 0.4 | | | |
| 0.442 | 0.2 | 0.2 | | | |
| 0.588 | 0.3 | 0.3 | | | |
| 0.618 | 0.3 | 0.2 | | | |
| 0.740 | 0.1 | 0.0 | | | |
| 0.806 | 0.7 | 0.6 | | | |
| 0.901 | 1.2 | 1.3 | | | |
| 1.000 | 0.0 | 0.6 | | | |
| 0.795 | 0.6 | 0.7 | | | |
| 0.904 | 1.2 | 0.4 | | | |
| 1.000 | 0.0 | 1.1 | | | |

**Table E3.** The values of $\Delta P$ and $\Delta y$ for n-hexane (1) + ethanol (2) + DMI (3)

| $x_1$ | $100\left\|y_i^{cal}-y_i^{\exp}\right\|$ | $100\left\|\frac{P_i^{cal}-P_i^{\exp}}{P_i^{\exp}}\right\|$ | $x_1$ | $100\left\|y_i^{cal}-y_i^{\exp}\right\|$ | $100\left\|\frac{P_i^{cal}-P_i^{\exp}}{P_i^{\exp}}\right\|$ |
|---|---|---|---|---|---|
| ***E/F = 1; 100.0 kPa*** | | | ***E/F = 3; 50.0 kPa*** | | |
| 0.000 | 0.0 | 0.2 | 0.000 | 0.0 | 0.9 |
| 0.051 | 0.0 | 0.0 | 0.046 | 0.3 | 3.0 |
| 0.109 | 0.2 | 0.4 | 0.116 | 0.6 | 2.2 |
| 0.209 | 2.5 | 2.2 | 0.243 | 0.3 | 0.6 |
| 0.370 | 1.2 | 0.9 | 0.358 | 0.8 | 1.1 |
| 0.516 | 0.9 | 0.7 | 0.561 | 0.5 | 0.6 |
| 0.569 | 0.8 | 0.6 | 0.645 | 0.5 | 0.6 |
| 0.701 | 0.8 | 0.6 | 0.694 | 0.5 | 0.6 |
| 0.835 | 0.3 | 0.3 | 0.861 | 0.1 | 0.1 |
| 0.878 | 0.1 | 0.0 | 0.914 | 0.2 | 0.2 |
| 0.967 | 0.3 | 0.2 | 1.000 | 0.0 | 0.6 |
| 1.000 | 0.0 | 1.5 | average | **0.5** | **0.9** |
| ***E/F = 1; 50.0 kPa*** | | | | | |
| 0.000 | 0.0 | 0.6 | | | |
| 0.064 | 1.6 | 4.2 | | | |
| 0.120 | 0.9 | 1.3 | | | |
| 0.237 | 0.9 | 0.8 | | | |
| 0.366 | 0.0 | 0.0 | | | |
| 0.516 | 0.2 | 0.2 | | | |
| 0.615 | 0.9 | 0.8 | | | |
| 0.690 | 0.6 | 0.5 | | | |
| 0.839 | 0.7 | 0.5 | | | |
| 0.881 | 1.1 | 0.9 | | | |
| 0.962 | 0.8 | 0.8 | | | |
| 1.000 | 0.0 | 2.3 | | | |

## Uncertainty Calculations

The calculation of the expanded combined uncertainties: The Guide to the Expression of Uncertainty in Measurement, ISO, October 1993 (updated in 2008)[6].

The calculation of the expanded combined uncertainties for the pseudo-ternary mixtures:

$$u_c(T) = \pm\sqrt{u^2(T_{fluctuation}) + u^2(T_{device\ specification})} \quad \text{E1)}$$

$$= \pm\sqrt{u^2(\frac{T_{fluctuation\ observed}}{\sqrt{n_T}}) + u^2(T_{device\ specification})}$$

$$= \pm\sqrt{u^2(\frac{0.4}{\sqrt{4}}) + 0.01^2}$$

$$= \pm\sqrt{0.2^2 + 0.01^2}$$

$$= 0.2\text{K}$$

$U(T)$ =>> 0.4K (level of confident 0.95 ($k$ = 2)

$n_T$ is the number of readings recorded for the value of $T$ within 15 minutes prior to sample collection.

$$u_c(P) = \pm\sqrt{u^2(P_{fluctuation}) + u^2(P_{device\ specification})} \quad \text{E2)}$$

$$= \pm\sqrt{u^2(\frac{P_{fluctuation\ observed}}{\sqrt{n_P}}) + u^2(P_{device\ specification})}$$

$$= \pm\sqrt{u^2(\frac{0.12}{\sqrt{4}}) + 0.01^2}$$

$$= \pm\sqrt{0.06^2 + 0.01^2}$$

$$= 0.11\ \text{kPa}$$

$U(P)$ =>> 0.23 kPa (level of confident 0.95 ($k$ = 2)

is the number of readings recorded for the value of $P$ within 15 minutes prior to sample collection.

$$u_c(x) = u_c(y) = \pm\sqrt{u^2(x_{repetition}) + u^2(x_{analytical\ balance}) + u^2(x_{GC})} \quad \text{E3)}$$

$$= \pm\sqrt{0.0001^2 + 0.0001^2 + 0.0027^2}$$

$$= 0.003$$

$U(x) = U(y)$ =>> 0.006 (level of confident 0.95 ($k$ = 2)

**References**


[1] R.C.. Weast, J.G. Grasselli, Handbook of Data on Organic Compounds, 2nd Editon, CRC Press, Inc., Boca Raton, FL, 1989.

[2] H. Kim, N.R. Vinueza, S.S. Kelley, S. Park, Correlation between solubility parameters and recovery of phenolic compounds from fast pyrolysis bio-oil by diesel extraction, Carbon Resour. Convers. 1 (2018) 238–244. https://doi.org/https://doi.org/10.1016/j.crcon.2018.08.004.

[3] European Chemical Agency, 1,4:3,6-dianhydro-2,5-di-O-methyl-D-glucitol, (n.d.). https://echa.europa.eu/nl/registration-dossier/-/registered-dossier/21446/4/4 (accessed July 3, 2025).

[4] A. Benazzouz, L. Moity, C. Pierlot, M. Sergent, V. Molinier, J.-M. Aubry, Selection of a Greener Set of Solvents Evenly Spread in the Hansen Space by Space-Filling Design, Ind. Eng. Chem. Res. 52 (2013) 16585–16597. https://doi.org/10.1021/ie402410w.

[5] O. Buken, K. Mancini, A. Sarkar, A sustainable approach to cathode delamination using a green solvent, RSC Adv. 11 (2021) 27356–27368. https://doi.org/10.1039/D1RA04922D.

[6] Working Group 1 of the Joint Committee for Guides in Metrology (JCGM/WG 1), Evaluation of measurement data — Guide to the expression of uncertainty in measurement, Int. Organ. Stand. Geneva ISBN. 50 (2008) 134.

## Appendix F

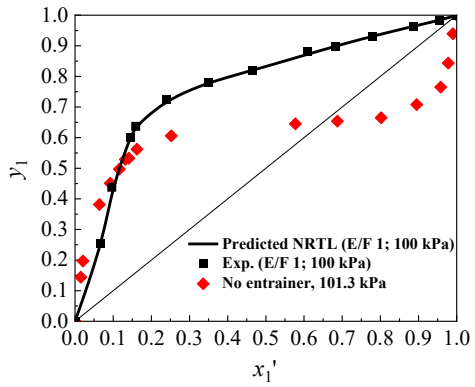


1-Methyl-2-Pyrrolidone (NMP)

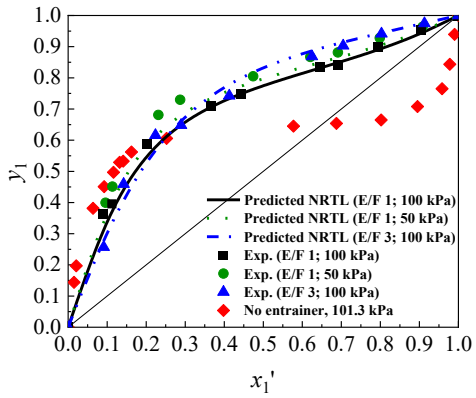


1-Butylpyrrolidin-2-one (NBP)

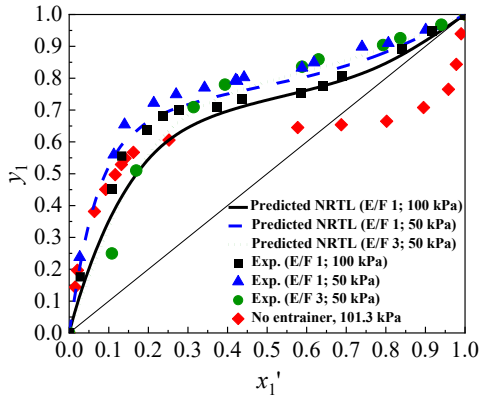


Guaiacol

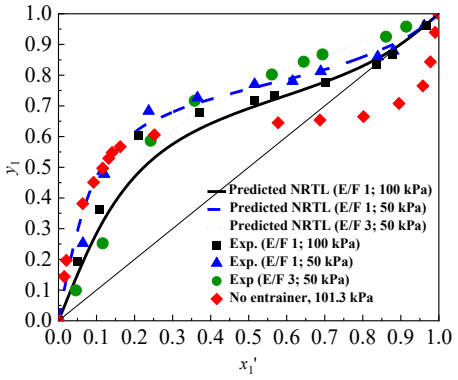


Dimethyl Isosorbide (DMI)

**Figure F1.** Comparison of the predicted and experimental VLE diagram for the n-hexane (1) + ethanol (2) mixture in the presence of various entrainers, where $x_1$ represents the mole fraction of n-hexane in the entrainer-free liquid phase, while $y_1$ indicates the mole fraction of n-hexane in the vapor phase. The experimental VLE data was obtained from our previous work, as discussed in Chapter 4.[1]

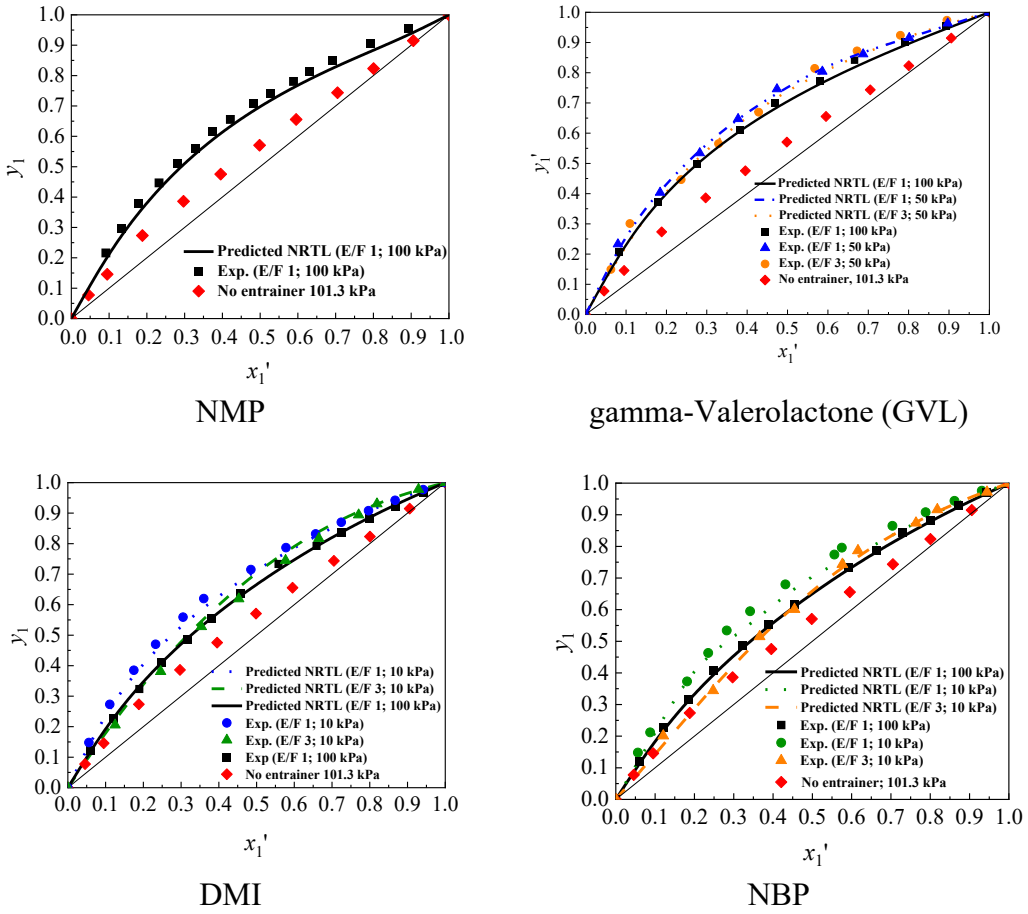


**Figure F2.** Comparison of the predicted and experimental VLE diagram for the methylcyclohexane (1) + toluene (2) mixture in the presence of various entrainers, where $x_1$ represents the mole fraction of methylcyclohexane in the entrainer-free liquid phase, while $y_1$ indicates the mole fraction of methylcyclohexane in the vapor phase. The experimental VLE data was obtained from our previous work, as discussed in Chapter 3.[2,3]

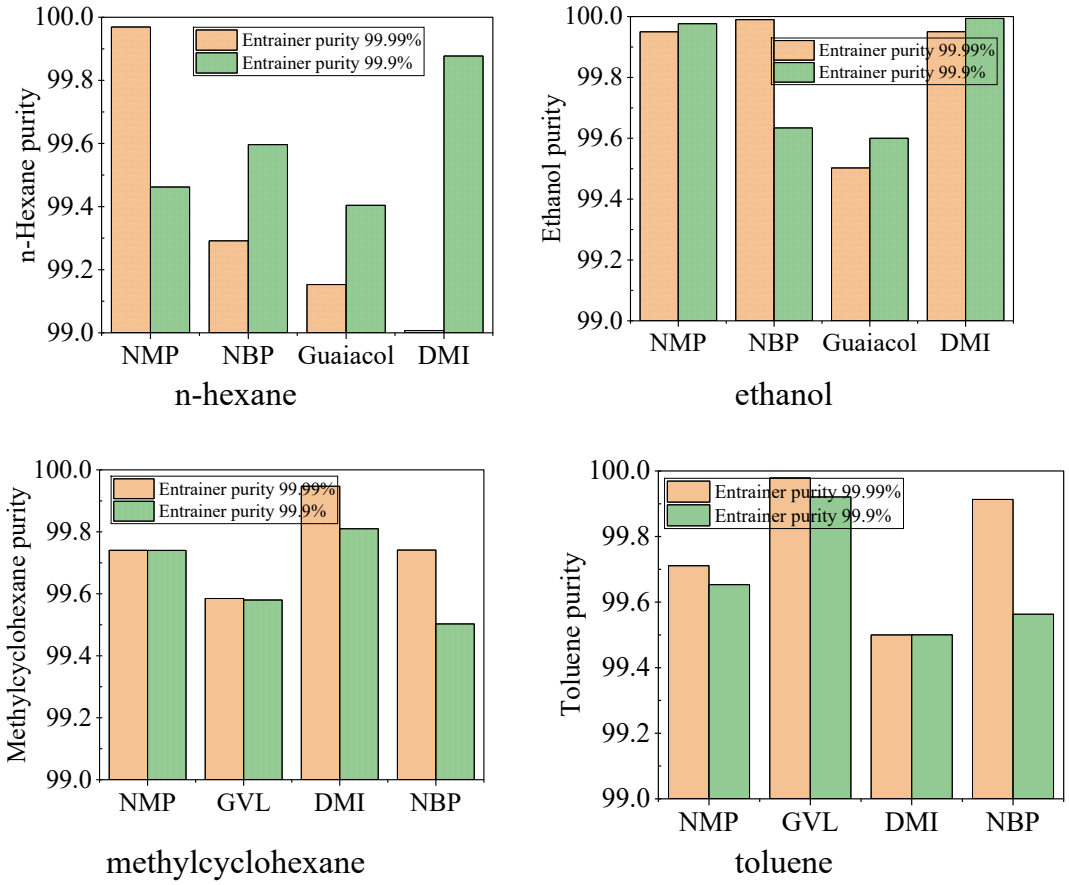


**Figure F3.** Sensitivity of recycled entrainer purity on product purity.

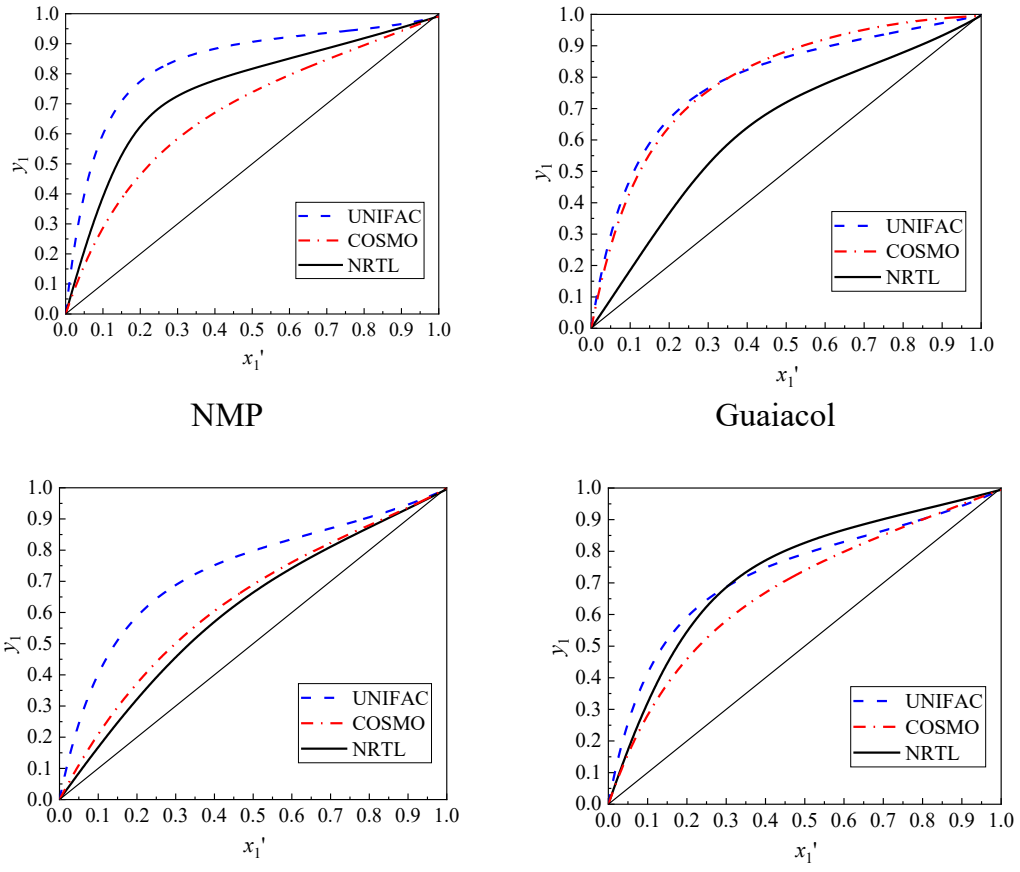


**Figure F4.** Comparison of VLE analysis (*x*-*y* diagram) obtained from NRTL, UNIFAC, and COSMO RS/SAC in the n-hexane (1) + ethanol (2) mixture at entrainer-to-feed ratio 1 and pressure of 101.3 kPa.

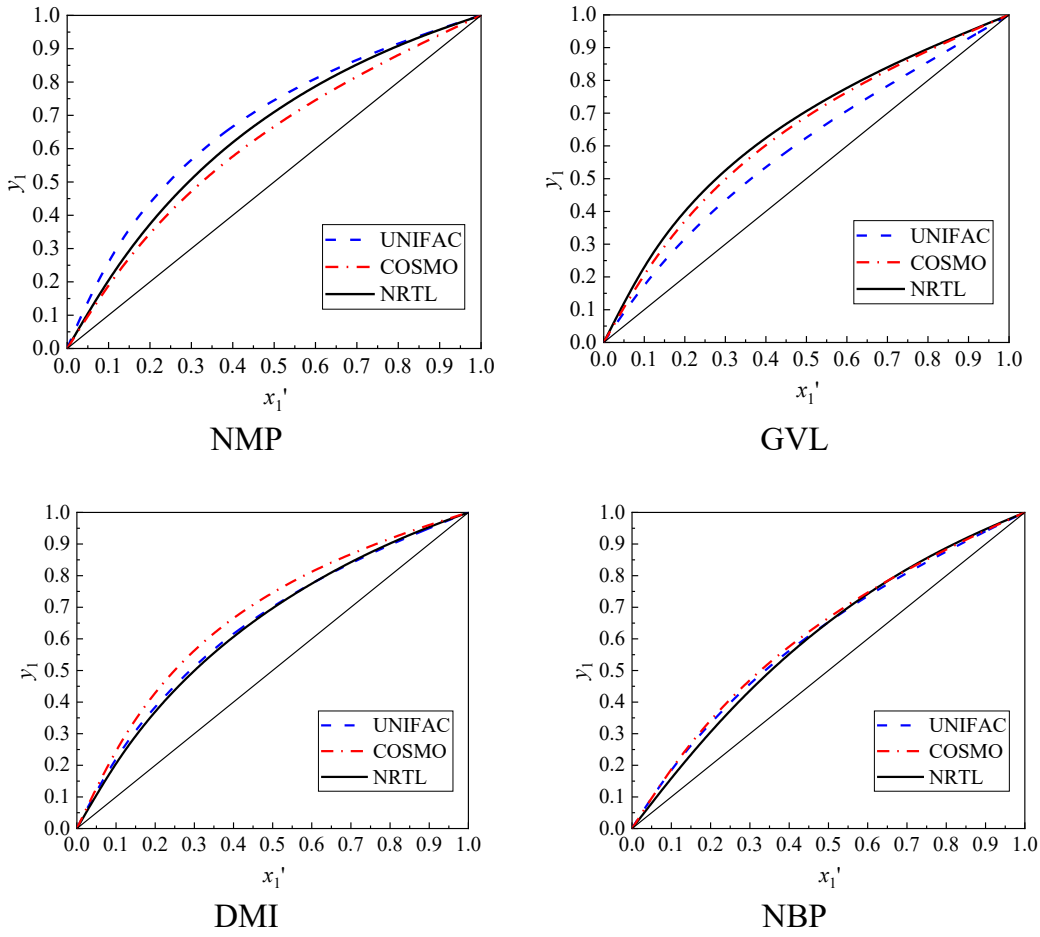


**Figure F5.** Comparison of VLE analysis (*x*-*y* diagram) obtained from NRTL, UNIFAC, and COSMO RS/SAC in the methylcyclohexane (1) + toluene (2) mixture at entrainer-to-feed ratio 1 and pressure of 101.3 kPa.

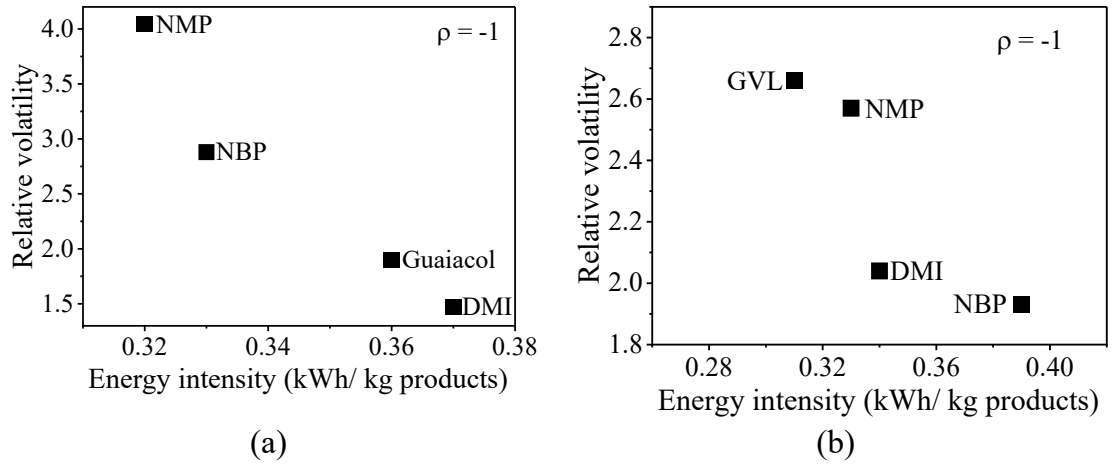


**Figure F6.** Correlation between energy intensity with relative volatility for a) n-hexane (1) + ethanol (2) mixture, and b) methylcyclohexane (1) + toluene (2) mixture. Spearman rank correlation coefficient (ρ = -1) with p-values = 0.083

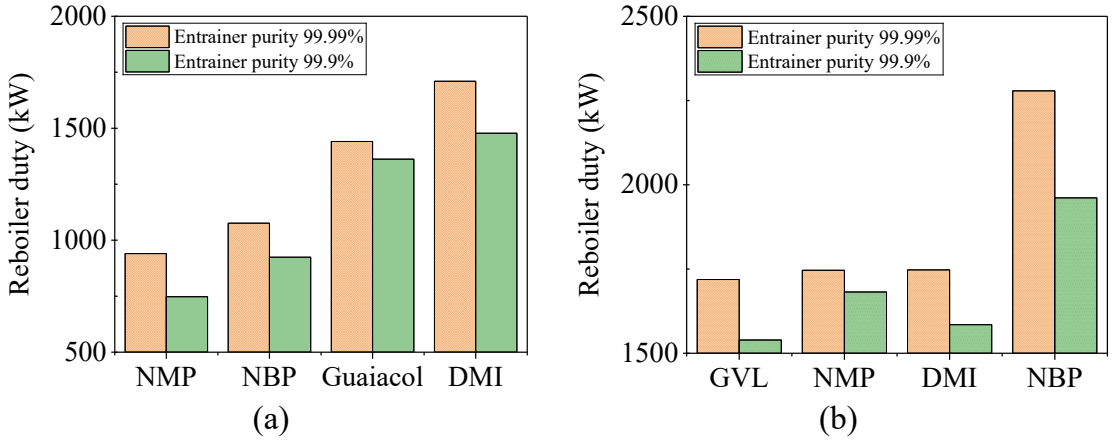


**Figure F7**. Effect of recycled entrainer purity on reboiler duty: a) n-hexane-ethanol, b) methylcyclohexane-toluene.

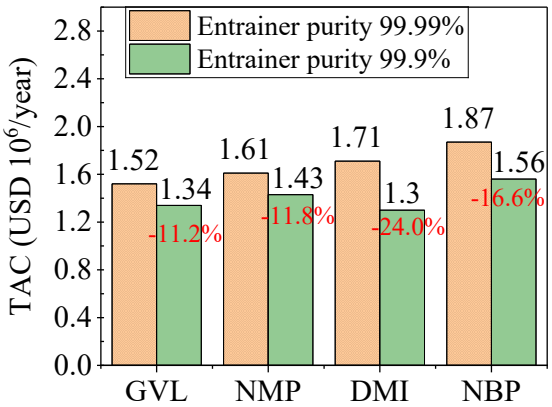


**Figure F8.** Sensitivity analysis of the recycled entrainer purity on the total annual cost (TAC) for the methylcyclohexane-toluene mixture.

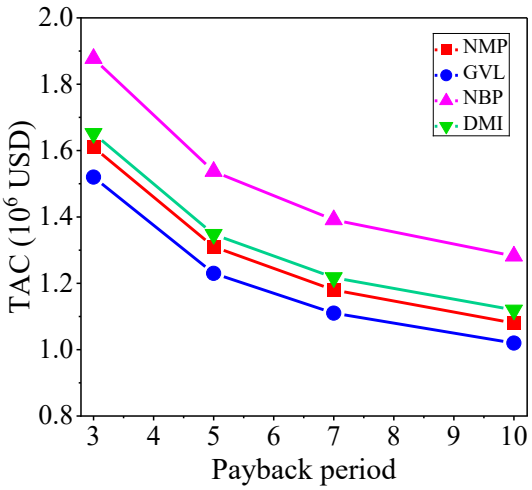


**Figure F9.** Sensitivity analysis of payback period vs TAC for the MCH-TOL mixture.

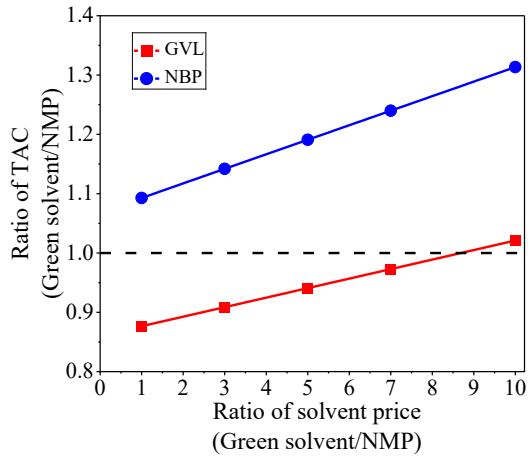


**Figure F10.** Sensitivity analysis for solvent price ratio (green solvent/NMP) vs TAC ratio (green solvent/NMP) for the MCH-TOL mixture.

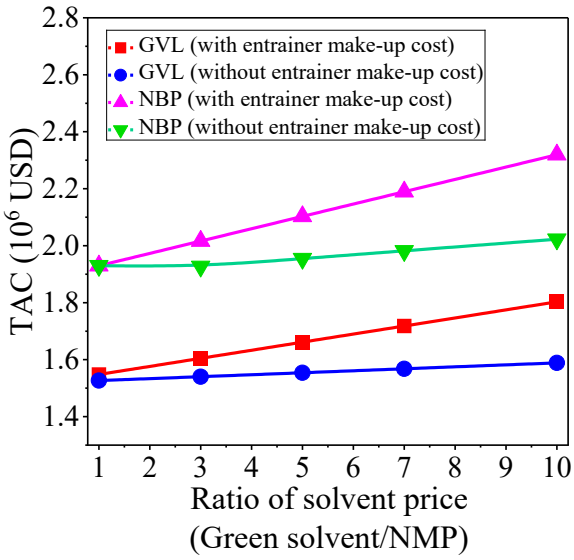


**Figure F11.** Sensitivity analysis for solvent price ratio (green solvent/NMP) with and without make up entrainer cost vs TAC for the MCH-TOL mixture.

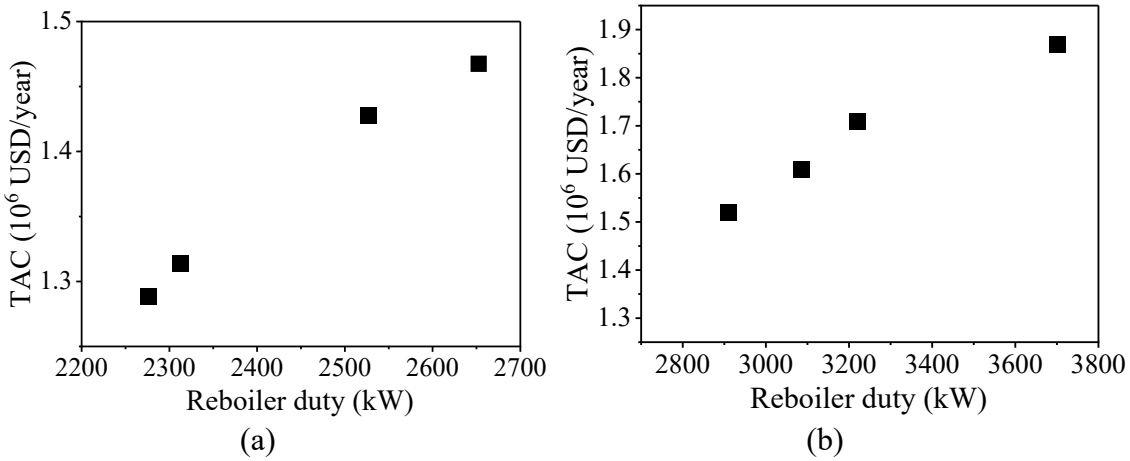


**Figure F12.** Correlation of the reboiler duty (kW) to total annual cost for a) n-hexane (1) + ethanol (2) mixture, and b) methylcyclohexane (1) + toluene (2) mixture.

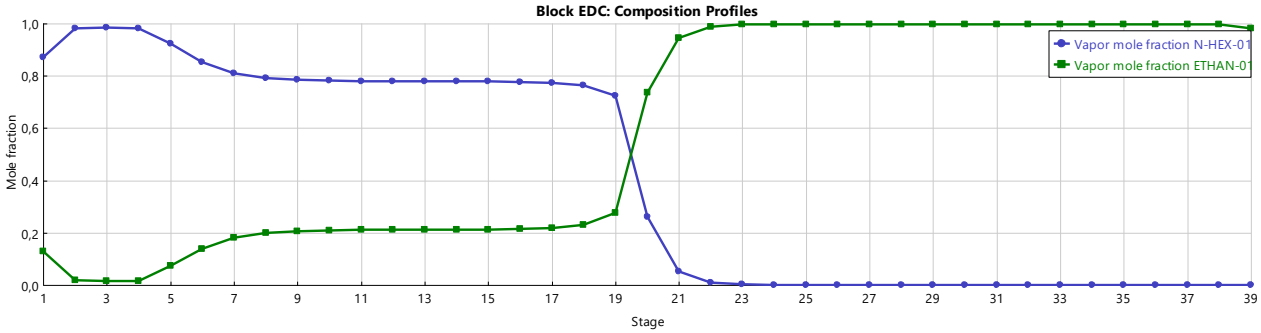


**Figure F13.** Composition profile in ED for n-hexane-ethanol-1-butylpyrrolidin-2-one at entrainer-to-feed ratio of 1 and pressure of 100.0 kPa.

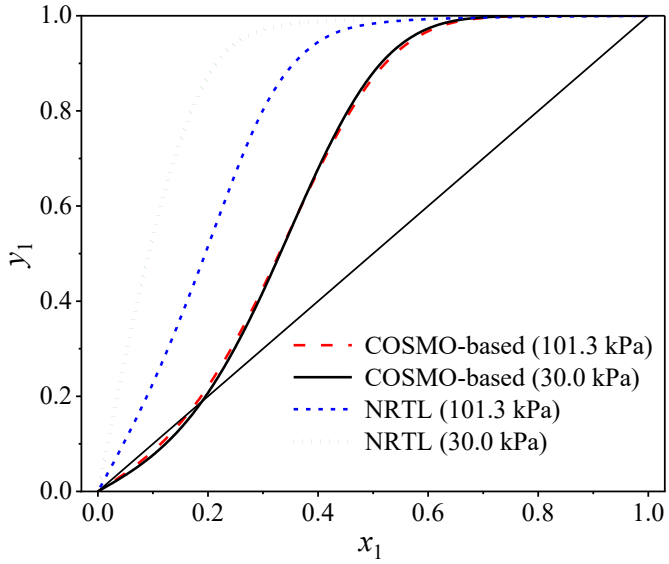


**Figure F14.** Predicted $x_1$-$y_1$ diagram for ethanol (1) + dimethyl isosorbide (2) mixture at 101.3 and 30.0 kPa.

**Table F1.** Binary interaction parameters (BIPs) of the NRTL model for the pseudo-ternary of n-hexane (1) + ethanol mixture in the presence of the investigated entrainers.[a,b]

| *i* component | *j* component | $A_{ij}$ | $A_{ji}$ | $B_{ij}$/K | $B_{ji}$/K | $C_{ij}$ |
|---|---|---|---|---|---|---|
| *n-hexane (1) + ethanol (2)* (entrainer: *1-butylpyrrolidin-2-one (3)* and *1-methylpyrrolidin-2-one (3)*) | | | | | | |
| [c]n-hexane (1) | ethanol (2) | -10.342 | -3.854 | 4120.934 | 1829.392 | 0.47 |
| n-hexane (1) | 1-butylpyrrolidin-2-one (3) | 1.748 | -13.206 | -581.379 | 5130.115 | 0.05 |
| ethanol (2) | 1-butylpyrrolidin-2-one (3) | 22.377 | -1.069 | -5518.982 | -133.055 | 0.45 |
| n-hexane (1) | 1-methylpyrrolidin-2-one (3) | -20.555 | 80.001 | 7813.650 | 9869.500 | 0.08 |
| ethanol (2) | 1-methylpyrrolidin-2-one (3) | 21.541 | 5.203 | -5845.412 | -2561.179 | 0.30 |
| *n-hexane (1) + ethanol (2)* (entrainer: *guaiacol (3)* and *dimethyl isosorbide (3)* ) | | | | | | |
| [c]n-hexane (1) | ethanol (2) | -10.342 | -3.854 | 4120.934 | 1829.392 | 0.47 |
| n-hexane (1) | guaiacol (3) | 24.967 | -14.786 | -7227.525 | 4793.393 | 0.26 |
| ethanol (2) | guaiacol (3) | 11.866 | -4.250 | -1934.061 | 1244.481 | 0.55 |
| n-hexane (1) | dimethyl isosorbide (3) | 11.988 | -12.067 | -2984.570 | 3932.560 | 0.30 |
| ethanol (2) | dimethyl isosorbide (3) | 11.537 | -11.680 | -3369.973 | 3639.305 | 0.30 |

[a] $A_{ij}$, $A_{ji}$, $B_{ij}$, and $B_{ji}$ asymmetric parameters; $C_{ij}$: the constant of non-randomness.

[b] NRTL Model: $\tau_{ij} = A_{ij} + B_{ij} / T$

[c] The BIPs for the hexane (1) – ethanol (2) pair were derived from the correlation of the VLE data at 101.3 kPa from this work combined with the VLE data at 61.3 kPa from literature.[4]

**Table F2.** Binary interaction parameters (BIPs) of the NRTL model for the pseudo-ternary of methylcyclohexane (1) + toluene mixture in the presence of the investigated entrainers.[a,b]

| *i* component | *j* component | $A_{ij}$ | $A_{ji}$ | $B_{ij}$/K | $B_{ji}$/K | $C_{ij}$ |
|---|---|---|---|---|---|---|
| *methylcyclohexane (1)+ toluene (2)* (entrainer: *gamma-valerolactone (3)* and *1-methylpyrrolidin-2-one (3)*) | | | | | | |
| [c]methylcyclohexane (1) | toluene (2) | -1.018 | 2.709 | 792.083 | -1248.381 | 0.30 |
| methylcyclohexane (1) | gamma-valerolactone (3) | 7.561 | -11.816 | -2200.111 | 4677.751 | 0.15 |
| toluene (2) | gamma-valerolactone (3) | 6.264 | -0.726 | -1783.554 | 329.415 | 0.88 |
| methylcyclohexane (1) | 1-methylpyrrolidin-2-one (3) | -3.548 | 4.113 | 1979.856 | 394.855 | 0.30 |
| toluene (2) | 1-methylpyrrolidin-2-one (3) | 13.533 | 13.858 | -5223.890 | -3020.539 | 0.30 |
| *methylcyclohexane (1)+ toluene (2)* (entrainer: *dimethyl isosorbide (3)* and *1-butylpyrrolidin-2-one (3)*) | | | | | | |
| [d]methylcyclohexane (1) | toluene (2) | -0.523 | -0.811 | -55.064 | 736.883 | 0.30 |
| methylcyclohexane (1) | dimethyl isosorbide (3) | 3.745 | 13.580 | -1626.755 | -2771.820 | 0.11 |
| toluene (2) | dimethyl isosorbide (3) | 5.206 | -1.493 | -2769.191 | 3938.608 | 0.11 |
| methylcyclohexane (1) | 1-butylpyrrolidin-2-one (3) | 12.977 | -3.019 | -3577.819 | 747.748 | 0.23 |
| toluene (2) | 1-butylpyrrolidin-2-one (3) | 4.372 | 4.247 | 2558.016 | 16.399 | 0.85 |

[a] $A_{ij}$, $A_{ji}$, $B_{ij}$, and $B_{ji}$ asymmetric parameters; $C_{ij}$: the constant of non-randomness.

[b] NRTL Model: $\tau_{ij} = A_{ij} + B_{ij} / T$

[c] The binary interaction parameters of methylcyclohexane (1) – toluene (2) pair were obtained from the correlation based on the combination of the binary VLE data measured in this work and literature.[5]

[d] Experimental VLE data for a binary system of methylcyclohexane (1) and toluene (2) at 101.3 kPa from our previous work[2] and at 26.7 and 53.3 kPa from reference[5] were combined and used to obtain the BIPs of methylcyclohexane and toluene pair.

**Table F3.** Equation for process performance calculations.

| Metric | Equation |
|---|---|
| Total annual cost | $TAC\,(USD/year) = \frac{Total\ Capital\ Cost}{Payback\ Period} + Total\ Operating\ Cost$ |
| Energy intensity | $Energy\ Intensity\,(kWh/kg) = \frac{Total\ Q_{reb.EDC} + Q_{reb.ERC}\,(kWh)}{Total\ products\ (kg)}$ |
| $CO_2$ emissions | $[CO_2]_{emission} = \left(\frac{Amt_{fuel}}{NHV}\right) \times \left(\frac{C\%}{NHV}\right)\alpha$<br>NHV: the net heating value of a fuel (for natural gas: 48,900 kJ/kg)<br>C%: the carbon content of the fuel, (for natural gas: 0.41 kg/kg)<br>$\alpha$: the molar mass ratio of $CO_2$ to carbon (3.67)<br><br>The term $Amt_{fuel}$ implies to the amount of fuel required (kJ/h).<br><br>$Amt_{fuel} = \frac{Q_{proc}}{\lambda_{proc}} \times (h_{proc} - 419) \times \frac{T_F - T_0}{T_F - T_S}$<br>$Q_{proc}$: the heat required in the reboiler duty<br>$\lambda_{proc}$ : the latent heat (kJ/kg) (low pressure steam (LP): 2081.3 kJ/kg; medium pressure steam (MP): 1995.2 kJ/kg, high pressure steam (HP): 1714.6 kJ/kg)<br>$h_{proc}$ : the enthalpy of steam (kJ/kg). LP steam: 2756.7 kJ/kg, MP steam: 2780.4 kJ/kg, HP steam: 2800.4 kJ/kg.<br><br>$T_S$: stack temperature (2073.15 K)<br>$T_F$: flame temperature in the reboiler (453.15 K)<br>$T_0$: ambient temperature (298.15 K). |

**Table F4.** Equation for equipment and utility cost calculations

| Equipment and Utility | Equation |
|---|---|
| Column cost | $= \frac{M\&S}{280} \times 937.636 \times ID^{1.0666} \times H^{0.802} \times (2.18 + F_c)$<br>$F_c = F_m\, F_p$ |
| Plate cost | $= \frac{M\&S}{280} \times 97.243 ID^{1.0666} \times F_c$<br>$F_c = F_s + F_t + F_m$ |
| Heat exchanger cost | $= \frac{M\&S}{280} \times 474.668 \times A^{0.65} \times (2.29 + F_c)$<br>$A = \frac{Q}{\Delta T \times k}$ |

| Equipment and Utility | Equation |
|---|---|
| | $F_c = (F_d + F_p) \times F_m$ |
| Steam cost (annual) | $= Q_R \times C_S$ |
| Cooling water cost (annual) | $= Q_C \times C_W$ |
| Utility cost | Low pressure (LP) steam (6 bar, 433 K) : 7.78 USD/GJ<br>Medium pressure (MP) steam (11 bar, 457 K): 8.22 USD/GJ<br>High pressure (HP) steam (42 bar, 527 K): 9.88 USD/GJ<br>Cooling water (1 bar, 310 K): 0.35 USD/GJ |
| Marshall & Swift Index (M&S) | 1773.4 (2021) |

**Symbol list:**

H: length (m)

ID: Diameter (m)

$F_c$: Correction factor

$F_m$: Material factor (3.67 for glass-lined steel in column and HE, 1.7 for plate)

$F_p$: Pressure factor (1 for column operating pressure below 3.4 atm and 0 for HE)

$F_s$: Tray spacing factor (0.6 for plate)

$F_t$: Tray type factor (0 for sieve plate column)

$F_d$: Heat exchange design factor (1)

$A$: Heat exchanger area ($m^2$)

$Q$: Heat exchanger duty (kW)

$\Delta T$ : Temperature difference (K)

$k$: Coefficient of heat transfers (kW/K $m^2$) 0.852 for the condenser and 0.568 for the reboiler

$Q_R$: reboiler duty (kW)

$C_S$ : Price of steam (USD/year)

$Q_C$: Condenser duty (kW)

$C_W$ : Price of Cooling water (USD/year)

## References


(1) Hartanto, D.; Schuur, B.; A. Kiss, A.; de Haan, A. B. Isobaric Vapor-Liquid Equilibrium of the Azeotropic Mixture n-Hexane + Ethanol with 1-Butylpyrrolidin-2-One as a Greener Entrainer and 1-Methylpyrrolidin-2-One as a Benchmark Entrainer. *J. Chem. Eng. Data* **2025**, *70* (10), 4091−4104.

(2) Hartanto, D.; Schuur, B.; Schuttevaer, T.; Kiss, A. A.; de Haan, A. B. Isobaric Vapor–Liquid Equilibrium of Methylcyclohexane + Toluene with Gamma-Valerolactone as a Biobased Entrainer and 1-Methylpyrrolidin-2-One as a Conventional Entrainer. *J. Chem. Eng. Data* **2025**, *70* (3), 1339−1351. https://doi.org/10.1021/acs.jced.4c00509.

(3) Hartanto, D.; Schuur, B.; Ammerlaan, M.; Kiss, A. A.; de Haan, A. B. Vapor–Liquid Equilibrium for the Separation of the Close-Boiling Mixture Methylcyclohexane–Toluene with Dimethyl Isosorbide as a Biobased Entrainer and 1-Butylpyrrolidin-2-One as a Greener Entrainer. *Ind. Eng. Chem. Res.* **2025**, *64* (38), 18927–18937. https://doi.org/10.1021/acs.iecr.5c01616.

(4) Ortega, J.; Espiau, F. A New Correlation Method for Vapor−Liquid Equilibria and Excess Enthalpies for Nonideal Solutions Using a Genetic Algorithm. Application to Ethanol + an n-Alkane Mixtures. *Ind. Eng. Chem. Res.* **2003**, *42* (20), 4978–4992. https://doi.org/10.1021/ie030327j.

(5) Weber, J. H. Vapor-Liquid Equilibria for System Methylcyclohexane-Toluene at Subatmospheric Pressures. *Ind. Eng. Chem.* **1955**, *47* (3), 454–457. https://doi.org/10.1021/ie50543a036.

(6) Gutierrez Hernandez, J. P. Extractive Distillation with Ionic Liquids as Solvents : Selection and Conceptual Process Design, Technische Universiteit Eindhoven, 2013. https://doi.org/10.6100/IR751728.

(*This page is intentionally left blank*)

# Acknowledgements

*Alhamdulillahi rabbil 'aalamiin*

Time has passed, and my PhD journey has finally reached its end. Looking back, this journey was a remarkable adventure, filled with tremendous challenges, unexpected turns, small victories, and wonderful rewards at almost every step. As I write this section, I still feel a strange mix of disbelief and deep gratitude. It is still hard for me to believe that I had opportunity to pursue and complete a PhD at Delft University of Technology, one of the most prestigious technical universities in the world. There was a time when I did not even dare to dream of obtaining a PhD from TU Delft. It felt too high and almost unreachable for me. But this journey happened. And it happened not because I walked alone, but because I was surrounded with many people who supported me a lot. They provided invaluable direct and indirect supports, help, advices and suggestions both in academic and in non-academic life. This PhD is therefore not an individual achievement. It is collective story, shaped by many generous and remarkable people who contributed in different ways. For that reason, I dedicate this chapter to everyone who has given me invaluable support throughout this journey. I am sincerely grateful to each of them. If I unintentionally forget one or two names, please accept my heartfelt apology.

My first acknowledgement is dedicated to my supervisors who provided amazing mentorship, thoughtful discussions, and genuine care throughout my PhD. I would like to express my deepest gratitude to **Prof. André** and **Prof. Tony**. It has truly been an honor to be supervised by both of you, your expertise in your fields, combined your extensive academic and industrial experience, has always been extraordinary for me. I was amazed that in almost every conference or course I attended, many people seemed to know both of you. Even before starting my PhD, when I learned that I would be supervised by both of you, I was very happy because your names appeared, in chemical engineering handbooks, important publications and works. It felt a little bit like being a fan who suddenly gets chance to meet and work with his favorite famous artist. Both of you were very encouraging and supportive, despite my experience and knowledge at the beginning were still very limited, and perhaps far from your academic standard. Beyond academic matters, both of you also consistently reminded me to care not only myself but also my family's well-being.

**Prof. André**, thank you very much for responding to my email when I was looking for a PhD position at TU Delft. To be honest, even now, I still cannot fully believe that I applied for a PhD at one of the leading technological universities in

the world and was accepted under your supervision. For me, the university once seemed unreachable. But you believe in me and gave me a chance to become your PhD student after the interview with you, Prof Tony and Prof. Valeria. Thanks for offering me this PhD position. I still remember that I had to postpone the start of my PhD for almost one year because my wife's health issue and the Covid outbreak. At that time, even before I officially start to become you PhD student, you had already given me a lot of support and understood my situation very well. When I eventually started my PhD, Covid protocols were still applied in both Indonesia and the Netherlands. It was a challenging beginning, but you always gave support and advice on how to start my PhD effectively. I also remember that within first month of my PhD, you had already given me a task to write an abstract for my first PhD conference, Distillation & Absorption 2022. Thank you for pushing me to write that abstract and sending me to that conference. It became my first scientific writing and conference experience during my PhD journey. It was also amazing that, at that time, you were already preparing me not only for DA2022, but even DA2026. I am also thankful that you involved me in the Transport Phenomena and Process System Engineering Group. Beyond academic work, you continuously supported me and showed your concern not only for my research but also myself and my family's well-being. Even during progress meetings, we did not only discuss research. We also chatted about vacation, culture, and even political and economic conditions both in Indonesia and the Netherlands. Those conversations made the meetings feel more relaxed. What I value most is your mentorship, which helped me not only to change how I think and act as a scientist, but also to grow as a person. I am truly grateful for your unwavering support throughout my PhD and as I move forward in my career as academia. It has been always a great honor for me to be your PhD student. Finally, I am glad to be your last PhD student, and I hope I can fulfill your expectation as your final PhD student.

I would also like to extend my deepest gratitude to **Prof. Tony**. I met you for the first time online when you interviewed me for my PhD application. You asked difficult questions and gave critical comments on my research proposal. At that moment, I was a bit worried that you might give a low score to my proposal. But you believed that I could improve it and finally I did. Thank you for accepting me as you PhD student. During my PhD, you provided invaluable support through your critical yet constructive feedback on my research and manuscript drafts. Your comments significantly improved the quality of my work. Thank you for always challenging me in my research, especially with your unique and unforgettable remarks such as "So what?", "Why? How? What?". At first, sometimes those questions were not always easy to answer, but for sure they improve me a lot. I also remember when you mentioned that you liked my research because it

combined both simulation and experimental work. During some discussions about predictive models and AI with colleagues at the ESCAPE34-PSE24 conference, and also during one of the PSE activities, you called me to join the conversation and share my opinion about the importance of experimental work. That moment gave me more motivation. Also, thank you for the chocolate that you always gave to me after I presented my progress. I am also glad to be part of the beginning member of the PSE group, which you lead. It taught me a lot about how to build and run the research group effectively. I will use PSE group activities as one of the benchmarks to apply at my home university in Indonesia. Also, you once told me that Indonesian humidity is terrible during your visit to Indonesia. Yet, I still might invite you to come to my home university in the near future.

My second acknowledgements is to **the Indonesia Endowment Fund for Education** (**LPDP**), Indonesia Ministry of Finance for providing me with a full PhD scholarship, with grant number SKPB-1597/LPDP/LPDP.3/2024. This scholarship means a lot to me, because my PhD journey would not have been possible without it. The full support and services from LPDP make my PhD filled with fruitful academic activities, and finally allowed me to finish this thesis and graduate. I hope LPDP scholarship will continue for a long time, so that it can nurture more Indonesians to reach their dreams of better education and a better life, and more importantly, to contribute and make an impact together for the society and for the development of Indonesia in every sector.

I would also like to thank **Prof. Valeria Garbin** for being one of the interviewers during my PhD application and also for being involved in my Go/No Go evaluation. I also thank to **Dr. Artur M. Schweidtmann** for being a committee member in my Go/No Go. Thank you both for your suggestions and feedback on my research. I would also like to express my sincere gratitude to graduate school of TU Delft for informing and organizing paperwork during my study as well for my defense ceremony, the doctoral committee include **Prof. Hester Bijl** (Rector Magnificus, Chairman), independent members: **Prof. Thijs Vlugt** (TU Delft), **Prof. Boelo Schuur** (University of Twente), **Prof. Meik B. Franke** (University of Twente), **Prof. John van der Schaaf** (Eindhoven University of Technology), and **Prof. Ferdinand Grozema** (TU Delft), for reviewing and assessing my dissertation.

I would like to sincerely thank to **Transport Phenomena (TP)** and **Process System Engineering (PSE)** groups, as well as the **Department of Chemical Engineering**, and the **Faculty of Applied Sciences** at TU Delft for their significant supports throughout my PhD journey. To **Sandra Paffen**, thank you for your crucial assistance at the beginning of my PhD, for providing detailed information regarding housing options, and for supporting all the paperwork and many other administrative matters. To my officemate **Matheus**, and **Artem,** thank

you for welcoming me into the office with such warm and friendly environment. To **Ruipeng,** thank you for the nice chats about food, culture, and many other things. To **Jorrit**, thanks for helping me acclimate and adapt to the TP group. I would also like to thank my colleagues in the PSE as my second group at TU Delft. To **Adinda Kohler**, many thanks for your extensive administration support, which made my PhD journey much smoother. To **Farzad**, thanks for the nice discussions, for working together in Aspen Workshop, and for the nice evening walk and chat during the conference in Florence. To **Qing**, thank you for nice discussions about distillation and related topics. In the Chemical Engineering Department, I was also glad to meet fellow Indonesians. Thanks for the chats and help, Mas **Albert,** Mbak **Amsal**, Mas **Helmi**, and Mas **Angga.** I also thank all TP and PSE colleagues for welcoming me into the groups. Also, many thanks to **Jochem**, **Merve**, **Matthijs**, and **Samar** for your contribution in the process simulation.

An important part of my PhD journey took place in Enschede, my second home in the Netherlands. I would therefore like to extend my appreciation to Sustainable Process Technology (SPT) group, University of Twente, for welcoming me so warmly and kindly. Thank you very much to **Prof. Boelo** for facilitating me to conduct experiments at SPT for almost two years. To **Erna**, **Benno**, **Ronald**, and **Raymond**, thank you for your guidance and help in ordering the chemical and preparing the VLE setup at the Meader and HPL labs. The problem was always beside the setup, but somehow you always provided effective solution. To **Yvonne**, thank you for setting up the paperwork and administration matters during my research visit at SPT. To **Hilbert**, thank you for giving me the tutorials on the VLE setup and COSMO-RS software. To **Tim**, thanks for helping me with GC. To Mbak **Helda**, Mas **Albertus**, and Mas **Dwi**, thanks for introducing me to SPT colleagues, and giving me detailed information, and of course for the chat. Also, thanks to **Tim Schuttevaer** for helping me with the experiment.

Beyond my academic activity, my second family in the Netherlands was always there for me. Many thanks to Mas **Goban** for welcoming me at Aart van der Leeuwlaan, to mukimin Delft and KMD, Pak **Deden**, Pak **Sigit** and Mbak **Wuri**, Mas **Aga** and Mbak **Kitty**, Kang **Jeje (Hariadi)**, Mas **Tofan**, Mas **Pandu**, Mas **Sindu**, Mas **Habib**, Kang **Mamin**, Bli **Wayan** and Mbak **Maeyta,** and Mas **Antra** and Mbak **Anni**. Special thanks to Mas **Ramzi** and Mbak **Mutiah** for your hospitality and for providing accommodation during my defense, and to all KMD fellows: Mas **Gilang**, Mas **Rifki**, Mbak **Fira**, Mbak **Hamida**, Mas **Widana**, Uda **Hanif**, Mbak **Sasa** (kecil), Mbak **Sasa** (besar) Mas **Habbie**, Mas **Fakhri**, Mas **Satria Galih**, Mas **Syakal**, Mas **Raihan**, Mas **Fafa**, Mas **Teddy**, Mas **Fahmi**, Mas **Budi**, Mbak **Adibah** and Mas **Yasa**, Uni **Reni**, Mas **Wildan**, Mbak **Dita**, Mas **Yafie**, Mas **Tono**, Mas **Faudy**, Mas **Fandi**, and Mas **Ardi**. Thank you for the invaluable support dan may Allah reward all of us. Aamiin. Also, to my Indonesian

colleague Mas **Arya**, Mas **Ardhan**, Mas **Maundri**, Mas **Jerry**, Mas **Aryesh**, and to all Indonesian students in Delft, PPI Delft, thanks a lot for the warm welcome and for providing detailed information for all of us. Good luck to all of us!

During my research visit in Enschede, I was surrounded by wonderful Indonesians. I would like to greatly appreciate the help of **Oma Sophie**, who gave me her permission to stay in her house during my two years experiments at UT. Thank you also for the delicious Indonesian and Dutch food that you cooked for me every day, and for sharing your beautiful life experience. To Oma Sophie's family, **Andre, Mareike, Dian, Yara**, Bu **Rumi**, thank you for very warm welcome. To Bu **Elly**, Bu **Enung**, Bu **Finfin**, **Bu Windie,** Bu **Yatie**, and other Ibu-Ibu Enschede who often visited Oma Sophie's home, chatted with me and of course provided and shared their delicious Indonesian snacks and food, thank you very much. Thank you for becoming my second family in the Netherlands. To Mas **Ega**, I first met you at Masjid IVEO, thank you for your recommendation and for letting me know about Oma Sophie's house. You opened the gate for me to know Indonesian families, IMEA, and friends in Enschede. Thank you also Mas **Hafidz,** Mas **Fidel,** Mas **Agung** for being my house mate, cooking, eating, and go to masjid together. To Mas **Candra,** Mas **Yasir,** Mas **Giri,** Mas **Ibnu**, and all IMEA members, thanks for helping me maintain my motivation and istiqomah in practicing Islam in Enschede. All of your support made my PhD balance. *Alhamdulillah*, I am also grateful for the EURO Muslim family. *Jazakumullah khairan katsiron* Pak **Said** and Ustadz **Agus** for guiding me and my wife during hajj pilgrimage. To my fellow hajj, Pak **Archi**, Mas **Niko**, Mas **Yusuf**, Mas **Shiddiq**, Mas **Herian,** Mas **Rihan**, Mas **Archie,** Mas **Fawaz**, and other jamaah, thank you for being part of that meaningful and beautiful journey.

I am deeply grateful to **Universitas Negeri Semarang**, the **Faculty of Engineering**, and the **Department of Chemical Engineering** for the tremendous support throughout the preparation and completion of of my PhD journey. Many thanks to my colleagues Bu **Selvi,** Bu **Prima**, Bu **Pita**, Bu **Widi**, Bu **Mega**, Bu **Dewi**, Bu **Lia**, Bu **Rini,** and Bu **Harianingsih**. I also thank Mas **Bayu**, Bu **Tanti**, Pak **Haniif,** Pak **Dieqi** for the insight, laughter, and support. Among others, Bu **Ria**, Bu **Nindi**, Bu **Rani**, Bu **Fafa**, Pak **Hanif**, Bu **Maulida**, Bu **Iin**, Bu **Ima**, Pak **Akbar**, Pak **Danang**, **Lala**, and **Reni**, thanks for your continuous support. I would also like to thank Prof. **Nur Qudus** (UNNES), Prof. **Pita** (UNNES), Prof. **Gede** (ITS), Prof. **Kuswandi** (ITS), Dr. **Ianatul** (University of Nottingham Malaysia) for providing recommendations during my scholarship application. My sincere gratitude also goes to Mbak **Saidah** who helped and shared information and suggestions during my PhD application, To **Annas** and Mbak **Anki**, many thanks for helping with paperwork at ITS, and to my colleagues K47 friends who have similar research areas with me, **Asalil** and **Agung,** for the discussion ranging from

thermodynamics topics to random talks. Look forward to continuing our collaboration, and I wish you success in your PhD journey! Thank you, Dr. Ardila Hayu Tiwikrama (**Tiwi)**, for the discussion, I look forward to collaborating with you in the near future. Thanks also to one of my best friends since bachelor's study, **M. Ali Fauzi**, for your inspiration and support, also for visiting me in the Netherlands.

Special thanks to one of the most important support systems during my PhD journey, which was accidentally established from an initial online discussion for PhD preparation in the Netherlands, and later named as "BNLB yg penting lulus". Thank you for sharing various topics and thoughts beyond academics, for the inspiration, insight, and laughter. Mas **Gilang,** Bu **Nuri,** Mas **Rifki**, I wish all the best for all of us and let's continue our fruitful, random, but necessary discussion. Additionally, I also thanks to the members of "Halan-Halan", Mas **Pras**, Mas **Rifko** and Mbak **Nafi**, Mbak **Rina**, and Mbak **Fera**. Thanks for making my PhD journey more colorful with delicious food, nice friendship, and wonderful adventures to explore NL and nearby countries. I hope our silaturahim will last for a long time and that we can meet again.

Pursuing PhD is not only about academic and professional things. It also part of deeply personal journey, filled with dreams, hopes, prayers, and abundant unconditional support and love from my beloved family. Thus, this work is dedicated to my families. To Bapak (Pak **Dori**) dan Ibu (Ibu **Sarti**), **Rohim**, Mbah **Somi**, Budhe **Tun**, Mbak **Ten**, Pak **Ipan,** Pak **Rom**, Mbak **Luk** and Mas **Akrom**, **Sekha**, and all Keluarga Sekaran. Also dedicated to my in-laws family, Bapak **Nuzul**, Ibu **Siti Maemunah (**Bu **Muk)**, **Septin**, **Ali**, **Dila**, **Rasyid**, and all Keluarga Mbakalan.

To my father Pak **Dori**, you are the one who has always believed that we can have dream and reach them, even when our resources are limited and we live as a middle- to low- income family. You always inspired me to believe that "nothing is impossible". You always believed that I could achieve my goals whenever I applied for scholarships or pursued higher study. In my professional work and PhD journey, I have tried to implement what you taught me. You, as a carpenter, told me that we should always work with integrity, passion, and perfection, no matter where we are and what kind of work we do. You also once said that when you were in elementary school, you were one of the outstanding students who always represented the school in various competitions. Unfortunately, you couldn't continue to go to high school and college because of financial situation. I hope this PhD degree can fulfill some of your dreams and hopes. To Ibu **Sarti**, since I was child, you went to overseas to work as a migrant worker for a better life for our family. I know it was not easy for you, but you always inspired me with how you fought for our dreams, worked hard, and sacrificed your own desires to achieve

more important goals for the family. You also didn't go to high school and college. I hope this PhD degree make you delighted, because together we have shown that we can reach our dream of better education and a better life. To my little and only brother, **Rohim**, thank you for all of your support, you do not talk too much, but I know that you always support me in your own way. Also, thanks for taking care of our parents at our home in Ponorogo. Wish all the best for your study, achieving your dreams and your future career! To Mbah **Somi**, you took care of me when I was child, and I remember our farewell before I started my PhD. You asked why it would take so long and expressed your worry about whether we would meet again. One month after I began my PhD, you passed away. It was a difficult time for me, but your inspiration, hard work, and patience remain in my memory and have helped me achieve this milestone. Many thanks also to my family **Keluarga Sekaran** for all of your kindness and help. Bapak **Nuzul** dan Ibu **Muk**, thank you for your endless support, prayers, and deep understanding of every condition I encountered, especially during my PhD journey. Thank you for taking care of dik Riyan and me with your unimaginable patient and tremendous support, so that I could pursue my PhD smoothly. You always supported whatever I needed, and gave invaluable suggestions and advices. **Septin**, **Ali**, **Rasyid**, many thanks for your helping hands. Without your help, my PhD would certainly not have gone as smoothly. All the best for you! For **Rasyid**, I hope someday you can also visit and study overseas, such as the Netherlands and many other countries. **Dila,** thank you for your continuous support. You were always ready to pick up Mbak Riyan and me, and help our family, whenever we needed your help. Wish all the best for your life and career! To **Keluarga Mbakalan**, I would like to thank for all of your tremendous support and for the very nice and warm togetherness.

I have saved this last and most special part of my acknowledgements for the person who means the most to me, my dearest wife, sayang, ta, **Riyan Zulmaniar Vinahari**. I am extremely grateful to have you by my side. Because of you, I have never truly felt lonely, even though for almost three years we were separated by oceans and continents with around 11,800 km distance. Our intensive communication truly supported me more than words can express. I am endlessly grateful for everything you have given me, your unconditional love, strength, and unwavering support, as well as for standing by my side, sharing every step, challenge, and moment of this journey with me. Our talks covered almost everything, from serious topics like, politics, economy, and statistics, to not-so-important but very necessary topics like, funny Instagram reels, artists, movies, and many random things. Those conversations made my PhD journey not only about experiments and scientific papers. They made it feel alive. More than that, I admire the person you are. You always think about and take care of other person more than yourself. You always think more about how I could eat and sleep well,

and whether my nutrition was fulfilled, than about your own comfort. I am sorry that we had to face LDM for almost three years during my PhD. I believe it was difficult for you to live alone in Indonesia with every single challenge around you, but you still gave your full and best support. Thank you very much for taking care of my parents and family in Indonesia. I am sorry that you had to abandon your own desires and always put our family first. When you went to Netherlands, I remember how much you struggled during your very first month, got ill and diarrhea during the flight from Surabaya and Jakarta to the Netherlands, and it took around one month for you to recover after arriving. You also has to adapt to an environment, culture, and language that were completely new to you. It was not easy, but you did very well. Everything you did was to support me in the Netherlands. I hope you also enjoyed every moment we shared, every adventure we had, and every new experience we unlocked together. And of course, thank you for the most delicious food you cooked for me, from rawon, soto, gado-gado, rempeyek and many more dishes with authentic Indonesian taste, even though it was hard to find authentic ingredients in the Netherlands. And thanks for the great and spicy sambal! No one can beat your sambal, believe me! We once thought that you could sell Indonesian sambal in the Netherlands, and I still believe many people would buy it. You also consistently researched discounted items in the supermarket before buying anything, all to help us save our expenses. Finally, we have passed through many challenges in our life, which I hope will shape us into stronger, wiser, and more patient person. Whatever the future brings, I know I will always have a place where I truly belong, with you. So, let us keep walking this life path together, growing, learning, and supporting each other. Also building our life side by side and strengthening our relationship just like the strong interaction between entrainer with the targeted compound I studied in my PhD. May Allah Subhanahu wa Ta'ala always grant us abundant blessing and guidance for a happy life in this world (*dunia*) and in the hereafter (*akhirat*), and may He reward us with His Jannah. *Aamiin Ya Rabbal'alamiin*.

**Kendal, 26 May 2026/09 Dzulhijjah 1446H**
**Dhoni Hartanto**

# List of publications and other portfolios

## List of Publications

### Journal publications

1. **Hartanto, D.**; Schuur, B.; Schuttevaer, T.; Kiss, A. A.; de Haan, A. B. Isobaric Vapor–Liquid Equilibrium of Methylcyclohexane + Toluene with Gamma-Valerolactone as a Biobased Entrainer and 1-Methylpyrrolidin-2-One as a Conventional Entrainer. J. Chem. Eng. Data 2025, 70 (3), 1339−1351.
2. **Hartanto, D.**; Schuur, B.; Ammerlaan, M.; Kiss, A. A.; de Haan, A. B. Vapor–Liquid Equilibrium for the Separation of the Close-Boiling Mixture Methylcyclohexane–Toluene with Dimethyl Isosorbide as a Biobased Entrainer and 1-Butylpyrrolidin-2-One as a Greener Entrainer. Ind. Eng. Chem. Res. 2025, 64 (38), 18927–18937.
3. **Hartanto, D.**; Schuur, B.; A. Kiss, A.; de Haan, A. B. Isobaric Vapor-Liquid Equilibrium of the Azeotropic Mixture n-Hexane + Ethanol with 1-Butylpyrrolidin-2-One as a Greener Entrainer and 1-Methylpyrrolidin-2-One as a Benchmark Entrainer. J. Chem. Eng. Data 2025, 70 (10), 4091-4104.
4. **Hartanto, D.**; Schuur, B.; A. Kiss, A.; de Haan, A. B. Vapor-Liquid Equilibrium for the Separation of the n-Hexane + Ethanol Azeotropic Mixture with Biobased Entrainers Guaiacol and Dimethyl Isosorbide. Fluid Phase Equilib. 2026, 605, 114694.
5. **Hartanto, D.**; Vonk S.; Kara M.; de Haan, A. B.; A. Kiss, A. Eco-efficient extractive distillation processes using biobased and greener entrainers for the separation of azeotropic and close-boiling mixtures. Separation and Purification Technology. 2026 (*submitted*)
6. **Hartanto, D.**; Schuur, B.; A. Kiss, A.; de Haan. Systematic selection of biobased, greener organic, and natural deep eutectic solvents (NADESs) for azeotropic and close-boiling mixtures separation by extractive distillation. (*work in progress*, *planned submission to Separation and Purification Technology*)

### Conference proceeding publications

1. Minor, A.-J.; **Hartanto, D.**; de Haan, A. B., Assessment of Deep Eutectic Solvents for Alcohol-Water Separations by Extractive Distillation. *The 12th International Conference on Distillation & Absorption Proceeding,* 2022, 1-6.

2. **Hartanto, D.**; Schuur, B.; Kiss, A. A.; de Haan, A. B. Effective Selection of Green Organics and Natural Deep Eutectic Solvents as Advanced Entrainers by COSMO-RS and Group Contributions Methods for Enhanced Design of Extractive Distillation. *Computer Aided Chemical Engineering*, 2024, 53, 1387–1392.
3. **Hartanto, D.**; Schuur, B.; A. Kiss, A.; de Haan, A. B. Comprehensive and Systematic Selection of Greener Entrainers for Enhanced Design of Extractive Distillation in Azeotropic Separations. *AIP Conference Proceedings*, 2026; *Accepted*.

### Oral conference presentations

1. **Hartanto, D.**; Schuur, B.; Kiss, A. A.; de Haan, A. B., European Symposium on Computer Aided Process Engineering and International Symposium on Process Systems Engineering, Florence, Italy, 2024.
2. **Hartanto, D.**; Schuur, B.; Kiss, A. A.; de Haan, A. B., 15th European Congress of Chemical Engineering (ECCE) & 8th European Congress of Applied Biotechnology (ECAB) & 3rd Iberoamerican Congress on Chemical Engineering (CIBIQ), Lisbon, Portugal, 2025.
3. **Hartanto, D.**; Schuur, B.; Kiss, A. A.; de Haan, A. B., The 14$^{th}$ International Conference on Thermofluids , Yogyakarta, Indonesia, 2025.
4. **Hartanto, D.**; Schuur, B.; Kiss, A. A.; de Haan, A. B., 13$^{th}$ International Conference on Distillation and Absorption, Salzburg, Austria, 2026 (*accepted*).

### Poster conference publications

1. Minor, A.-J.; **Hartanto, D.**; de Haan, A. B., *The 12th International Conference on Distillation & Absorption*, Touluse, France, 2022.
2. **Hartanto, D.**; Keestra, H.; Schuur, B.; Kiss, A. A.; de Haan, A. B.,*The Netherlands Process Technology Symposium - NPS2023,* Enschede, The Netherlands, 2023.

## Other portfolios

### Speaker at the Industrial Forum

**Hartanto, D.** *Thermal Separation Technology Symposium* by Het kennisnetwerk NL GUTS (Netherlands Separation Process Network)*,* Ede, The Netherlands, 2025. (*Invited speaker*)

## PhD visiting researcher

at Sustainable Process Technology (SPT), University of Twente (2022-2024)

## Reviewer

Served as a reviewer for the reputable international journals/proceeding:

1. Renewable Energy (Elsevier): 3 papers
2. Industrial & Engineering Chemistry Research (Amerian Chemical Society (ACS) Publications): 3 papers
3. ACS Omega (Amerian Chemical Society (ACS) Publications): 1 paper
4. Journal of Chemical Engineering & Data (Amerian Chemical Society (ACS) Publications): 5 papers
5. Environmental Quality Management (Wiley): 2 papers
6. Computer Aided Process Engineering (proceeding) (Elsevier): 2 papers

## Supervision

1. **Jochem Bank**. Performance assessment of green organic entrainers and natural deep eutectic solvents (NADESs) for azeotropic mixture separations by extractive distillation. *MSc Thesis of TU Delft*, 2024.
2. **Merve Kara**. Assessment of extractive distillation using green entrainers and development of an entrainer selection methodology. *MSc Thesis of TU Delft*, 2024.
3. **Matthijs Ammerlaan**. Extractive Distillation Process Design and Simulation for Separating the Close-Boiling Methylcyclohexane-Toluene Mixture using Bio-based and Organic Entrainers with Aspen Plus. *MSc Thesis of TU Delft*, 2024.
4. **Samar Vonk**. Comparison of predictive thermodynamic models with NRTL in process simulation of green entrainers for extractive distillation. *MSc Thesis of TU Delft*, 2025.
5. **Tim Schuttevaer**. On the use of cyrene-gammavalerolactone mixtures as entrainer in extractive distillation: application and solvent regeneration studies. *MSc Thesis of University of Twente (Tutor on VLE experimental work)*, 2024.
6. **Alifia Rahma Wahyudi**. Ferrofluids Regeneration via Distillation. *MSc Thesis of University of Twente (Tutor on VLE experimental work)*. 2024.

**Teaching duty**

1. CH3803 Product and Process Design (Aspen Plus Software Workshop) 2022
2. CH3803 Product and Process Design (Aspen Plus Software Workshop) 2023
3. CH3803 Product and Process Design (Aspen Plus Software Workshop) 2024
4. CH3803 Product and Process Design (Aspen Plus Software Workshop) 2025

# Curriculum Vitae

Dhoni Hartanto was born on November 11, 1987, in Ponorogo, East Java Province, Indonesia. He obtained his bachelor's degree in chemical engineering from Institut Teknologi Sepuluh Nopember (ITS), Indonesia, in 2011. During his undergraduate studies, he was selected as one of the 40 outstanding students in Indonesia by the Sampoerna Foundation and received a full scholarship for his bachelor's degree. During his study, he was awarded the 1st rank of outstanding student in the Department of Chemical Engineering and the 5th rank of outstanding student at ITS. During this period, he also won several national scientific competitions. He was awarded a BSc degree with distinction (Cum Laude) with the thesis "*Isobaric Vapor - Liquid Equilibria for Binary Systems Ethanol + Ethyl Acetate and Ethanol + Isoamyl Alcohol at 101,33 kPa, 79,99 kPa and 26,67 kPa"*

In 2011, he continued his studies in chemical engineering through a double degree master's program between ITS, Indonesia, and National Taiwan University of Science and Technology (NTUST), Taiwan, with a full scholarship from both universities. He completed his master's degree in 2013 and was awarded an MSc degree with distinction (Cum Laude) for his thesis entitled *"Vapor-Liquid Equilibrium of Aqueous Alcohol Mixtures in the Presence of Biological Buffer TRIS or EPPS".* After completing his master's degree, he began his academic career as a junior lecturer in the Chemical Engineering Department, Universitas Negeri Semarang (UNNES), Indonesia.

After several years in academia as a junior lecturer, he applied for doctoral study and was awarded a PhD scholarship from the Indonesia Endowment Fund for Education (LPDP), Ministry of Finance, Republic of Indonesia, in September 2019. He started his PhD in December 2021 at Delft University of Technology (TU Delft), the Netherlands, under the supervision of Prof. Dr. Ir. André B. de Haan and Prof. Dr. Ir. Anton A. Kiss. His doctoral research focuses on developing *"A systematic and validated framework for selecting greener entrainers towards eco-efficient extractive distillation".*


TUDelft
lpdp